Journal of Applied Mechanics

(Contributions of the ASME Applied Mechanics Division)

...		1
..., and Heat-Transfer Measurements	D. S. Johnson	2
...covery Spaced Radial Diffuser	H. V. Worland	9
...Through a Cyclone Dust Separator	M. E. Weber and J. H. Keenan	16
...Mechanisms by Method of Components	J. Blackburn	22
...Number	B. R. G. Baker and T. F. Irvine, Jr.	23
...	S. J. Kline and R. O. Kenny	29
...of a Simple Built-Up Beam	T. H. H. Pian	35
...Sensors of Induction Motors	E. Erdelyi and G. Hevesy	39
...and Plates to Random Loads	A. G. Bergen	46
...Stationary Spectrum of Circular Disk on Flexible Base	R. L. Sharpe	53
...Body on an Elastic Foundation	G. B. Warburton	55
...of Solid-Infinite Circular Elastic Bar	Richard Skalak	59
...Phenomena	J. H. Huth, J. S. Thompson, and M. E. Van Valkenburg	65
...Two-Dimensional Sweep and Strain Distributions	A. J. Durelli and W. F. Riley	69
...for Fracture of Metals	Takeo Yokobori	77
...ations of Blasius-Frankl Nets	E. G. Thomsen	81
...With Reinforced Cutouts	P. C. Hodge, Jr., and Nicholas Perrone	88
...of Laplace's and Poisson's Equation	H. G. Landau	95
...Stresses in an Elastic-Plastic Wedge	P. M. Naghdi	99
...Strength Subjected to Bending	W. A. Green and J. P. Li	103
...Plane of Stationary Crack	M. L. Williams	109
...Loads on Plane Twist of Infinite Strip	Osamu Tamate	115
...Problem of Elasticity	Gene-Shay Pan'kov	122
...Imperfect Cylindrical Shells	W. A. Nash	125
...for Linear Mass-Spring System	Eugene Sevin	131
...		
...Nozzle Flows	E. E. Zwikle and Bernhold Schneider	137
...Bending of Circular Plates	Yi-Yuan Yu	141
...Symmetrical Ring Glaciers	G. P. Fisher	144
...		
...a Sphere Pack	A. Fisk	148
...Stress Conditions for a Rotating Solid	L. V. King	149
...Solution for Clamped Circular Plate	K. D. Cowper	151
...Viscoelastic-Beam Impact Problem	E. A. Bilby	152
...briefly published papers by P. G. Kafka and M. B. Bieber; A. M. Wahl; F. Per... ...Hoff; A. C. Hoge and G. O. Seaburg; O. E. Hagenbuch; A. K. Head; T. C. Li... ...Murray; James Walters and John Elliott		155
...		168

MARCH, 1957

VOL. ... NO. ...

... of The American Society of Mechanical Engineers

rnal of Applied Mechanics

Papers Submitted for Publication by the ASME Applied Mechanics Division

[illegible] Chairman,
[illegible] Editor

W. Ramberg, Secretary
D. C. Drucker and J. Kestin, Technical Editors

Published Quarterly by

The American Society of Mechanical Engineers

Publication Office, 20th and Northampton Streets, Easton, Pa.
Executive Offices at the Headquarters of the Society, 29 West Thirty-Ninth Street, New York 18, N. Y.
Communications should be addressed to the Technical Editors, Journal of Applied Mechanics, ASME,
Division of Engineering, Brown University, Providence 12, R. I.

OFFICERS OF THE SOCIETY

W. F. Klein, President

[illegible], Secretary
C. E. Davies, Secretary
O. B. Schier, 2nd, Assistant Secretary

[illegible] Committee

J. J. Jakosky, Jr., Editor
H. E. Wessman, Publisher

Statement of the Society not responsible for statements or opinions advanced in papers or . . . printed in its publications (B13, Par. 4)

Subscription [illegible] Engineers, Incorporated, 29 West Thirty-Ninth Street, New York 18, N. Y. The principal office of the Society is located at 29 West Thirty-Ninth Street, New York 18, N. Y. Checks should be drawn to the order of the Society. Price per copy [illegible] $1.50 [illegible] postage to all countries outside the United States. [illegible] Society [illegible] Engineers, [illegible] they are so by elections on the mailing [illegible] Society [illegible] Engineers [illegible] Society [illegible] Engineers or exchanges advanced in papers or . . . [illegible] Society [illegible] Engineers [illegible] Society [illegible] Engineers [illegible] Society [illegible] Engineers

John M. Lessells

PAPERS in the field of Applied Mechanics have appeared in Transactions, ASME, ever since the first volume (1880). It was not until 1927, however, that the ASME Applied Mechanics Division was organized. In that year, and for a few years thereafter, the papers contributed to Transactions by the Professional Divisions were grouped in separate issues according to the Division sponsorship. Papers of the Division appeared quarterly as a part of Transactions.

When Transactions became a monthly periodical an attempt was made to devote the February issue to the papers of the Applied Mechanics Division until 1935, when the *Journal of Applied Mechanics* was authorized by the Publications Committee at the request of that Division. Decision to set up the *Journal* as a separate quarterly, but also as a part of Transactions ASME, was based on a demand for an international journal in the field of applied mechanics which none of the societies involved, except ASME, offered to undertake.

Perhaps the most important element in the success of the *Journal* from the point of view of the Publications Committee was the appointment, on recommendation of the Division, of John M. Lessells as technical editor. As one of the organizers of the Division and an enthusiastic proponent of the *Journal*, he devoted his time and talents to the task of centralizing authority and responsibility in his office without remuneration for his services, with the result that the Editorial Department was relieved of all duties except those of styling manuscripts and producing the finished publication.

In 1956 Lessells asked to be relieved of the editorship of the *Journal*, but his interest in it and his advice and long experience are still available.

John Moyes Lessells was born in Dunfermline, Scotland, in 1888. As an apprentice in his father's concern he attended engineering classes at the Lauder Technical School, Dunfermline, where he obtained a Carnegie Scholarship to continue his studies at the Heriot-Watt College, Edinburgh, and the University of Glasgow, which awarded him the degree of Bachelor of Science in Engineering in 1915. During the first World War he served at Rolls-Royce, Ltd., in Derby, and at the Whitworth Company, Ltd., Newcastle-on-Tyne, where his work dealt mostly with inspection of aero-engine parts. In 1918 he became special engineer to the works manager of Rolls-Royce, Ltd., and was engaged in design and production.

Lessells came to the United States in 1920 to enter the employ of the Westinghouse Electric and Manufacturing Company where he organized the Mechanics Division of the Research Laboratories. Nearly a decade earlier Benjamin G. Lamme had organized an electrical design school for the training of gifted young college graduates employed by the Company. George M. Eaton, a Member of ASME, organized a similar training plan for mechanical engineers at Westinghouse in the early 1920's and in this work Lessells played an important part. Many men of outstanding ability were attracted to the Westinghouse Company, among whom were such ASME Members as Timoshenko, Den Hartog, and Nadai.

When Lessells was offered the position of Manager of Engineering of the Turbine and Diesel Engine Department of Westinghouse at South Philadelphia, he was successful in attracting such men as Ormondroyd, Soderberg, Karelitz, Kroon, and others.

Lessells engaged in consulting practice of his own in 1935, and in 1936 became an Associate Professor of Mechanical Engineering at the Massachusetts Institute of Technology. In 1946 he organized Lessells and Associates, Inc.

Lessells joined ASME in 1923 and was made a Fellow in 1952. He became an Honorary Member, ASME, in 1952, "for outstanding contributions to the development of Applied Mechanics within The American Society of Mechanical Engineers."

Lessells is a stocky, sandy-haired, blue-eyed Scotsman whose speech still shows strong traces of a native burr. As a colleague he possesses a solid stability that inspires confidence and a friendliness that has the warmth of affection. An explosive chuckle punctuates his lighter conversation. Interest in and affection for his adopted country have given him a better knowledge of it and more profound understanding of its history and institutions than most native-born citizens can boast. He is enticed to return to Great Britain for summer holidays which he spends renewing old acquaintances, building good will, and taking pictures.

The relationships of Lessells with the ASME Editorial Department have been, from the start, on a basis of friendly cordiality. Should difficulties arise between the Department and authors, a call to him would assure prompt and effective treatment. He was a frequent and welcomed visitor in the office of the Managing Editor, the late Katherine Clendinning, who looked upon the *Journal* as her special pride and members of the Applied Mechanics Division as her best and most respected friends. To the complete mutual understanding and co-operation of these two a large measure of the success of the *Journal* rested from its beginning. Nor should mention be omitted of the loyal and effective service of Miss Gwendoline M. Jackson, secretary to Lessells, who was always helpfully on the other end of the telephone when need arose.

As a fellow editor who has been associated with Lessells for at least two decades and has watched the *Journal of Applied Mechanics* grow from an experimental venture to a respected engineering quarterly with the highest international reputation, the writer of this tribute is confident that he speaks for a great multitude of other friends and co-workers in the field of applied mechanics in wishing John Lessells long life, sound health, and the satisfactions he has earned.

GEORGE A. STETSON, *Editor Emeritus ASME*

Velocity, Temperature, and Heat-Transfer Measurements in a Turbulent Boundary Layer Downstream of a Stepwise Discontinuity in Wall Temperature[1]

By D. S. JOHNSON,[2] WHIPPANY, N. J.

Results are presented of an experimental investigation of the concomitant thermal and velocity fields occurring when there is a small stepwise discontinuity in the temperature of the wall on which a zero-pressure-gradient, low-speed, turbulent boundary layer has formed. The mean velocity and temperature fields have been measured and local heat-transfer-coefficient values in the streamwise direction have been obtained in the region where the thermal boundary layer has not yet reached the free stream. No over-all similarity between the thermal and velocity fields was found.

Nomenclature

The following nomenclature is used in the paper:

$c_f \equiv \tau_1 \Big/ \frac{1}{2}\rho U_0^2$ = wall skin-friction coefficient
c_p = specific heat at constant pressure
k = thermal conductivity
Nu_a = Nusselt number formed using any length a
P = instantaneous value of static pressure
Pe_a = Péclet number formed using any length a
p = instantaneous value of static-pressure fluctuation
Q = heat flux per unit area
Re_a = Reynolds number formed using any length a
St = Stanton number
T = absolute temperature
$T_* \equiv Q_1/\rho c_p U_*$ = friction temperature
t = time
U, V, W = instantaneous values of velocity components in direction of x, y, z-axes, respectively
$U_* \equiv \sqrt{\tau_1/\rho}$ = friction velocity
u, v, w = instantaneous values of turbulent velocity fluctuations in direction of x, y, z-axes, respectively
x, y, z = co-ordinate axes (see Fig. 1)
$\alpha \equiv k/\rho c_p$ = thermal diffusivity
$\delta_c \equiv \int_0^\infty \frac{\bar{U}}{U_0}\frac{\bar{T}-T_0}{T_1-T_0}\,dy$ = convection thickness of thermal boundary layer
δ_Θ = geometric thickness of thermal boundary layer
$\delta^{**} \equiv \int_0^\infty \frac{\bar{U}}{U_0}\left(1-\frac{\bar{U}}{U_0}\right)dy$ = momentum thickness of momentum boundary layer
ϑ = instantaneous value of turbulent temperature fluctuation
μ = dynamic viscosity
$\nu \equiv \mu/\rho$ = kinematic viscosity
ρ = density
$\sigma \equiv \mu c_p/k$ = Prandtl number
τ = shearing stress

Notation

$(\ )_i$ = ith co-ordinate axis (Cartesian tensor notation)
$(\ )_0$ = free-stream condition
$(\ )_1$ = condition at wall
$(\ )' \equiv \sqrt{\overline{(\ )^2}}$, root-mean-square value
$\overline{(\ )}$ = time (or ensemble) average; i.e., mean value

Introduction

Turbulent flows with mean shear (e.g., the boundary layer, jet, wake, and fully developed pipe and channel flows) are of importance in several fields of interest. In many cases where such flows are encountered in practice, they are accompanied by heat or mass transfer; the situation can be much more complex than the flow in the absence of transfer if there are appreciable effects of the transferred quantity back upon the flow. Consequently, studies of such cases have been primarily experimental and usually have been directed toward the measurement of over-all properties and the formulation of empirical relationships.

The investigation reported here was intended to provide some basic information on the transfer of heat through a turbulent boundary layer. To this end, the number of controlling factors was reduced by making the measurements in an air flow having simple, reproducible boundary conditions and whose speed was low enough to permit neglecting the effects of compressibility. In particular, the static pressure was constant and the parameter $(\bar{T}_M - T_0)/T_0$, where $\bar{T}_M$ is the maximum mean temperature encountered and T_0 is a reference temperature such as that of the

---

[1] Based on part of a dissertation submitted to The Johns Hopkins University in August, 1955, in conformity with the requirements for the degree of Doctor of Engineering. The investigation was supported by the Office of Scientific Research, Air Research and Development Command, under Contract AF 18(600)-671.

[2] Member of Technical Staff, Bell Telephone Laboratories, Inc.; formerly, Research Assistant, Department of Aeronautics, The Johns Hopkins University, Baltimore, Md.

Contributed by the Applied Mechanics Division and presented at the Annual Meeting, New York, N. Y., November 25–30, 1956, of The American Society of Mechanical Engineers.

Discussion of this paper should be addressed to the Secretary, ASME, 29 West 39th Street, New York, N. Y., and will be accepted until April 10, 1957, for publication at a later date. Discussion received after the closing date will be returned.

Note: Statements and opinions advanced in papers are to be understood as individual expressions of their authors and not those of the Society. Manuscript received by ASME Applied Mechanics Division, May 28, 1956. Paper No. 56—A-19.

ambient or free stream, was restricted to a small enough value that the dynamical properties of the flow were unchanged, within experimental accuracy, from their values in the absence of heat transfer.[2]

Previous measurements of heat transfer in a turbulent boundary layer usually have been for the purpose of obtaining heat-transfer data only. The investigations most similar to the work reported here have been those of Élias (1)[4] and of Scesa and Sauer (2). Élias obtained mean velocities and temperatures in the turbulent boundary layer over a heated plate; although the momentum and thermal layers started at slightly different streamwise locations, he concluded that the latter quickly became fully developed (i.e., reached the free stream) so that the majority of his turbulent-layer measurements corresponded to effectively simultaneous initial points. The results of his measurements are discussed in terms of momentum-transport theory by Squire (3). Scesa and Sauer obtained local heat-transfer data for a flat-plate turbulent boundary layer with the thermal layer starting at several distances from the leading edge of the plate. Their results have been compared with semiempirical theory by Rubesin (4).

The present paper reports some results of an experimental investigation of the velocity and thermal fields sketched in Fig. 1.

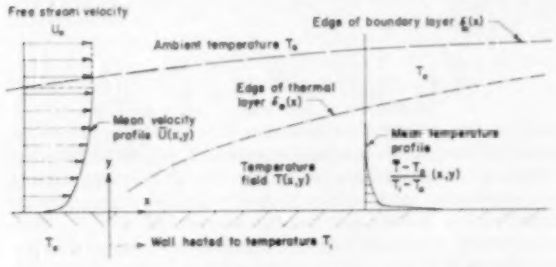

FIG. 1 SKETCH OF VELOCITY AND TEMPERATURE FIELDS

With the present experimental configuration, the heated wall is not long enough for the thermal boundary layer to grow out to the momentum free stream. At the time of writing, an extended heated section is under construction, and measurements farther downstream are planned.

ANALYTICAL CONSIDERATIONS

Equations of Mean Motion. In Cartesian co-ordinates, the steady turbulent flow of a viscous incompressible fluid is governed by the Reynolds equations

$$\rho \bar{U}_j \frac{\partial \bar{U}_i}{\partial x_j} = -\frac{\partial \bar{P}}{\partial x_i} + \frac{\partial}{\partial x_k}\left(\mu \frac{\partial \bar{U}_i}{\partial x_k} - \overline{\rho u_i u_k}\right) \quad [1]$$

where a repeated index indicates summation and the Reynolds restriction has been applied, namely

$$U_i(t) = \bar{U}_i + u_i(t); \quad P(t) = \bar{P} + p(t); \quad \bar{u}_i = \bar{p} \equiv 0 \quad [2]$$

Conservation of mass for the mean flow is expressed by the continuity equation

$$\frac{\partial \bar{U}_j}{\partial x_j} = 0 \quad [3]$$

(The fluctuating velocities also satisfy the continuity equation at any instant.)

Replacing the tensor notation by the conventional x, y, and z-axes and corresponding mean and fluctuation velocity components ($\bar{U}$, $\bar{V}$, $\bar{W}$) and (u, v, w), and applying the conventional boundary-layer-type approximation for two-dimensional mean motion in the x, y-plane with mean flow in the direction of the x-axis, Equations [1] and [3] become

$$\rho\left(\bar{U}\frac{\partial \bar{U}}{\partial x} + \bar{V}\frac{\partial \bar{U}}{\partial y}\right) = -\frac{\partial \bar{P}}{\partial x} + \mu\frac{\partial^2 \bar{U}}{\partial y^2} - \rho\frac{\partial \overline{uv}}{\partial y} \quad [4]$$

$$\frac{\partial \bar{U}}{\partial x} + \frac{\partial \bar{V}}{\partial y} = 0 \quad [5]$$

where the term $\partial\overline{u^2}/\partial x$ was neglected, relative to $\partial \bar{U}^2/\partial x$ or $\partial\overline{uv}/\partial y$, for example.

As is well known, these equations differ in form from the corresponding equations for the laminar layer only by the additional term involving the Reynolds or turbulent shearing stress $-\rho\overline{uv}$. The total shearing stress is

$$\tau = \mu\frac{\partial \bar{U}}{\partial y} - \rho\overline{uv} \quad [6]$$

Since the static-pressure gradient was negligible for measurements reported here, the term $\partial \bar{P}/\partial x$ is omitted in the remainder of this section.

Taking the origin and orientation of axes as shown in Fig. 1, Equation [4] can be integrated with respect to y to give the turbulent shearing stress as a function of y. The result is

$$\overline{uv}(y) = \nu\left[\left(\frac{\partial \bar{U}}{\partial y}\right)_y - \left(\frac{\partial \bar{U}}{\partial y}\right)_1\right] + \bar{U}(y)\int_0^y \frac{\partial \bar{U}}{\partial x}\,dy' - \int_0^y \frac{\partial \bar{U}^2}{\partial x}\,dy' \quad [7]$$

(y' is a variable of integration), where the boundary conditions

$$\bar{U} = 0 \text{ and } \overline{uv} = 0 \text{ at } y = 0 \quad [8]$$

have been applied and $\bar{V}$ has been eliminated with the continuity Equation [5]. Using Equation [6] and letting $y \to \infty$ in Equation [7], the well-known von Karman integral equation for the boundary layer with zero pressure gradient is obtained

$$\frac{d\delta^{**}}{dx} = \frac{c_f}{2} \quad [9]$$

Equations [7] and [9] permit estimates of the turbulent shearing stress and skin-friction coefficient to be made from mean-flow measurements alone.

Mean Heat-Transfer Equations. The heat-transfer (energy) equation for incompressible flow with no heat sources and constant fluid properties is

$$\frac{DT}{Dt} = \alpha\nabla^2 T \quad [10]$$

where $$\frac{D}{Dt} \equiv \frac{\partial}{\partial t} + U_i\frac{\partial}{\partial x_i}$$

Equation [10] is linear in T if the temperature range is small enough to permit assuming the diffusivity α to be constant. If a Reynolds restriction is assumed for the temperature as well as the velocity

$$T(t) = \bar{T} + \vartheta(t); \quad U_i(t) = \bar{U}_i + u_i(t); \quad \bar{\vartheta} = \bar{u}_i \equiv 0 \quad [11]$$

[2] A result of this latter restriction is the equivalence, due to governing equations of the same form, of mass transfer at low contaminant concentrations and heat transfer at low temperatures; such equivalence would permit a mass-transfer problem to be studied with heat transfer as an analog, for example.

[4] Numbers in parentheses refer to the Bibliography at the end of the paper.

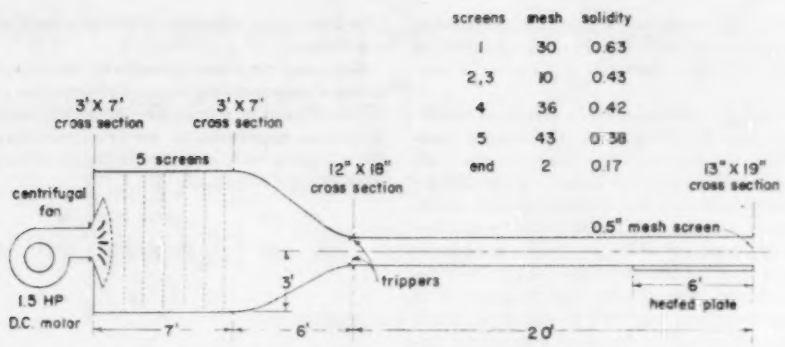

FIG. 2 SKETCH OF WIND TUNNEL

substitution into Equation [10] followed by averaging yields the mean heat-transfer equation for turbulent flow (5)

$$\bar{U}_i \frac{\partial \bar{T}}{\partial x_i} = \alpha \nabla^2 \bar{T} - \frac{\partial (\overline{\vartheta u_k})}{\partial x_k} \quad [12]$$

The equation for flow in a boundary layer with two-dimensional mean motion follows from the usual laminar-boundary-layer-type of approximation plus the neglecting of $\partial \overline{u\vartheta}/\partial x$

$$\bar{U} \frac{\partial \bar{T}}{\partial x} + \bar{V} \frac{\partial \bar{T}}{\partial y} = \alpha \frac{\partial^2 \bar{T}}{\partial y^2} - \frac{\partial \overline{v\vartheta}}{\partial y} \quad [13]$$

Equation [13] differs in form from the laminar case by the addition of the turbulent heat-transfer term $-\overline{v\vartheta}$ in the same way the Reynolds equation differed from the laminar momentum equation by the addition of the turbulent shearing stress. Furthermore, the turbulent heat-transfer and Reynolds equations have the same general appearance when the gradient of the average static pressure $\bar{P}$ is zero. In the past, this fact has led to semiempirical analyses assuming complete analogy between heat and momentum transfer, a situation requiring that the Prandtl number σ be unity as well as equating a vector transport to a scalar transport.

Just as the boundary-layer-momentum equation can be integrated to determine the distribution of the turbulent shearing stress or to obtain the skin friction, similar procedures yield the distribution of turbulent heat transfer and the heat-transfer coefficient at the wall. Integrating Equation [13] with respect to y and applying the boundary conditions

$$\bar{T} = T_1, \quad \bar{V} = 0, \quad \overline{v\vartheta} = 0 \quad \text{at} \quad y = 0 \quad [14]$$

together with the continuity Equation [5], the turbulent heat-transfer rate is given by

$$\overline{v\vartheta}(y) = \alpha \left[\left(\frac{\partial \bar{T}}{\partial y} \right)_y - \left(\frac{\partial \bar{T}}{\partial y} \right)_1 \right] + \bar{T}(y) \int_0^y \frac{\partial \bar{U}}{\partial x} dy' - \int_0^y \frac{\partial}{\partial x} (\bar{U}\bar{T}) dy' \quad [15]$$

Writing the total heat transfer as the sum of molecular and turbulent contributions

$$Q = k \frac{\partial \bar{T}}{\partial y} - \rho c_p \overline{v\vartheta} \quad [16]$$

and substituting into Equation [13], integration with respect to y yields the thermal integral equation[5]

$$\rho c_p \frac{d}{dx} \int_0^{\delta_\Theta} \bar{U}(\bar{T} - T_0) dy = Q_1 \quad [17]$$

where δ_Θ, the geometric thickness of the thermal layer, is not necessarily the same as that of the momentum layer. If the mean static pressure and the wall temperature are constant, Equation [17] can be written as

$$\frac{d}{dx} \int_0^\infty \frac{\bar{U}}{U_0} \frac{\bar{T} - T_0}{T_1 - T_0} dy = \frac{Q_1}{\rho c_p U_0 (T_1 - T_0)} \quad [18]$$

where the upper limit of integration has been extended to infinity since the integrand vanishes for values of y greater than δ_Θ. Equation [18] is quite similar in form to the momentum integral equation for the boundary layer with zero pressure gradient, Equation [9]; the integral has the dimension of length and is characteristic of the thermal convection field. In analogy with the momentum thickness, Eckert (7) has called this the "convection thickness," denoted here by δ_c. The quantity on the right-hand side of the equation is the local value of the Stanton number, a convective heat-transfer coefficient. In these terms, Equation [18] assumes the form

$$\frac{d\delta_c}{dx} = \mathrm{St} \quad [19]$$

In past analyses of turbulent flow with a fixed boundary, it has been found that the so-called friction velocity U_* is a useful reference quantity, especially for the flow in the neighborhood of the wall. For such flows involving heat transfer, Squire (8) has suggested the use of an "analogous" reference temperature which he calls the "friction temperature" T_*, and defines by the relation $T_* U_* \equiv Q_1/(\rho c_p)$. Convenient expressions for the friction velocity and temperature are

$$\frac{U_*}{U_0} = \sqrt{\frac{\overline{c_f}}{2}} \quad [20]$$

$$\frac{T_*}{T_1 - T_0} = \frac{\mathrm{St}}{\sqrt{\frac{\overline{c_f}}{2}}} \quad [21]$$

By choosing an appropriate reference length, the Nusselt number can be obtained as the product of the Stanton and Péclet numbers; the latter, of course, is itself the product of Prandtl and Reynolds numbers.

EXPERIMENTAL EQUIPMENT AND PROCEDURES

The wind tunnel, Fig. 2, is an open-return blowing type which

[5] The derivation of this equation is given, for example, in (6), pp. 614–615.

was constructed for the present investigation. The settling chamber and test section are connected by a contraction which is slightly asymmetric in vertical section to permit the test section to be a convenient height from the floor. The test-section area increases slightly from entrance to exit to maintain constant static pressure with boundary-layer growth. The side walls of this portion are of plate glass while the top and bottom are plastic-faced plywood. While the boundary layer on the floor was utilized for measurements, $^1/_8$-in. rods were taped to all four walls transverse to the flow about 2 in. upstream of the end of the contraction to insure simultaneous transition of the boundary layers and hence similar growth rates. The entire tunnel is pressurized slightly by a $^1/_4$-in.-mesh, low-density screen at the outlet. All measurements were made at a free-stream velocity of 25 fps, at which condition the free-stream turbulence level u'/U_0 is 0.07 per cent at the entrance to the test section.

The last 6 ft of floor of the test section, where the boundary layers on all walls are between 4 and 5 in. thick, is $^1/_4$-in.-thick aluminum-alloy plate whose temperature can be raised as much as 35 deg C above ambient by means of electrical resistance coils directly beneath. Buckling due to the temperature gradient through the plate is prevented by longitudinal steel channels attached to the bottom of the plate assembly. The heating elements are helical coils of nichrome resistance wire supported by ceramic rods transverse to the flow direction and about $^1/_2$ in. below the plate. The longitudinal spacing of the coils is uniform except in the neighborhood of the leading edge, where they are closer together to allow for the higher heat-transfer rates in that region. The coils are enclosed to reduce excessive and variable extraneous heat losses. The total heating current is controlled by a variable autotransformer and local adjustments are made by rheostats in series with the coils heating each 6-in. length of plate.

The temperature distribution over the area of the plate is given by 25 copper-constantan thermocouple junctions whose voltages are measured with reference to a junction in the free stream ahead of the plate. The junctions in the plate are soft-soldered into brass plugs pressed into holes in the aluminum; after finishing, the junction is flush with the plate surface. Immediately prior to installation in the tunnel, the plate surface was given a "satin" finish by polishing all over with fine abrasive paper. All measurements were made with the plate heated 15 deg C above free-stream temperature; this gives a value of 0.05 for the parameter $(T_1 - T_0)/T_0$ and was chosen after comparing mean velocity and longitudinal turbulence-level profiles at several overheats with those obtained over the unheated plate.

Probes are positioned normal to the floor of the test section by a device similar to a vernier height gage; for the first inch of travel from the floor, the location is given by a dial indicator reading to 0.001 in., and beyond 1 in., the position is read by means of cross hairs and a magnifier on a scale divided to 0.01 in. The zero reading for any traverse is obtained by measuring the distance between the probe and its reflection in the plate through a telescope having a reticle scale. A clear reflection results when the axis of the telescope is at a grazing angle to the plate surface. The estimated accuracy of location is ±0.0015 in. in the first inch of travel and ±0.004 in. beyond. No deflection of the probes due to airloading of them or their supports could be detected; zero settings were generally made with the tunnel running, however.

The distributions of mean velocity and mean temperature through the boundary layer were determined at a number of points on the center line of the heated plate. Mean velocities were obtained with a total-head probe consisting of a flattened hypodermic needle with an opening 0.010 × 0.055 in. and wall thickness 0.010 in.; the pressures were read on an inclined alcohol manometer having a ten-to-one slope where the position of the meniscus could be read to an accuracy of ±0.01 mm by means of a vernier. Results were corrected for the effect of varying mean temperature (hence density) in the boundary layer. Several mean velocity profiles also were obtained from hot-wire measurements as an independent check on the values given by the total-head probe; these were found to agree within experimental accuracy. Corrections for the effects of turbulence, mean velocity gradient, or proximity of the wall have not been applied to the data as presented.

Mean temperatures were measured with 0.00005-in-diam platinum wires mounted on conventional hot-wire anemometer probes but operated as resistance thermometers. These had resistances of the order of 80 ohms and were used in pairs in a bridge arrangement to compensate for any gradual drifting of the ambient temperature; one probe was fixed in the free stream while the other was traversed through the boundary layer.

Results of Measurements

Mean velocity profiles over the heated plate as determined from total-head tube measurements are plotted in dimensionless form in Fig. 3. There is reasonably close similarity, considering that the boundary-layer Reynolds number increases with dis-

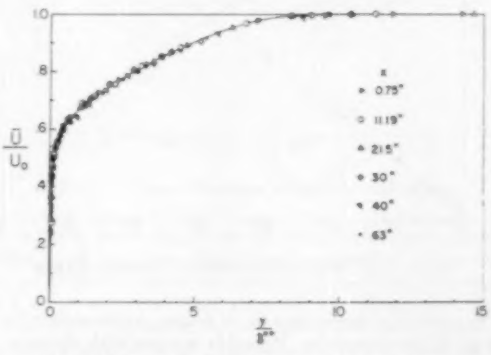

Fig. 3 Mean Velocity Profiles Along Plate

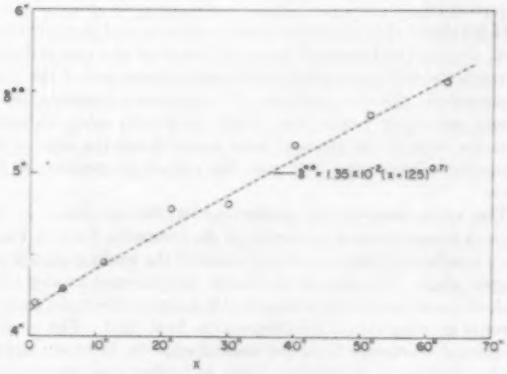

Fig. 4 Momentum Thickness of Boundary Layer

tance along the plate. The distribution with x of the momentum thickness δ^{**} is given in Fig. 4; the dashed line is a simple power-law fitting of the experimental data and is represented by

$$\delta^{**}(x) = 0.0135(x + 125)^{0.71} \quad [22]$$

with δ^{**} and x in inches.

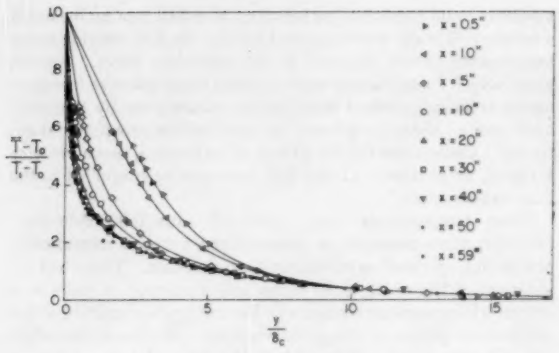

FIG. 5 MEAN TEMPERATURE PROFILES ALONG PLATE

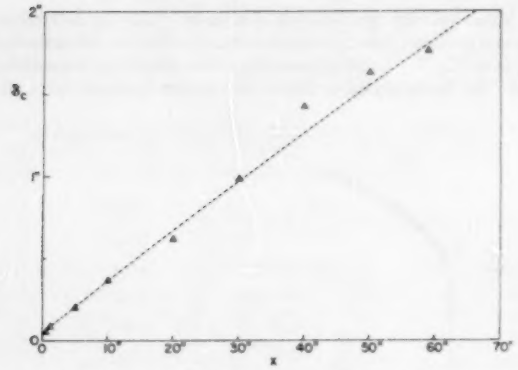

FIG. 6 CONVECTION THICKNESS OF THERMAL LAYER

The power-law approximation, of course, does not allow for the change of boundary-layer Reynolds number with distance (9), but it is simple and permits explicit rough estimates of skin-friction coefficients through application of the von Karman integral Equation [9].

It developed that at the free-stream velocity and plate overheat used, the thermal boundary layer did not grow at a rate sufficient to reach the free stream before the downstream end of the plate was reached. An extrapolation of the apparent geometric thicknesses, assuming power laws for both growth rates, indicated that the edge of the thermal layer would reach the edge of the momentum layer some 2 ft past the end of the present heated plate.

The mean temperature profiles under the conditions of the present measurements are shown in dimensionless form in Fig. 5 for a number of distances downstream of the leading edge of the heated plate. No over-all similarity is evidenced among these and, of course, none is to be expected in a region where the thermal layer is growing into a inhomogeneous flow field. The profiles farthest downstream from the leading edge do, however, appear to be tending to a limiting form, indicating the approach to the fully developed state—presumably attainable in another 2 ft.

Values of the convection thickness δ_c defined by Equation [18] as determined from mean velocity and mean temperature profiles at several points along the plate are plotted in Fig. 6. Owing to the amount of scatter in these points, no attempt was made to fit an analytical expression giving the variation of δ_c with x; the dashed curve was faired in by eye, however.

Of course, the von Karman integral method can be applied to estimation of boundary-layer-type heat-convection problems just as to momentum (6). For the present problem, however, an explicit analytical solution for $\delta_c(x)$ with the given velocity field is simple only with a restriction to similar temperature profiles $\bar{T}$ for all x—an assumption not consistent with Fig. 5. The rather laborious job of calculating $\delta_c(x)$ with $\bar{T}$-curves assumed to be a one-parameter family has not been undertaken.

DISCUSSION OF RESULTS

In the absence of a fully developed thermal boundary layer, no significant comparison can be made between the forms of the mean velocity and mean temperature profiles. For the situation studied, the two are not similar even near the downstream end of the heated plate; this is demonstrated in Fig. 7 where the mean curve through the velocity profiles of Fig. 3 is compared with the mean curve of the downstream temperature profiles of Fig. 5. [The dimensionless mean temperature has been plotted as $(T_1 - \bar{T})/(T_1 - T_0)$ to give it the same values as the dimensionless mean velocity at the end points.] In Fig. 8 typical velocity and temperature data are plotted in semilogarithmic co-ordinates to indicate the extent of possible logarithmic regions in the two profiles.

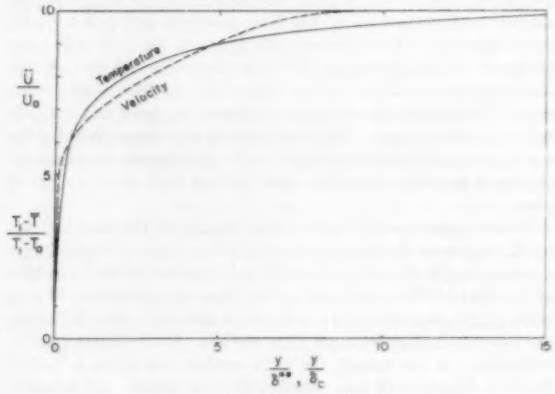

FIG. 7 COMPARISON OF FORMS OF MEAN-VELOCITY AND TEMPERATURE PROFILES

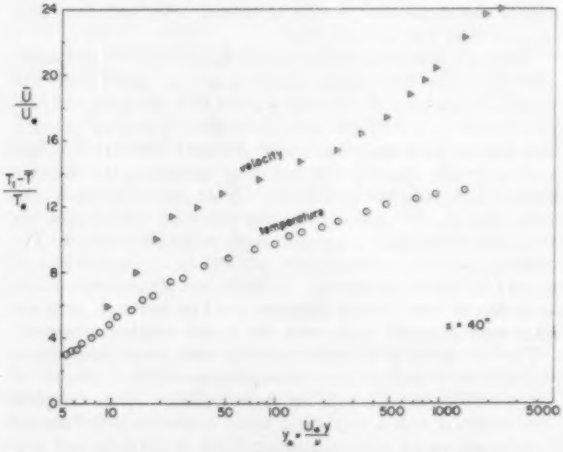

FIG. 8 MEAN VELOCITY AND TEMPERATURE IN SEMI-LOGARITHMIC CO-ORDINATES

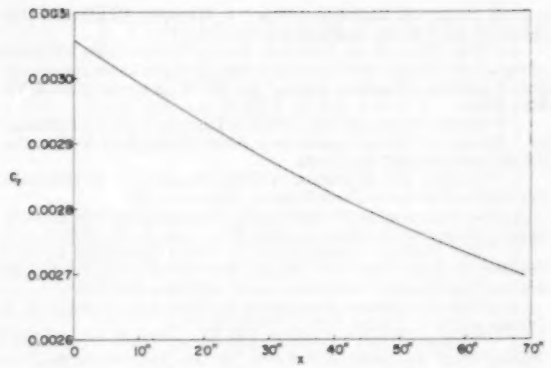

FIG. 9 SKIN-FRICTION COEFFICIENT ALONG HEATED WALL

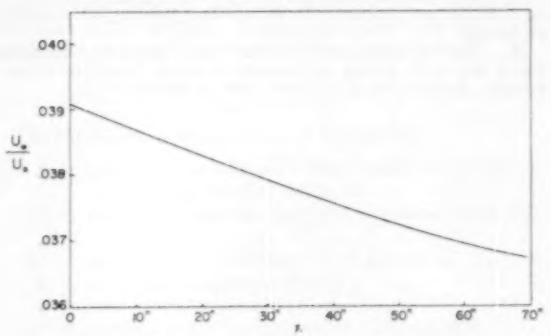

FIG. 10 FRICTION VELOCITY ALONG PLATE

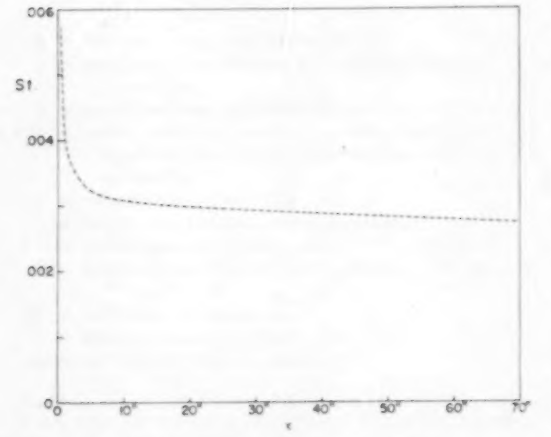

FIG. 11 STANTON NUMBER ALONG PLATE

A comparison was made among the values obtained for the skin-friction coefficient c_f at one location where independent determinations could be made from extrapolation to the wall of the turbulent shearing stress $-\rho\overline{uw}$ as directly measured (10) and as computed from Equation [7], from the "law of the wall" (11) and from the semiempirical relation of Squire and Young (12) as well as from the use of Equations [9] and [22]. These did not agree within experimental accuracy and, in fact, the largest value was more than twice the magnitude of the smallest. Examination of

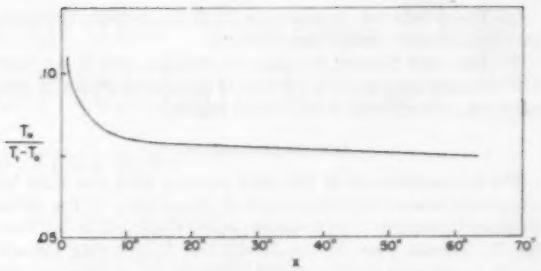

FIG. 12 FRICTION TEMPERATURE ALONG PLATE

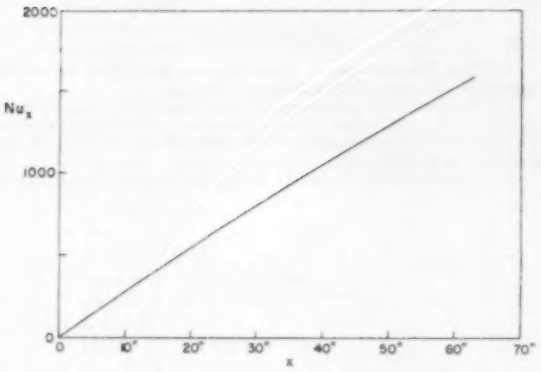

FIG. 13 NUSSELT NUMBER ALONG HEATED WALL

factors which might contribute to such a discrepancy, such as possible small deviations from two-dimensionality of the mean flow, led to the conclusion that the actual skin-friction coefficient has a value very near that given by the Squire and Young formula (10). The variation of c_f along the heated plate was therefore determined to be as shown in Fig. 9; the distribution of the friction velocity as computed from Fig. 9 by means of Equation [20] is given in Fig. 10.

The local Stanton number along the plate is presented in Fig. 11; the values were obtained from application of Equation [19] to the data of Fig. 6. The friction temperature T_* as defined by Equation [21] is plotted in Fig. 12 from the data of Figs. 9 and 11. It is seen that this quantity remains almost constant with distance along the plate following a sharp drop in the leading-edge region. This behavior is to be contrasted with the monotonic decrease of the friction velocity, the analogous quantity pertaining to skin friction.

The local heat-transfer coefficient was computed in the form of the Nusselt number based on distance from the leading edge and is presented in Fig. 13. The values were obtained from the relation $\mathrm{Nu}_x = \mathrm{Pe}_x \mathrm{St} = \sigma \mathrm{Re}_x \mathrm{St}$ where the material properties were evaluated at the free-stream temperature.

CONCLUSION

The experimental investigation of the velocity and thermal fields existing downstream of a stepwise discontinuity in the temperature of a flat plate on which a turbulent boundary layer has been formed has constituted a first step in the study of the details of heat transfer through turbulent boundary layers. The following general results may be stated in connection with the region where the thermal boundary layer has not become fully developed; i.e., of the same order of thickness as the existing momentum boundary layer:

(*a*) There does not appear to be similarity between the mean velocity and mean temperature profiles.

(*b*) The local friction temperature remains almost constant with distance from the leading edge of the heated section of wall following a sharp drop in the initial region.

Acknowledgments

The accomplishment of the work reported here was aided by many members of the Department of Aeronautics of The Johns Hopkins University. In particular, acknowledgment is due Prof. Stanley Corrsin (now in the Mechanical Engineering Department), under whose guidance and direction the project was carried out, and Mr. W. Furth, who performed much of the reduction of data.

BIBLIOGRAPHY

1 "The Transference of Heat From a Hot Plate to an Air Stream," by F. Élias, NACA TM 614, 1931.

2 "An Experimental Investigation of Convective Heat Transfer to Air From a Flat Plate With a Stepwise Discontinuous Surface Temperature," by S. Seesa and F. M. Sauer, Trans. ASME, vol. 74, 1952, pp. 1251–1255.

3 "Heat Transfer," by H. B. Squire, in "Modern Developments in Fluid Dynamics, High-Speed Flow," L. Howarth, Ed., Oxford University Press, London, England, vol. 2, 1953.

4 "The Effect of an Arbitrary Surface-Temperature Variation Along a Flat Plate on the Convective Heat Transfer in an Incompressible Turbulent Boundary Layer," by M. W. Rubesin, NACA TN 2345, 1951.

5 "Sur les Equations de la Diffusion Thermique par Turbulence," by J. Kampé de Fériet, *Annales de la Société Scientifique de Bruxelles*, vol. 57, series 1, 1937, pp. 67–72.

6 "Modern Developments in Fluid Dynamics," S. Goldstein, Ed., Oxford University Press, London, England, 1938.

7 "Introduction to the Transfer of Heat and Mass," by E. R. G. Eckert, McGraw-Hill Company, Inc., New York, N. Y., 1950, p. 119.

8 "The Friction Temperature: A Useful Parameter in Heat Transfer Analysis," by H. B. Squire, IME-ASME General Discussion on Heat Transfer, September 11–13, 1951, pp. 185–186.

9 "The Free-Stream Boundaries of Turbulent Flows," by S. Corrsin and A. L. Kistler, NACA TN 3133, 1954.

10 "Turbulent Heat Transfer in a Boundary Layer With Discontinuous Wall Temperature," by D. S. Johnson, Department of Aeronautics, The Johns Hopkins University, Baltimore, Md., OSR Technical Note 55-289, August, 1955.

11 "Turbulent Boundary Layers in Adverse Pressure Gradients," by F. H. Clauser, *Journal of the Aeronautical Sciences*, vol. 21, 1954, pp. 91–108.

12 "The Calculation of the Profile Drag of Aerofoils," by H. B. Squire and A. D. Young, Aeronautical Research Committee (Great Britain), Reports and Memoranda 1838, November, 1937.

A Theoretical Analysis of the Viscous Flow in a Narrowly Spaced Radial Diffuser[1]

By HENRY W. WOOLARD,[2] BUFFALO, N. Y.

A theoretical method for calculating the radial pressure distribution for laminar viscous flow in a narrowly spaced radial diffuser having arbitrarily shaped walls deviating only moderately from a plane surface is developed. The analysis as it stands is also directly applicable to turbulent flow in the initial inlet region of a diffuser. Additional work is necessary to obtain a complete turbulent-flow analysis. Pressure distributions calculated by the laminar-flow theory show reasonably good agreement with the limited experimental pressure distributions available at the time of the analysis. Fairly good agreement also is obtained for the performance of a disk-valve element.

Nomenclature

The following nomenclature is used in the paper:

r, y, ϕ = cylindrical co-ordinates; radial, axial, and peripheral directions respectively (Fig. 1)
h = local displacement or gap between diffuser walls (Fig. 2)
h^* = nondimensional displacement or gap, (h/h_i)
R = outer radius of diffuser (Fig. 1)
δ = local boundary-layer thickness (Fig. 1)
δ^* = nondimensional boundary-layer thickness, $2\delta/h$
δ^D = boundary-layer displacement thickness, $\int_0^\delta (1 - u/U)dy$
Λ = nondimensional local radius, (r/r_i)
ζ = nondimensional distance from diffuser entrance, $(r - r_i)/r_i$
η = nondimensional y-co-ordinate, $(y + h/2)/\delta$, $y < 0$
u, v, w = radial, axial, and peripheral velocity components, respectively, in cylindrical co-ordinate system; $w = 0$ herein (Fig. 1)
U = velocity along $y = 0$ (Fig. 1)
U_i = velocity on $y = 0$ at inner radius (Fig. 1)
U^* = nondimensional velocity along $y = 0$, (U/U_i)
$\mathcal{U}$ = nondimensional perturbation velocity along $y = 0$, $(U^* - 1)$
H = total pressure (absolute)
p = static pressure (absolute)
p_a = atmospheric pressure (absolute)
μ = absolute viscosity
ρ = mass density, slugs/cu ft
ν = kinematic viscosity, (μ/ρ)
w = specific weight
W = total weight of the upper disk
Q = flow quantity
a_L = boundary-layer-profile parameter (Equation [12])
b = laminar boundary-layer-profile parameter (Equation [29])
J = laminar boundary-layer-profile parameter (Equation [30])
$\mathcal{J}$ = boundary-layer-profile parameter (Equation [9])
$\mathcal{J}_2$ = boundary-layer-profile parameter (Equation [11])
Γ = $(\mathcal{J} - 1)/(\mathcal{J} - \mathcal{J}_2)$
k = $1 + K_6\delta_i^*$
K_0 = $(\mathcal{J}_2 - 1)_L$
K_f = $(r_i/h_i)(\nu/U_ih_i)$
K_2 = $4a_LK_f(\mathcal{J}_2 - 1)^2/(\mathcal{J} - \mathcal{J}_2)$
K_4 = $[K_2(T_1 + 1)^2 + 2(T_1 + 1) - k]/k$
K_5 = $1 + kK_2$
T_1 = $[\Gamma k - (1 + \Gamma)]/(1 + \Gamma)$
T_2 = $k - 1$
$O(\ )$ = order of magnitude of ( )

Subscripts

i = conditions at inner radius (Fig. 1)
L = conditions at end of inlet region (Fig. 1)
s = conditions where separation begins (Fig. 1)
R = conditions at outer radius (Fig. 1)
w = conditions at diffuser wall; i.e., at $y = \pm h/2$
p = conditions in supply pipe (Fig. 2)
ζ = derivative with respect to ζ

Superscripts

$'$ = derivatives with respect to the independent variable

Introduction

This paper is concerned with the theoretical determination of the pressure distribution for the flow of a viscous fluid in a narrowly spaced radial diffuser having arbitrarily shaped walls deviating only moderately from a plane surface, Fig. 1. A narrowly spaced radial diffuser is defined herein as one in which the displacement effect of the wall boundary layers is strong enough to restrict the nondimensional perturbation velocity along the central stream surface, i.e. $(U/U_i - 1)$, and the absolute value of its first derivative with respect to r/r_i, to values small in comparison to unity.

This analysis was developed originally for the purpose of understanding and predicting the behavior of a simple double-disk valve element of the type shown in Fig. 2. Elements of this type occasionally are used in hydraulic servos or in other hydraulic devices. Justification for the analysis can be made, however, on the basis that it deals with a fundamental-type flow as well as on the fact that it has possible usefulness in the study of the flow in certain types of centrifugal-compressor diffusers (1),[3] radial bear-

[1] Based on the author's Master of Science thesis, "A Study of the Flow in a Narrowly-Spaced Radial Diffuser," University of Buffalo, Buffalo, N. Y., February, 1954.

[2] Research Aerodynamicist, Cornell Aeronautical Laboratory; Lecturer, University of Buffalo, Buffalo, N. Y.

Contributed by the Applied Mechanics Division and presented at the Annual Meeting, New York, N. Y., November 25–30, 1956, of The American Society of Mechanical Engineers.

Discussion of this paper should be addressed to the Secretary, ASME, 29 West 39th Street, New York, N. Y., and will be accepted until April 10, 1957, for publication at a later date. Discussion received after the closing date will be returned.

Note: Statements and opinions advanced in papers are to be understood as individual expressions of their authors and not those of the Society. Manuscript received by ASME Applied Mechanics Division, May 1, 1956. Paper No. 56—A-18.

[3] Numbers in parentheses refer to the Bibliography at the end of the paper.

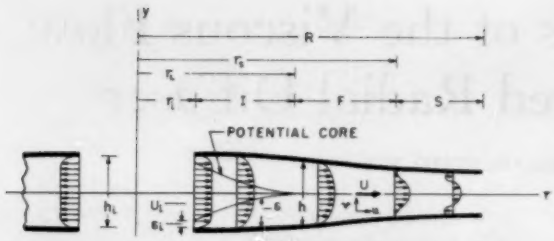

FIG. 1 ILLUSTRATION OF THE RADIAL-FLOW REGIONS. CONFIGURATION IS ROTATIONALLY SYMMETRIC ABOUT THE y-AXIS. THE INLET, FILLED, AND SEPARATED REGIONS ARE DENOTED RESPECTIVELY BY *I*, *F*, AND *S*.

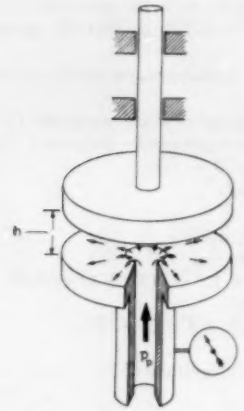

FIG. 2 DOUBLE-DISK VALVE ELEMENT

ings (2, 3), spherical bearings (4), or pneumatic gages (5).

Radial diffusers in one form or another have been investigated experimentally by Brown (1), Allen (5), Comolet (8), Willis (9), Eck (10), Mohn (11), Mohn and Connelly (12), Paivanas (13), and Welanetz (14); and theoretically by Fuller (2), Shaw and Macks (3), Purday (6), Comolet (7, 8), Brown (1), Mohn (11), Welanetz (14), and Woolard (15).

The theoretical analyses of Fuller, Shaw and Macks, Purday, and Comolet are for a laminar viscous flow in which the acceleration terms in the equations of motion are assumed to be small in comparison to the viscous terms, and are therefore neglected. This is a special case of the problem analyzed in this paper and is analogous to the Poiseuille type flow for straight channels and pipes.

Mohn (11), Brown (1), Welanetz (14), and Woolard (15) have dealt with various aspects of the problem using the classical hydraulic method. The hydraulic method treats the flow as one-dimensional and utilizes a modified Bernoulli equation which includes an additional term accounting for the pressure drop due to friction by means of a friction factor or coefficient.

Pressure distributions calculated[4] by the author using the hydraulic method for laminar and turbulent flow[5] in a radial diffuser with parallel walls are shown in Fig. 3, where they are compared with an experimental pressure distribution obtained by Mohn (11) for the flow of water in a double-disk valve element. A pressure distribution for one-dimensional frictionless flow also is shown. It is seen here that the turbulent-flow calculation agrees fairly well with the experiment.

For a number of reasons, one is apt to suspect that this agreement is fortuitous. First, it is not known in Mohn's experiments whether the flow in the diffuser is laminar or turbulent. There is good reason to suspect that it is laminar even when the flow in the supply pipe is turbulent. This suspicion is based on the fact that the flow experiences a large contraction in cross-sectional area in passing from the supply pipe to the diffuser inlet. Large area contractions are effective in reducing turbulence.[6] Sternberg (17), in a very interesting paper, has shown that the conversion of a turbulent boundary layer to a laminar one can actually occur.

Regardless of whether the flow is laminar or turbulent there are numerous reasons why the hydraulic method is open to suspicion. The hydraulic method assumes that the boundary layer fills the gap at the entrance of the diffuser, whereas it probably requires some finite radial distance for the boundary layer to span the gap. The term accounting for the pressure drop due to friction in the hydraulic method is obtained for flows in which there is no acceleration or deceleration in the flow direction. This, of course, is not the case for the radial diffuser. For the turbulent case, the hydraulic method uses friction coefficients obtained for circular pipes. The applicability of these friction coefficients, through the hydraulic-radius concept, to the greatly differenat boundary conditions of the radial diffuser is certainly questionable. Finally, the hydraulic method provides no means for predicting a separation point.

Using the inlet flow into straight pipes and channels[7] as a guide, the radial-flow regions of a radial diffuser are assumed in this analysis to be as shown in Fig. 1. Here it is seen that the boundary layer does not completely fill the gap near the inlet, and consequently, there exists a flow region, called the potential core, in which there is no viscous shearing action. As we follow the flow in the radial direction, the boundary-layer thickness increases until the boundary layer completely fills the gap. The region from the inner radius r_i up to this point is called the inlet region. In a straight pipe or channel, once the boundary layer fills the pipe or channel, the flow will continue to have about the same general character as one proceeds in the flow direction, except where the boundary layer is initially laminar, in which case transition to a turbulent layer may occur eventually. The radial-flow case, however, will be somewhat different because of

[4] For further details see author's thesis (15).

[5] The author's original thesis (15) contains an error for the turbulent case which may be corrected by dividing by 2.0 those terms containing the friction coefficient f.

[6] Reference (16), pp. 201–203.

[7] Ibid., pp. 299–311.

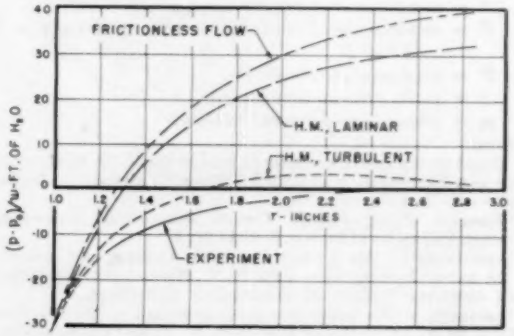

FIG. 3 COMPARISON OF PRESSURE DISTRIBUTIONS CALCULATED BY THE HYDRAULIC METHOD WITH AN EXPERIMENTAL PRESSURE DISTRIBUTION OBTAINED BY MOHN (11) FOR THE FLOW OF WATER IN A RADIAL DIFFUSER WITH PARALLEL WALLS

(R = 2.85 in., r_i = 1.00 in., h_i = 0.023 in., and U_i = 72.3 ft/sec. Experimental data at $(p_p - p_o)/w$ = 50.0 ft of water.)

the positive pressure gradient in the radial direction. This gradient eventually will cause the boundary layer to separate from the wall, a phenomenon which does not occur in straight pipes and channels where the pressure gradient in the flow direction is relatively small.

This representation of the radial-flow regions is valid for flows in which the boundary layer is either laminar or turbulent throughout the whole region. Naturally, the case of transition from a laminar to a turbulent layer cannot be treated theoretically.

All of the regions described may not necessarily exist in a given case. The flow conditions may be such that the exit of the diffuser is reached before the boundary layer separates or before it fills the gap.

In solving a case where all three regions exist, it is only necessary, of course, to obtain a solution up to r_s, since the pressure is constant in the separated region.

The analysis herein is for incompressible flow and uses the "integral method" of solution (18, 19). For laminar flow, it is possible that a slightly more exact method of analysis could have been performed in the inlet region by generalizing Blasius' solution for the two-dimensional boundary layer in a manner analogous to that for channels (20) and circular pipes (16). However, a cursory examination of this method of approach indicated that it would be fraught with many more difficulties than the simpler and more flexible integral method. The integral method has the advantage that it is applicable to both laminar and turbulent flow and is easier to adapt to curved-wall diffusers. Its use permits the treatment of the boundaries in a somewhat gross manner. That is, if it is desired to analyze a diffuser in which the upper and lower walls are not symmetric about the surface $y = 0$, Fig. 1, we may, within the spirit of the integral method, replace the nonsymmetric configuration by a symmetric one having the same height h at a given radial station providing, of course, that the original nonsymmetry is not too great.

This paper deals with the laminar-flow case. The turbulent-flow solution was completed only for the inlet region in the author's thesis (15). However, it should be possible to obtain a turbulent-flow solution in the filled and separated regions without undue difficulty (15). The laminar-boundary-layer solution was given prior treatment in this investigation for two reasons: (*a*) The mathematical analysis is simpler than for the turbulent case; and (*b*) the boundary layer in the radial diffuser actually may be laminar, even when the supply-pipe flow is turbulent, for the reason previously stated.

Since the analysis is for an incompressible fluid it ceases to be valid in a gas when the local velocity approaches the local velocity of sound, or in a liquid when the vapor pressure is reached.

Theory

The Governing Differential Equations. If one writes the differential equations, in the cylindrical co-ordinates r, y, ϕ (Fig. 1), for the steady radial flow ($w = 0$) of a viscous, incompressible fluid,[1] and applies the usual order-of-magnitude analysis (19) for boundary-layer flows, one determines that the static pressure is a function of r only, and that the governing equations are

$$u\frac{\partial u}{\partial r} + v\frac{\partial u}{\partial y} = -\frac{1}{\rho}\frac{dp}{dr} + \nu\frac{\partial^2 u}{\partial y^2} \quad \text{(momentum)} \ldots [1]$$

$$\frac{\partial u}{\partial r} + \frac{u}{r} + \frac{\partial v}{\partial y} = 0 \quad \text{(continuity)} \ldots [2]$$

These are the boundary-layer equations that must be solved subject to the given boundary conditions. Before proceeding with their solution, it is of interest to emphasize two important characteristics of the flow.

Two Important Characteristics of the Theoretical Flow. It is assumed, as an approximation, that $(\partial^2 u/\partial y^2) = 0$ at $y = 0$. We then have the following useful relations

At $y = 0$

$$\partial u/\partial y = 0, \quad v = 0, \text{ due to symmetry}$$

$$\partial^2 u/\partial y^2 = 0, \text{ by assumption}$$

Then from Equation [1]

$$\rho U dU/dr = -dp/dr \ldots [3]$$

Upon integration, this becomes

$$p + \rho U^2/2 = H \ldots [4]$$

That is, Bernoulli's equation is valid on the surface $y = 0$.

At $y = \pm h/2$

$$u = v = 0$$

Substituting these values, and Equation [3] in Equation [1], we obtain, at the wall

$$-UdU/dr = \nu\partial^2 u/\partial y^2 \ldots [5]$$

It is emphasized here that the curvature of the diffuser walls is considered to be small, so that the distance along the wall is essentially equal to $(r - r_i)$, and the distance normal to the wall equal to y; i.e., the cosine of the local angle of inclination of the diffuser wall is taken to be unity.

Integral Form of Boundary-Layer Equations for Present Problem. If we apply the averaging process outlined by Schlichting (19) to Equation [1], and substitute Equations [2] and [3] in the result, we obtain the following integral form of the boundary-layer momentum equation

$$\rho\frac{\partial}{\partial r}\int_{-\frac{h}{2}}^{0} u^2 dy + \frac{\rho}{r}\int_{-\frac{h}{2}}^{0} u^2 dy - \frac{h}{4}\rho\frac{dU^2}{dr} + \mu\left(\frac{\partial u}{\partial y}\right)_w = 0 \ldots [6]$$

The continuity equation in integral form is

$$Q = 2\pi r U(h - 2\delta) + 4\pi r\int_{-\frac{h}{2}}^{-\frac{h}{2}+\delta} u dy \ldots [7]$$

Since u/U is assumed to be a function of η, where $\eta = (y + h/2)/\delta$, it is convenient to write Equations [6] and [7] in terms of these quantities. On this basis, these equations become, respectively

$$\rho\frac{d}{dr}\left\{U^2\left[(\vartheta - 1)\delta + \frac{h}{2}\right]\right\} + \frac{\rho}{r}U^2\left[(\vartheta - 1)\delta + \frac{h}{2}\right] - \rho\frac{h}{4}\frac{dU^2}{dr} + \frac{\mu U}{\delta}\left[\frac{\partial(u/U)}{\partial\eta}\right]_w = 0 \ldots [8]$$

where

$$\vartheta = \int_0^1 (u/U)^2 d\eta \ldots [9]$$

and

$$Q = 2\pi r U[h + 2\delta(\vartheta_2 - 1)] \ldots [10]$$

where

[1] See, for example, Goldstein (16), p. 103.

$$\mathcal{J}_2 = \int_0^1 (u/U)d\eta \quad [11]$$

These equations are valid for either a laminar or a turbulent boundary layer in both the filled and inlet regions. The parameters $\mathcal{J}$ and $\mathcal{J}_2$ obviously have different values for laminar and turbulent boundary layers.

Solution in Inlet Region—Laminar or Turbulent Boundary Layer. In the inlet regions it is assumed, for both laminar and turbulent boundary layers, that the boundary-layer profiles are similar to each other at different radial stations. It is realized that this is a somewhat bold assumption. Solutions possibly could be obtained without making this assumption, but they would be rather involved and probably would require complicated iterative procedures. Physically, the assumption is aided somewhat by the fact that we are dealing with narrowly spaced diffusers. In this case, the displacement effect[9] of the growing boundary layer tends to reduce the pressure gradient considerably over that which occurs in the nonviscous case, Fig. 3, and hence the profiles in the inlet region tend to behave more nearly like those on a flat plate. In any case, the solutions obtained from the theory based upon this assumption agree fairly well with experiment, and it is believed that the assumption is justified for the purpose of obtaining an approximate solution.

For similar profiles, $\mathcal{J}$ is a constant and not a function of r in Equation [8]. The quantity $[\partial(u/U)/\partial\eta]_w$ is also a constant. Denote this by

$$a_L \equiv [\partial(u/U)/\partial\eta]_{wL} \quad (r_i \leq r \leq r_L) \quad [12]$$

The parameter a_L has different values for laminar and turbulent boundary layers. In the theory for the laminar boundary layer, an analytical expression for the velocity profile can be derived so that the profile shapes join smoothly at r_L in passing from the inlet region to the filled region. For this reason, the expressions for $\mathcal{J}$ and a_L depend upon the analysis in the section entitled "Laminar-Boundary-Layer Profile Characteristics in the Filled Region." A smooth joining of the turbulent-boundary-layer profiles at r_L cannot be achieved, since there does not yet exist an analytical expression for the turbulent-boundary-layer profile which accounts for the external pressure gradient. Explicit formulas for $\mathcal{J}$ and a_L for a laminar boundary layer in the inlet region are given in the Appendix. The corresponding formulas for a turbulent boundary layer may be found in the author's thesis (15).

If we apply the conditions that $\mathcal{J}$ and $[\partial(u/U)/\partial\eta]_w$ are constant in the inlet region, combine Equations [8] and [10], and introduce the nondimensional quantities

$$\Lambda = r/r_i, \quad U^* = U/U_i, \quad h^* = h/h_i, \quad \text{and} \quad \delta^* = 2\delta/h$$

we obtain, after some algebra

$$[2K_0^2(\mathcal{J}-1)\Lambda^2U^*\delta^{*2} - K_0(\mathcal{J}-1)k\Lambda\delta^*/h^* + K_0^2\Lambda^2h^*U^*\delta^*]dU^*/d\Lambda + K_0^2(\mathcal{J}-1)\Lambda U^{*2}\delta^{*2} + K_0^2(\Lambda^2h^{*\prime} + \Lambda h^*)U^{*2}h^* - K_0(\mathcal{J}-1)k(1 + \Lambda h^{*\prime}/h^*)U^*\delta/h^* + 4a_LK_0^2K_f\Lambda^2U^* = 0 \quad [13]$$

The nondimensional boundary-layer thickness becomes

$$\delta^* = (k/\Lambda U^* - h^*)/K_0h^* \quad [14]$$

Now define $\bar{U}$ as

$$U^* = 1 + \bar{U} \quad [15]$$

Further assume that $|\bar{U}| \ll 1$ and $|d\bar{U}/d\Lambda| \ll 1$.

These approximations are valid only for a narrowly spaced radial diffuser, in which the displacement effect of the growing boundary layer tends to make $\bar{U}$ and $d\bar{U}/d\Lambda$ considerably less than in the nonviscous case.

The foregoing assumptions regarding $\bar{U}$ permit linearization of Equation [13]. If we substitute Equations [14] and [15] in Equation [13], introduce the variable ζ, restrict h^*_ζ to values less than unity, and neglect nonlinear terms in $\bar{U}$, $d\bar{U}/d\zeta$, and h^*_ζ, we obtain

$$g_1(\zeta)d\bar{U}/d\zeta + g_2(\zeta)\bar{U} = g_3(\zeta) \quad [16]$$

where

$$g_1(\zeta) = (\mathcal{J}-1+M)h^{*2}(\zeta+1)^2 - (2\mathcal{J}-2+M)kh^*(\zeta+1) + (\mathcal{J}-1)k^2 \quad [17]$$

$$g_2(\zeta) = K_2(\mathcal{J}-\mathcal{J}_2)h^{*2}(\zeta+1)^2 + 2Mh^{*2}(\zeta+1) - Mkh^* \quad [18]$$

$$g_3(\zeta) = -[K_2(\mathcal{J}-\mathcal{J}_2) - K_0h^*_\zeta]h^{*2}(\zeta+1)^2 - [Mh^{*2} + (M+2K_0)kh^*_\zeta](\zeta+1) + Mkh^* + (\mathcal{J}-1)k^2h^*_\zeta/h^* \quad [19]$$

$$M = (\mathcal{J}-1-K_0h^*)$$

The solution to Equation [16] is

$$\bar{U} = \frac{\int_0^\zeta f_1(\zeta)[g_3(\zeta)/g_1(\zeta)]d\zeta}{f_1(\zeta)} + \frac{K_2}{f_1(\zeta)} \quad [20]$$

where

$$f_1(\zeta) = \exp\int[g_2(\zeta)/g_1(\zeta)]d\zeta \quad [21]$$

If $\zeta = 0$ is not a singular point of the differential Equation [16], $K_2 = 0$ will satisfy the required boundary condition $\bar{U}(0) = 0$. It is shown in the author's thesis (15) that when $\delta^*_i = 0$, $\zeta = 0$ becomes a singular point and it is not possible to satisfy the boundary condition. This behavior is more or less to be expected, since the original boundary-layer equations are valid only for large local Reynolds numbers (based on the length $r - r_i$). It is not the purpose here to resolve the problem of the behavior of the boundary layer at a leading edge. This is a difficult problem within itself, and has not yet been resolved completely (21, 22) even for the simpler case of the flat plate at zero angle of attack in a uniform stream. In addition, $\delta^*_i = 0$ is an idealization, and in any actual case some initial boundary layer will probably exist so that δ^*_i will not be zero. The procedure will be to estimate δ^*_i when possible, and when not possible, use a value arbitrarily small compared to unity. The following suggests itself: Since in the usual flat-plate boundary-layer theory, the local boundary-layer thickness is assumed to be small in comparison to the distance from the plate leading edge, we are assured of obtaining a value of δ_i small in comparison to $h_i/2$, if we use for δ_i the value of δ obtained from flat-plate theory when based upon a Reynolds number equal to $U_ih_i/2\nu$. This yields

$$\delta^*_i = 7.07(\nu/U_ih_i)^{1/5} \quad [22]$$

for a laminar boundary layer.

The integrals indicated in Equation [20] must be evaluated by numerical methods. The simple trapezoidal rule is usually adequate for this purpose if small enough increments are taken. The integration stops at $\delta^* = h^*$, hence it is necessary to make a running calculation of δ^* in order to determine where the integration should be stopped.

The parameter K_2 depends upon a_L, which is unknown a priori and must be determined by an iteration process. The procedure for determining a_L is described in the Appendix for a laminar boundary layer and in the author's thesis (15) for a turbulent boundary layer.

[9] Reference (19), p. 109.

An analytical expression for $f_f(\zeta)$ can be obtained for the case of a diffuser with flat parallel walls; i.e., $h^* = 1.0$. The resulting expression is

$$f_f(\zeta) = (\zeta - T_1)^{-K_4}(\zeta - T_2)^{K_3} \exp\,[K_3/(1 + \Gamma)]\zeta \quad [23]$$

The parameters K_4, K_3, T_1, and T_2 are defined in the nomenclature.

Laminar-Boundary-Layer Profile Characteristics in the Filled Region. Since $u(y) = u(-y)$, we need consider only $0 \leq y \leq h/2$ or $-h/2 \leq y \leq 0$. For $-h/2 \leq y \leq 0$, we assume, in a manner similar to Pohlhausen (19), that the boundary-layer velocity profile is given by

$$u/U = a\eta + b\eta^3 + c\eta^3 + d\eta^4 + e\eta^5 \quad [24]$$

where $$\eta = 2y/h + 1$$

since $\delta = h/2$ in the filled region.

Since the boundary condition $u = 0$ at $y = -h/2$ is automatically satisfied by Equation [24], the five free constants a, b, c, d, and e are determined by the following remaining conditions

$$\int_0^1 (u/U)d\eta = Q/2\pi rhU \quad \text{(continuity)} \quad [25]$$

$$y = 0\text{: } u = U;\ \partial u/\partial y = 0;\ \partial^3 u/\partial y^3 = 0 \quad [26]$$

$$y = -h/2\text{: } \nu\partial^3 u/\partial y^3 = -UdU/dr \quad [27]$$

These yield

$$u/U = F(\eta) + bG(\eta) + JL(\eta) \quad [28]$$

where

$$b = -(h^2/8\nu)dU/dr = -(h^{*2}/8)(U_e h_e/\nu)(h_e/r_e)d\bar{U}/d\zeta \quad [29]$$

$$J = Q/\pi rhU \quad (r_L \leq r \leq r_e) \quad [30]$$

$$F(\eta) = -5\eta + 40\eta^3 - 55\eta^4 + 21\eta^5 \quad [31]$$

$$G(\eta) = -\eta/6 + \eta^3 - 2\eta^3 + 5\eta^4/3 - \eta^5/2 \quad [32]$$

$$L(\eta) = 5\eta - 30\eta^3 + 40\eta^4 - 15\eta^5 \quad [33]$$

The functions $F(\eta)$, $G(\eta)$, and $L(\eta)$ are analogous to the well-known Pohlhausen functions (19) for the boundary-layer flow about a body immersed in an infinite stream.

Boundary-layer separation occurs when $[\partial(u/U)/\partial\eta]_w = 0$, hence the criterion for separation obtained from Equation [28] is

$$J - b/30 = 1 \quad \text{(separation)} \quad [34]$$

Solution in Filled Region—Laminar Boundary Layer. In this region, $\delta = h/2$, and ϑ is variable. Substituting Equation [28] in Equation [9], we obtain

$$\vartheta = I_1 + bI_2 + JI_3 + b^2I_5 + bJI_6 + J^2I_4 \quad [35]$$

where

$$\left.\begin{aligned} I_1 &= \int_0^1 F^2(\eta)d\eta = 0.4401 & I_2 &= 2\int_0^1 F(\eta)G(\eta)d\eta = 0.002285 \\ I_3 &= 2\int_0^1 F(\eta)L(\eta)d\eta = -0.4235 & I_5 &= \int_0^1 G^2(\eta)d\eta = 0.001102 \\ I_6 &= 2\int_0^1 G(\eta)L(\eta)d\eta = -0.0000001 & I_4 &= \int_0^1 L^2(\eta)d\eta = 0.3752 \end{aligned}\right\} \quad [36]$$

Let $r_i = 0(1)$, then the orders of magnitude are $\ldots\ h^2,\ h,\ 1,\ 1/h,\ 1/h^2, \ldots\ldots$ Now $\delta = O(h)$, $r = 0(r_i) = O(1)$, $U^* = 0(1)$, and $Q = O(U_i h_i)$. Boundary-layer theory requires $\nu/U_i h_i = O(\delta^2)$, hence, $\nu/U_i = O(h^2)$. It follows that $b = O(1)$ and $J = O(1)$. Hence we finally have

$$O(\vartheta) = O(I_1) + O(I_2) + O(I_3) + O(I_5) + O(I_6) + O(I_4)$$

One is tempted at this point to drop in Equation [35] all terms small in comparison to I_1; i.e., $O(I_2)$, $O(I_3)$, and $O(I_5)$. This, however, will yield only a first-order differential equation for the filled region and will not provide for the smooth joining of $\bar{U}$ at the juncture of the two regions, since it will allow only one boundary condition on $\bar{U}$ to be stipulated. The term containing I_5 can be dropped in Equation [41], however, since, in addition to being very small compared to the other terms, its omission does not reduce the order of the differential equation.

We now substitute $\delta = h/2$, Equation [28], and the modified Equation [35] into Equation [8], and introduce the nondimensional quantities ζ, U^*, and h^*. If, we let $U^* = 1 + \bar{U}$, assume $|\bar{U}| \ll 1$, $|d\bar{U}/d\Lambda| \ll 1$, restrict h^*_ζ to values less than unity, and neglect nonlinear terms in the small quantities $\bar{U}$, $d\bar{U}/d\Lambda$, and h^*_ζ, we obtain, after considerable algebra

$$d^2\bar{U}/d\zeta^2 + g_6(\zeta)d\bar{U}/d\zeta + g_0(\zeta)\bar{U} = g_6(\zeta) \quad [37]$$

where

$$g_6(\zeta) = \left(\frac{1}{K_f} + \frac{C_1}{h^{*2}}\right)\frac{1}{(1+\zeta)} + \frac{C_2}{h^{*2}} \quad [38]$$

$$g_0(\zeta) = \frac{C_2}{h^{*2}(1+\zeta)^3} - \left(\frac{C_6K_f}{h^{*6}} + \frac{3C_2}{h^{*2}}\right)\frac{1}{(1+\zeta)} + \frac{2C_6K_f}{h^{*4}} \quad [39]$$

$$g_0(\zeta) = -\frac{C_3}{h^{*4}(1+\zeta)^3} - \frac{2C_3h^*_\zeta}{h^{*5}(1+\zeta)^3} + \left(\frac{C_3h^*_\zeta}{h^{*4}} + \frac{C_4K_f}{h^{*2}} + \frac{C_5}{h^{*2}}\right)\frac{1}{(1+\zeta)} - \frac{C_6K_f}{h^{*4}} \quad [40]$$

$$\left.\begin{aligned} C_1 &= -16I_3k/I_2 & C_4 &= 320k/I_2 \\ C_2 &= 8(11/12 - 2I_1)/I_2 & C_5 &= 8I_1/I_2 \\ C_3 &= 32I_3k^2/I_2 & C_6 &= 160/I_2 \end{aligned}\right\} \quad [41]$$

The differential Equation [37] must be integrated numerically. There are numerous methods for doing this. The author used the Runge-Kutta method. Kamke (23) gives explicit formulas for applying the Runge-Kutta method directly to a second-order differential equation of the form $y'' = f(x, y, y')$. His formulas are more convenient than the usual method of applying the Runge-Kutta method simultaneously to two first-order differential equations.

Since it is necessary to integrate Equation [37] numerically, one might question the necessity of linearizing, since the Runge-Kutta method is valid for a nonlinear differential equation.[10] In practice, the labor involved in numerically solving the nonlinear equation by the Runge-Kutta method is considerably greater than that required in solving the linearized Equation [37]. In addition, since the solution in the inlet region of the diffuser is based upon a linearized equation, the same degree of accuracy should be retained in the filled region for the sake of consistency.

It will be recalled that in the development for ϑ the terms containing b were not dropped, even though their coefficients were very small compared to those of the other terms, because such a

[10] The nonlinear equation is presented in the author's thesis (15).

procedure would reduce the order of the differential equation and thus cause the loss of a boundary condition.

The boundary conditions in the present problem stipulate that $\bar{U}(\zeta_L)$ and $(d\bar{U}/d\zeta)_L$ be equal to the values obtained at ζ_L from the inlet-flow solution; that is, the two solutions must join smoothly.

If an order-of-magnitude analysis is made of $g_4(\zeta)$ and $g_5(\zeta)$ it may be shown that they are $O(10)$, whereas the coefficient of $d^2\bar{U}/d\zeta^2$ is unity. This suggests that the boundary condition on $(d\bar{U}/d\zeta)_L$ has only a localized influence which diminishes rapidly as $(\zeta - \zeta_L)$ increases. This conjecture can be tested by comparing solutions of the first-order and second-order differential equations.

If we now neglect terms containing I_2 and I_5 in Equation [35] before substituting in Equation [8], the following first-order differential equation is obtained in place of Equation [37]

$$g_7(\zeta)d\bar{U}/d\zeta + g_8(\zeta)\bar{U} = g_6(\zeta) \ldots\ldots\ldots\ldots [42]$$

where

$$g_7(\zeta) = C_1/h^{*3}(1 + \zeta) + C_2/h^{*3} \ldots\ldots\ldots [43]$$

and $g_6(\zeta)$ and $g_8(\zeta)$ are as defined in Equations [39] and [40], respectively. Equation [42] may be solved by numerical quadrature in the same manner as Equation [16].

Two examples were computed in the author's thesis (15), using both the second-order and first-order differential equations for the filled region; i.e., Equations [37] and [42], respectively. The solutions obtained were practically identical for both equations and in both cases. This limited evidence seems to indicate that solutions based upon a first-order differential equation, although theoretically questionable, may be satisfactory from a practical standpoint.

Application

In order to determine whether the theoretical analysis gives reasonable results, three examples have been calculated for comparison with the experimental results of Mohn (11). The calculations were made for the laminar flow of water in a basic double-disk valve element of the type shown in Fig. 2. The disk surfaces (diffuser walls) are flat and parallel. The inner radius r_i is 1.00 in., and the outer radius R is 2.85 in. Two of the cases were calculated using both the second-order and first-order differential equations in the filled region. In both cases, the two different procedures yielded practically identical results. Because of this close agreement the calculation of the remaining case is based on the first-order differential equation. All calculations were carried only to the second approximation in the inlet region. The linearized Bernoulli equation is used to calculate the pressure distribution for the sake of consistency. Further details may be found in the author's thesis (15).

A pressure distribution calculated by the present theory is compared with one of Mohn's experimental pressure distributions in Fig. 4, where it is seen that the agreement is reasonably good in view of the geometric differences between the actual device and the theoretical model. The theory predicts flow separation at a radius of 2.41 in., hence the static pressure is constant from here on out to the exit radius of 2.85 in. The corresponding pressure distribution calculated by the hydraulic method, Fig. 3, of course, does not yield a separation point. Knowledge of the separation point is of interest for at least two reasons: (*a*) If a diffuser is being used to recover static pressure, it is useless to make the outer radius greater than the radius at which separation occurs. (*b*) If separation occurs in a flow system it is apt to cause flow instability. This is undesirable in any case, but especially so in a double-disk valve being used as a control device in a hydraulic system.

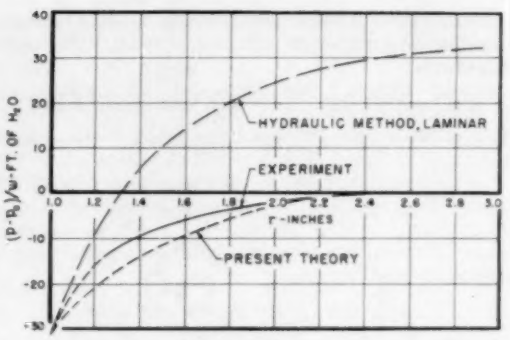

Fig. 4 Comparison of Pressure Distributions Calculated by Two Methods With an Experimental Pressure Distribution Obtained by Mohn (11) for the Flow of Water in a Radial Diffuser With Parallel Walls

(R = 2.85 in., r_i = 1.00 in., h_i = 0.023 in., and U_i = 72.3 ft/sec. Values of $(p_p - p_s)/w$ are 50.0 and 50.2 ft of water for the experiment and the present theory, respectively.)

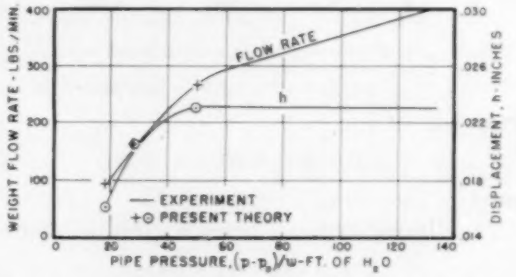

Fig. 5 Comparison of the Theoretically Calculated Weight-Flow Rates and Disk Displacements With Mohn's (11) Experimental Results for the Flow of Water in a Double-Disk Valve Element

(R = 2.85 in. and r_i = 1.00 in. Experimental and theoretical upper disk weights are 32.7 and 25.1 lb, respectively.)

The agreement between theory and experiment shown in Fig. 4 is fairly representative of the relative agreement obtained for the other two cases calculated at lower flow rates.

It will be recalled that the theory is based upon the assumptions that $|\bar{U}| \ll 1$ and $|d\bar{U}/d\Lambda| \ll 1$. In the three examples calculated it was found that these conditions were satisfied in general. The largest deviation in $\bar{U}$ occurred for the case shown in Fig. 4. For this case $\bar{U}$ decreased monotonically from zero at the inner radius to a value of -0.190 at the separation point. The $\bar{U}$ distribution for Fig. 4 may be reproduced easily, using the linearized Bernoulli equation and the data in Fig. 4. Plots of $\bar{U}$ for all three cases may be found in the author's thesis (15).

The theoretical weight flow rate and displacement curves for a double-disk valve element as obtained from the three calculated cases are compared with experiment in Fig. 5. It is seen in this figure that although the flow rate and displacement curves agree closely with experiment, the corresponding upper disk weights are different. The experimental upper disk weight is 32.7 lb, while the theoretical weight is 25.1 lb. In view of the acknowledged differences between the actual model and the theoretical model, this agreement seems reasonably good.

It will be observed that the experimental curves in Fig. 5 exhibit an abrupt change in slope at a supply-pipe pressure head of about 50 ft of water. This is a typically characteristic behavior of the double-disk valve with water flow. It is believed to be due to a cavitation phenomenon since it occurs when the pressure at

the inner radius approaches absolute zero. If one uses the criterion that the slope changes in the flow rate and displacement curves occur when the pressure at the inner radius reaches absolute zero, the present theory predicts the position of the slope change for the example calculated.

It should be noted that, if computational facilities were available, a family of curves of $\bar{U}$ as a function of ζ (up to ζ_L) for various values of the parameters r_i/h_i, and $U_i h_i/\nu$ could be calculated once and for all for radial diffusers with flat and parallel walls. In addition to providing immediate data for calculating radial pressure distributions, these curves also would provide information as to the range of the parameters r_i/h_i and $U_i h_i/\nu$ which yield narrowly spaced radial diffusers. As the situation now stands, one must actually calculate the $\bar{U}$ distribution for any given case and then determine whether the given diffuser is a narrowly spaced one on the basis of whether or not the conditions $|\bar{U}| \ll 1$ and $|d\bar{U}/d\Lambda| \ll 1$ are violated.

Acknowledgment

The author would like to acknowledge interesting discussions with Dean Paul E. Mohn and Dr. Theodor Ranov of The School of Engineering, University of Buffalo.

BIBLIOGRAPHY

1 "Friction Coefficients in a Vaneless Diffuser," by W. B. Brown, NACA TN 1311, 1947.

2 "Hydrostatic Lubrication," by D. D. Fuller, *Machine Design*, vol. 19, 1947, June, p. 110; July, p. 117; August, p. 115; September, p. 127.

3 "Analysis and Lubrication of Bearings," by M. C. Shaw and Fred Macks, McGraw-Hill Book Company, Inc., New York, N. Y., 1949, pp. 559 and 582.

4 "Behavior of Air in the Hydrostatic Lubrication of Loaded Spherical Bearings," by T. L. Corey, H. H. Rowand, Jr., E. M. Kipp, and C. M. Tyler, Jr., ASME Paper No. 54—LUB-8.

5 "Theory of Gaging," by W. F. Allen, *Mechanical Engineering*, vol. 75, 1953, pp. 199–204.

6 "An Introduction to the Mechanics of Viscous Flow," by H. F. P. Purday, Dover Publications, New York, N. Y., 1949, p. 30.

7 "Radial Flow of a Compressible Viscid Fluid Between Two Parallel Planes" (in French), by R. Comolet, *Comptes Rendus*, Academy of Sciences, Paris, France, vol. 235, November 17, 1952, pp. 1190–1193.

8 "Experimental Study of a Radial Flow of Viscous Fluid Between Two Parallel Planes" (in French), by R. Comolet, *Comptes Rendus*, Academy of Sciences, Paris, France, vol. 235, December 1, 1952, pp. 1366–1369.

9 "On the Pressure Produced on a Flat Plate When Opposed to a Stream of Air Issuing From an Orifice in a Plane Surface," by Rev. R. Willis, Transactions of the Cambridge Philosophical Society, vol. 3, part 1, April 21, 1828, pp. 121–140. (Microfilm or photostat copy available from the Library of Congress.)

10 "Technische Strömungslehre," by Bruno Eck, Julius Springer, Berlin, Germany, 1941, p. 217.

11 "Some Phenomena of Radial Flow Between Discs," by P. E. Mohn, MS thesis, Graduate School of the University of Illinois, Urbana, Ill., 1930.

12 "An Investigation of the Properties of a Variable Lift Radial Diffuser," by P. E. Mohn and J. R. Connelly, University of Illinois, Urbana, Ill., 1929.

13 "A Study of the Flow of Air in a Radial Diffuser," by J. A. Paivanas, MS thesis, University of Buffalo, Buffalo, N. Y., June, 1955.

14 "A Suction Device Using Air Under Pressure," by L. F. Welanetz, JOURNAL OF APPLIED MECHANICS, Trans. ASME, vol. 78, June, 1956, pp. 269–272.

15 "A Study of the Flow in a Narrowly Spaced Radial Diffuser," by H. W. Woolard, MS thesis, University of Buffalo, Buffalo, N. Y., February, 1954. (Copies obtainable from the Library, Cornell Aeronautical Laboratory, Buffalo, N. Y.)

16 "Modern Developments in Fluid Dynamics," by S. Goldstein, Oxford University Press, vols. 1 and 2, 1938.

17 "The Transition From a Turbulent to a Laminar Boundary Layer," by Joseph Sternberg, BRL Report No. 906, Ballistic Research Laboratories, Aberdeen Proving Ground, Md., May, 1954.

18 "Integral Methods in the Theory of the Boundary Layer," by L. G. Loitsianskii, NACA TM 1070, 1944.

19 "Boundary Layer Theory," by H. Schlichting, translated by J. Kestin, McGraw-Hill Book Company, Inc., New York, N. Y., 1955.

20 "Laminare Kanaleinlaufströmung," by H. Schlichting, *Zeitschrift für angewandte Mathematik und Mechanik*, Bd. 14, 1934, pp. 368–373.

21 "Second Approximation to the Laminar Boundary-Layer Flow Over a Flat Plate," by H. L. Alden, *Journal of Mathematics and Physics*, vol. 27, no. 2, 1948, pp. 91–104.

22 "On the Flow of an Incompressible Viscous Fluid Past a Flat Plate at Moderate Reynolds Numbers," by Y. H. Kuo, *Journal of Mathematics and Physics*, vol. 32, nos. 2 and 3, 1953, pp. 83–101.

23 "Differentialgleichungen, Lösungsmethoden und Lösungen," by E. Kamke, Chelsea Publishing Company, New York, N. Y., third edition, 1948, pp. 149–150.

Appendix

The Parameters b_L, J_L, $\mathcal{J}$, and $\mathcal{J}_2$ in the Inlet Region for a Laminar Boundary Layer

Since the boundary-layer profiles for the inlet and filled regions should join smoothly, the parameter a_L for the inlet region as determined from Equations [12] and [28] is

$$a_L = 5(J_L - 1) - b_L/6 \quad [44]$$

where b and J are defined by Equations [29] and [30], and L denotes conditions at $r = r_L$. The question of determining J_L and b_L now arises. This is done as follows:

Consider a flow in which J_L is finite when $r_L \to \infty$. In this case $b_L \to 0$, and the flow is like the two-dimensional flow between two parallel plates. It is therefore assumed that J_L has the same numerical value that exists for the two-dimensional flow between two parallel plates. On this basis, the parameter b_L reflects the difference between the profile shape in a radial flow and in a two-dimensional flow between parallel plates.

The boundary-layer displacement thickness δ^D is related to the thickness δ as follows

$$\delta^D/\delta = 1 - \int_0^1 (u/U)d\eta \quad [45]$$

For radial-flow profiles in the inlet region, Equation [45] yields

$$J_L = 2(1 - \delta^D/\delta) \quad [46]$$

The velocity profile for the two-dimensional flow between two parallel plates has a parabolic form (19). In terms of η, this gives $u/U = 2\eta - \eta^2$. Substituting this expression in Equation [45], we obtain $\delta^D/\delta = 1/3$. Hence we have

$$J_L = 4/3 \qquad \mathcal{J} = 8/15 \qquad \mathcal{J}_2 = 2/3$$

These are the values of J_L, $\mathcal{J}$, and $\mathcal{J}_2$ which will be used in the inlet region for a laminar boundary layer.

The parameter b_L remains to be determined. This is done by an iteration process in which b_L is first taken as zero and the corresponding $\bar{U}$ curve is calculated up to $\zeta = \zeta_L$. A new value of b_L is obtained and the solution is repeated. In the examples calculated thus far, sufficient convergence was obtained at the second approximation.

Head Loss in Flow Through a Cyclone Dust Separator or Vortex Chamber

By H. E. WEBER[1] and J. H. KEENAN[2]

An analysis for predicting the head loss in flow through a cyclone dust separator is presented. The effect of wall friction is indicated by consideration of two cases—one for zero wall friction, the other for wall friction great enough to eliminate the angular momentum of the stream. Comparisons of the analysis are made with the experimental data obtained from a test cyclone in which the flow rate, the depth of the inlet area, the radius of the exhaust pipe, and the extension of the exhaust pipe into the cyclone were variable. In general the agreement between the theoretical and experimental results is good. The regions of deviation between the two results are evaluated qualitatively with respect to the effects of wall friction on the head loss.

Nomenclature

The following nomenclature is used in the paper:

- a_e = cross-sectional area of cyclone-exhaust pipe
- a_i = cross-sectional area of cyclone-inlet port
- c_1, c_2 = constants in solution of equations of motion for an inviscid fluid
- H = head of fluid neglecting body forces, where $H = p + \frac{1}{2}\rho V^2$ in consistent units
- H_l = difference in head between fluid entering cyclone and same fluid at rest after leaving cyclone and expanding to atmospheric pressure, where

$$H_l \equiv p_i + \frac{1}{2}\rho V_i^2 - p_a$$

- p = static pressure
- p_a = static pressure of atmosphere, final static pressure of fluid stream
- p_i = static pressure of fluid stream at inlet to cyclone and at radii equal to inlet radius
- p_r = static pressure at any radius over top and bottom plates of vortex chamber or cyclone
- p_{rc} = static pressure at any radius over cross section of the vena contracta
- r, θ, z = cylindrical co-ordinates
- r_c = radius of vena contracta
- r_e = radius of cyclone exhaust pipe measured to outside of pipe
- r_i = radius at which inlet stream enters cyclone or vortex chamber as determined by angular momentum of inlet stream about axis of chamber—assumed to lie at radius of vertical center line of inlet port
- r_0 = radius of cyclone cylinder
- u, v, w = fluid velocities in cylindrical co-ordinates r, θ, z, respectively
- V = total fluid velocity
- V_c = total fluid velocity at r_c of vena contracta
- V_i = total fluid velocity at r_i of cyclone inlet
- v_c = θ-velocity at r_c of vena contracta
- v_r = θ-velocity at r at surfaces of top and bottom plates of a vortex chamber
- v_{rc} = θ-velocity at r in plane of vena contracta
- w_c = z-velocity at vena contracta
- ρ = density of fluid

Introduction

In a cyclone a flow of gas enters a cylindrical vortex chamber through an inlet port which is tangential to the outside of the chamber. This inlet port, usually of rectangular cross section, may have either its inner or outer side tangential to the outside of the cylindrical chamber. One end of the cylinder is in the shape of a cone, cut off before the vertex to form a hole which leads to the particle collector or hopper. The other end of the cylinder is usually a flat plate around an axial exhaust pipe extending into and concentric with the cylinder. The entering gas forms a vortex which approximates a potential vortex outside of a central core and a solid-body vortex in the core. The diameter of this core is approximately 60 per cent of the exhaust-pipe diameter[3] in the cylindrical region below the exhaust pipe. In the conical section of the cyclone this core diameter decreases with the diameter of the cone. A discussion of the core is reserved for later in this treatment of the head loss.

Theoretical Approach

In the following analysis the flow through a simple vortex chamber of the shape shown in Fig. 1 is considered. The total head loss H_l, if the flow through the vortex chamber expands into a large volume on leaving the chamber, is the difference between the head at the inlet and the head where the final velocity is zero.[4] For this case a control volume is taken as shown in Fig. 1. The steady-flow energy and momentum equations can be applied to any control volume, and the quantities involved in the equations need be evaluated only at the boundaries of the control volume. Therefore, regardless of how the flow properties vary inside the control volume, the end result as determined from the energy and momentum equations remains unaltered.

The principal assumption made in this analysis is that potential

---

[1] Shell Development Company, Emeryville, Calif. Now with General Electric Company, Danville, Calif.

[2] Professor of Mechanical Engineering, Massachusetts Institute of Technology, Cambridge, Mass. Fellow ASME.

Contributed by the Applied Mechanics Division and presented at the Annual Meeting, New York, N. Y., November 25–30, 1956, of The American Society of Mechanical Engineers.

Discussion of this paper should be addressed to the Secretary, ASME, 29 West 39th Street, New York, N. Y., and will be accepted until April 10, 1957, for publication at a later date. Discussion received after the closing date will be returned.

Note: Statements and opinions advanced in papers are to be understood as individual expressions of their authors and not those of the Society. Manuscript received by ASME Applied Mechanics Division, May 4, 1956. Paper No. 56—A-8.

[3] "Investigations Into Cyclone Dust Separators," by A. J. Ter Linden, Proceedings of the Institution of Mechanical Engineers, vol. 160, no. 2, 1949, p. 233.

[4] Gravitational, surface tension, and electrical effects are neglected, and the head is defined at any point in the flow as

$$H \equiv p + \left(\frac{1}{2}\right)\rho V^2$$

where p is the static pressure and V the total velocity at the point.

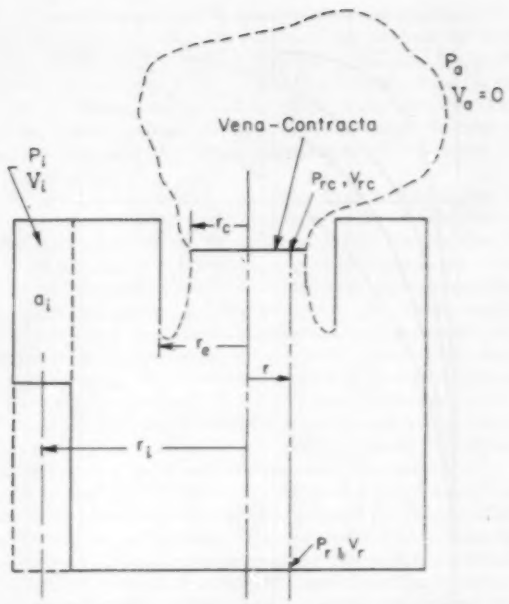

FIG. 1 VORTEX CHAMBER AND CONTROL VOLUME

flow exists in the vortex chamber from the inlet port to the vena contracta in the exhaust pipe, and that all of the head loss occurs in the expansion to the atmosphere after the vena contracta. The foregoing assumption, of course, implies the following: No axial or tangential shear forces exist at the boundaries of the control volume or in the interior of the fluid. The validity of this assumption is considered later in "Discussion of Theoretical Results." It is also assumed that the flow is axially symmetric.

THEORETICAL ANALYSIS

For the control volume inside of the walls of the vortex chamber and the dotted line shown in Fig. 1 the head loss between inlet and exit of a fluid stream is defined as

$$H_l \equiv p_i - p_a + \frac{1}{2}\rho V_i^2 \equiv \Delta p_{\text{stag}} \quad \ldots\ldots [1]$$

since $V_a = 0$. The quantity H_l is the head loss or stagnation-pressure drop from the inlet port to the atmosphere. If an expression for the pressure drop $p_i - p_a$ can be found in terms of the geometric and flow parameters of the vortex chamber, the head loss or stagnation-pressure drop can be evaluated. To do this we shall apply the momentum and energy equations to a control volume from the inlet port to the vena contracta as shown in Fig. 1 by the walls of the vortex chamber and the boundary of the stream after separation from the exhaust-pipe edge. For the axial momentum equation the pressure distributions across the bottom plate, across the top plate, and across the vena contracta will be required. These pressure distributions will be obtained from the equations of motion for an inviscid fluid.

For inviscid or potential flow in the control volume the tangential velocity distribution is a potential vortex (vr = const). Over the surface of the top and bottom plates of the control volume the radial velocities are assumed to be small compared to the tangential velocities. Such is the case if the inlet-port area is small compared to the circumferential area of the control volume. The incoming streamlines expand axially and the stream flows radially inward over a circumferential area normally much larger than the inlet-port area. By using the continuity equation and a potential vortex for the tangential velocity we find that u/v is of the order of magnitude of $a_i/(2\pi r_i L)$, where L is the depth of the chamber. This quantity and, hence, u/v is small compared to unity for the normal cyclone-separator dimensions; and near the walls u/v becomes still smaller.

Neglecting, therefore, the radial velocities over the surfaces of the top and bottom plates, the pressure distributions over these plates may be obtained from the equations of motion, and

$$\frac{dp}{dr} = \rho\frac{v^2}{r} \quad \ldots\ldots [2]$$

Using vr = const = $V_i r_i$ and integrating we obtain these pressure distributions as

$$p_i - p_r = \frac{1}{2}\rho V_i^2\left(\frac{r_i^2}{r^2} - 1\right) \quad \ldots\ldots [3]$$

In addition the pressure distribution over the plane of the vena contracta is required. The diameter of the vena contracta is that diameter to which the inviscid stream must contract such that its outflow of axial momentum is balanced by the net axial pressure force acting on the control volume of Fig. 1 from the inlet port to the vena contracta. The final pressure to which the stream expands is constant along its outer edge or free streamlines. Hence, in this portion of the flow field the solution to the equations of motion becomes

$$\left.\begin{aligned} vr &= v_c r_c = c_1 \\ w &= w_c = c_2 \\ u &= 0 \end{aligned}\right\} \quad \ldots\ldots [4]$$

The constants c_1 and c_2 can be determined from the moment-of-momentum equation and the continuity equation, respectively, for the control volume from the inlet port to the vena contracta, Fig. 1. The moment-of-momentum equation for no loss of angular momentum yields

$$V_i r_i = v_c r_c \quad \ldots\ldots [5]$$

The continuity equation for the control volume considered yields

$$w_c \pi r_c^2 = V_i a_i \quad \ldots\ldots [6]$$

since the axial velocity is uniform over the vena contracta.

The pressure distribution across the vena contracta can now be obtained from Equations [2] and [5] as

$$p_a - p_{rc} = \frac{1}{2}\rho V_i^2 r_i^2\left(\frac{1}{r^2} - \frac{1}{r_c^2}\right) \quad \ldots\ldots [7]$$

To obtain an expression for the pressure drop $p_i - p_a$, which is required as a function of the vortex-chamber dimensional and flow parameters, we first apply the axial-momentum equation to the control volume from the inlet port to the vena contracta. This equation can be written under the assumptions made as

$$\int_0^{r_c}(p_r - p_{rc})2\pi r dr + \int_{r_c}^{r_e}(p_r - p_a)2\pi r dr = \rho w_c^2 \pi r_c^2 \quad \ldots [8]$$

For $r > r_c$ the pressure forces on the fluid over the top and bottom plates cancel and contribute nothing to the net axial force.

At the radius r the tangential component of the velocity is the same in the plane of the vena contracta as along the bottom plate. Therefore, the difference between the pressure on the bottom plate and that in the vena contracta is given by Bernoulli's equation as

$$p_r - p_{re} = \frac{1}{2}\rho w_e^2 \quad [9]$$

which is independent of the tangential velocity and the radius for $r < r_e$. Therefore, with Equation [9] Equation [8] becomes

$$\int_{r_0}^{r_e} (p_r - p_a) 2\pi r dr = \frac{1}{2}\rho w_e^2 \pi r_e^2 \quad [10]$$

which is independent of the distribution of tangential velocity for $r < r_e$. The only conditions required to satisfy Equation [10] are that for $r < r_e$

$$v_{re} = v_r$$

and

$$w_e = \text{const}$$

The pressure distribution in the plane of the vena contracta given by Equation [7] is not required. Substituting the pressure distribution over the bottom plate given by Equation [3] and the continuity Equation [6] into Equation [10] we obtain

$$\frac{p_i - p_a}{\frac{1}{2}\rho V_i^2} + 1 = \frac{2r_i^2}{r_e^2 - r_c^2}\ln\frac{r_e}{r_c} + \frac{a_i^2}{\pi^2 r_c^2(r_e^2 - r_c^2)} \quad [11]$$

A different form of this expression leading to the same end result is obtained by using Equations [3], [6], [7], and [8].

To obtain an expression for the radius of the vena contracta in terms of the dimensional parameters of the vortex chamber we may write Bernoulli's equation for any streamline from the inlet port to the vena contracta, since all streamlines have the same total head or Bernoulli constant. For convenience we may select a streamline that lies at the radius of the vena contracta (i.e., at the outside edge of the stream at the vena contracta where the pressure is p_a). This equation is expressed as

$$p_i + \frac{1}{2}\rho V_i^2 - p_a - \frac{1}{2}\rho V_c^2 = 0 \quad [12]$$

where V_c is the total velocity at the vena-contracta radius and is given by

$$V_c^2 = v_c^2 + w_c^2 \quad [13]$$

Equation [13] may be expressed in terms of the inlet velocity by use of Equations [5] and [6]; then substituting this into Equation [12] we obtain

$$\frac{p_i - p_a}{\frac{1}{2}\rho V_i^2} + 1 = \left(\frac{r_i}{r_c}\right)^2 + \left(\frac{a_i}{\pi r_c^2}\right)^2 \quad [14]$$

Finally we combine Equations [11] and [14] to obtain

$$\left(\frac{a_i}{a_e}\right)^2\left(\frac{r_e}{r_c}\right)^4 + \left(\frac{r_e}{r_c}\right)^2\left[\left(\frac{r_i}{r_e}\right)^2 - 2\left(\frac{a_i}{a_e}\right)^2\right] - \left(\frac{r_i}{r_e}\right)^2\left(1 + 2\ln\frac{r_e}{r_e}\right) = 0 \quad [15]$$

From this last equation the ratio of the vena-contracta radius to the exhaust-pipe radius is determined as a function of the vortex-chamber dimensions. This ratio is plotted in Fig. 2 as a function of the square of the ratio of the inlet-port area to the exhaust-pipe area for various ratios of the inlet radius to exhaust-pipe radius.

The left-hand member of each of Equations [11] and [14] is the head loss per unit inlet-velocity head or the head-loss coefficient for the flow through the vortex chamber (see Equation [1]). Either of these equations may be used with Fig. 2 or Equation [15] to determine the head loss. Rewriting Equation [14] we obtain an expression for the head-loss coefficient in terms of the geometric parameters of the vortex chamber. Equation [14] becomes

$$\frac{H_l}{\frac{1}{2}\rho V_i^2} = \left(\frac{r_i}{r_e}\right)^2\left(\frac{r_e}{r_c}\right)^2 + \left(\frac{a_i}{a_e}\right)^2\left(\frac{r_e}{r_c}\right)^4 \quad [16]$$

where a_e is the cross-sectional area of the exhaust pipe and values of r_e/r_c are obtained from Fig. 2. Equation [16] is plotted in Figs. 3 and 4.

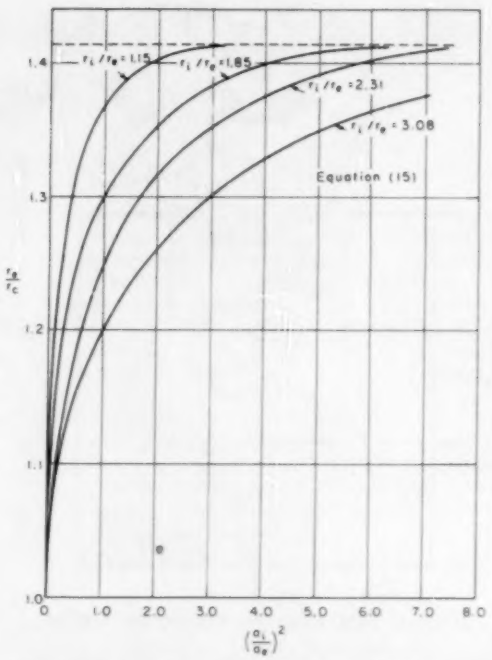

FIG. 2 VENA-CONTRACTA RADIUS IN SWIRL FLOW

DISCUSSION OF THEORETICAL RESULTS

In the flow of a real fluid through the control volume of Fig. 1 shear forces exist both at the boundaries and in the fluid. It is noted that the assumption of inviscid flow to the vena contracta is very good in head-loss determinations for ordinary flow (without swirl) through a Borda mouthpiece.[5] One restriction on the validity of the results is that the interior edge of the mouthpiece must be "far" from the wall of the chamber. In such a case the velocities, and hence the shear stresses at the walls of the chamber, are very small. We are justified, therefore, in neglecting the shear forces when writing the axial-momentum equation. The same is true for the axial shear forces when swirl flow is superimposed on the axial flow as in a cyclone vortex chamber. However, the tangential velocities are now, in general, much greater than the axial and radial velocities. Therefore, the tangential shear forces may not be negligible in the analysis as presented in this paper. The tangential shear stresses at the walls of the vortex chamber or

[5] Personal communication from Prof. A. H. Shapiro of Massachusetts Institute of Technology, Cambridge, Mass.

boundaries of the control volume will affect the angular momentum Equation [5] which was used to obtain the velocity at the vena contracta. Any internal fluid shear will alter the tangential velocities and affect the pressure distributions across the ends of the cylindrical chamber and across the vena contracta. These pressure and velocity distributions in turn alter the axial-momentum equation. Finally, of course, Bernoulli's Equation [12] is not valid.

It becomes of interest then to evaluate the limitations that the assumption of no tangential shear places on the solution obtained when it is applied to the flow of a real fluid. We can show the relative importance of the loss of angular momentum due to wall shear near the inlet as compared to the loss of angular momentum only in the atmosphere after the vena contracta. In this case it is assumed that all angular momentum of the incoming stream about the axis of the control volume is lost in wall friction with no change in pressure at r_i. Downstream of r_i the flow is without swirl and is assumed to be inviscid. It is noted that at the vena contracta the streamlines become straight and parallel for frictionless subsonic flow. That this must be true may be shown in the following manner:

The pressure of the fluid in the vortex chamber is higher than that of the atmosphere into which the stream discharges. Therefore the stream must contract causing its velocity to increase until the pressure of the stream decreases to that of the atmosphere. At all points farther downstream the streamlines must be straight and parallel in order that the pressure in the stream be equal to that outside of the stream, since this latter is the final pressure which the stream attains. By definition the vena contracta is the minimum cross-sectional area of the discharging stream. Therefore the streamlines become straight and parallel at the vena contracta. In addition all of the streamlines originate in a reservoir with the same total head and all suffer the same discontinuity in head; therefore, they all have the same total head at the vena contracta. Finally, since the pressure and total head become constant at the vena contracta, the axial velocity there must become uniform across the stream.

In order to determine the head loss for flow through the chamber of Fig. 1 with no swirl, we may make use of Equations [8] or [10] and [12] and specialize them for the case of zero tangential velocity. The pressure across the top and bottom plates becomes a constant equal to the inlet static pressure p_i; and the pressure across the vena contracta becomes a constant equal to the atmospheric pressure p_a. Hence, Equation [8] may be written as

$$(p_i - p_a)\pi r_c^2 = \rho w_c^2 \pi r_c^2 \quad \ldots\ldots [17]$$

If we assume that the interior edge of the re-entrant exhaust pipe is "far" from the walls of the control volume or chamber, the assumption of frictionless flow to the vena contracta is good because the velocities and the shear forces at the walls of the control volume are very small compared with the pressure forces. Equation [12] may then be written as

$$p_i - p_a - \frac{1}{2}\rho w_c^2 = 0 \quad \ldots\ldots [18]$$

The axial velocity w_c, at the vena contracta can be expressed in terms of the inlet velocity v_i by the continuity Equation [6]. Then by combining Equations [17] and [18] we can eliminate the pressure drop $p_i - p_a$. Thus the ratio of the exhaust-pipe radius to the vena-contracta radius is determined as

$$r_e/r_c = \sqrt{2} \quad \ldots\ldots [19]$$

The total head loss for flow through the chamber (zero swirl) is obtained from Equations [1], [18], and [19] as

$$\frac{H_i}{\frac{1}{2}\rho V_e^2} = 1 + 4\left(\frac{a_i}{a_e}\right)^2 \quad \ldots\ldots [20]$$

This equation is plotted in Figs. 3 and 4, from which it may be seen that the head loss is much larger for the combination of swirl flow and through-flow than for ordinary through-flow.

In both flows analyzed the pressure decreases from the inlet to the vena contracta as the velocity increases. Then after the vena contracta the entire velocity head, which is obtained at the expense of pressure head, is lost. Without swirl the total head loss is the axial velocity head at the vena contracta plus the velocity head at the inlet. With swirl the total head loss is the axial velocity head plus the tangential velocity head at the radius of the vena contracta. The latter head loss is larger because the total velocity head with swirl at the vena-contracta radius is larger than the sum of the velocity heads without swirl at the inlet and vena contracta. The reverse is true of the head loss in a small region of vortex-chamber geometry. This region is of little practical value and is considered later. Since in both flow cases the total head is constant between the inlet radius and the vena contracta, the pressure drop from r_i to r_e is greater with swirl flow. Consequently, we may expect that any loss of angular momentum due to wall friction will result in a head loss less than that predicted in the case of no loss of angular momentum upstream of the vena contracta.[6] However, a further examination of this premise is required.

As mentioned previously, there exists a small region of vortex-chamber geometry in which the head loss for ordinary through-flow is greater than that for swirl flow. In this region r_i/r_e is near unity, a_i/a_e is near zero, and

$$H_i \Big/ \left(\frac{1}{2}\rho V_e^2\right)$$

is near unity. For these values of r_i/r_e and a_i/a_e the axial-velocity head at r_e is larger in ordinary through-flow than the total velocity head at r_e in swirl flow. This difference in velocity heads is due to the difference in sizes of the vena contractas. Fig. 2 and Equation [19] show that the vena contracta is always larger in swirl flow than in ordinary through-flow and asymptotically approaches that of the latter as $(a_i/a_e)^2$ increases. In the axial-momentum Equation [10] which is valid in both cases the integration of the pressure that contributes to the net axial force extends only over the interval $r_e \geqslant r \geqslant r_c$. At the top of the control volume in this interval the pressure is a constant p_a. The integrated pressure force over the bottom of the control volume in the same interval is smaller in a pressure field that decreases radially inward than in one that is radially constant. Therefore the outflow of axial momentum, which is equal to the net axial pressure force, is smaller and the vena contracta is larger in swirl flow than in ordinary through-flow.

Real Fluid Flow

In the case of wall and internal fluid friction the vena contracta may also change in size owing to a redistribution of the velocities and pressures. In fact, a central core of approximately solid-body rotation exists in the flow of a real fluid through a cyclone. The radius of this core is found experimentally to be approximately uniform axially in the cylindrical portion of the cyclone and equal to about 0.6 of the exhaust-pipe radius. Consequently, the core radius is less than the minimum radius of the vena contracta. The minimum radius of the vena contracta is obtained from

[6] It is found that increasing the dust loading or roughening the cyclone walls, which decrease the angular momentum of the fluid, decreases the head loss or pressure drop through the cyclone.

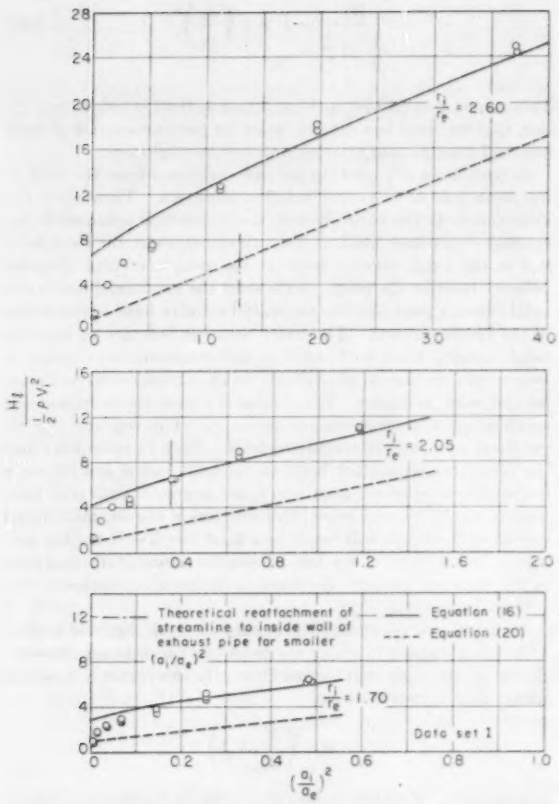

FIG. 3 HEAD-LOSS COEFFICIENT; DATA ON 0.7-IN. EXTENSION OF EXHAUST PIPE IN A CHAMBER 6.0 IN. DEEP

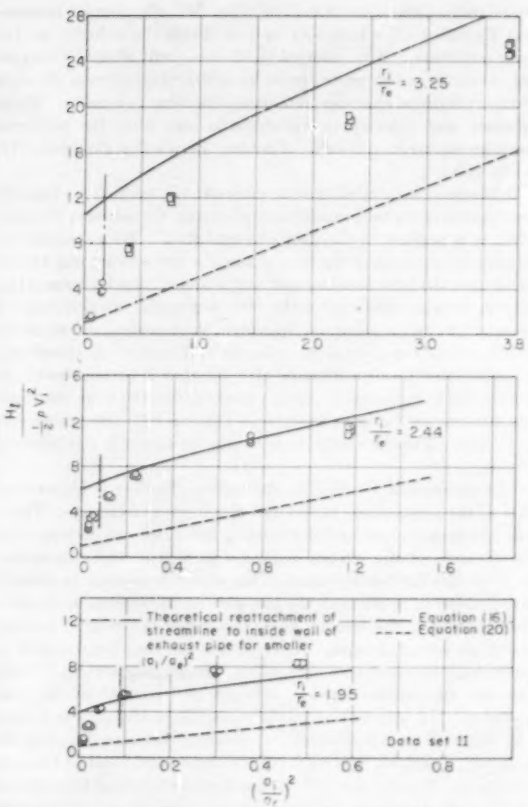

FIG. 4 HEAD-LOSS COEFFICIENT; DATA ON 3.0-IN. EXTENSION OF EXHAUST PIPE IN A CHAMBER 6.0 IN. DEEP

Equation [15] as

$$r_{cmin} = r_e/\sqrt{2}$$

which is the same as that obtained in the case of no swirl in the flow. The core of solid-body rotation has an angular momentum which is less than that of the fluid outside of the core. Therefore, most of the axial outflow of fluid must occur near the outside of the leaving stream in order to accommodate the total angular momentum in the body of fluid outside of the core. This behavior of the leaving stream does occur, and the axial velocity is much higher near the outside than near the center of the leaving stream. A nonuniform axial velocity for a given flow over a given cross-sectional area represents a greater flow of linear momentum than a uniform velocity. Therefore a nonuniform axial velocity over the vena contracta would in itself tend to increase the radius of the vena contracta over that given in Fig. 2. However, the radial pressure gradient over the bottom of the control volume is not as great for real flow as for inviscid flow. Therefore from the discussion given previously, the net axial pressure force over the bottom plate in the interval $r_e \geq r \geq r_c$ is greater in the case of real flow with a smaller radial pressure gradient. A greater net axial pressure force would in itself tend to decrease the radius of the vena contracta under that given in Fig. 2. Hence we have two phenomena in real flow that tend to cancel their separate effects on the size of the vena contracta. However, wall and internal fluid friction alter the pressure distribution in a different way over each end of the control volume. Therefore the axial pressures over the entire top and bottom surfaces, and not only in the interval $r_e \geq r \geq r_c$ will contribute to the net axial force. Finally, the tangential velocity head at r_c is smaller in real flow than in inviscid flow due to the loss of angular momentum in wall friction.

In the discussion between real and inviscid flows some of the differences may have little effect on the head losses for the two flows, whereas other differences may have a large effect. The entire problem of real flow through the vortex chamber becomes very complex, and we turn to some experimental results for comparison with the theory. Before doing so we may see one additional fact from the two cases analyzed for inviscid flow.

An examination of Fig. 3 reveals that as $(a_i/a_e)^2$ approaches zero, the difference between Equations [16] and [20] becomes equal to $(r_i/r_e)^2 - 1$. If we examine the physical nature of the flow as the inlet-port area a_i approaches zero, we see that this becomes the case of a small jet discharging into a reservoir having a wall area which is large compared to the area of the jet. In this case all angular momentum of the inlet stream is dissipated in wall friction near the radius of the inlet. Hence, we would expect the head loss for the flow of a real fluid to approach the head loss given by Equation [20] as $(a_i/a_e)^2$ approaches zero; i.e., the total head loss for the flow approaches one inlet-velocity head. It should be noted, however, that the percentage loss of angular momentum at the outside wall of the cyclone is probably a function of the ratio of the wall shear force to the momentum of the inlet stream. Consequently the ratio of the wall area to the inlet area may become important for determining the head loss as the inlet area approaches zero.

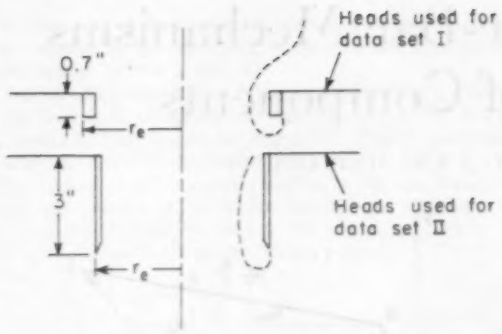

FIG. 5 RE-ENTRANT EXHAUST-PIPE DETAILS

COMPARISON OF EXPERIMENT WITH THEORY

Experimental results for short square-ended exhaust pipes as shown in Fig. 5 are presented in Fig. 3. The correspondence with the theoretical curves is very good except in the region where $(a_i/a_e)^2$ approaches zero. In this region the deviation of the actual head loss from the theoretical follows the expected course as explained previously. In the analysis we assumed, as indicated by Equation [8], that separation occurs at radius r_e. Our assumption is not necessarily confirmed by the good agreement between experimental and analytical results.

Turning now to data from longer sharp-edged exhaust pipes as shown in Fig. 5 we note from Fig. 4 for $r_i/r_e = 3.25$ (smallest exhaust pipe) that the experimental data give values of head loss lower than the theoretical curve of Equation [16]. This behavior is expected as was discussed previously, since Equation [16] should give the maximum values of head loss obtainable, if the flow properties are axially the same upstream of r_e along the top and bottom plates of the chamber. However, we also note that as r_i/r_e decreases (larger exhaust pipes), the observed head loss becomes higher than the theoretically expected maximum. The head loss unaccounted for by the analysis in this case may be attributable to the large axial components of velocity in the constricted space between the exhaust pipe and the cylinder wall. These result in wall friction which adds to the net axial force on the control volume in the direction of momentum outflow.

CONCLUSION

The comparisons of experimental and analytical data of Figs. 3 and 4 indicate that for relatively large ratios of inlet area to exhaust area a momentum analysis omitting all friction forces gives a good representation of the head loss in a cyclone separator. As the ratio of inlet area to exhaust area approaches zero, the experimental results show a transition from the analytical results for vortex flow to those for flow without rotation about the axis.

ACKNOWLEDGMENT

The work reported herein was sponsored by Jabez Burns and Sons, Inc., New York, N. Y.

The Synthesis of Four-Bar Mechanisms by the Method of Components

By J. HIRSCHHORN,[1] SYDNEY, N. S. W., AUSTRALIA

The synthesis of four-bar mechanisms based on the vectorial representation of links in complex form was first suggested by S. Bloch.[2] His work was further developed by R. Beyer[3] and N. Rosenauer.[4,5] These kinematicians investigated the synthesis of the four-bar mechanism for prescribed instantaneous angular velocities and accelerations of the three moving links. This paper presents a somewhat different approach to the problem, in that the vectors are being resolved into Cartesian components. This method permits the synthesis for prescribed conditions concerning angular velocities, accelerations, and lengths of links. The author believes that the simpler treatment will make this method more readily acceptable to engineers.

The configuration, velocity, and acceleration diagrams of the four-bar mechanism shown in Fig. 1 are defined by the following vector equations

Configuration diagram, Fig. 1(*a*) . . . . $\bar{p} + \bar{s} = \bar{q} + \bar{r}$

Velocity diagram, Fig. 1(*b*) . . . . . $\bar{v}_S = \bar{v}_Q + \bar{v}_{SQ}$

Acceleration diagram, Fig. 1(*c*) . . . . . $\bar{a}_S = \bar{a}_Q + \bar{a}_{SQ}$

By resolving each vector into components in the directions of the x and y-axes these vector equations can be replaced by six algebraic equations

$$q_x + r_x = s_x + p \quad \ldots\ldots [1]$$

$$q_y + r_y = s_y \quad \ldots\ldots [2]$$

$$q_y\omega_q + r_y\omega_r = s_y\omega_s \quad \ldots\ldots [3]$$

$$q_x\omega_q + r_x\omega_r = s_x\omega_s \quad \ldots\ldots [4]$$

$$q_x\omega_q^2 + q_y\alpha_q + r_x\omega_r^2 + r_y\alpha_r = s_x\omega_s^2 + s_y\alpha_s \quad \ldots\ldots [5]$$

$$q_y\omega_q^2 - q_x\alpha_q + r_y\omega_r^2 - r_x\alpha_r = s_y\omega_s^2 - s_x\alpha_s \quad \ldots\ldots [6]$$

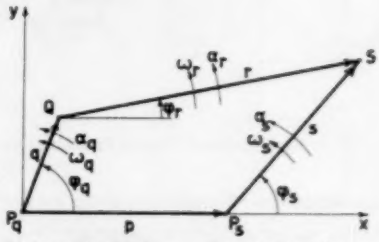

Links: Fixed link p Connecting link r
Driving link q Driven link s

FIG. 1(*a*) CONFIGURATION DIAGRAM

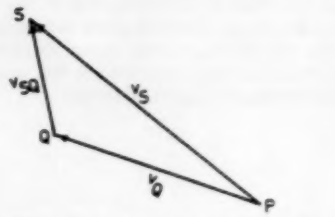

Velocities: $v_Q = q\omega_q$, $v_{SQ} = r\omega_r$, $v_S = s\omega_s$

FIG. 1(*b*) VELOCITY DIAGRAM

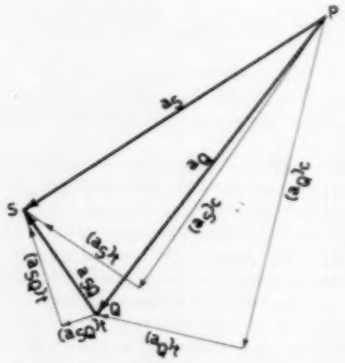

Centripetal-acceleration components:

$(aQ)_c = q\omega_q^2$, $(aSQ)_c = r\omega_r^2$, $(aS)_c = s\omega_s^2$

Tangential-acceleration components:

$(aQ)_t = q\alpha_q$, $(aSQ)_t = r\alpha_r$, $(aS)_t = s\alpha$.

FIG. 1(*c*) ACCELERATION DIAGRAM

These equations contain 13 variables, viz.:

The projections q_x and q_y of the driving link, its angular velocity ω_q, and angular acceleration α_q.

The projections r_x and r_y of the connecting link, its angular velocity ω_r, and angular acceleration α_r.

The projections s_x and s_y of the driven link, its angular velocity ω_s, and angular acceleration α_s.

The length of the fixed link, p.

[1] Senior Lecturer in Mechanical Engineering, New South Wales University of Technology.

[2] "On the Synthesis of Four-Bar Linkages," by S. Bloch, Bulletin of the Academy of Sciences, USSR, 1940, N1, pp. 47–54.

[3] "Gelenkvierecke mit vorgeschriebenen Geschwindigkeits- und Beschleunigungsverhaltnissen," by R. Beyer, *Getriebetechnik*, vol. 11, 1943, pp. 193–195.

[4] "Gelenkvierecke mit vorgeschriebenen Grösst- und Kleinstwerten der Abtriebswinkelgeschwindigkeit," by N. Rosenauer, *Getriebetechnik*, vol. 12, 1944, N1.

[5] "Complex Variable Method for Synthesis of Four-Bar Linkages," by N. Rosenauer, *Australian Journal of Applied Science*, vol. 5, 1954, pp. 305–308.

Contributed by the Applied Mechanics Division and presented at the Annual Meeting, New York, N. Y., November 25–30, 1956, of THE AMERICAN SOCIETY OF MECHANICAL ENGINEERS.

Discussion of this paper should be addressed to the Secretary, ASME, 29 West 39th Street, New York, N. Y., and will be accepted until April 10, 1957, for publication at a later date. Discussion received after the closing date will be returned.

NOTE: Statements and opinions advanced in papers are to be understood as individual expressions of their authors and not those of the Society. Manuscript received by ASME Applied Mechanics Division, April 9, 1956. Paper No. 56—A-3.

With the aid of these equations, problems in which seven of these variables are prescribed may be solved either directly or by the method of "gradual approach."

Case A. The following particulars are prescribed: Length of the fixed link: instantaneous angular velocities and angular accelerations of the driving and driven links; length and position of either the driven or the driving link.

The procedure to be outlined applies to the case where the length and position of the driven member are prescribed. A similar approach would be used in the second case, where the driving link is specified in magnitude and position.

Data:

Fixed link: Length p

Driving link: Angular velocity ω_q, angular acceleration α_q

Driven link: Length s and position φ_s, defined by s_x and s_y, angular velocity ω_s, angular acceleration α_s

Solution: By combining Equation [1] with Equation [4], and Equation [2] with Equation [3] the following equations are obtained in which q_x, q_y, r_x, and r_y are expressed in terms of ω_r and the prescribed quantities

$$q_x = \frac{s_x(\omega_s - \omega_r) - p\omega_r}{\omega_q - \omega_r} \quad [7]$$

$$q_y = \frac{s_y(\omega_s - \omega_r)}{\omega_q - \omega_r} \quad [8]$$

$$r_x = \frac{-s_x(\omega_s - \omega_q) + p\omega_q}{\omega_q - \omega_r} \quad [9]$$

$$r_y = \frac{-s_y(\omega_s - \omega_q)}{\omega_q - \omega_r} \quad [10]$$

Equations [5] and [6] are then combined to eliminate α_r, thus

$$\omega_q^2(q_x r_x + q_y r_y) + \alpha_q(q_y r_x - q_x r_y) + \omega_r^2(r_x^2 + r_y^2) = \omega_r^2(r_x s_x + r_y s_y) + \alpha_s(r_x s_y - r_y s_x) \quad [11]$$

By substituting Equations [7] to [10] into Equation [11] a quadratic equation in ω_r is obtained, of the form

$$A\omega_r^2 - B\omega_r + C = 0$$

One root of this equation is equal to ω_q, giving infinitely long links q and r, while the other root, which represents the actual angular velocity of the connecting link, is given by the expression

$$\omega_r = \frac{B}{A} - \omega_q \quad [12]$$

Example 1. The following values are prescribed:

Fixed link: $p = 3.375$ in.

Driving link: $\omega_q = 10$ radians/sec, $\alpha_q = 0$

Driven link: $s_x = 4$ in., $s_y = 4.625$ in., $\omega_s = 5$ rad/sec

$\alpha_s = 10$ rad/sec^2

From Equation [7]

$$q_x = \frac{160 - 59\omega_r}{8(10 - \omega_r)}$$

From Equation [8]

$$q_y = \frac{185 - 37\omega_r}{8(10 - \omega_r)}$$

From Equation [9]

$$r_x = \frac{430}{8(10 - \omega_r)}$$

From Equation [10]

$$r_y = \frac{185}{8(10 - \omega_r)}$$

Equation [11] reduces to

$$8765\omega_r^2 - 104{,}259\omega_r + 166{,}090 = 0$$

from which, by Equation [12]

$$\omega_r = \frac{104{,}259}{8765} - 10 = 1.895 \text{ rad/sec}$$

$$\left.\begin{aligned} q_x &= 0.745 \text{ in.} \\ q_y &= 1.77 \text{ in.} \end{aligned}\right\} \; q = 1.92 \text{ in.}$$

$$\left.\begin{aligned} r_x &= 6.64 \text{ in.} \\ r_y &= 2.85 \text{ in.} \end{aligned}\right\} \; r = 7.22 \text{ in.}$$

Case B. The following particulars are specified: Length of the fixed link; instantaneous angular velocities and angular accelerations of the driving and driven links; length of the driving and position of the driven link, or vice versa.

Illustrated in the following is the procedure adopted in the case where the length of the driving and the position of the driven member are prescribed. A similar method of solution would be used in the inverse problem.

Data:

Fixed link: Length p

Driving link: Length q, angular velocity ω_q, angular acceleration α_q

Driven link: Position, defined by the ratio $\frac{s_y}{s_x} = \tan \varphi_s$; angular velocity ω_s, angular acceleration α_s

Solution: In this case the gradual elimination of the unknown quantities would finally yield an equation of the fourth degree in q_x, thus making advisable the use of the gradual-approach method of solution:

A value of q_x is assumed and the corresponding values of ω_r and $\tan \varphi_s = s_y/s_x$ are calculated, using the procedure outlined in Case A. This step is repeated a number of times and the results are plotted against q_x. From the graphs thus obtained the correct results may be read. It should be noted that the physical limits of q_x are $\pm q$.

Example 2. The mechanism shall satisfy the following requirements:

Fixed link: $p = 5$ in.

Driving link: $q = 2$ in., $\omega_q = 10$ rad/sec, $\alpha_q = 0$

Driven link: $\tan \varphi_s = s_y/s_x = 4/3$, $\omega_s = 5$ rad/sec, $\alpha_s = 0$

Table 1 shows the results of the preliminary approach. It can

TABLE 1 PRELIMINARY RESULTS FOR EXAMPLE 2

q_x	q_y	ω_r	s_y/s_x
+2.0	0	+2.85	0
+1.5	±1.323	+2.61	± 0.41
+1.0	±1.732	+2.31	± 0.69
+0.5	±1.936	+1.90	± 1.15
0	±2.000	+1.38	± 2.35
−0.418	±1.956	+0.772	∞
−0.5	±1.936	+0.625	∓11.6
−1.0	±1.732	−0.525	∓ 1.38
−1.5	±1.323	−2.50	∓ 0.53
−2.0	0	−6.67	0

be seen that the required value of $s_y/s_x = 4/3$ will be given by two values of q_x, one between 0 and +0.5, the other between −1.0 and −1.5.

There are, therefore, two mechanisms which satisfy the pre-

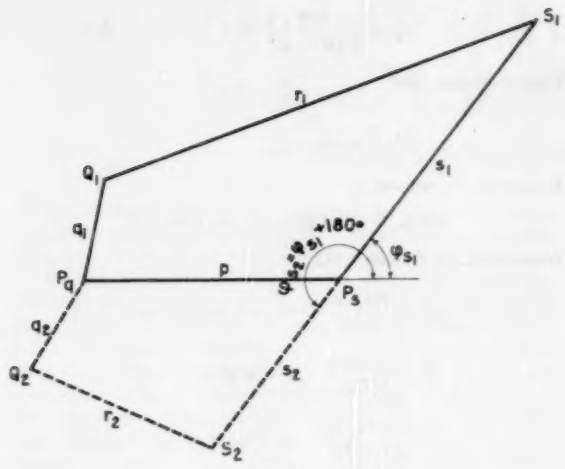

FIG. 2

scribed requirements of p, q, ω_q, α_q, ω_r, α_r, and $\tan \varphi_s$, but only one of these gives the correct *position* φ_s.

The final results are given in the following, and the two mechanisms are shown in Fig. 2:

Mechanism 1

$q_x = 0.38$ in.	$q_y = 1.97$ in.	$q = 2.00$ in.
$r_x = 8.40$ in.	$r_y = 3.08$ in.	$r = 8.95$ in.
$s_x = 3.78$ in.	$s_y = 5.04$ in.	$s = 6.30$ in.

Mechanism 2

$q_x = -1.02$ in.	$q_y = -1.72$ in.	$q = 2.00$ in.
$r_x = +3.57$ in.	$r_y = -1.55$ in.	$r = 3.89$ in.
$s_x = -2.45$ in.	$s_y = -3.27$ in.	$s = 4.09$ in.

Case C. A four-bar mechanism is to be designed to give prescribed instantaneous values of angular velocity and angular acceleration of the three moving links.

This problem has been solved by N. Rosenauer[4, 5] by the method of "complex variables," and its solution by the "component method" is presented only for the sake of completeness.

Solution: The method of attack consists in the progressive elimination of the unknown quantities from Equations [1] to [6].

Example 3. The mechanism shall satisfy the following requirements:

Fixed link: Length p

Driving link: $\omega_q = 10$ rad/sec, $\alpha_q = 0$

Connecting link: $\omega_r = 2$ rad/sec, $\alpha_r = 15$ rad/sec^2

Driven link: $\omega_s = 5$ rad/sec, $\alpha_s = 10$ rad/sec^2

From Equation [1]

$$q_x + r_x = s_x + p \quad \ldots\ldots [a]$$

From Equation [2]

$$q_y + r_y = s_y \quad \ldots\ldots [b]$$

From Equation [3]

$$10q_y + 2r_y = 5s_y \quad \ldots\ldots [c]$$

From Equation [4]

$$10q_x + 2r_x = 5s_x \quad \ldots\ldots [d]$$

From Equation [5]

$$100q_x + 4r_x + 15r_y = 25s_x + 10s_y \quad \ldots\ldots [e]$$

From Equation [6]

$$100q_y + 4r_y - 15r_x = 25s_y - 10s_x \quad \ldots\ldots [f]$$

In the first step q_y is eliminated.

Equation [b] combined with Equation [c] gives

$$8r_y = 5s_y \quad \ldots\ldots [g]$$

Equation [b] combined with Equation [f] gives

$$96r_y + 15r_x = 75s_y + 10s_x \quad \ldots\ldots [h]$$

This reduces the system to five Equations [a], [d], [e], [g], [h] containing five unknown quantities q_x, r_x, r_y, s_x, s_y.

Next, s_y is eliminated:

Equation [g] combined with Equation [e] gives

$$100q_x + 4r_x - r_y = 25s_x \quad \ldots\ldots [i]$$

Equation [g] combined with Equation [h] gives

$$-24r_y + 15r_x = 10s_x \quad \ldots\ldots [k]$$

The field has been reduced to four Equations [a], [d], [i], [k] containing the unknown quantities q_x, r_x, r_y, s_x.

The next quantity eliminated is r_y:

Equation [i] combined with Equation [k] gives

$$2400q_x + 81r_x = 590s_x \quad \ldots\ldots [l]$$

Term s_x is eliminated by the following steps:

Equation [a] combined with Equation [l] gives

$$1810q_x - 509r_x = -590p \quad \ldots\ldots [m]$$

Equation [d] combined with Equation [l] gives

$$1220q_x - 155r_x = 0 \quad \ldots\ldots [n]$$

Term r_x is finally eliminated by combining Equation [m] with Equation [n], giving

$$(1220 \times 509 - 1810 \times 155)q_x = 590 \times 155p \quad \ldots\ldots [o]$$

and

$q_x = 0.268p$,	$q_y = 0.449p$	$q = 0.523p$
$r_x = 2.110p$,	$r_y = 0.746p$	$r = 2.240p$
$s_x = 1.380p$,	$s_y = 1.195p$	$s = 1.825p$

A New Method to Measure Prandtl Number and Thermal Conductivity of Fluids[1]

By E. R. G. ECKERT[2] and T. F. IRVINE, JR.,[3] MINNEAPOLIS, MINN.

A new method is described by which the Prandtl number and indirectly the thermal conductivity of fluids can be measured. The method is based on the fact that a well-established, unique relation exists between the Prandtl number and the recovery factor for laminar high-velocity boundary-layer flow. The test setup is described which has been devised for such measurements, and test results are presented for air at atmospheric pressure and temperatures between 60 and 350 F.

Introduction

THE Prandtl number is a dimensionless property value which is of importance in high-speed fluid mechanics and in convective heat-transfer processes. In the past no attempt has been made to measure it directly, but it was calculated from other properties by which it can be expressed according to the relation

$$\mathrm{Pr} = \frac{\mu c_p}{k} \qquad [1]$$

(μ viscosity, c_p specific heat at constant pressure, k thermal conductivity). The purpose of this paper is to describe a method by which the Prandtl number can be measured directly. This method was proposed several years ago by the senior author.[4] Acting upon this suggestion, an apparatus was built by Seban, Scesa, and Levy (1).[5] Design difficulties, however, made corrections to the measured results necessary, which were estimated by the authors to be of order 2 per cent. The results of measurements on air which have been obtained in the meantime by the junior author with a different design are presented here.

Method

Any method for measuring property values has to be based on a relation which contains, in addition to the property sought for, only quantities which can be measured readily. For thermal and dynamic properties such relations are usually obtained by an integration of Fourier's or Navier-Stokes' equations for certain geometries and boundary conditions. The well-known method of measuring viscosity by the pressure drop which a fluid experiences in flowing through a capillary tube, for instance, is based on Poisson's solution of the Navier-Stokes equations. There are several such solutions available which contain the Prandtl number and which, in principle, can be used for a measurement of this property. One which looks especially attractive from an experimental viewpoint is offered by the relation describing the temperature which a flat plate assumes in high-velocity, steady, two-dimensional flow when it exchanges heat with the fluid only by convective heat transfer. This temperature, which may be referred to as the recovery temperature t_r, is usually described by a recovery factor

$$r = \frac{t_r - t_s}{t_t - t_s} \qquad [2]$$

(t_s static, t_t total temperature in the flow at sufficient distance from the plate). The value for this recovery factor was for the first time calculated by E. Pohlhausen (2) by an integration of the laminar boundary-layer equations assuming that the properties appearing in these equations can be considered as constants. It was found that under these conditions the recovery factor is a function of Prandtl number only. A. Busemann pointed out that for Prandtl numbers between 0.5 and 5, this relation, which is tabulated in Pohlhausen's paper, can be expressed with very good accuracy by the simple expression

$$r = \mathrm{Pr}^{1/2} \qquad [3]$$

In the meantime these calculations have been checked many times and were extended to study the effects of a pressure variation in the flow along the surface, of surface curvature, and of property variations (3, 4, 5, 6, 7, 8). Also, the validity of the boundary-layer equations which were obtained by L. Prandtl by an order-of-magnitude argument from the Navier-Stokes equations has been well established. Therefore, the temperature recovery may be considered as an effect which is very well known today and Equation [3] may be used to determine the Prandtl number by measuring the recovery factor. In principle, only temperature measurements are required according to Equation [2]. However, since a measurement of the static temperature in a high-velocity flow is very difficult, it is advisable to transform Equation [3] by the introduction of the relation

$$t_t - t_s = \frac{V^2}{2c_p} \qquad [4]$$

defining the total temperature t_t (obtained by adiabatic deceleration of the flow with velocity V in a fluid for which the specific heat can be considered as constant in the range between t_t and t_s). In this way, the working relation

$$\mathrm{Pr}^{1/2} = 1 - \frac{t_t - t_r}{\frac{V^2}{2c_p}} \qquad [5]$$

---

[1] Publication from the Heat Transfer Laboratory, University of Minnesota. Financial support by the Graduate School of the University is gratefully acknowledged.

[2] Professor of Mechanical Engineering, University of Minnesota. Mem. ASME.

[3] Assistant Professor of Mechanical Engineering, University of Minnesota.

[4] For instance, at the luncheon talk, "Problems and Progress in Aircraft Heat Transfer," given to the Heat Transfer Division of The American Society of Mechanical Engineers at Atlantic City, N. J., November 4, 1951.

[5] Numbers in parentheses refer to Bibliography at end of paper.

Contributed by the Applied Mechanics Division and presented at the Annual Meeting, New York, N. Y., November 25–30, 1956, of The American Society of Mechanical Engineers.

Discussion of this paper should be addressed to the Secretary, ASME, 29 West 39th Street, New York, N. Y., and will be accepted until April 10, 1957, for publication at a later date. Discussion received after the closing date will be returned.

Note: Statements and opinions advanced in papers are to be understood as individual expressions of their authors and not those of the Society. Manuscript received by ASME Applied Mechanics Division, February 9, 1956. Paper No. 56—A-32.

is obtained; it connects the Prandtl number with quantities which can all be measured readily.

It may be advisable to review the conditions for which Equation [5] is valid. The relation holds for laminar, steady, two-dimensional flow of the boundary-layer type (i.e., with sufficiently large Reynolds number) with constant velocity V of a fluid with constant properties over a smooth flat surface which exchanges heat with this fluid only (no radiation and heat sources or sinks below the surface). The constant-property condition can be approximated by making the velocity reasonably small, and the degree to which this is necessary can be checked with the help of relations available for fluids with variable properties (7, 8).

It has been mentioned before that the Prandtl number has been calculated in the past with Equation [1] from the values for viscosity, specific heat, and heat conductivity. The accuracy with which the Prandtl number is known depends in this way on the accuracy of information on the other properties. For gases, measurement of the heat conductivity causes great difficulties, and this is reflected in the limited present-day knowledge of this property. The results of measurements which have been published recently deviate, even for air, in a temperature range between 60 and 600 F by approximately 4 per cent. The methods used for these measurements are based on Fourier's equation which describes heat flow through a stagnant gas body.

The one quantity which causes the main difficulties in these measurements is the heat flow. Because of the low heat conductivity of gases, it is impossible to keep heat losses small. At higher temperatures the radiative heat exchange between the surfaces is especially troublesome. In addition, natural convection currents have to be avoided. All these sources of error are radically reduced in the present method for the measurement of Prandtl numbers, because it employs a high-velocity flow in which the convective heat transfer is large and in which heat losses easily can be kept small. Hence it can be expected that heat conductivities of gases calculated from measured Prandtl numbers will be more accurate than the directly measured values. This conclusion also is based on the fact that viscosity and specific heat are known with considerably better accuracy than heat conductivity and will be borne out by the results presented later on in this paper.

Test Setup

Fig. 1 shows the apparatus which has been devised to fulfill the conditions required for the use of Equation [5] and to permit the necessary measurements. The test setup is designed for Prandtl-number measurements in gases. The high-velocity flow is generated by the expansion of the gas in a rotationally symmetrical nozzle a. The nozzle diameter is only 0.4 in. This makes it possible to work with relatively small amounts of gas in an open system. A field of uniform velocity is in this way set up in the conically shaped region b. The surface on which recovery conditions are to be established is the surface of a thermocouple c which is strung coaxially through the nozzle. Its one junction d reads the recovery temperature t_r, the second junction e, the total temperature t_t in the gas stream since it is located in an area where the gas velocity is low. This arrangement has the advantage that the temperature difference $t_t - t_r$ which appears in Equation [5] is indicated directly.

The total temperature which also is required is measured by another thermocouple f, the other junction of which is placed in melting ice. Radiation errors are kept small by radiation shields g, h, and i and by guard heating of the walls k of the vessel upstream of the nozzle. Heat conduction along the thermocouple is minimized by choice of low-heat-conductivity material (manganin-constantan) and of a small wire diameter (0.018 in.). The joint d is carefully butt-welded and reworked to the wire thickness. This, together with the length dimension of nozzle and wire to junction d and with the fact that the wire is led through the nozzle into a region of low velocity, insures laminar boundary-layer flow along the wire up to and beyond junction d. On the other hand, the flow condition upstream from the cylindrical nozzle section does not agree with the flow assumed in the derivation of Equation [5]. A calculation of the development of the boundary layer along the wire as the flow approaches the nozzle and through the convergent-nozzle portion showed, however, that the boundary layer at the junction d is still quite thin compared to the wire diameter. The calculations in reference (4) show also that the recovery factor in accelerated flow deviates very little from the value at constant velocity. This insures that the influence of the accelerated-flow region on condition at junction d is negligibly small.

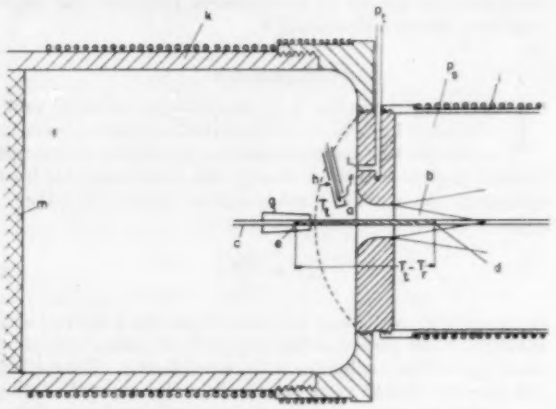

a—nozzle
b—field of constant velocity and pressure
c—thermocouple with junctions d and e
f—thermocouple
g, h, i—radiation shields
k—guard heating
l—measurement of total pressure
m—storage-type heat exchanger

Fig. 1 Apparatus for Measurement of Prandtl Number of Gases

Equation [5] requires additionally the knowledge of the velocity V outside the boundary layer along the thermocouple wire. This velocity is obtained from two pressure readings and the total-temperature measurement. One pressure is measured at location l chosen so that the kinetic energy of the gas is negligibly small. This reading, therefore, is identical with the total pressure p_t. The pressure is also read in the large space surrounding the gas jet behind the nozzle. This pressure determines with a slight correction the static pressure p_s in the jet at the cross section of junction d as long as the flow velocities are subsonic. It was also carefully checked that the expansion of the gas in the nozzle from pressure p_t to p_s is isentropic. In the temperature and pressure range in which the measurements described in the next section were carried out, the gas could be considered as an ideal one. Therefore, the following relation was used to calculate the velocity parameter in Equation [5]

$$\frac{V^2}{2c_p} = T_t\left[1 - \left(\frac{p_s}{p_t}\right)^{\frac{\gamma-1}{\gamma}}\right] \qquad [6]$$

with γ representing the ratio of specific heats at constant pressure and volume.

A storage-type heat exchanger is used to heat the gas to the

required temperature. It consists of a ceramic matrix *m* packed into the vessel upstream of the nozzle. The matrix is electrically heated prior to the tests. During the experiments gas from a storage bottle is blown through the matrix and in this way heated to a temperature which was found to be locally, and during a period of approximately one minute timewise, very constant.

A careful analysis of possible systematic errors like conduction or radiation errors in temperature measurements showed that the largest deviation from the true Prandtl value is caused by the fact that a rotationally symmetrical flow situation is used in the experiment instead of the two-dimensional one for which Equation [5] was derived. This will cause an error which depends on the ratio of boundary-layer thickness to wire diameter. Using the results of an analysis by Seban and Bond (6), it was found that under the conditions of the experiments the resulting error may have a value up to 0.7 per cent. This, therefore, is considered to be the accuracy for the measurements presented in the next section. In future work this error can be reduced easily and substantially by giving the thermocouple the shape of a thin-walled tube of larger diameter.

Test Results

A series of measurements has been made with the apparatus described in the previous section in which the Prandtl number of air was determined at atmospheric pressure and in a temperature range between 60 and 350 F. The results obtained are shown in Fig. 2 as full points. A mean line also is drawn through the test points as a full line and the two dashed curves indicate 0.5 per cent deviation from the mean line. It may be recognized that all data points except one are within this range.

The thermal conductivities also were calculated from the measured Prandtl numbers, from specific heats in reference (9) and viscosities from reference (10). The results are shown in Fig. 3 as full points. Also inserted in the figure are the results of three of the latest direct experimental determinations of the thermal conductivity of air (11, 12, 13). The full line is the curve recommended by the National Bureau of Standards (14) which extended the work of Keyes (15). Keyes used a modified type of Sutherland equation to fit existing experimental data to 660 F. The National Bureau of Standards extended this work up to 1340 F.

It may be observed that the scatter of the data has been substantially reduced in the present measurements and that a satisfactory agreement exists with the National Bureau of Standards recommended curve. In the temperature range covered in the present work it is felt that the reliability of 4 per cent ascribed to the thermal conductivity of air by the National Bureau of Standards may be re-evaluated to 1 per cent.

The main engineering interest lies today in heat-conductivity values for high temperatures. An investigation by Glassman and Bonilla (16) extended such measurements to temperatures as high as 860 F. No principal difficulty can be foreseen which would prevent use of the method described in this paper for Prandtl-number measurements at very high temperatures, and such an investigation is planned for the near future.

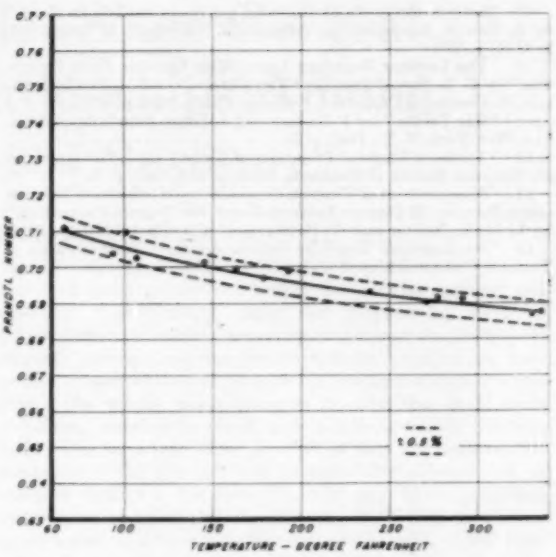

Fig. 2 Prandtl Number of Air at Atmospheric Pressure

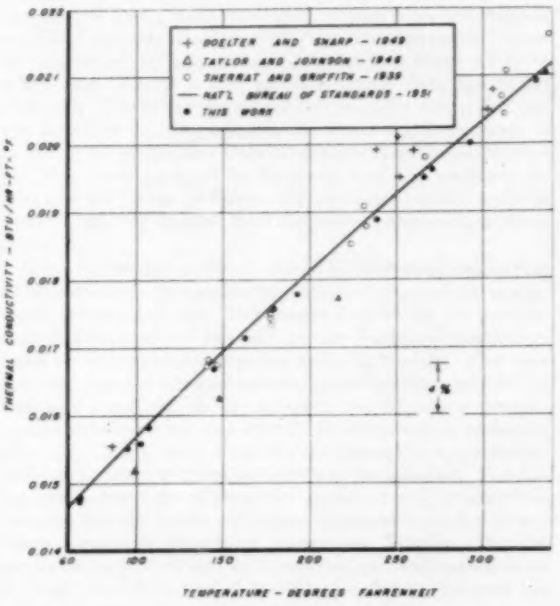

Fig. 3 Thermal Conductivity of Air at Atmospheric Pressure

BIBLIOGRAPHY

1 "Prandtl Number Determination by Means of Recovery Factor Measurements," by R. A. Seban, S. Scesa, and A. Levy, Project SQUID, University of California, Technical Report UCB-1-R, 1954.

2 "Der Wärmeaustausch zwischen festen Körpern und Flüssigkeiten mit kleiner Reibung und kleiner Wärmeleitung," by E. Pohlhausen, *Zeitschrift für angewandte Mathematik und Mechanik*, vol. 1, 1921, pp. 115–121.

3 "Der Wärmeübergang an eine mit grosser Geschwindigkeit längs angeströmte Platte," by E. Eckert and O. Drewitz, *Forschung auf dem Gebiete des Ingenieurwesens*, vol. 11, 1940, pp. 116–124.

4 "Effect of Large Temperature Changes (Including Viscous Heating) Upon Laminar Boundary Layers With Variable Free-Stream Velocity," by Solomon Levy, *Journal of the Aeronautical Sciences*, vol. 21, July, 1954, p. 459.

5 "Heat Transfer in Laminar Boundary Layers Subject to Surface Pressure and Temperature Distributions," by A. N. Tifford and S. T. Chu, Proceedings of the Second Midwestern Conference on Fluid Mechanics, 1952, p. 363.

6 "Skin Friction and Heat Transfer Characteristics of a Laminar Boundary Layer on a Cylinder in Axial Incompressible Flow," by R. A. Seban and R. Bond, *Journal of the Aeronautical Sciences*, vol. 18, October, 1951, p. 671.

7 "Sullo strato limite laminare nei gas lungo una lamina plana," by L. Crocco, Rendiconti di Matematica, Università di Roma, vol. 2, 1941, p. 138.

8 "The Laminar Boundary Layer With Variable Fluid Properties," by E. R. Van Driest, Heat Transfer and Fluid Mechanics Institute, University of California, Berkeley, Calif., 1954, p. 127.

9 "Gas Tables," by J. Keenan and J. Kaye, John Wiley & Sons, Inc., New York, N. Y., 1949, p. 34.

10 "Tables of Thermal Properties of Gases," by J. Hilsenrath, et al., National Bureau of Standards, Circular 564, 1955, p. 69.

11 "Measurement of Thermal Conductivity of Air and of Exhaust Gases Between 50 Degrees Fahrenheit and 900 Degrees Fahrenheit," by L. M. K. Boelter and W. H. Sharp, NACA TN 1912, July, 1949.

12 "An Improved Hot-Wire Cell for Accurate Measurements of Thermal Conductivities of Gases Over a Wide Temperature Range. Results for Air Between 87 Degrees K and 375 Degrees K," by W. J. Taylor and H. L. Johnston, *Journal of Chemistry and Physics*, vol. 14, 1946, p. 219.

13 "A Hot Wire Method for the Thermal Conductivity of Gases," by G. G. Sherratt and E. Griffiths, *Philosophical Magazine*, vol. 27, 1939, p. 68.

14 Reference (10), p. 70.

15 "A Summary of Viscosity and Heat-Conduction Data for He, A, H_2, O_2, N_2, CO, CO_2, H_2O, and Air," by F. G. Keyes, Trans. ASME, vol. 73, 1951, p. 589.

16 "The Thermal Conductivity and Prandtl Number of Air at High Temperature," by I. Glassman and C. F. Bonilla, Heat Transfer Symposium, American Institute of Chemical Engineers, December, 1951.

The State Principle—Some General Aspects of the Relationships Among the Properties of Systems

By S. J. KLINE[1] and F. O. KOENIG,[2] STANFORD, CALIF.

An independent generalization, here called the "State Principle," is necessary for the development of thermodynamics. Previously, this principle has been either tacitly assumed, or at best stated incompletely. A discussion and explicit formulation of this principle are given. The Phase rule is deduced from the State Principle and certain related empirical information. In this derivation no reference whatsoever is made to the First Law or the Second Law of Thermodynamics. A new, simple, systematic means for counting the number of components in the phase rule, which has no known exceptions and which does not rely on either advanced thermodynamics or the First and Second Laws, is presented. Examples of its use are included.

Nomenclature

The following nomenclature is used in the paper:

- C = number of components in a certain type of list of chemical components
- F = maximum number of independent intensive properties of a certain class of systems
- m = mass of system
- n = maximum number of independent properties in a given system
- P = number of phases in system
- r = an intensive property of system
- U = internal energy of a certain class of system

Introduction

In most treatises on the subject, thermodynamics is defined as the study of energy, its transformations, and the relationships among the properties of systems. Recently two papers concerned entirely with the history and epistemology of the Laws governing energy transformations, the First and Second Laws of Thermodynamics, have been published by Keenan and Shapiro[3] and Emmons.[4] Work of this type serves to make thermodynamics a more precise and useful tool for the engineer and scientist. Unfortunately, since the monumental work of Gibbs,[5] little attention has been given to the general aspects of the relations among the properties of systems. And it has been generally assumed that no fundamental principle is needed in this area. The present paper attempts to show that there is an underlying principle involved, and that this principle has been tacitly used for a long time. It is hoped that this more explicit treatment of the principle and its underlying concepts will be useful to workers in this field. The authors fully recognize that this will not be the last word on the subject. But, if the present paper serves to stimulate further active discussion, it will have served its purpose well.

In order to give an adequate formulation of the principle, which will hereafter be referred to as the State Principle, it is necessary to give first a more thorough discussion of the definitions of state and property than previously has been available. After formulation of the state principle, further definitions are given which make possible a new, accurate, simple deduction of the phase rule. These new definitions also provide a simple and precise means for counting correctly the number of components to be used in the phase rule. Detailed analysis of systems more complex than those governed by the phase rule, and combined applications employing the First and Second Laws together with the State Principle are omitted from the present paper owing to space limitations.

In the following discussion it should be understood clearly that all remarks apply only within the domain of conventional macroscopic thermodynamics. This means that we do not consider any relativistic effects nor rely on any statistical calculations based on assumptions concerning molecular models. This does not mean that the relations between properties are unaffected by molecular structure; on the contrary, the differences between various substances are due entirely to differences in molecular structure. But it does mean that we choose to focus attention solely on the phenomenological aspects of the behavior. This has the usual advantages of simplicity combined with generality in the sense that the results will remain unaltered in the face of any future discoveries concerning microscopic behavior. It also carries the restriction that we cannot deal with systems which are so small that the action of individual molecules becomes important.

In classical thermodynamics all considerations of state are confined to systems in complete equilibrium. The extensions by Onsager, et al., now allow these same considerations to be applied to systems near equilibrium. The following discussion applies to systems in equilibrium[6] or near equilibrium in the sense of Onsager. In the examples actually discussed we will limit our-

---

[1] Associate Professor of Mechanical Engineering, Stanford University. Mem. ASME.

[2] Professor of Chemistry, Stanford University.

[3] "History and Exposition of Thermodynamics," by J. H. Keenan and A. H. Shapiro, *Mechanical Engineering*, vol. 69, 1947, pp. 915–921.

[4] "Re-Examination of Thermodynamic Fundamentals," by H. W. Emmons, *Mechanical Engineering*, vol. 72, 1950, p. 475.

Contributed by the Applied Mechanics Division and presented at the Annual Meeting, New York, N. Y., November 25–30, 1956, of The American Society of Mechanical Engineers.

Discussion of this paper should be addressed to the Secretary, ASME, 29 West 39th Street, New York, N. Y., and will be accepted until April 10, 1957, for pulbication at a later date. Discussion received after the closing date will be returned.

Note: Statements and opinions advanced in papers are to be understood as individual expressions of their authors and not those of the Society. Manuscript received by ASME Applied Mechanics Division, April 9, 1956. Paper No. 56—A-4.

[5] "Collected Works," by J. W. Gibbs, Yale University Press, vol. 1, 1948.

[6] The operational test of equilibrium, of course, is to isolate the system; if no changes then occur the system is said to have been in equilibrium.

selves to situations of complete equilibrium, but we make the foregoing remarks to retain all possible generality.

Terminology—Property and State

The usual procedure in giving a statement of a principle is to define certain key terms which are then used in stating the principle. Usually, these key terms cannot be defined with a satisfactory degree of rigor. The whole process is then one which starts from vague qualitative notions based on physical perceptions and proceeds by a stepwise process to a condition of relative exactitude embodied in certain quantitative relations between well-defined symbols. One of the real problems in the present case is that the two key terms employed, namely, "state" and "property," have been defined only very loosely, even more loosely than is usually the case. An attempt is therefore now made to improve these definitions.

The concepts of property and state are inextricably connected. Either can be defined quite easily if the other is known. There are, therefore, five possible courses of action open: (1) Define either property or state and use the definition in turn to define the other; (2) assume that either one is known intuitively and use it to define the other; (3) define both together by successive stages; (4) define both at once; (5) define each in terms of the other. Of these alternatives, (4) and (5) are logically fallacious, and (3) is undesirable. In addition, there appears to be no adequate definition for either state or property alone. The only remaining course of action open, and it is not an altogether satisfactory one, is to assume that either state or property is known and then to define the other in terms of it. In this case we shall assume that we understand the term property in its general significance. We then define a class called "primary property"; it in turn is used to define state.[1] Finally, the definition of state is used to define our final and useful class of properties called "macroscopic."

The first step in this process, which must never be omitted under any circumstances, is the specification of the system. For the sake of clarity we will take as the system, for the moment, an arbitrary amount of pure liquid water, in equilibrium, at rest with respect to the observer, and in the absence of effects of external fields,[2] capillarity, motion, and fluid shear. By well-established procedures we can measure the pressure, temperature, mass, and volume of this water. We also can measure, if we choose, such things as its surface area, elevation with respect to the earth, and acoustic velocity. Evidently, the number of such things that we can measure is indefinitely large. We might heat the water or compress it until the temperature and pressure had changed substantially and then repeat all of the previous measurements. After each of many observers has made many such measurements, which is our present status, we would discover that not all of the values determined were independent. That is, if we establish, say, the pressure, temperature, and mass of this system, its color, thermal conductivity, acoustic velocity, volume, and an indefinitely large number of other measurable quantities are fixed. Since, in this system, the observer is stationary with respect to the system and there is no effect of gravity, the velocity and elevation of the system relative to other co-ordinates, say, the earth, are not fixed. Similarly, the external surface area of the system is not fixed. Nevertheless, velocity, elevation, and surface area are measurable characteristics of the system.

This discussion suggests the definition of a subclass which we now call "primary property." A primary property is any property of a system which satisfies the following three conditions: (1) At any instant it has a quantitative numerical value; (2) it is defined without use of statistical calculations applied to molecular models; (3) it is defined and its value can be found by the type of experimental measurements described in the foregoing. It is to be clearly understood that the particular empirical observations just described form an example rather than a definitive procedure.

Using the definition of primary property just given, we can now form an adequate definition of state as follows: "When a sufficient number of primary properties are fixed so that in addition an indefinitely large number of other primary properties of the system are fixed, the state of the system is fixed." Using this definition of state we now define a new class called "macroscopic property." Any property which satisfies conditions (1) and (2) in our definition of primary property and which is also fixed when state is fixed, is called a macroscopic property. For the sake of brevity, the term macroscopic property will be referred to simply as property in the remainder of this paper.

It is to be noted that, in the entire foregoing treatment, the term "property of the system," in contradistinction to "property of the substance" is employed. It is this that gives point to the remark that elevation, velocity, and surface area are not fixed in the case of the system of pure water discussed. It is clear that since thermodynamics is the analysis of systems (and control volumes), it is the properties of systems that we need. A very clear example of this need is the analysis of the pressure of radiation in a total vacuum. What has perhaps not been so clear is the fact that it is difficult, if not impossible, to speak of the properties of substances in any meaningful way without an adequate definition of the system in which the substance is to be found, including the reference of co-ordinates for the system and the operations that are allowable. Superficially, it might appear that some equations of state, for example the steam tables, do speak of properties without a definition of the system, but this is certainly not so. In fact, no intelligent use of the steam tables can be made until one is quite clear that they apply only to 1 lb of water, in equilibrium, with the observer riding on the system, and in the absence of effects of external fields, capillarity, and fluid shear.

It often has been assumed that the two classes, primary property and macroscopic property, are the same. Since macroscopic property is essentially "any quantity which is fixed when state is fixed" and primary property is essentially "any observable characteristic," this need not be so. And, indeed, a closer observation reveals that they are not the same; the two classes do contain many quantities in common, but each contains some quantities that are not included in the other. In the example given it was stated that elevation, velocity, and surface area were not fixed when state was fixed; this is essentially true for the system defined in that case, and it is thus an example of primary properties which are not macroscopic properties. Even clearer examples can be framed. Observable geometric shape factors, such as maximum thickness, are clearly primary properties, but rarely, if ever, would they be useful in fixing state or necessarily be fixed when state is fixed.

Internal energy and entropy are examples of macroscopic properties that are not primary properties. Item (3) in the definition of primary property, as given, requires that the quantity be defined and its value found by experimental measurement; that is, an operational definition is given a priori and without any reference to the concept of state. This is not true of energy and entropy. Both logically and historically they are defined in terms of the concept of state utilizing the First Law and the Second Law, respectively. It is noted that in both of these definitions what is shown is not that energy or entropy is an observable characteristic but that they are fixed when state is fixed. Considerable discussion has been held between the authors and with colleagues on whether entropy, energy, and certain other quantities are observable. But, in actuality, this not only depends on the exact interpretation given to the word "observable," but it is also irrelevant. The point is that primary properties are defined operationally in terms of laboratory measurements and without

[2] Electricity, magnetism, gravity.

reference to state. Primary property is then used to define state, and finally, certain macroscopic properties are introduced which cannot be given adequate definitions without the concept of state. This last step is clearly an extension beyond the idea of a primary property, and it is by this extension that we include all the properties which we now need, or may need in the future, in the class which we call macroscopic property.

A more fundamental corollary to the statements just made is as follows: Which primary properties are fixed by state depends only on the specification of the system. For those readers who have considerable experience the concept that a given quantity may be a property of some systems, but not of other systems, may seem difficult to accept. But upon close examination it will be found that it is true and, furthermore, that the difficulty in accepting it springs primarily from long experience with the very special class of system which is used in defining the properties of substances. Some examples may aid in clarifying this point.

A very simple case is the matter of elevation or position in the gravity field. To the observer who rides on the system, elevation is not a property; thus we do not need elevation to use the steam tables, nor can we find any entry of elevation therein. Consider, on the other hand, a system including a dam with water behind it driving a hydraulic turbine. In this system the property with which we are most concerned is elevation; it is change in elevation alone that makes possible the work output we are trying to achieve. And it is certainly most necessary to know the elevation of the water if we are to know the energy available in the system. Here of course the observer stands at some fixed level and does not move with the water, but the only real change between this case, in which elevation is a property, and the steam tables, in which it is not, is the definition of the system being considered.

Another example is surface area. If our system is that employed in the steam tables again, surface area is not considered; it is not tabulated, and generally would not be considered as a property. However, in the cases of a surface layer at which adsorption, heat transfer, or chemical changes are occurring, the area is a highly significant property. It is also well known that the surface area must be fixed to calculate the energy of any system containing material that is stretched out very thin.

In these examples it has been pointed out to the authors by several colleagues that another view can be taken. Put very briefly, this view holds that all observable characteristics are always properties, but that they have either no effect or negligible effect in some systems. This viewpoint is an adequate one and it leads to the same answers as that obtained by the mode of thinking discussed in the foregoing. On careful inspection it appears that the difference lies essentially in whether we want to rule out the irrelevant quantities at the point where we define the system, or later on. It is the authors' opinion that the former course is more in keeping with the facts and with what is actually done and that it agrees better with what follows later. The authors' suggestion has the added advantages of emphasizing the need for clear definition of the system and providing for a single uniform treatment of all kinds and classes of properties.

Formulation of the State Principle

Utilizing the definitions of state and property just given, we now formulate the generalization which we call the State Principle in three parts:

1 Given any macroscopic system in equilibrium, there exists a group of functional relations among its properties.

2 The number of independent properties in each of these relations for a given system is usually equal to, and in no case greater than, a positive integer n.

3 The maximum number of independent properties n for a given system depends only on the specification of the system and is found by empirical observation.

For convenience in applying the State Principle we shall call any one of the functional relations among properties, referred to in item 1 of the principle, an "equation of state." Item 3 of the State Principle implies that at the present stage of knowledge we are not able to give one rule for the determination of the number n for any system whatever, merely on the basis of its specification.

The State Principle is a fundamental postulate of thermodynamics in the same sense as are the First and Second Laws. It is not new; thermodynamicists have understood these facts for many years. However, it has been employed tacitly rather than explicitly in the vast majority of cases. No exposition of it appears to have been published previously in any form. Like the First and Second Laws of Thermodynamics, the State Principle cannot be deduced from any other fundamental macroscopic postulate, nor can it be proved by any other deductive means. Its sole proof lies in the fact that the principle and all of its deductive consequences are in accord with laboratory observations.

Certain general remarks concerning the nature of the functional relations described by the State Principle should be made.

We note that in the various equations of state for a given system, the number of independent variables is by no means always equal to the maximum number n but may frequently be less than n. There are two important cases. The first, and perhaps most important, is the case of intensive state which requires a lesser number of independent variables. We shall discuss this case in detail later in connection with the phase rule. The second type arises from the fact that certain properties can take on zero values. Perhaps the commonest example is the specific internal energy of a perfect gas which, for suitably defined systems, is a function of temperature only although normally it would be expected to be a function of two variables.

It also has been shown by Gibbs[4] and Kline and Shapiro[5] that, even in the simplest cases, some of the functions in the equations of state are single-valued, others are not. Similarly, there is no guarantee that the functions in the equation of state or their derivatives are everywhere continuous. In fact, many examples of discontinuous properties, such as the specific heats of a vaporizing liquid, are well known.

The Simple System and the Phase Rule

One type of system that is treated frequently by use of thermodynamics belongs to a class which we shall call "simple system" and define in the following. The maximum number of independent intensive properties in a simple system, under proper conditions, is given by the phase rule which is familiar as one of the most important laws relating to state. We shall now illustrate the use of the State Principle by a discussion of the phase rule, including a new precise means for counting the number of components.

Our discussion begins with the definitions of a series of terms. The following group of definitions is not new, but is restated for completeness and in some cases to increase the rigor.

Homogeneous system. A system is homogeneous if any subsystem has the same set of properties as the system itself, and each of these properties has the same value in each subsystem of the same volume.

Intensive property of a homogeneous system. A property of a homogeneous system is intensive if, for any given state of the

[5] "On the Normal Shock Wave in Any Single Phase Fluid Substance," by S. J. Kline and A. H. Shapiro, papers of the Heat Transfer and Fluid Mechanics Institute, Stanford University Press, 1953.

system, the property has the same value in the system itself and in all its subsystems.

Extensive property. A property of a homogeneous system is extensive if its value, for fixed values of all the intensive properties, is proportional to the mass of the system.

Phase. Any part, or parts, of a system in which all intensive properties are identical in both kind and value is called a phase of the system. The existence of a phase is independent of the amount of mass in the phase, and a given phase may exist in any finite number of distinct parts.

Intensive property of a system. A property of the type of system governed by the phase rule is intensive if, and only if, it is an intensive property of any of its phases. (Thus in the case of several phases the density of each is an intensive property of the system.)

Intensive state. When all intensive properties of a system are fixed, its intensive state is fixed.

Component. A set of components of a system is a set of chemicals, each of known chemical formula, from which the system in any of its states can be prepared, using a mixing procedure which is specified. Any member of any set of components is called a component of the system.

The following definitions are new, but, as will be demonstrated, they are necessary to a careful treatment of the phase rule.

Simple system. A system is simple if (1) it is homogeneous or consists of a finite number of homogeneous parts in contact; (2) it is in equilibrium; and (3) external fields, capillarity, motion, fluid shear, and anisotropic stress are absent or of negligible effect; a simple system may be either open or closed. This is merely a name for the class of systems to which the phase rule applies and for which most existing tables have been prepared. The utility of such a name is obvious.

Independent, and determinate set of components. A set of components is independent if the mixing procedure permits addition to, and withdrawal from, the system of each member of the set alone in such a way that all of the states thus preparable are states of the system as specified. A set of components is determinate if the mass of each member required to prepare the system, under the mixing procedure, is fixed when the state of the system is fixed.

Free simple system. A simple system is free if (1) it has a set of components that is both independent and determinate, and (2) when its intensive state is fixed, the mass of each phase is variable independently.

A full understanding of the operational significance of each of the three preceding definitions is of great importance in proper use of the phase rule. While they in no way relieve the individual from thinking, they do make easier and more accurate the application of the rule. The best way to grasp their significance is through examples. For this reason two are included in the following.

To these definitions we append for clarity the following comments:

(1) It is readily shown that the ratio of any two of the extensive properties of a homogeneous system is an intensive property.

(2) Not all properties are necessarily either intensive or extensive, but for homogeneous systems most properties of physical interest belong to one or the other of these two classes.

(3) The intensive state of a simple system is not the same thing as its state. When state is fixed, intensive state is fixed, but the converse state is not in general true. This appears plainly from the definition of the free simple system in which, when the intensive state is fixed, the state is still variable by varying the masses of the phases.

(4) For any free simple system all sets of components that are both determinate and independent have the same number of members; we shall denote this number by C.[9]

In regard to the need for these new definitions, it will be shown by counter examples that the phase rule will not necessarily produce correct answers unless we are dealing with a simple system, and each of the three conditions implied, respectively, by use of an independent list of components, a determinate list of components, and a free system is fulfilled. In this sense these three definitions are logically necessary to the statement of the phase rule. The authors have attempted to reduce them to less than three definitions, but these attempts have failed, and it is our present opinion that each of the three conditions, in effect, bars out a distinctly different kind of a difficulty in use of the phase rule; hence it is unlikely that any further reduction can be realized. The authors recognize also that the conditions required by use of a determinate list and an independent list have been understood by most chemists for a long time; however, the rigor with which this understanding has been applied often has left much to be desired. This all too frequently meant that only a sophisticated chemist "skilled in the art" could obtain proper answers. These new definitions minimize the hueristic aspects by giving precise explicit tests. The definition of free system, on the other hand, covers certain rare cases that have troubled even the chemist in the past, and it would appear that no scheme for systematic treatment of this difficulty has been published previously. It is the authors' belief, based on teaching experience, that these new definitions make the use of the phase rule easier to grasp and more accurate in application both for the chemist and for the engineer.

We shall now write down the Phase rule: For any given free simple system, the maximum number of independent intensive properties F is given by

$$F = C + 2 - P$$

where C is the number of items in a list of components that is both determinate and independent and P is the number of phases.

Next we shall deduce this result from the following premises: (a) the State Principle, (b) the foregoing definitions, (c) the empirical fact that for any free simple system having one or more sets of components that are both determinate and independent, the maximum number of independent properties n is C + 2. Note that the information in premise (c) is empirical and is of the type mentioned under part (3) of the State Principle as given previously.

The deduction is as follows: For any simple system the total number of intensive properties is indefinitely great. But since, by part (2) of the State Principle, the total number of independently variable properties of any kind cannot exceed a maximum value n, the number of intensive properties independently variable also must have a maximum. This latter maximum we denote by F. It then follows, from its definition, that the intensive state of any simple system is fixed by F independently variable intensive properties which we may denote by $r_1 \ldots r_F$. We denote the masses of the P phases of the simple system by $m_1 \ldots m_P$.

Since this discussion is limited to free simple systems, it follows by definition of this class of system that the mass of each phase is independently variable when intensive state is fixed. Furthermore, the following argument shows that intensive state

[9] This statement can be proved in either of two ways: Examination of sets that are not independent and determinate, including the restricting conditions and internal reactions possible in such sets, shows that a theorem can be constructed proving the assertion. It also can be proved simply by constructing many examples, all of which will show it to be true. Since space does not permit the inclusion of the more exact and complex method in the present paper, it is left to the reader to construct enough examples to convince himself of the truth of the assertion.

plus the mass of each phase is sufficient to fix all intensive and extensive properties of the system. For each extensive property, a corresponding intensive property can be formed by dividing the extensive property by the mass of the phase; for example, the volume of any phase divided by its mass yields its specific volume. Consequently, if the intensive state and the mass of each phase are known, any desired extensive property can be found by multiplying an appropriately defined intensive property, which is fixed by intensive state, by the mass of the phase in question. As we already have pointed out, the number of intensive properties is indefinitely large even in the simplest systems. Consequently, any required number of extensive properties can be formed in this way. It then follows that intensive state plus the mass of each phase is always sufficient to fix state.

On combining the conclusion just derived with the definition of the free simple system, it follows that the set of $F + P$ properties comprised of $r_1 \ldots r_F$, and $m_1 \ldots m_p$ always contains the maximum number of independent properties n characterizing the system; that is, the number n for all such systems is $F + P$. But from item (c) of the premises, the number n for such systems is also $C + 2$. Equating these two values for n yields

$$F + P = C + 2$$

or

$$F = C + 2 - P$$

which is the phase rule—the desired result.

It should be noted that this derivation differs strikingly in two ways from any that has previously been given: (1) It is much simpler and shorter; (2) no use whatsoever is made of either the First Law or the Second Law of Thermodynamics. These facts can be seen most clearly by outlining for comparison the steps followed in the usual derivations. These all start with premises and definitions which are logically entirely equivalent to ours[10] and in addition employ the First and Second Laws.

Typically, the usual proofs proceed via the Gibbs criteria of equilibrium and the Gibbsian equations for the simple system (both of which are derived using all of the State Principle, the First Law and the Second Law), to the special conditions, expressed in terms of pressures, temperatures, and chemical potentials, respectively, for the mechanical, thermal, and chemical equilibrium of the system. By subtracting the total number of these equilibrium conditions from the total number of intensive variables, which would be independent if the system were separated into its constituent phases, and these were varied independently, the phase rule is finally obtained. In addition to its sheer length and complexity, this type of deduction has the drawback that the two Laws of Thermodynamics loom so large as to obscure the role of the State Principle and the premises, immediately related to it, namely, items (b) and (c) of the authors' premises. Whereas, in fact, it is the State Principle and its related premises that are essential and the First and Second Laws which are unnecessary.

Examples will now be given illustrating the use of the new definitions in applications of the phase rule.

Example 1. Definition of system: An aqueous solution of NaCl prepared by dissolving solid salt in distilled water at room temperature and pressure (Table 1).

[10] The premises in the usual derivations are frequently not stated explicitly and it may appear that we have made an additional assumption in item (c) of our premises. However, an equivalent assumption, in the form of an empirical fact concerning the number of independent properties of some specific type of system, is always made. Often this assumption is implied by the use of the special symbol U for the internal thermal energy where it is understood that U is the energy of only certain very restricted systems, and it is assumed at the outset that the number of independent intensive properties in these restricted systems is two. This assumption concerning U is based on empirical observation, and logically it is identical in kind (although not in scope) to premise (c) in the foregoing.

TABLE 1 DATA FOR EXAMPLE 1

	Possible list of components	Is list determinate	Is list independent	Number in list
1	$NaCl$, H_2O	Yes	Yes	2
2	Na, Cl, H_2O	Yes	No	3
3	$NaCl$, $NaCl{\cdot}2H_2O$, H_2O	No	Yes	3
4	HCl, $NaOH$, $NaCl$, H_2O	No	No	4
5	H_2, O_2, Na, Cl_2	Yes	No	4
6	$NaCl$, H_2O, $(H_2O)_2$	No	Yes	3
7	H_2O, $NaCl{\cdot}2H_2O$	Yes	Yes	2

The correct answer here, of course, is $C = 2$. This gives by the phase rule

$$F = 2 + 2 - 1 = 3$$

and intensive state is indeed fixed by three intensive variables, say, temperature, pressure, and concentration of sodium. This example shows clearly that wrong answers can be obtained easily by use of the phase rule in cases where the list is not both independent and determinate.

It is suggested that the reader can easily invent new lists of components and try them using the tests of independence and determinary both on this example and on others. It will be found that in general the number of items in the list of components will be greater than the correct number C unless the list is both determinate and independent.

Some discerning readers also may invent lists for systems of two or more phases, which pass the tests for both independence and determinacy, but which contain a number of items less than the correct number C. This arises from an implied or stated restriction in the means by which the system is prepared, and this difficulty is avoided by applying the third test of the free system. Let us illustrate with an example.

Example 2. Consider now the simple system of two phases, consisting, respectively, of solid BiOCl and an aqueous solution, and prepared by mixing arbitrary amounts of H_2O and $BiCl_3$. For this system a determinate and independent set of components is clearly H_2O, $BiCl_3$. Hence $C = 2$. Since $P = 2$ the phase rule gives

$$F = 2 + 2 - 2 = 2$$

But actually for this system $F = 3$ (e.g., temperature, pressure, and concentration of Bi in the solution). The explanation lies in the fact that the system as specified is not free because the masses of the phases will always be found in the ratio fixed by the reaction

$$H_2O + BiCl_3 \rightarrow 2HCl + BiOCl(S)$$

A corresponding free system for this case is, for instance, one made of the same two phases as before but prepared by mixing arbitrary amounts of H_2O, $BiCl_3$, and HCl. Here $C = 3$, whence $F = 3$, the correct result. This example suffices to show that it is also necessary to make sure that the system as specified is free when applying the phase rule.

Let us return for a moment to the very simple case of greatest interest to the engineer, the simple system of one pure substance. It is obvious, on any basis, that the number C is 1. From premise (c), used in deriving the Phase rule, it follows that the total number of independent properties n is 3 regardless of the number of phases. From the Phase rule it is also clear that the number of independent intensive properties F for 1, 2, and 3 phases is, respectively, 2, 1, and 0. All of this is correct, and it provides a means for treating this simplest and commonest type of system that is entirely consistent with what ultimately must be done in more complex systems, and, surprisingly, it has been the authors' experience that this scheme is easier to teach even beginning students than the other treatments often given.

Let us now extend this example slightly so that we no longer have a simple system. For example, we might take again the system made up of the water stored behind a dam. To specify

the intensive state of this water it is certainly necessary to give temperature, pressure, and elevation; hence $F = 3$. Here the phase rule fails because the system is not simple; an effect of gravity is important in this system. It is equally easy to envisage systems for which the phase rule will not work if any of the other restrictions of the simple system concerning external fields, capillarity, anisotropic stress, and fluid shear are removed.

This naturally leads to the question, can a statement be given which specifies n or F for systems more general than those to which the phase rule applies? In so far as the authors know, no completely general statement is available; however, one somewhat broader than the phase rule can be postulated. Space requirements preclude this more general development in the present paper, but the authors hope to include a discussion of this point along with illustrations of combined applications of the State Principle, the First Law, and the Second Law of Thermodynamics in a subsequent paper.

Conclusions

1 The State Principle is necessary to the logical development of thermodynamics. Its explicit statement is useful in clarifying the principle and its underlying concepts.

2 By use of the State Principle and certain new definitions, a derivation of the phase rule is obtained which is simple and rigorous and which requires no resort to advanced thermodynamics or to the First and Second Laws.

Structural Damping of a Simple Built-Up Beam With Riveted Joints in Bending[1]

By T. H. H. PIAN,[2] CAMBRIDGE, MASS.

A theoretical study is made of the structural damping in the bending of a simple built-up beam with thin reinforcing spar caps in which the rivets or screws prevent the sliding motion between the cap and the beam. An analytical expression of the energy loss per cycle of static loading is derived in terms of amplitude of load, stiffness of rivets, and tightness of joint. Experimental measurements on a test beam provide a qualitative verification of the theory.

Nomenclature

The following nomenclature is used in the paper:

A = cross-sectional area of one spar cap
A_n = amplitude of vibration of tip mass at nth cycle
a = length of spar cap
b = length of spar cap along which sliding motion between cap and beam occurs
e = elongation of outer fiber of beam without caps
E = modulus of elasticity
F = shear force at end of beam
$(\Delta F)_{max}$ = amplitude of alternating shear load
h = depth of beam
I = moment of inertia of beam without caps
I_{total} = moment of inertia of beam including caps
K = stiffness of beam, load per unit tip deflection
k = distributed shear load per unit length required for unit displacement of continuous joint
M = bending moment on beam without caps
Q = static moment with respect to neutral axis of spar-cap cross section
q = distributed shear force between cap and beam
q_M = limiting friction force per unit length between cap and beam
r = relative displacement between cap and beam
s = shear load in continuous joint per unit length
ΔW = energy loss
x = distance along beam
x_n = amplitude of nth cycle of vibration as shown by oscillograph record
σ = normal stress in spar cap
$\lambda = 2I/Ah^2$
$\mu = [2EI/kh^2(1+\lambda)]^{1/2}$
$\phi = F/q_M h$
$\Delta\delta$ = additional deflection at tip of built-up beam due to sliding motion between caps and beam

Introduction

In a previous paper,[3] the author made a theoretical study of the bending of a simple built-up beam with its reinforcing spar caps fastened by screws. This analysis assumes that the spar caps and the beam are held together by pressures which depend upon the tightness of the screw joints and that the screws in the holes have sufficient lateral clearance so as not to hinder any sliding motion between the cap and the beam. Thus, whenever the shear force between the two surfaces has reached the limiting friction force, a sliding motion begins, and the shear force is redistributed. The load-deflection relation and the energy loss per cycle of static loading were then determined. It was found that the nonlinear component of the load-deflection curve contains mainly a second-power term and that the energy loss per cycle varies approximately as the third power of the amplitude of vibration.

The same paper also describes an experimental investigation of the structural damping in built-up cantilever beams with spliced joints. It is shown that for a beam with screw joints the experimental results check quite favorably with the analytical solution. The present paper describes an extension of the theoretical analysis to the case where the sliding motion between the cap and the beam is prevented by the tight fit of the screws or rivets.

Theoretical Analysis

Bending of a Riveted Built-Up Beam. The problem to be considered here is that of a cantilever beam with reinforcing spar caps, shown in Fig. 1, subjected to a vertical shear load F at the free end. The reinforcing cap is attached to the beam by rivets or by tightly fitted screws. The sliding motion between the cap and the beam is resisted by friction forces which depend upon the pressure between the two surfaces, the smoothness of the two surfaces, and the elastic forces associated with the shear

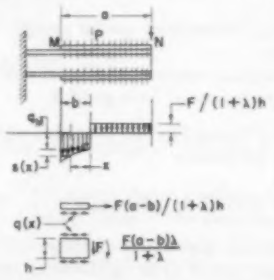

Fig. 1 Cantilever Beam With Reinforcing Spar Caps

---

[1] The results presented in this paper were obtained in the course of research sponsored by the Office of Naval Research, under Contract N5-ori-07833, with Massachusetts Institute of Technology.

[2] Assistant Professor of Aeronautical Engineering, Massachusetts Institute of Technology.

Contributed by the Applied Mechanics Division and presented at the Annual Meeting, New York, N. Y., November 25–30, 1956, of The American Society of Mechanical Engineers.

Discussion of this paper should be addressed to the Secretary, ASME, 29 West 39th Street, New York, N. Y., and will be accepted until April 10, 1957, for publication at a later date. Discussion received after the closing date will be returned.

Note: Statements and opinions advanced in papers are to be understood as individual expressions of their authors and not those of the Society. Manuscript received by ASME Applied Mechanics Division, March 20, 1956. Paper No. 56—A-2.

[3] "Structural Damping in a Simple Built-Up Beam," by T. H. H. Pian and F. C. Hallowell, Jr., Proceedings of the First U. S National Congress of Applied Mechanics, ASME, 1952, pp. 97–102.

rigidity of the rivets. To simplify the analysis, it is assumed that the rivets are so closely spaced that they can be replaced by a continuous shear joint. The shear deformation of the rivets varies linearly with the shearing force applied.

The beam is assumed to be very slender so that the transverse shear deformation can be neglected. It is further assumed that the thickness of the caps is small in comparison to the depth of the beam so that the moment of inertia of the laminated section can be expressed by

$$I_{\text{total}} = I + Ah^2/2 \quad [1]$$

where

I = moment of inertia of beam without caps
A = cross-sectional area of one cap
h = depth of beam

Following the reasoning given in the author's previous paper,[3] it is concluded that, for the given beam subjected to a shear force F at the end, the shear-force distribution along the plane MN between the cap and the beam may be divided into two regions (see Fig. 1). In the region between M and P the distributed shear force is negative and there is a sliding motion between the two surfaces. Beyond this region no sliding motion occurs, and the shear distribution is the same as that of a solid beam.

The distributed shear force in the region PN can be determined by the elementary theory

$$q = FQ/I_{\text{total}} \quad [2]$$

where Q is the static moment with respect to the neutral axis of the cross section of the spar cap. This is reduced to

$$q = F/(1 + \lambda)h \quad [3]$$

where

$$\lambda = 2I/Ah^2 \quad [4]$$

The distributed shear force in the region MP can be expressed by

$$q(x) = q_M + s(x) \quad [5]$$

where

q_M = limiting friction force per unit length between cap and beam
$s(x)$ = shear load in continuous joint per unit length
x = distance measured from point P

By considering the equilibrium condition of the segment MP of the spar cap, one obtains

$$F(a - b)/(1 + \lambda)h = q_M b + \int_0^b s(x)dx \quad [6]$$

In the present case, the relative displacement between the spar cap and the beam $r(x)$ is equal to the shear deformation of the joint at the point x. If k is the spring constant, defined by the distributed shear load per unit length required for a unit displacement, one obtains

$$r(x) = s(x)/k \quad [7]$$

The unknown function $s(x)$ can be determined by the condition of consistency of deformation.

The elongation of the outer fiber for the length x of the beam can be written as

$$e(x) = \int_0^x (Mh/2EI)dx \quad [8]$$

where M is the bending moment on the beam without caps and is given by

$$M = F(a - b)\lambda/(1 + \lambda) + Fx + q_M hx + h\int_0^x s(x)dx \quad [9]$$

The corresponding elongation of the spar cap is

$$e(x) = (1/E)\int_0^x \sigma(x)dx \quad [10]$$

where $\sigma(x)$ is the normal stress in the spar cap and is given by

$$\sigma(x) = \frac{1}{A}\left[\frac{F(a - b)}{(1 + \lambda)h} - q_M x - \int_0^x s(x)dx\right] \quad [11]$$

The introduction of the condition that the elongation of the outer fiber is equal to the sum of the elongation of the spar cap and the joint deformation, obtained from Equations [7] to [11] yields

$$\frac{h}{2EI}\left\{[F + q_M h(1 + \lambda)]\frac{x^2}{2} + h(1 + \lambda)\int_0^x\int_0^x s(x)dx\,dx\right\} = \frac{s(x)}{k} \quad [12]$$

Differentiating Equation [12] twice produces the following equivalent differential equation

$$\frac{d^2s}{dx^2} - \frac{kh^2(1 + \lambda)}{2EI}s = \frac{kh}{2EI}[F + q_M h(1 + \lambda)] \quad [13]$$

with the boundary conditions that

$$\text{at } x = 0, \quad s = ds/dx = 0 \quad [14]$$

The solution of Equation [13] is

$$s(x) = q_M[1 + \phi/(1 + \lambda)]\,[\cosh(x/\mu) - 1] \quad [15]$$

where

$$\mu = \left[\frac{2EI}{kh^2[1 + \lambda)}\right]^{1/2} \quad [16]$$

$$\phi = F/q_M h \quad [17]$$

The substitution of Equations [15] into [6] and solution for b, the region where the sliding motion occurs, gives

$$b = \mu \sinh^{-1}[\phi a/(1 + \lambda + \phi)\mu] \quad [18]$$

In studying the damping characteristics of a built-up beam, it is necessary to determine the load-deflection characteristics of the beam. Here, the additional deflections which result from the sliding motion between the cap and the beam are investigated. The only difference in the stress distribution between the solid and the built-up beam is the difference in the bending-moment distribution within the segment MP. The additional moment at x of the built-up beam is

$$\left.\begin{aligned}\Delta M(x) &= [q_M + F/(1 + \lambda)h]\,hx + h\int_0^x s(x)dx \\ &= q_M h[(1 + \lambda + \phi)/(1 + \lambda)]\,\mu \sinh(x/\mu)\end{aligned}\right\} \quad [19]$$

Hence, the additional deflection at the tip of the built-up beam is

$$\Delta\delta = \frac{1}{EI}\left[(a - b)\int_0^b \Delta M\,dx + \int_0^b\int_0^b \Delta M\,dx\,dx\right] \quad [20]$$

Substitution of the expressions for b and ΔM from Equations [18] and [19] gives

$$\Delta\delta = \frac{q_M h(1+\lambda+\phi)\mu^2}{EI(1+\lambda)}\left\{a\left[\left(\left[\frac{\phi a}{(1+\lambda+\phi)\mu}\right]^2+1\right)^{1/2} - \frac{1+\lambda+2\phi}{1+\lambda+\phi}\right] + \mu\sinh^{-1}\frac{\phi a}{(1+\lambda+\phi)\mu}\right\} \quad [21]$$

It should be remarked that the load-deflection relation just derived is limited to the case when there is no residual stress in the structure. During a process of cyclic loading, residual stress exists in the beam and a different load-deflection relation will hold. The effect of decreasing the load after a maximum load F_{max} has been reached, is to superimpose upon the shear distribution at the maximum-load condition a shear distribution resulting from a negative shear force. When the spar cap starts to slide from the left end the friction force is in the opposite direction. This shear distribution to be superimposed must be of the same form shown in Fig. 1, except that the limiting shear force is $2q_M$ instead of q_M. Therefore, after the reproducible state has been reached in cyclic loading, the additional beam deflection resulting from the slippage of the joint can be expressed again by Equation [21] except that ϕ is now defined by

$$\phi = (\Delta F)_{max}/2q_M h \quad [22]$$

where $(\Delta F)_{max}$ is the amplitude of the alternating shear load.

It also can be seen that for a very large value of μ, i.e., for the case where the rivets offer very little resistance, Equation [21] becomes

$$\Delta\delta = \frac{(\Delta F)_{max}a^2\phi}{6EI(1+\lambda)(1+\lambda+\phi)^2}[3(1+\lambda)+2\phi] \quad [23]$$

This equation is equivalent to Equation [7] of the previous paper.[3]

Energy Loss per Cycle of Static Loading. The energy loss per cycle of static loading is equal to the area of the hysteresis loop of the load-deflection curve. This area is the same as the area of ΔF versus $\Delta\delta$ curve, shown in Fig. 2. In this figure, the

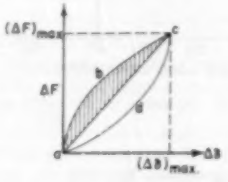

FIG. 2 HYSTERESIS LOOP

curve *a-b-c* is represented by Equation [21]. The energy loss per cycle of static loading is equal to the area enclosed by the curve *a-b-c-d-a*, which is equal to twice the shaded area shown in Fig. 2. It can be expressed as

$$\Delta W/\text{cycle} = (\Delta F)_{max}(\Delta\delta)_{max} - 2\int_0^{(\Delta F)_{max}}(\Delta\delta)d(\Delta F) \quad [24]$$

By introducing the expression for $\Delta\delta$ in Equation [21] and by substituting

$$(\Delta F)_{max} = 2q_M h\phi$$

one obtains

$$\Delta W/\text{cycle} = \frac{4q_M^2h^2\mu^2(1+\lambda+\phi)}{EI}\left[\frac{\phi a}{(1+\lambda+\phi)\mu} - \sinh^{-1}\frac{\phi a}{(1+\lambda+\phi)\mu}\right] \quad [25]$$

It can be seen that for small values of ϕ/μ, the expression

$$\phi a/(1+\lambda+\phi)\mu - \sinh^{-1}\phi a/(1+\lambda+\phi)\mu$$

approaches

$$\frac{1}{6}[\phi a/(1+\lambda+\phi)\mu]^3$$

and Equation [25] reduces to

$$\Delta W/\text{cycle} = \frac{(\Delta F)^3_{max}a^2}{12EI\,q_M h(1+\lambda+\phi)^2} \quad [26]$$

This indicates that, if the rivets of the built-up beam are very flexible and the amplitude of vibration is not too large, the energy loss per cycle varies approximately as the third power of the load amplitude and is roughly inversely proportional to the tightness of the joint.

For large values of ϕ/μ, $\sinh^{-1}\phi a/[(1+\lambda+\phi)\mu]$ is small compared with $\phi a/[(1+\lambda+\phi)\mu]$, and Equation [25] then becomes

$$\Delta W/\text{cycle} = 2(\Delta F)_{max}q_M h\mu^2 a/EI \quad [27]$$

This shows that, if the rivets are somewhat flexible to very stiff and the amplitude of vibration is very large, the energy loss per cycle becomes proportional to both the load amplitude and the tightness of the joint.

EXPERIMENTAL INVESTIGATION

Description of Tests. To verify the foregoing theory, an experimental investigation of the effects of amplitude of load and

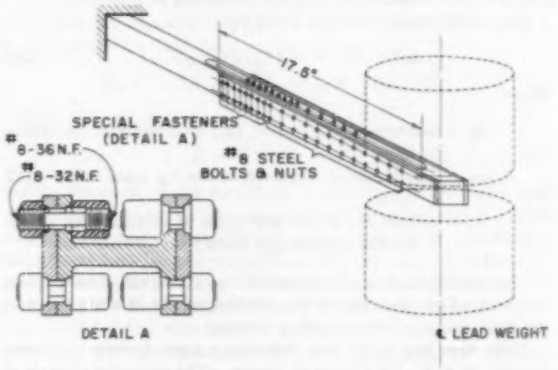

FIG. 3 EXPERIMENTAL TEST SETUP

of joint tightness on the energy loss in cyclic loading was carried out with a simple built-up beam. The test beam was made of steel and had a cantilever support, Fig. 3. The cross section of the major part of the beam was I-shaped and reinforced on both sides by spar caps which were fastened with screws. It was expected that the sliding motion would occur in the first 4 in. from the inboard end of the reinforcing caps, and special fasteners shown in Detail A of Fig. 3 were used in this region. The special fastener consisted of a long screw which had enough flexibility to permit sliding motion between the cover plate and the beam. The spar caps and beam were joined together with the screws, and the nuts were then fastened tightly so that any sliding motion between spar caps and beam would cause bending of the screws. The screw joint is used here in place of a rivet connection because there is no way to control the tightness and flexibility of rivets.

The stiffness of the individual fasteners was determined by using a pair of sliding blocks which were held together by a single fastener. A shear force was applied to the sliding block, and the relation between the shear displacement and the applied force was determined. It was found that the stiffness of each screw varied between 16,700 and 12,500 lb per in. with an average of 15,000 lb per in. for various tightnesses of the screws. An equivalent joint of continuous properties would have a stiffness k of 60,000 lb/in/in.

The limiting friction between the beam and the plate is a function of the tightness of the fastener which is determined from the torque applied to the screws. Lap-joint specimens with a different number of screws and different tightnesses were tested by a tensile testing machine under controlled strain rate. It was found that the limiting sliding friction is directly proportional to the torque applied to the screws and approximately proportional to the number of screws per unit length. By referring to an equivalent joint of continuous properties, the limiting friction q_M was given by

$$q_M(\text{in-lb/in.}) = 20 \times (\text{tightness of screw measured in torque of in-lb})$$

The structural damping, in terms of the loss of energy per cycle of vibration, was measured by the rate of decay of free vibration.

A 60-lb lead mass was bolted to the free end of the beam. The beam was deflected to one side by string and then released by cutting the string. The decay of the beam was obtained from readings from a pair of electric strain gages mounted on the opposite sides of the beam close to the root. The readings were recorded on Consolidated dynamic recording equipment.

The energy loss per cycle is given by

$$\Delta W/\text{cycle} = KA^3_{n+1/2} l_a(x_n/x_{n+1}) \ldots\ldots\ldots [28]$$

where

K = stiffness of the beam; i.e., load per unit tip deflection

$A_{n+1/2}$ = amplitude of vibration of the tip mass at $n + 1/2$ cycle

x_n = amplitude of the nth cycle of vibration as shown by the oscillograph record

The amplitude $A_{n+1/2}$ is related to $x_{n+1/2}$ through a calibration constant which depends on the location of the strain gages and the attenuation of the recording system.

Tests were run under four different values of screw tightness; namely, 2, 4, 6, and 8 in-lb of torque. The equivalent values of limiting sliding friction q_M, are 40, 80, 120, and 160 lb per in., respectively.

Results of Tests and Comparison With Theoretical Analysis. The results of the experimental investigation are presented by log-log plots of the energy loss per cycle against the double amplitude of the load at the end of the beam for four values of screw tightness, Fig. 4. For small amplitudes of vibration the energy loss is approximately proportional to the third power of the stress amplitude, while for larger amplitudes of vibration it is proportional to a lower power of the stress amplitude. Fig. 4 also presents the theoretical solutions obtained from Equation [25] for comparison. This figure shows that the experimental

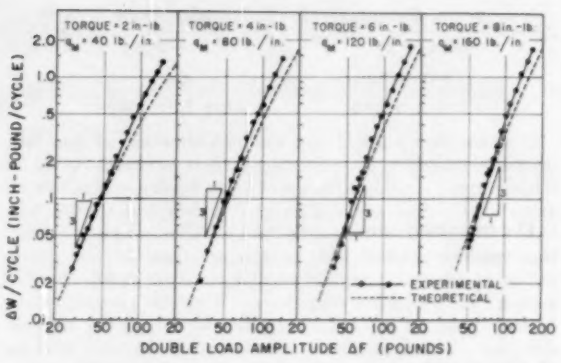

FIG. 4 VARIATION OF ENERGY LOSS IN VIBRATING BUILT-UP BEAMS

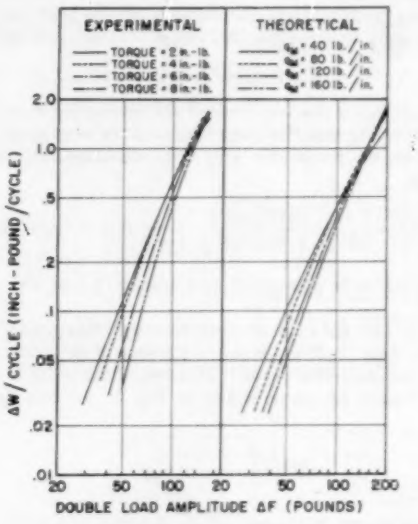

FIG. 5 DAMPING IN BUILT-UP BEAMS

results are in qualitative agreement with the theoretical solution. In all cases, the agreement between the two curves is fair at the lower amplitude region while the deviation becomes large at higher amplitudes.

The effect of the screw tightness on the structural damping is shown by redrawing the test curves so as to produce the single plot of Fig. 5. This figure reveals that for low-amplitude vibration, the energy loss is higher with lower screw tightness, while at high amplitudes the effect of screw tightness on the energy loss becomes less important. In fact, at very high amplitudes the energy loss tends to become lower for lower screw tightness. This phenomenon has been predicted already by the theoretical analysis. The experimental and theoretical curves are plotted side by side in Fig. 5 for comparison. The similarity of the two families of curves affords a qualitative proof of the foregoing theory.

Vibration Modes of Stators of Induction Motors

By E. ERDELYI,[1] ERIE, PA., and G. HORVAY,[2] SCHENECTADY, N. Y.

The increased emphasis placed on the design of "noiseless" machinery has led to the requirements of better evaluation of the magnetic attractive forces developed between rotor and stator of induction motors, better evaluation of stator response to such forces, and better evaluation of the sound waves radiated by the vibrating stator frame. This paper treats the crucial phase of the problem, determining the vibration characteristics of two concentric shells (stator core inside the stator frame) coupled by nonrigid ribs. The vibration theory of such coupled structures is developed and the theoretical results are compared with the experimental measurements obtained for a 30-hp, 3-phase, induction motor. The agreement is within 7 per cent. Parts 1 and 3 of the problem, determination of the airgap force waves and of the sound radiated, are discussed in separate papers.

1 Geometry of the Stator

THE stator of an induction motor is illustrated schematically in Fig. 1. It consists essentially of a rather thin outer frame (the "outer ring") approximately cylindrical in shape, mounted on supports. A cylindrical inner core (the "inner ring") is connected to the outer shell by ribs. This core is made up of steel laminations parallel to the plane of the paper, in order to reduce the effect of eddy currents. Outside the long-dashed circle the core may be regarded as a homogeneous body, fully contributing to the structural strength (rigidity) of the ring. The stator teeth and windings, inside the dashed circle, contribute to the weight (inertia) but not to the strength of the ring.

The stator for which the tests discussed in Section 5 were carried out was that of a

30-hp, 4-pole, 440-volt, 1780-rpm, 38-amp, 40 C temperature rise..... [1]

medium induction motor. Numerical values given here and elsewhere refer to this "experimental motor."[3] Inner ring (i), outer ring (o), supports (s), ribs (r) have the following lengths L in the z-direction (into the plane of the paper)

$$L_i = 5.75, \quad L_o \cong L_s = 10.4, \quad L_r = 5.2 \ldots\ldots [2a]$$

The dimensions

$$R = 7.89, \quad r = 6.2 \ldots\ldots [2b]$$

denote the radii of the structural center lines of the outer and inner rings. Although the structure of the outer ring is rather irregular because of openings for access and better ventilation, end shields with bearing supports at the two ends for rotor support, and departure from circular cross section for structural purposes, it will be regarded nevertheless as a uniform, thin-walled, cylindrical structure. The same approximation also has been made for the inner ring. For this component the approximation is, of course, less drastic. The "structural" widths of outer ring, inner ring, upper and lower ribs of the motor to be used in the strain energy expressions are

$$h_o = 0.31, \quad h_i = 1.1, \quad h_r = 0.9 \ldots\ldots [3]$$

The "inertial" widths to be used in the kinetic-energy expressions are

$$\tilde{h}_o = 0.31, \quad \tilde{h}_i = 1.1, \quad \tilde{h}_r = 0.75 \ldots\ldots [4]$$

These widths enter the formulas of moment of inertia and cross-section area

$$I_r = h_r^3 L_r/12, \quad A_r = h_r L_r, \quad \tilde{A}_r = \tilde{h}_r L_r, \text{ etc.} \ldots\ldots [5]$$

of the various components. If greater accuracy is desired, distinction also may be made between an effective h to be used in the area formula and an effective h to be used in the moment-of-inertia formula. However, such refinements will not be considered in this paper.

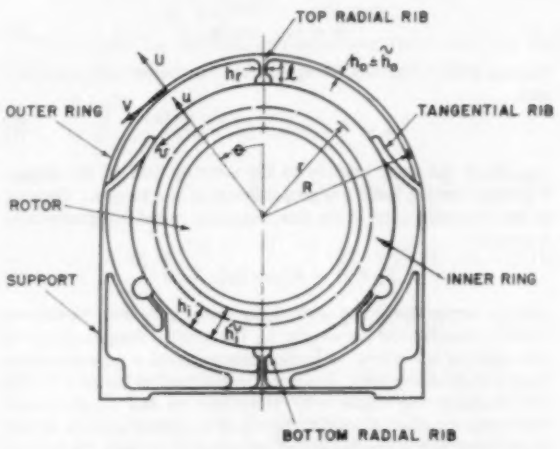

Fig. 1 Illustration of Experimental Motor

---

[1] Advance Engineering, Direct-Current Motor and Generator Department, General Electric Company.

[2] Metallurgy and Ceramics Research Department, Research Laboratory, General Electric Company. Mem. ASME.

[3] Mechanical quantities are given in inch, pound, second units unless otherwise indicated. Frequencies are given in cps (symbol f) or rad/sec (symbol ω or Ω).

Contributed by the Applied Mechanics Division and presented at the Annual Meeting, New York, N. Y., November 25–30, 1956, of The American Society of Mechanical Engineers.

Discussion of this paper should be addressed to the Secretary, ASME, 29 West 39th Street, New York, N. Y., and will be accepted until April 10, 1957, for publication at a later date. Discussion received after the closing date will be returned.

Note: Statements and opinions advanced in papers are to be understood as individual expressions of their authors and not those of the Society. Manuscript received by ASME Applied Mechanics Division, December 13, 1955. Paper No. 56—A-28.

Inside the inner ring, supported by bearings at $z = -L_s/2, +L_s/2$ is the squirrel-cage rotor.[4] Its outline is indicated by the innermost circle in Fig. 1.

When a balanced, 3-phase supply is connected to the windings of the stator, a rotating magnetic flux is created in the air gap. This flux induces voltages in the rotor bars. The interaction of the currents caused by these voltages with the magnetic flux in the airgap manifests itself as a tangential force. The angular speed (rps) of the rotation is given by

$$n = (1 - s)f/p \quad \ldots\ldots [6]$$

where f is the frequency (60 cps), p the number of pole pairs (1),[5] and

$$s = 1 - n/n_s, \quad (n_s = f/p) \quad \ldots\ldots [7]$$

the slip of the rotor relative to the rotating field in the airgap. For small torque loads s is proportional to the torque. Because of the nonuniformity of the flux, rotating, radial, magnetic-force waves (1)

$$F_k(\theta, t) = F_k \cos(\omega_k t - k\theta) \quad \ldots\ldots [8]$$

develop across the airgap and set the stator core into vibrations. Here F_k denotes the amplitude, ω_k the angular frequency of the kth mode of the wave. θ is the distance from a reference cross section (the stator top), measured in mechanical radians.[6] The ribs transmit the stator core vibrations to the stator frame. The latter attenuates most of the sound pressures emitted by the stator core, but generates sound pressures of its own. The noise experienced in the surroundings of the motor originates largely from these stator-frame vibrations.

Analytical and experimental methods of determining the sound waves sent out from the vibrating stator frame are described in (2), and the methods used for calculating the airgap force, Equation [8], and the various schemes used for diminishing its intensity are described in (1). A comprehensive description of past and present theoretical and experimental approaches is contained in (3). In this paper we shall be concerned only with the central phase of the problem, determination of the stator response to the given exciting force, $F_k(\theta, t)$.[7]

2 Strain Energy of the System

The problem of motor-frame vibrations caused by rotating airgap force waves attracted attention of motor designers as much as 40 years ago. It was soon recognized that the proper slot combination bears critically on noiseless operation. The paper by M. Krondl (4) represents a particularly enlightening early effort in the field of noise abatement. The modern approach to the problem was pioneered by P. L. Alger (5), who showed that reasonable qualitative results may be obtained by considering the stator core as a thin-walled cylinder of infinite length, excited by the airgap force waves in small-amplitude inextensional ring modes (i.e., two-dimensional modes, independent of z). These vibrations, in turn, cause radiation of sound. Jordan (6), in Germany, proceeded along similar lines.

Clearly, disregard of the motor frame to which the inner core is coupled implies a crude approximation. Vigorous noise-elimination programs more recently instituted have rendered mandatory a re-examination of the vibration analysis of stator frame and core.

Using the notation of Fig. 1, and still assuming small-amplitude vibrations (linearized system) and z-independence (two-dimensional modes), we may write the radial and tangential displacements of inner and outer rings (represented by their center lines) in the form

$$\left.\begin{aligned} u(\theta, t) &= \sum_2^\infty u_m(\theta, t) \\ &= \sum_2^\infty [a_m(t) \cos m\theta + b_m(t) \sin m\theta] \\ v(\theta, t) &= \sum_2^\infty [c_m(t) \cos m\theta + d_m(t) \sin m\theta] \\ U(\theta, t) &= \sum_2^\infty [A_m(t) \cos m\theta + B_m(t) \sin m\theta] \\ V(\theta, t) &= \sum_2^\infty [C_m(t) \cos m\theta + D_m(t) \sin m\theta] \end{aligned}\right\} \quad \ldots [9]$$

The calculations are simplified considerably if the assumption of inextensional deformations is made

$$dv/d\theta = -u, \quad dV/d\theta = -U \quad \ldots\ldots [10a]$$

i.e.

$$c_m = b_m/m, \quad d_m = -a_m/m, \quad C_m = B_m/m, \quad D_m = -A_m/m \quad \ldots\ldots [10b]$$

Since the adequacy of the results is not impaired, the foregoing assumption will be used. Then, during a deformation, the inner and outer rings acquire the strain energies (7)[8]

$$\mathfrak{U}_i = \frac{1}{2} \int_{-\pi}^{\pi} \frac{E_i I_i}{(1 - \nu_i^2) r^3} \left(\frac{d^2 u}{d\theta^2} - u \right)^2 d\theta = \frac{\pi}{2} \frac{E_i I_i}{(1 - \nu_i^2) r^3} \Sigma (1 - m^2)^2 (a_m^2 + b_m^2) \quad \ldots\ldots [11a]$$

$$\mathfrak{U}_o = \frac{\pi}{2} \frac{E_o I_o}{(1 - \nu_o^2) R^3} \Sigma (1 - m^2)^2 (A_m^2 + B_m^2) \quad \ldots [11b]$$

$$\left.\begin{aligned} \frac{\pi}{2} \frac{E_i I_i}{(1 - \nu_i^2) r^3} &= 1.25 \times 10^6 \\ \frac{\pi}{2} \frac{E_o I_o}{(1 - \nu_o^2) R^3} &= 3.34 \times 10^6 \end{aligned}\right\} \quad \ldots\ldots [12]$$

The supports of the motor frame are fastened to the foundation by means of bolting. The bolts provide relatively loose attachment (slight rigidity), and the support strain energy may be ignored in first approximation (8). For other motors different methods of support may be contemplated, and for this reason the Appendix discusses some of the extensions to be made in the theory when support strain energy is not negligible. The outer ring is joined to the inner rings by two radial and four tangential ribs. In first approximation the tangential ribs do not contribute restraint (strain energy). Of vital importance, however, are the strain energies of the top and bottom ribs, as these are the

[4] Co-ordinate z is measured from the rotor mid-plane.

[5] Numbers in parentheses refer to the Bibliography at the end of the paper.

[6] The circumference of the stator comprises 2π mechanical radians, $2\pi p$ electrical radians.

[7] The authors are greatly indebted to Dr. R. Plunkett of the General Engineering Laboratory of the General Electric Company for stimulating discussions about the various aspects of the problem.

[8] The accuracy of the analysis may be improved by regarding I_i, I_o under the integral signs as variables in θ. Such a refinement will not be considered here. In Equations [12] $E_i = 30 \times 10^6$, $\nu_i = 0.3$, $E_o = 16 \times 10^6$, $\nu_o = 0.3$ denote Young's modulus and Poisson ratio of inner and outer rings; the moments of inertia are $I_i = 5.73$, $I_o = 0.592$.

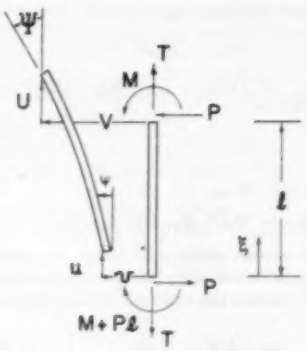

FIG. 2 DEFORMATION OF A RADIAL RIB UNDER ACTIONS OF T, P, M

elements which provide the coupling between inner and outer shells. By Fig. 2 a moment M, shear force P, and tensile force T cause a tip rotation, deflection, and extension of a rib with respect to the base

$$\left.\begin{aligned} \Psi - \psi &= \frac{Ml}{D_r} + \frac{Pl^2}{2D_r} \\ V - v &= l\psi + \frac{Ml^2}{2D_r} + \frac{Pl^3}{3D_r} \\ U - u &= Tl/EA_r \end{aligned}\right\} \quad \ldots\ldots\ldots [13]$$

$$D_r = EI_r/(1-\nu_r^2) = 3.8 \times 10^6,\ EA_r = 34.5 \times 10^6,\ l = 0.75 \quad \ldots\ldots [14]$$

The assumption of small deflections makes it possible to ignore, as is customary, the interaction between bending and stretching. On noting the relations converse to Equations [13]

$$\left.\begin{aligned} M &= \frac{D_r}{l}\left[-6\,\frac{V-v}{l} + 4\Psi + 2\psi\right] \\ Pl &= \frac{D_r}{l}\left[\,12\,\frac{V-v}{l} - 6\Psi - 6\psi\right] \\ T &= \frac{EA_r}{l}\,[U-u] \end{aligned}\right\} \quad \ldots\ldots [15]$$

we find that the strain energy of the rib may be written as

$$\begin{aligned} \mathfrak{U}_{rib} &= \frac{1}{2D_r}\int_0^l [M + P(l-\xi)]^2\,d\xi + \frac{1}{2EA_r}\int_0^l T^2\,d\xi \\ &= \frac{l}{2D_r}\left[M^2 + MPl + \frac{P^2l^2}{3}\right] + \frac{l}{2EA_r}\,T^2 \\ &= \frac{6D_r}{l}\left[\left(\frac{V-v}{l}\right)^2 - \frac{V-v}{l}\,(\Psi+\psi) + \frac{\Psi^2+\psi^2+\Psi\psi}{3}\right] \\ &\quad + \frac{EA_r}{2l}\,(U-u)^2 \quad \ldots\ldots [16] \end{aligned}$$

where

$$\left.\begin{aligned} \Psi &= -dU/Rd\theta \\ &= R^{-1}\sum_2^\infty m(A_m \sin m\theta - B_m \cos m\theta) \\ \psi &= -du/rd\theta = r^{-1}\sum_2^\infty m(a_m \sin m\theta - b_m \cos m\theta) \end{aligned}\right\} \quad \ldots [17]$$

Expression [16] is to be formed for both the upper rib (introduce Equations [9], [10], [17] into [16]), using $\theta = 0$, and for the lower rib (introduce Equations [9], [10], [17] into [16]), using $\theta = \pi$. The sum of the two expressions will be labelled $\mathfrak{U}_{ribs}$. In contrast to the very simple Expressions [11], where no cross products $a_m a_n$, $a_m b_n$, $a_m A_n$ etc., occur, $\mathfrak{U}_{ribs}$ will contain, with the exception of products between even and odd terms, all types of cross products.

3 EQUATIONS OF MOTION

The formulas for the inner and outer-ring kinetic energies are (10)

$$\mathfrak{K}_i = \frac{w_i}{2g}\int_{-\pi}^{\pi} (\dot{u}^2 + \dot{v}^2)\,d\theta = \frac{\pi w_i}{2g}\sum_m \frac{m^2+1}{m^2}\,(\dot{a}_m^2 + \dot{b}_m^2) \quad \ldots\ldots [18a]$$

$$\mathfrak{K}_o = \frac{\pi w_o}{2g}\sum_m \frac{m^2+1}{m^2}\,(\dot{A}_m^2 + \dot{B}_m^2) \quad \ldots\ldots [18b]$$

$$\frac{\pi w_i}{2g} = 7.78 \times 10^{-3},\quad \frac{\pi w_o}{2g} = 6.15 \times 10^{-3} \quad \ldots [19a, b]$$

In the foregoing expressions w denotes the weight per radian of the rings, and g the gravitational acceleration. The kinetic energy of the support and ribs is incorporated in the numerical Expression [19b]. The mass distribution around the periphery is assumed to be constant. A somewhat more accurate approach is outlined in the Appendix. The Lagrangian equations of motion of the system are now given by

$$\frac{d}{dt}\,\frac{\partial \mathfrak{K}}{\partial \dot{a}_m} - \frac{\partial \mathfrak{U}}{\partial a_m} = \frac{\partial \mathfrak{W}}{\partial a_m},$$

$$\frac{d}{dt}\,\frac{\partial \mathfrak{K}}{\partial \dot{b}_m} - \frac{\partial \mathfrak{U}}{\partial b_m} = \frac{\partial \mathfrak{W}}{\partial b_m} \quad \ldots\ldots [20a, b]$$

$$\frac{d}{dt}\,\frac{\partial \mathfrak{K}}{\partial \dot{A}_m} - \frac{\partial \mathfrak{U}}{\partial A_m} = 0,\quad \frac{d}{dt}\,\frac{\partial \mathfrak{K}}{\partial \dot{B}_m} - \frac{\partial \mathfrak{U}}{\partial B_m} = 0 \quad \ldots [20c, d]$$

$$m = 2, 3, \ldots$$

where $\mathfrak{U} = \mathfrak{U}_i + \mathfrak{U}_o + \mathfrak{U}_{ribs},\quad \mathfrak{K} = \mathfrak{K}_i + \mathfrak{K}_o \quad \ldots\ldots [21]$

are the total strain energy and kinetic energy of the system, respectively, and $\mathfrak{W}$ denotes the force potential

$$\mathfrak{W} = \sum_m \int_{-\pi}^{\pi} F_k(\theta, t)u_m(\theta, t)\,d\theta = \pi F_k a_k \cos \omega_k t + \pi F_k b_k \sin \omega_k t \quad \ldots\ldots [22]$$

The forces

$$\left.\begin{aligned} F_{ak}\cos\omega_k t &\equiv \partial\mathfrak{W}/\partial a_k = \pi F_k \cos\omega_k t \\ F_{bk}\sin\omega_k t &\equiv \partial\mathfrak{W}/\partial b_k = \pi F_k \sin\omega_k t \end{aligned}\right\} \quad \ldots\ldots [23]$$

are the generalized forces representing airgap excitation. They are discussed in greater detail in (3). As an example, the $m = 4$ Equation [20b] assumes the form

$$\begin{aligned} &M_4 b_4 + K_{42}a_2 + K_{44}b_2 + K_{46}A_2 + K_{48}B_2 \\ &\quad + K_{4,10}a_4 + K_{4,12}b_4 + K_{4,14}A_4 + K_{4,16}B_4 + K_{4,18}a_4 + \ldots \\ &\quad = \begin{cases} F_k \sin\omega_k t & \text{for } k = m \\ 0 & \text{for } k \neq m \end{cases} \quad \ldots\ldots [24] \end{aligned}$$

where M_4, K_{42}, K_{44}, . . . are certain constants of the system. It may be noted that the matrix of the equation system is symmetric; $K_{mn} = K_{nm}$, etc.

4 Natural Modes of Vibration

The forced response of the system can be calculated best by prior solution of the problem of natural modes. This is done most conveniently by the Rayleigh-Ritz method. Placing the right-hand sides in Equations [20] equal zero, regarding $a_m(t)$, $b_m(t)$ of Equations [9] as sinusoidally varying quantities

$$a_m(t) = a_m \sin \Omega t, \quad b_m(t) = b_m \sin \Omega t \ldots\ldots\ldots [25]$$

of amplitudes a_m, b_m, etc., and replacing, correspondingly, $\ddot{a}_m^2$ in Equations [18] by $-\Omega^2 a_m^2$, $(d/dt)\partial\mathfrak{K}/\partial\dot{a}_m$ by $-\Omega^2\partial\mathfrak{K}/\partial a_m$, etc., a determinantal equation may be obtained

$$\mathfrak{D}_{even}(\Omega^2) = \begin{vmatrix} K_{22} - M_2\Omega^2 & K_{24} & & \\ K_{42} & K_{44} - M_4\Omega^2 & & \\ & & \cdot & \\ & & & \cdot \end{vmatrix} = 0 \ldots [26a]$$

for the even modes, and a similar equation

$$\mathfrak{D}_{odd}(\Omega^2) = \begin{vmatrix} K_{33} - M_3\Omega^2 & K_{35} & & \\ K_{53} & K_{55} - M_5\Omega^2 & & \\ & & \cdot & \\ & & & \cdot \end{vmatrix} = 0 \ldots . [26b]$$

for the odd modes. Here

$$K_{22} - M_2\Omega^2, \; K_{24}, \; K_{26}, \; K_{28}, \; K_{2,10}, \ldots$$

represent the a_2a_2, a_2b_2, a_2A_2, a_2B_2, a_2a_4, . . . elements of $\mathfrak{D}_{even}$. The literal expressions of the elements are exceedingly cumbersome; as an illustration the expressions for a few of the elements are given

$$\left.\begin{aligned} K_{22} &= \frac{9\pi}{r^3}\frac{E_i I_i}{1-\nu_i^2} + \frac{2EA_r}{l}, \quad M_2 = \frac{5}{4}\frac{\pi w_i}{g} \\ K_{24} &= K_{42} = 0, \quad K_{26} = K_{62} = -\frac{2EA_r}{l} \\ K_{44} &= K_{66} = -\frac{6D_r}{l^2} - \frac{12D_r}{l^2R} + \frac{12D_r}{l^2r} + \frac{16D_r}{lRr} \end{aligned}\right\} . [26c]$$

TABLE 1(a) NATURAL FREQUENCIES (CPS) AND EIGENVECTORS OF EVEN MODES

$f_{theor.}$	Mode	a_2	b_2	A_2	B_2	a_4	b_4	A_4	B_4	a_6	b_6	A_6	B_6	$f_{exper.}$
460	X_{21c}	1.0000	-.2630	1.0634	-.2239	.0115	-.0005	-.0387	.0221	.0020	.0001	-.0043	-.0010	468 482
490	X_{21s}	.2138	1.0000	0.2161	.7504	.0015	.0015	.0017	-.0017	+.0003	-.0003	-.0013	-.0094	473
10,430	X_{2cc}	-.7981	-.0000	1.0000	.0002	-1.0160	-.0000	1.2136	-.0005	-1.7438	+.0000	1.4399	.0009	-
1,140	X_{2cs}	.0631	-.6024	-.0402	1.0000	-.0103	.0100	.0820	.5480	.0016	.0058	.0042	.0763	1,220
2,560	X_{41c}	-.3079	-.0015	.3775	.0005	1.0000	.0009	+.8155	.0138	.0546	-.0001	-.2889	.0334	
2,940	X_{41s}?	.0000	.0087	.0003	-.0167	-.0005	1.0000	-.0004	-.0304	.0000	-.0002	-.0003	.0251	
1,295	X_{4cc}	.6236	.0479	-.7139	-.1006	-.1471	-.0013	1.0000	.0258	-.0225	-.0006	.0953	.0154	
2,060	X_{4cs}?	.0057	-.1863	.0156	.3167	-.0616	.0326	.0061	1.0000	-.0006	-.0054	.0065	-.0884	
6,240	X_{61c}	-.2080	+.0000	.2607	.0003	-.3113	-.0000	.3303	-.0056	1.0000	-.0000	.5506	.0015	
6,980	X_{61s}	.0000	-.0038	+.0000	.0057	.0000	.0003	-.0000	.0039	.0000	1.0000	.0000	.0044	
3,660	X_{6cc}	.1652	.0008	-.2088	-.0000	.5637	.0006	-.3175	-.0633	-.0747	+.0001	1.0000	-.0153	
4,240	X_{6cs}	.0020	-.0322	.0006	.0637	.0047	-.0166	-.0078	.0535	-.0014	-.0414	.0093	1.0000	

TABLE 1(b) NATURAL FREQUENCIES (CPS) AND EIGENVECTORS OF ODD MODES

$f_{theor.}$	Mode	a_3	b_3	A_3	B_3	a_5	b_5	A_5	B_5	a_7	b_7	A_7	B_7	$f_{exper.}$
1,170	X_{31c}	1.0000	-.1201	1.2740	-.3940	.0372	.0013	-.1302	+.0325	.0088	.0045	-.0437	.0118	1080 1156
1,580	X_{31s}	.1145	.2653	.1969	1.0000	.0062	.0034	.0314	.1016	.0015	.0028	.0043	-.0257	1540
8,200	X_{3cc}	.8074	.0000	1.0000	-.0017	-1.2502	-.0000	1.1779	.0020	2.3523	.0000	2.0114	-.0036	--
1,225	X_{3cs}	.0097	1.0000	.0058	-.3280	-.0001	.0040	.0046	.0965	.0000	.0021	-.0010	.0230	1240
3,950	X_{51c}	-.4732	.0003	.5236	.0047	1.0000	-.0006	1.0978	-.0118	.0908	-.0000	-.5339	-.0485	
4,750	X_{51s}	+.0000	-.0025	-.0000	.0050	.0001	1.0000	.0001	.0003	-.0000	-.0015	.0001	.0020	
2,240	X_{5cc}	.7774	-.0033	.6602	.0215	-.1291	.0001	1.0000	.0152	-.0265	-.0001	.1257	-.0039	
2,940	X_{5cs}	-.0057	-.0429	.0096	.1071	.0027	-.0007	-.0040	1.0000	.0005	.0006	-.0055	-.0446	
5,200	X_{71c}	+.1335	-.0002	-.1515	-.0024	.7691	-.0001	-.2466	.0053	.0557	-.0001	1.0000	.1660	
9,780	X_{71s}	-.0000	-.0010	-.0000	.0037	-.0000	.0014	+.0000	.0004	-.0000	1.0000	-.0000	.0034	
11,650	X_{7cc}	.3001	-.0000	-.3751	.0003	.3774	+.0000	-.4207	-.0002	1.0000	+.0000	-.5271	.0003	
5,580	X_{7cs}	-.0018	-.0114	.0011	.0314	-.0058	-.0017	.0053	.0395	.0010	-.0028	-.0091	1.0000	

Restricting each system to 12 equations each (i.e., neglecting a_8, b_8, A_8, B_8, a_9, . . .), the following natural frequencies f_m, even modes

$$X_m = [a_2, b_2, A_2, B_2, a_4, b_4, A_4, B_4, a_6, b_6, A_6, B_6]_{\{m\}} \quad [27a]$$

and odd modes

$$X_m = [a_3, b_3, A_3, B_3, a_5, b_5, A_5, B_5, a_7, b_7, A_7, B_7]_{\{m\}} \quad [27b]$$

are obtained for the experimental motor.

The extreme left column in Table 1 shows the theoretically obtained frequencies, the extreme right column the experimentally obtained frequencies. It will be noted that there are four second modes (four possibilities for two full waves in 360 deg)

$$\{m\} = 2_{ic}, 2_{is}, 2_{cc}, 2_{cs}$$

four third modes (four possibilities for three full waves in 360 deg) $\{m\} = 3_{ic}, 3_{is}, 3_{cc}, 3_{cs}$

and so on, corresponding to whether $\theta = 0$ is an antinode ("cosine mode"), or a node ("sine mode"), and whether inner and outer rings move in unison ("in-tact," i.e., in phase), or oppositely ("counter-tact," i.e., in antiphase).[9] The privileged position of the vertical axis is due to the deviation of the shell structures from precise circularity, but almost precise retention of the vertical axis of symmetry. (The slight departure from symmetry, as occasioned by various openings in the frame, explains the occurrence of two measured natural modes of the same shape, as illustrated by the two frequencies f_{2ic}, etc.) The comparison for the even modes in Table 2 indicates that for the fundamental modes, 8-row or even 4-row determinants provide ample accuracy. Similar results hold for odd modes.

TABLE 2 COMPARISON OF NATURAL FREQUENCIES

Determinant	f_{2ic}	f_{2is}	f_{2cc}	f_{2cs}
4 × 4	464	500	5140	1123
8 × 8	461	492	6870	1164
12 × 12	460	490	10430	1140

Once the natural modes X_m of the System [24] are known, the forced response X to excitation by the generalized force

$$F_{bk} \sin \omega_b t = [0, 0, 0, 0, 0, \ldots, 0, \pi F_k, 0, \ldots]_{\substack{a_2\ b_2 A_2 B_2 a_4 \quad a_k \quad b_k A_k}} \sin \omega_b t \quad [28]$$

may be written explicitly as [see Reference (9)[10]]

$$X = \Im\left\{\left\langle \frac{F_{bk}}{M_k\omega_b^2} \frac{X_2}{|X_2|^2}\right\rangle \frac{X_{2c}e^{i\omega_b t}}{(\Omega_2/\omega_b)^2 - 1 + ic_2\Omega_2/\omega_b} + \left\langle \frac{F_{bk}}{M_k\omega_b^2} \frac{X_4}{|X_4|^2}\right\rangle \frac{x_4 e^{i\omega_b t}}{(\Omega_4/\omega_b)^2 - 1 + ic_4\Omega_4/\omega_4} + \ldots\right\} \quad [29]$$

[9] In some instances the abridged subscripts $\{2\}$, $\{4\}$, $\{6\}$, $\{8\}$, $\{10\}, \ldots, \{3\}, \ldots$ or just $\{m\}$ are used in place of 2_{ic}, 2_{is}, 2_{cc}, 2_{cs}, 4_{ic}, . . . , 3_{ic}, . . . to indicate the various modes. In other cases, where there can be no confusion, as in Equation [29], the braces around m are omitted altogether.

[10] $\Im$ = imaginary part of. For the sake of generality the damping constants of the various modes were also here included in Equation [29]. They may be ignored, except at resonance. Response to the force $F_{ak}\cos\omega_a t$ involves, similarly, the real part of the brace in Equation [29], with F_{ak} replacing F_{bk}.

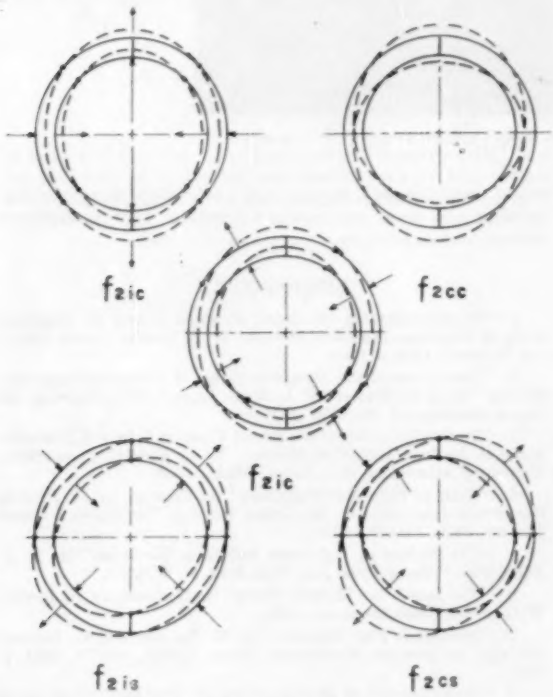

FIG. 3 TWO-WAVE MODES

(Dashed-line curves represent theoretical results. For simplicity, higher harmonic ripples of modes are not shown. Arrows indicate observed locations of maximum amplitudes, dots indicate observed locations of nodes. f_{2ic} = 460 [theoretical], 468 cps [experimental]; f_{2is} = 490 cps [theoretical], 473 [experimental]; f_{2cc} = 10,430 [theoretical], not found experimentally; f_{2cs} = 1140 cps [theoretical], 1220 [experimental]. A second in-tact cosine mode, f_{2ic} = 482 [experimental], illustrated in center diagram also was measured.)

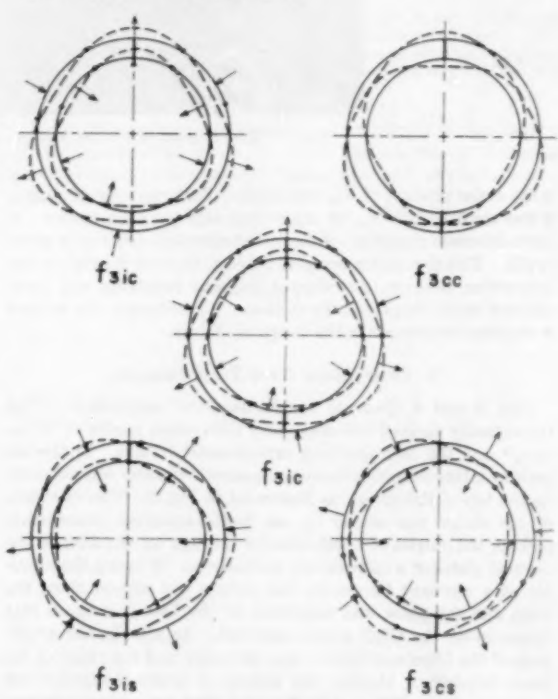

FIG. 4 THREE-WAVE MODES

(Dashed-line curves represent theoretical results. For simplicity, higher harmonic ripples of modes are not shown. Arrows indicate observed locations of maximum amplitudes, dots indicate observed location of nodes. f_{3ic} = 1170 cps [theoretical], 1080 cps [experimental]; f_{3is} = 1225 [theoretical], 1240 [experimental]; f_{3cc} = 8200 [theoretical], not found experimentally; f_{3cs} = 1580 [theoretical], 1540 [experimental]. A second in-tact cosine mode, f_{3ic} = 1156 [experimental] illustrated in the center diagram also was measured.)

where Ω_m are the natural frequencies

$$\Omega_{2ic}(=2\pi f_{2ic}),\ \Omega_{2is},\ \Omega_{2sc},\ \Omega_{2ss},\ \Omega_{4ic}\ldots$$

X_m the corresponding modes, and c_m the corresponding damping constants. $< F_{kk}, X_m >$ denotes the scalar product of the forcing function with the m^{th} natural mode

$$< F_{kk}, X_m > = \pi F_k b_{k\{m\}} \ldots\ldots\ldots\ldots [30a]$$

(subscript $\{m\}$ indicates that the Fourier coefficient b_k belongs to mode m) and

$$|X_m|^2 = (a_2^2 + b_2^2 + A_4^2 + B_2^2 + a_4^2 + \ldots)_{\{m\}} \quad [30b]$$

is the scalar product of X_m with itself. For simplicity of writing it was assumed that $F_{kk} \sin \omega_k t$ excites only the even modes. A more elaborate discussion of the forced-vibration response is given in (3). This is a rather complex subject, because it involves the interaction between complicated exciting functions and complicated mode shapes of the system. Nevertheless, the subject is of prime importance in the design of motors.

5 Comparison With Test Results

Figs. 3 and 4 illustrate the fundamental component of the theoretically derived two-wave and three-wave modes of vibration,[11] and the corresponding experimental results. In the experimental investigation an electromagnetic vibrator was mounted on the top of the motor, as illustrated in Fig. 5. The vibration of the stator was sensed by an inertia-operated piezoelectric pickup, the output of which was fed through an amplifier to the vertical plates of a cathode-ray oscilloscope. Keeping the vibrator at a resonant frequency, the pickup was moved along the rings and the phase and amplitude of the Lissajous figure that appeared on the CRO screen observed. At a node, the amplitude of the Lissajous figure was a minimum and the phase of the trace indefinite. Moving the pickup, a phase change became apparent, depending on the direction that the pickup has been moved. The amplitude of the Lissajous figure increased steadily until the position of maximum displacement was reached. This procedure was continued until the whole stator had been sensed. The arrows in Figs. 3 and 4 indicate the location of the experimentally observed amplitudes and the dots indicate the experimentally located nodes.

The instrumentation for the determination of the natural frequencies and the location of amplitudes and nodes may be regarded as reliable in the frequency range of 400 cps to 2000 cps. Because of departure from circular symmetry of the shells there is some deviation between the theoretical and experimental node and amplitude locations. While the tests have not duplicated all theoretical nodes, in particular the cosine countertact modes f_{2sc}, f_{3sc}, f_{4sc} were not observable, and higher than third modes were not looked for, the agreement between theoretical prediction and experimental observation of natural frequencies and node and antinode locations may nevertheless be deemed as satisfactory.

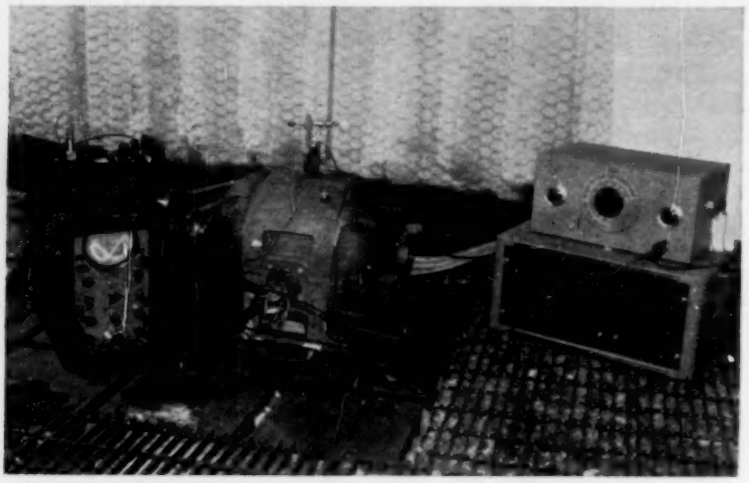

Fig. 5 Excitation of Stator Frame and Core by Electromagnetic Vibrator

[11] The higher harmonic components add small ripples to the mode shapes, without changing their character.

BIBLIOGRAPHY

1 "Predetermination of Sound Pressure Levels of Magnetic Noise of Polyphase Induction Motors," by E. Erdelyi, Trans. AIEE, vol. 74, part 3, 1955, p. 1269.

2 "Calculation of the Magnetic Noise of Polyphase Induction Motors," by E. Erdelyi and P. L. Alger, *Journal of the Acoustical Society of America*, vol. 28, 1956, p. 1063.

3 "Predetermination of the Sound Pressure Levels of Magnetic Noise in Medium Induction Motors," by E. Erdelyi, dissertation, University Microfilms, Ann Arbor, Mich., 1955.

4 "Noise of Electrical Machinery" (in French), by M. Krondl, Conférence Internationale des Grand Réseaux Electriques à Haute Tension, Paris, France, 1933.

5 "The Nature of Polyphase Induction Machines," by P. L. Alger, John Wiley & Sons, Inc., New York, N. Y., 1951.

6 "The Low Noise Electric Motor" (in German), by H. Jordan, W. Girardet, Essen, Germany, 1950.

7 "Stresses in Pipe Bundles," by H. Poritsky and G. Horvay, Journal of Applied Mechanics, Trans. ASME, vol. 73, 1951, p. 241.

8 "Measurement of Mobility," by R. Plunkett, Journal of Applied Mechanics, Trans. ASME, vol. 76, 1954, p. 250.

9 "Solution of Large Equation Systems and Eigenvalue Problems by Lanczos' Matrix Method," by G. Horvay, Office of Technical Service, U. S. Government Printing Office, Washington, D. C., 1953, Report KAPL-1004.

10 "Vibration Problems in Engineering," by S. Timoshenko, D. Van Nostrand Company, Inc., New York, N. Y., 1947.

Appendix

Rigid Body Modes

If the attachment of the stator to the foundation is very rigid (support springs K_x, K_y in Fig. 6*a* are stiff), the rigid body modes x, y, α, Fig. 6(*b*), representing horizontal displacement of stator center of gravity, vertical displacement, pitching about center of gravity, cannot be ignored. It may be assumed for generality that the rotor center C, the stator frame center of gravity G, and the spring center of the supports S no longer coincide.

The displacements U, V must now be modified to

$$\left.\begin{aligned} \bar{U}(\theta) &= U + x\sin\theta - y\cos\theta + \alpha\eta\sin\theta \\ \bar{V}(\theta) &= V - x\cos\theta + y\sin\theta \\ &\quad + \alpha R[1 + (\eta/R)\cos\theta] \end{aligned}\right\} \ldots [31]$$

and similar expressions hold also for $\bar{u}$ and $\bar{v}$. (The last terms of $\bar{U}$, $\bar{V}$ are the displacements caused by pitching, as illustrated in Fig. 6*b*.)

The kinetic energy of the frame is now modified to

$$\mathcal{K}_s = \frac{w_0}{2g}\int_{-\pi}^{\pi}(\dot{\bar{U}}^2 + \dot{\bar{V}}^2)d\theta \ldots\ldots\ldots\ldots [32]$$

and similar alterations are performed in other expressions. The spring energy of the supports

$$\begin{aligned} \mathcal{U}_{sup} = \frac{1}{2}K_x[\{-\bar{U}(-\gamma)\sin\gamma + \bar{V}(-\gamma)\cos\gamma\}^2 \\ + \{-\bar{U}(\gamma)\sin\gamma - \bar{V}(\gamma)\cos\gamma\}^2] \\ + \frac{1}{2}K_y[\{\bar{U}(-\gamma)\cos\gamma + \bar{V}(-\gamma)\sin\gamma\}^2 \\ + \{-\bar{U}(\gamma)\cos\gamma - \bar{V}(\gamma)\sin\gamma\}^2] \ldots\ldots [33] \end{aligned}$$

is to be added to the other strain-energy Expressions [21], and the equations of motion are now formed not only with respect to a_2, b_2, A_2, B_2, a_3, . . . , but also with respect to x, y, α.

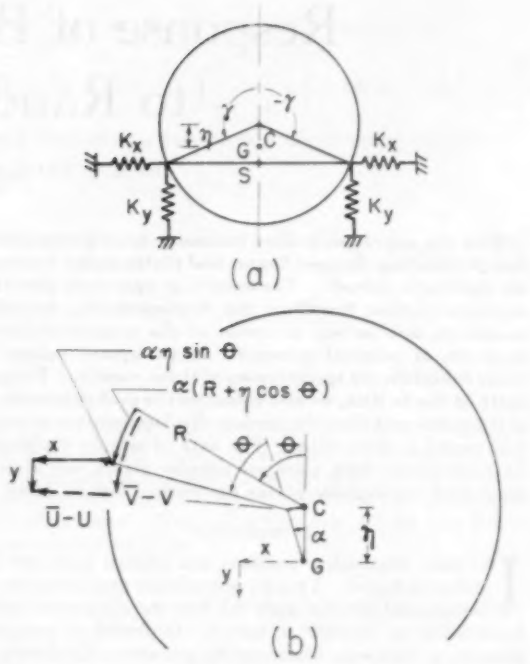

Fig. 6 Case When Rotor Center C, Stator Frame Center of Gravity G, and Spring Center S Do Not Coincide

(Diagram *a* illustrates support springs K_x, K_y; diagram *b* illustrates displacements caused by pitching α, horizontal center of gravity motion x, and vertical center of gravity motion y.)

Since this study was directed mainly at proper understanding of the experimental motor for which the analysis of the main text was found to be adequate, no use was made of the foregoing refinements.

Response of Beams and Plates to Random Loads

By A. C. ERINGEN,[1] LAFAYETTE, IND.

With the use of generalized harmonic analysis the problem of vibrating damped beams and plates under stochastic loading is solved. The resulting equations give the cross-correlation functions for displacements, stresses, moments, and so on, in terms of the cross-correlation function of external pressure. Mean square values of these functions are special cases of these results. Using a method due to Rice, we also calculate the probable number of times per unit time the random displacements or stresses will exceed a given value. The case of simply supported bars, cantilever bars, clamped circular plates, and simply supported rectangular plates are worked out in detail.

Introduction

In many engineering problems the external loads are not definitely known. Thus all deterministic analyses based on well-defined external loads fall into the category of being hypothetical or academic in nature. In almost all instances, however, we have some idea about the probability distribution of external loads, or at least we can calculate the cross-correlation functions of the loads from the data based on experimental measurement over a long period of time. Having only these correlation functions, we ask the question: Is it possible to determine the cross-correlation functions, hence the mean square values of the displacements or stresses? The present paper is aimed at providing a partial answer to this question.

The methods of statistical mechanics have long provided very successful results in kinetic theory, thermodynamics, theory of homogeneous turbulence, random walk, random flight, noise, and the theory of Brownian motion. In the literature we already find the work of Van Lear and Uhlenbeck (1)[2] which treats the Brownian motion of strings and cantilever beams. Earlier, Ornstein (2) and Houdijk (3) treated the same problems. For systems having a single degree of freedom we have the Langevin solution and for a discrete system such as coupled harmonic oscillators Wang and Uhlenbeck (4) give historical developments in an excellent paper. Reference (5) contains (4) and important articles in stochastic processes and noise theory such as those of Chandrasekhar, S. O. Rice, and others. More recently we find articles by Liepmann (6), Press and Houboldt (7) which take up the buffeting problem and gust loads which are one of the headaches of the aircraft industry.

In what follows we apply the generalized Fourier analysis developed by Wiener (8) to the problem of vibrating bars and plates under stochastic loads. We are thus able to calculate cross-correlation functions, the mean square values of the displacement, and the stresses.

We also have the method of Rice (9) available to predict the probable number of times per unit time; the random function (for example, displacement or stress) will exceed a given value. The solution of these problems and the method presented, we believe, will throw some light on this very important problem.

Formal Solution

Consider a beam or a plate which is subjected to a known transverse-force distribution, random in time. The beam or plate is of classical type. Let us select the origin of pressure $p(x, t)$ for a beam or $p(x, y, t)$ for a plate so that it has zero time average

$$< p(x, y, t) > = 0 \quad [1]$$

where $< >$ represents the time average of pressure, defined by

$$< p > = \lim_{T \to \infty} \frac{1}{2T} \int_{-T}^{T} p(x, y, t)dt \quad [2]$$

From the statistical calculation made on experimental data one knows the cross-correlation function of pressure. In stationary random processes this is independent of the origin of time. Moreover the dependence on the time interval is very small when the interval is large.[3] Hence we may assume that the cross correlation of pressure is given by

$$<p(x, y, t + \tau)p(\xi, \eta, t) > = d(x, y, \xi, \eta)\delta(\tau) \quad [3]$$

where $\delta(\tau)$ is the Dirac delta function. Later we shall consider special forms for d.

The differential equation of classical damped linear plate theory is

$$\nabla^4 u + \frac{\partial^2 u}{\partial t^2} + 2\beta \frac{\partial u}{\partial t} = p(x, y, t) \quad [4]$$

Here u is the transverse displacement; x, y, rectangular coordinates; t, β, p reduced time, damping coefficient, and the transverse pressure which are related to corresponding actual time t_0, damping coefficient β_0, and pressure p_0 by

$$\left.\begin{aligned} t &= (gD/\rho)^{1/2} t_0, \quad \beta = \frac{1}{2}\,\beta_0 (g/\rho D)^{1/2} \\ p &= p_0/D, \qquad\quad D = Eh^3/12(1 - \nu^2) \end{aligned}\right\} \quad [5]$$

where E is Young's modulus, h is the thickness, ρ is the weight density per unit area, g is the acceleration of gravity. Equation [4] reduces to the beam equation if one takes EI for D and $y = \partial/\partial y = 0$. In this case ρ and p_0 must be interpreted as the weight density and the load per unit length, respectively.

In the following analysis, beam and plate problems are treated

[1] Professor, Division of Engineering Sciences, Purdue University.

[2] Numbers in parentheses refer to the Bibliography at the end of the paper.

Contributed by the Applied Mechanics Division and presented at the Annual Meeting, New York, N. Y., November 25–30, 1956, of The American Society of Mechanical Engineers.

Discussion of this paper should be addressed to the Secretary, ASME, 29 West 39th Street, New York, N. Y., and will be accepted until April 10, 1957, for publication at a later date. Discussion received after the closing date will be returned.

Note: Statements and opinions advanced in papers are to be understood as individual expressions of their authors and not those of the Society. Manuscript received by ASME Applied Mechanics Division, May 2, 1956. Paper No. 56—A-5.

[3] There exist problems in which pressure correlation of the Form [3] is not acceptable. However, often approximation in this form is possible. White noise, Brownian motion, more generally all perfectly random processes are included in [3].

as one. For specific cases resulting formulas are explicitly given.

We formally try a solution for Equation [4] of the type

$$u = \frac{1}{2\pi}\int_{-\infty}^{\infty} U(x, y, \zeta)e^{i\zeta t}d\zeta \quad \ldots\ldots [6]$$

Substitution of Equation [6] into [4] gives

$$\nabla^4 U - (\zeta^2 - 2i\beta\zeta)U = P(x, y, \zeta) \quad \ldots\ldots [7]$$

In Equation [4] we used the Fourier integral representation of $p(x, y, t)$

$$p(x, y, t) = \frac{1}{2\pi}\int_{-\infty}^{\infty} P(x, y, \zeta)e^{i\zeta t}d\zeta \quad \ldots\ldots [8]$$

The solution of Equation [7] under appropriate, time-independent boundary conditions has the form

$$U = \sum_{m,n} a_{mn}(\zeta)V_{mn}(x, y) \quad \ldots\ldots [9]$$

where a_{mn} are arbitrary and the eigenfunctions $V_{mn}(x, y)$ are free of arbitrary constants and satisfy all boundary conditions and the differential equation

$$\nabla^4 V_{mn} - \lambda^4_{mn} V_{mn} = 0 \quad \ldots\ldots [10]$$

where λ_{mn} are the eigenvalues and are determined from a frequency equation which will be known when the boundary conditions are given explicitly. The eigenfunction expansion for P is

$$P(x, y, \zeta) = \sum_{m,n} Q_{mn}(\zeta)V_{mn}(x, y) \quad \ldots\ldots [11]$$

If we now use Equations [9] to [11] in [7] we obtain

$$a_{mn} = \frac{Q_{mn}(\zeta)}{\lambda_{mn}^4 - \zeta^2 + 2i\beta\zeta} \quad \ldots\ldots [12]$$

Thus the solution of Equation [7] now reads

$$U(x, y, \zeta) = \sum_{m,n} \frac{Q_{mn}(\zeta)V_{mn}(x, y)}{\lambda_{mn}^4 - \zeta^2 + 2i\beta\zeta} \quad \ldots\ldots [13]$$

This is formal, since the stochastic pressure does not lend itself to a series expansion. However, we make these results rigorous with the help of generalized harmonic analysis.

Generalized Harmonic Analysis

Let us, for the moment, assume that the records of u and p are cut off outside $t = -T$ and $t = T$; that is, they are zero outside this interval. The inverse Fourier transform of Equations [6] and [8] now reads

$$U_T(x, y, \zeta) = \int_{-T}^{T} u(x, y, t)e^{-i\zeta t}dt \quad \ldots\ldots [14]$$

$$P_T(x, y, \zeta) = \int_{-T}^{T} p(x, y, t)e^{-i\zeta t}dt \quad \ldots\ldots [15]$$

where subscript T indicates that u and p are zero outside of the interval $(-T, T)$. We now define power spectrums $\widetilde{PP}$ and $\widetilde{UU}$ and the cross-correlation function $<pp>$ and $<uu>$ of pressure and displacements by

$$\left.\begin{aligned} \widetilde{PP} &= \lim_{T\to\infty}\frac{1}{2\pi T} P_T(x, y, \zeta)P_T(\xi, \eta, -\zeta) \\ <pp> &= \lim_{T\to\infty}\frac{1}{2T}\int_{-T}^{T} p(x, y, t+\tau)p(\xi, \eta, t)dt \end{aligned}\right\} \quad \ldots [16]$$

$$\left.\begin{aligned} \widetilde{UU} &= \lim_{T\to\infty}\frac{1}{2\pi T} U_T(x, y, \zeta)U_T(\xi, \eta, -\zeta) \\ <uu> &= \lim_{T\to\infty}\frac{1}{2T}\int_{-T}^{T} u(x, y, t+\tau)u(\xi, \eta, t)dt \end{aligned}\right\} \quad \ldots [17]$$

From Parseval's theorem we have the reciprocal relations

$$\widetilde{PP} = \frac{1}{\pi}\int_{-\infty}^{\infty} <pp>\, e^{-i\zeta\tau}d\tau, \quad <pp> = \frac{1}{2}\int_{-\infty}^{\infty} \widetilde{PP}\, e^{i\zeta\tau}d\zeta \quad \ldots\ldots [18]$$

$$\widetilde{UU} = \frac{1}{\pi}\int_{-\infty}^{\infty} <uu>\, e^{-i\zeta\tau}d\tau, \quad <uu> = \frac{1}{2}\int_{-\infty}^{\infty} \widetilde{UU}\, e^{i\zeta\tau}d\zeta \quad \ldots\ldots [19]$$

If we now assume that the previous analysis up to Equation [13] was made with the data on u and p taken zero outside $(-T, T)$, we can use the generalized harmonic analysis to calculate the cross-correlation function of displacements in terms of power spectrum of pressures. Substituting Equation [13] into the first of Equations [17] we obtain

$$\widetilde{UU} = \sum_{mnrs} \frac{V_{mn}(x, y)V_{rs}(\xi, \eta)\widetilde{Q_{mn}Q_{rs}}(\zeta)}{(\lambda_{mn}^4 - \zeta^2 + 2i\beta\zeta)(\lambda_{rs}^4 - \zeta^2 - 2i\beta\zeta)} \quad \ldots [20]$$

where

$$\widetilde{Q_{mn}Q_{rs}}(\zeta) = \lim_{T\to\infty}\frac{1}{2\pi T} Q_{mnT}(\zeta)Q_{rsT}(-\zeta) \quad \ldots\ldots [21]$$

The second of Equations [19] now gives the cross-correlation function $<uu>$ for displacements, which is all we can calculate with the information available.

Evaluation of $\widetilde{Q_{mn}Q_{rs}}(\zeta)$

Fortunately in most physical problems eigenfunctions $V_{mn}(x, y)$ are orthogonal; i.e.

$$\int_A V_{mn}(x, y)V_{rs}(x, y)dA = \begin{bmatrix} b_{mn} \text{ for } r = m,\ n = s \\ 0 \text{ for } r \neq m \text{ or } n \neq s \end{bmatrix} \quad \ldots [22]$$

where the integral is taken over the total area of the plate (total length of the beam). Thus, multiplying both sides of Equation [11] by $V_{rs}(x, y)$ and integrating over the area A, we obtain

$$Q_{mn}(\zeta) = \frac{1}{b_{mn}}\int_A P(x, y, \zeta)V_{mn}(x, y)dA \quad \ldots\ldots [23]$$

If we use P_T instead of P in this equation, we obtain $Q_{mnT}(\zeta)$.

Upon substitution of Q_{mnT} so calculated into Equation [21] and using the first of Equations [16] we get

$$\widetilde{Q_{mn}Q_{rs}} = \frac{1}{b_{mn}b_{rs}}\int_A\int_A \widetilde{PP}\, V_{mn}(x, y)V_{rs}(\xi, \eta)\, dA(x, y)dA(\xi, \eta) \quad \ldots\ldots [24]$$

This shows that we need to calculate $\widetilde{PP}$. To this end we use Equation [3] which means

$$<pp> = d(x, y, \xi, \eta)\delta(\tau) \quad \ldots\ldots [25]$$

The first of Equations [18] now gives

$$\widetilde{PP} = \frac{1}{\pi}\, d(x, y, \xi, \eta) \quad \ldots\ldots\ldots\ldots\ldots [26]$$

Equation [24] now gives $\widetilde{Q_{ms}Q_{rs}}$

$$\widetilde{Q_{ms}Q_{rs}} = \frac{1}{\pi b_{ms} b_{rs}} \int_A \int_A d(x, y, \xi, \eta)$$
$$V_{ms}(x, y) V_{rs}(\xi, \eta) dA(x, y) dA(\xi, \eta) \quad \ldots\ldots [27]$$

We notice that $\widetilde{Q_{ms}Q_{rs}}$ is independent of ζ. Therefore $\widetilde{UU}$, given by Equation [20], when substituted into the second of Equations [19] can be integrated with respect to ζ by means of contour integration. For the case of $\tau \geq 0$, we select the half circle with center at O in the upper half of the ζ-plane, and the real axis as our contour. Of the four poles, the two, namely

$$\zeta = i\beta \pm (\lambda_{ms}^4 - \beta^2)^{1/4}$$

are located on the upper half plane. The integral vanishes on the semicircular arc as the radius of the arc tends to ∞. Hence our integral is equal to $2\pi i$ times the sum of the residues in the upper half plane.

$$\langle uu \rangle = \frac{1}{2} \sum_{mnrs} T_{mnrs} V_{ms}(x, y) V_{rs}(\xi, \eta) \widetilde{Q_{ms}Q_{rs}} \ldots [28]$$

where T_{mnrs} is the Fourier transform of $\widetilde{UU}$ with respect to ζ which is obtained by the contour integration described

$$T_{mnrs} = \frac{2\pi}{\omega_{ms}}\, e^{-\beta\tau}$$
$$\left[\frac{(\lambda_{rs}^4 - \lambda_{ms}^4 + 4\beta^2) \sin \omega_{ms}\tau + 4\beta\omega_{ms} \cos \omega_{ms}\tau}{(\lambda_{rs}^4 - \lambda_{ms}^4 + 4\beta^2)^2 + (4\beta\omega_{ms})^2}\right] \ldots\ldots [29]$$
$$\omega_{ms} = (\lambda_{ms}^4 - \beta^2)^{1/4}, \quad \tau \geq 0.$$

The value of T_{mnrs} for $\tau < 0$ is obtained by carrying out the contour integration in the lower half plane. The result follows from Equation [29] by taking $-\tau$ for τ and interchanging λ_{rs} and λ_{ms}.

For $\lambda_{ms}^4 \leq \beta^2$ the procedure is similar and the expression for T_{mnrs} contains hyperbolic functions for $\lambda_{ms}^4 < \beta^2$ and τ for $\lambda_{ms}^4 = \beta^2$. However, for higher modes of vibrations the frequencies will be large enough making $\lambda_{ms}^4 > \beta^2$ for sufficiently large m and n. Here we consider the interesting case in which β is small enough making $\lambda_{ms}^4 > \beta^2$ for all m and n.

Any further computation requires the explicit form of $d(x, y, \xi, \eta)$. Two special cases of practical importance are given

$$\left.\begin{aligned} d &= d_1 \delta(x - \xi)\delta(y - \eta) \\ d &= d_2 \delta(x - a)\delta(\xi - a)\delta(y - b)\delta(\eta - b) \end{aligned}\right\} \ldots [30]$$

Here d_i are constants and δ represents the delta function. Substitution of Equations [30] into [27], respectively, gives

$$\left.\begin{aligned} \widetilde{Q_{ms}Q_{rs}} &= d_1/\pi b_{ms} \\ \widetilde{Q_{ms}Q_{rs}} &= (d_2/\pi b_{ms} b_{rs}) V_{ms}(a, b) V_{rs}(a, b) \end{aligned}\right\} \ldots [31]$$

In each case, all other components of $\widetilde{Q_{ms}Q_{rs}}$ not given above are zero. The first of Equations [30] represents a stochastic load which has infinite correlation at $x = \xi$, $y = \eta$ while the second is a concentrated load at the point (a, b). Further special cases are possible.

Correlation of Stresses and Bending Moments

The maximum flexural stresses are given by

$$\left.\begin{aligned} \sigma_x &= 6M_x/h^2, \quad \sigma_y = 6M_y/h^2 \\ \tau_{xz} &= 3Q_x/2h, \quad \tau_{yz} = 3Q_y/2h \end{aligned}\right\} \ldots\ldots [32]$$

where M_x, M_y are the bending moments and Q_x, Q_y are the transverse shearing forces. In the classical theory these are given by

$$\left.\begin{aligned} M_x &= -D\left(\frac{\partial^2 u}{\partial x^2} + \nu \frac{\partial^2 u}{\partial y^2}\right), \qquad M_y = -D\left(\frac{\partial^2 u}{\partial y^2} + \nu \frac{\partial^2 u}{\partial x^2}\right) \\ Q_x &= -D \frac{\partial}{\partial x}\left(\frac{\partial^2 u}{\partial x^2} + \nu \frac{\partial^2 u}{\partial y^2}\right), \qquad Q_y = -D \frac{\partial}{\partial y}\left(\frac{\partial^2 u}{\partial y^2} + \nu \frac{\partial^2 u}{\partial x^2}\right) \end{aligned}\right\} \ldots [33]$$

Calculation of power spectrums $\widetilde{M_xM_x}$, $\widetilde{M_xQ_y}$, etc., ... are sufficient to obtain power spectrums $\widetilde{\sigma_x\sigma_x}$, $\widetilde{\sigma_x\tau_{yz}}$, ..., since, for example, they are given by equations of the form

$$\widetilde{\sigma_x\sigma_x} = 36\widetilde{M_xM_x}/h^4, \quad \widetilde{\sigma_x\tau_{yz}} = 9\widetilde{M_xQ_y}/h^3 \ldots\ldots [34]$$

where

$$\widetilde{M_xM_x} = D^2 \sum_{mnrs} \widetilde{Q_{ms}Q_{rs}} \left(\frac{\partial^2 V_{ms}}{\partial x^2} + \nu \frac{\partial^2 V_{ms}}{\partial y^2}\right) \times \left(\frac{\partial^2 V_{rs}}{\partial \xi^2} + \nu \frac{\partial^2 V_{rs}}{\partial \eta^2}\right) (\lambda_{ms}^4 - \zeta^2 + 2i\beta\zeta)^{-1} \times (\lambda_{rs}^4 - \zeta^2 - 2i\beta\zeta)^{-1}$$

$$\widetilde{M_xQ_y} = D^2 \sum_{mnrs} \widetilde{Q_{ms}Q_{rs}} \left(\frac{\partial^2 V_{ms}}{\partial x^2} + \nu \frac{\partial^2 V_{ms}}{\partial y^2}\right) \times \left(\frac{\partial^2 V_{rs}}{\partial \eta^2} + \nu \frac{\partial^2 V_{rs}}{\partial \xi^2 \partial \eta}\right) (\lambda_{ms}^4 - \zeta^2 + 2i\beta\zeta)^{-1} \times (\lambda_{rs}^4 - \zeta^2 - 2i\beta\zeta)^{-1} \ldots\ldots [35]$$

The cross-correlation functions $\langle M_xM_x \rangle$, $\langle M_xQ_y \rangle$, . . . are obtained by taking one half the Fourier transforms of $\widetilde{M_xM_x}$, $\widetilde{M_xQ_y}$, . . . with respect to ζ. These correlation functions are given by equations of the form

$$\left.\begin{aligned} \langle M_xM_x \rangle &= \frac{1}{2} D^2 \sum_{mnrs} T_{mnrs} \widetilde{Q_{ms}Q_{rs}} \left(\frac{\partial^2 V_{ms}}{\partial x^2} + \nu \frac{\partial^2 V_{ms}}{\partial y^2}\right)\left(\frac{\partial^2 V_{rs}}{\partial \xi^2} + \nu \frac{\partial^2 V_{rs}}{\partial \eta^2}\right) \\ \langle M_xQ_y \rangle &= \frac{1}{2} D^2 \sum_{mnrs} T_{mnrs} \widetilde{Q_{ms}Q_{rs}} \left(\frac{\partial^2 V_{ms}}{\partial x^2} + \nu \frac{\partial^2 V_{ms}}{\partial y^2}\right) \frac{\partial}{\partial \eta}\left(\frac{\partial^2 V_{rs}}{\partial \eta^2} + \nu \frac{\partial^2 V_{rs}}{\partial \xi^2}\right), \ldots \end{aligned}\right\} \ldots [36]$$

Probability Calculations

With the knowledge available in the present problem it is not possible to calculate the probability distribution function. However, for a distribution symmetrical with respect to time we have Gauss's inequality leading to an upper bound for the probability that $u - \langle u \rangle$ be greater than some multiple of the mean

deviation. In the problems treated, we have $\langle u \rangle = 0$. Hence Gauss's inequality reads

$$P(|u| \geq k\sigma) \leq 4/9k^2 \quad \ldots\ldots\ldots\ldots\ldots [37]$$

where P means probability, k is any constant, and σ is the mean deviation which can be calculated from the cross-correlation function $\langle uu \rangle$ by taking $x = \xi$, $y = \eta$, and $\tau = 0$; i.e.

$$\sigma^2 = \langle u^2 \rangle - \langle u \rangle^2 = \langle u^2 \rangle = \langle u(x, y, t)u(x, y, t) \rangle \quad [38]$$

Very often the distribution function can be approximated by the Gaussian distribution. In this case, using the asymptotic expansion we can show that (10)

$$P(|u| \geq k\sigma) \cong e^{-k^2/2}/k(2\pi)^{1/2} \quad k \gg 1 \quad \ldots\ldots [39]$$

S. O. Rice has given a formula to calculate the probable number of times, $N_0(u_a)$, per unit time the random function u will exceed the value $u = u_a$, where u_a may be the maximum allowable displacement or some component of stress, and so on. The formula of Rice for u_a taken as the displacement is

$$N_0(u_a) = \frac{1}{\pi} e^{-u_a^2/2\sigma^2} \left[\int_{-\infty}^{\infty} \zeta^2 \widetilde{UU} d\zeta \Big/ \int_{-\infty}^{\infty} \widetilde{UU} d\zeta \right]^{1/2} \quad [40]$$

For the case of stress we need to use power spectrum of the stress component desired in place of $\widetilde{UU}$ in Equation [40].

We can calculate the integrals occurring in Equation [40] by the contour integration used previously. In fact we can calculate these integrals directly from $\langle uu \rangle$ given by Equation [28]. Since $\langle uu \rangle$ is $^1/_2$ the Fourier transform of $\widetilde{UU}$, all we need to do is to differentiate $-2\langle uu \rangle$ with respect to τ twice and set $\tau = 0$. This gives the integral in the numerator inside of the bracket in Equation [40]. The integral in the denominator is obtained by setting $\tau = 0$ in $2\langle uu \rangle$.

Hence

$$\left.\begin{aligned} \int_{-\infty}^{\infty} \zeta^2 \widetilde{UU} d\zeta &= 4\pi\beta \sum_{mnrs} \frac{V_{ms}(x, y)V_{rs}(\xi, \eta)\widetilde{Q_{ms}Q_{rs}}(\lambda_{ms}^4 + \lambda_{rs}^4)}{(\lambda_{rs}^4 - \lambda_{ms}^4 + 4\beta^2)^2 + (4\beta\omega_{ms})^2} \\ \int_{-\infty}^{\infty} \widetilde{UU} d\zeta &= 8\pi\beta \sum_{mnrs} \frac{V_{ms}(x, y)V_{rs}(\xi, \eta)\widetilde{Q_{ms}Q_{rs}}}{(\lambda_{rs}^4 - \lambda_{ms}^4 + 4\beta^2)^2 + (4\beta\omega_{ms})^2} \end{aligned}\right\} \quad [41]$$

Determination of the distribution function, of course, is the ideal in stochastic problems. Sometimes with additional assumptions on correlation functions of pressure and considering a canonical ensemble of plates or bars and assuming that the distribution tends to a Maxwellian one as $t \to \infty$, one can obtain a distribution function. This is also possible for a Markoffian process [Chandrasekhar, Wang, and Uhlenbeck (5)]. It, however, requires much effort. Since it is hard to justify the underlying assumptions it is felt that further effort in this direction would be fruitless. Finally it is possible to calculate the cross-correlation functions for the systems starting from an initial configuration and velocity distribution. These calculations are also lengthy. Moreover, from the engineering point of view, they are only useful in measuring the pressure correlations from the measurement of displacement of the systems. In engineering systems the transient effect in statistical computations occupies small value. Thus such computations in the present work are avoided.

Beams and Plates With Different Edge Conditions

Eigenfunctions $V_{ms}(x, y)$ and eigenvalues λ_{ms} of several beams and plates with different edge conditions are listed in (11). Our V_{ms}, λ_{ms}, and b_{ms} are, respectively, equal to g_{ms}, p_{ms}, and b_{ms} of (11). Here we work out only the following cases:

(*a*) *Simply supported beams*

$$V_n(x) = \sin(n\pi x/L), \quad b_n = L/2, \quad \lambda_n = n\pi/L \quad \ldots [42]$$

Hence

$$\widetilde{Q_sQ_r} = \frac{4}{\pi L^2} \int_0^L \int_0^L d(x, \xi) \sin(n\pi x/L) \sin(r\pi\xi/L) dx d\xi \quad \ldots [43]$$

The two cases corresponding to Equations [30] respectively give

$$\widetilde{Q_sQ_r} = (2d_1/\pi L)\delta_{sr}, \quad \widetilde{Q_sQ_r} = (4d_2/\pi L^2) \sin(n\pi a/L) \sin(r\pi a/L) \quad \ldots\ldots [44]$$

We give cross-correlation functions only for the first case

$$\langle uu \rangle = (d_1/\pi L) \sum_n T_{ns} \sin(n\pi x/L) \sin(n\pi\xi/L) \quad \ldots [45]$$

where

$$T_{ns} = \frac{L^4 e^{-\beta\tau}}{2\pi^3 n^4} \left(\frac{\sin \omega_n \tau}{\omega_n} + \frac{\cos \omega_n \tau}{\beta} \right)$$

$$\omega_n = \left(\frac{n^4\pi^4}{L^4} - \beta^2 \right)^{1/2}, \quad \tau \geq 0.$$

For $\tau = 0$ we were able to sum the terms in $\langle uu \rangle$

$$\langle uu \rangle = (d_1L^3/24\beta) \left[\frac{1}{L^4} (x^2\xi + x\xi^2) - \frac{1}{L^3} (3x^2\xi + \xi^3) + 2\frac{x\xi}{L^2} \right] \quad \ldots\ldots [46]$$

valid for $\quad 0 \leq x + \xi \leq 2L, \quad 0 \leq x - \xi \leq 2L$

For the case of $x < \xi$ the sum would be obtained by interchanging x and ξ in Equation [46]. The case $x = \xi$ follows from Equation [46]

$$\langle uu \rangle = (d_1L^3/12\beta)(x/L)^2(1 - x/L)^2 \quad \ldots\ldots [47]$$

$$0 \leq x \leq L, \quad \tau = 0, \quad x = \xi$$

For the mid-point $x = \xi = L/2$ and arbitrary τ the autocorrelation function reads

$$\left\langle u\left(\frac{L}{2}, t + \tau\right) u\left(\frac{L}{2}, t\right) \right\rangle = \frac{d_1L^3}{2\beta\pi} e^{-\beta\tau} \sum_{1, 3, \ldots} \frac{1}{n^4} \left(\cos \omega_n \tau + \frac{\beta}{\omega_n} \sin \omega_n \tau \right), \quad \tau \geq 0 \quad [48]$$

This is strongly convergent. Taking only the first term, we will have less than 2 per cent error.

The correlation function $\langle M_sM_s \rangle$ of the bending moment in accordance with Equation [36] at $x = \xi$ is

$$\langle M_sM_s \rangle = (D^2d_1/\pi L) \sum_n T_{ns}(n\pi/L)^4 \sin^2(n\pi x/L). \quad [49]$$

For $\tau = 0$ this becomes

$$\langle M_s(x, t)M_s(x, t) \rangle = (D^2d_1/2\beta L) \sum_n \sin^2(n\pi x/L). \quad [50]$$

Similar to Equation [48] for the case of $\tau \neq 0$ but $x = L/2$ we have

$$<M_x\left(\frac{L}{2}, t+\tau\right)M_x\left(\frac{L}{2}, t\right)> = (D^2d_1/2\beta L)e^{-\beta\tau} \sum_{1,3,\ldots}\left(\cos\omega_n\tau + \frac{\beta}{\omega_n}\sin\omega_n\tau\right), \quad \tau \geq 0 \ldots\ldots [51]$$

Both Equations [50] and [51] diverge. This is because of the delta function appearing in Equation [3] and also because of the severeness of the assumptions underlying the classical beam-and-plate theory. It is desirable to carry out the calculations for the Timoshenko beam theory to ascertain this point.

Similar behavior occurs for the second case of Equations [30]. The situation here is similar to the case of a plucked cantilever beam where the classical theory leads to infinite strain.

For the case of $\tau = 0$, $x = \xi$ by using Equation [47] which is the value of σ^2 and Equations [41], [42], and [43] we can calculate $N_\theta(u_n)$. We find that

$$\int_{-\infty}^{\infty} \zeta^2\widetilde{UU}\, d\zeta = (d_1/\beta L)\sum_n \sin^2(n\pi x/L)$$

$$\int_{-\infty}^{\infty} \widetilde{UU}\, d\zeta = \sigma^2/2 = (d_1L^3/6\beta)(x/L)^2(1 - x/L)^2$$

We again find divergence. Hence in classical beam theory for the first case of Equations [30] $N_\theta(u_n)$ grows beyond limit.

(*b*) *Cantilever beam, clamped at* $x = 0$

$$V_n(x) = \frac{\cosh\lambda_n x - \cos\lambda_n x}{\cosh\lambda_n L + \cos\lambda_n L} - \frac{\sinh\lambda_n x - \sin\lambda_n x}{\sinh\lambda_n L + \sin\lambda_n L} \ldots [52]$$

where λ_n is the nth positive root of the equation

$$\cos\lambda L \cosh\lambda L + 1 = 0 \ldots\ldots [53]$$

We also can show easily that (12)

$$b_n = \frac{L}{4}\,[V_n^2(x)]_{x=L} \ldots\ldots [54]$$

The two cases corresponding to Equations [30] now give

$$\widetilde{Q_nQ_r} = (d_1/\pi b_n)\delta_{nr}, \quad \widetilde{Q_nQ_r} = (d_2/\pi b_n b_r)V_n(a)V_r(a)$$

The cross-correlation function for the first case is

$$<uu> = (d_1/2\pi)\sum_n \frac{1}{b_n} T_{nn}V_n(x)V_n(\xi) \ldots\ldots [55]$$

In the case of $\tau = 0$ and $x = \xi = L$ we are able to perform the summation indicated in Equation [55]. For this case we have

$$<uu> = (d_1/4\beta)\sum_n V_n^2(L)/\lambda_n^4 b_n = (d_1/\beta L)\Sigma\lambda_n^{-4} \ldots [56]$$

in view of Equation [54]. Lord Rayleigh (13) gives the value of this sum

$$<u(L, t)u(L, t)> = d_1/12\beta L \ldots\ldots [57]$$

The general case for $x = \xi = L$, but any τ may be calculated approximately from Equation [55]. Since the series is strongly convergent, by taking the first term only, we have

$$<u(L, t+\tau)u(L, t)> \cong (d_1/12\beta L)e^{-\beta\tau}\left(\cos\omega_1\tau + \frac{\beta}{\omega_1}\sin\omega_1\tau\right) \ldots\ldots [58]$$

Here we used the value $1/12$ for $1/\lambda_1^4$ instead of $1/12.35$, since this makes the value for $\tau = 0$ correct.

We also could calculate cross-correlation functions $<M_xM_x>$ and $<M_xQ_x>$, . . . by combining Equations [35] and [52].

(*c*) *Circular plates clamped at outer edge*

$$\left.\begin{aligned} V_{mn}(r, \theta) &= [J_n(\lambda_{mn}r) + BI_n(\lambda_{mn}r)]\sin(n\theta + \gamma_0) \\ B &= -J_n(\lambda_{mn}a)/I_n(\lambda_{mn}a), \quad b_{mn} = 2\pi a^2 J_n^2(\lambda_{mn}a) \end{aligned}\right\} \ldots [59]$$

where λ_{mn} is the mth root of

$$\frac{J_{n+1}(\lambda a)}{J_n(\lambda a)} + \frac{I_{n+1}(\lambda a)}{I_n(\lambda a)} = 0 \ldots\ldots [60]$$

where J_n and I_n are the Bessel functions of first kind with real and imaginary arguments, respectively, and a is the radius of the plate. The cross-correlation function $<uu>$ is obtained from Equations [28] and [59]. For the first case of Equation [31] and for $\tau \geq 0$ it reads

$$<uu> = (d_1/4\beta)e^{-\beta\tau}\sum_{m,n}\frac{1}{b_{mn}\lambda_{mn}^4}\left(\cos\omega_{mn}\tau + \frac{\beta}{\omega_{mn}}\sin\omega_{mn}\tau\right)V_{mn}(r, \theta)V_{mn}(\rho, \varphi) \ldots\ldots [61]$$

At the center of the disk, Equation [61] reduces to a single series. Thus for $r = \rho = 0$, $\tau \geq 0$ we get

$$<u(0, \theta, t+\tau)u(0, \varphi, t)> = \frac{d_1a^2\sin^2\gamma_0}{8\pi\beta}\,e^{-\beta\tau}\sum_m \frac{1}{(a\lambda_{m0})^4}\left[\frac{1}{J_0(\lambda_{m0}a)} - \frac{1}{I_0(\lambda_{m0}a)}\right]^2 \left(\cos\omega_{m0}\tau + \frac{\beta}{\omega_{m0}}\sin\omega_{m0}\tau\right) \ldots\ldots [62]$$

This series is rapidly convergent. For engineering purposes it is sufficient to consider only the first term. Since $(\lambda_{00}a)^4 = 104.2$ we have approximately

$$<u(0, \theta, t+\tau)u(0, \varphi, t)> \cong \frac{d_1a^2\sin^2\gamma_0}{8(104.2)\pi\beta}\,e^{-\beta\tau}\left[\frac{1}{J_0(\lambda_{00}a)} - \frac{1}{I_0(\lambda_{00}a)}\right]^2 \left(\cos\omega_{00}\tau + \frac{\beta}{\omega_{00}}\sin\omega_{00}\tau\right) \ldots\ldots [63]$$

For other points we need to use Equation [61], which also converges. However, more than one term is needed for an acceptable accuracy.

The calculation of the cross-correlation function for moments follows the same line as that given in (*a*). Here we compute only $<M_rM_r>$. The bending moment M_r is given by

$$M_r = -D\left[\frac{\partial^2 u}{\partial r^2} + \nu\left(\frac{1}{r}\frac{\partial u}{\partial r} + \frac{1}{r^2}\frac{\partial^2 u}{\partial\theta^2}\right)\right]$$

Parallel to Equation [35] we will have

$$<M_rM_r> = \frac{1}{2}D^2\sum_{mnjk} T_{mnjk}\widetilde{Q_{mn}Q_{jk}}\left[\frac{\partial^2 V_{mn}}{\partial r^2} + \nu\left(\frac{1}{r}\frac{\partial V_{mn}}{\partial r} + \frac{1}{r^2}\frac{\partial^2 V_{mn}}{\partial\theta^2}\right)\right]\left[\frac{\partial^2 V_{jk}}{\partial\rho^2} + \nu\left(\frac{1}{\rho}\frac{\partial V_{jk}}{\partial\rho} + \frac{1}{\rho^2}\frac{\partial^2 V_{jk}}{\partial\varphi^2}\right)\right] \ldots\ldots [64]$$

Combining Equations [31], [64] for $\rho = r = 0$ and $\tau \geq 0$ we obtain

$$<M_r M_r> = \frac{d_1 D^2 e^{-\beta\tau}}{32\pi a^2 \beta} \left\{ (1+\nu^2)\sin^2\gamma_0 \sum_m \left[\frac{1}{J_0(\lambda_{m0}a)} + \frac{1}{I_0(\lambda_{m0}a)}\right]^2 \left(\cos\omega_{m0}\tau + \frac{\beta}{\omega_{m0}}\sin\omega_{m0}\tau\right) + \frac{(1-\nu)^2}{4}\sin(2\theta+\gamma_0)\sin(2\varphi+\gamma_0)\sum_m \left[\frac{1}{J_2(\lambda_{m2}a)} - \frac{1}{I_2(\lambda_{m2}a)}\right]^2 \left(\cos\omega_{m2}\tau + \frac{\beta}{\omega_{m2}}\sin\omega_{m2}\tau\right)\right\} \quad \ldots\ldots [65]$$

For other types of cross-correlation functions involving known distributions in r and θ computation of $<uu>$, $<M_r M_r>$, $<M_r M_\theta>$, . . . must be based on the general formulas such as Equations [28] and [35].

(d) Rectangular plates simply supported at all edges

$$V_{ms}(x, y) = \sin(m\pi x/a)\sin(n\pi y/b), \quad b_{ms} = ab/4$$

$$\lambda_{ms} = [(m\pi/a)^2 + (n\pi/b)^2]^{1/2}$$

where a and b are edge lengths.

For the first case of Equation [31] and for $\tau \geq 0$ we obtain

$$<uu> = (d_1/ab\beta)e^{-\beta\tau} \sum_{m,n} \frac{\sin(m\pi x/a)\sin(n\pi y/b)\sin(m\pi\xi/a)\sin(n\pi\eta/b)}{[(m\pi/a)^2 + (n\pi/b)^2]^2} \left(\cos\omega_{ms}\tau + \frac{\beta}{\omega_{ms}}\sin\omega_{ms}\tau\right)$$

Similar to Equation [65] we can compute cross correlation of moments.

The autocorrelation Function [47] for a simply supported beam at $\tau = 0$ is plotted in Fig. 1. It gives a maximum at $x/L = 1/2$. The autocorrelation Functions [48] at $x = L/2$ for the simply supported beam, [58] at $x = L$ for the cantilever beam, and [63] at $r = 0$ for the clamped circular plates are plotted in Fig. 2. Since we consider only the first term in each series they all have the same shapes in terms of parameters $\beta\tau$ and Ω_1 defined in Fig. 2. All these curves lie between the curve marked $\Omega_1 = 0$ and the R-axis. The curve marked $\Omega_1 = 0$ does not oscillate. All other curves begin oscillating faster and faster as Ω_1 increases.

Acknowledgment

The contents of this paper were obtained in the course of research sponsored by the U. S. Office of Naval Research. The author is indebted to Dr. W. A. Beck for checking the analysis.

BIBLIOGRAPHY

1 "Brownian Motion of Strings and Elastic Rods," by G. A. Van Lear and G. E. Uhlenbeck, *Physical Review*, vol. 38, 1931, p. 1583.

2 "Zur Theorie der Brownschen Bewegung fur Systeme, worin mehrere Temperaturen vorkommen," by L. S. Ornstein, *Zeitschrift für Physik*, vol. 41, 1927, p. 848.

3 "Brownian Motion of a Wire," by A. Houdijk, *Archives Neerlandaises des Sciences Exactes et Naturelle*, series IIIA, vol. 11, 1928, p. 212.

4 "On the Theory of Brownian Motion," by M. C. Wang and G. E. Uhlenbeck, *Reviews of Modern Physics*, vol. 17, nos. 2 and 3 1945, pp. 323–342.

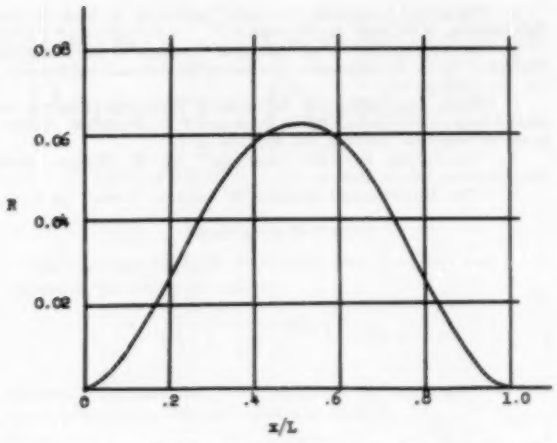

Fig. 1 Autocorrelation Function for Simply Supported Beam at $\tau = 0$
$R = <u(x, t)u(x, t)> /(d_1 L^3/12\beta)$

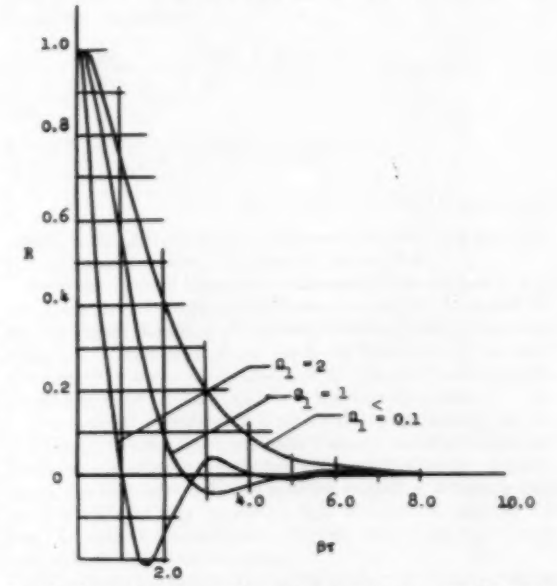

Fig. 2 Autocorrelation Functions for Beams and Circular Plates

Simply supported beam

$$R = <u(L/2, t+\tau)u(L/2, t)> /(d_1 L^3/2\beta\pi^4)$$

$$\Omega_1 = (\pi^4 L^{-4}\beta^{-2} - 1)^{1/2}$$

Cantilever beam

$$R = <u(L, t+\tau)u(L, t)> /(d_1/12\ \beta L)$$

$$\Omega_1 = (\lambda_1^4\beta^{-2} - 1)^{1/2}$$

Clamped circular plates

$$R = <u(0, \theta, t+\tau)u(0, \varphi, t)> /K$$

$$K = d_1 a^2 \sin^2\gamma_0 \left[\frac{1}{J_0(\lambda_{00}a)} - \frac{1}{I_0(\lambda_{00}a)}\right]^2 \Big/ (833.6\pi\beta)$$

$$\Omega_1 = (\lambda_{00}^4\beta^{-2} - 1)^{1/2}$$

5 "Noise and Stochastic Processes," edited by N. Wax, Dover Publications, New York, N. Y., 1954.

6 "On the Application of Statistical Concepts to the Buffeting Problem," by H. W. Liepmann, *Journal of the Aeronautical Sciences*, vol. 19, 1952, p. 793.

7 "Some Applications of Generalized Harmonic Analysis to Gust Loads on Airplanes," by H. Press and J. C. Houboldt, *Journal of the Aeronautical Sciences*, vol. 22, 1955, p. 17.

8 "Generalized Harmonic Analysis," by N. Wiener, *Acta Mathematica*, vol. 55, 1930, p. 117.

9 "The Mathematical Analysis of Random Noise," by S. O. Rice, *Bell System Technical Journal*, vol. 23, 1944, p. 282; vol. 24, 1945, p. 46.

10 "Engineering Cybernetics," by H. S. Tsien, McGraw-Hill Book Company, Inc., New York, N. Y., 1954.

11 "Transverse Impact on Beams and Plates," by A. C. Eringen, JOURNAL OF APPLIED MECHANICS, Trans. ASME, vol. 75, 1953, p. 461.

12 "Applied Elasticity," by J. Prescott, Dover Publications, New York, N. Y., 1946, p. 226.

13 "The Theory of Sound," by J. W. S. Rayleigh, Dover Publications, New York, N. Y., vol. 1, 1945, p. 279.

Dependence of the Frequency Spectrum of a Circular Disk on Poisson's Ratio

By R. L. SHARMA,[1] TORONTO, ONTARIO, CANADA

The results of computations of frequencies of axially symmetric flexural vibrations of circular disks are given for an intermediate frequency range and for several values of Poisson's ratio.

Nomenclature

The following nomenclature is used in the paper:

- d = diameter
- g = material constant related to Poisson's ratio
- h = thickness
- p = resonant frequency in radians per second
- $\bar{p}$ = frequency in radians per second of the first thickness-shear mode of an infinite plate of thickness h
- β_1 = parameter depending upon the ratio $p/\bar{p}$ and the material constant g
- γ = parameter depending upon β_1, g, and the mode of axially symmetric flexural vibrations
- μ = shear modulus
- ν = Poisson's ratio
- ρ = density
- π = ratio of circumference to diameter of any circle = 3.1416

Introduction

The problem of free, axially symmetric, flexural vibrations of a circular disk was considered, recently, by Deresiewicz and Mindlin[2] as a solution of equations of motion, taking into account the effects of rotatory inertia and transverse-shear deformation. These authors obtained the frequency equation and gave the results of computations of frequencies, for Poisson's ratio = 0.312, in the range $0.80 \leqslant p/\bar{p} \leqslant 1.12$ where p and $\bar{p}$ are the circular frequencies of the disk and of the first thickness-shear mode of an infinite plate, respectively.

In the recent past some devices making use of thick, vibrating disks have appeared. The applications required the computation of frequencies of the first three modes in the range $0.2 \leqslant p/\bar{p} \leqslant 0.95$. This exceeds the range of applicability of the classical equations of the thin plates but lies well within the range of the solutions by Deresiewicz and Mindlin. In addition it was found desirable to study the dependence of frequency on slight variations of Poisson's ratio.

Frequency Spectrum

The complete solution of the frequency problem[2] can be expressed in the following manner

$$\frac{d}{h} = \gamma \left(\frac{p}{\bar{p}}\right)\left[\frac{(1-\beta_1^2)}{3(1+g)}\right]^{1/2} \quad \text{for } p < \bar{p} \qquad [1]$$

where d is the diameter, h the thickness, and g the material constant, is related to Poisson's ratio ν as follows

$$g = \frac{\pi^2}{24}(1-\nu^2) \qquad [2]$$

Also β_1 and γ are the parameters obtained from the following equations, respectively

$$\frac{p}{\bar{p}} = \left[1 + \frac{\beta_1^2(1+g)^2}{g(1-\beta_1^2)^2}\right]^{-1/2} \quad \text{for } p < \bar{p} \qquad [3]$$

and

$$\frac{g+\beta_1^2}{1+g}\gamma\frac{J_0(\gamma)}{J_1(\gamma)} + \frac{1+g\beta_1^2}{1+g}\beta_1\gamma\frac{I_0(\beta_1\gamma)}{I_1(\beta_1\gamma)} - (1-\nu)(1+\beta_1^2) = 0 \quad \text{for } p < \bar{p} \qquad [4]$$

where $J_0(x)$, $J_1(x)$ are Bessel functions of the first kind and $I_0(x)$ $I_1(x)$ are modified Bessel functions of the first kind.

With the value of ν specified, a choice of β_1 determines $p/\bar{p}$ by Equation [3] and yields an infinite set of roots γ by Equation [4]. For the chosen β_1 each of these roots furnishes a ratio d/h through Equation [1] and hence there results an infinite set of values of d/h corresponding to each value of $p/\bar{p}$. We shall limit ourselves to the first three modes of axially symmetric vibrations.

The material considered is a nickel alloy commercially known as Ni-Span C which has a constant Young's modulus over an extended temperature range and has a high mechanical Q. Depending on the heat-treatment and solution annealing, Poisson's ratio for this material may vary from 0.25 to 0.35. In view of the large amount of computations involved, only three values of ν, 0.25, 0.30, 0.35, will be considered.

To facilitate the task of finding the roots γ of Equation [4] for a series of values of $p/\bar{p}$, tables were computed of the functions

$$x\frac{J_0(x)}{J_1(x)} \text{ for } 0(0.01)10, \quad 2.8(0.001)3.3, \quad 6.0(0.001)6.3, \quad 9.0(0.001)9.5$$

$$x.\frac{I_0(x)}{I_1(x)} \text{ for } 0.0(0.001)10.0$$

to six significant places.[3]

The subsequent numerical work was carried out on a desk calculator. The results are shown in Table 1.

Making use of the definition

$$\bar{p} = \frac{\pi}{h}\left(\frac{\mu}{\rho}\right)^{1/2} \qquad [5]$$

---

[1] Collins Radio Company of Canada Ltd., Toronto, Ontario, Canada. Now with Collins Radio Company, Western Division, Burbank, Calif.

[2] "Axially Symmetric Flexural Vibrations of a Circular Disk," by H. Deresiewicz and R. D. Mindlin, Journal of Applied Mechanics, Trans. ASME, vol. 75, 1953, pp. 86–88.

Contributed by the Applied Mechanics Division and presented at the Annual Meeting, New York, N. Y., November 25–30, 1956, of The American Society of Mechanical Engineers.

Discussion of this paper should be addressed to the Secretary, ASME, 29 West 39th Street, New York, N. Y., and will be accepted until April 10, 1957, for publication at a later date. Discussion received after the closing date will be returned.

Note: Statements and opinions advanced in papers are to be understood as individual expressions of their authors and not those of the Society. Manuscript received by ASME Applied Mechanics Division, May 23, 1956. Paper No. 56—A-10.

[3] Computations were performed by J. B. Rea Company, Los Angeles, Calif. All tables are stored in the library of Collins Radio Company, Burbank, Calif.

TABLE 1 $p/\bar{p}$ VERSUS d/h

$p/\bar{p}$	Ratio d/h								
	First Mode			Second Mode			Third Mode		
	ν =0.25	0.30	0.35	0.25	0.30	0.35	0.25	0.30	0.35
0.10	6.929	7.091	7.272	14.341	14.587	14.887	21.680	22.031	22.462
0.15	5.520	5.654	5.795	11.403	11.608	11.831	17.237	17.529	17.843
0.20	4.670	4.782	4.903	9.626	9.797	9.981	14.550	14.791	15.049
0.25	4.084	4.183	4.288	8.399	8.547	8.704	12.694	12.900	13.120
0.30	3.649	3.737	3.832	7.485	7.614	7.753	11.312	11.492	11.683
0.35	3.309	3.390	3.475	6.769	6.886	7.008	10.230	10.388	10.558
0.40	3.035	3.109	3.187	6.189	6.294	6.405	9.354	9.494	9.646
0.45	2.807	2.876	2.948	5.706	5.802	5.902	8.624	8.751	8.887
0.50	2.614	2.679	2.746	5.296	5.383	5.476	8.004	8.120	8.244
0.55	2.450	2.510	2.572	4.944	5.022	5.108	7.474	7.575	7.688
0.60	2.304	2.363	2.421	4.631	4.707	4.787	7.001	7.099	7.202
0.65	2.177	2.230	2.287	4.357	4.430	4.502	6.586	6.678	6.772
0.70	2.064	2.118	2.169	4.112	4.180	4.248	6.215	6.306	6.387
0.75	1.963	2.013	2.063	3.890	3.953	4.019	5.878	5.957	6.039
0.80	1.872	1.920	1.967	3.689	3.749	3.812	5.572	5.646	5.722
0.85	1.790	1.836	1.881	3.505	3.564	3.622	5.289	5.358	5.431
0.90	1.715	1.758	1.802	3.335	3.390	3.448	5.026	5.091	5.160
0.95	1.646	1.688	1.730	3.177	3.229	3.287	4.778	4.843	4.905

TABLE 2 PER CENT DEVIATION IN DIAMETER FROM THE CASE $\nu = 0.30$

$p/\bar{p}$	Deviation					
	First Mode		Second Mode		Third Mode	
	ν = 0.25	0.35	0.25	0.35	0.25	0.35
0.2	-2.40	+2.53	-1.78	+1.89	-1.66	+1.74
0.5	-2.49	+2.50	-1.84	+1.73	-1.45	+1.53
0.8	-2.56	+2.45	-1.63	+1.68	-1.33	+1.35

TABLE 3 PER CENT DEVIATION IN FREQUENCY FROM THE CASE $\nu = 0.30$

First Mode			Second Mode			Third Mode		
d/h	Deviation		d/h	Deviation		d/h	Deviation	
	ν =0.25	0.35		0.25	0.35		0.25	0.35
1.75	-3.4	+3.4	3.5	-2.0	+2.0	5.0	-1.4	+1.4
2.00	-3.7	+3.3	4.0	-2.3	+2.1	6.0	-1.8	+1.8
2.50	-3.7	+3.5	4.5	-2.2	+2.1	7.0	-1.9	+1.8
3.00	-3.7	+3.7	5.0	-2.2	+2.3	8.0	-2.1	+2.1
4.00	-4.0	+4.1	6.0	-2.4	+2.4	9.0	-2.1	+2.3
5.00	-3.7	+3.7	8.0	-2.7	+2.8	12.0	-2.5	+2.8

where the constants μ and ρ are the shear modulus and the density, respectively, we find:

1 For disks vibrating at the same frequency, those disks with larger Poisson's ratio will also have larger diameter. Table 2 shows deviations from the case $\nu = 0.30$ for some representative ratios of $p/\bar{p}$.

2 For disks having the same dimensions, those disks with larger Poisson's ratio will vibrate at higher frequencies. Table 3 shows percentage deviation in frequency from the case $\nu = 0.30$ for some representative ratios of d/h.

Such an analysis was found helpful in explaining the frequency deviation due to variations in material constants. This study thus makes available the upper and lower limits of (1) the disk sizes for a certain frequency or (2) the disk frequencies for a certain dimension. Such information can be used for the proper selection or the design of precision equipment to be used for fabricating the circular disks.

Acknowledgments

The author wishes to express his gratitude to Collins Radio Company for permitting the publication of this study. His sincerest thanks are also due to Kirk Dickens for his help in the calculations.

Forced Vibration of a Body on an Elastic Stratum

By G. B. WARBURTON,[1] EDINBURGH, SCOTLAND

The paper considers the forced vibration of a body with a circular base resting on a homogeneous elastic stratum of infinite surface area and constant depth. The body is subjected to a vertical disturbing force along the axis of symmetry. After evaluating an integral given by Arnold, Bycroft, and Warburton,[2] curves are given showing the dependence of the resonant frequency on three parameters. Good agreement is obtained between theoretical values of the resonant frequency and experimental values taken from the previous paper.[2]

Nomenclature

The following nomenclature is used in the paper:

$a_0 = kr_0$ = frequency factor
A = amplitude of vibration
$b = m_0/\rho r_0^3$ = mass ratio
E = Young's modulus
f_1, f_2 = functions of a_0, ν, and R
$h = [\rho/(\lambda + 2\mu)]^{1/2}p$
$k = (\rho/\mu)^{1/2}p$
m_0 = mass resting on surface of stratum
n = integer
p = circular frequency of force applied to mass
P = amplitude of exciting force
r = radial distance from center of base of mass m_0
r_0 = radius of base of mass m_0
$R = \delta/r_0$ = depth factor
s = dimensionless variable
t = time
w = displacement of mass in vertical direction
$\alpha = (k^2s^2 - h^2)^{1/2}$
$\beta = (k^2s^2 - k^2)^{1/2}$
δ = depth of stratum
$\eta = \dfrac{h}{k} = \left(\dfrac{\mu}{\lambda + 2\mu}\right)^{1/2} = \left[\dfrac{1 - 2\nu}{2(1 - \nu)}\right]^{1/2}$
$\lambda = \dfrac{E\nu}{(1 + \nu)(1 - 2\nu)}$ = Lamé's elastic constant
μ = modulus of rigidity
ν = Poisson's ratio
ρ = density of material of stratum
σ_z = normal stress in vertical direction

[1] Senior Lecturer, Head of Post-Graduate School of Applied Dynamics, Department of Engineering, University of Edinburgh.

[2] "Forced Vibrations of a Body on an Infinite Elastic Solid," by R. N. Arnold, G. N. Bycroft, and G. B. Warburton, JOURNAL OF APPLIED MECHANICS, Trans. ASME, vol. 77, 1955, pp. 391–400.

Contributed by the Applied Mechanics Division and presented at the Annual Meeting, New York, N. Y., November 25–30, 1956, of THE AMERICAN SOCIETY OF MECHANICAL ENGINEERS.

Discussion of this paper should be addressed to the Secretary, ASME, 29 West 39th Street, New York, N. Y., and will be accepted until April 10, 1957, for publication at a later date. Discussion received after the closing date will be returned.

NOTE: Statements and opinions advanced in papers are to be understood as individual expressions of their authors and not those of the Society. Manuscript received by ASME Applied Mechanics Division, May 9, 1956. Paper No. 56—A-35.

Introduction

The paper considers a body with a circular base resting on an elastic stratum of infinite area and constant depth. The body is subjected to a harmonic disturbing force in the vertical direction; the line of action of this force passes through the center of gravity of the body and through the center of its circular base, Fig. 1. The paper is an extension of the work of Arnold, Bycroft, and Warburton,[2] who considered the forced vibration of a body on a

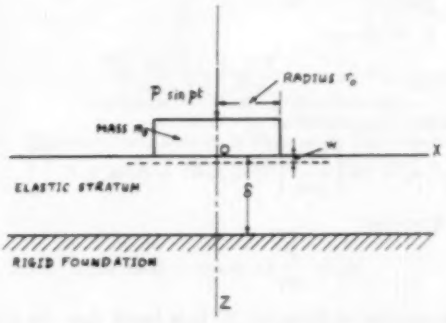

FIG. 1 MASS ON AN INFINITE ELASTIC STRATUM

semi-infinite elastic medium and on an elastic stratum for the four modes of vibration; namely, vertical translation, horizontal translation, torsion, and rocking. Computed theoretical results for a stratum were given only for the torsional mode. The present paper gives the results of calculations for the mode of vibration—vertical translation—for a stratum and compares them with experimental results given previously.[2]

Theory

This is a mixed boundary-value problem, as the conditions to be satisfied for a body with a rigid circular base of radius r_0 resting on a stratum are (*a*) zero stress at the surface for $r > r_0$; (*b*) constant amplitude of displacement of the surface for $0 \leq r \leq r_0$; (*c*) no reflection of waves from the boundaries at infinity ($r = \infty$). It is assumed that the stratum rests on a rigid infinite foundation and that no friction exists between the stratum and the foundation and between the circular base and the surface of the stratum.

The mixed boundary conditions are not satisfied rigorously. Instead, the distribution of direct stress under the base is assumed to be similar to that between a rigid base and a semi-infinite medium for a static load. Thus for a periodic disturbing force Pe^{ipt} the direct stress :

$$\sigma_z = \frac{Pe^{ipt}}{2\pi r_0(r_0^2 - r^2)^{1/2}} \quad \text{for } r \leq r_0 \qquad [1]$$

$$= 0 \qquad \text{for } r > r_0$$

The analysis of the earlier paper[2] is followed, leading to an expression for the displacement w, which consists of an infinite integral plus terms corresponding to free waves in the stratum. The latter terms are added to satisfy the boundary conditions at

infinity. This solution does not give a constant value for the amplitude of w over the range $0 \leq r \leq r_0$. A weighted-average value of the dynamic displacement is defined[2] by

$$w_a = \int_0^{r_0} \frac{w r\, dr}{r_0(r_0^2 - r^2)^{1/2}} \quad \ldots\ldots [2]$$

This leads to the following expression for the displacement (Equation [29] of paper[2])

$$w_a = Re\left[\frac{Pe^{ipt}}{8\pi\mu r_0}\int_0^\infty \frac{(s^2-\eta^2)^{1/2}\sin^2 a_0 s\, ds}{a_0 s\, l(s)} - \frac{Pe^{ipt}i}{8\mu r_0}\sum \frac{(s_n^2-\eta^2)^{1/2}\sin^2 a_0 s_n}{a_0 s_n\, l'(s_n)}\right] \ldots [3]$$

where s_n are the real roots of $l(s) = 0$

$$l(s) = (s^2 - 1/2)^2 \coth \alpha\delta - s^2(s^2-\eta^2)^{1/2}(s^2-1)^{1/2}\coth \beta\delta$$

$$l'(s_n) = \left[\frac{dl(s)}{ds}\right]_{s=s_n}$$

$$a_0 = pr_0(\rho/\mu)^{1/2} \text{ and } \eta = \frac{h}{k} = \left[\frac{1-2\nu}{2(1-\nu)}\right]^{1/2}$$

This can be expressed as

$$w_a = Re\left[\frac{Pe^{ipt}}{\mu r_0}\left\{f_1(a_0, \nu, R) + if_2(a_0, \nu, R)\right\}\right] \ldots\ldots [4]$$

where $R = \delta/r_0$

or

$$w_a = \frac{P}{\mu r_0}(f_1 \cos pt - f_2 \sin pt) \ldots\ldots [5]$$

By inspection of Equation [3] it is found that the integral is real and thus gives f_1; the summation gives f_2. Equation [5] gives the displacement for a rigid massless base; for a mass m_0 the amplitude of vibration of the mass is given by Reissner[3] as

$$A = \frac{P}{\mu r_0}\left[\frac{f_1^2 + f_2^2}{(1 + ba_0^2 f_1)^2 + (ba_0^2 f_2)^2}\right]^{1/2} \ldots\ldots [6]$$

where $b = m_0/\rho r_0^3$.

Values of f_1 and f_2

In Figs. 2 and 3 the functions f_1 and f_2 have been plotted against frequency factor a_0 for specific values of R and for $\nu = 1/4$ and $\nu = 0$, respectively. Inspection of the integral in Equation [3] shows that it diverges at $s = 0$ if $\cot(a_0 R\eta) = 0$; i.e., if

$$a_0 = (2n-1)\pi/2\eta R,\ n = 1, 2, 3 \ldots$$

Only the lowest root, corresponding to $n = 1$, lies within the range of values of a_0 considered here. The form of functions f_1 and f_2 depends on the value of Poisson's ratio ν.

(*a*) $0 < \nu < 1/4$. In Fig. 2, f_1 and f_2 are plotted for $\nu = 1/4$; their form for other values of ν in this range will be similar. For $\nu = 1/4$, $f_1 \to -\infty$ as $a_0 R \to 2.5742$ and also as $a_0 R \to 2.7208$; the former is caused by the existence of two identical roots of $l(s) = 0$ for $a_0 R = 2.5742$, the latter by the divergence of the integral at $s = 0$ for $a_0 R = 2.7208$. For the small range of values of a_0 from $2.5742/R$ to $2.7208/R$, the fluctuations of f_1 and f_2 have not been given and f_1 is shown by a dotted line in Fig. 2.

(*b*) $\nu = 0$. The behavior of f_1 is similar to that just described; $f_1 \to -\infty$ as $a_0 R \to 2.1582$ and also as $a_0 R \to 2.2215$. The approximate form of f_1 in this range is shown in Fig. 4. Function f_2 is zero for $a_0 < 2.1582/R$ and varies rapidly in the range $2.1582/R < a_0 < 2.2215/R$, as shown approximately by the dotted lines in Fig. 3.

(*c*) $1/3 < \nu < 1/2$. Function $f_1 \to -\infty$ as $a_0 R \to \pi/2\eta$; f_2 is finite for $a_0 > 0$.

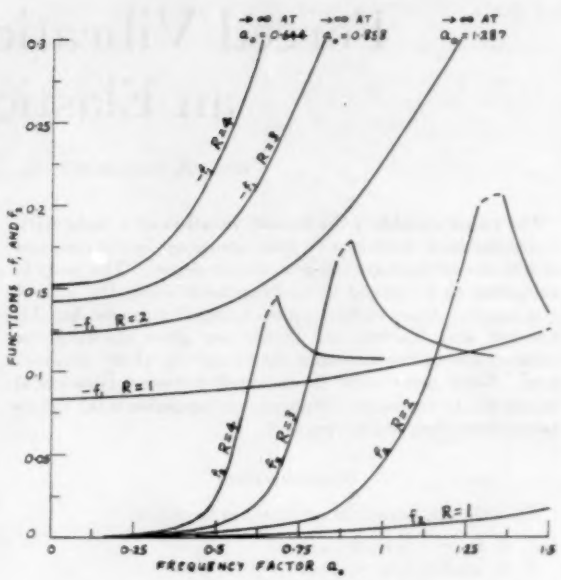

FIG. 2 FUNCTIONS f_1 AND f_2, $\nu = 1/4$

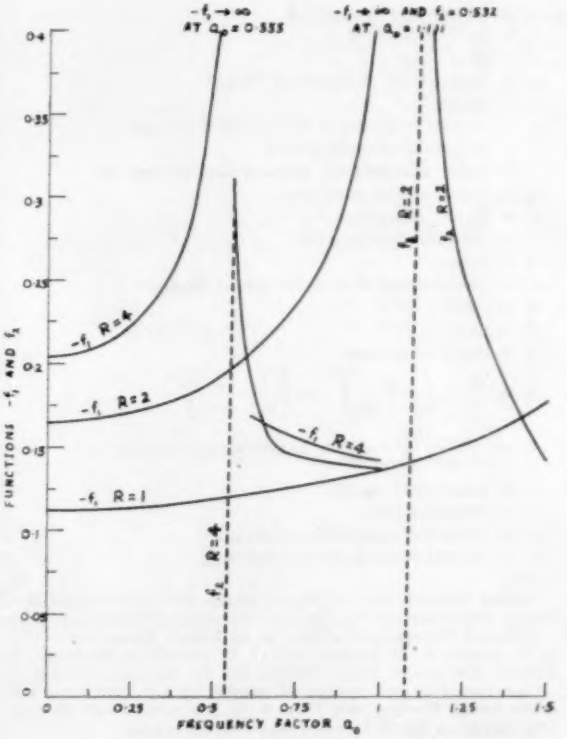

FIG. 3 FUNCTIONS f_1 AND f_2, $\nu = 0$

[2] "Stationäre, axialsymmetrische, durch eine schüttelnde Masse erregte Schwingungen eines homogenen elastischen Halbraumes," by E. Reissner, *Ingenieur-Archiv*, vol. 7, 1936, pp. 381–396.

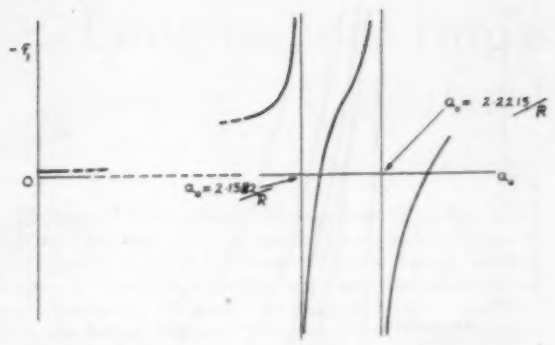

FIG. 4 VARIATION OF f_1 IN CRITICAL RANGE, $\nu = 0$

(*d*) $\nu = 1/2$. Functions f_1 and f_2 are finite for $a_0 > 0$.

For $b > 0$, the amplitude factor $A\mu r_0/P \to 1/ba_0^2$ as $f_1 \to \infty$. Thus the required response curves can be plotted without an exact knowledge of the variation of f_1 and f_2 in the vicinity of the foregoing critical values of a_0.

RESPONSE CURVES

In Figs. 5–7, curves are given showing the relation between the frequency factor at which the amplitude is a maximum and the value of the mass ratio b. For the curves of Figs. 5 and 6, Poisson's ratio equals zero; for those of Fig. 7, $\nu = 1/4$. Each curve represents a different value of the depth ratio R. The experimental points shown in Fig. 6 are taken from Fig. 8(*a*) of Arnold, Bycroft, and Warburton.[1] The experimental values of the physical constants μ and ρ, which are required to convert resonance frequencies into nondimensional frequency factors at resonance, are taken from Table 1 of that paper.

For $\nu > 0$, the theoretical response curves for different values of b have finite maximum amplitudes, except that the curve for a rigid massless plate ($b = 0$) has a maximum at infinity. For $\nu = 0$, each theoretical response curve has an infinite peak at a frequency factor given by

$$1 + ba_0^2 f_1 = 0 \qquad [7]$$

In Table 1, values of the magnification factor are given for various values of the depth factor R and the mass ratio b for $\nu = 1/4$; the magnification factor is $(1/f_1)_{a_0=0} \times$ (maximum value of $A\mu r_0/P$), as $A\mu r_0/P = -f_1$ when the frequency is zero. Magnification factors for a semi-infinite medium for the same values of b (from paper[2]) are also given in Table 1.

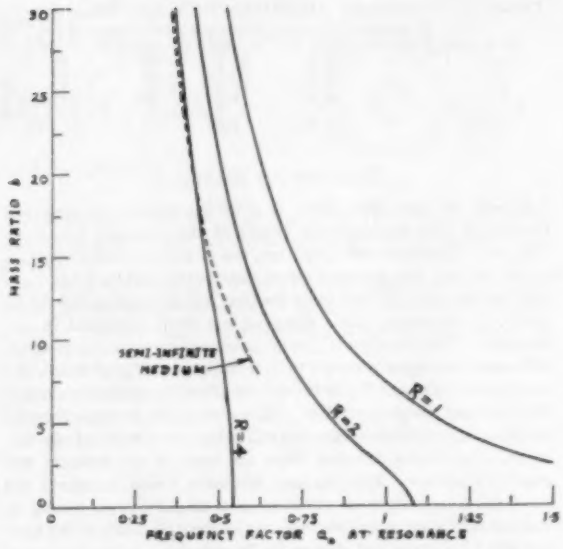

FIG. 5 VARIATION OF FREQUENCY FACTOR AT RESONANCE WITH b AND R, $\nu = 0$

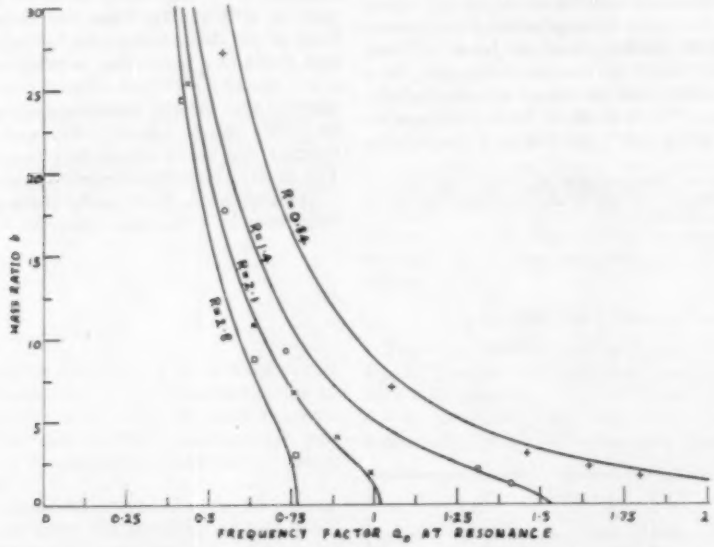

FIG. 6 VARIATION OF FREQUENCY FACTOR AT RESONANCE WITH b AND R, $\nu = 0$

TABLE 1 VALUES OF MAGNIFICATION FACTOR. $\nu = 1/4$

$R = \delta/r_0$	b = 0	5	10	20	30
1	∞	13.0	25.7	46	65
2	∞	11.7	23.7	45	60
3	∞	6.1	12.4	31	47
4	∞	14.2	7.2	19	34
Semi-infinite medium	1	1.21	1.60	2.22	2.72

Discussion of Results

It will be seen that there is good agreement between the theoretical and experimental values of the resonant frequency (Fig. 6). There are two major sources of error in the derivation of the theory; the assumed stress distribution between the mass and the stratum will lead to errors that will increase as the depth factor R decreases; also damping has been neglected in the analysis. The presence of damping in an experimental medium will cause the response curves to have finite peaks for all values of ν but for low values of R this should not affect the derived values of the resonant frequency. For high values of R, an experimental medium with moderate damping will behave as a semi-infinite medium, as no waves reflected from the base of the stratum will reach its surface. Runyan and Anderson,[4] who measured the mechanical impedance of a system consisting of a mass resting on a stratum of sand, concluded that an increase of depth of the sand beyond 8 in. would not change the impedance. As their value of r_0 was 1.435 in., this suggests that for sand a stratum will behave as a semi-infinite medium if $R \geq 5.6$.

In the analysis of this paper damping is neglected and thus waves reflected at the stratum-foundation boundary will return to the surface; this will occur even for large values of the stratum depth. For a semi-infinite medium there can be no reflected waves. Thus the limiting case of the analysis of this paper for a stratum as $R \rightarrow \infty$ is not that of the comparable semi-infinite medium with no damping; this is shown in Table 1 and also by the dotted curves in Figs. 5 and 7, relating to a semi-infinite medium (results taken from the earlier paper[3]). The theoretical curve for $R = 6$ in Fig. 7 has been included in order to show the trend of the theoretical results for higher values of R, but has been shown by a broken line, as this curve alone of those in Figs. 5 to 7 should not be used to predict resonant frequencies for a practical medium with moderate damping. The analysis should be applied only to a stratum with such low values of R and of damping that waves are reflected from the base of the stratum. This could be investigated experimentally for any particular case.

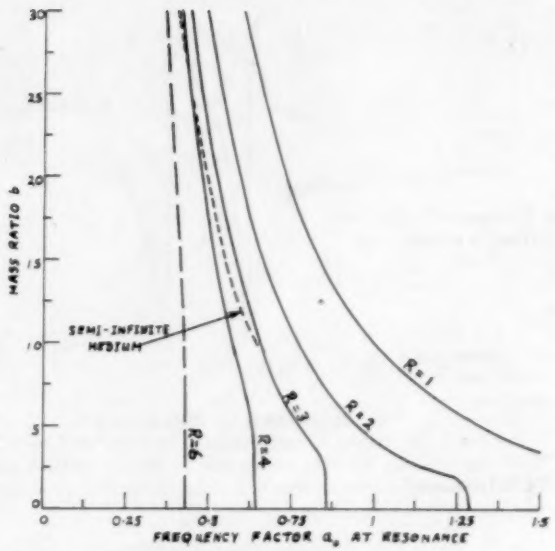

Fig. 7 Variation of Frequency Factor at Resonance With b and R, $\nu = 1/4$

The application of the results of this paper to predict resonant frequencies for a soil-mass system will be published later.

[4] "Mechanical Impedance Measurement of Soils," by W. R. Runyan and R. E. Anderson, *Journal of the Acoustical Society of America*, vol. 28, 1956, pp. 73–76.

Longitudinal Impact of a Semi-Infinite Circular Elastic Bar

By RICHARD SKALAK,[1] NEW YORK, N. Y.

The impact of a semi-infinite elastic bar of circular cross section is studied using the equations of motion of linear-elasticity theory and a method of double-integral transforms. An evaluation of the solution is obtained using approximations which are valid for large values of the time after the initial impact. The numerical results show a continuous dispersion of the wave front and an oscillation which are not found in the usual elementary-theory solution.

Introduction

THE classical theory of the longitudinal motions of an elastic bar leads to the one-dimensional wave equation

$$c_e^2 \frac{\partial^2 u_z}{\partial z^2} = \frac{\partial^2 u_z}{\partial t^2} \quad \ldots\ldots [1]$$

where u_z is the displacement parallel to the axis z of the bar. The constant c_e is the elementary wave velocity

$$c_e^2 = \frac{E}{\rho} \quad \ldots\ldots [2]$$

where E is Young's modulus and ρ is the density. According to this theory the displacements resulting from the impact of a semi-infinite bar have a comparatively simple form. Choosing the origin of z to be at a rigid surface which a bar moving toward the left with velocity v strikes at $t = 0$, there is a step wave of strain set up given by

$$\frac{\partial u_z}{\partial z} = \left\{ \begin{array}{ll} -\dfrac{v}{c_e}, & 0 < z < c_e t \\ 0, & c_e t < z < \infty \end{array} \right\} \quad \ldots\ldots [3]$$

The lateral surfaces of the bar are assumed free of traction and hence there is implied a strain in any direction perpendicular to the axis equal to the negative of Equation [3] times Poisson's ratio ν. This leads to a step wave also in the displacements perpendicular to the axis. Of course, such a discontinuity cannot take place in an actual bar.

The present paper investigates the impact of a semi-infinite bar of uniform circular section using the equations of the linear theory of elasticity. The solution is derived in terms of a double-integral transform and evaluated approximately for large values of the time after the initial impact. The displacements and strains of this solution are continuous and the wave front shows a gradual dispersion over an increasing length of the bar as it progresses.

The dispersive nature of a bar in the three-dimensional theory is known from an exact solution for sinusoidal waves by Pochhammer (1, p. 287).[2] The phase velocities of the various modes of

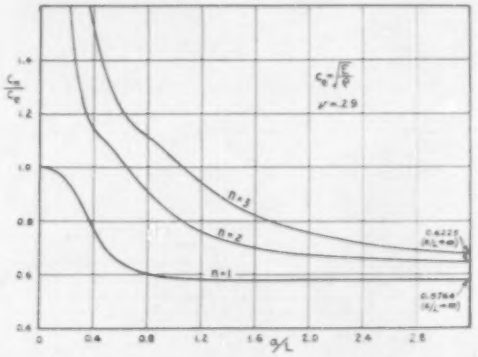

Fig. 1 Phase Velocities of an Infinite Circular Bar

motion in an infinite circular bar vary with the wave length as shown in Fig. 1 for $\nu = 0.29$. Data for this figure are taken from Davies (2). The elementary velocity c_e appears as the first approximation of the phase velocity of the first mode of the exact solution for waves which are long in comparison to the radius of the bar. The c_e appears again in this role in the solution which follows.

Solution by Integral Transforms

The initial conditions of the problem considered are shown in Fig. 2. Two semi-infinite circular bars, moving in opposite directions with speed v, are assumed to meet at the origin of z at time $t = 0$. After time $t = 0$ the bars are assumed to behave as a single, solid, infinite bar. Because of the symmetry, the traction

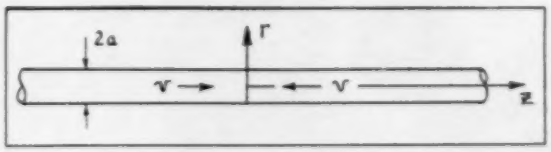

Fig. 2 Initial Conditions

across the plane $z = 0$ is normal to it and the displacements normal to this plane are zero. Each of the original bars is thus confronted by the same boundary conditions as if it had struck a rigid frictionless surface at $z = 0$.

The solution is derived by superposition of two parts. The first part is the solution of the original problem with the further

[1] Assistant Professor, Department of Civil Engineering and Engineering Mechanics, Columbia University.

Contributed by the Applied Mechanics Division and presented at the Annual Meeting, New York, N. Y., November 25–30, 1956, of The American Society of Mechanical Engineers.

Discussion of this paper should be addressed to the Secretary, ASME, 29 West 39th Street, New York, N. Y., and will be accepted until April 10, 1957, for publication at a later date. Discussion received after the closing date will be returned.

Note: Statements and opinions advanced in papers are to be understood as individual expressions of their authors and not those of the Society. Manuscript received by ASME Applied Mechanics Division, December 13, 1955. Paper No. 56—A-37.

[2] Numbers in parentheses refer to the Bibliography at the end of the paper.

condition that a lateral restraint is applied so that the radial displacement u_r is everywhere zero. This results in a compression wave for which

$$u_z = \left\{ \begin{array}{ll} \mp vt, & |\pm z| > c_e t \\ -\dfrac{z}{c_e} v, & -c_e t < z < c_e t \end{array} \right\} \quad \ldots\ldots [4]$$

where c_e is the velocity of dilatational waves in an infinite medium

$$c_e^2 = \frac{\lambda + 2\mu}{\rho}$$

and λ and μ are Lamé constants. In this case the assumed lateral restraint must apply a radial traction to the surface of bar, directed inward, and of magnitude

$$\lambda \frac{\partial u_z}{\partial z} \quad \ldots\ldots [5]$$

The conditions for any time $t > 0$ are shown in Fig. 3.

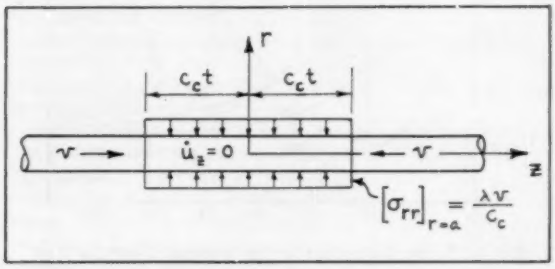

FIG. 3 SOLUTION WITH LATERAL RESTRAINT

The second part of the solution is the response of an infinite bar, initially at rest and unstressed, to a radial traction applied to the surface of the bar, directed outward, and starting from the origin $z = 0$ at $t = 0$. This loading is chosen to be exactly the negative of the traction shown in Fig. 3. When the two parts of the solution are superimposed, their surface tractions cancel and the sum of the two sets of displacements satisfies all conditions and equations governing the original problem.

It remains to find the second part of the solution, the response to the radial loading. The displacement equations of motion for axially symmetric cases are, as given by Love (1, p. 288)

$$\rho \frac{\partial^2 u_r}{\partial t^2} = (\lambda + 2\mu) \frac{\partial \Delta}{\partial r} + 2\mu \frac{\partial \omega_\theta}{\partial z} \quad \ldots\ldots [6]$$

$$\rho \frac{\partial^2 u_z}{\partial t^2} = (\lambda + 2\mu) \frac{\partial \Delta}{\partial z} - \frac{2\mu}{r} \frac{\partial}{\partial r} (r\omega_\theta) \quad \ldots\ldots [7]$$

where

$$\Delta = \frac{1}{r} \frac{\partial (r u_r)}{\partial r} + \frac{\partial u_z}{\partial z} \quad \ldots\ldots [8]$$

and

$$\omega_\theta = \frac{1}{2} \left(\frac{\partial u_r}{\partial z} - \frac{\partial u_z}{\partial r} \right) \quad \ldots\ldots [9]$$

The boundary conditions on the surface of the bar are

$$[\sigma_{rr}]_{r=a} = R(z, t) = \left\{ \begin{array}{ll} \dfrac{\lambda v}{c_e}, & -c_e t < z < c_e t \\ 0, & |z| > c_e t \end{array} \right\} \quad \ldots [10]$$

and

$$[\sigma_{rz}]_{r=a} = 0 \quad \ldots\ldots [11]$$

where σ_{rr} and σ_{rz} are the components of stress and a is the radius of the bar.

The double-integral transform $\bar{g}(\gamma, p)$ of a function $g(z, t)$ is now defined by

$$\bar{g}(\gamma, p) = \frac{1}{4\pi^2} \int_{-\infty}^{\infty} e^{-i\gamma z} dz \int_0^{\infty} g(z, t) e^{-ipt} dt \quad \ldots [12]$$

The inversion formula of this transformation is

$$g(z, t) = \int_{-\infty}^{\infty} e^{i\gamma z} d\gamma \int_{-\infty - ia}^{\infty - ia} \bar{g}(\gamma, p) e^{ipt} dp \quad \ldots [13]$$

The transformation from t to p is the Laplace transform with the usual transform variable replaced by ip. The transformation from z to γ is a Fourier integral transform. Provided $g(z, t)$ and its time derivatives are zero at $t = 0$, the double transform of

$$\frac{\partial^{n+s} g(z, t)}{\partial z^n \partial t^s}$$

is $(i\gamma)^n (ip)^s \bar{g}(\gamma, p)$.

Four equations involving the double transforms $\bar{u}_r$, $\bar{u}_z$, $\bar{\Delta}$, and $\bar{\omega}_\theta$ are obtained by applying the transformation [12] to Equations [6], [7], [8], and [9]. From the transformed equations, $\bar{u}_r$ and $\bar{u}_z$ may be eliminated, yielding two equations in $\bar{\Delta}$ and $\bar{\omega}_\theta$

$$\frac{\partial^2 \bar{\Delta}}{\partial r^2} + \frac{1}{r} \frac{\partial \bar{\Delta}}{\partial r} + h^2 \bar{\Delta} = 0 \quad \ldots\ldots [14]$$

$$\frac{\partial^2 \bar{\omega}_\theta}{\partial r^2} + \frac{1}{r} \frac{\partial \bar{\omega}_\theta}{\partial r} + \left(k^2 - \frac{1}{r^2} \right) \bar{\omega}_\theta = 0 \quad \ldots\ldots [15]$$

where

$$h^2 = \frac{\rho p^2}{\lambda + 2\mu} - \gamma^2 \quad \ldots\ldots [16]$$

$$k^2 = \frac{\rho p^2}{\mu} - \gamma^2 \quad \ldots\ldots [17][3]$$

From Equations [14] and [15] it follows that $\bar{\Delta}$ and $\bar{\omega}_\theta$ are of the form

$$\bar{\Delta} = BJ_0(hr) \quad \ldots\ldots [18]$$

$$\bar{\omega}_\theta = DJ_1(kr) \quad \ldots\ldots [19]$$

where B and D are functions of γ and p and J_0 and J_1 are the Bessel functions of order 0 and 1. Equations [18] and [19] are used to replace $\bar{\Delta}$ and $\bar{\omega}_\theta$ in the transforms of Equations [6] and [7]. These equations are then solved for $\bar{u}_r$ and $\bar{u}_z$. Thus

$$\bar{u}_r = A \frac{\partial}{\partial r} [J_0(hr)] + C\gamma J_1(kr) \quad \ldots\ldots [20]$$

$$\bar{u}_z = i\gamma A J_0(hr) + \frac{i}{r} C \frac{\partial}{\partial r} [rJ_1(kr)] \quad \ldots\ldots [21]$$

where A and C are functions of γ and p.[4]

The Boundary Conditions [10] and [11] determine the functions A and C. The stresses σ_{rr} and σ_{rz} are first expressed in terms of the displacements u_r, u_z. These equations are transformed by [12] and $\bar{u}_r$ and $\bar{u}_z$ are replaced by Equations [20] and [21]. The results are

[3] Reference (1), p. 289, equation [51].
[4] Ibid., (1), p. 289, equation [53].

$$A\left[2\mu\frac{\partial^2 J_0(ha)}{\partial a^2}-\frac{p^2\rho\lambda}{\lambda+2\mu}J_0(ha)\right]+2\mu C\gamma\frac{\partial J_1(ka)}{\partial a}=\overline{R}\quad[22]$$

$$2\gamma A\frac{\partial J_0(ha)}{\partial a}+C\left(2\gamma^2-\frac{\rho p^2}{\mu}\right)J_1(ka)=0\quad[23]$$

where $\overline{R}$ is the transform of the load function $R(z, t)$ in Equation [10].[5] Solving Equations [22] and [23] simultaneously

$$A=\frac{\overline{R}}{F}\left(2\gamma^2-\frac{\rho p^2}{\mu}\right)J_1(ka)\quad[24]$$

$$C=-\frac{2\overline{R}\gamma}{F}\frac{\partial J_0(ha)}{\partial a}\quad[25]$$

where

$$F=\left[2\mu\frac{\partial^2 J_0(ha)}{\partial a^2}-\frac{p^2\rho\lambda}{\lambda+2\mu}J_0(ha)\right]\left(2\gamma^2-\frac{\rho p^2}{\mu}\right)J_1(ka)-2\mu\gamma\frac{\partial J_1(ka)}{\partial a}2\gamma\frac{\partial J_0(ha)}{\partial a}\quad[26]$$

The equation $F = 0$ is the frequency equation for free vibrations derived by Pochhammer.[6] This fact is utilized in the subsequent development.

The solution for u_r and u_z is completed by substituting the values of A and C, Equations [24] and [25], into Equations [20] and [21] and then inverting according to Equation [13]. This yields u_r and u_z as double integrals for any loading $R(z, t)$. In the case at hand R is specified by Equation [10] and

$$\overline{R}=\frac{\lambda v}{2\pi^2 c_e^2\left(\gamma^2-\frac{p^2}{c_e^2}\right)}\quad[27]$$

Hence the second part of the solution of the original problem is given by

$$u_r=\frac{v}{2\pi^2}\int_{-\infty}^{\infty}\int_{-\infty-i\alpha}^{\infty-i\alpha}\frac{-\lambda\left(2\gamma^2-\frac{\rho p^2}{\mu}\right)hJ_1(ka)J_1(hr)+2\lambda\gamma^2 hJ_1(ha)J_1(kr)}{c_e^2\left(\gamma^2-\frac{p^2}{c_e^2}\right)F}e^{i(\gamma z+pt)}d\gamma dp\quad[28]$$

$$u_z'=\frac{v}{2\pi^2}\int_{-\infty}^{\infty}\int_{-\infty-i\alpha}^{\infty-i\alpha}\frac{-\gamma^2\lambda\left(2\gamma^2-\frac{\rho p^2}{\mu}\right)J_1(ka)J_0(hr)-\gamma^2 2\lambda hkJ_1(ha)J_0(kr)}{c_e^2\left(\gamma^2-\frac{p^2}{c_e^2}\right)F}e^{i(\gamma z+pt)}d\gamma dp\quad[29]$$

[5] Reference (1), p. 289, equation [54].
[6] Ibid., p. 289.

Equation [29] is for the strain in the axial direction u_z' where the prime indicates differentiation with respect to z. The strain is computed rather than u_z itself because this simpifies the subsequent work.

The first integral involving p in Equations [28] and [29] may be evaluated by Cauchy's residue theorem applied in the complex p-plane. The computation for u_z' is typical. The path of integration is closed by a semicircle of infinite radius about the origin in the upper half of the p-plane. The integral over the semicircle is zero so the original integral is equal to $2\pi i$ times the sum of the residues at the poles enclosed.

If the numerator and the denominator of Equation [29] are each multiplied by k and the various Bessel functions are replaced by their respective infinite series, it is found that only even powers of h and k appear. Hence there are no branch points in the complex p-plane in spite of the fact that h and k are irrational functions of p.

On the infinite semicircle, the various Bessel functions may be replaced by the asymptotic forms which they approach for large arguments. In the limit it is found that the magnitude of the integrand of Equation [29], excluding the exponential factor, is proportional to $(p^2)^{-2}$. This insures that the integral over the infinite semicircle vanishes.

There are poles of the integrand of Equation [29] at $p = \pm\gamma c_e$ due to the factor

$$[\gamma^2-(p/c_e)^2]$$

in the denominator. The residues at these poles yield contributions to u_z' which are

$$u_z'=\frac{v}{2\pi i c_e}\int_{-\infty}^{\infty}\frac{e^{i\gamma(z-c_e t)}}{\gamma}d\gamma-\frac{v}{2\pi i c_e}\int_{-\infty}^{\infty}\frac{e^{i\gamma(z+c_e t)}}{\gamma}d\gamma=\frac{v}{c_e}H(z+c_e t)-\frac{v}{c_e}H(z-c_e t)\quad[30]$$

where H is the Heaviside unit step function. The strain expressed by Equation [30] exactly cancels the strain due to the first part of the solution expressed by Equation [4].

The remaining poles of Equation [29] for any values of γ are at the points in the p-plane at which $F(\gamma, p) = 0$. These points are designated

$$p_n=p_n(\gamma)=\pm c_n\gamma\quad[31]$$

The functions $p_n(\gamma)$ are the circular frequencies of free vibration for an infinite bar in terms of the wave number $\gamma = 2\pi/L$ where L is the wave length. This follows from the fact that $F = 0$ is the frequency equation. The frequencies p_n may be expressed in terms of the phase velocities c_n as indicated in Equation [31]. The phase velocities are shown in Fig. 1 for $\nu = 0.29$.

The contributions from the poles due to the zeros of F are

$$u_z'=\frac{vi}{\pi}\int_0^{\infty}\sum_n\left[\frac{-\gamma^2\lambda\left(2\gamma^2-\frac{\rho p^2}{\mu}\right)J_1(ka)J_0(hr)-\gamma^2 2\lambda hkJ_1(ha)J_0(ka)}{c_e^2\left(\gamma^2-\frac{p^2}{c_e^2}\right)\frac{\partial F}{\partial p}}e^{i(\gamma z+pt)}\right]_{p=p_n}d\gamma\quad[32]$$

Equation [32] is the complete expression for the axial strain in the original problem. A similar expression may be derived from Equation [28] for u_r.

$$u_r = \frac{vi}{\pi}\int_0^\infty \sum_n \left[\frac{-\lambda\left(2\gamma^2 - \frac{\rho p^2}{\mu}\right) hJ_1(ka)J_1(hr) + 2\lambda\gamma^2 hJ_1(ha)J_1(kr)}{c_e^2\left(\gamma^2 - \frac{p^2}{c_e^2}\right)\frac{\partial F}{\partial p}} e^{i(\gamma z + pt)}\right]_{p=p_n} d\gamma \quad [33]$$

Evaluation of u_z' and u_r for Large Values of t

It would be difficult to carry out the integrations in Equations [32] and [33] because the p_n are known only through the transcendental equation $F = 0$. Some information can be obtained by making approximations valid for large values of t.

If z is chosen equal to $c't$ in Equation [32], where c' is an arbitrary constant velocity, the integrals take on a form to which the method of stationary phase[7] may be applied for large values of t. According to this method the integrals over the various p_n-curves will all be at most of order $1/\sqrt{t}$ when t is sufficiently large except for contributions arising from points where the denominator of the integrand approaches zero.

This denominator would be zero if $\partial F/\partial p$ were zero at any point on the p_n versus γ curves. However, this does not occur. Consider F as a function of γ and p defined by Equation [26]. In the p, γ-plane, the lines $F(p, \gamma) = 0$ are the lines p_n versus γ; i.e., the natural frequencies. Along any such curve $\partial F/\partial S_1 = 0$, S_1 being the direction along the curve. If at any point $\partial F/\partial p = 0$ also, then it is easily shown $\partial F/\partial S = 0$ for any direction S through this point, provided the curve $F = 0$ does not have a tangent parallel to the p-axis at this point. The condition $\partial F/\partial S = 0$ means that the function $F(p, \gamma)$ is either at a maximum, a minimum, or a stationary point. If it is maximum or minimum, a curve $F(p, \gamma) = 0$ could not pass through it. If it were a stationary point, there would be two lines $F(p, \gamma) = 0$ passing through it. But it is known that there are no such branch points by inspection of the p_n versus γ curves. Also, there is no point where a p_n versus γ curve is parallel to the p-axis. Hence there are no points on the p_n versus γ curves at which $\partial F/\partial p = 0$.

The denominator in Equation [32] is, however, zero at the point which is at $\gamma = 0$ in the integral over p_1, the first mode frequencies. At this point the factor $[\gamma^2 - (p_1/c_e)^2]$ is zero because p_1 approaches zero with γ. The essential contribution to u_z' which does not decay with time is

$$u_z' = \frac{vi}{2\pi}\int_{-\epsilon}^{+\epsilon} \frac{N}{G}\left[e^{i(\gamma z + c_1\gamma t)} - e^{i(\gamma z - c_1\gamma t)}\right] d\gamma \quad [34]$$

where N and G are the numerator and denominator, respectively, of the integrand of Equation [32] with p replaced by $c_1\gamma$ and ϵ is a small positive number. The two exponential terms are derived from the fact that there are two solutions of $F = 0$ for the first mode, namely, $p_1 = \pm c_1\gamma$ where c_1 is the magnitude of the phase velocity. The functions N and G in Equation [34] are replaced by their limiting values as γ approaches zero since ϵ may be chosen indefinitely small. The ratio N/G may be shown to have a limit of $1/\gamma c_e$, after considerable algebra not shown here. Two terms of the expansion of c_1 about $\gamma = 0$ are used to approximate c_1 in the exponential terms of Equation [34]. If only one term is used, the end results are exactly the elementary theory solution (3). The two terms used here are given by Love[8]

$$c_1 = c_e - d\gamma^2 \quad [35]$$

where

$$d = \frac{1}{4}\nu^2 a^2 c_e \quad [36]$$

With the foregoing approximations, Equation [34] becomes

$$u_z' = \frac{vi^2}{2\pi c_e}\int_{-\infty}^{\infty}\left[\frac{\sin(\gamma z + c_e\gamma t - d\gamma^3 t)}{\gamma} - \frac{\sin(\gamma z - c_e\gamma t + d\gamma^3 t)}{\gamma}\right] d\gamma \quad [37]$$

where the limits have been extended from $\pm\epsilon$ to $\pm\infty$. This is permissible because the integrals so added are of order $1/\sqrt{t}$ which is negligible in the present approximation.

Equation [37] may be written in the form

$$u_z' = \frac{v}{\pi c_e}\int_0^\infty \left[\frac{\sin(\gamma z'' + d\gamma^3 t)}{\gamma} + \frac{\sin(\gamma z' + d\gamma^3 t)}{\gamma}\right] d\gamma \quad [38]$$

where

$$\left.\begin{aligned} z'' &= -z - c_e t \\ z' &= z - c_e t \end{aligned}\right\} \quad [39]$$

The new co-ordinate z' measures the distance of any given point (z, t) ahead or behind a point starting from $z = 0$ at $t = 0$ and moving in the positive direction with velocity c_e. The latter is the location of the wave front in the elementary-theory solution (3) and will be called the wave-front point. The z'' has a similar significance for a wave-front point moving in the negative direction.

By a change of the variable of integration, Equation [38] becomes

$$u_z' = \frac{v}{c_e}\left[\frac{1}{\pi}\int_0^\infty \frac{\sin\left(\alpha''\eta + \frac{1}{3}\eta^3\right)}{\eta} d\eta + \frac{1}{\pi}\int_0^\infty \frac{\sin\left(\alpha'\eta + \frac{1}{3}\eta^3\right)}{\eta} d\eta\right] \quad [40]$$

where

$$\alpha'' = \frac{z''}{\sqrt[3]{(3dt)}} \qquad \alpha' = \frac{z'}{\sqrt[3]{(3dt)}} \quad [41]$$

The integrals in Equation [40] are functions of α'' and α' which are related to Airy's integral $Ai(\alpha)$

$$Ai(\alpha) = \frac{1}{\pi}\int_0^\infty \cos\left(\alpha\eta + \frac{1}{3}\eta^3\right) d\eta \quad [42]$$

Airy's integral has been tabulated by Airy and others (4). $Ai(\alpha'')$ is the derivative with respect to α'' of the first integral in Equation [40]. Similarly, $Ai(\alpha')$ is the derivative of the second integral. Hence

[7] Reference (3), p. 505.
[8] Reference (1), p. 290.

$$u_z' = \frac{v}{c_e}\left[\frac{1}{6} + \int_0^{\alpha''} Ai(\alpha)d\alpha + \frac{1}{6} + \int_0^{\alpha'} Ai(\alpha)d\alpha\right] \quad [43]$$

where the 1/6 terms are the values of the first and second integrals of Equation [40] for $\alpha'' = 0$ and $\alpha' = 0$, respectively, which may be obtained by a contour integration. The values of the integrals in Equation [40] also may be obtained directly for points far ahead or far behind the wave-front point by neglecting the term η^3 in the numerators and performing a contour integration. The results show that far ahead and far behind the wave-front point the present solution agrees with the elementary solution (3). For points near $z'' = 0$ or $z' = 0$, Equation [43] is used. The integrals of Airy's integral indicated in Equation [43] are computed numerically using the tables of Airy's integral given by Miller (4).

The same approximations that have been used in evaluating u_z' may be used for u_r. The final result is

$$u_r = -\gamma r u_z' \quad [44]$$

where u_z' is given by Equation [43]. This shows that in the present approximation the relationship of the radial strain to the longitudinal strain at any point is the same as in a longitudinally stressed bar at rest. The numerical results for u_z' and u_r are shown in Figs. 4 and 5.

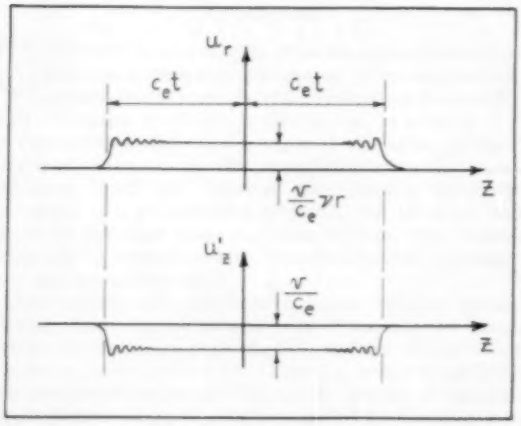

FIG. 4 LONG TIME APPROXIMATION OF u_z' AND u_r

In the natural co-ordinates of (z, t), the wave form shown in Fig. 5 gradually spreads out around the moving wave-front point, $z' = 0$. Consider a point moving so that the strains at its location are constant. This requires $\alpha' = \text{const}$, say α_0', which by Equation [41] requires

$$z' = \alpha_0' \sqrt[3]{(3dt)} \quad [45]$$

Equation [45] states that, for constant strain, a point must continually move away from the wave-front point. This shows the dispersion of the wave form.

The overshooting of the elementary-theory value by the initial rise in the wave form of Fig. 5 is attributed to radial inertia. This and the subsequent oscillations are discussed later.

APPROXIMATE THEORIES AND EXPERIMENTS

The complexity of working with the equations of elasticity (5) and (6), has led to the development of various approximate theories. The first improvement in Equation [1] was suggested

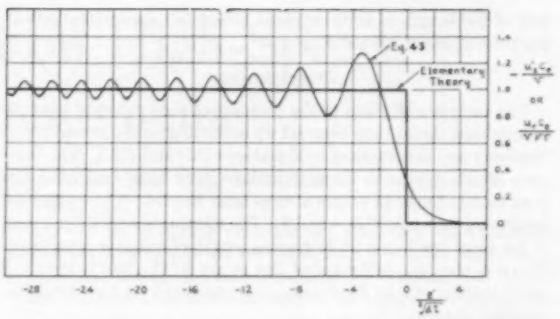

FIG. 5 SHAPE OF TYPICAL WAVE FRONT

by Rayleigh (6) and takes into account the radial inertia. The corresponding equation of motion

$$c_e^2 \frac{\partial^2 u_z}{\partial z^2} = \frac{\partial^2 u_z}{\partial t^2} - \frac{\nu^2 a^2}{2}\frac{\partial^4 u_z}{\partial z^2 \partial t^2} \quad [46]$$

appears in Love.[9] A more complete theory incorporating two degrees of freedom is given by Mindlin and Herrmann (5, 7). Another approximate theory has been given by Sutton (8).

If an approximate theory is used to solve the impact problem treated previously, similar results may be expected if the same long-time approximations are used. The information essential to the foregoing development is primarily the first two terms of the expansion of the phase velocity of the first mode c_1, about $\gamma = 0$. If these two terms are preserved by the approximate theory, it may be expected to yield results quite similar to the solution just given.

In the case of Rayleigh's correction leading to Equation [46], the first two terms of the expansion of the phase velocity about $\gamma = 0$ are identical to those of the Pochhammer solution for the first mode. Davies (2) has used Equation [46] to solve for the displacements at one end of a bar when the other end is subjected to a suddenly applied force. He derives the "pressure in the bar" by differentiation of the displacement curve. This pressure curve, shown in his Fig. 32,[10] is comparable to Fig. 5 of the present paper which shows the axial strain. If the horizontal scale of Fig. 5 is adjusted to agree with the particular radius and length used by Davies for his bar A, the two figures agree quite closely. The bar A was 193.5 cm long and 1.27 cm in radius. Davies used a trignometric series or mode approach retaining 80 to 90 terms. His results are limited to the particular ratio of length to radius selected for computation, while the result shown in Fig. 5 is more general.

The agreement of the Davies' and the present solution indicates that the effects described by the present solution are due to the radial inertia since this is the only factor included by Davies which is not contained in the elementary Equation [1].

Davies also shows some experimental results which confirm the existence of the oscillations and of the overshooting of the elementary-theory value by the initial rise as shown in Fig. 5. Some further experimental results are given by Curtis (9). The wave forms he shows have a leading portion closely resembling Fig. 5. However, the wave forms obtained at a moderate distance from the impact end of the bar ($z/a = 79$), show additional components which are identified by Curtis as a contribution of the second mode of vibration and an effect due to the fact that the first mode has a certain minimum group velocity. These results give an indica-

[9] Reference (1), p. 428.
[10] Reference (2), p. 441.

tion of the length of time required before the approximations of the present paper are valid.

Conclusions

The complete solution of the problem of the impact of a semi-infinite circular bar has been set up according to the equations of elasticity and is contained in Equations [32] and [33]. The integrals which appear in these equations have been evaluated approximately for large values of time after impact. The numerical results are shown in Figs. 4 and 5. The solution shows a dispersion of the wave front over an increasing length of bar as it progresses. There is also an oscillation of the strain in the bar behind the wave front about its final value, not predicted by the usual elementary theory.

BIBLIOGRAPHY

1 "Theory of Elasticity," by A. E. H. Love, Cambridge University Press, Cambridge, England, fourth edition, 1927, p. 287.

2 "A Critical Study of the Hopkinson Pressure Bar," by R. M. Davies, Transactions of the Royal Society of London, England, series A, vol. 240, 1948, p. 375.

3 "Methods of Mathematical Physics," by H. Jeffreys and B. S. Jeffreys, Cambridge University Press, Cambridge, England, second edition, 1950.

4 "The Airy Integral," by J. C. P. Miller, Mathematical Tables, published for the British Association at the Cambridge University Press, Part-Volume B, 1946.

5 "A One-Dimensional Theory of Compressional Waves in an Elastic Rod," by R. D. Mindlin and G. Herrmann, Proceedings of the First U. S. National Congress of Applied Mechanics, June, 1951, p. 187.

6 "Theory of Sound," by Lord Rayleigh, Dover Publications, New York, N. Y., 1945, p. 251.

7 "Application of Green's Method in Deriving Approximate Theories of Elasticity," by G. Herrmann, ONR Project NR-064-388, Contract Nonr-266(09), Technical Report No. 13, February, 1954.

8 "An Intermediate Theory of Longitudinal Stress Waves in Bars," by G. W. Sutton, ONR Project NR 062-059, Contract N6onr-24420, Report No. 21-18, September, 1954.

9 "Second Mode Vibrations of the Pochhammer-Chree Frequency Equation," by C. W. Curtis, *Journal of Applied Physics*, vol. 25, July, 1954, p. 928.

Some New Data on High-Speed Impact Phenomena

By J. H. HUTH,[1] J. S. THOMPSON,[2] and M. E. VAN VALKENBURG[3]

This paper presents a summary of some recent experimental work aimed at evaluating the role of various physical parameters in high-speed impact phenomena. It is shown that penetration into thick targets by projectiles of the same material, for certain common metals, can be expressed approximately through a single relationship of the form $(p/d) = 2.5(V/c)^{1.4}$ in a range of about $0.1 \leq (V/c) \leq 1.0$. Here p represents penetration (crater depth) measured from the initial target surface, d a characteristic dimension of the projectile, and V the impact velocity. c is the "sonic" velocity in the projectile and target material as expressed by the formula $c = \sqrt{E/\rho}$, where E is Young's modulus and ρ the density. Experimental results are given for steel, aluminum, brass, lead, magnesium, and a magnesium-lithium alloy.

Introduction

CURRENT interest in space flight raises the question of possible damage from meteoric impacts. If one accepts the hypothesis that all meteoric orbits are elliptical, the possibility exists of impacts at relative speeds as high as about 2×10^5 fps (the parabolic speed in the region of the earth's orbit). A number of penetration theories are available for impact velocities well below 10,000 fps. However, they generally involve the assumption of a nondeforming projectile, and hence are inapplicable in the speed range of current interest. (For example, see chapter 12 of reference 1.[4]) Therefore, further experimental work was deemed desirable.

Unfortunately any experimental impact research program utilizing present-day equipment must of necessity be content with accelerating macroscopic particles to fairly modest velocities—of the order of 10,000 fps. However, even with this limitation, some fundamental knowledge of the physics of high-speed impact phenomena can be obtained provided the experiments are specifically designed with this goal in mind. An analysis of the problem is presented in the next section, followed by a description of such experiments.

Analysis

Although many phenomena (such as spalling, perforation, etc.) are of interest, the experiments reported herein were aimed specifically at studying cratering in relatively thick targets. In order to extrapolate the results of such a complex occurrence, or even offer a scientific interpretation, it is necessary to reduce to an absolute minimum the number of parameters involved.

The simplest cratering experiment possible can be formulated as follows: Fire a sphere in a vacuum at normal incidence against a semi-infinite target, and make the target and sphere of the same material. Under these circumstances the penetration p (crater depth measured from the original surface level) should be a function of the sphere diameter d, the impact velocity V, and various properties of the material. In dimensionless form one possible relationship might be

$$\left(\frac{p}{d}\right) = f\left\{\left(\frac{V}{c}\right), \left(\frac{V^2}{Q}\right), \left(\frac{Vd}{\alpha}\right)\right\} \quad \text{[1]}$$

where

- c may be interpreted as either a shock or sonic speed in the target and pellet material.
- Q is the energy per unit mass required to either melt, vaporize, or otherwise remove the material that originally occupied the crater.
- α is the thermal diffusivity.

(The foregoing definitions are still quite general. Exact definitions of c and Q as actually used will be given at the end of this section.)

Equation [1] is obviously a gross simplification, inasmuch as many other material properties might have been included. However it can encompass at least two current theories of cratering. For example, if the effect of (V^2/Q) predominates, then Equation [1] can agree phenomenologically with the "high velocity" theory of Rinehart (1) in which crater volume is proportional to the kinetic energy of the pellet, and the craters themselves are of constant shape.[5] On the other hand, if (V/c) predominates, and c is taken as equal to $\sqrt{k/\rho}$ where k represents a target "strength parameter" and ρ the mass density, then Equation [1] can agree with Öpiks (2) modified hydrodynamic theory. (In this case c would correspond to Öpiks V'.) This explains the choice of Equation [1] as an interesting relationship.

Specifically, experiments were then designed to determine if (p/d) could, for a variety of metals, be expressed solely in terms of either (V/c) or (V^2/Q) when c and Q are defined as follows: Let the symbol c represent $\sqrt{E/\rho}$ where E is Young's modulus and ρ the density, while Q represents the energy per unit mass required to heat and melt a given metal.

Experimental Program

Experiments essentially based on the model expressed by Equation [1] have been carried out by two separate groups. One such program was carried out at the Naval Research Laboratory by Mr. Thompson, while the other was conducted at the University of Utah.[6]

---

[1] Engineer, Rand Corporation, Santa Monica, Calif. Mem. ASME.

[2] Engineer, Rand Corporation, Santa Monica, Calif.

[3] Associate Professor of Electrical Engineering, University of Utah, Salt Lake City, Utah.

[4] Numbers in parentheses refer to the Bibliography at the end of the paper.

Contributed by the Applied Mechanics Division and presented at the Annual Meeting, New York, N. Y., November 25–30, 1956, of The American Society of Mechanical Engineers.

Discussion of this paper should be addressed to the Secretary, ASME, 29 West 39th Street, New York, N. Y., and will be accepted until April 10, 1957, for publication at a later date. Discussion received after the closing date will be returned.

Note: Statements and opinions advanced in papers are to be understood as individual expressions of their authors and not those of the Society. Manuscript received by ASME Applied Mechanics Division, May 15, 1956. Paper No. 56—A-15.

[5] If $(p/d) = (V^2/Q)^{1/2}$ then Q would be directly proportional to Rinehart's k_1 factor.

[6] This research was supported by the U.S. Air Force, through the Office of Scientific Research of the Air Research and Development Command.

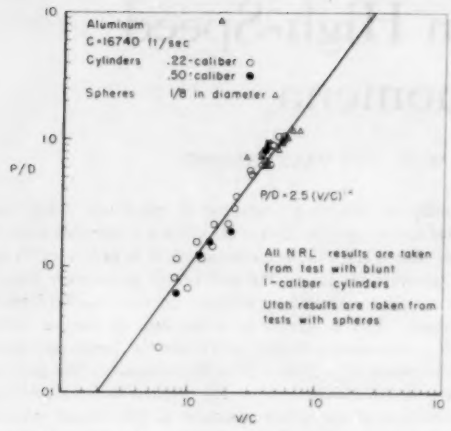

FIG. 1 CALIBERS OF PENETRATION AS A FUNCTION OF MACH NUMBER

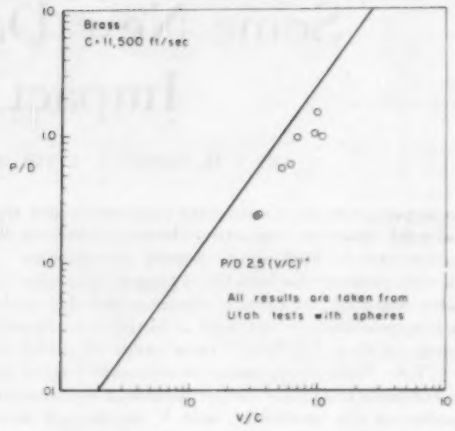

FIG. 4 CALIBERS OF PENETRATION AS A FUNCTION OF MACH NUMBER

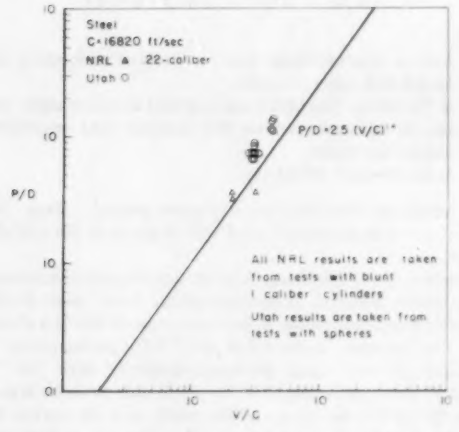

FIG. 2 CALIBERS OF PENETRATION AS A FUNCTION OF MACH NUMBER

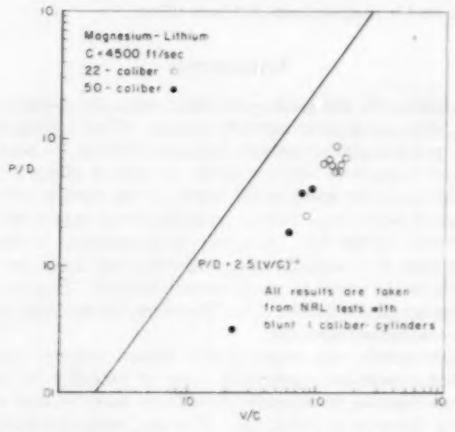

FIG. 5 CALIBERS OF PENETRATION AS A FUNCTION OF MACH NUMBER

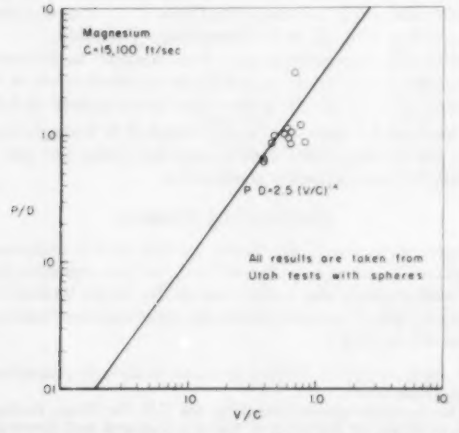

FIG. 3 CALIBERS OF PENETRATION AS A FUNCTION OF MACH NUMBER

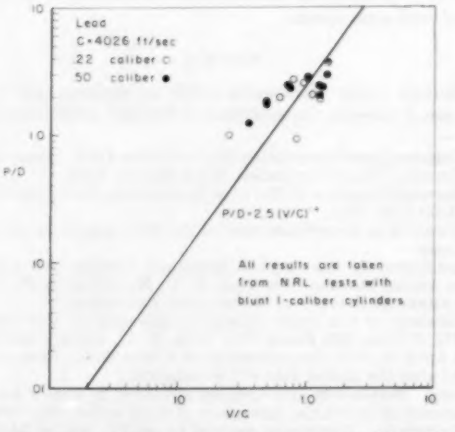

FIG. 6 CALIBERS OF PENETRATION AS A FUNCTION OF MACH NUMBER

The technique used by the two groups were quite different. At NRL the pellets were fired from guns, and the speeds measured photographically. The use of guns dictated a switch from spheres to cylinders one caliber long (length/diameter = 1), but gave results with remarkably little scatter. The firing program included lucite, teflon, lead, aluminum, a magnesium-lithium alloy,[7] and steel. Lucite, through its transparency, also permitted motion pictures to be taken of the actual cratering. The camera used was the University of Rochester Institute of Optics high-speed camera and Printer, Model II (3). This device provided frame frequencies of 20×10^3 and 4×10^6 frames per sec.

At Utah, $^1/_8$-in-diam spheres were accelerated by means of a cylindrical explosive charge. Their technique has been described in a recent publication (4). They fired brass, aluminum, magnesium, and steel pellets. In both cases, most firings were made in air.

In principle, the materials should be chosen so as to separate the effects of the three parameters in Equation [1]. (For example, tin and platinum have nearly identical c, but quite different Q.) However, in this preliminary work selection was made more on the practical basis of availability.

Results

The results of the experimental investigations are shown in Figs 1–12. First it was found that, for various metals, (p/d) could be correlated fairly well on the basis of the Mach number (V/c), where c is the sound speed as defined previously.[8]

Penetration in calibers apparently may be expressed in terms of the Mach number, for most metals, as follows

$$\left(\frac{p}{d}\right) = k\left(\frac{V}{c}\right)^n \quad \ldots\ldots\ldots\ldots\ldots\ldots\ldots\ldots\ldots\ldots [2]$$

where $k = 2.5$, $n = 1.4$, and (V/c) is in the range of about $0.1 \leq (V/c) \leq 1.0$.

(The fact that for the lithium-magnesium alloy, k would have to be altered is not too surprising. Lithium itself is also an anomaly in that it melts at 0.9 of its characteristic temperature (5) which, by Debye's approximation, is directly related to mean velocity of sound for long waves in a crystal.) The lithium-magnesium and brass results taken together indicate a possible alloying effect on k.

Figs. 8 and 9 indicate that the crater volume is not precisely proportional to either energy or momentum. Also a marked size effect is apparent. However, a direct dependence on energy would be an approximation over selected intervals. For lead[9] the constant of proportionality (between kinetic energy and mass of displaced material) is about 3.5 gm cal/gm (heat of fusion of lead is 5.9 gm cal/gm), while for aluminum it is 367 gm cal/gm (heat of fusion of aluminum is 76.8 gm cal/gm). However, a subsequent sectioning and etching of the Al and Mg-Li craters ($V = 7600$ fps) revealed no evidence of melting. A similar conclusion was reached in the case of lead ($V = 5000$ fps). (The lead pellets apparently vaporized.)

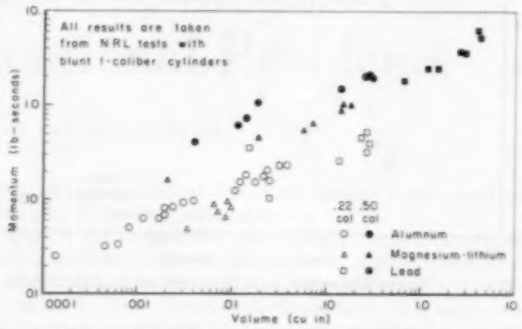

Fig. 8 Crater Volume as a Function of Momentum of the Impacting Particle

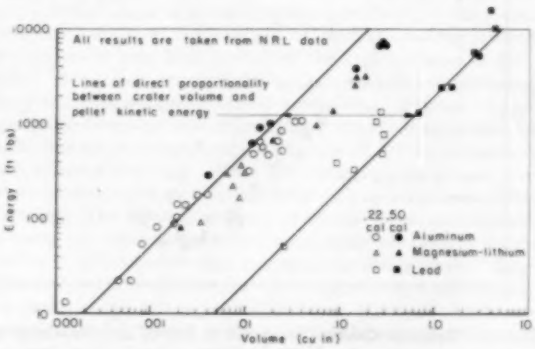

Fig. 9 Crater Volume as a Function of Energy of the Impacting Particle

The tendency toward a lessening of penetration in lead as (V/c) exceeds 1 (see Fig. 6) is interesting, but should be checked by further experimentation. In this connection, plastics with low sonic speeds also were fired in an effort to investigate the supersonic regime. Unfortunately the plastics chosen, lucite and teflon, tended to crater quite differently from metals and the results could not be used to predict metal performance.

However the lucite was of interest in an attempt to photograph an actual crater in the process of formation. The resulting pictures indicated a shock-wave velocity in lucite of the order of 9000 fps.

It is of interest also to compare the cratering with Baldwin's (6) correlations for explosion pits and lunar craters. (These correlations relate crater diameters and depths, and explosion-pit

[7] The ratio of magnesium to lithium by weight was about 6.

[8] However, it should be noted that for the metals chosen, c and $\sqrt{Q}$ tend to vary together.

[9] Rinehart (1) gives a value of 5.26 gm cal/gm for lead.

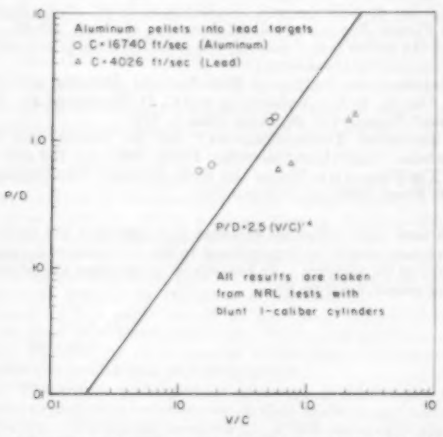

Fig. 7 Calibers of Penetration as a Function of Mach Number

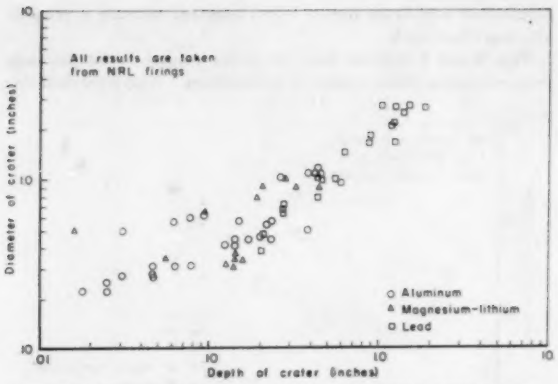

FIG. 10 CRATER DIAMETER AS A FUNCTION OF CRATER DEPTH

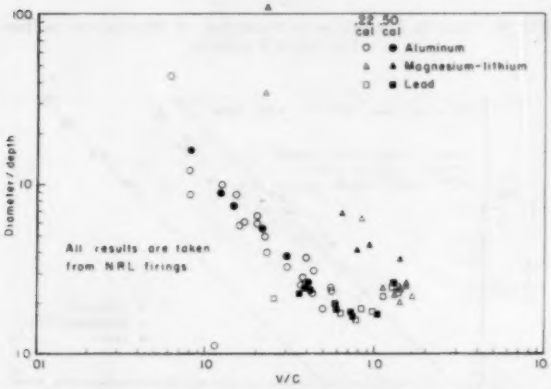

FIG. 11 RATIO OF CRATER DIAMETER TO DEPTH AS A FUNCTION OF MACH NUMBER

diameters with energy release.) The relationship of diameters to depths of the current series of craters, Figs. 10 and 11, is similar to the corresponding relationship for explosion pits, but of course on a reduced scale. Specifically, Figs. 10 and 11 first show that at low velocities the crater is just an indentation with a nearly constant diameter equal to that of the impacting cylinder. At high velocities, the craters again begin to become relatively shallower. Fig. 12 relating crater diameter to energy is also similar to Baldwin's corresponding correlation if the energy scaling is the square of the linear scaling.

CONCLUSIONS

It has been rather well established that the approach suggested in this paper will lead to meaningful experiments, that within the range of speeds tested melting or vaporization does not play a large role in target cratering, and that penetration by metallic pellets into targets of the same material can be expressed through Equation [2]. Fig. 8 gives some indication of the error to be expected from this relationship when widely different metals are involved. It is interesting to note that the exponent of V in

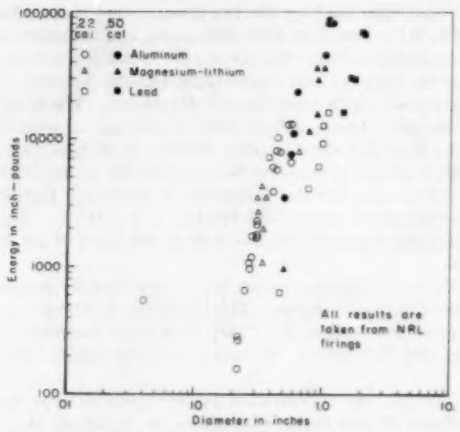

FIG. 12 CRATER DIAMETER AS A FUNCTION OF ENERGY OF THE IMPACTING PARTICLE

Equation [2] lies between the exponents in Rinehart's (1) low- and high-velocity approximations.[10] Quite possibly the dependence of p on V will further decrease at higher speeds, as a result of increasingly shallow craters.

Also, within the limit of experimental error, penetration has been shown to be directly proportional to a characteristic dimension of the pellet. Small changes in the shape of the pellet also have proved inconsequential.

ACKNOWLEDGMENTS

The authors wish to express their appreciation to Dr. Irwin of Naval Research Laboratory for making test facilities available; to Mr. Atkins of the Applied Physics Laboratory for much technical assistance; to Dr. Milne of the University of Rochester for his assistance in the photographic program; to Dr. Eyring of the University of Utah for many helpful comments and suggestions; and to Dr. Schapiro of Douglas Aircraft for sectioning, etching, and examining the craters.

BIBLIOGRAPHY

1 "Behavior of Metals Under Impulsive Loads," by J. S. Rinehart and J. Pearson, The American Society for Metals, 1954, p. 202.

2 "The Formation of Craters by High-Speed Particles," by M. Rostoker, *Meteoritics*, vol. 1, no. 1, 1953, pp. 11–27.

3 "Motion Picture Photography at Ten Million Frames per Second," by B. O'Brien and G. Milne, *Journal of the Society of Motion Picture Engineers*, vol. 52, January, 1949, pp. 20–40. (This refers to the earlier type I camera, but gives the main principles of the apparatus used in these tests.)

4 "Method for Producing High-Velocity Metallic and Plastic Pellets," by M. E. Van Valkenburg and C. D. Hendricks, Jr., *Journal of Applied Physics*, vol. 26, June, 1955, p. 776.

5 "Statistical Thermodynamics," by R. Fowler and E. A. Guggenheim, Cambridge University Press, 1949, pp. 133 and 330.

6 "The Face of the Moon," by R. B. Baldwin, The University of Chicago Press, 1948, pp. 132 and 225.

[10] At very high velocities Rinehart indicates that the penetration of a fragment should be proportional to the $^1/_3$ power of its mass and $^2/_3$ power of its velocity. At low velocities he takes the penetration as being proportional to V^2.

Experiments for the Determination of Transient Stress and Strain Distributions in Two-Dimensional Problems

By A. J. DURELLI[1] and W. F. RILEY,[2] CHICAGO, ILL.

The object of this investigation was to develop a method utilizing photoelasticity for determining transient stress and strain distributions in two-dimensional problems. Numerous investigators have approached this problem using the common photoelastic materials which have a relatively high modulus of elasticity and correspondingly high velocity of wave propagation. However, many difficulties were encountered in photographically recording data, and only a few reliable stress patterns were obtained. In order to avoid these difficulties, a material with a low modulus of elasticity and a correspondingly low velocity of wave propagation was developed. As a result the 8-mm. Fastax camera is capable of recording precise fringe patterns. The material used was a member of the epoxy-resin family, modified to give the desired properties. Both its static and dynamic properties were determined as accurately as possible. It was found that the strain-fringe value of the material is approximately constant, but the modulus of elasticity and stress-fringe value are different for static and dynamic loadings. Preliminary studies were conducted to develop the method using a circular disk under a radially applied concentrated impact load as the model. A simply supported beam under central impact was then studied, and deflection curves obtained were compared with curves theoretically predicted by Saint Venant and Flamant. The comparisons showed good agreement. An analysis of the formation of the fringe pattern for various times after impact also was made.

Introduction

THE PROBLEM of determining the distribution of stress and strain in a two-dimensional specimen subjected to an impact type of loading is difficult to solve mathematically. Very few theoretical solutions can be found in the literature, and in most cases those which are available deal only with a specific phase of the problem such as deflections in beams. Complete stress or strain distributions are seldom available, and those results which have been obtained are usually not in a readily usable form. The mathematical difficulties make an experimental approach to the problem highly desirable.

Much of the experimental work done in the field of dynamic loading has been conducted using electrical resistance-wire strain gages. At best this method limits the observations to a relatively few isolated points. Presently, considerable work is being done by numerous investigators in an attempt to apply photoelasticity to the study of dynamic loadings, but only a few satisfactory stress patterns have been obtained. The majority of the researchers have approached the problem using the common photoelastic materials, such as CR-39, bakelite, etc., in which the velocity of wave propagation is very high because of the high modulus of elasticity. As a result, commercially available cameras are not capable of recording adequately the dynamic fringe patterns. In an attempt to overcome this difficulty new recording equipment in the form of streak cameras and ultrahigh-speed, full-frame cameras were designed and built. When the streak camera is used, the dynamic phenomena are recorded across only a narrow zone of the specimen. The patterns obtained are cumbersome and difficult to interpret. When ultrahigh-speed cameras are used, it is difficult to obtain sufficient light to expose the film properly. Usually a uniform field of light cannot be obtained; i.e., when the central region of the film is properly exposed, the model boundary regions are underexposed, and many of the phenomena are missed. A second limitation of many ultrahigh-speed cameras is the relatively few consecutive frames they are capable of recording.

In this paper a method for obtaining clear fringe patterns for the entire model eliminating many of the difficulties and objections of the previously stated methods is described. This development has been made possible by selecting as the model material a specially prepared plastic with a very low modulus of elasticity and unusually good photoelastic properties. In a material with a low modulus of elasticity the velocity of wave propagation is low, and the commercially available 8-mm Fastax camera is capable of recording satisfactory fringe patterns. A previous contribution in this line of approach was made by H. C. Perkins (1)[3] who used gelatin and rubber as model materials. The research reported in the present paper was developed independently of this contribution.

A grid method for determining strains also was used in this study, but at the present time it has not been developed completely for dynamic work. Its final development and application will be the subject of a future paper. The photographs presented in this paper show the grid network in its early stages of development. These grid lines were used only as an aid in the plotting of fringes. No data were used which were obtained by measuring changes in these grid distances. The presence of a fixed reference line in the field of the photographs allowed the determination of boundary displacements with either a micrometer-microscope or an optical comparator. A micrometer-microscope was used to measure deflections in this study.

---

[1] Supervisor, Stress Analysis Section, Armour Research Foundation of Illinois Institute of Technology. Assoc. Mem. ASME.

[2] Associate Engineer, Stress Analysis Section, Armour Research Foundation of Illinois Institute of Technology.

Contributed by the Applied Mechanics Division and presented at the Annual Meeting, New York, N. Y., November 25–30, 1956, of The American Society of Mechanical Engineers.

Discussion of this paper should be addressed to the Secretary, ASME, 29 West 39th Street, New York, N. Y., and will be accepted until April 10, 1957, for publication at a later date. Discussion received after the closing date will be returned.

Note: Statements and opinions advanced in papers are to be understood as individual expressions of their authors and not those of the Society. Manuscript received by ASME Applied Mechanics Division, April 20, 1956. Paper No. 56—A-11.

[3] Numbers in parentheses refer to the Bibliography at the end of the paper.

The authors believe that the method presented allows the study of wave-propagation phenomena with a thoroughness and precision that were previously impossible. The soundness of the new approach is verified by comparing the results of some simple beam tests with theoretical predictions by Saint Venant and Flamant (2).

The Photoelastic Model Material

The requirements of the material to be used can be stated briefly as follows: It must be transparent, birefringent, and elastic. It must be relatively easy to manufacture, machine, and handle, and have a low modulus of elasticity.

Gelatin meets most of the requirements listed, and it was used in the initial studies of the photoelastic techniques. However, its detrimental time-edge effect, poor machinability, and high strain fringe value, i.e., strain necessary to produce one fringe in a model of unit thickness, made advisable the development of another material.

A survey of the literature was conducted in an attempt to find a plastic which would satisfy the previously stated requirements. This survey revealed that several investigators had made use of a clear epoxy resin as a photoelastic material and had reported good results (3, 4). This material was developed by the Ciba Company and is sold in England under the name Araldite Casting Resin "B." A somewhat similar member of the epoxy-resin family, manufactured by the Ciba Company, Inc., Kimberton, Pa., and sold in liquid form under the name Araldite 502, also was investigated, and it was found that its properties can be varied over a wide range by adding suitable amounts of a compatible plasticizer, such as dibutyl phthalate, and small amounts of cyclohexanol. The manufacturer recommends the use of Araldite Hardener HN-951 as the curing agent for this cold-setting resin.

The material used in the subject study was obtained by adding 20 parts of a mixture consisting of 5 parts cyclohexanol and 3 parts dibutyl phthalate, to 30 parts resin and 3 parts hardener. It was found that this material loaded statically follows Hooke's law and the stress-optic law up to a strain of about 6 per cent, has a modulus of elasticity (which changes with composition and age) of about 375 psi, and has a material fringe value of approximately 0.52 psi-in/fringe.

The material can be cast between glass plates into sheets of any desired size and thickness if a thin layer of cellulose acetate is used to prevent bonding. The model can be rough cut from the sheet by using a jig saw, and the boundaries can be finished with a router. The boundaries of the model when prepared in this way are remarkably free of machining stresses but develop some time-edge stresses which can be considerably retarded by applying a film of petrosene wax. In the tests conducted the material did not exhibit any optical or mechanical creep during a 24-hr period of investigation.

Equipment and Techniques for Dynamic Work

The Dynamic Polariscope. One of the polariscopes in the Armour Research Foundation photoelasticity laboratory is of the diffused-light type with a 12-in-diam field. This polariscope is completely described in a paper by one of the authors (5). In order to convert this polariscope for dynamic work, it was necessary to increase the intensity of the light source. This was accomplished by using four simultaneously triggered Sylvania Type 2A (focal plane) flash bulbs in place of the green fluorescent lamps used for static work. The intensity of the flash from these bulbs rises to a peak of 1,500,000 lumens in 20 millisec. A Wratten 77A filter plus a Corning Glass 4-72 filter was used to approximate a monochromatic source of light.

High-Speed Photographic Equipment and Techniques. While several high-speed cameras are commercially available, today the 8-mm Fastax WF1 camera (which uses 16-mm film) was found to be satisfactory. This camera is capable of recording at the rate of 14,000 frames per sec when used in conjunction with the Model J-410 Fastax control unit. When operating at this speed the exposure time is approximately 14 microsec and the interval between frames is approximately 70 microsec. This is sufficiently fast to give clear fringe patterns. Kodak Linagraph Ortho, Linagraph Pan, and Tri-X films are commercially available and sufficiently fast to be exposed properly. The Ortho film is difficult to obtain in the 16-mm size, and the Linagraph Pan film does not give clear enlargements. Kodak Tri-X gives the best results and should be developed using Kodak DK-50 developer.

The Loading Mechanism. Impact loadings used in this study were obtained by using falling weights. Partial control of the impact can be exercised by varying the height from which the striker falls and by varying the weight of the striker.

Synchronization. When the Fastax control unit is used, the synchronization of the camera and the impact can be obtained by means of the camera timer and the event timer. In this way the camera is permitted to get up to its maximum speed before the impact occurs. The flashing of the bulbs is controlled by a switch which is activated by the falling striker.

Preliminary Studies for Developing the Method

The circular disk was chosen as a convenient model to be used in developing the techniques, because it is easy to machine and to load. Also the fringe order at all points of the model can be determined from a single frame, since a zero-order fringe is present in every frame, and the high concentrations near the points of application of the load permit the evaluation of the photographic techniques. Fig. 1 shows a series of photographs of a circular disk in one of the preliminary tests. It is interesting to note that the time required to photograph approximately eight frames is the time necessary for the stress wave to propagate across the disk. It is obvious from the photographs that the material is sufficiently sensitive to permit the stress distribution to be determined throughout the disk during this interval. If less sensitive materials are used, it may not be possible to observe the wave propagation.

The fringe pattern begins to form at the point of impact, and only after several fringes have formed does the fringe pattern begin to develop at the point of support. Between the moment the impact takes place and the moment the reaction begins, many of the more interesting features of the phenomena develop. The fringe order at the point of application of the load is approximately $9^1/_2$ at the time the reaction begins at the other end of the diameter. After 26 frames the fringe order at the point of application of the load decreases to $8^1/_2$ while the fringe order at the point of support is several fringes higher (approximately $10^1/_2$). From this time on the pattern slowly becomes symmetric, and the maximum fringe order (about 12 fringes near both top and bottom) is eventually reached. The fringe pattern then decays in a symmetric manner, and eventually the disk is left completely stress-free, indicating that the impact was within the elastic limit of the material. This complete cycle of events required approximately 0.03 sec.

For this test the 0.5-order fringe propagated with a constant velocity (3050 in. per sec) across the vertical diameter of the disk. A modulus of elasticity for the material of 825 psi was obtained by using the two-dimensional wave equation

$$V = \sqrt{\frac{E}{(1 - \nu^2)\,\rho}}$$

where

V = velocity of propagation of 0.5-order fringe

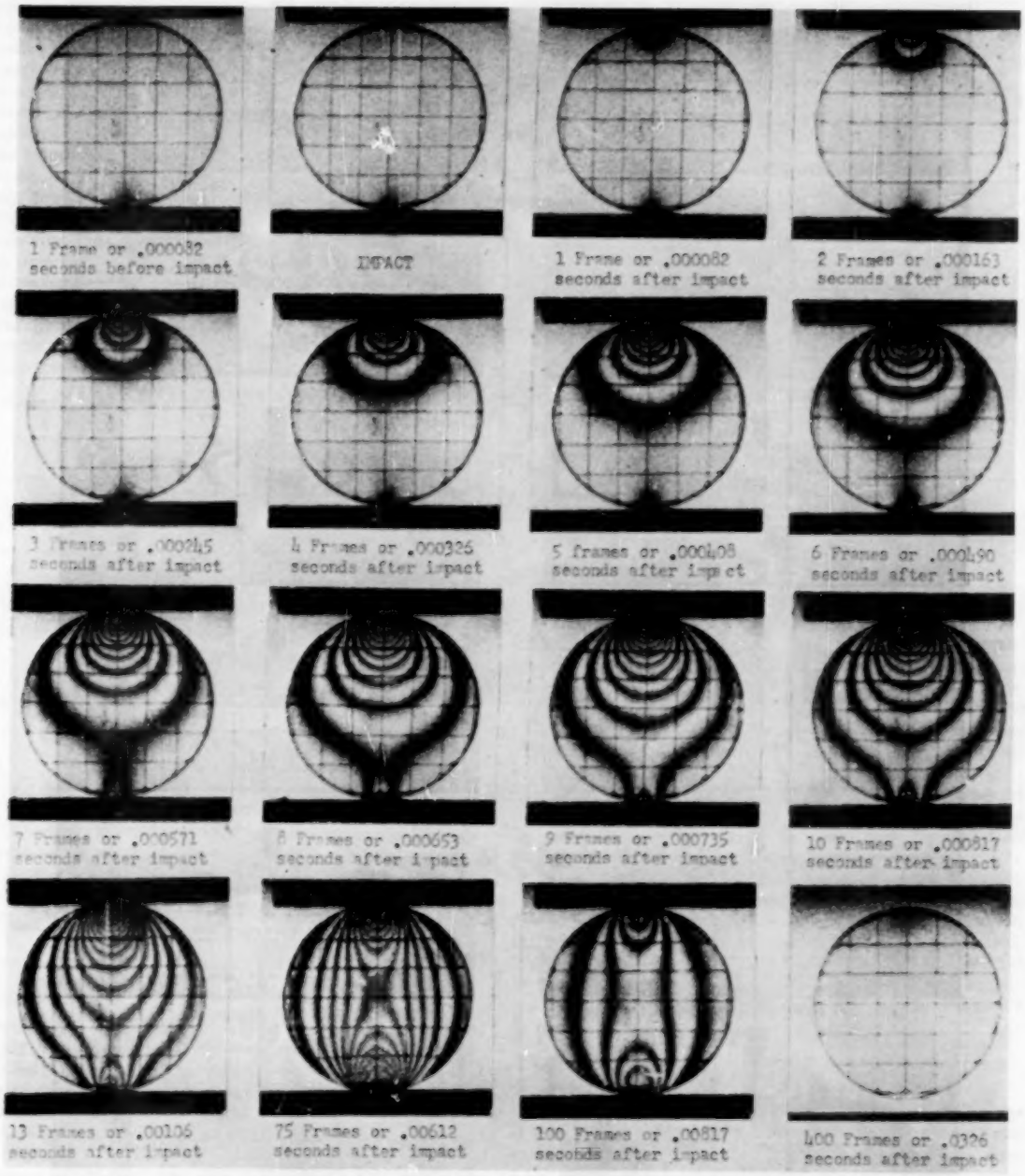
1 Frame or .000082 seconds before impact
IMPACT
1 Frame or .000082 seconds after impact
2 Frames or .000163 seconds after impact
3 Frames or .000245 seconds after impact
4 Frames or .000326 seconds after impact
5 Frames or .000408 seconds after impact
6 Frames or .000490 seconds after impact
7 Frames or .000571 seconds after impact
8 Frames or .000653 seconds after impact
9 Frames or .000735 seconds after impact
10 Frames or .000817 seconds after impact
13 Frames or .00106 seconds after impact
75 Frames or .00612 seconds after impact
100 Frames or .00817 seconds after impact
400 Frames or .0326 seconds after impact

FIG. 1 ARALDITE EPOXY RESIN DISK 2½ IN. DIAM UNDER IMPACT OF A 4-OZ WEIGHT FALLING FROM A HEIGHT OF 8 IN.
(Views were taken with an 8-mm Fastax camera with a 2-in. lens at a speed of 12,240 frames per sec.)

E = modulus of elasticity
ν = Poisson's ratio
ρ = density

Other tests also were conducted to develop the method, among them several beams of different spans. Fig. 2 illustrates the photographs obtained from one of these tests.

DYNAMIC PROPERTIES OF THE MATERIAL

To determine the dynamic properties of the modified epoxy resin, a method was employed similar to that used by Taylor and Volterra (6, 7). The equipment consisted of two steel cylinders, each weighing 29 lb, suspended as ballistic pendulums and the 8-mm Fastax camera. A short bar of the material to be tested was

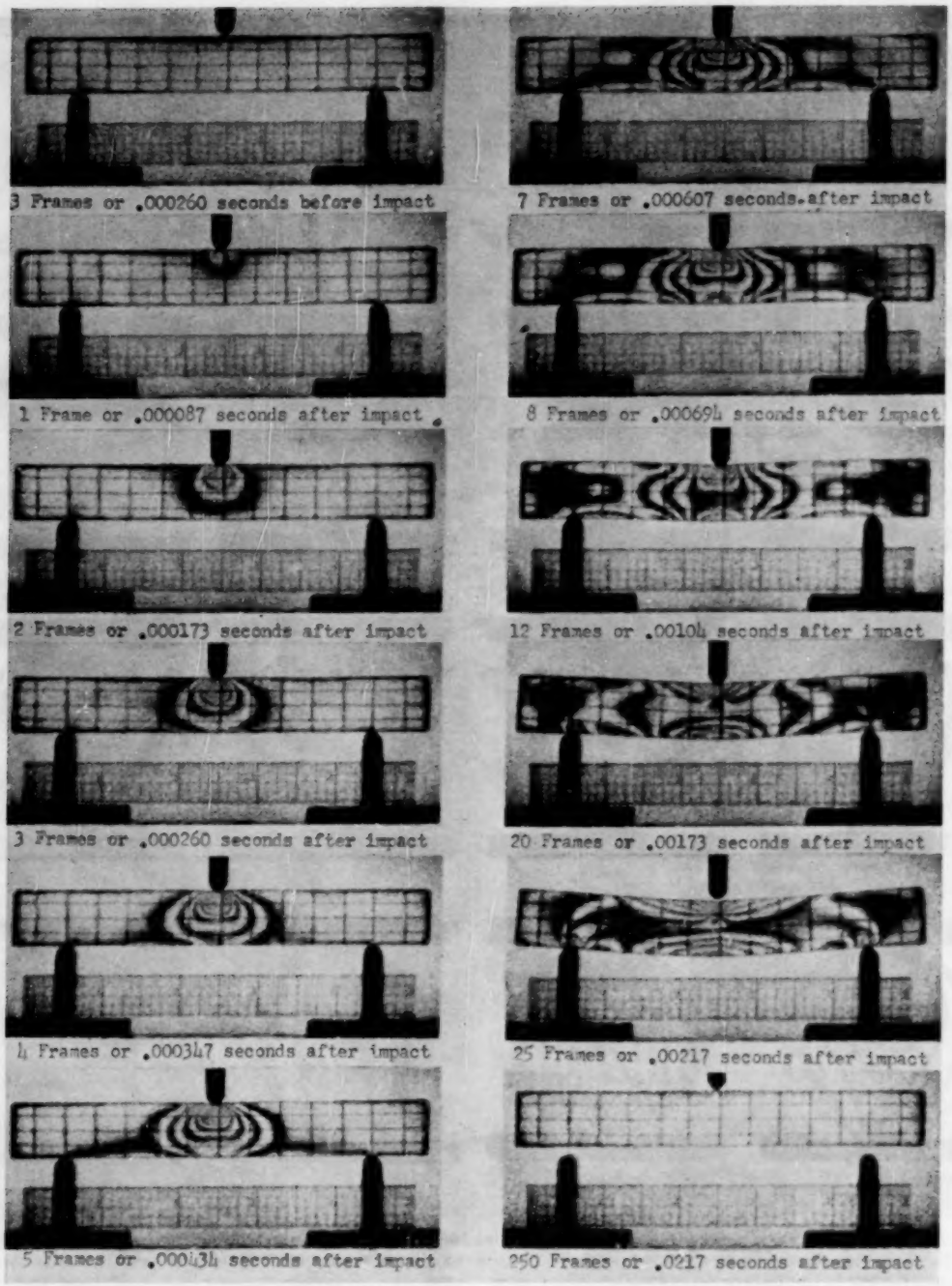
3 Frames or .000260 seconds before impact
7 Frames or .000607 seconds after impact
1 Frame or .000087 seconds after impact
8 Frames or .000694 seconds after impact
2 Frames or .000173 seconds after impact
12 Frames or .00104 seconds after impact
3 Frames or .000260 seconds after impact
20 Frames or .00173 seconds after impact
4 Frames or .000347 seconds after impact
25 Frames or .00217 seconds after impact
5 Frames or .000434 seconds after impact
250 Frames or .0217 seconds after impact

FIG. 2 ARALDITE EPOXY RESIN BEAMS 5 1/8 IN. × 1/4 IN. × 1/2 IN. UNDER IMPACT OF A 4-OZ WEIGHT FALLING FROM A HEIGHT OF 8 IN.

(Beam is simply supported and views were taken with an 8-mm Fastax camera with a 2-in. lens operating at a speed of 11,520 frames per sec.)

placed on the plane end of one of the cylinders such that the longitudinal axes of the specimen and cylinder coincided. The second cylinder was then released from a predetermined height to strike the free end of the specimen. During impact, the displacements of the pendulums in respect to a fixed reference wire placed in the field of the photographs were recorded. The displacement-time curves for the pendulums were then plotted from measurements made directly on the film with a micrometer-microscope. The strain-time curve for the specimen was computed from these displacement-time curves, assuming that the strain is uniform throughout the body at every instant. The stress-time curve for the specimen was determined by differentiation from the displacement-time curve of the pendulum holding the specimen. From the stress-time and strain-time relations a dynamic stress-strain curve was then plotted, Fig. 3, which is linear up to a strain of approximately 4 per cent. The dynamic modulus of elasticity obtained this way was 1180 psi, and corresponds to a strain rate of about 25 in/in/sec.

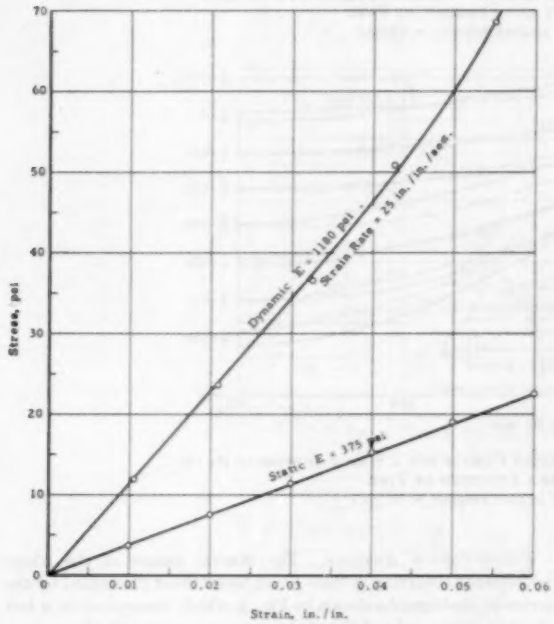

FIG. 3 STATIC AND DYNAMIC STRESS-STRAIN CURVES

In addition to the displacement data, the fringe patterns during impact also were recorded on the film. At the beginning of the impact the propagating and reflecting stress waves made the fringe pattern fairly complex, but after a few frames the fringe order throughout the specimen became uniform. For the next 12 frames the pattern became dark every third frame, and after that the fringes were not sufficiently clear to make observations. Since the stress level in the bar at every instant was known, it was possible to compute the dynamic fringe value. These data are plotted in Fig. 4 with the values corresponding to the first few frames being omitted. The slope of this curve indicates that the material has a dynamic material fringe value in shear of 1.75 psi-in/fringe. This compares with a static value of only 0.52 psi-in/fringe.

In this same test a grid network placed on the surface of the specimen allowed an approximate determination of transverse strains, using a micrometer-microscope. These measurements show that the dynamic value for Poisson's ratio is about 0.50,

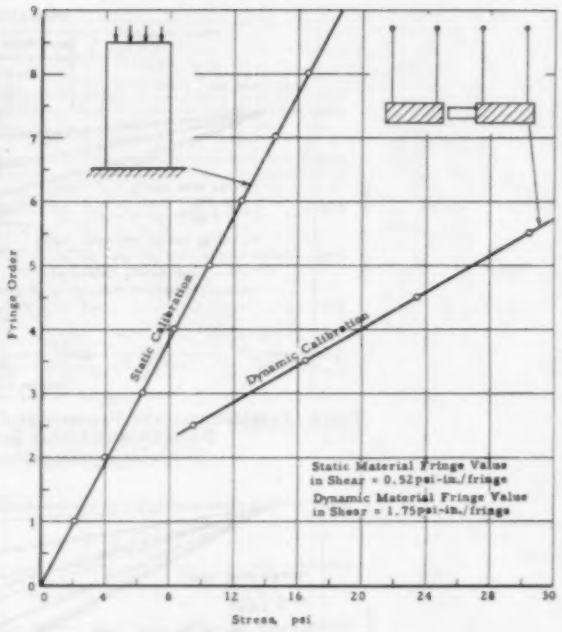
Fringe Order
Stress, psi
Static Calibration
Dynamic Calibration
Static Material Fringe Value in Shear = 0.52 psi-in./fringe
Dynamic Material Fringe Value in Shear = 1.75 psi-in./fringe

FIG. 4 STATIC AND DYNAMIC STRESS OPTIC CALIBRATION

while the static value was determined as 0.40. These results should not be considered final, and a more accurate measurement should be made using embedded grids instead of cemented grids.

The static value of the strain-fringe constant was determined to be 1.9×10^{-3} in/fringe, and the dynamic value at 25 in/in/sec was determined to be 2.0×10^{-4} in/fringe. The strain-fringe value is therefore essentially independent of the rate of loading.

It should be pointed out that the values reported herein are for the softest material developed for use in the study of wave propagation. The material used for the beam tests reported later was made harder to avoid excessive beam deflections.

It was found in this study that the velocity of propagation varied for fringes of different order. The high-order fringes propagate at lower velocities than the low-order fringes. However, the velocity of propagation for a given fringe order is constant. This phenomenon requires further investigation. The method of translating the results obtained from a material of this kind to results expected in materials with different properties also should be considered in future work.

STUDY OF A SIMPLY SUPPORTED BEAM UNDER CENTRAL IMPACT

Deflection Study. In order to evaluate the new method, a series of tests were conducted for the case of a simply supported beam under central impact. This problem was selected for study, since a theoretical solution was available in the literature which could be used as a basis of comparison for the experimentally determined results. Saint Venant and Flamant determined mathematically the deflection of a bar under transverse central impact at various times after impact. Numerical results in the form of curves are presented for the cases in which the beam-striker weight ratios are 0.5, 1, and 2. Some experimental results by L. Foeppl (8) also were available.

In this paper the results of two tests are presented and are compared with the theoretically predicted deflection curves. Fig. 5 shows the experimental and theoretical deflection curves for a

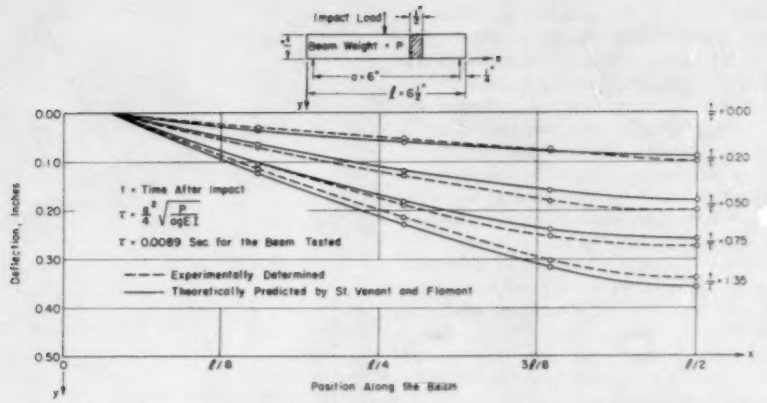
Impact Load
Beam Weight = P
a = 6"
ℓ = 6½"
t = Time After Impact
τ = 0.0089 Sec. for the Beam Tested
Experimentally Determined
Theoretically Predicted by St. Venant and Flamant
Deflection, Inches
Position Along the Beam

FIG. 5 EXPERIMENTAL AND THEORETICAL DEFLECTION CURVES FOR A SIMPLY SUPPORTED BEAM UNDER CENTRAL IMPACT AS A FUNCTION OF TIME
(Striker-beam weight ratio = 2; impact velocity = 55 ips.)

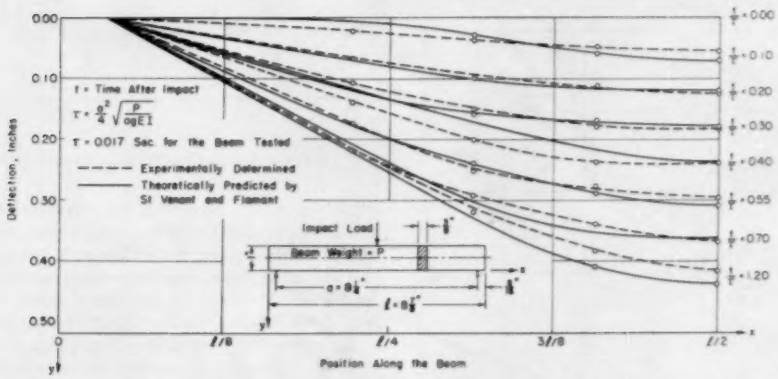
t = Time After Impact
τ = 0.017 Sec. for the Beam Tested
Experimentally Determined
Theoretically Predicted by St. Venant and Flamant
Impact Load
Beam Weight = P
a = 9½"
ℓ = 9½"
Deflection, Inches
Position Along the Beam

FIG. 6 EXPERIMENTAL AND THEORETICAL DEFLECTION CURVES FOR A SIMPLY SUPPORTED BEAM UNDER CENTRAL IMPACT AS A FUNCTION OF TIME
(Striker-beam weight ratio = 1; impact velocity = 55 ips.)

beam under central impact in which the weight of the striker is twice the weight of the beam. The deflections for four different times after impact were measured directly on the film. As can be seen from the curves, the comparisons are in good agreement. A maximum deflection of 0.34 in. occurred at a time between 0.010 sec (135 frames) and 0.013 sec (165 frames) after impact. Since the deflection changes are very small during this interval, it was not possible to determine the exact frame or time at which the maximum deflection occurred. This compares very favorably with the theoretically predicted maximum of 0.36 in. which should occur 0.0126 sec (149 frames) after impact. The modulus of elasticity of the material used in this test was determined to be 1100 psi from measurements of the static deflection of the beam. Since the strain rate at most points in the beam is less than 1.7 in/in/-sec, the static value of the modulus of elasticity was used, Fig. 5, for the comparison with Saint Venant's formula.

In the second test a longer beam was used with the weight of the striker equal to the weight of the beam. The results of this test are shown in Fig. 6. As in the previous test the theoretical results were computed using the statically determined value of E, which for this beam was 1300 psi. In this test the experimentally determined maximum deflection of 0.44 in. occurs at 0.020 sec (250 frames) after impact.

Fringe-Pattern Analysis. The general nature of the fringe movements occurring in these beam tests is best illustrated by the series of photographs shown in Fig. 2, which correspond to a test in which the weight of the striker was approximately three times the weight of the beam. In the first photograph the beam is shown prior to impact. The striker has entered the field but has not touched the upper surface of the beam. For four frames after impact the fringe pattern builds up under the striker but no pattern forms near the supports. In the fifth frame the first reaction from the supports begins to form. For the next 15 frames a very complex state of stress is seen to exist in the beam, and the pattern is very different from the static fringe pattern for a centrally loaded simply supported beam. After 25 frames the pattern begins to resemble the static pattern. The last photograph (after 250 frames) shows the beam completely stress-free, indicating that the impact has been completely elastic and no residual stresses remain.

Referring now to the fringe pattern for the second beam test: The fringe order along the lower edge, horizontal center line, upper edge, and vertical center line of the beam was plotted for various times after impact. In Fig. 7 the fringe order along the lower edge of the beam is shown. At the center, the fringe order increases to about $3^1/_2$ very rapidly. It then remains constant

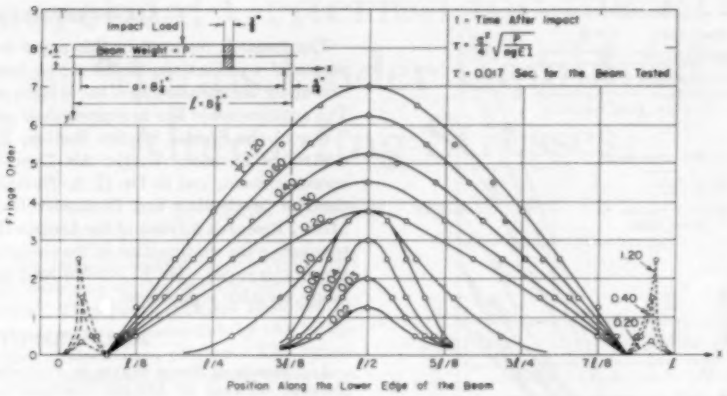
Impact Load
Beam Weight = P
t = Time After Impact
τ = 0.017 Sec. for the Beam Tested
Fringe Order
Position Along the Lower Edge of the Beam

FIG. 7 PHOTOELASTIC FRINGE ORDER ALONG LOWER EDGE OF A SIMPLY SUPPORTED BEAM UNDER CENTRAL IMPACT AS A FUNCTION OF TIME
(Striker-beam weight ratio = 1; impact velocity = 55 ips.)

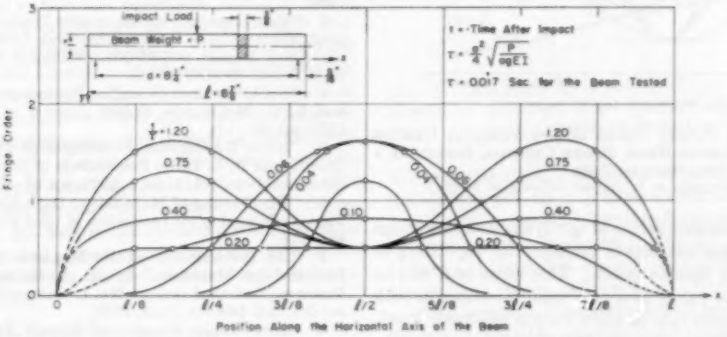
Impact Load
Beam Weight = P
t = Time After Impact
τ = 0.017 Sec. for the Beam Tested
Fringe Order
Position Along the Horizontal Axis of the Beam

FIG. 8 PHOTOELASTIC FRINGE ORDER ALONG HORIZONTAL AXIS OF A SIMPLY SUPPORTED BEAM UNDER CENTRAL IMPACT AS A FUNCTION OF TIME
(Striker-beam weight ratio = 1; impact velocity = 55 ips.)

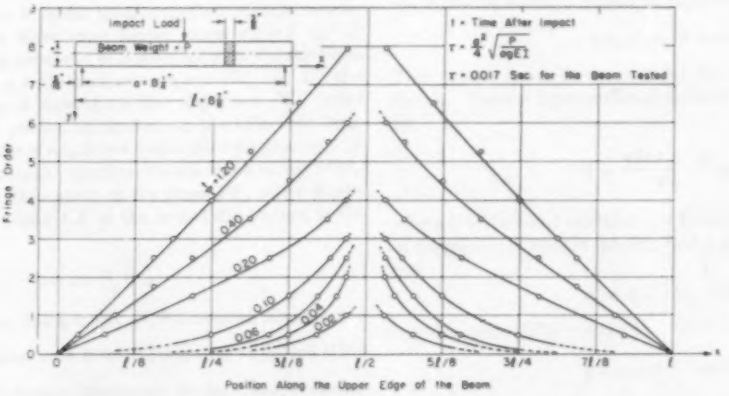
Impact Load
Beam Weight = P
t = Time After Impact
τ = 0.017 Sec. for the Beam Tested
Fringe Order
Position Along the Upper Edge of the Beam

FIG. 9 PHOTOELASTIC FRINGE ORDER ALONG UPPER EDGE OF A SIMPLY SUPPORTED BEAM UNDER CENTRAL IMPACT AS A FUNCTION OF TIME
(Striker-beam weight ratio = 1; impact velocity = 55 ips.)

until a reaction begins at the support, then increases to a maximum when the deflection is a maximum. In Fig. 8 the fringe order along the horizontal center line is plotted. Note here that the maximum fringe order shifts from the center of the beam toward the points of support. In Fig. 9 the fringe order is plotted for the upper edge of the beam. In Fig. 10 the fringe order is plotted for the vertical center line under the point of application of the load. As can be seen from this figure the fringe pattern builds up in a very complex manner.

These patterns could be evaluated in terms of strains and

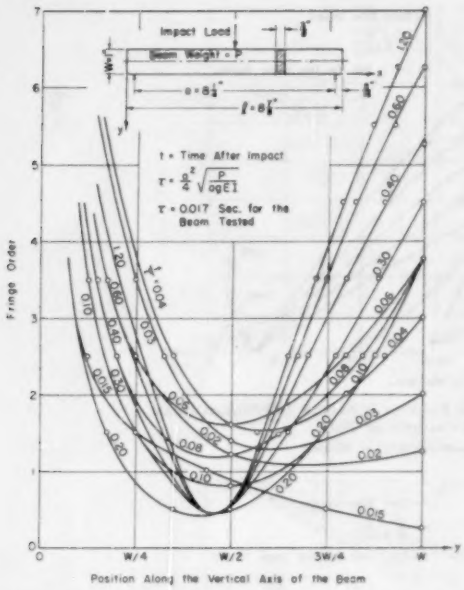

FIG. 10 PHOTOELASTIC FRINGE ORDER ALONG VERTICAL CENTER LINE OF A SIMPLY SUPPORTED BEAM UNDER CENTRAL IMPACT AS A FUNCTION OF TIME
(Striker-beam weight ratio = 1; impact velocity = 55 ips.)

stresses, using the appropriate values of the dynamic-strain fringe constant and the dynamic modulus of elasticity corresponding to the strain rate at each specific point. This value of E can be taken equal to the static value, as a first approximation, in both beam tests, since the strain rate in these tests is relatively small. The dynamic-strain fringe value for the materials used in the beam tests has not been determined.

ACKNOWLEDGMENTS

The research reported in this paper is an outgrowth of some phases of a project conducted at the Armour Research Foundation under the sponsorship of the Wright Air Development Center. The authors would like to express their appreciation to Mr. E. H. Wang of the Special Studies Section, Engineering Branch, Installations Division, Wright Air Development Center, for his encouragement, and to Dr. G. A. Nothmann, Manager, Department of Mechanism and Dynamics Research, and Mr. K. W. Miller, Research Advisor of the Armour Research Foundation, for sponsoring the continuation of the research leading to the publication of this paper. Mr. E. Phillips read the manuscript and made many valuable suggestions.

BIBLIOGRAPHY

1 "Movies of Stress Waves in Photoelastic Rubber," by H. C. Perkins, JOURNAL OF APPLIED MECHANICS, Trans. ASME, vol. 75, 1953, p. 140.

2 "Courbes Representatives des Lois du Choc Longitudinal et du Choc Transversal d'une Barre Prismatique," by de Saint Venant and M. Flamant, *Journal de l'École Polytechnique*, Paris, France, vol. 59, 1889.

3 "Experiments With Composite Models," by C. Mylonas, Technical Report No. 8, Ballistic Research Laboratories, Department of the Army Project 503-06-005, Ordnance Project TB3-0122, Contract DA-19-020-ORD-798.

4 "An Ethoxylene Resin for Photoelastic Work," by H. Spooner and L. C. McConnell. *British Journal of Applied Physics*, vol. 4, 1953, pp. 181–184.

5 "Some Unorthodox Procedures in Photoelasticity," by A. J. Durelli and R. L. Lake, Proceedings of the Society for Experimental Stress Analysis, vol. 9, no. 1, 1951, pp. 97–122.

6 "The Testing of Materials at High Rates of Loading," by G. I. Taylor, *Journal of the Institution of Civil Engineers*, vol. 26, 1946, pp. 486–518.

7 "An Investigation on the Dynamic Properties of Plastics and Rubber-Like Materials," by R. A. Eubanks, D. Muster, and E. Volterra, Technical Report No. 1, Contract No. N7-onr-32911, Project No. NR 064369, June, 1952.

8 "Slow-Motion Pictures of Impact Tests by Means of Photoelasticity," by L. Foeppl, JOURNAL OF APPLIED MECHANICS, Trans. ASME, vol. 71, 1949, pp. 173–177.

A Theoretical Criterion for the Fracture of Metals Under Combined Alternating Stresses

By TAKEO YOKOBORI,[1] SENDAI, JAPAN

A criterion for the fracture of metals under combined alternating stresses is developed on the basis of the present concepts of dislocations. These concepts are modified by taking into account the stress concentration by the inclusion itself against which dislocations pile up. The agreement is good with the experimental data in the literature.

Introduction

In A previous paper (1),[2] a simple dislocation model for the fatigue fracture of metals was developed, and *S-N* curves and the temperature dependence of fatigue strength were calculated on the basis of nucleation theory. By using the same order of magnitude of the number n of piled-up dislocations and the value q of the stress-concentration factor by an obstacle itself, respectively, the calculations of *S-N* curves and the temperature dependence of fatigue strength were in good agreement with the experimental data in the literature. In the present paper the dislocation model is slightly modified, and it has been shown that the stress condition of fracture under combined alternating stresses agrees fairly well with the data in the literature when the same order of magnitude of n and q, respectively, as those used for the calculation of *S-N* curves and the temperature dependence of fatigue strength were used.

Theoretical Considerations

The limit of cold-working in fatigue process was assumed to correspond to the saturated state of piling up of dislocations at an obstacle such as a hard inclusion or a precipitate (1). Let us suppose that the specimen is under axially applied uniform tensile-stress range S. Then there exist tensile stress $\sigma_\varphi (= S \sin^2 \varphi)$ normal to and shearing stress $\tau_\varphi (= S \cos \varphi \sin \varphi)$ in the slip plane XX making an angle φ with the specimen axis ZZ, Fig. 1. If n similar edge dislocations moving on this slip plane XX under shearing stress τ_φ are pushed up against an obstacle, then large tensile stress of the order of $n\tau_\varphi$ arises near a piled-up group of dislocations (2). Consequently, the total tensile stress in the neighborhood of the locked dislocation on the plane YY, which is perpendicular to the slip plane XX at the locked dislocation, is the sum of

$$\sigma_{\varphi+\pi/2} + n\tau_\varphi \quad \ldots\ldots [1]$$

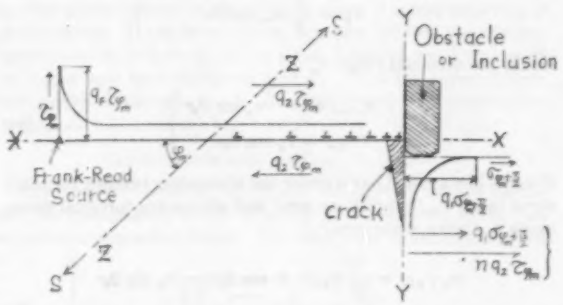

Fig. 1 Initiation of Fatigue Crack Based on Dislocation Model as Affected With Stress Concentration Due to Obstacle or Inclusion Itself

The obstacle itself in the form of a hard particle against which dislocations pile up may have a notch effect in many cases, Fig. 1. Let the stress-concentration factor at the edge of the obstacle be denoted by q_1 as shown in Fig. 1. The stress-concentration factor q_F at the region where the Frank-Read source (3) begins to be operated may be as large as q_1. However, the averaged value q_2 of the stress-concentration factors over the whole length of slip line which contains piled-up dislocations is expected to be much smaller than q_F. The stress-concentration factor falls off rapidly in the region remote from the source of the stress concentration (in the present case, Frank-Read source, reference 3). Thus, we get the following formula instead of Equation [1]

$$q_1\sigma_{\varphi+\pi/2} + nq_2\tau_\varphi \quad \ldots\ldots [2]$$

This tensile stress is assumed as determining the fracture of metals. Term n is proportional to shear stress and is represented by

$$n = \frac{\pi L(1-\nu)}{Gb} q_2\tau_\varphi \quad \ldots\ldots [3]$$

where G is the shear modulus, ν is Poisson's ratio, b is of the order of magnitude of atomic spacing, and L is slip distance (4). If we put

$$c_0 = \pi L(1-\nu)/Gb$$

then Equation [2] is written as

$$q_1\sigma_{\varphi+\pi/2} + c_0 q_2^2 \tau_\varphi^2 \quad \ldots\ldots [4]$$

The value of

$$q_1\sigma_{\varphi+\pi/2} + c_0 q_2^2 \tau_\varphi^2$$

has a maximum on the plane making an angle φ_m with ZZ, which satisfies the condition

$$\frac{\partial}{\partial\varphi}\left| q_1\sigma_{\varphi+\pi/2} + c_0 q_2^2 \tau_\varphi^2 \right| = 0 \quad \ldots\ldots [5]$$

---

[1] Assistant Professor, Department of Mechanical Engineering, Tohoku University.

[2] Numbers in parentheses refer to the Bibliography at the end of the paper.

Contributed by the Applied Mechanics Division and presented at the Annual Meeting, New York, N. Y., November 25–30, 1956, of The American Society of Mechanical Engineers.

Discussion of this paper should be addressed to the Secretary, ASME, 29 West 39th Street, New York, N. Y., and will be accepted until April 10, 1957, for publication at a later date. Discussion received after the closing date will be returned.

Note: Statements and opinions advanced in papers are to be understood as individual expressions of their authors and not those of the Society. Manuscript received by ASME Applied Mechanics Division, April 5, 1956. Paper No. 56—A-21.

Hence if the effect of thermal fluctuations is neglected, the condition for fatigue fracture will be given by

$$q_1\sigma_{\varphi_m+\pi/2} + cq_2^2\tau_{\varphi_m}^2 = \alpha E \quad \ldots\ldots [6]^3$$

where E is Young's modulus, and α is a numerical value of the order of magnitude of one tenth.

Under the tensile stress σ_{wb}

$$\left.\begin{aligned} \sigma_{\varphi+\pi/2} &= \frac{1}{2}\,\sigma_{wb}(1+\cos 2\varphi) \\ \tau_\varphi &= \frac{1}{2}\,\sigma_{wb}\sin 2\varphi \end{aligned}\right\} \quad \ldots\ldots [7]$$

Under the torsional stress τ_w

$$\left.\begin{aligned} \sigma_{\varphi+\pi/2} &= -\tau_w \sin 2\varphi \\ \tau_\varphi &= \tau_w \cos 2\varphi \end{aligned}\right\} \quad \ldots\ldots [8]$$

Hence when a round bar is under the alternating bending (tensile) stress range σ_{wb} (mean stress zero) and alternating torsional stress range τ_w (mean stress zero)

$$\left.\begin{aligned} \sigma_{\varphi+\pi/2} &= \frac{1}{2}\,\sigma_{wb}(1+\cos 2\varphi) - \tau_w \sin 2\varphi \\ \tau_\varphi &= \frac{1}{2}\,\sigma_{wb}\sin 2\varphi + \tau_w \cos 2\varphi \end{aligned}\right\} \quad \ldots [9]$$

From Equations [5] and [9] we can get φ_m. Substituting this value of φ_m in Equation [9] and using Equation [6], we can obtain the relation between σ_{wb} and τ_w. However, the graphical method will be simpler and this method is used in this paper. Eliminating φ from Equation [9], we get

$$\left(\sigma_{\varphi+\pi/2} - \frac{1}{2}\,\sigma_{wb}\right)^2 + \tau_\varphi^2 = \left(\frac{1}{2}\,\sigma_{wb}\right)^2 + \tau_w^2 \quad \ldots [10]$$

Equation [10] represents the Mohr stress circle with $\sigma_{\varphi+\pi/2}$ as

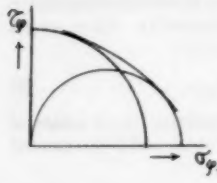

FIG. 2 MOHR'S CIRCLES FOR $\sigma_{\varphi+\pi/2}$ AND τ_φ

abscissa and τ_φ as ordinate, Fig. 2. The relation between σ_{wb} and τ_w can be obtained by using the condition that Equation [6] should be the envelope of these Mohr stress circles.

COMPARISON WITH EXPERIMENTAL DATA IN LITERATURE

Steel. In Fig. 3 the experimental data in the literature (5) were replotted so that alternating (tensile) stress range σ_{wb} and alternating shearing stress range τ_w at fracture may be expressed, respectively, in the term of the ratio to the fatigue strength σ_0 under alternating bending (mean stress zero). From the condition that Equation [6] should be the envelope of the Mohr stress circles obtained from experimental data (5), q_1 is calculated as shown in Table 1. In this paper α in Equations [4] and [6] is assumed to be $^1/_{10}$. Let us attempt to estimate the value of n, the average number of piled-up dislocations corresponding to shearing stress $\bar{\tau}_{\varphi_m}$, the average value of τ_{φ_m} over all the cases of combined stresses ranging from the case under alternating bending stress σ_{wb} only, to the case under alternating shearing stress τ_w only. For that purpose the following approximation was assumed; that is, the parabola expressed by Equation [6] was approximated by the following straight line as the envelope of the Mohr stress circles above described

$$q_1\sigma_{\varphi_m+\pi/2} + \bar{n}q_2\tau_{\varphi_m} = \alpha E \quad \ldots\ldots [11]$$

where

$$\bar{n} = \frac{\pi L(1-\nu)q_2\bar{\tau}_{\varphi_m}}{Gb} \quad \ldots\ldots [12]$$

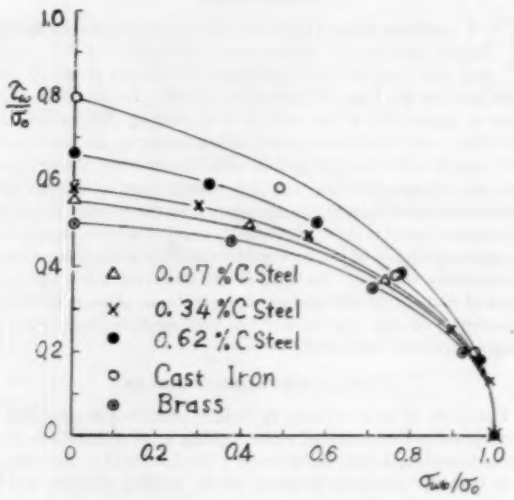

FIG. 3 COMPARISON WITH DATA OF FATIGUE STRENGTH UNDER COMBINED ALTERNATING STRESSES

(Data were compiled from reference 5. Full lines show theoretical curves calculated by Equation [6]. σ_{wb} = alternating bending [tensile] stress range at fracture. τ_w = alternating shearing-stress range at fracture. σ_0 = fatigue strength under alternating bending [mean stress zero]. σ_{wb}, τ_w, and σ_0 correspond to endurance limit for steel and cast iron, and to fatigue strength at 10^7 cycles for brass.)

Hence the negative reciprocal n_0 of the inclination of the tangent of the Mohr stress circles represents

$$\frac{q_2}{q_1}\bar{n} \quad \ldots\ldots [13]$$

Since q_2 is expected to be very small, we assume q_2 as unity.[4] Thus $\bar{n}$ is calculated by using the values of q_1, q_2, and n_0 as in Table 1. The calculated values of $\bar{n}$ are not unreasonable. Then L is also calculated from Equation [12] by using the values of $\bar{n}$, $\bar{\tau}_{\varphi_m}$, q_2, G, ν, and b as shown in Table 1. In the case of steel, L may be assumed to be the mean ferrite path[5] (6), according to the

[3] When the value of q_1 and q_2 are assumed to be equal, the number n of piled-up dislocations are calculated as 1.5 or 2.5 for steel (1). (Since in the calculation of n in reference 1 the numerical factor of 2 was omitted, in the value of n, 1.5 or 2.5 applies rather than 3 or 5.) Since q_1 is the value very near the periphery of the inclusion, and q_2 is the averaged value remote from the source of the stress concentration (in this case, Frank-Read source), q_1 is expected to be much larger than q_2. Hence, the true value of n is considered much larger than 1.5 or 2.5 (q_1/q_2 times as large, Table 1). However, the calculation of S-N curves and the temperature dependence of fatigue strength are not formally affected by the inequality of the value of q_1 and q_2.

[4] In a case where the second term of Equation [6] predominates, q_2 can be found experimentally by measuring L.

[5] It may be more reasonable to assume L as the largest among the ferrite paths contained in the specimen, and consequently the scatter of fatigue life may be partly attributed to the extreme-value problem such as treated by Weibull (14) and Freudenthal and Gumbel (15).

present theoretical considerations, and the obstacles may correspond to grain boundaries, inclusions, or pearlite patches. It seems to be justified by the fact that the calculated values of L in Table 1 are approximately equal to the observed mean distance from one pearlite patch to the next in the case of 0.62 per cent carbon steel (ferrite-pearlite structure), and equal to the observed mean distance between grain boundaries in the case of 0.07 per cent carbon steel (ferrite structure) as revealed in the metallographic observations (5).[6]

It is interesting that the calculated curve in Fig. 3 is in good agreement with experiments and that by using the same order of magnitude of n_0 and the value of q_1 as in Table 1, respectively, the calculations of S-N curves and the temperature dependence of the fatigue strength are also in accordance with experimental data (1).

TABLE 1 CALCULATED VALUES OF NUMBER OF PILED-UP DISLOCATIONS $\bar{n}$, AND SLIP DISTANCE L
($G = 8.28 \times 10^{11}$ dyne/cm², $\nu = 0.28$, $b = 2.48 \times 10^{-8}$ cm)

Material	q_1	q_2	$\tau_{\varphi m}$, kg/mm², from observations	$n_0 = \frac{q_2}{q_1}\bar{n}$, observed value	$\bar{n}$	L, cm
0.62% carbon steel	55	1	17.0	3.0	165	8.8×10^{-4}
0.07% carbon steel	27	1	14.7	9.4	254	1.57×10^{-4}

It should be noted that the values of τ_w/σ_0 plotted as a function of σ_{wb}/σ_0 increase with increase in carbon content from 0.07 per cent to 0.62 per cent. Consequently the absolute value of the inclination of the envelope of the Mohr stress circles of $\sigma_{\varphi+\pi/2}$ and τ_φ increases with the increase of carbon content, Figs. 2 and 3. This phenomenon may be explained as follows: The mean ferrite path may be expected to decrease with the increase of carbon content. Consequently, with the increase of carbon content, the value of L in Equation [5] and of c_0 in Equation [6] decreases. It can be seen from Equation [6] that the square root of c_0 is inversely proportional to the absolute value of inclination of the envelope of the Mohr stress circles in accord with the formula

$$\frac{d\tau_{\varphi m}}{d\sigma_{\varphi m+\pi/2}} = -q_1/2\sqrt{c_0}\, q_2\sqrt{E - q_1\sigma_{\varphi m+\pi/2}} \quad \ldots [14]$$

Thus the phenomenon can be well understood.

Cast Iron. In the case of cast iron, c_0 may be expected to be much smaller and hence the effect of the term of c_0 in Equation [6] may be smaller than in steel, and the criterion for fracture approaches that of the maximum tensile stress. The experimental data are in good agreement with this concept, Fig. 3. The calculated curve also agrees well with the data of Gough and Pollard (7).

Brass and Other Nonferrous Metals. In the case of brass in which piled-up dislocations may be expected to be very large, the term of $q_1\sigma_{\varphi m+\pi/2}$ is negligible as compared with the term $c_0q_2^2\tau_{\varphi m}^2$ in Equation [6]. In such a case, Equation [6] reduces to

$$c_0q_2^2\tau_{\varphi m}^2 = \alpha E \quad \ldots [15]$$

which is apparently the maximum shear-stress condition. The criterion is in good agreement with the data for brass, Fig. 3 (5) and for certain aluminum alloys (8). However, it must be noted that this criterion is only a special case of Equation [6] and is the same formula as that proposed by Mott (9) and Stroh (10). For example, in the case of aluminum and almite (11), the τ_w/σ_0 versus σ_{wb}/σ_0 curves lie above the maximum shear-stress curve. This fact means that in Equation [6] the term of $q_1\sigma_{\varphi m+\pi/2}$ is not negligible compared with $c_0q_2^2\tau_{\varphi m}^2$.

Apparent Nonuniqueness of Criterion for Fracture of Steel Under Alternating Combined Stresses. Maier (12) reported that the maximum tensile-stress condition holds for mild steel under combined alternating stresses according to experiments by himself and by Morikawa and Griffis (13). This criterion seems to be inconsistent with the experimental results of Nishihara and Kawamoto (5) described in the foregoing. The inconsistency may be resolved on the basis of the present theory as follows:

In steels of the same order of magnitude of carbon content, some steels may contain a larger number of inclusions than others and hence possess smaller values of c_0 corresponding to shorter mean free paths of inclusions, or some steels may have larger values of q_1 than others because of the nature or shape of inclusions acting as notch effects. It can be seen from Equation [6] that the criterion approaches the maximum tensile-stress condition if c_0 is very small or if q_1 is very large compared with q_2. Thus the apparent nonuniqueness of the criterion for the fracture of steel under alternating combined stresses is not surprising.

Fatigue Strength of Various Metals

The absolute value of the fatigue strength of various metals may be qualitatively shown as in Fig. 4; for example, in the case of uniaxial alternating stress. The trend may be understood from the relative magnitude of c_0 and q, when q_1 and q_2 were assumed to be equal for convenience. It is to be noted that the effect of the following fact is also involved in the trend of the curve of Fig. 4: Young's modulus of copper and cast iron is smaller than that of steel.

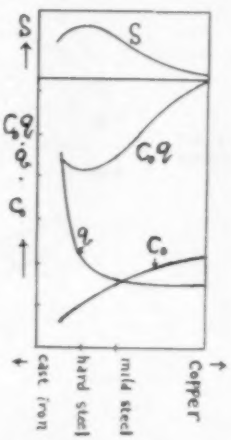

FIG. 4 SCHEMATIC REPRESENTATION OF RELATIVE FATIGUE STRENGTH OF VARIOUS METALS AND ALLOYS
(cq is a measure of relative shear participation in fracture assuming $q_1 = q_2$, where $c_0 = \pi L[1 - \nu]/Gb$, and q is stress-concentration factor. S = fatigue strength.)

Acknowledgment

The present work is part of a research project of the Committee on Fatigue of the Japan Society of Testing Materials, under the leadership of Prof. M. Kawamoto, and was carried out with the financial aid of the Ministry of Education of Japan. The author wishes to express his thanks to Prof. F. Numachi for his interest in this work and for his kindness during the preparation of the manuscript.

BIBLIOGRAPHY

1 "The Theory of Fatigue Fracture of Metals" (in English), by T. Yokobori, *Journal of the Physical Society of Japan*, vol. 10, May, 1955, p. 368.

[6] If there are actually 165 or 250 dislocations piled up, as suggested in the paper, they may perhaps be revealed by x-ray measurements of the internal stresses. No such measurements are known to the author.

2 "The Production of Large Tensile Stresses by Dislocations," by J. S. Koehler, *Physical Review*, vol. 85, 1952, p. 480.

3 "Multiplication Processes for Slow Moving Dislocations," by F. C. Frank and W. T. Read, Jr., *Physical Review*, vol. 79, 1950, p. 722.

4 "The Equilibrium of Linear Arrays of Dislocations," by J. D. Eshelby, F. C. Frank, and F. R. N. Nabarro, *Philosophical Magazine*, series 7, vol. 42, 1951, p. 351.

5 "The Strength of Metals Under Combined Alternating Bending and Torsion" (in Japanese), by T. Nishihara and M. Kawamoto, Transactions of the Japan Society of Mechanical Engineers, vol. 6, 1940, p. 8; ibid., vol. 7, 1941, p. 85.

6 "The Initiation of Plastic Strain in Plain Carbon Steels," by C. S. Roberts, R. C. Carruthers, and B. L. Averbach, Trans. ASM, vol. 30, 1952, p. 1150.

7 "Strength of Metals Under Combined Alternating Stresses," by H. J. Gough and H. V. Pollard, Proceedings of The Institution of Mechanical Engineers, vol. 131, 1935, p.3.

8 "The Fatigue Test of Duralumin Under Combined Bending and Torsion" (in Japanese), by T. Nishihara and M. Kawamoto, *Nippon Kinzoku Gakkai-Si*, vol. 5, 1941, p. 110.

9 "Dislocations, Plastic Flow and Creep," by N. F. Mott, Proceedings of the Royal Society of London, England, series A, vol. 220, 1953, p. 1.

10 "The Formation of Cracks as a Result of Plastic Flow," by A. N. Stroh, Proceedings of the Royal Society of London, England, series A, vol. 223, 1954 p. 404.

11 "The Effect of Almite on the Fatigue Properties of Aluminum Under the Combined Alternating Bending and Torsion" (in Japanese), by T. Nishihara and M. Kawamoto, *Nippon Kinzoku Gakkai-Si*, vol. 7, 1943, p. 539.

12 "Wechselbeanspruchung von Rohren unter Innendruck," by A. F. Maier, *Stahl und Eisen*, vol. 54, 1934, p. 1289.

13 "The Biaxial Fatigue Strength of Low-Carbon Steels," by G. K. Morikawa and L. Griffis, *Welding Journal Research Supplement*, vol. 24, 1945, p. 167.

14 "Statistical Representation of Fatigue Failures in Solids," by W. Weibull, Transactions of the Royal Institute of Technology, Stockholm, Sweden, No. 27, 1949.

15 "On the Statistical Interpretation of Fatigue Tests," by A. M. Freudenthal and E. J. Gumbel, Proceedings of the Royal Society of London, England, series A, vol. 216, 1953, p. 309.

A New Method for the Construction of Hencky-Prandtl Nets

By E. G. THOMSEN,[1] BERKELEY, CALIF.

A graphical method for the rapid construction of Hencky-Prandtl nets has been developed. The principle employed has been stated in a theorem. It is shown that the method may be used for nets on both the physical plane and on the velocity plane or hodograph. The use is illustrated by examples.

Introduction

SPECIFIC solutions of plane problems of perfectly plastic solids are likely to become important in metal-forming technology. This is due to the fact that recent experiments (1, 2, 3)[2] seem to indicate that the perfectly plastic solid may be a suitable model for solving actual metal-forming problems. The study of plane flow of perfectly plastic solids is a branch of applied mathematics and is encompassed in the theory of plasticity. As a tool, however, the theory is not readily usable by the practicing engineer because of mathematical complexities and the consumption of time usually encountered in the solution of problems. For a discussion of general treatments of plastic-flow problems by analytical and numerical methods, the reader is referred to the literature and in particular to books by Hill (4) and Prager and Hodge (5).

An important step forward in the practical solution of forming problems was made when Prager (6) in 1953 published an article on the general geometrical interrelationships of the maximum-shear directions or slip lines in the physical plane, on velocities in the hodograph, and on stresses in the stress plane. He further showed in this treatise, which undoubtedly will come to be recognized as a milestone of progress in forming technology, that approximate solutions can be obtained by relatively simple graphical means.

The purpose of this paper is to point out some additional features of the slip-line field and hodograph which heretofore apparently have not been used for graphical construction.

Some Properties of Slip-Line Fields

Let Fig. 1 represent a general slip-line solution of two centered fans symmetrically spaced about a center line. Slip-line solutions of this kind are known as Hencky-Prandtl nets (7) and consist of orthogonal families of α and β slip lines. The properties of these nets have been formulated in the theorems of Hencky (8) and Prandtl (9) and in the following sections use will be made of these properties.

Consider the β_2 slip line of Fig. 1 which crosses the α_2 slip line at D. The local radius of curvature of the α_2-line at D is given by $Dd = R_D$ and is tangent to the β_2-line because of orthogonality. In accordance with the equations derived by Hencky (8), the radius of curvature of a slip line of one family changes by the distance traveled along the intersecting slip line of the other family. Hence the radius of curvature of the α_1 slip line, as we travel along the β_2 slip line from D to A, is given by $R_D + DA = R_A$. A statement of this property of slip lines is known as Hencky's second theorem, which has been extended by Prandtl (9) to read that the center of the radius of curvature lies on the

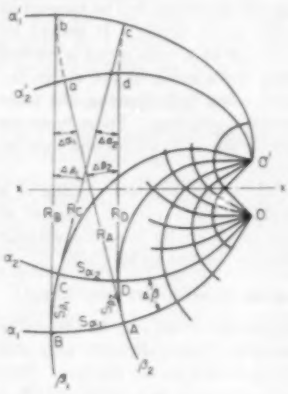

Fig. 1 Portion of a Centered-Fan-Type Hencky-Prandtl Net

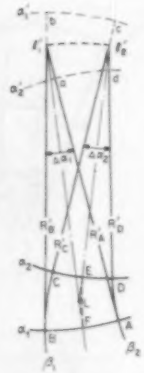

Fig. 2 Portion of a Curvilinear Square Formed When Two Pairs of Slip Lines of Each Family Cross Each Other

involute da which has been identified as the α_2'-line in Fig. 1. If the Hencky-Prandtl theorems also are applied as we travel along the β_1-line, it is at once evident that the radius of curvature changes from R_C to R_B and that its center moves along the involute cb.

Hencky's first theorem may now be applied to show that the angle between the tangents or radii of curvature of two fixed

---

[1] Professor of Metal Processing, University of California. Mem. ASME.

[2] Numbers in parentheses refer to the Bibliography at the end of the paper.

Contributed by the Applied Mechanics Division and presented at the Annual Meeting, New York, N. Y., November 25–30, 1956, of The American Society of Mechanical Engineers.

Discussion of this paper should be addressed to the Secretary, ASME, 29 West 39th Street, New York, N. Y., and will be accepted until April 10, 1957, for publication at a later date. Discussion received after the closing date will be returned.

Note: Statements and opinions advanced in papers are to be understood as individual expressions of their authors and not those of the Society. Manuscript received by ASME Applied Mechanics Division, May 23, 1956. Paper No. 56—A-14.

shear lines of the same family remains constant, hence $\Delta\beta_1 = \Delta\beta_2$ and similarly $\Delta\alpha_1 = \Delta\alpha_2$. It should be noted that the center of the radius of curvature of an α-line, as for example α_2, as we travel from D to C, moves along the involute dc.

Let Fig. 2 represent the curvilinear square A-B-C-D of Fig. 1 and let the tangents at the points of intersection of the α and β slip lines of this square intersect at l_2' and l_1', respectively. This modification requires an extension of the tangents at A and D, but a shortening of those at B and C without altering the angle $\Delta\alpha$. This geometrical construction establishes the two geometrically similar polygons D-E-C-l_1' and A-F-B-l_1', which may be provided with center lines El_2' and Fl_1', respectively, which intersect at L. These two polygons become congruent as the spacing of the α-lines approaches zero, and in the limit when $\alpha = 0$ the α_1 and α_2-lines are coincident and hence the points E and F coincide with the point of intersection L of two imaginary center lines. From this it is clear that the Hencky relationships may be applied to the point of intersection of the center lines and that the length of the center line, as it rolls from E to F along the curved path, increases exactly by the length of path traveled, namely E-F. Thus, if the polygons are thought of as a portion of a wedge, then the center line of this wedge can be made to roll along a curved path, such that the edges of the wedge will be tangent at all times to two slip lines of the same family. It should be noted that the center line of a wedge as it rolls along a curved path, traces a slip line only when the spacing of the wedge becomes infinitesimal; for slip lines having finite spacing, the trace of the center line apparently is not a slip line. These facts are of importance in graphical construction of slip lines and may be expressed in the following theorem:

A wedge having the same angle as the slip-line spacing of a centered fan-type Hencky-Prandtl net will remain tangent to the slip lines of the same family, as its center line rolls without sliding along a curved path which is tangent to this line.

Graphical Determination of Hencky-Prandtl Nets

The geometrical relationships just described may be utilized in a graphical technique for obtaining Hencky-Prandtl nets and hodographs. Let line OB_1B_n of Fig. 3 be a known slip line. This slip line as shown in the figure may belong to a family which is centered at O. Let it be required to find the other slip lines of

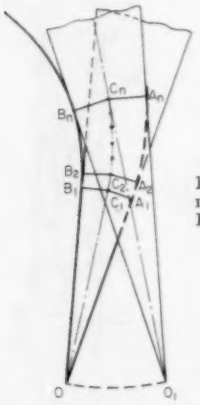

Fig. 3 Graphical Method of Establishing Slip Lines, When One Slip Line Is Known, by Use of Cardboard Wedges

the same family at any arbitrary angular spacing of either an α or β slip line. In order to accomplish this, a cardboard wedge of manila folder thickness is cut, having the correct wedge angle and having been provided with an arbitrary series of lines normal to the edge of the wedge which meet on a common center line. These intersecting normal lines can be imagined as tangents to a slip line which intersects the edges of the wedge if this slip line as an approximation is replaced by a circular arc. One side of this wedge is then made to coincide with points OB_1 of the slip line OB_1B_n with the center point of the wedge located at O. This permits drawing of the straight portion OA_1 of the slip line OA_1A_n. A pencil point may now be used as a center of rotation by pressing down at point C_2. The wedge is then rotated counterclockwise until B_2 becomes tangent to the given slip line. This permits drawing a short element of the required slip line at A_2. It is seen that by repeating this process, as point B moves from B_1 to B_n, the center C_1 moves to C_n by rolling without sliding along a fictitious center line, and n short segments of the required slip line can be drawn at A_1 to A_n. It should be noted that it is permissible to use segments of wedges as shown in Fig. 4 in order to establish slip lines, in the event the slip-line spacing

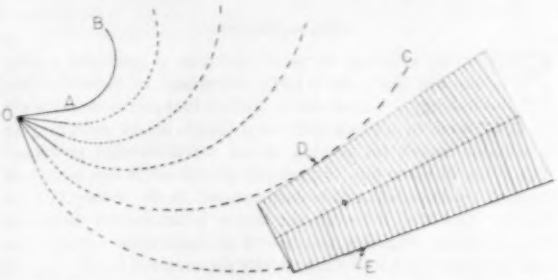

Fig. 4 Use of a Wedge Segment During Determination of Slip-Line Fields

becomes too large and hence the wedge too long and unwieldy to handle. To use such a wedge segment it is necessary merely to lay it tangent to the already drawn slip-line segments, as, for example, at points D and E of Fig. 4. The slip lines of the other family are drawn in a similar manner, utilizing the center of the second centered fan.

To get some measure of the accuracy of the graphical method, a two-centered fan (15-deg equiangular) Hencky-Prandtl net has been drawn with this method and is compared with the same net computed by Hill (10) using numerical methods. The net obtained graphically is shown in Fig. 5. The α and β slip lines were

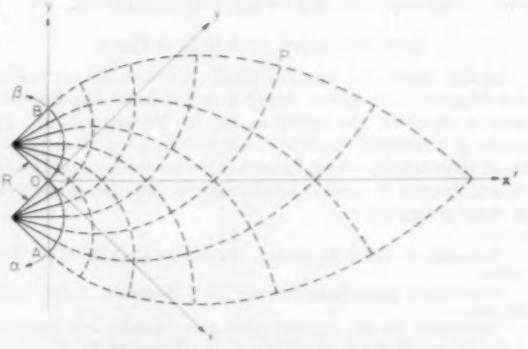

Fig. 5 General Two-Centered-Fan Solution

obtained independently and it is to be noted that the slip lines meet at 45 deg on the center line OX'. This was accomplished without trial and error and shows the reproducibility of the method without requiring excessive care. A comparison of the measured results, using an actual radius of 2 in. for the centered

TABLE 1 COMPARISON OF HILL'S (10) NUMERICAL SOLUTION OF A PROBLEM OF SYMMETRIC-CENTERED FANS WITH GRAPHICAL SOLUTION

Coordinate	x' Numerical	x' Graphical	y' Numerical	y' Graphical
1.1	0.428	0.44	0	0
1.2	0.647	0.66	0.286	0.29
1.3	0.792	0.80	0.639	0.64
1.4	0.845	0.85	1.040	1.05
1.5	0.789	0.80	1.464	1.46
1.6	0.617	0.63	1.880	1.90
2.2	1.018	1.02	0	0
2.3	1.333	1.34	0.413	0.41
2.4	1.552	1.57	0.944	0.94
2.5	1.634	1.65	1.571	1.57
2.6	1.545	1.58	2.256	2.21
3.3	1.867	1.87	0	0
3.4	2.338	2.37	0.615	0.62
3.5	2.673	2.70	1.429	1.44
3.6	2.804	2.85	2.414	2.43
4.4	3.13(4)	3.17	0	0
4.5	3.85	3.90	0.937	0.93
4.6	4.37	4.43	2.205	2.21
5.5	5.06	5.08	0	-0.01
5.6	6.17	6.22	1.453	1.45
6.6	8.04	8.08	0	-0.01

fans and a 15-deg wedge angle, is given in Table 1. The co-ordinates, after Hill, are referred to the rectangular axes (x', y') passing through O and are directed along the perpendicular to the axis of symmetry. These nodal points are also identified by integers measured along the x and y-axis as m and n, respectively. Thus the co-ordinates of point $P(x, y)$ are $m = 4$, $n = 6$. It is seen by referring to Table 1 that the errors are approximately 1 to 2 per cent, which is in most instances equal to the width of a fine pencil line and hence is an inherent inaccuracy in any graphical method. Then, too, the fact that second-order quantities are neglected in the use of circular arcs between families even when spaced as far apart as 15 deg contributes to inaccuracy, but appears to be of minor consequence. This was demonstrated by the use of a 30-deg wedge, which gave approximately the same net but was clumsier to use than a smaller wedge.

If a general Hencky-Prandtl net has been established, as, for instance, that of Fig. 5, the solution does not become specific until another boundary condition has been introduced. Let *G-G* of Fig. 6 be a boundary across which the slip lines cannot be continued, as, for example, a surface of a rigid container. Let it be assumed further that the slip lines must meet this container at 45 deg and that this slip line lies between the *E-E* and *F-F* slip lines already established. The required slip line is found by placing a wedge tangent to points *A* and *B* so that one of the equally spaced radial lines, as, for example, *C-D*, emanating from the center of the wedge, is at 45 deg to the surface *G-G*. If it is required to obtain a more accurate angle of this new slip line with an already drawn neighboring line, it will be necessary to apply a correction. This correction is necessary because of the fact that slip lines spaced at equal finite angles are not spaced at equal distances, when measured along a slip line of the other family. A correction is, however, conveniently found from a graph of the angular spacing between slip lines as a function of

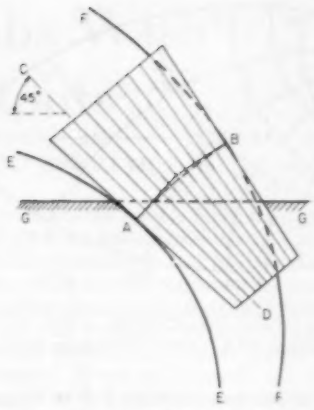

FIG. 6 DETERMINATION OF A SLIP LINE AT A BOUNDARY BY MEANS OF A WEDGE SEGMENT

distance along a slip line of the other family. The corrected angle can be read from this graph and another wedge having this angle may be used to establish the corrected slip line by the method already described.

GRAPHICAL DETERMINATION OF HODOGRAPH

Fig. 7 shows a general 15-deg equiangular Hencky-Prandtl net, which was obtained graphically and which has been applied to a problem in sheet extrusion through a sharp-edged die. This general solution also can be applied to other problems in plane strain, as, for example, piercing and forging. For convenience in discussing this problem, the β-lines have been numbered and the α-lines have been given lower-case letters as shown in Fig. 7. This permits easy identification of points of intersection of two slip lines by combinations of numbers and letters.

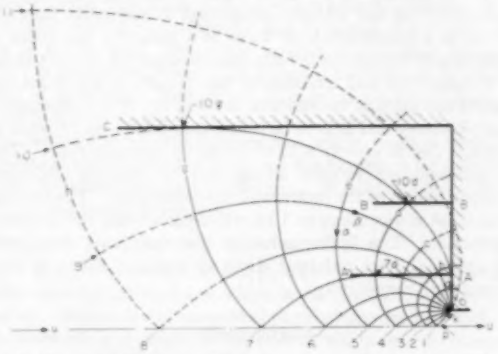

FIG. 7 SEVERAL POSSIBLE SOLUTIONS FOR A PROBLEM OF STRIP EXTRUSION

Referring to Fig. 7 it is seen that the billet moves with a velocity u to the right of the figure and that the extruded product leaves the die opening at 0-1 with a uniform velocity U. The billet is confined in the container by the die *O-A-B-C* and by three possible container walls *A-A*, *B-B*, or *C-C* shown shaded in the figure. These three boundaries have intersecting slip lines at 7*d*, 10*d*, and 10*g*, respectively, as discussed by Hill (4, 11) under the following conditions:

1 Slip line 7 is tangent to boundary *A-A* at 7*d* and at an angle of 45 deg to die *O-A* at *O* for maximum container wall friction.

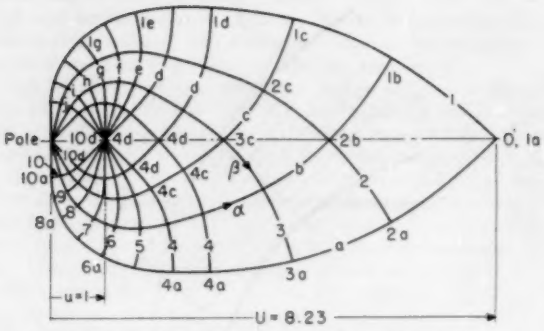

FIG. 8 HODOGRAPH SATISFYING BOUNDARY *B-B* OF FIG. 7

2 Slip line 10 intersects boundary *B-B* at 10*d* at an angle of 45 deg and gives a condition for zero container-wall friction.

3 Slip line 10 is parallel to boundary *C-C* at 10*g* and hence represents a condition for maximum friction, without having line 10 cross the rigid container wall and hence enter into a forbidden zone.

In the discussion to follow it is assumed that the reader is familiar with hodographs since this subject has been discussed adequately elsewhere (1, 6, 12). Fig. 8 shows the hodograph for the solution given by the frictionless boundary *B-B*. The hodograph was constructed entirely with 15-deg wedges in a manner analogous to the one used for the Hencky-Prandtl net. This is possible because the properties of the network of lines on the physical plane have identical properties with those on the hodograph. The hodograph is started by laying off a velocity of unity from the pole to the point 10*d* from which lines 4 to 10 and *d* to *j* radiate as a 15-deg centered fan. It is to be noted that the same identification system has been used as for the slip lines of Fig. 7. A number or letter identical with a slip line has the significance that the velocity component is normal to that slip line, while a combination of these two indicates the point of intersection of normals to the slip lines; it also gives a direct measure of magnitude and direction of the velocity if a straight line connects the point of intersection to the pole. The hodograph is self-explanatory and it is to be noted that lines *a* and 1 meet on the center line at exactly 8.23 which is the extrusion ratio. This was accomplished without adjustment by treating the upper and lower halves of the hodograph independently. The velocity of the billet *u* was taken as 1 in. when performing the graphical construction. The hodographs for the remaining boundaries *A-A* and *C-C* were obtained similarly and are shown in Figs. 9(*b*) and 9(*a*), respectively.

CONCLUSIONS

1 The graphical method developed in the paper for constructing Hencky-Prandtl nets is both practical and rapid.

2 The method may be used for nets on both physical planes and hodographs.

3 A comparison of a two-centered fan solution with that obtained numerically by Hill shows that the error of the graphical solution is of the order of 1–2 per cent, which in most cases is of the width of a fine pencil line.

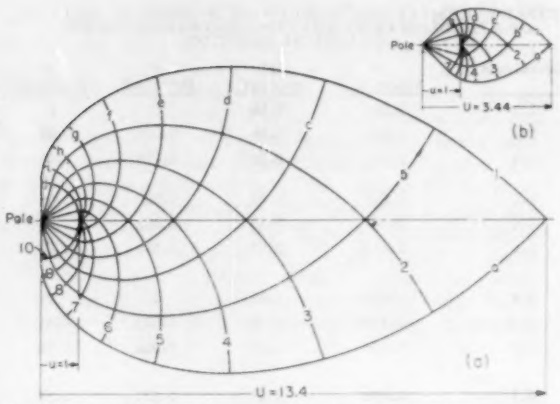

FIG. 9 HODOGRAPHS SATISFYING NETS OF FIG. 7: (*a*) BOUNDARY *C-C*; (*b*) BOUNDARY *A-A*

ACKNOWLEDGMENT

The author wishes to acknowledge the support given by the National Science Foundation (grant G-1002) and the University of California for this investigation.

BIBLIOGRAPHY

1 "The Theory of Plasticity in Relation to Its Engineering Applications," by Hugh Ford, *Zeitschrift für angewandte Mathematik und Physik*, vol. 5, Fas. 1, 1954, pp. 1–35.

2 "Comparison of Slip-Line Solutions With Experiment," by E. G. Thomsen, JOURNAL OF APPLIED MECHANICS, Trans. ASME, vol. 78, 1956, pp. 225–230.

3 "Comparison of an Unsymmetric Slip Line Solution in Extrusion With Experiment," by T. F. Jordan and E. G. Thomsen, *Journal of the Mechanics and Physics of Solids*, vol. 4, 1956, pp. 184–190.

4 "The Mathematical Theory of Plasticity," by R. Hill, Oxford, at the Clarendon Press, Amen House, London, England, 1950, pp. 129–160.

5 "Theory of Perfectly Plastic Solids," by W. Prager and P. G. Hodge, John Wiley & Sons, Inc., New York, N. Y., 1951, pp. 123–168.

6 "A Geometric Discussion of the Slip Line Field in Plane Plastic Flow," by W. Prager, Transactions of the Royal Institute of Technology, Stockholm, Sweden, no. 65, 1953, pp. 1–25.

7 "Über die Hencky-Prandtlschen Kurven," by C. Caratheodory and E. Schmidt, *Zeitschrift für angewandte Mathematik und Mechanik*, vol. 3, 1923, pp. 468–475.

8 "Über Einige Statisch bestimmte Fälle des Gleichgewichts in Plastischen Körpern," by H. Hencky, ibid., vol. 3, 1923, pp. 241–251.

9 "Anwendungsbeispiele zu einem Henckyschen Satz über das Gleichgewicht," by L. Prandtl, ibid., vol. 3, 1923, pp. 401–406.

10 "The Mathematical Theory of Plasticity," by R. Hill, Oxford, at the Clarendon Press, Amen House, London, England, 1950, pp. 156, 350.

11 "A Theoretical Analysis of the Stresses and Strains in Extrusion and Piercing," by R. Hill, *Journal of the Iron and Steel Institute*, vol. 158, 1948, pp. 177–185.

12 "On Unsymmetrical Extrusion in Plane Strain," by A. P. Green, *Journal of the Mechanics and Physics of Solids*, vol. 3, 1955, pp. 189–196.

Yield Loads of Slabs With Reinforced Cutouts[1]

By P. G. HODGE, JR.,[2] and NICHOLAS PERRONE,[3] BROOKLYN, N. Y.

A method of computing upper and lower bounds on the carrying capacity of a plane slab with a reinforced cutout is presented. The slab is subjected to a uniaxial load which is either uniform or applied by means of a perfectly rigid clamp. The results are applied to several examples and are found to agree quite well with experimental values.

1 Introduction

IN STRUCTURAL design it is frequently necessary to utilize plane slabs as tensile carrying members. If the slab is uniform, then the usual techniques of the theory of elasticity furnish a practical method for designing the plate. For example, the maximum uniaxial load which can be carried by a uniform slab is simply the maximum allowable stress multiplied by the cross-sectional area. However, if it is necessary to interrupt the slab with a cutout, the analysis or design becomes considerably more complex. For example, a re-entrant corner in a plate under a tensile load gives rise to an elastic design load of zero while a pin-point hole gives a stress-concentration factor of 3. Even if the re-entrant corners are filleted, elasticity theory still predicts relatively high stress concentrations in the neighborhood of the fillets. These factors are legitimate design criteria for a brittle material which will crack when the maximum allowable stress is reached. However, for a ductile material, a small amount of local plastic flow usually will relieve such concentrations. Therefore, from a practical point of view, the formation of these local plastic regions will not in itself impair the load-carrying capacity of the plate.

Of course, as the load is further increased the plastic regions will spread and eventually the resulting deformations will render the slab no longer serviceable. However, there is frequently a substantial difference between the maximum elastic load and the maximum serviceable load. For a ductile material which is not subjected to repeated alternating loads, the latter load may well be a more realistic design criterion.

This paper is concerned with the determination of this maximum serviceable load for uniform slabs with various shapes of reinforced cutouts. For definiteness the maximum serviceable load will be identified with the "yield load" of the theory of limit analysis. For an ideal rigid, perfectly plastic material this is the smallest load for which any deformations can occur; for a real material it represents the load at which relatively small increments of load produce relatively large increments in deformation.

Comparatively little previous work has been done in this field. Weiss, Prager, and Hodge (1)[4] considered the problem of determining the uniform circular cylindrical reinforcement necessary to restore a slab with a circular cutout to full strength. Levin (2) extended their work to include more general reinforcements for circular cutouts. Hodge and others (3, 4, 5, 6) and Gaydon and his associates (7, 8) have considered various cases of slabs with unreinforced cutouts. Some experimental work has been done by Vasarhelyi and Hechtman (9, 10, 11, 12).

In the present paper some of the theoretical results previously obtained will be extended to somewhat more general types of reinforced cutouts. In particular, estimates of the yield load will be made for some of the particular specimens considered by Vasarhelyi and Hechtman for the purpose of comparing theoretical and experimental results.

In the next section, the problem will be clearly stated and the basic assumptions enumerated. Also, the limit-analysis theorems of Drucker, Greenberg, and Prager will be expressed in an appropriate form.

Section 3 will be concerned with the determination of upper and lower bounds on the yield loads of slabs with unreinforced cutouts by assuming conditions of plane stress. In Section 4 the reinforcement will be treated as a curved beam, and lower bounds on some particular shaped reinforcements will be found. These results will be combined with those of Section 3 to furnish lower bounds on the yield loads of slabs with reinforced cutouts. If the load is introduced to a reinforced slab by means of a uniform motion of the boundary, then the method of obtaining the lower bound is altered somewhat. This type of loading will be investigated in Section 5. Next, upper bounds on reinforced slabs are found in Section 6.

In Section 7 a numerical comparison will be made between the theoretical results obtained here and the experimental values obtained by Vasarhelyi and Hechtman. Finally, the conclusions will be discussed in Section 8.

2 Statement of the Problem

The paper is concerned with a square slab containing a centered cutout of some given shape which is reinforced in a prescribed manner. Regardless of the actual physical process by which the reinforcement is attached to the slab, it will prove convenient to regard any reinforcing material, together with that part of the slab which is under the reinforcement, as the "hub." The remainder of the slab will be referred to as the "base slab," Fig. 1.

Equal and opposite loads are applied to two opposing edges of the slab. In practice, the method of applying these loads may vary and, in any case, it is difficult to analyze the exact stress distribution at the edge of the slab. Therefore, in the analysis two extreme situations will be assumed. In one case the load will be taken as uniform and of intensity $2k\lambda\lambda_T$ per unit length, where λ is the thickness of the base slab and $2k$ is the tensile yield stress. Since a slab without any cutout can support an edge load of $2k\lambda$, the "cutout factor" $\lambda_T(\lambda_T \leq 1)$ represents the relative tensile capacity of the slab under uniform tension. The other

[1] The material presented in this paper was obtained in the course of research sponsored by the Office of Naval Research. This paper is part of a thesis submitted by one of the authors (NP) in partial fulfillment of requirements for the degree of Doctor of Philosophy in Applied Mechanics at the Polytechnic Institute of Brooklyn.

[2] Professor of Applied Mechanics, Polytechnic Institute of Brooklyn. Mem. ASME.

[3] Research Associate in Applied Mechanics, Polytechnic Institute of Brooklyn.

Contributed by the Applied Mechanics Division and presented at the Annual Meeting, New York, N. Y., November 25–30, 1956, of The American Society of Mechanical Engineers.

Discussion of this paper should be addressed to the Secretary, ASME, 29 West 39th Street, New York, N. Y., and will be accepted until April 10, 1957, for publication at a later date. Discussion received after the closing date will be returned.

Note: Statements and opinions advanced in papers are to be understood as individual expressions of their authors and not those of the Society. Manuscript received by ASME Applied Mechanics Division, May 3, 1956. Paper No. 56—A-7.

[4] Numbers in parentheses refer to Bibliography at end of paper.

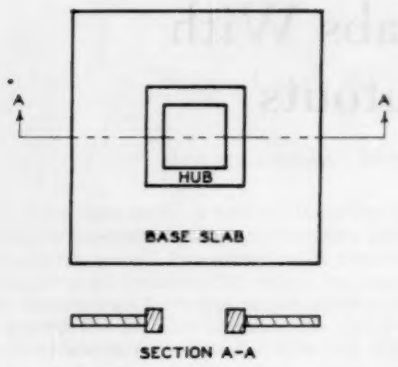

FIG. 1 SLAB WITH REINFORCED CUTOUT

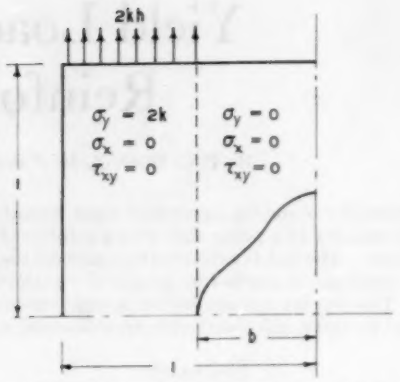

FIG. 2 AN EXTREME LOAD CONDITION ASSOCIATED WITH UNIFORM EDGE MOVEMENT

extreme load condition is to assume a uniform velocity at the edges. In this case the actual pressure distribution across the edge is unknown, but the cutout factor $\lambda_P(\lambda_P \leq 1)$ can be defined by $2kh\lambda_P L = P$, where P is the total applied load and L the total width of the slab.

It will be assumed that the dimensions of the hub and slab are such that the stress distribution in the base slab may be characterized by "plane stress," while the hub may be analyzed by general beam theory. Both the hub and slab are assumed to be made of a perfectly plastic material which satisfies the Tresca yield condition and the associated flow law. For such a material in a state of plane stress, the theorems of limit analysis (13, 14) state that:

1 The yield load is the largest load for which it is possible to find any equilibrium stress field which satisfies the yield restriction

$$\max\ [|\sigma_1|,\ \ |\sigma_2|,\ \ |\sigma_1 - \sigma_2|] - 2k \leq 0 \qquad [1]$$

2 The yield load is the smallest load for which the internal rate of dissipation of energy

$$D_i = 2k \max\ |\dot{\epsilon}| \qquad [2]$$

is less than the rate at which the surface tractions do work on the surface velocities.

The two theorems can be used together to provide upper and lower bounds on the yield load. In the event that these bounds coincide, the exact yield load must be their common value. However, even when they do not coincide, the limits may be sufficiently close together to provide a reasonable basis for engineering analysis and design.

3 YIELD LOAD OF UNREINFORCED SLAB

The yield load for a slab with an unreinforced cutout subject to uniform boundary motion is easily determined to be

$$\lambda = 1 - b \qquad [3]$$

where $2b$ is the maximum width of the cutout. Indeed, the stress distribution shown in Fig. 2 is evidently statically admissible, so that $1 - b$ is a lower bound. An upper bound is obtained by considering sliding out of the plane at an angle $\beta = 45$ deg (Fig. 3). In this case, the internal rate of energy dissipation must be computed by a limiting process, and is readily found to be

$$D_i = kAv = 2khv\,(1 - b)\sqrt{2} \qquad [4]$$

Since the external energy-dissipation rate is $(2k\lambda)\,(2h)\,(v/\sqrt{2})$,

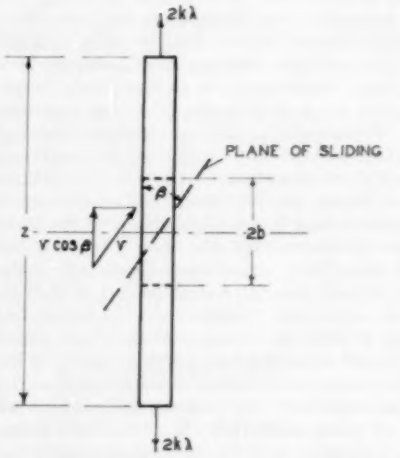

FIG. 3 SLIDING OUT OF PLANE FOR UNREINFORCED SLAB

it follows from the second theorem of limit analysis that $1 - b$ is also on upper bound, and hence the exact cutout factor.

If the edge load is uniform, then Equation [3] still provides an upper bound, but Fig. 2 no longer satisfies the stress-boundary conditions. In this case, it is found profitable to use a discontinuous stress field (4, 6, 7), as illustrated for a square cutout in Fig. 4. In view of later applications, the general case of internal and external loads is considered. The discussion is best conducted in terms of the principal stresses $2kr$ and $2ks$, and the angle θ between a principal stress and the x-axis. For the example of Fig. 4 it may be verified that the stress solution

$$r_1 = [(\lambda - \mu)b]/[(1 - b)(1 - y)],\ s_1 = \lambda,\ \ \theta_1 = 0 \qquad [5]$$

$$\left.\begin{aligned} r_2 + s_2 &= (\lambda - \mu)/(1 - b) \\ &\quad [(\lambda - \mu b)/(\lambda - \mu) - 2b/y] \\ r_2 - s_2 &= \{[y(\lambda - \mu b)]^2 + [2b(\lambda - \mu)]^2\}^{1/2}/y(1 - b) \end{aligned}\right\} \qquad [6]$$

$$\theta_2 = 1/2 \cos^{-1} \{y(\lambda - \mu b)/\left[[y(\lambda - \mu b)]^2 + [2b(\lambda - \mu)]^2\right]^{1/2}\}$$

$$r_3 = (\lambda - \mu)b/[(b - y)(1 - b)],\ \ s_3 = \mu,\ \ \theta_3 = 0 \qquad [7]$$

$$r_4 = 0,\ \ s_4 = (\lambda - \mu b)/(1 - b),\ \ \theta_4 = 0 \qquad [8]$$

satisfies equilibrium and boundary conditions.

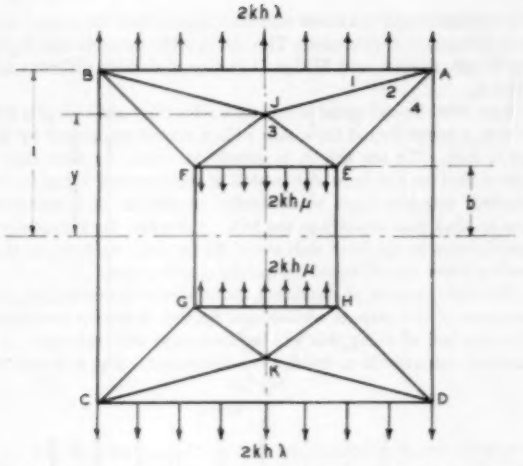

FIG. 4 STATICALLY ADMISSIBLE STRESS FIELD FOR SQUARE SLAB WITH CENTERED SQUARE CUTOUT

The yield Inequality [1] may now be written as

$$\max [|r_i|, \quad |s_i|, \quad |r_i - s_i|] \leq 1, \quad i = 1, 2, 3, 4 \ldots . \quad [9]$$

Since each of the six Inequalities [9] must be satisfied in each of the four regions, there is a total of 24 inequalities to be satisfied if the stress field is to be statically admissible. However, it can be shown that for any choice of y which satisfies the geometrical requirement

$$b \leq y \leq 1 \ldots \ldots \ldots

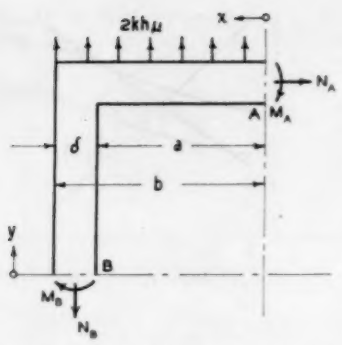

FIG. 7 QUARTER SECTION OF A SQUARE HUB FOR A SQUARE CUTOUT

As a first example a square reinforcement of a square cutout will be considered, Fig. 7.

Equilibrium of generic Cartesian sections x or y is clearly satisfied if

$$\left.\begin{aligned} M(x) &= kh\mu(ab - x^2) - M_B \\ N(x) &= 0 \end{aligned}\right\} \quad 0 \leq x \leq a \ldots\ldots [13a]$$

$$\left.\begin{aligned} M(y) &= M_B \\ N(y) &= 2kh\mu b \end{aligned}\right\} \quad 0 \leq y \leq a \ldots\ldots\ldots [13b]$$

where M_B is an arbitrary redundant moment. Substitution of Equations [13] into the yield Inequality [12] results in

$$-(2kH\delta)^2 + 8k^2Hh\mu(ab - x^2) \leq 8kHM_B \leq (2kH\delta)^2 + 8k^2Hh\mu(ab - x^2) \ldots\ldots [14a]$$

$$-(2kH\delta)^2 + (2kh\mu b)^2 \leq 8kHM_B \leq (2kH\delta)^2 - (2kh\mu b)^2 \ldots [14b]$$

The extreme right and left-hand sides of Inequality [14a] could be considered as separate functions of x for the interval $0 \leq x \leq a$. Obviously, the absolute minimum value of the right-hand side occurs at $x = a$; the maximum value of the left-hand side occurs at $x = 0$. Hence, Inequalities [14] will be satisfied provided that

$$-(2kH\delta)^2 + 8k^2Hh\mu\, ab \leq 8kHM_B \leq (2kH\delta)^2 + 8k^2Hh\mu a(b - a) \ldots\ldots [15a]$$

$$-(2kH\delta)^2 + (2kh\mu b)^2 \leq 8kHM_B \leq (2kH\delta)^2 - (2kh\mu b)^2 \ldots [15b]$$

Since M_B is a redundant quantity its value need not be specified to obtain a statically admissible stress field; it is only necessary to guarantee that its value will be such that the Inequalities [15] are not inconsistent. A necessary and sufficient condition that this be so is that each lower limit on M_B be less than each upper limit. It is readily verified that the largest value of μ which satisfies the resulting inequalities is

$$\mu = (a/b)(H/h)[-1 + \sqrt{1 + 2(\delta/a)^2}] \text{ if } \delta/a \leq 2. [16a]$$

$$\mu = (\delta/b)(H/h) \quad \text{if} \quad \delta/a \geq 2 \ldots\ldots\ldots [16b]$$

Equations [16] represent a solution to the square reinforcement problem obtained by utilizing Cartesian co-ordinates. Hodge (6) has shown that the identical result is produced if cylindrical co-ordinates and stress resultants are employed.

The case of a circular cutout of radius a, reinforced by a circular reinforcement of constant thickness δ, may be more conveniently solved with cylindrical co-ordinates, but leads, in fact, to exactly the same Equations [16] for μ. If μ is set equal to 1, the reinforcement thickness sufficient to reinforce the cutout slab to full strength is obtained. The result is the same as that found by Weiss, Prager, and Hodge (1) using a slightly different approach.

Any lower bound equal or less than 1 for the yield load of a hub is also a lower bound for a slab with a cutout reinforced by the given hub. To see this it is merely necessary to note that a stress field in the base slab which is uniform and equal to the applied external load is statically admissible and transmits the applied load directly to the hub. However, the actual stress distribution in the base slab would be far from uniform, so that such a lower bound would be unduly conservative.

For the purpose of obtaining an improved lower bound, the analyses of the present section and Section 3 can be combined. The method of doing this will be illustrated with reference to a circular cutout with a circular reinforcement. Fig. 8 shows the statically admissible stress field to be considered. Regions 1, 2, 3, 4 are the same as in Fig. 4 and the stress field is defined by Equations [5] to [8]. Region 5 is the uniform-stress field

$$r_5 = 0, \qquad s_5 = \mu, \qquad \theta_5 = 0$$

Obviously, this is in equilibrium with regions 3 and 4. Further, a uniform vertical traction of $2k\mu h$ per unit length is transmitted from region 5 to the hub, region 6.

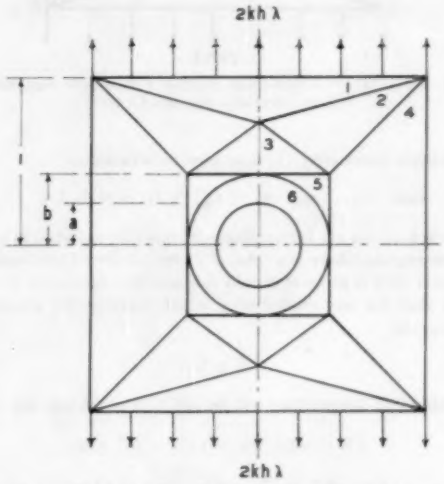

FIG. 8 STATICALLY ADMISSIBLE STRESS FIELD FOR SQUARE SLAB WITH CENTERED CIRCULAR REINFORCED CUTOUT

The analysis is as follows: The maximum value of μ which can be supported by the hub is given by Equations [16]. This value of μ is then substituted into Equations [11] to give a lower bound for the load factor λ. The extension to the other shapes considered is obvious.

5 LOWER BOUNDS FOR REINFORCED SLABS—UNIFORM-VELOCITY BOUNDARY CONDITIONS

The uniform-velocity boundary condition could be realized experimentally by means of a rigid clamping device on the edge. Since the reinforced cutout cannot strengthen the slab it is intuitively clear that the greater portion of the load will be taken by those portions of the slab somewhat removed from the slab center line. Therefore, a plausible loading system for a slab with a circular cutout and circular reinforcement is as shown in Fig. 9. Regions 1 and 2 are stressed to full yield, while region 3 is stress-

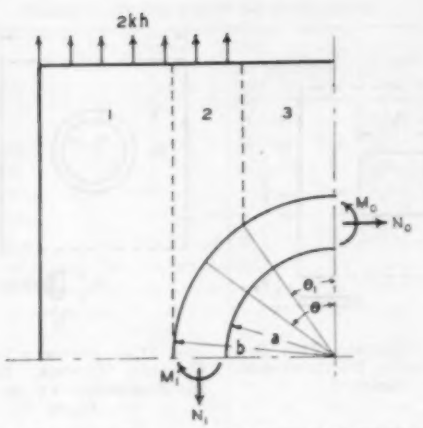

FIG. 9 CIRCULAR CUTOUT WITH CIRCULAR REINFORCEMENT

free. The problem resolves to finding the smallest value of θ_1 for which a statically admissible system will exist in the hub.

As in any closed bent-beam problem there is a single redundant which will be taken as M_0 (Fig. 9). Equilibrium then demands that the bending moment and axial force at any section be given by

$$\left.\begin{aligned} M &= M_0 \\ N &= 0 \end{aligned}\right\} \text{ for } 0 \leq \xi \leq \xi_1 \ldots\ldots\ldots\ldots [17a]$$

and

$$\left.\begin{aligned} M &= M_0 + Khb^2(\alpha\xi - \xi_1)(\xi - \xi_1) \\ N &= 2kHb\xi(\xi - \xi_1) \end{aligned}\right\} \text{ for } \xi_1 \leq \xi \leq 1 \ldots [17b]$$

where

$$\xi = \sin\theta, \qquad \xi_1 = \sin\theta_1$$

It is convenient to reformulate the problem in terms of dimensionless quantities

$$\alpha = a/b, \quad \eta = h/H$$

$$m = M/(khb^2), \quad m_0 = M_0/(khb^2) \ldots\ldots\ldots [18]$$

and to define three functions of ξ by

$$f_0(\xi) = (1 - \alpha)^2/2\eta$$

$$f_1(\xi) = (\eta/2)\xi^2(\xi - \xi_1)^2 \ldots\ldots\ldots\ldots\ldots [19]$$

$$f_2(\xi) = (\alpha\xi - \xi_1)(\xi - \xi_1)$$

Substitution of Equations [17], [18], [19] into Inequality [12] then yields

$$-f_0 + f_1 - f_2 \leq m_0 \leq f_0 - f_1 - f_2 \ldots\ldots [20a]$$

$$-f_0 \leq m_0 \leq f_0 \ldots\ldots\ldots\ldots\ldots [20b]$$

Inequality [20a] must be valid for all $\xi_1 \leq \xi \leq 1$, while [20b] is independent of ξ.

A necessary and sufficient condition that a solution of Inequalities [20] exist is that the minimum upper bound on m_0 is equal or greater than the maximum lower bound. Since f_1 is of the fourth power in ξ, the maximum and minimum values are not easily found in closed form, and since ξ_1 is unknown it is difficult to use numerical methods even in a specific example. However, since f_1 is positive and is to be added on the left and subtracted on the right, sufficient conditions on the existence of m_0 will be obtained if f_1 is replaced by any function which is pointwise greater than f_1. For $|\xi| < 1$ an obvious such choice is

$$f_1^* = (\eta/2)(\xi - \xi_1)^2$$

Therefore, it is desired to eliminate m_0 from the inequalities

$$-f_2 + f_1^* - f_2 \leq m_0 \leq f_0 - f_1^* - f_2 \ldots\ldots [21a]$$

$$-f_0 \leq m_0 \leq f_0 \ldots\ldots\ldots\ldots\ldots [21b]$$

If $\alpha > \eta$, $\alpha > \xi_1$, then it can be shown that a necessary and sufficient condition that Inequalities [21] possess a solution is that

$$-f_0 + f_1^*(\xi_0) - f_2(\xi_0) \leq m_0 \leq f_0 - f_1^*(1) - f_2(1) \ldots [22]$$

where

$$\xi_0 = \xi_1(1 + \alpha - \eta)/(2\alpha - \eta)$$

These inequalities obviously possess a solution if and only if the left-hand side is equal to or less than the right-hand side. After some computation it is seen that this is equivalent to the inequality

$$\left[\frac{(1-\alpha)^2}{2(2\alpha - \eta)} + 1 + \eta/2\right]\xi_1^2 - (1 + \alpha + \eta)\xi_1 + \left[\alpha + \frac{\eta}{2} - \frac{(1-\alpha)^2}{\eta}\right] \leq 0 \ldots\ldots [23]$$

Therefore, the desired value of ξ_1 is the smallest positive number satisfying Inequality [23]. For any given values of α and η this may be easily found. Finally, it follows from over-all equilibrium that the cutout factor is related to ξ_1 by

$$\lambda_{VL} = 1 - b\xi_1 \ldots\ldots\ldots\ldots\ldots [24]$$

By using the procedure just outlined, uniform-velocity lower bounds were found for six different specimens. These are listed in Table 1 under λ_{VL}. For all specimens considered, the assumed conditions $\alpha > \eta$, $\alpha > \xi_1$ were not violated.

Uniform-velocity lower bounds for a square cutout with square reinforcement can be found in a similar manner. In Fig. 10 a

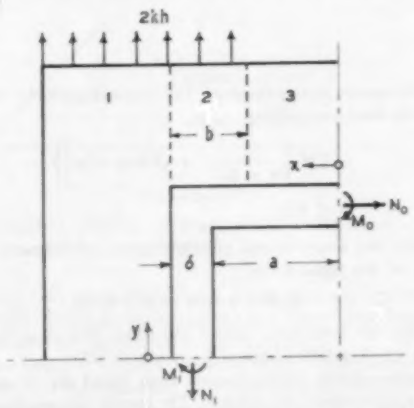

FIG. 10 SQUARE CUTOUT WITH SQUARE REINFORCEMENT

proposed load scheme is suggested for which it is required to find the maximum value of b that will support a statically admissible system. The stress fields 1, 2, 3 are the same as in the previous case. Because of the geometry of the problem it is expedient to use here a Cartesian co-ordinate system. Again, all force resultants can be expressed in terms of a single redundant-force re-

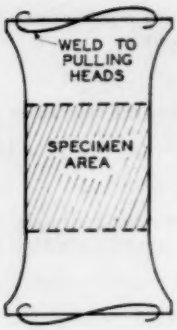

FIG. 11(a) PLANFORM OF TYPICAL TEST SPECIMEN

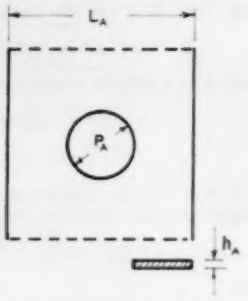

FIG. 11(b) SPECIMEN TYPE A—CIRCULAR CUTOUT, NO REINFORCEMENT

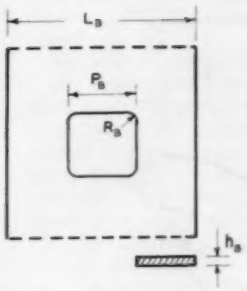

FIG. 11(c) SPECIMEN TYPE B—SQUARE CUTOUT, NO REINFORCEMENT

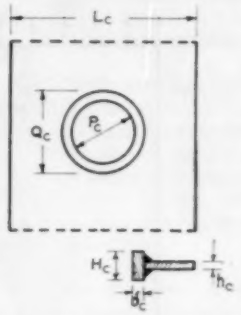

FIG. 11(d) SPECIMEN TYPE C—CIRCULAR CUTOUT, CIRCULAR REINFORCEMENT BY AN INSERT PLATE

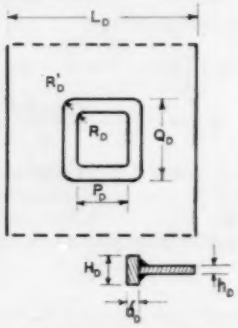

FIG. 11(e) SPECIMEN TYPE D—SQUARE CUTOUT, SQUARE REINFORCEMENT BY AN INSERT PLATE

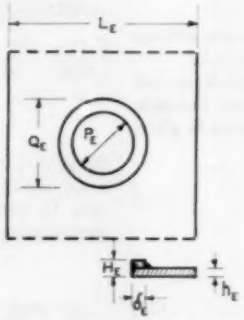

FIG. 11(f) SPECIMEN TYPE E—CIRCULAR CUTOUT, CIRCULAR REINFORCEMENT BY A SINGLE DOUBLER PLATE

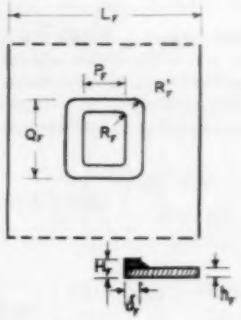

FIG. 11(g) SPECIMEN TYPE F—SQUARE CUTOUT, SQUARE REINFORCEMENT BY A SINGLE DOUBLER PLATE

sultant. Application of the yield Inequality [12] for the regions

$$0 \leq x \leq a$$

$$0 \leq y \leq a$$

and subsequent elimination of the redundant-force resultant, yields two final inequalities

$$b \leq \delta \left\{ \frac{1}{\eta + 2} \left[1 + \sqrt{3 + 4/\eta} \right] \right\} \quad [25a]$$

$$b \leq \delta/\eta \quad [25b]$$

Finally, the lower bound emerges upon enforcement of equilibrium of the rigid clamp

$$\lambda_{VL} = 1 - a - \delta + b \quad [26]$$

Obviously, the best lower bound will occur when b is the largest number which satisfies both of Inequalities [25].

Uniform-velocity lower bounds were found for 10 specimens having square reinforced cutouts. The results also are enumerated in Table 1 under λ_{VL}.

6 Upper Bounds on Reinforced Slabs

An upper bound for a slab with a reinforced cutout is easily obtained by a slight modification of the analysis for an unreinforced slab to account for the different thicknesses of the hub and slab (3). It is readily verified that the upper bound in this case is

$$\lambda = 1 - b + \delta/\eta \quad [27]$$

7 Comparison of Experimental and Theoretical Results

Vasarhelyi and Hechtman have carried out a series of tests on steel slabs with both reinforced and unreinforced cutouts (9). All specimens were stressed under uniaxial tension. The test sections of the slabs were square and had centered cutouts with various shaped reinforcements. The results showed that as the load was slowly increased the elongations remained small until a critical value of the load referred to as the general yielding load was reached. Thereafter a small increase of the load was accompanied by a disproportionately large increase of displacement. Finally the slab would fracture at a load referred to as the ultimate load. Obviously, the yield load defined in the preceding analysis should correspond to the experimentally observed general yielding load.

The specimens tested are shown schematically in Fig. 11. Since the cutout factor λ was defined as the ratio of the load carried by the slab with a reinforced cutout to the uncut slab, the experimental value λ_E has been computed in this fashion, using the test results from specimen 1 as a basis. The theoretical bounds on the cutout factor have been computed by the methods of Sections 3, 4, 5, and 6. The resulting comparisons are shown in Table 1 (the specimen numbering is that of Vasarhelyi and Hechtman). The second column in Table 1 gives the type of specimen (see Fig. 11), and the next group of columns lists its various associated dimensions. The last 4 columns list the experimental cutout factor λ_E, and the theoretical bounds.

Fig. 12 gives a pictorial representation of the results under the

TABLE 1 COMPARISON OF SPECIMENS

SPECIMEN NUMBER	TYPE	SPECIMEN DIMENSIONS (IN INCHES) L	a	h	H	R	A	T	Q	TEST TEMP (°F)	TERMINAL YIELDING LOAD (KIPS)	YIELD LOAD OF UNCUT SPEC. (KIPS)	λ_E	λ_{TL}	λ_U	λ_{TL}
2	A	36	–	1/4	–	–	–	9	–	76	281.5	390	.75	.59	.75	.75
3	D	36	–	1/4	–	1/32	–	9	–	72	292	390	.75	.59	.75	.75
4	D	36	–	1/4	–	1 1/8	–	9	–	78	292	390	.75	.59	.75	.75
5	C	36	1/4	1/4	2	–	–	9	9 1/2	74	324	390	.83	.62	.86	.70
6	C	36	1/4	1/4	1	–	–	9	9 1/2	73	324	390	.83	.62	.79	.77
7	D	36	1/4	1/4	2	1/4	1/4	9	9 1/2	75	322	390	.83	.62	.85	.78
8	D	36	1/4	1/4	1	3/16	3/16	9	9 1/2	74	293	390	.74	.62	.79	.77
9	D	36	1/4	1/4	2	1 1/8	1 1/8	9	9 1/2	72	319	390	.82	.62	.85	.78
10	D	36	1/4	1/4	1	1 1/8	1 1/8	9	9 1/2	75	323	390	.80	.62	.79	.77
11	E	36	4 1/2	1/4	1/2	–	–	9	28	75	360.5	390	.92	.74	1.00	.93
12	E	36	2 1/4	1/4	1/2	–	–	9	23 1/2	73	331.5	390	.85	.66	.88	.84
13	F	36	4 1/2	1/4	1/2	1/32	1 1/8	9	28	76	337.5	390	.86	.74	1.00	.93
14	F	36	2 1/4	1/4	1/2	1/32	1 1/8	9	23 1/2	71	300	390	.77	.65	.88	.84
15	F	36	4 1/2	1/4	1/2	1 1/8	1 1/8	9	28	76	362	390	.93	.84	1.00	.93
16	F	36	2 1/4	1/4	1/2	1 1/8	1 1/8	9	23 1/2	73	300	390	.77	.65	.88	.84
17	C	36	1 7/8	1/4	1/2	–	–	9	22 3/4	74	322	390	.83	.62	.85	.82
18	C	36	3/4	1/4	1	–	–	9	20 1/2	75	340	390	.87	.62	.76	.81
20	D	36	1 7/8	1/4	1/2	1/32	1 1/8	9	22 3/4	72	320	390	.82	.62	.85	.83
22	D	36	1 7/8	1/4	1/2	1 1/8	1 1/8	9	22 3/4	73	319	390	.82	.62	.85	.83

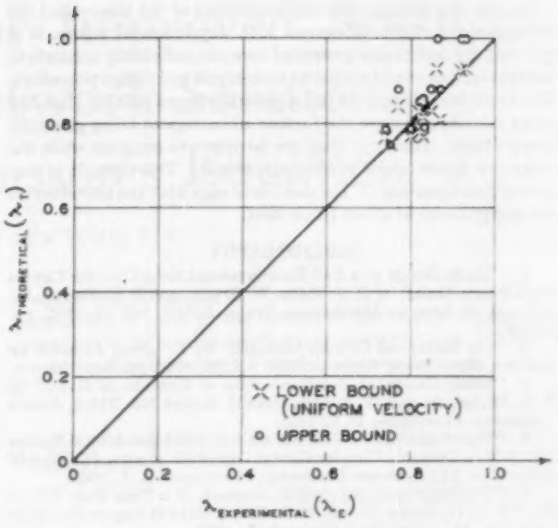

FIG. 12 GRAPHIC DISPLAY OF RESULTS (UNIFORM-VELOCITY LOWER BOUNDS)

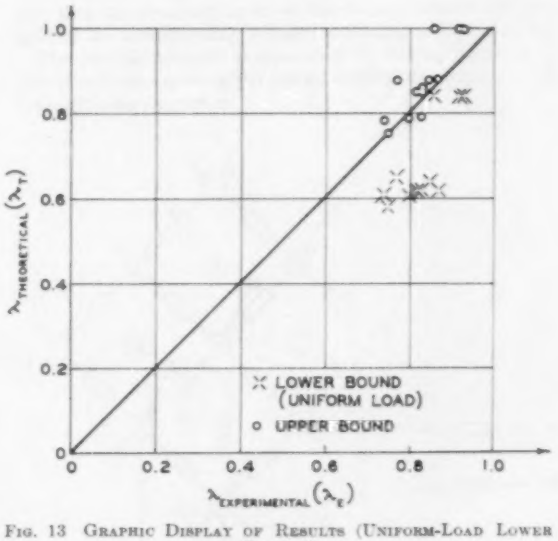

FIG. 13 GRAPHIC DISPLAY OF RESULTS (UNIFORM-LOAD LOWER BOUNDS)

assumption that the test corresponds to uniform edge velocity, while Fig. 13 does the same for uniform edge tension. In each case the experimentally observed value λ_E is taken as abscissa and the theoretical value as ordinate. The extent to which the two ordinates coincide is a measure of the closeness of the theoretical bounds, while the extent to which the points cluster about the line $\lambda = \lambda_E$ is a measure of the agreement between theory and experiment.

8 CONCLUSIONS

In comparing experimental results with theoretical predictions, it is necessary to analyze closely the extent to which the assumptions of the theory agree with the conditions of the experiments. In the present case, two different sets of theoretical results are available, corresponding to two different types of loading conditions. In the experiments of Vasarhelyi and Hechtman, the square "test section" was part of a larger specimen which was welded to pulling heads. Relative to the deformations undergone by the slab, the pulling heads are comparatively rigid, and the effect of the added length of material is to give further room for the stresses to distribute themselves in the most favorable fashion. Therefore, it appears reasonable to expect that the assumption of uniform boundary velocity would yield better agreement than the assumption of uniform load, and a comparison of Figs. 12 and 13 shows that this is indeed the case.

An examination of Fig. 12 shows that in only two cases does the experimentally observed load fall noticeably below the predicted lower bound, and in only one case is it noticeably above the predicted upper bound. Even in these cases the discrepancy is less than might be due to variations in the yield stress of different slabs. However, it may be due in part to the limitations of the theory; so that it is worth while to examine some of these limitations more carefully.

In using beam theory, which is essentially one dimensional, to describe the three-dimensional state of stress in the hub, certain stresses were neglected entirely, and others were averaged over the hub. In particular, in cases where the hub is thick relative to the base slab, the assumption that the stress is uniform over the width is obviously in error. As a result, the most favorable stress distributions were implicitly assumed to be statically admissible, while in reality the material might fail at a lower bound because it could not achieve this favorable distribution.

The same objection applies to a lesser degree to the assumption of plane stress in the base slab. The net effect of these assumptions is to predict an unconservative yield load, and hence they may partially account for those specimens which failed at loads less than those predicted.

On the other hand, the assumption of perfect plasticity neglects the additional carrying capacity due to strain-hardening of the material, which may partially explain the specimen which was stronger than predicted. Of course, the comparatively small number of specimens for which obvious inconsistencies existed might be attributed to some degree to experimental error.

Despite the afore-mentioned limitations of the theory and the accompanying slight differences with experimental values, it is felt that the techniques presented here are sufficiently accurate to warrant serious consideration as an analysis and design procedure. The lower bounds appear to be generally more reliable than the upper bounds and have the further advantage of being generally conservative. However, they are laborious to compute while the suggested upper bound is absurdly simple. Therefore, it is suggested that Equation [27] be used for design with the introduction of a design factor of about 10 per cent.

BIBLIOGRAPHY

1 "Limit Design of a Full Reinforcement for a Circular Cutout in a Uniform Slab," by H. J. Weiss, W. Prager, and P. G. Hodge, Jr., JOURNAL OF APPLIED MECHANICS, Trans. ASME, vol. 74, 1952, pp. 397–401.

2 "On Reinforced Circular Cutouts," by E. Levin, JOURNAL OF APPLIED MECHANICS, Trans. ASME, vol. 75, 1953, pp. 546–552.

3 "Limit Design of Reinforcements of Cutouts in Slabs," by P. G. Hodge, Jr. and W. Prager, GDAM Report No. B11-2, Brown University, Providence, R. I., 1951.

4 "Upper and Lower Bounds on the Yield Load of a Square Slab With a Centered Circular Cutout," by P. G. Hodge, Jr., GDAM Report No. B11-7, Brown University, Providence, R. I., 1952.

5 "The Reinforcement to Full Strength of a Thin Slab With a Slit," by P. G. Hodge, Jr. and B. K. Froyd, GDAM Report No. B11-10, Brown University, Providence, R. I., 1953.

6 "Final Report on Yield Loads of Slabs With Reinforced Cutouts," by P. G. Hodge, Jr., GDAM Report No. B11-22, Brown University, Providence, R. I., 1953.

7 "A Theoretical Investigation of the Yield Point Loading of a Square Plate With a Central Circular Hole," by F. A. Gaydon and A. W. McCrum, *Journal of the Mechanics and Physics of Solids*, vol. 2, 1953, pp. 156–169.

8 "On the Yield-Point Loading of a Square Plate With Concentric Circular Hole," by F. A. Gaydon, *Journal of the Mechanics and Physics of Solids*, vol. 2, 1954, pp. 170–176.

9 "Welded Reinforcement of Openings in Structural Steel Members," by D. Vasarhelyi and R. A. Hechtman, *The Welding Journal Research Supplement*, vol. 30, 1951, pp. 182s–192s.

10 "Welded Reinforcement of Openings in Structural Steel Members," by D. Vasarhelyi and R. A. Hechtman, *The Welding Journal Research Supplement*, vol. 31, 1952, pp. 169s–180s.

11 "Welded Reinforcement of Openings in Structural Steel Members," by D. Vasarhelyi and R. A. Hechtman, Third Progress Report, University of Washington, Seattle, Wash., 1953.

12 "Welded Reinforcement of Openings in Structural Steel Members," by D. Vasarhelyi and R. A. Hechtman, and Y. T. Yoshimi, Fourth Progress Report, University of Washington, Seattle, Wash., 1953.

13 "The Safety Factor of an Elastic-Plastic Body in Plane Strain," by D. C. Drucker, H. J. Greenberg, and W. Prager, JOURNAL OF APPLIED MECHANICS, Trans. ASME, vol. 73, 1951, pp. 371–378.

14 "Extended Limit Analysis Theorems for Continuous Media," by D. C. Drucker, W. Prager, and H. J. Greenberg, *Quarterly of Applied Mathematics*, vol. 9, 1952, pp. 381–389.

A Simple Procedure for Improved Accuracy in the Resistor-Network Solution of Laplace's and Poisson's Equation

By H. G. LANDAU,[1] NEW YORK, N. Y.

The necessity for practical solutions of Laplace's and Poisson's equations arises frequently in engineering; for example, in problems of steady-state temperature, electric and gravitational potential, incompressible fluid flow, elastic torsion, and other problems of elasticity. It is well known that these equations can be solved by resistor networks (1).[2] In this note it is shown that in solving the equation

$$\nabla^2 u = f(x, y), \quad [1]$$

where $\nabla^2 u = \frac{\partial^2 u}{\partial x^2} + \frac{\partial^2 u}{\partial y^2}$

by a resistor network, it is possible to reduce greatly the lumping or truncation error by simply adding additional resistors to the usual arrangement, without any increase in the number of mesh points.

Resistor Network With Improved Accuracy

THE usual resistor network for solving Equation [1] uses the setup indicated in Fig. 1(*a*). The values v of an approximation to $u(x, y)$ are to be calculated at the nodes of a square net of spacing h. In the electric network each node representing a point in the interior of the region considered is connected to its nearest neighbors by equal resistors R, and v is proportional to the voltage V at the corresponding node

$$v = cV \quad [2]$$

where c is the scale factor. The input current I to each node is determined by $f(x, y)$ from the relation

$$I = -\frac{h^2 f(x, y)}{cR} \quad [3]$$

If we are concerned with the Dirichlet problem, i.e., Equation [1] is to be solved subject to u having specified values on the boundary, then the boundary nodes of the electric network are to be held at the corresponding voltages according to Equation [2].

This electric network is equivalent to solving Equation [1] numerically by replacing the partial differential equation by the finite-difference equation

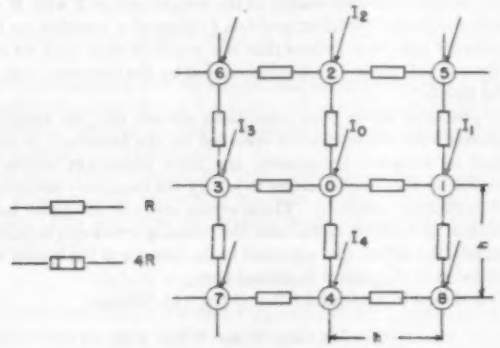

Fig. 1(*a*) Network for *H*-Operator

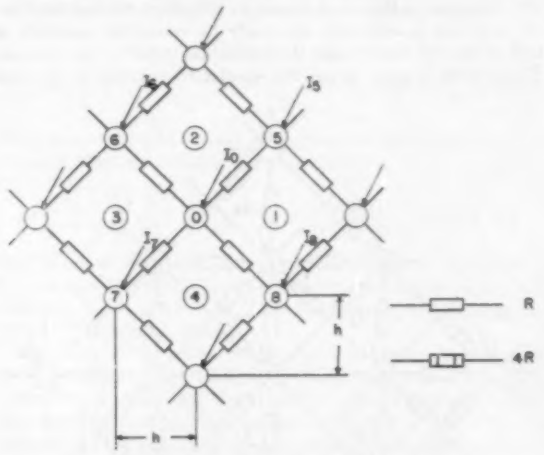

Fig. 1(*b*) Network for 2*X*-Operator

$$\frac{1}{h^2}[v(x + h, y) + v(x, y + h) + v(x - h, y) + v(x, y - h) - 4(x, y)] = f(x, y) \quad [4]$$

or, with the notation of Fig. 1, Equation [1] is approximated at node 0 by

$$v_1 + v_2 + v_3 + v_4 - 4v_0 = h^2 f_0$$

where f_0 is the value of $f(x, y)$ at node 0.

It is convenient to represent the left-hand side of Equation [4] by an operator, which, following Milne (2), we call H and represent by the stencil

---

[1] Mathematician, Heat and Mass Flow Analyzer Laboratory, Columbia University.

[2] Numbers in parentheses refer to the Bibliography at the end of the paper.

Contributed by the Applied Mechanics Division and presented at the Annual Meeting, New York, N. Y., November 25–30, 1956, of The American Society of Mechanical Engineers.

Discussion of this paper should be addressed to the Secretary, ASME, 29 West 39th Street, New York N. Y., and will be accepted until April 10, 1957, for publication at a later date. Discussion received after the closing date will be returned.

Note: Statements and opinions advanced in papers are to be understood as individual expressions of their authors and not those of the Society. Manuscript received by ASME Applied Mechanics Division, May 11, 1956. Paper No. 56—A-13.

$$H = \begin{array}{|c|c|c|}\hline 0 & 1 & 0 \\ \hline 1 & -4 & 1 \\ \hline 0 & 1 & 0 \\ \hline \end{array} \quad \ldots\ldots\ldots\ldots\ldots [5]$$

where the number in each position is the coefficient multiplying the value of v at that position. Then Equation [4] can be written

$$Hv = h^2 f \ldots\ldots\ldots\ldots\ldots [6]$$

Now it is well known, and physically apparent, that the same problem can be solved by using the network of Fig. 1(*b*), which is equivalent to merely rotating the network of Fig. 1(*a*). The corresponding operator and equation are

$$2X = \begin{array}{|c|c|c|}\hline 1 & 0 & 1 \\ \hline 0 & -4 & 0 \\ \hline 1 & 0 & 1 \\ \hline \end{array} \quad \ldots\ldots\ldots\ldots\ldots [7]$$

$$2Xv = 2h^2 f \ldots\ldots\ldots\ldots\ldots [8]$$

It is also known, in the theory of the numerical solution of differential equations (2, 3), that the operators H and X can be combined to obtain an operator that gives a considerably closer approximation to Equation [1]. The proper combination is

$$K = 4H + 2X = \begin{array}{|c|c|c|}\hline 1 & 4 & 1 \\ \hline 4 & -20 & 4 \\ \hline 1 & 4 & 1 \\ \hline \end{array} \quad \ldots\ldots\ldots [9]$$

giving the finite-difference equation

$$Kv = 6h^2 f \ldots\ldots\ldots\ldots\ldots [10]$$

The objection to the use of Equation [10] when solving the Poisson equation numerically, especially by relaxation methods, is that it greatly complicates the individual steps in the process. Therefore it is usual to use the simpler H-operator, and if this does not give a sufficiently accurate result, to use H again with a finer spacing; and then, perhaps, use Richardson's h^2 extrapolation procedure (1, 4).

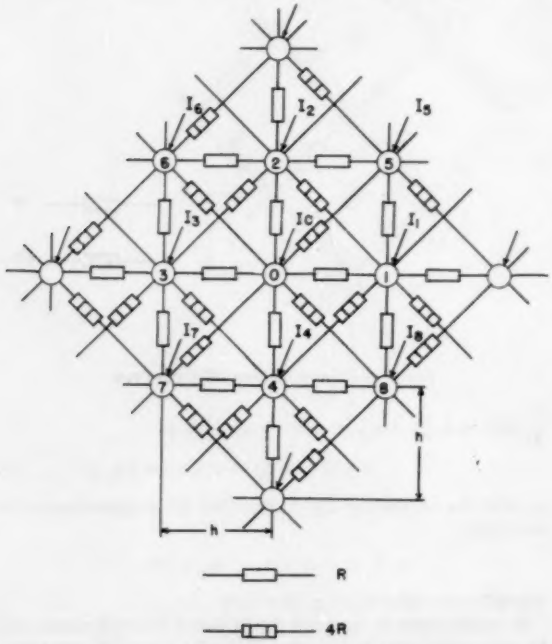

FIG. 1(*c*) NETWORK FOR *K*-OPERATOR

The main point here, however, is that when the Poisson equation is solved by an electric network, the use of a network equivalent to the K-operator instead of H requires only a trivial addition. This consists in adding diagonal resistors to the network of Fig. 1(*a*) as indicated in Fig. 1(*c*). Each diagonal resistor has a resistance of $4R$, and they are connected to the network only at the original nodes.

To check that this network is equivalent to using the K-operator, we write the equation for the currents flowing into node 0 in Fig. 1(*c*)

$$\frac{1}{R}\sum_{i=1}^{4}(V_i - V_0) + \frac{1}{4R}\sum_{i=5}^{8}(V_i - V_0) + I_0 = 0 \ldots [11]$$

and then use Equation [2] and make the input current

$$I_0 = -\frac{3h^2 f_0}{2cR} \ldots\ldots\ldots\ldots\ldots [12]$$

This gives

$$-20v_0 + 4(v_1 + v_2 + v_3 + v_4) + v_5 + v_6 + v_7 + v_8 = 6h^2 f_0 \ldots [13]$$

which is Equation [10] for this point of the net.

ACCURACY

The slight complication of the network introduced by the addition of the diagonal resistors is more than justified by the great improvement in the accuracy of the result due to reduction in the lumping error.[3] It does not seem to be generally recognized how much of an improvement in accuracy the use of K instead of H introduces. Milne (2) has given the maximum error for the case when $f(x, y)$ is zero or a constant, and it is shown here that the same or a similar bound on the error holds for a wider class of $f(x, y)$. In order not to complicate the analysis too much, and because we are interested mainly in the comparison of K with H, we consider only the Dirichlet problem (values of u specified on the boundary) and also assume that our region is such that we can set up a square mesh which is intersected by the boundary only at nodal points.

In problems where these conditions are not met, for example, problems with the derivative specified on the boundary or with curved or irregular boundaries, the most important source of error will be that due to failure to satisfy the boundary conditions with sufficient accuracy. These errors are not discussed here. However, in these problems also, the lumping errors due to failure to satisfy the differential equation in the interior of the region will be reduced to the extent indicated here.

It is shown in Appendix 1 that if $f(x, y)$ is bilinear

$$f(x, y) = a_0 xy + a_1 x + a_2 y + a_3 \ldots\ldots\ldots [14]$$

then the maximum difference between $u(x, y)$ which satisfies Equation [1] and v which satisfies Equation [10], and has the same values at the nodal points on the boundary, is given by

$$\max |u - v| \leq \frac{h^6 \rho^2 M_3}{12096} \ldots\ldots\ldots [15]$$

where ρ is the radius of the smallest circle containing the region, and

$$M_3 = \max |D_x^3 u| = \max \left| \frac{\partial^3 u}{\partial x^3} \right|$$

[3] There also may be a reduction in error of measurement (as observed in the example described later), but this reduction has not yet been analyzed.

This difference is to be compared with the corresponding error when the simpler operator H is used; this is (2), without restriction on $f(x, y)$

$$\max |u - v| = \frac{h^2 \rho^2 M_4}{24} \quad [16]$$

where M_4 is the maximum of the fourth-order partial derivatives of u.

Without going into the question of how M_4 and M_8 are to be estimated,[4] it can be seen that Equation [15] is a very great improvement over Equation [16], the error being of order h^4 instead of h^2. In the following an example is given in which the actual errors were calculated.

Extended Applicability of Error Bound

When $f(x, y)$ is not bilinear as in Equation [14], we can often use the same error estimate as in Equation [15] by the device of reducing Poisson's equation to Laplace's. Suppose it is possible to find some function $w(x, y)$ which satisfies

$$\nabla^2 w = f(x, y) \quad [17]$$

without regard to the boundary values. Then putting

$$u = W + w \quad [18]$$

we have to find $W(x, y)$ satisfying

$$\nabla^2 W = 0$$

and $W = u - w$ on the boundary.

In engineering problems the form of $f(x, y)$ is frequently simple enough to allow w to be found easily. A formula for w which is exact if $f(x, y)$ is a polynomial in x and y can be obtained as follows: With the operator notation D_x and D_y

$$w = \frac{1}{D_x^2 + D_y^2} f = D_y^{-2}(1 + D_y^{-2} D_x^2)^{-1} f$$
$$= (D_y^{-2} - D_y^{-4} D_x^2 + D_y^{-6} D_x^4 - \ldots) f \quad [19]$$

Here $D_y^{-1} f$ is to be interpreted as $\int^y f(x, y')dy'$. It is easy to see that Equation [19] terminates and gives a value for w which satisfies Equation [17] if $f(x, y)$ is a polynomial in x and y or any integrable function of y only. A similar formula with x and y interchanged also can be used.

In the electric network the shift from solving for u to solving for W means that no current needs to be introduced at interior nodes. This simplifies the procedure and should reduce experimental errors.

Error for Other Forms of $f(x, y)$

If this reduction of Poisson's equation is not possible or is inconvenient, the error in the solution using the K-operator may be of lower order than h^6. We can see what the order will be from Equation [33] in Appendix 1, since if $u(x, y)$ satisfies Equation [1], then

$$Ku - 6h^2 \nabla^2 u = \frac{1}{2} h^4 \nabla^2 f$$
$$+ \frac{1}{60} h^6 [\nabla^4 f + 2 D_x^2 D_y^2 f] + \frac{1}{8!} G^{(8)}(s) \quad [20]$$

where $G(s)$ is defined by Equation [29]. The error $u - v$ where v satisfies Equation [10] and has the same boundary values as u, will be of order lower by two in h than the first nonvanishing term on the right in Equation [20].

[4] There are some suggestions in Milne (2)

An important case is that for $f(x, y)$ harmonic

$$\nabla^2 f = 0 \quad [21]$$

Then the lumping error using K will be at least of order h^4 [written $O(h^4)$]. It will be again $O(h^6)$ if in addition

$$\frac{\partial^4 f}{\partial x^2 \partial y^2} = 0$$

and in this case, a calculation of $G^{(8)}(s)$ shows that instead of Equation [15] we have

$$\max |u - v| \leq \frac{13 h^6 \rho^2 M_8'}{12{,}096} \quad [22]$$

where now M_8' is the maximum of the eighth-order partial derivatives of u.

This case occurs when the biharmonic equation of elasticity

$$\nabla^4 \psi = 0 \quad [23]$$

is treated by factorization into two second-order equations

$$\nabla^2 \psi = \phi(x, y) \quad [24]$$

$$\nabla^2 \phi = 0 \quad [25]$$

A procedure for solving the biharmonic equation by this method using coupled-resistor networks has been proposed by several writers (5, 6, 7). If we use the diagonal resistors as proposed here, then the lumping error in the computed values of ϕ will be $O(h^6)$, and those for ψ will be at least $O(h^4)$. Both errors are, of course, $O(h^2)$ if the usual (H) network is used as suggested by the writers.

Another procedure for making the lumping error of order h^6 in the solution of Equation [1] can be seen by writing Equation [20] in the form

$$\frac{1}{6h^2} Ku = \left\{ f + \frac{h^2}{12} \nabla^2 f + \frac{h^4}{360} [\nabla^4 f + 2 D_x^2 D_y^2 f] \right\} + O(h^6)$$

If we make the input current proportional to the quantity in the brackets, that is, instead of Equation [12] use

$$I_0 = -\frac{3h^2}{2cR} \left\{ f_0 + \frac{h^2}{12} \nabla^2 f_0 + \frac{h^4}{360} [\nabla^4 f_0 + 2 D_x^2 D_y^2 f_0] \right\}$$

then the error will be of order h^6. This is directly applicable if $f(x, y)$ is a function whose derivatives are readily calculated; otherwise $\nabla^2 f$, $\nabla^4 f$, and $D_x^2 D_y^2 f$ can be approximated by using the values of f at the net points.

This kind of correction to the input has been suggested by Southwell (8) and others. Southwell suggested it for his network of equilateral triangles, which is similar to the K-operator here in that the first error term is proportional to $\nabla^4 u = \nabla^2 f$. The K-operator has the advantage of making possible the elimination of the next error term also. The equilateral-triangle network has an advantage where the shape of the region is such as to make it fit more exactly.

Experimental Test of Method

To test this diagonal-resistor network, a problem in the elastic torsion of a square section was run on the Heat and Mass Flow Analyzer at Columbia University. This problem is part of the elastoplastic torsion problem previously treated in this laboratory (9). The problem is to find $\phi(x, y)$ satisfying

$$\nabla^2 \phi = -2G\theta \quad [26]$$

in a square of side a, where G and θ are constants, and $\phi = 0$ on the boundary of the square. Introducing dimensionless variables

$$\xi = \frac{x}{a}, \quad \eta = \frac{y}{a}, \quad u = \frac{\phi}{G\theta a^2} \ldots\ldots\ldots [27]$$

the equation becomes

$$\frac{\partial^2 u}{\partial \xi^2} + \frac{\partial^2 u}{\partial \eta^2} = -2 \ldots\ldots\ldots [28]$$

in the unit square with $u = 0$ on the boundary. This was solved with $h = 1/6$, and because of symmetry only one eighth of the square need be treated. The network is shown in Fig. 2(*a*). In order to have comparable values the problem was run again with the usual H-network, which had been used before (9), Fig. 2(*b*).

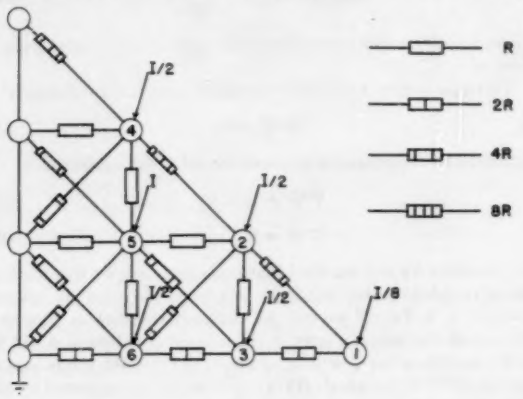

FIG. 2(*a*) NETWORK FOR ELASTIC TORSION PROBLEM USING DIAGONAL RESISTORS (K)

The finite-difference equations for this problem, using the H- and K-operators, were solved numerically. The differences between these and the electric-network solutions give the experimental errors. For this problem the analytic solution in series form is also known (10, 11), so that the exact values of u can be computed for comparison with the finite-difference solutions, thus giving the lumping error alone. All these comparisons are given in Table 1.

The improvement effected by the use of the diagonal-resistor network K is apparent. Lumping errors are about 1 per cent of those using the usual network and are negligible in comparison with the experimental errors. The accuracy of the K-network here, using only six points, is quite adequate for engineering purposes as can be seen by evaluating the torque and maximum stress from the network values. For example, for the torque

$$M_\theta = 2 \iint_A u d\xi d\eta$$

we get $M_\theta = 0.1406$, using the K-resistor-network values and the approximate integration formula given in Appendix 2. This agrees exactly with the value calculated from the series solution in Timoshenko and Goodier (11). The same accuracy could be obtained with the H-network only by making runs with $h = 1/12$ as well as $h = 1/6$ and then using h^2 extrapolation (9).

The experimental errors given by the usual H-network, about 1 per cent, are what is to be expected on problems of this type (9). The fact that the K-network shows smaller experimental errors may be due to the extra care which is expected whenever a special test is run. However, it is believed that there is an additional effect toward the reduction of experimental errors as a result of the added resistors. Further study will be needed to establish the existence of this effect

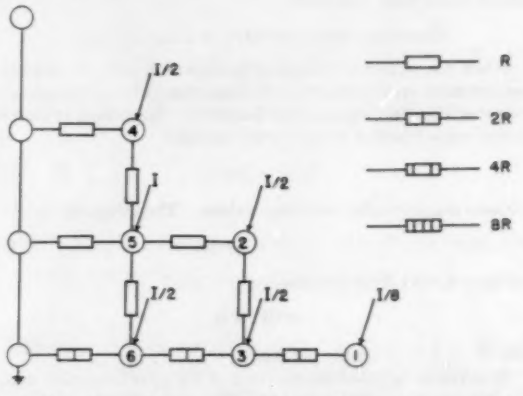

FIG. 2(*b*) USUAL NETWORK FOR ELASTIC TORSION PROBLEM (H)

ACKNOWLEDGMENT

The resistor-network experiments were performed by Mr. Joseph W. Hlinka of the Heat and Mass Flow Analyzer Laboratory, Columbia University.

This work was made possible by a grant from the Higgins Fund and is part of a continuing study of the solution of engineering problems on electric-network computers. The first report on this study was the previously cited paper (9) by Weiner, Salvadori, and Paschkis on elastoplastic torsion, and further reports will be made as the study develops.

BIBLIOGRAPHY

1 "Analog Methods in Computation and Simulation," by W. W. Soroka, McGraw-Hill Book Company, Inc., New York, N. Y., 1954, pp. 280–285.

2 "Numerical Solution of Differential Equations," by W. E. Milne, John Wiley & Sons, Inc., New York, N. Y., 1953, chapter 10.

3 "Numerical Analysis," by D. R. Hartree, Oxford University Press, London, England, 1955, p. 218.

4 "Numerical Methods on Engineering," by M. G. Salvadori and M. L. Baron, Prentice-Hall, Inc., New York, N. Y., 1952, chapter 5.

5 "Sur la détermination numérique de fonctions biharmoniques

TABLE 1 CALCULATED SOLUTIONS OF EQUATION [28] AND ERRORS, BY DIFFERENT METHODS ($h = 1/6$)

Node no.		1	2	3	4	5	6
Solution							
1	Series	0.14734	0.12069	0.13317	0.05456	0.07983	0.08730
2	Finite difference: K	0.14737	0.12072	0.13320	0.05465	0.07986	0.08732
3	Finite difference: H	0.1442	0.1180	0.1303	0.0529	0.0780	0.0854
4	Resistor network: Diagonal (K)	0.1472	0.1206	0.1328	0.0547	0.0800	0.0875
5	Resistor network: Usual (H)	0.1426	0.1170	0.1289	0.0528	0.0778	0.0852
Lumping errors							
6	K (line 2 − line 1)	+0.00003	+0.00003	+0.00003	+0.00009	+0.00003	+0.00002
7	H (line 3 − line 1)	−0.0031	−0.0027	−0.0029	−0.0017	−0.0018	−0.0019
Experimental errors							
8	K (line 4 − line 2)	−0.0002	−0.0001	−0.0004	+0.00005	+0.0001	+0.0002
9	H (line 5 − line 3)	−0.0016	−0.0010	−0.0014	−0.0001	−0.0002	−0.0002

par un procédé analogique de réseaux superposés," by J. Boscher, Comptes Rendus de l'Académie des Sciences, vol. 236, 1953, pp. 44–46.

6 "Experiments With an Electrical Analogue for the Extension and Flexure of Flat Plates," by P. J. Palmer and S. C. Redshaw, *Aeronautical Quarterly*, vol. 6, 1955, pp. 13–30.

7 "The Solution of Plane Stress Problems by an Electrical Analogue Method," by G. Liebmann, *British Journal of Applied Physics*, vol. 6, 1955, pp. 145–157.

8 "Relaxation Methods in Theoretical Physics," by R. V. Southwell, Oxford University Press, London, England, 1946, p. 24.

9 "A Resistor-Network Solution for the Elasto-Plastic Torsion Problem," by J. H. Weiner, M. G. Salvadori, and V. Paschkis, Proceedings of the American Society of Civil Engineers, vol. 81, 1955, Separate No. 671, 10 pp.

10 "Mathematical Theory of Elasticity," by I. S. Sokolinikoff, McGraw-Hill Book Company, Inc., New York, N. Y., 1946, p. 149.

11 "Theory of Elasticity," by S. Timoshenko and J. N. Goodier, McGraw-Hill Book Company, Inc., New York, N. Y., 1951, p. 276.

Appendix 1

To arrive at a bound for the error using the K-operator, we define an auxiliary function

$$G(t) = 4[u(x+th, y) + u(x, y+th) + u(x-th, y) + u(x, y-th)] + u(x+th, y+th) + u(x-th, y+th) + u(x-th, y-th) + u(x+th, y-th) \quad [29]$$

Then
$$G(0) = 20u(x, y) \quad [30]$$

and
$$G(1) - G(0) = Ku(x, y) \quad [31]$$

We use Taylor's series with remainder

$$G(1) = G(0) + G'(0) + \frac{1}{2!}G''(0) + \ldots + \frac{1}{7!}G^{(7)}(0) + \frac{1}{8!}G^{(8)}(s) \quad [32]$$

where $0 < s < 1$, and the existence of the eighth partial derivatives of $u(x, y)$ is assumed. To evaluate Equation [31] in terms of $u(x, y)$, we use the operators

$$D_x = \frac{\partial}{\partial x}, \quad D_y = \frac{\partial}{\partial y}, \quad D_xD_y = \frac{\partial^2}{\partial x \partial y}, \text{ etc.}$$

Then

$$G^{(n)}(t) = h^n\{4[D_x^n u(x+th, y) + D_y^n u(x, y+th) + (-D_x)^n u(x-th, y) + (-D_y)^n u(x, y-th)] + (D_x+D_y)^n u(x+th, y+th) + (-D_x+D_y)^n u(x-th, y+th) + (-D_x-D_y)^n u(x-th, y-th) + (D_x-D_y)^n u(x+th, y-th)\}$$

where, for example

$$(D_x - D_y)^3 u(x+th, y-th) = \frac{\partial^3 u}{\partial x^3} - 3\frac{\partial^3 u}{\partial x^2 \partial y} + 3\frac{\partial^3 u}{\partial x \partial y^2} - \frac{\partial^3 u}{\partial y^3}$$

evaluated at the point $(x+th, y-th)$.

Now, calculating Equation [32] and using Equation [31], we get the desired expression for the difference between Ku and $\nabla^2 u$

$$Ku - 6h^2\nabla^2 u = \frac{1}{2}h^4\nabla^4 u + \frac{1}{60}h^6[\nabla^6 u + 2D_x^2 D_y^2 \nabla^2 u] + \frac{1}{8!}G^{(8)}(s) \quad [33]$$

where

$$\nabla^4 u = \nabla^2\nabla^2 u = (D_x^2 + D_y^2)^2 u(x, y)$$

Equation [33] holds for any function u having eighth derivatives. If we now consider a function u which satisfies Equation [1] with

$$f(x, y) = a_0xy + a_1x + a_2y + a_3 \quad [34]$$

then in the interior of the region

$$D_x^4 u = -D_x^2 D_y^2 u = D_y^4 u$$
$$D_x^6 u = -D_x^4 D_y^2 u = D_x^2 D_y^4 u = -D_y^6 u \quad [35]$$
$$D_x^8 u = -D_x^6 D_y^2 u = D_x^4 D_y^4 u = -D_x^2 D_y^6 u = D_y^8 u$$

and we find

$$|G^{(8)}(s)| \leq 80h^8 M_8 \quad [36]$$

where

$$M_8 = \max |D_x^8 u|$$

(for $D_x^8 u$ we can substitute any of the eighth-order derivatives in Equation [35]).

It follows that

$$|Ku - 6h^2\nabla^2 u| \leq \frac{h^8 M_8}{504} \quad [37]$$

We do not know $u(x, y)$, which satisfies Equation [1], but instead v, which satisfies Equation [10] and has the same values at the nodal points on the boundary. Using a theorem of Milne (2), we get the result which he stated for Laplace's equation

$$\max |u - v| \leq \frac{h^8 \rho^3 M_8}{12{,}096} \quad [38]$$

where ρ is the radius of the smallest circle containing the region.

Appendix 2

The following approximate integration formula is useful for functions satisfying Poisson's equation:

To evaluate

$$I = \int_{-h}^{h}\int_{-h}^{h} u(x, y)dxdy = h^2\int_{-1}^{1}\int_{-1}^{1} u(sh, th)dsdt$$

we expand the integrand, and write u_0 for $u(0, 0)$, then

$$I = h^2\int_{-1}^{1}\int_{-1}^{1}\left[u_0 + h(sD_x + tD_y)u_0 + \frac{h^2}{2!}(sD_x + tD_y)^2 u_0 + \frac{h^3}{3!}(sD_x + tD_y)^3 u_0 + \ldots\right]dsdt$$
$$= 4h^2\left[u_0 + \frac{h^2}{3!}(D_x^2 + D_y^2)u_0 + \frac{h^4}{4!}\left(\frac{D_x^4}{5} + \frac{6}{9}D_x^2 D_y^2 + \frac{D_y^4}{5}\right)u(\theta_1 h, \theta_2 h)\right]$$
$$= 4h^2\left(u_0 + \frac{1}{6}h^2\nabla^2 u_0\right) + R, \quad \text{with} \quad |R| \leq \frac{8}{45}h^6 M_4$$

So if

$$\nabla^2 u = f(x, y)$$
$$I = 4h^2\left(u_0 + \frac{h^2}{6}f_0\right) + O(h^6)$$

Stresses and Displacements in an Elastic-Plastic Wedge[1]

By P. M. NAGHDI,[2] ANN ARBOR, MICH.

An elastic, perfectly plastic wedge of an incompressible isotropic material in the state of plane strain is considered, where the stress-strain relations of Prandtl-Reuss are employed in the plastic domain. For a wedge (with an included angle β) subjected to a uniform normal pressure on one boundary, the complete solution is obtained which is valid in the range $0 < \beta < \pi/2$; this latter limitation is due to the character of the initial yield which depends on the magnitude of β. Numerical results for stresses and displacements are given in one case ($\beta = \pi/4$) for various positions of the elastic-plastic boundary.

Introduction

ALTHOUGH the general theory of plane strain for rigid, perfectly plastic material (unrestricted plastic flow) and its application have been explored successfully in recent years,[3] complete solutions to problems of plane elastic-plastic strain (contained plastic deformation) have been possible in only a few cases, where the elastic-plastic boundary is determined a priori by symmetry considerations. References to existing solutions of plane elastic-plastic strain (in the theory of perfectly plastic solids) may be found in Prager and Hodge (1, Ch. 4 and 7), Hill (2, Ch. 5), Koiter (3), and in a recent paper by Shaffer and House (4).[4] Even for axisymmetric problems, such as the thick-walled circular cylinder subjected to internal pressure (1, Ch. 4), a complete solution in closed form can be deduced (by using the stress-strain relations of Prandtl-Reuss) only if the material is assumed to be incompressible in both the elastic and the plastic ranges; otherwise, the integration of the differential equations involved is accomplished by numerical methods.[5]

The present paper, employing the stress-strain relations of Prandtl-Reuss, is concerned with the elastic, perfectly plastic solution of an incompressible isotropic wedge in the state of plane strain, subjected to a uniform normal pressure (assumed to be monotonically increasing with time) on one boundary only. As the character of the initial yield and the locus of the elastic-plastic boundary depend on the nature of the load, as well as on the included wedge angle β, the present analysis is confined primarily to wedge regions where $\beta < \pi/2$. A complete solution (stresses and displacements) is given for a wedge region $0 \leq \theta \leq \beta < \pi/2$ subjected to a uniform normal pressure, as shown in Fig. 1, and numerical results are plotted for the case when $\beta = \pi/4$. In the limit, the stress distribution reduces to the solution of the corresponding problem of a rigid, perfectly plastic material (1, pp. 156–158).

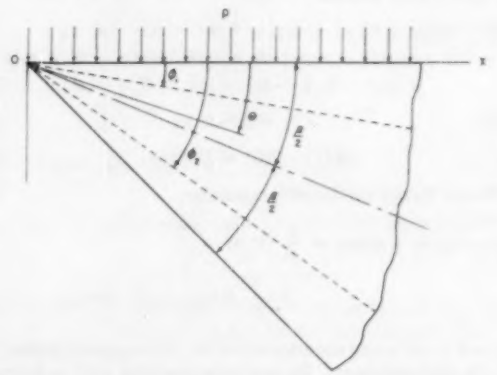

FIG. 1 NARROW WEDGE UNDER A UNIFORM LATERAL PRESSURE

We recall that in the state of plane strain, here referred to cylindrical co-ordinates (r, θ, z), the radial and tangential displacements u_r and u_θ are at all times independent of z (the z-axis is taken perpendicular to the plane of the cross section in Fig. 1), and that $u_z = 0$. The nonvanishing components of strain are given by

$$\epsilon_r = \frac{\partial u_r}{\partial r}, \quad \epsilon_\theta = \frac{u_r}{r} + \frac{1}{r}\frac{\partial u_\theta}{\partial \theta},$$

$$2\epsilon_{r\theta} = \frac{1}{r}\frac{\partial u_r}{\partial \theta} + \frac{\partial u_\theta}{\partial r} - \frac{u_\theta}{r} \quad \ldots\ldots [1]$$

and since $\epsilon_z = 0$, it follows that

$$\epsilon_r = -\epsilon_\theta \quad \ldots\ldots [2]$$

for an incompressible material. In the absence of body forces, the stress-differential equations of equilibrium which are not identically satisfied may be written as

---

[1] The results presented in this paper were obtained in the course of research sponsored by the Office of Naval Research, under Contract Nonr-1224 (01), Project NR-064-408, with the University of Michigan.

[2] Professor of Engineering Mechanics, University of Michigan. Mem. ASME.

[3] See, for example, reference (1), Chapters 5 and 6; and reference (2), Chapters 6, 7, 8, and 9. Numbers in parentheses refer to the Bibliography at the end of the paper.

[4] Available solutions obtained by total strain (deformation) theories of plasticity, as in (12) and the first portion of (13) are ruled out here. It also should be mentioned that the results given in the last portion of (13) as well as (14), both dealing only with the stresses in an elastic-plastic wedge as a statically determinate problem, are incorrect. Reference (12) was called to the author's attention by Prof. W. Prager.

[5] An exception is Koiter's solution in closed form for a thick-walled cylinder of a compressible elastic-plastic material, subjected to internal pressure (3); this solution was obtained by employing Tresca's singular yield condition and associated flow rules. For an exposition of the use of singular yield conditions and associated flow rules, see also reference (5).

Contributed by the Applied Mechanics Division and presented at the Annual Meeting, New York, N. Y., November 25–30, 1956, of THE AMERICAN SOCIETY OF MECHANICAL ENGINEERS.

Discussion of this paper should be addressed to the Secretary, ASME, 29 West 39th Street, New York, N. Y., and will be accepted until April 10, 1957, for publication at later date. Discussion received after the closing date will be returned.

NOTE: Statements and opinions advanced in papers are to be understood as individual expressions of their authors and not those of the Society. Manuscript received by ASME Applied Mechanics Division, May 28, 1956. Paper No. 56—A-20.

$$\frac{\partial s_r}{\partial r} + \frac{1}{r}\frac{\partial \sigma_{r\theta}}{\partial \theta} + \frac{s_r - s_\theta}{r} + \frac{\partial s}{\partial r} = 0 \quad \ldots\ldots [3a]$$

$$\frac{\partial \sigma_{r\theta}}{\partial r} + \frac{1}{r}\frac{\partial s_\theta}{\partial \theta} + 2\frac{\sigma_{r\theta}}{r} + \frac{1}{r}\frac{\partial s}{\partial \theta} = 0 \quad \ldots\ldots [3b]$$

where the components of the stress-deviation tensor are related to the nonvanishing components of the stress tensor $\{\sigma_r, \sigma_\theta, \sigma_z, \sigma_{r\theta}\}$ by

$$s_r = \sigma_r - s, \quad s_\theta = \sigma_\theta - s, \quad s_z = \sigma_z - s = -(s_r + s_\theta). \quad [4]$$

and the mean normal stress s, on account of the condition of incompressibility, is determined from the differential equations of equilibrium.

While Equations [1] to [4] are valid in the elastic, as well as the plastic domain, the stress-strain relations in the elastic and plastic ranges are furnished respectively by Hooke's law, and the stress-strain law of Prandtl-Reuss which, for an incompressible material, reads[6]

$$2G\{\dot{e}_r, \dot{e}_\theta, \dot{e}_z, \dot{e}_{r\theta}\} = \{\dot{s}_r, \dot{s}_\theta, \dot{s}_z, \dot{\sigma}_{r\theta}\} + \lambda\{s_r, s_\theta, s_z, \sigma_{r\theta}\} \quad [5]$$

In Equations [5], λ is a scalar factor which, in general, depends on the co-ordinates as well as time t; dot denotes differentiation with respect to time, and G is the shear modulus of elasticity. In addition, the Mises yield condition for the state of plane strain reduces to

$$s_r^2 + s_r s_\theta + s_\theta^2 + \sigma_{r\theta}^2 = k^2 \quad \ldots\ldots [6]$$

where k is the yield limit in simple shear.

The Fully Elastic Solution

The displacement field for an elastic incompressible isotropic material in the state of plane strain, referred to cylindrical co-ordinates (r, θ, z) is characterized by[7]

$$G\left[\nabla^2 u_r - \frac{1}{r}\left(\frac{u_r}{r} + \frac{2}{r}\frac{\partial u_\theta}{\partial \theta}\right)\right] + \frac{\partial s}{\partial r} = 0 \quad \ldots [7a]$$

$$G\left[\nabla^2 u_\theta + \frac{1}{r}\left(\frac{2}{r}\frac{\partial u_r}{\partial \theta} - \frac{u_\theta}{r}\right)\right] + \frac{1}{r}\frac{\partial s}{\partial \theta} = 0 \quad \ldots [7b]$$

$$\left(\frac{\partial}{\partial r} + \frac{1}{r}\right) u_r + \frac{1}{r}\frac{\partial u_\theta}{\partial \theta} = 0 \quad \ldots\ldots [7c]$$

where

$$\nabla^2 \equiv \frac{\partial^2}{\partial r^2} + \frac{1}{r}\frac{\partial}{\partial r} + \frac{1}{r^2}\frac{\partial^2}{\partial \theta^2}$$

The solution of Equations [7] for a wedge subjected to uniform tractions may be written as

$$Gu_r = -r(a \cos 2\theta + c \sin 2\theta) \quad \ldots\ldots [8a]$$

$$Gu_\theta = r(a \sin 2\theta - c \cos 2\theta) - d\, r \log r \quad \ldots\ldots [8b]$$

[6] It should be noted that the stress-strain relations of Prandtl-Reuss in the form Equation [5] have been criticized by Truesdell (6) and Thomas (7), who have contended that the "stress rate" (on the right-hand side of [5]) should be defined with respect to convected co-ordinates, in order to render [5] as a dynamically correct system. While this is true in principle, the present use of the Prandtl-Reuss stress-strain relations presupposes infinitesimal displacements, in which case the refinement proposed in (6, 7) is unnecessary; hence, at a fixed point of observation, the partial derivative of the stress with respect to time can be used instead. In this connection, see also references (8) and (9), where the question of stress rate is discussed.

[7] For a discussion of the general equations of linear elasticity for an incompressible material, see (10, section 3).

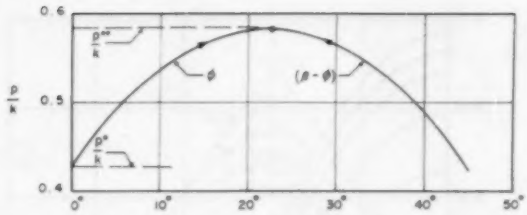

Fig. 2 Lateral Pressure p Versus Elastic-Plastic Boundaries, $0 < \phi < \beta/2$ and $\beta/2 < (\beta - \phi) < \beta$ for $\beta = \pi/4$

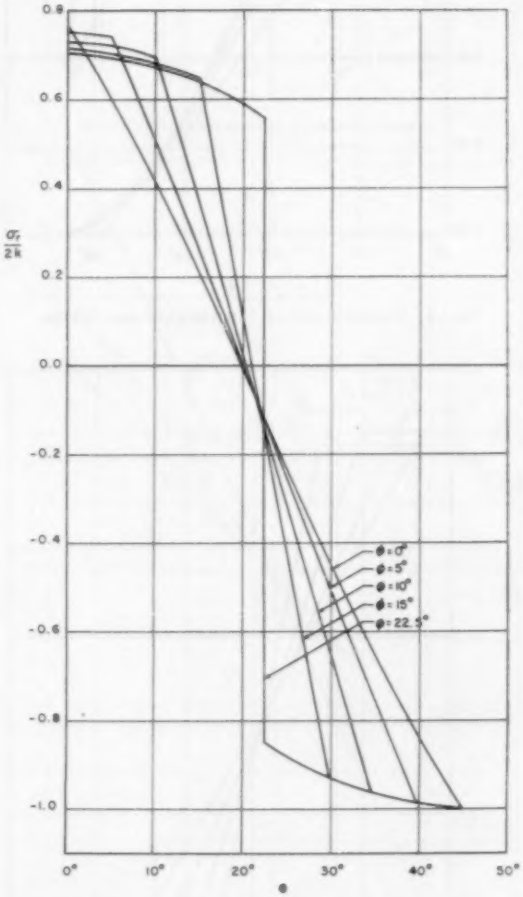

Fig. 3 Distribution of Radial Stress

$$s = 2(b + d\theta) \quad \ldots\ldots [9]$$

from which, by Equations [4] and Hooke's law, we have[8]

$$\left.\begin{aligned} s_r &= -s_\theta = -2(a \cos 2\theta + c \sin 2\theta) \\ \sigma_{r\theta} &= -d + 2(a \sin 2\theta - c \cos 2\theta) \\ s_z &= 0 \end{aligned}\right\} \quad \ldots\ldots [10]$$

[8] The components of the stress tensor, as given by Equations [9] and [10], together with the special results [14], are given in (11, pp. 123–125).

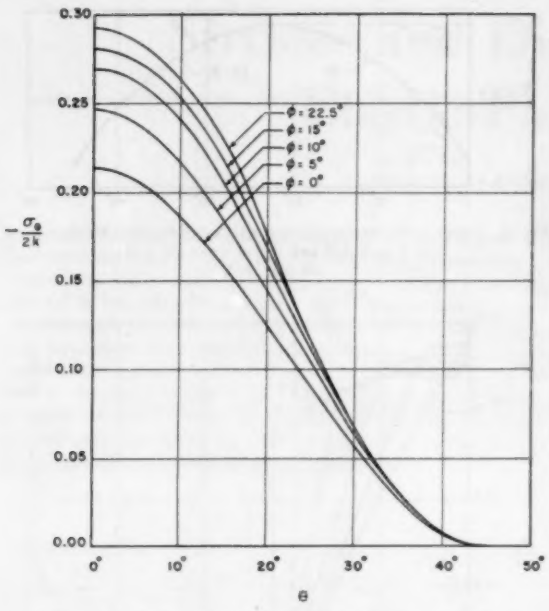

FIG. 4 DISTRIBUTION OF CIRCUMFERENTIAL STRESS

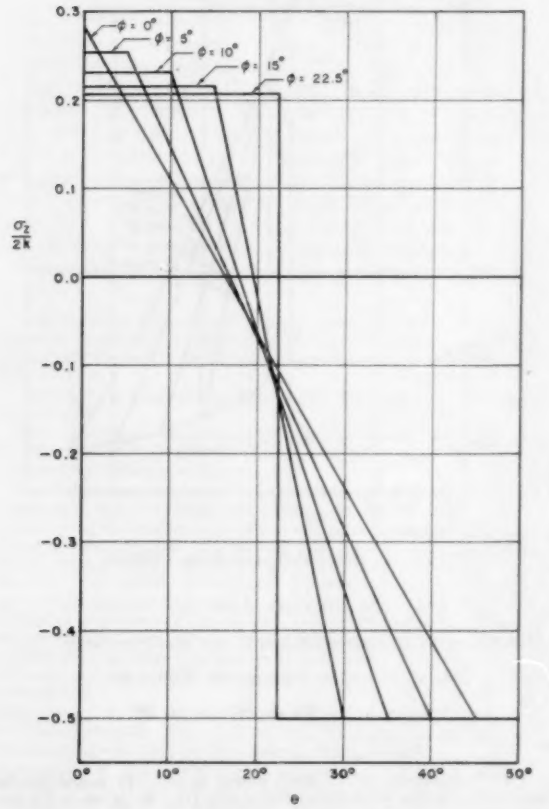

FIG. 5 DISTRIBUTION OF AXIAL STRESS

For future purposes, we first record the values of the constants a, b, c, and d when Solutions [9] and [10] are subjected to the boundary conditions

$$\left.\begin{aligned} \sigma_\theta(\theta_1) &= \sigma_1, \qquad \sigma_{r\theta}(\theta_1) = \tau_1 \\ \sigma_\theta(\theta_2) &= \sigma_2, \qquad \sigma_{r\theta}(\theta_2) = \tau_2 \end{aligned}\right\} \quad \ldots\ldots\ldots [11]$$

and then deduce, as a special case, the values of the constants appropriate for a wedge of included angle $0 < \beta < 2\pi$ uniformly loaded on one boundary, as shown in Fig. 1. Thus the constants of integration determined by Equations [11] are

$$\left.\begin{aligned} a &= \frac{1}{D}\{(\sigma_2 - \sigma_1)[\cos 2\theta_2 - \cos 2\theta_1] \\ &\quad + \tau_1[\sin 2\theta_1 - \sin 2\theta_2 + 2(\theta_2 - \theta_1)\cos 2\theta_2] \\ &\quad + \tau_2[\sin 2\theta_2 - \sin 2\theta_1 - 2(\theta_2 - \theta_1)\cos 2\theta_1]\} \\ c &= \frac{1}{D}\{(\sigma_2 - \sigma_1)[\sin 2\theta_2 - \sin 2\theta_1] \\ &\quad + \tau_1[\cos 2\theta_2 - \cos 2\theta_1 + 2(\theta_2 - \theta_1)\sin 2\theta_2] \\ &\quad + \tau_2[\cos 2\theta_1 - \cos 2\theta_2 - 2(\theta_2 - \theta_1)\sin 2\theta_1]\} \\ b &= -\frac{1}{D}\{\sigma_1[-1 + \cos 2(\theta_2 - \theta_1) \\ &\quad + 2\theta_2 \sin 2(\theta_2 - \theta_1)] + \sigma_2[-1 + \cos 2(\theta_2 - \theta_1) \\ &\quad - 2\theta_1 \sin 2(\theta_2 - \theta_1)] + \tau_1[-2\theta_1 - \sin 2(\theta_2 - \theta_1) \\ &\quad + 2\theta_2 \cos 2(\theta_2 - \theta_1)] + \tau_2[-2\theta_2 + \sin 2(\theta_2 - \theta_1) \\ &\quad + 2\theta_1 \cos 2(\theta_2 - \theta_1)]\} \\ d &= \frac{1}{D}\{-2(\sigma_2 - \sigma_1)\sin 2(\theta_2 - \theta_1) \\ &\quad + 2\tau_1[-1 + \cos 2(\theta_2 - \theta_1)] \\ &\quad + 2\tau_2[-1 + \cos 2(\theta_2 - \theta_1)]\} \end{aligned}\right\} \quad \ldots [12]$$

where

$$D = 4\sin 2(\theta_2 - \theta_1)[\tan(\theta_2 - \theta_1) - (\theta_2 - \theta_1)] \ldots [13]$$

For the special case shown in Fig. 1, i.e., when $\theta_1 = 0$, $\theta_2 = \beta$, $\sigma_1 = -p$, and $\sigma_2 = \tau_1 = \tau_2 = 0$, the foregoing results reduce to

$$\left.\begin{aligned} a &= -p\frac{\tan\beta}{4\kappa}, \quad c = \frac{p}{4\kappa} \\ b &= -p\left(\frac{1}{2} + \frac{\tan\beta}{4\kappa}\right), \quad d = -\frac{p}{2\kappa} \\ \kappa &= \tan\beta - \beta \end{aligned}\right\} \quad \ldots\ldots [14]$$

INITIAL YIELD AND THE ELASTIC-PLASTIC BOUNDARY

Since $s_r = -s_\theta$, the Yield Condition [6] becomes

$$s_\theta^2 + \sigma_{r\theta}^2 = k^2 \ldots\ldots\ldots\ldots\ldots [15]$$

the left-hand side of which, by Equations [10] and [14] for the wedge shown in Fig. 1, can be written as $(p/2\kappa)^2 f(\theta)$, where

$$f(\theta) = [\tan^2\beta + 2(1 - \cos 2\theta) - 2\tan\beta \sin 2\theta] \ldots [16]$$

Hence, yielding begins at the values of θ for which $f(\theta)$ attains its maximum value. An examination of Equation [16], together with its first and second derivatives, reveals that, depending on the magnitude of the wedge angle β, f assumes its maximum at different values of θ. Thus, in the range $0 < \beta < 2\pi$, plastic flow will first set in at one or more values of $\theta (0 \leq \theta \leq \beta)$, as given in Table 1. For example, in the range $0 < \beta < \pi/2$, f is a minimum at $\theta = \beta/2$, and will attain its maximum simultaneously at $\theta = 0$

and $\theta = \beta$. For $\beta = \pi/2$, the right-hand side of Equation [16] is independent of θ and the entire region becomes plastic when the load reaches the value $(2k)$.

In the remainder of this paper, attention will be confined to wedge regions of which the included angle has the range $0 < \beta < \pi/2$. As seen in Table 1, yielding for this range of β will begin simultaneously at the outside surfaces when the pressure has reached the value

$$p^* = 2k\kappa(\tan \beta)^{-1} \quad \ldots\ldots [17]$$

TABLE 1 VALUES OF θ FOR WHICH f IN EQUATION [16], IN THE RANGE $0 < \beta < 2\pi$, IS A MAXIMUM

Range of wedge angle	Values of θ, where yielding will initiate
$0 < \beta < \frac{\pi}{2}$	$\theta = 0, \beta$
$\beta = \frac{\pi}{2}$	all $0 \leq \theta \leq \frac{\pi}{2}$
$\frac{\pi}{2} < \beta < \frac{3\pi}{2}$	$\theta = \frac{\beta}{2}$
$\beta = \frac{3\pi}{2}$	all $0 \leq \theta \leq \frac{3\pi}{2}$
$\frac{3\pi}{2} < \beta < 2\pi$	$\theta = \frac{\beta}{2} \pm \frac{\pi}{2}$

For a pressure $p > p^*$, a portion of the wedge region becomes plastic, and since the yield condition is independent of r, the elastic-plastic boundary must be a wedge bounded by $\theta = \phi_1$ and $\theta = \phi_2$, as indicated in Fig. 1.

Elastic-Plastic Solution

In the elastic region $\phi_1 \leq \theta \leq \phi_2$, the solution is still of the form of Equations [8], [9], and [10], but the boundary conditions are now

$$\left.\begin{aligned} s_\theta^2(\phi_1) + \sigma_{r\theta}^2(\phi_1) &= k^2 \\ s_\theta^2(\phi_2) + \sigma_{r\theta}^2(\phi_2) &= k^2 \end{aligned}\right\} \quad \ldots\ldots [18]$$

as well as the conditions for continuity of stresses in the form of Equations [11] with θ_1 and θ_2 replaced, respectively, by ϕ_1 and ϕ_2. With the use of the latter four conditions, the coefficients a, b, c, and d (as functions of ϕ_1 and ϕ_2) may still be written in the form of Equations [12], where now σ_1, τ_1, σ_2, and τ_2 refer to the normal and shearing components of stress at the elastic-plastic boundaries. Here, we also note that according to Equations [10], [8], and [2], at a generic point P in the elastic domain

$$s_r : s_\theta : s_z = \epsilon_r : \epsilon_\theta : \epsilon_z = 1 : -1 : 0; \quad \phi_1 \leq \theta \leq \phi_2 \quad \ldots [19]$$

Since, by Equations [9] and [10], the components of stress in the elastic region do not involve r, continuity of the stresses at the elastic-plastic boundaries demands that these quantities remain independent of r throughout the wedge. Hence, the stress-differential equations of equilibrium, Equations [3], reduce to

$$\frac{\partial \sigma_{r\theta}}{\partial \theta} + (s_r - s_\theta) = 0 \quad \ldots\ldots [20a]$$

$$\frac{\partial s_\theta}{\partial \theta} + 2\sigma_{r\theta} + \frac{\partial s}{\partial \theta} = 0 \quad \ldots\ldots [20b]$$

which hold in the elastic as well as the plastic regions $0 \leq \theta \leq \phi_1$ and $\phi_2 \leq \theta \leq \beta$. Differentiating the first of the foregoing with respect to t, combining (after multiplication by λ) the resulting equation with Equation [20a], and making use of the stress-strain relations of Prandtl-Reuss and the incompressibility Relation [7c], there results the following differential equation for the radial displacement in the plastic domain

$$\frac{1}{r}\frac{\partial^2 \dot{u}_r}{\partial \theta^2} - r\frac{\partial^2 \dot{u}_r}{\partial r^2} + 3\frac{\partial \dot{u}_r}{\partial r} + \frac{\dot{u}_r}{r} = \frac{\sigma_{r\theta}}{G}\frac{\partial \lambda}{\partial \theta} \quad \ldots\ldots [21]$$

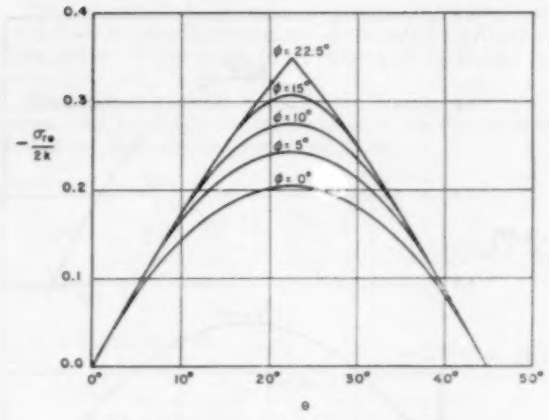

FIG. 6 DISTRIBUTION OF SHEARING STRESS

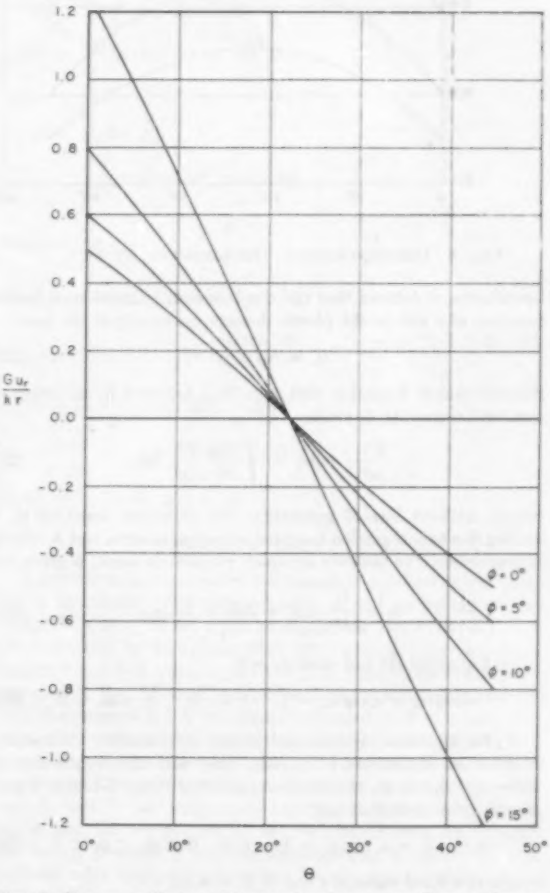

FIG. 7 RATIO OF RADIAL DISPLACEMENT TO r OR RADIAL STRAIN

Since the loading is assumed to increase monotonically with time, as in previous elastic-plastic investigations, it is convenient to interpret the dot as indicating differentiation with respect to ϕ, which, when necessary, will be identified with either ϕ_1 or ϕ_2.

As radial slip is not permissible along the elastic-plastic

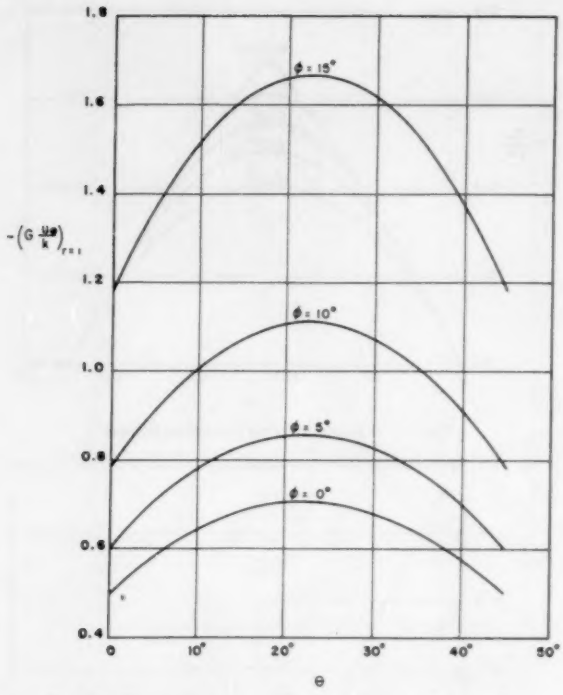

FIG. 8 CIRCUMFERENTIAL DISPLACEMENT AT $r = 1$

boundaries, it follows that the displacement u_r must be a linear function of r also in the plastic domain, or simply of the form

$$u_r = r\epsilon_r(\theta, \phi) \quad \ldots [22]$$

Substitution of Equation [22] into [21], followed by an integration with respect to ϕ, yields

$$\frac{\partial^2 \epsilon_r}{\partial \theta^2} + 4\epsilon_r = \int \frac{\sigma_{r\theta}}{G}\frac{\partial \lambda}{\partial \theta}\,\partial\phi \quad \ldots [23]$$

where, without loss of generality, the arbitrary function of θ arising due to integration has been set equal to zero, and λ, which is proportional to the rate at which stresses do work, is given by

$$\lambda = \frac{G}{k^2}(s_r\dot{\epsilon}_r + s_\theta\dot{\epsilon}_\theta + 2\sigma_{r\theta}\dot{\epsilon}_{r\theta}) \quad \ldots [24]$$

By Equation [2] and since $\epsilon_z = 0$

$$\epsilon_r : \epsilon_\theta : \epsilon_z = \dot{\epsilon}_r : \dot{\epsilon}_\theta : \dot{\epsilon}_z = 1 : -1 : 0; \quad 0 < \phi_1 < \phi_2 < \beta \ldots [25]$$

at P, for all states of contained plastic deformation. Moreover, in view of Equations [19], [24], [25] and the continuity of stresses at ϕ_1 and ϕ_2, the stress-strain law of Prandtl-Reuss, Equation [6], demands that at P

$$\dot{s}_r : \dot{s}_\theta : \dot{s}_z = s_r : s_\theta : s_z = 1 : -1 : 0; \quad 0 < \phi_1 < \phi_2 < \beta \ldots [26]$$

where at a fixed value of r and θ, $\lambda = \lambda(\phi)$.

According to Equations [26], s_r and s_θ have the same absolute value throughout the wedge. Hence, the quantity $(s_r - s_\theta) = -2s_\theta$ and, with the aid of the Mises Yield Condition, Equation [20a] in the plastic domain becomes

$$\frac{\partial \sigma_{r\theta}}{\partial \theta} = \pm 2[k^2 - \sigma_{r\theta}^2]^{1/2} \quad \ldots [27]$$

Integration of Equation [27], together with [15] and [26], results in

$$\left.\begin{aligned} \sigma_{r\theta}(\theta, \phi) &= \pm k \sin 2(\theta - \gamma) \\ s_\theta(\theta, \phi) &= -s_r(\theta, \phi) = \pm k \cos 2(\theta - \gamma) \end{aligned}\right\} \ldots [28]$$

where $\gamma = \gamma(\phi)$, and the question of the appropriate signs in each of the two plastic regions will be disposed of presently. The mean normal stress, in the plastic domain, is determined by substituting Equations [28] into [20b], which leads to $\partial s/\partial\theta = 0$, or

$$s = s(\phi) \quad \ldots [29]$$

The stress tensor in the plastic regions $0 \leq \theta \leq \phi_1$ and $\phi_2 \leq \theta \leq \beta$, in addition to fulfilling the continuity requirements at ϕ_1 and ϕ_2, also must conform to the boundary conditions

$$\left.\begin{aligned} \sigma_\theta(0, \phi_1) &= -p, \quad \sigma_{r\theta}(0, \phi_1) = 0 \\ \sigma_\theta(\beta, \phi_2) &= \sigma_{r\theta}(\beta, \phi_2) = 0 \end{aligned}\right\} \quad \ldots [30]$$

respectively. Substitution of Equations [28] and [29] into each of the Conditions [30] yields, respectively

$$\gamma = 0, \quad s = -p \mp k; \quad 0 \leq \theta \leq \phi_1 \quad \ldots [31a]$$

and

$$\gamma = \beta, \quad s = \mp k; \quad \phi_2 \leq \theta \leq \beta \quad \ldots [31b]$$

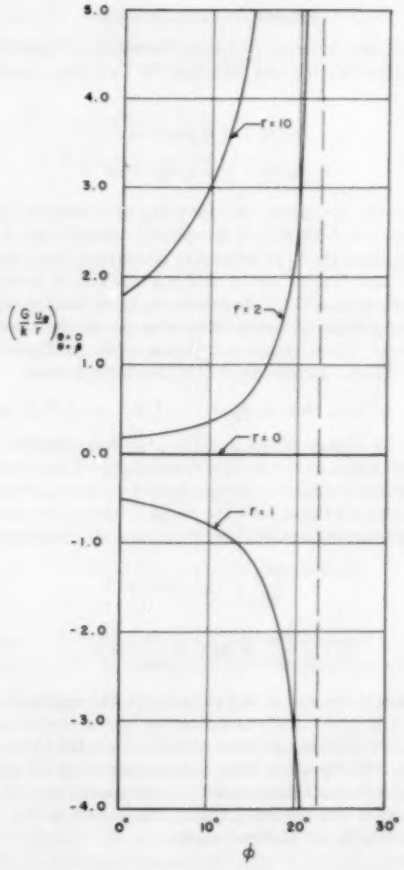

FIG. 9 RATIO OF CIRCUMFERENTIAL DISPLACEMENT TO r AT VARIOUS POSITIONS ALONG OUTSIDE BOUNDARIES

in each of the two plastic regions. Guided by the fact[9] that the lateral pressure bends the wedge so as to produce a tensile radial stress on $\theta = 0$, and a compressive radial stress on $\theta = \beta$, we choose the lower sign in Equations [28] and [31a] for the plastic region $0 \leq \theta \leq \phi_1$, and the upper sign in Equation [28] and [31b] for the region $\phi_2 \leq \theta \leq \beta$. In this manner, we finally obtain the following stress distribution in the two plastic regions

$$\left.\begin{aligned} s_r &= -s_\theta = k\cos 2\theta, \quad s_z = 0 \\ \sigma_{r\theta} &= -k\sin 2\theta \\ s &= -p + k \end{aligned}\right\};\ 0 \leq \theta \leq \phi_1 \ldots [32]$$

and

$$\left.\begin{aligned} s_r &= -s_\theta = -k\cos 2(\theta - \beta), \quad s_z = 0 \\ \sigma_{r\theta} &= k\sin 2(\theta - \beta) \\ s &= -k \end{aligned}\right\};\ \phi_2 \leq \theta \leq \beta . [33]$$

Continuity of the stresses at the elastic-plastic boundaries, together with Boundary Conditions [18] for the stresses in the elastic region $\phi_1 \leq \theta \leq \phi_2$, require the continuity of the mean normal stress at ϕ_1 and ϕ_2. Hence, by Equations [10], [32], and [33], we have

$$\left.\begin{aligned} 2(b + d\phi_1) &= -p + k \\ 2(b + d\phi_2) &= -k \end{aligned}\right\} \ldots\ldots\ldots [34]$$

where b and d are of the form given in Equations [12], with θ_1 and θ_2 replaced by ϕ_1 and ϕ_2; also, by Equations [32] and [33], the quantities σ_1, τ_1, σ_2, and τ_2 in Equation [12] are

$$\sigma_1 = -p + k(1 - \cos 2\phi_1), \quad \tau_1 = -k\sin 2\phi_1 \ldots [35a]$$

and

$$\sigma_2 = -k[1 - \cos 2(\phi_2 - \beta)], \quad \tau_2 = k\sin 2(\phi_2 - \beta) \ldots [35b]$$

Elimination of p from Equations [34] leads to a single equation which, after considerable manipulation, reduces to

$$\phi_1 + \phi_2 = \beta \ldots\ldots\ldots\ldots\ldots [36]$$

revealing the interdependence of ϕ_1 and ϕ_2. Thus, in what follows, one of the elastic-plastic boundaries, i.e., ϕ_1, will be identified with ϕ, and the other ϕ_2, with $(\beta - \phi)$.

We now return to Equation [23] and proceed to determine the displacements in one of the two plastic regions, i.e., $0 \leq \theta \leq \phi$. Since by the first of Equations [32], $\epsilon_r = -\epsilon_\theta$, and by Equations [5] $\dot{\epsilon}_{r\theta} = -\tan 2\theta\dot{\epsilon}_r$, then with the aid of Equations [2], [24], and [32], Equation [23] becomes[10]

$$\frac{\partial^2\epsilon_r}{\partial\theta^2} + 2\tan 2\theta\,\frac{\partial\epsilon_r}{\partial\theta} + 4\sec^2 2\theta\,\epsilon_r = 0 \ldots\ldots [37]$$

the solution of which may be written as

$$\epsilon_r = \cos 2\theta[A_1(\phi) + B_1(\phi)\log|\sec 2\theta + \tan 2\theta|] \ldots [38]$$

Equations [38], [22], and the incompressibility condition [7c], together with the observation that $\epsilon_{r\theta}$ is independent of r, lead to the following displacements for the plastic region $0 \leq \theta \leq \phi$

$$\left.\begin{aligned} u_r &= r\cos 2\theta[A_1 + B_1\log|\sec 2\theta + \tan 2\theta|] \\ u_\theta &= -r\sin 2\theta[A_1 + B_1\log|\sec 2\theta + \tan 2\theta|] + r[B_1\log|\sec 2\theta| - 2B_1\log r + C_1(\phi)] \end{aligned}\right\};\ 0 \leq \theta \leq \phi \ldots [39]$$

[9] This remark is similar to that offered in (1, p. 157) for a wedge of rigid, perfectly plastic material.

[10] Differential equation [37] can also be derived by means of Equations [5] and the appropriate equation of compatibility.

The displacements for the region $(\beta - \phi) \leq \theta \leq \beta$, which may be deduced in a similar manner, are of the same form as Equations [39] except that A_1, B_1, C_1 are replaced by A_2, B_2, and C_2, respectively, and θ by $(\theta - \beta)$.

The coefficient functions A_i, B_i, and C_i $(i = 1, 2)$ are determined from the continuity requirements of the displacement field at the elastic-plastic boundaries. Thus

$$\left.\begin{aligned} A_1(\phi) &= P_1\sec 2\phi - \frac{d}{2G}\log|\sec 2\phi + \tan 2\phi| \\ B_1(\phi) &= \frac{d}{2G} \\ C_1(\phi) &= P_1\tan 2\phi + Q_1 - \frac{d}{2G}\log|\sec 2\phi| \\ P_1(\phi) &= -\frac{1}{G}[a\cos 2\phi + c\sin 2\phi] \\ Q_1(\phi) &= \frac{1}{G}[a\sin 2\phi - c\cos 2\phi] \end{aligned}\right\};\ 0 \leq \theta \leq \phi \ldots [40]$$

and

$$\left.\begin{aligned} A_2(\phi) &= P_2\sec 2\phi - \frac{d}{2G}\log|\sec 2\phi - \tan 2\phi| \\ B_2(\phi) &= \frac{d}{2G} \\ C_2(\phi) &= -P_2\tan 2\phi + Q_2 - \frac{d}{2G}\log|\sec 2\phi| \\ P_2(\phi) &= -\frac{1}{G}[a\cos 2(\beta - \phi) + c\sin 2(\beta - \phi)] \\ Q_2(\phi) &= \frac{1}{G}[a\sin 2(\beta - \phi) - c\cos 2(\beta - \phi)] \end{aligned}\right\};\ (\beta - \phi) \leq \theta \leq \beta \ldots [41]$$

In summary, a statement of the complete solution of the problem is as follows: The displacements u_r and u_θ throughout the wedge $(0 \leq \theta \leq \beta)$ are given by Equations [8a, b] for $\phi \leq \theta \leq (\beta - \phi)$, and by Equations [39], [40], and [41] for the plastic regions $0 \leq \theta \leq \phi$ and $(\beta - \phi) \leq \theta \leq \beta$; the stresses in the elastic region $\phi \leq \theta \leq (\beta - \phi)$ are of the form of Equations [10] and [9]; the stresses in the two plastic regions $0 \leq \theta \leq \phi$ and $(\beta - \phi) \leq \theta \leq \beta$ are given, respectively, by Equations [32] and [33]; and the coefficient functions a, b, c, and d are of the form of Equations [12], with σ_1, τ_1, σ_2, τ_2 given by Equations [35], and θ_1 and θ_2 (as well as ϕ_1 and ϕ_2) replaced, respectively, by ϕ and $(\beta - \phi)$. Also, the functional relation between the lateral pressure p and the elastic-plastic boundary $\theta = \phi$, deduced with the aid of Equation [36] from either of Equations [34], is given by

$$\left.\begin{aligned} \frac{p}{k} &= \frac{2}{\tan\alpha}[\alpha\sin 2\phi(\tan\alpha + \tan\phi) + (\tan\alpha - \alpha)] \\ \alpha &= \beta - 2\phi \end{aligned}\right\} \ldots [42]$$

In the limit of fully plastic state, the components of stress in the two plastic regions, given by Equations [32] and [33], reduce to the known results for a wedge of a rigid, perfectly plastic material, where $\phi = \phi_1 = \phi_2 = \beta/2$ (separating the two plastic regions) is a line of stress discontinuity. It may be noted, however, that this limiting result (as in the analogous case of the bending of a wide beam by terminal couples) is achieved only after an infinite amount of straining.

Numerical Example—Conclusion

We now consider a numerical example and assume $\beta = \pi/4$. For this particular case, Fig. 2 shows the values of the elastic-plastic boundaries ϕ and $(\beta - \phi)$ corresponding to given values of p/k which, in the range of contained plastic deformation, is bounded by p^*/k and p^{**}/k. The resulting stress distributions and displacements, in this case $(\beta = \pi/4)$, for various positions of ϕ are shown in Figs. 3 to 9.

In conclusion, it may be mentioned that while the validity of the foregoing elastic-plastic solution is limited to wedge regions with included angle $\beta < \pi/2$, many features of the analysis presented are also applicable to other ranges of values of β and may be extended to cover wedge regions exposed to more general uniform surface tractions.

BIBLIOGRAPHY

1 "Theory of Perfectly Plastic Solids," by W. Prager and P. G. Hodge, Jr., John Wiley & Sons, Inc., New York, N. Y., 1951.

2 "The Mathematical Theory of Plasticity," by R. Hill, Oxford University Press, London, England, 1950.

3 "On Partially Plastic Thick-Walled Tubes," by W. T. Koiter, Biezeno Anniversary Volume on Applied Mechanics, Haarlem, Holland, 1953, pp. 233–251.

4 "The Elastic-Plastic Stress Distribution Within a Wide Curved Bar Subjected to Pure Bending," by B. W. Shaffer and R. N. House, Jr., Journal of Applied Mechanics, Trans. ASME, vol. 77, 1955, pp. 305–310; also, "Displacements in a Wide Curved Bar Subjected to Pure Elastic-Plastic Bending," by B. W. Shaffer and R. N. House, Jr., New York University Technical Report prepared for Army Office of Ordnance Research, September, 1955.

5 "On the Use of Singular Yield Conditions and Associated Flow Rules," by William Prager, Journal of Applied Mechanics, Trans. ASME, vol. 75, 1953, pp. 317–320.

6 "The Simplest Rate Theory of Pure Elasticity," by C. Truesdell, *Communications on Pure and Applied Mathematics*, vol. 8, 1955, pp. 123–132.

7 "Characteristic Surfaces in the Prandtl-Reuss Plasticity Theory," by T. Y. Thomas, *Journal of Rational Mechanics and Analysis*, vol. 5, 1956, pp. 251–262.

8 "Hypo-Elasticity and Plasticity," by A. E. Green, Proceedings of the Royal Society of London, England, series A, vol. 234, 1956, pp. 46–59.

9 "Hypo-Elastic Shear," by C. Truesdell, *Journal of Applied Physics*, vol. 27, 1956, pp. 441–447.

10 "Drang und Zwang," by A. L. Föppl, R. Oldenbourg, Berlin, Germany, vol. 1, 1924.

11 "Theory of Elasticity," by S. Timoshenko and J. N. Goodier, McGraw-Hill Book Company, Inc., New York, N. Y., second edition, 1951, pp. 123–125.

12 "A Concentrated Force Applied to a Half-Plane," by K. N. Shevchenko, *Prikladnaia Matematika i Mekhanika*, vol. 12, 1948, pp. 385–388; also, "The Elastic-Plastic State Due to a Concentrated Force Applied to a Half-Plane," by K. N. Shevchenko, *Dokladi Akademii Nauk USSR* (New Series), vol. 61, 1948, pp. 29–30.

13 "Plane Equilibrium of a Plastic Wedge," by V. V. Sokolovskii, Akademii Nauk USSR, *Prikladnaia Matematica i Mekhanika*, vol. 14, 1950, pp. 391–404.

14 "Elastic-Plastic Equilibrium of a Wedge and Discontinuous Solutions in the Theory of Plasticity," by G. S. Šapiro, Nauk USSR, *Prikladnaia Matematica i Mekhanika*, vol. 16, 1952, pp. 101–106.

Beams of Uniform Strength Subjected to Uniformly Distributed Loading[1]

By W. A. GROSS[2] and J. P. LI[3]

Beams with uniform strength subjected only to bending have the same maximum flexural stress at any cross section. The shapes, deflections, and weights are given for cantilever, simple, and fixed beams of uniform strength and appreciable weight subjected to uniformly distributed loadings. Explicit solutions are given for beams having rectangular cross sections and constant height. Solutions in integral form are provided for rectangular beams of constant width. This method is also applicable to beams with constant ratio of height to width, as well as beams with circular cross sections. Examples illustrate the large material savings over uniform cross-section beams which may be achieved.

Introduction

A BEAM of uniform strength in bending has the same maximum flexural stress at every cross section when subjected to pure bending.

Blasius[4] first published, but did not solve, the fundamental integral equation for a beam of uniform strength in bending taking into consideration the weight of the beam. At that time solutions neglecting the weight of the beam were available. Gaede[5] provided solutions for beams having rectangular cross sections and constant height loaded by their own weight. Recently Opatowski[6,7] has investigated the general problem and provided techniques for deriving solutions to various cantilever problems. In every case elementary beam theory is assumed valid.

Beams of this type are useful when a design requires them to contain a minimum quantity of homogeneous material. This can account for a significant material savings over the beam of uniform cross section designed to handle the same load.

Comparatively simple results are developed here for rectangular beams with constant height, and methods of solution are indicated for rectangular beams with constant width and constant ratio of height to width as well as for circular beams. In all cases, the effects of shear are neglected so that, at sections where the bending moment vanishes, the cross section of the beam becomes zero. Practical design requires that additional material be provided to withstand shearing loads and that buckling be considered if, in a rectangular beam, h/b becomes large.

Deflections

The radius of curvature ρ for a beam subject only to bending is $EI(x)/M(x)$ in which E is Young's modulus, $I(x)$ the moment of inertia at section x with respect to the neutral axis, and $M(x)$ the moment at the same section. For a beam of constant strength, $M(x) = \pm 2\sigma I(x)/h(x)$, so that $\rho(x) = \mp h(x)E/2\sigma$. For beams of constant height, $\rho(x)$ is constant in absolute value and changes sign at points of inflection; σ is the assigned maximum flexural stress at a section, and ρ is the radius of curvature. This relation holds for large deflections, so long as stresses remain less than the proportional limit.

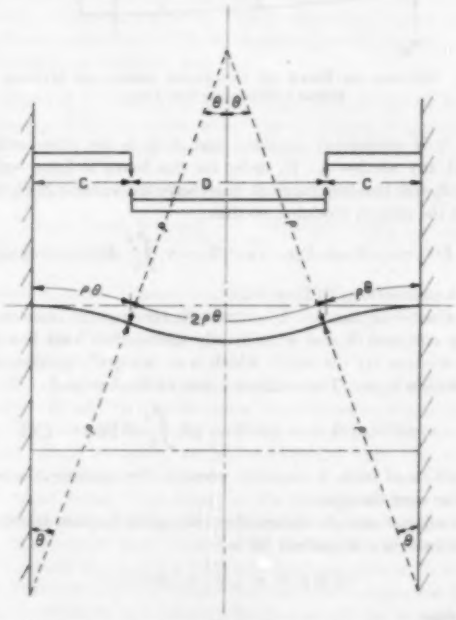

Fig. 1 Fixed Beam With Rectangular Cross Section and Constant Height

Deflections of cantilever and simple beams are easily visualized. A single fixed beam of uniform strength is impossible in accordance with the assumptions. Instead, fixed beams may be considered to be combinations of simple and cantilever beams connected at points of zero moment. At these points the cross section must be zero so that the "beam" in effect is composed of three parts. Fig. 1 illustrates the case of the rectangular beam

[1] The results presented in this paper were obtained while the authors were Assistant Professors of Theoretical and Applied Mechanics at Iowa State College, Ames, Iowa.

[2] Member of the Technical Staff, Bell Telephone Laboratories, Inc., Murray Hill, N. J. Now with International Business Machines Corporation, San Jose, Calif.

[3] Research Engineer, Scientific Laboratory, Ford Motor Company, Dearborn, Mich.

[4] "Träger kleinster durch biegung und Stabe gröster Knickfestigkeit bei gegebenen Materialverbrauch," by H. Blasius, *Zeitschrift für Mathematik und Physik*, vol. 62, 1914, pp. 182–197.

[5] "Balkenträger von gleichen Widerstande gegen Biegung," by K. Gaede, *Bautechnik*, vol. 15, 1937, pp. 120–123.

[6] "Cantilever Beams of Uniform Strength," by I. Opatowski, *Quarterly of Applied Mathematics*, vol. 3, no. 1, 1945, pp. 76–81.

[7] "Design of Beams of Long Span and Low Specific Strength," by I. Opatowski, Journal of Applied Mechanics, Trans. ASME, vol. 67, 1945, pp. A-156–A-158.

Contributed by the Applied Mechanics Division and presented at the Annual Meeting, New York, N. Y., November 25–30, 1956, of The American Society of Mechanical Engineers.

Discussion of this paper should be addressed to the Secretary, ASME, 29 West 39th Street, New York, N. Y., and will be accepted until April 10, 1957, for publication at a later date. Discussion received after the closing date will be returned.

Note: Statements and opinions advanced in papers are to be understood as individual expressions of their authors and not those of the Society. Manuscript received by ASME Applied Mechanics Division, May 16, 1956. Paper No. 56—A-9.

with constant height for which ρ has a fixed magnitude. The radius of curvature is reduced for clarity. Since the slope y', is required to be continuous, by geometry the points of inflection, marking the ends of the cantilever sections, occur at one quarter of the span from either end. If, through some strategem, discontinuous slopes can be tolerated at the points of zero moment of a constant-strength beam fixed at both ends, the mid-section can be made to take any length from zero up to, but less than, full span. To provide for the practical support of shear additional material must be provided, or even a pin-type connection may be used at the points of zero moment.

Rectangular Beams of Uniform Strength Having Constant Height

Fig. 2 shows a beam having specific weight γ subjected to a uniformly distributed load of intensity q. The bending moment is negative when the upper fiber is in tension. At any section x

$$M(x) = -M_0 + R_0 x - qx^2/2 - \gamma \int_0^x A(\xi)(x - \xi)d\xi \quad [1]$$

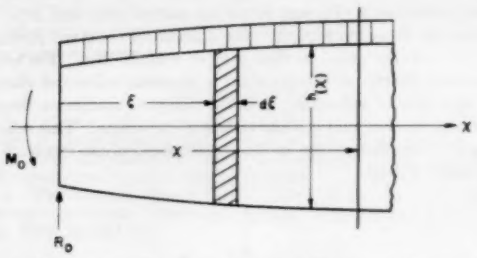

Fig. 2 Section of Beam of Constant Strength Having Uniformly Distributed Load

where γ is considered constant and $A(\xi)$ is the cross-sectional area at any section ξ. In order for the beam to have uniform strength, this bending moment must have the value $\sigma Z(x)$, where $Z(x)$ is the section modulus, so that

$$\pm 2\sigma I/h = -M_0 + R_0 x - qx^2/2 - \gamma \int_0^x A(\xi)(x - \xi)d\xi \quad [2]$$

Since h is constant, $A(\xi) = hb(\xi)$.

(*a*) *Cantilever Beam.* A beam with rectangular cross section having constant h and a uniformly distributed load has a defining relation for the width which is an integral equation of the convolution type. The origin is taken at the free end

$$-\sigma h^2 b(x)/6 = -qx^2/2 - \gamma h \int_0^x b(\xi)(x - \xi)d\xi \quad [3]$$

The left-hand term is negative because the bending moment is negative over the span.

The solution may be obtained readily using Laplace transforms. The transform of Equation [3] is

$$\sigma h^2 b(s)/6 = q/s^3 + \gamma h b(s)/s^2 \quad [4]$$

Therefore

$$b(s) = 6q/\sigma h^2 s(s^2 - 6\gamma/\sigma h) \quad [5]$$

The inverse transform of Equation [5] gives the equation for the width

$$b(x) = q(\cosh ax - 1)/\gamma h \quad [6]$$

In this and subsequent equations

$$a = (6\gamma/\sigma h)^{1/2} \quad [7]$$

The weight of the beam is

$$W = \gamma \int_0^L A(x)dx = (q/a)(\sinh aL - aL) \quad [8]$$

(*b*) *Simply Supported Beam.* The defining relation for the simply supported beam of rectangular cross section with constant height is, with origin taken at one end

$$\sigma h^2 b(x)/6 = R_0 x - qx^2/2 - \gamma h \int_0^x b(\xi)(x - \xi)d\xi \quad [9]$$

in which

$$R_0 = \frac{1}{2}(qL + W) \quad [10]$$

The Laplace transform of Equation [9] is

$$\sigma h^2 b(s)/6 = R_0/s^2 - q/s^3 - \gamma h b(s)/s^2 \quad [11]$$

in which R_0 for any particular beam is a constant. Solving for $b(s)$ gives

$$b(s) = 6R_0/\sigma h^2(s^2 + a^2) - 6q/\sigma h^2 s(s^2 + a^2) \quad [12]$$

so that

$$b(x) = (aR_0/\gamma h)\sin ax + (q/\gamma h)(\cos ax - 1) \quad [13]$$

The weight is given by

$$W = \int_0^L [aR_0 \sin ax + q(\cos ax - 1)]dx \quad [14]$$

After integrating, and using Equation [10], it follows that

$$W = \frac{q}{a}\left(2\tan\frac{aL}{2} - aL\right) \quad [15]$$

and

$$R_0 = \frac{q}{a}\tan(aL/2) \quad [16]$$

Now Equation [13] may be written

$$b(x) = (q/\gamma h)[\tan(aL/2)\sin ax + \cos ax - 1] \quad [17]$$

(*c*) *Fixed Beam.* We consider here the symmetrical fixed beam having rectangular cross section and fixed height. (The treatment for an unsymmetrical beam is similar.)

By reversing the sign of R_0 and σ, which changes a to ia in Equations [11] and [12], and using Equation [13] (R_0 is computed from the simply supported center section of length D by Equation [16] in which a does not change to ia), the width of the cantilever portions may be written directly

$$b(x) = (q/\gamma h)[\tan(aD/2)\sinh ax + \cosh ax - 1] \quad [18]$$

As seen in Fig. 1, D is the length of the simply supported middle portion of the beam. The x-co-ordinate increases from zero at the ends of the cantilever sections going toward the supporting walls.

The weight of each cantilever section is

$$W_c = (q/a)[\tan(aD/2)(1 - \cosh aC) + \sinh aC - aC] \quad [19]$$

where C is the length of the cantilever portions.

The moment at any cross section of the cantilever may be obtained by putting Equation [18] into Equation [1] (in which $M_0 = 0$ and R_0 is replaced by $-R_0$) and integrating

$$M(x) = -(q/a^2)[\tan(aD/2)\sinh ax + \cosh ax - 1] \quad [20]$$

At the wall

$$M_0 = -(q/a^2)[\tan(aD/2)\sinh aC + \cosh aC - 1] \quad [21]$$

For $D = 2C = L/2$, the appropriate relations for cross section,

weight, and moment of cantilever and mid-section may be written directly.

Rectangular Beams of Uniform Strength Having Constant Width

The deflection relations hold for the neutral plane of a beam. For a rectangular beam of constant width, the height must vary from zero at points of zero moment to maximums at points where the moment is maximum. The radius of curvature approaches zero along with the height.

The description of the beam sections may be obtained, as pointed out by Opatowski, by successive approximations, power series, or reduction to convenient integral forms.

(*a*) *Cantilever Beam.* The variation of the rectangular cross section of a cantilever beam of uniform strength with constant width is defined by

$$-\sigma bh^2(x)/6 = -qx^2/2 - \gamma b \int_0^x h(\xi)(x-\xi)d\xi \quad [22]$$

in which the origin is at the free end.

Differentiate Equation [22] twice with respect to x

$$(\sigma/6\gamma)[h^2]'' = h + q/\gamma b \quad [23]$$

and note that substituting

$$p(h) = h' \text{ and } p\frac{dp}{dh} = h''$$

transforms this relation into a Bernoulli equation.

Two integrations give

$$\sqrt{\frac{\sigma}{2\gamma}} \int_0^h \frac{h\,dh}{H} = \int_0^x dx \quad [24]$$

where

$$H = (h^2 + 3qh^2/2\gamma b + K^2)^{1/2}$$

in which K^2 is the constant introduced by the first integration.

The constant of integration may be evaluated in the following manner:

From Equation [24] note that

$$\frac{dx}{dh} = \sqrt{\frac{\sigma}{2\gamma}}\frac{h}{H} \quad [25]$$

Since

$$M(x) = -\frac{\sigma h^2(x)b}{6} = -\frac{qx^2}{2} - \gamma \int_0^x A(\xi)(x-\xi)d\xi$$

$$M'(x) = -\frac{\sigma hh'b}{3} = -qx - \gamma \int_0^x A(\xi)d\xi \quad [26]$$

Using Equation [25]

$$hh' = H\sqrt{\frac{2\gamma}{\sigma}} = -\frac{3M'}{\sigma b} \quad [27]$$

When $x = 0$, $M' = h = H = 0$. It follows that $K = 0$. The solution from Equation [24] is therefore

$$x = \sqrt{\frac{\sigma}{2\gamma}} \int_0^h (h^2 + 3qh^2/2\gamma b)^{-1/2} h\,dh \quad [28]$$

so that

$$h = \gamma x^2/2\sigma + \sqrt{3q/\sigma b}\,x \quad [29]$$

It follows that the weight of the beam is

$$W = \gamma^2 bL^3/6\sigma + L^3\sqrt{3bq\gamma^2/4\sigma} \quad [30]$$

(*b*) *Simply Supported Beam.* The defining equation for the simply supported beam of constant width is

$$\sigma bh^2(x)/6 = R_0 x - qx^2/2 - \gamma b \int_0^x h(\xi)(x-\xi)d\xi \quad [31]$$

This relation may be treated similarly to Equation [22] and we have

$$K^2 = 9R_0^2/2b^2\sigma\gamma \quad [32]$$

so that the solution in integral form is (using Equation [24])

$$x = \sqrt{\sigma/2\gamma} \int_0^h (9R_0^2/2b^2\sigma\gamma - 3qh^2/2\gamma b - h^2)^{-1/2} h\,dh \quad [33]$$

Since this equation cannot be integrated directly, other means must be used.

The most practical method of determining the shape of the beam from Equation [33] is to use numerical integration. R_0 must first be approximated. A reasonably close guess may, however, be made by utilizing easily calculable data. The problem reduces to determining the difference in weight of a beam described by Equation [33] and that of a comparable simple beam for which specific gravity is neglected when determining shape. A close approximation of this weight difference (with which the total weight and end reaction are easily obtainable) may be determined by comparison with the weight difference of other types of uniform-strength beams. It is convenient to do this using ratios in the following manner: Let

$$r = \frac{\text{weight of a beam of uniform strength with particular loading}}{\text{weight of similar beam whose specific gravity was neglected}}$$
for the shape determination

then using Equation [10], obtain R_0 using W calculated from

$$\frac{r\,(\text{simple beam, } b = c_1)}{r\,(\text{cantilever beam, } b = c_1)} = \frac{r\,(\text{simple beam, } h = c_2)}{r\,(\text{cantilever beam, } h = c_2)}$$

in which c_1, c_2 are appropriate constants. This first approximation should be close enough that only one, or at the most, two further trials should be necessary. The weight may be verified numerically.

If the relations between the constants warrant, it may be convenient to obtain the solution using Weierstrassian elliptical functions. Since these functions are only selectively tabulated, this method would generally be less convenient than the straight numerical integration.

(*c*) *Fixed Beam.* The design of the fixed beam may be based on a center portion simply supported by the two cantileverlike ends. The cantilever sections may be treated like the simply supported section of Equation [31], save that the signs of R_0 and the stress σ are reversed. It follows that the defining equation for the cantilever sections, each taken to be one quarter the span length is

$$x = (\sigma/2\gamma)^{1/2} \int_0^h (9R_0^2/2b^2\sigma\gamma + 3qh^2/2b\gamma + h^2)^{-1/2} h\,dh \quad [34]$$

Rectangular beams having constant ratio of width to height and beams with circular cross sections may be treated in a similar fashion.

Examples

Results are given in Table 1 for 50 in. of 100-in-long rectangular simple and cantilever beams. Fixed constants are $\gamma = 150$ pcf, $\sigma = 100$ psi, $q = 20$ lb/in., either $b = 10$ in., or $h = 10$ in.

TABLE 1 RECTANGULAR CROSS-SECTION BEAMS OF UNIFORM STRENGTH

(q = 20 lb/in., either [b] or [h] = 10 in., σ = 100 psi, γ = 150 pcf, L (simple beam) = 100 in.)

Distance from end of beam (in.)	0	10	20	30	40	50	Weight, lb
Beams with h = 10 in.							
Cantilever	0	0.61	2.46	5.67	10.35	16.88	232
Cantilever (neglecting γ)	0	0.60	2.40	5.40	9.60	15.00	(1875)[a]
Simple	0	10.90	20.00	26.80	30.80	32.30	1930
Simple (neglecting γ)	0	5.40	9.60	12.60	14.40	15.00	(3750)[a]
Beams with b = 10 in.							
Cantilever	0	2.49	5.07	7.74	10.49	13.33	281
Cantilever (neglecting γ)	0	2.45	4.90	7.35	9.80	12.25	(692)[a]
Simple	0	9.85	12.75	13.85	14.90	15.50	1052
Simple (neglecting γ)	0	7.36	9.81	11.24	12.01	12.27	(1384)[a]

[a] These are weights of 50-in. cantilever beams and 100-in. symmetrical simple beams having uniform cross section (b = 10 in., h = 15.9 in., or h = 10 in., b = 43.2 in.), which have maximum fiber stress = 100 psi.

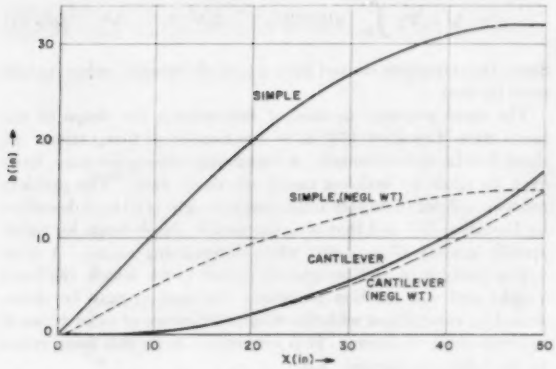

FIG. 3 BEAM WIDTH (CONSTANT HEIGHT)

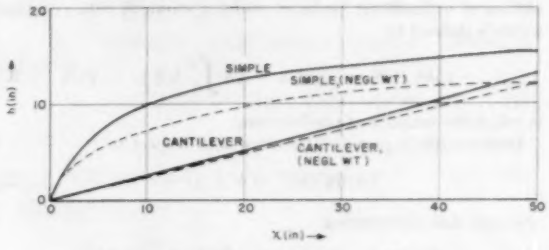

FIG. 4 BEAM HEIGHT (CONSTANT WIDTH)

Fig. 3 shows the variation of width with length for cantilever and simple beams of constant height with and without consideration of weight. Fig. 4 shows the variation of height for beams of constant width.

The difference between the shapes of the simple beams of constant height with and without weight consideration is largely due to the fact that, in this example, the weight of the beam is of the same order of magnitude as the total loading. Hence R_0 for the beam with weight considered is appreciably more than that of the beam with weight neglected.

For purposes of comparison, the end 50 in. of cantilever beams, or 100 in. simple beams having uniform rectangular cross sections of b = 10 in., h = 15.9 in., or b = 43.2 in., h = 10 in. will, when loaded identically to the example beams, have fiber stresses which vary to a maximum of 100 psi. The cantilever beam of uniform strength with constant height is the only example which differs in maximum size appreciably from the comparable dimensions of the uniform beam.

One expects the weights of uniform-cross-section beams to differ appreciably from those of uniform-strength beams. This is indeed the case, as may be seen by reference to Table 1. The uniform-section beam may require several times as much material.

ACKNOWLEDGMENT

The authors acknowledge gratefully a derivation suggested by the reviewers which has been incorporated in the revised form of the paper.

On the Stress Distribution at the Base of a Stationary Crack[1]

By M. L. WILLIAMS,[2] PASADENA, CALIF.

In an earlier paper it was suggested that a knowledge of the elastic-stress variation in the neighborhood of an angular corner of an infinite plate would perhaps be of value in analyzing the stress distribution at the base of a V-notch. As a part of a more general study, the specific case of a zero-angle notch, or crack, was carried out to supplement results obtained by other investigators. This paper includes remarks upon the antisymmetric, as well as symmetric, stress distribution, and the circumferential distribution of distortion strain-energy density. For the case of a symmetrical loading about the crack, it is shown that the energy density is not a maximum along the direction of the crack but is one third higher at an angle $\pm \cos^{-1}(1/3)$; i.e., approximately ±70 deg. It is shown that at the base of the crack in the direction of its prolongation, the principal stresses are equal, thus tending toward a state of (two-dimensional) hydrostatic tension. As the distance from the point of the crack increases, the distortion strain energy increases, suggesting the possibility of yielding ahead of the crack as well as ±70 deg to the sides. The maximum principal tension stress occurs on ±60 deg rays. For the antisymmetrical stress distribution the distortion strain energy is a relative maximum along the crack and 60 per cent lower ± 85 deg to the sides.

MANY previous investigators have studied the elastic-stress distributions around cracks with some of the earliest contributions being from Inglis (1)[3] who studied an internal crack using elliptical bounding surfaces, Griffith (2) who set up an energy criterion for crack instability, Westergaard who initially treated the crack problem in the same way to be exploited in this paper (3), as well as by the complex variable technique in a later paper (4). The stress distribution at the base of cracks also has been examined photoelastically with the first attempt to measure isochromatic-fringe patterns in this specific application apparently being accomplished by Hollister (5). Recently Post (6) has published some interesting results of his photoelastic observations for the case of an edge crack.

It is the purpose of this paper to supplement the results of these investigators in certain respects which it is hoped will aid in the further understanding of the elastic-stress distribution at the base of a stationary crack.

In a previous investigation (7) the plane-stress distribution near the vertex of an infinite sector of included angle α was considered for various combinations of boundary conditions. For the particular purpose of this paper it is desired to consider the case where the two radial edges of the plate are unloaded and the included angle approaches 2π. It has been shown that stress functions, i.e., solutions of $\nabla^4\chi(r, \theta) = 0$, of the form

$$\chi(r, \theta, \lambda) \equiv r^{\lambda+1}F(\theta; \lambda) = r^{\lambda+1}[c_1 \sin(\lambda+1)\theta + c_2 \cos(\lambda+1)\theta + c_3 \sin(\lambda-1)\theta + c_4 \cos(\lambda-1)\theta] \quad [1]$$

will satisfy the conditions of stress-free edges along $\theta = 0$ and $\theta = \alpha$ if the λ are chosen as the positive roots of

$$\sin(\lambda\alpha) = \pm\lambda \sin\alpha \quad [2]$$

For the case where $\alpha = 2\pi$, corresponding to the case of a crack with flank angle $\omega = \alpha - 2\pi = 0$, the eigenequation takes the particularly simple form $\sin(2\pi\lambda) = 0$, thus requiring $\lambda = n/2$, $n = 1, 2, 3, \ldots$, and yielding the stress function

$$\chi(r, \theta; n/2) = r^{(n/2)+1}\left[c_1 \sin\left(\frac{n}{2}+1\right)\theta + c_2 \cos\left(\frac{n}{2}+1\right)\theta + c_3 \sin\left(\frac{n}{2}-1\right)\theta + c_4 \cos\left(\frac{n}{2}-1\right)\theta\right] \quad [3]$$

From the general definition of the stress function

$$\sigma_r = \frac{1}{r^2}\frac{\partial^2\chi}{\partial\theta^2} + \frac{1}{r}\frac{\partial\chi}{\partial\theta} = r^{\lambda-1}[F''(\theta) + (\lambda+1)F(\theta)] \quad [4]$$

$$\sigma_\theta = \frac{\partial^2\chi}{\partial r^2} = r^{\lambda-1}[\lambda(\lambda+1)F(\theta)] \quad [5]$$

$$\tau_{r\theta} = -\frac{1}{r}\frac{\partial^2\chi}{\partial r\partial\theta} + \frac{1}{r^2}\frac{\partial\chi}{\partial\theta} = r^{\lambda-1}[-\lambda F'(\theta)] \quad [6]$$

one proceeds to require for this case that σ_θ and $\tau_{r\theta}$ vanish on $\theta = 0$ and $\theta = \alpha = 2\pi$. By reference to Equations [3–6] this implies that

$$F(0, n/2) = F'(0, n/2) = F(2\pi, n/2) = F'(2\pi, n/2) = 0$$

Ordinarily, that is, if $\alpha < 2\pi$, the four homogeneous boundary conditions permit three of the four c_i constants to be determined in terms of the fourth. In this case, however, all four boundary conditions can be satisfied by

$$\chi(r, \theta) = r^{(n/2)+1}\left\{c_2\left[\sin\left(\frac{n}{2}-1\right)\theta - \frac{n-2}{n+2}\sin\left(\frac{n}{2}+1\right)\theta\right] + c_4\left[\cos\left(\frac{n}{2}-1\right)\theta - \cos\left(\frac{n}{2}+1\right)\theta\right]\right\} \quad [7]$$

where the first term is equivalent to that used by Westergaard (3).

Turning now to a more convenient alternate form of expressing Equation [7] in terms of the bisector angle $\psi = \theta - \pi$, the stress

---

[1] This investigation was sponsored in part by the National Advisory Committee for Aeronautics, under Contract NAw-6431.

[2] Associate Professor, California Institute of Technology.

[3] Numbers in parentheses refer to the Bibliography at the end of the paper.

Contributed by the Applied Mechanics Division and presented at the Annual Meeting, New York, N. Y., November 25–30, 1956, of THE AMERICAN SOCIETY OF MECHANICAL ENGINEERS.

Discussion of this paper should be addressed to the Secretary, ASME, 29 West 39th Street, New York, N. Y., and will be accepted until April 10, 1957, for publication at a later date. Discussion received after the closing date will be returned.

NOTE: Statements and opinions advanced in papers are to be understood as individual expressions of their authors and not those of the Society. Manuscript received by ASME Applied Mechanics Division, March 21, 1956. Paper No. 56—A-16.

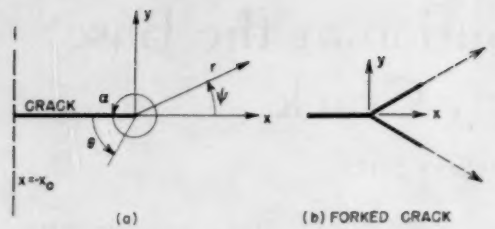

FIG. 1 GEOMETRY

function $\chi(r, \psi)$ can be split into its even $\chi_e(r, \psi)$ and odd $\chi_o(r, \psi)$ parts with respect to ψ (Fig. 1)

$$\chi_e(r, \psi) = \sum_{n=1,2,3,\ldots} \left\{ (-1)^{n-1} a_{2n-1} r^{n+\frac{1}{2}} \left[-\cos\left(n-\frac{3}{2}\right)\psi + \frac{2n-3}{2n+1}\cos\left(n+\frac{1}{2}\right)\psi \right] + (-1)^n a_{2n} r^{n+1} \left[-\cos\left(n-\frac{3}{2}\right)\psi + \cos\left(n+\frac{1}{2}\right)\psi \right] \right\} \quad [8]$$

$$\chi_o(r, \psi) = \sum_{n=1,2,3,\ldots} \left\{ (-1)^{n-1} b_{2n-1} r^{n+\frac{1}{2}} \left[\sin\left(n-\frac{3}{2}\right)\psi - \sin\left(n+\frac{1}{2}\right)\psi \right] + (-1)^n b_{2n} r^{n+1} \left[-\sin\left(n-\frac{3}{2}\right)\psi + \frac{2n-3}{2n+1}\sin\left(n+\frac{1}{2}\right)\psi \right] \right\} \quad [9]$$

It should be observed that even though the field equation and the boundary conditions along the radial edges are satisfied, the constants a_i and b_i are undetermined. Their values of course depend upon the loading conditions; more specifically, either upon the boundary conditions at infinity in the case of an infinite sector, or upon those at some fixed radius when the plate has finite dimensions. For the latter practical case, which includes the problem under consideration, all the higher eigenfunctions in general will be present in order to determine a solution in the large.

Upon writing out the first few terms

$$\chi(r, \psi) = r^{3/2}\left[a_1\left(-\cos\frac{\psi}{2} - \frac{1}{3}\cos\frac{3\psi}{2}\right) + b_1\left(-\sin\frac{\psi}{2} - \sin\frac{3\psi}{2}\right)\right] + a_2 r^2[1 - \cos 2\psi] + 0(r^{5/2}) + \ldots \quad [10]$$

from which the associated stresses may be found from Equations [4–6] as

$$\sigma_r(r, \psi) = \frac{1}{4r^{1/2}}\left\{ a_1\left[-5\cos\frac{\psi}{2} + \cos\frac{3\psi}{2}\right] + b_1\left[-5\sin\frac{\psi}{2} + 3\sin\frac{3\psi}{2}\right]\right\} + 4a_2\cos^2\psi + 0(r^{1/2}) + \ldots \quad [11]$$

$$\sigma_\psi(r, \psi) = \frac{1}{4r^{1/2}}\left\{ a_1\left[-3\cos\frac{\psi}{2} - \cos\frac{3\psi}{2}\right] + b_1\left[-3\sin\frac{\psi}{2} - 3\sin\frac{3\psi}{2}\right]\right\} + 4a_2\sin^2\psi + 0(r^{1/2}) + \ldots \quad [12]$$

$$\tau_{r\psi}(r, \psi) = \frac{1}{4r^{1/2}}\left\{ a_1\left[-\sin\frac{\psi}{2} - \sin\frac{3\psi}{2}\right] + b_1\left[\cos\frac{\psi}{2} + 3\cos\frac{3\psi}{2}\right]\right\} - 2a_2\sin 2\psi + 0(r^{1/2}) + \ldots \quad [13]$$

Before proceeding further, it is convenient to identify the stress state which is multiplied by the constant a_2, viz.

$$a_2 r^2(1 - \cos 2\psi) = 2a_2 r^2\sin^2\psi = 2a_2 y^2$$

In the Cartesian co-ordinates analog of Equations [4–6], the stresses are

$$\sigma_x = 4a_2, \quad \sigma_y = 0, \quad \text{and } \tau_{xy} = 0$$

For most cases of interest, including the usual tension and bending specimens, σ_x along the edge $x = -x_0$ (see Fig. 1) is zero; hence for these cases $\sigma_x = 4a_2 = 0$ and thus Equations [11–13] with respect to the radial variation are all of the form $r^{-1/2} + 0(r^{1/2})$, and the local stress variations in the vicinity of the base of the crack, $r \to 0$, are proportional, up to vanishing terms in r, to the contribution of the first term. If the boundary $x = -x_0$ were loaded, however, say by a uniform pressure, this contribution would have to be superimposed.

It is convenient at this point to compute two quantities useful in photoelastic analysis; specifically, the sum of the normal stresses, which is proportional to the isopachic lines, and the difference of the principal stresses, which is proportional to the isochromatic lines.

Thus

$$\sigma_r + \sigma_\psi = \frac{1}{4r^{1/2}}\left\{ a_1\left[-8\cos\frac{\psi}{2}\right] + b_1\left[-8\sin\frac{\psi}{2}\right]\right\} + \ldots = \sigma_1 + \sigma_2 \quad [14]$$

$$\sigma_1 - \sigma_2 = [(\sigma_r - \sigma_\psi)^2 + 4\tau_{r\psi}^2]^{1/2} = \frac{\pm 1}{4r^{1/2}}\left\{ 16a_1^2\sin^2\psi + 64b_1^2\left(1 - \frac{3}{4}\sin^2\psi\right)\right\}^{1/2} + \ldots \quad [15]$$

The direction of principal stress is found from the condition that the shear stress, $\tau_{n\alpha}$, on a plane whose normal is inclined at an angle α to the radius vector vanishes

$$\tau_{n\alpha} = \tau_{r\psi}\cos 2\alpha - (1/2)(\sigma_r - \sigma_\psi)\sin 2\alpha = 0$$

$$0 = -r^{-1/2}\left\{\left[\sin\frac{\psi}{2}\cos^2\frac{\psi}{2}\cos 2\alpha - \cos\frac{\psi}{2}\sin^2\frac{\psi}{2}\sin 2\alpha\right]a_1 + \left[\cos\frac{\psi}{2}\left(2 - 3\cos^2\frac{\psi}{2}\right)\cos 2\alpha + \sin\frac{\psi}{2}\left(2 - 3\sin^2\frac{\psi}{2}\right)\sin 2\alpha\right]b_1\right\} + \ldots \quad [16]$$

The angle β of a stress trajectory with the x-axis, Fig. 1, is then $\beta = \psi + \alpha$. Also the total strain-energy density

$$W = \frac{1}{2E}\left[\sigma_r^2 + \sigma_\psi^2 - 2\nu\sigma_r\sigma_\psi + 2(1+\nu)\tau_{r\psi}^2\right] \ldots [17]$$

and the strain energy due to distortion alone, i.e., the total strain energy less that due to change in volume

$$W_d = \frac{1}{12G}\left[(\sigma_1-\sigma_2)^2 + (\sigma_2-\sigma_3)^2 + (\sigma_3-\sigma_1)^2\right]$$

$$= \frac{1}{12G}(3\tau_{oct})^2 \ldots [18]$$

where the expression is given in terms of principal stresses ($\sigma_3 = 0$ in this case), and the definition of the octahedral shearing stress has been used, may be written, respectively, as

$$32ErW = a_1^2\left[(34-30\nu)\cos^2\frac{\psi}{2} + 2(1+\nu)\sin^2\frac{\psi}{2} + 2(1+\nu) - 4(1+\nu)\cos 2\psi\right] + b_1^2\left[(34-30\nu)\sin^2\frac{\psi}{2} + 2(1+\nu)\cos^2\frac{\psi}{2} + 18(1+\nu) + 12(1+\nu)\cos 2\psi\right] + 2a_1b_1\left[(32-22\nu)\sin\frac{\psi}{2}\cos\frac{\psi}{2} - 8(1+\nu)\sin 2\psi\right] + \ldots [19]$$

$$6GrW_d = a_1^2\left(1+3\sin^2\frac{\psi}{2}\right)\cos^2\frac{\psi}{2} + 2b_1^2\left[3+\left(1+3\cos\frac{\psi}{2}\right)\left(1-3\cos\frac{\psi}{2}\right)\sin^2\frac{\psi}{2}\right] + 2a_1b_1\sin\psi + \ldots [20]$$

In the foregoing expressions it is seen that the term multiplied by the coefficient a_1b_1 represents a coupling between the symmetric and antisymmetric variations with respect to ψ.

Finally, the displacements (see reference 7) are found to be

$$2\mu U_r(r,\psi) = r^{1/2}\left\{a_1\left[\left(-\frac{5}{2}+4\sigma\right)\cos\frac{\psi}{2} + \frac{1}{2}\cos\frac{3\psi}{2}\right] + b_1\left[(-3+4\sigma)\sin\frac{\psi}{2} + \sin\frac{3\psi}{2}\right]\right\} + \ldots [21]$$

$$2\mu U_\psi(r,\psi) = r^{1/2}\left\{a_1\left[\left(\frac{7}{2}-4\sigma\right)\sin\frac{\psi}{2} - \frac{1}{2}\sin\frac{3\psi}{2}\right] + b_1\left[-\left(\frac{7}{2}-4\sigma\right)\cos\frac{\psi}{2} + \frac{3}{2}\cos\frac{3\psi}{2}\right]\right\} + \ldots [22]$$

where

$$\sigma \equiv \nu/(1+\nu)$$

Symmetrical Stress Distribution

For the sake of simplicity it is convenient to analyze the two types of solutions separately; the symmetric solutions, i.e., $b_i = 0$, are perhaps the more common, occurring, for example, in the case of an edge crack in a thin plate subjected to bending or tension.

Specializing the stresses and the other quantities to this case gives

$$\sigma_r(r,\psi) = \frac{1}{4r^{1/2}}\left[-5\cos\frac{\psi}{2} + \cos\frac{3\psi}{2}\right]a_1 + \ldots [23]$$

$$\sigma_\psi(r,\psi) = \frac{1}{4r^{1/2}}\left[-3\cos\frac{\psi}{2} - \cos\frac{3\psi}{2}\right]a_1 + \ldots [24]$$

$$\tau_{r\psi}(r,\psi) = \frac{1}{4r^{1/2}}\left[-\sin\frac{\psi}{2} - \sin\frac{3\psi}{2}\right]a_1 + \ldots [25]$$

$$2\mu U_r(r,\psi) = r^{1/2}\left[\left(-\frac{5}{2}+4\sigma\right)\cos\frac{\psi}{2} + \frac{1}{2}\cos\frac{3\psi}{2}\right]a_1 + \ldots [26]$$

$$2\mu U_\psi(r,\psi) = r^{1/2}\left[\left(\frac{7}{2}-4\sigma\right)\sin\frac{\psi}{2} - \frac{1}{2}\sin\frac{3\psi}{2}\right]a_1 + \ldots [27]$$

$$\sigma_1 + \sigma_2 = \frac{1}{4r^{1/2}}\left[-8\cos\frac{\psi}{2}\right]a_1 + \ldots [28]$$

$$\sigma_1 - \sigma_2 = \frac{1}{4r^{1/2}}\left[4a_1\sin\psi\right] + \ldots [29]$$

$\beta_{\sigma=1} = (3\psi/4) \pm (\pi/4)$; also isotropic foci at $\psi = 0$.. [30]

$$W = \frac{a_1^2}{Er}\cos^2\frac{\psi}{2}\left[1-\nu+(1+\nu)\sin^2\frac{\psi}{2}\right] + \ldots [31]$$

$$W_d = \frac{a_1^2}{Er}\cos^2\frac{\psi}{2}\left[\frac{1+\nu}{3} + (1+\nu)\sin^2\frac{\psi}{2}\right] + \ldots [32]$$

It is observed that, for this elastic behavior in an isotropic homogeneous material, the stress system represented by the first term possesses the characteristic square-root singularity found by Inglis (1), Westergaard (4), and others; also, the shapes of the isopachics and isochromatic fringes are in agreement with photoelastic data obtained by Post (6) and corroborated independently at GALCIT. In addition, however, there are certain other interesting features which, because of the relative simplicity of the previous expressions, become readily apparent.

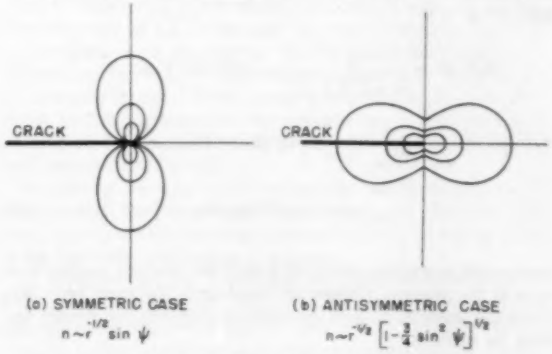

Fig. 2 Isochromatic-Fringe Patterns

The first of these relates to the observation that the shear stress is zero along the line of propagation of the crack ($\psi = 0$). The σ_r and σ_ψ stresses must therefore be principal stresses as expected, but moreover from Equation [29] the stresses are equal

$$\sigma_1(0) \to \sigma_2(0) = (-a_1)r^{-1/2} + \ldots$$

In other words, at the base of the crack there exists a strong tend-

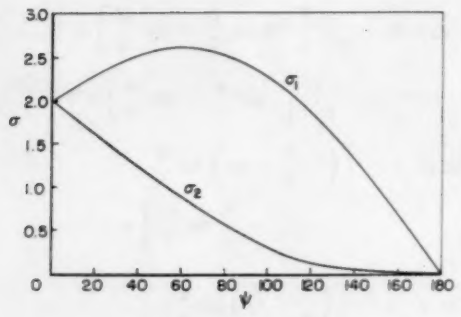

(a) SYMMETRIC CASE

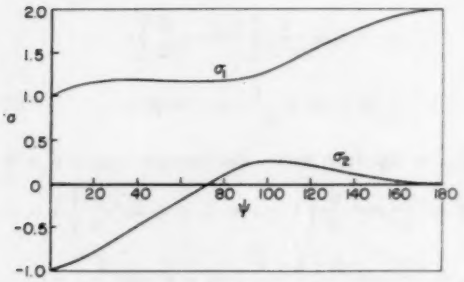

(b) ANTISYMMETRIC CASE

FIG. 3 PRINCIPAL-STRESS VARIATIONS

ency toward a state of (two-dimensional) hydrostatic tension which consequently may permit the elastic analysis to apply closer to the point of the crack that was hitherto supposed, notwithstanding the square-root stress singularity.

In order to investigate this point a bit more fully, particularly for the higher terms in r, i.e., further away from the crack point, more terms can be considered in Equations [23] and [24] to obtain, for $\psi = 0$

$$\sigma_r(r, 0) = \sum_{n = 1, 2, 3 \ldots} (-1)^n (2n - 1) a_{2n-1} r^{n - \frac{3}{2}} \quad [33]$$

$$\sigma_\psi(r, 0) = \sum_{n = 1, 2, 3 \ldots} \left\{ (-1)^n (2n - 1) a_{2n-1} r^{n - \frac{3}{2}} + (-1)^{n+1} 2a_{2n} (2n - 1) r^{n-1} \right\} \quad [34]$$

from which it may be concluded that, if the constant loading term $a_1 = 0$, the principal stresses are equal up to the linear term in r. From the previous relation the difference between the stresses can then be written

$$\sigma_r - \sigma_\psi = \sum_{n = 1, 2, 3 \ldots} (-1)^n 2a_{2n} (2n - 1) r^{n-1} \quad [35]$$

Therefore the principal stresses will become progressively unequal and the tendency toward hydrostatic tension reduced as the distance from the crack increases. As a matter of interest the stress trajectories for the lowest eigensolution, $n = 1$, are shown in Fig. 5 and they are observed to be of the interlocking type which explains the apparent contraction that $\beta = \pm\pi/4$ for $\psi = 0$ from

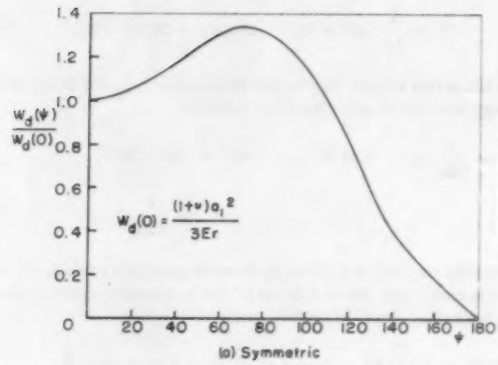

(a) Symmetric

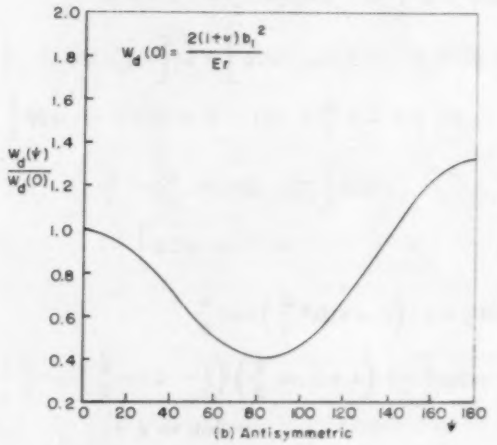

(b) Antisymmetric

FIG. 4 STRAIN-ENERGY-DENSITY DISTRIBUTIONS

Equation [30]. The equality of the principal stresses leads to a locus of isotropic points.

Another interesting characteristic of the solution is shown in Fig. 4 which shows the variation of distortion strain energy as a function of angle for a fixed radius. Because of the afore-mentioned hydrostatic tendency, the maximum energy of distortion does not occur along the line of crack direction, but rather at

$$\psi^* = \pm\cos^{-1}(1/3) \approx \pm 70 \text{ deg}$$

where it is one third higher.

The previous results also give the principal stress as

$$\sigma_{1,2} = -\frac{a_1}{r^{1/2}} \cos\frac{\psi}{2} \left[1 \mp \sin\frac{\psi}{2} \right]$$

for which the maximum value of $(3\sqrt{3}/4)(-a_1)r^{-1/2}$ occurs at $\bar{\psi} = \cos^{-1}(1/2) = \pi/3$ at which angle the stress trajectories are parallel to the x, y-co-ordinates; i.e., $\beta = 0, \pi/2$. The maximum shear stress $\tau_{max} = 1/2\,(\sigma_1 - \sigma_2)$ oriented at $\beta = \pi/8, 5\pi/8$, $\psi = \pi/2$ and equals exactly one half the hydrostatic tension value to which the normal stresses are subjected along $\psi = 0$ at the same radial distance. Some of the foregoing properties are summarized in Fig. 6.

Finally, the radial and circumferential displacements on the free edges from Equations [23] and [24] are found to be zero and $\pm 4(1 + \nu)^{-1} a_1 r^{1/2}$, thus leading to the expected fact that the two faces will have closed together and overlapped under a compression loading, an impossible situation by itself requiring $a_1 = 0$.

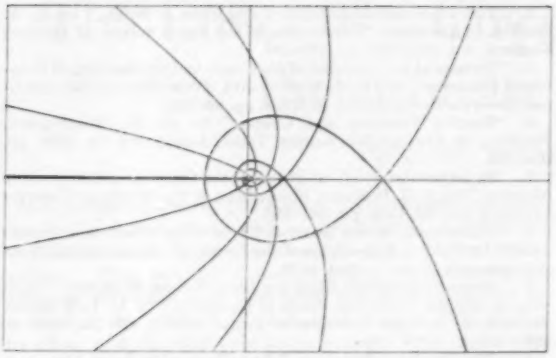

FIG. 5 STRESS TRAJECTORIES FOR LOWEST EVEN EIGENFUNCTION $\beta = (3\psi/4) \pm (\pi/4)$

In this case one is led to the contact problem treated by Westergaard (4) wherein there is no stress singularity at the point of the crack.

ANTISYMMETRICAL STRESS DISTRIBUTION

When the stress distribution is antisymmetric, which is a case that does not seem previously to have been treated explicitly, such as may exist about a crack parallel to the neutral axis of a beam in pure bending, there results

$$\sigma_r(r, \psi) = \frac{1}{4r^{1/2}}\left[-5 \sin^2 \frac{\psi}{2} + 3 \sin \frac{3\psi}{2}\right] b_1 + \ldots \quad [36]$$

$$\sigma_\psi(r, \psi) = \frac{1}{4r^{1/2}}\left[-3 \sin \frac{\psi}{2} - 3 \sin \frac{3\psi}{2}\right] b_1 + \ldots \quad [37]$$

$$\tau_{r\psi}(r, \psi) = \frac{1}{4r^{1/2}}\left[\cos \frac{\psi}{2} + 3 \cos \frac{3\psi}{2}\right] b_1 + \ldots \quad [38]$$

$$2\mu U_r(r, \psi) = r^{1/2}\left[(-3 + 4\sigma) \sin \frac{\psi}{2} + \sin \frac{3\psi}{2}\right] b_1 + \ldots \quad [39]$$

$$2\mu V_\psi(r, \psi) = r^{1/2}\left[-\left(\frac{7}{2} - 4\sigma\right)\cos \frac{\psi}{2} + \frac{3}{2} \cos \frac{3\psi}{2}\right] b_1 + \ldots \quad [40]$$

$$\sigma_1 + \sigma_2 = \frac{1}{4r^{1/2}}\left[-8 \sin \frac{\psi}{2}\right] b_1 + \ldots \quad [41]$$

$$\sigma_1 - \sigma_2 = \frac{1}{4r^{1/2}}\left[8\left(1 - \frac{3}{4} \sin^2 \psi\right)^{1/2}\right] b_1 + \ldots \quad [42]$$

$$W = \frac{b_1^2}{Er}\left[(1 - \nu) \sin^2 \frac{\psi}{2} + (1 + \nu)\left(1 - \frac{3}{4} \sin^2 \psi\right)\right] + \ldots \quad [43]$$

$$W_d = \frac{b_1^2}{Er}\left[\frac{1 + \nu}{3} \sin^2 \frac{\psi}{2} + (1 + \nu)\left(1 - \frac{3}{4} \sin^2 \psi\right)\right] + \ldots \quad [44]$$

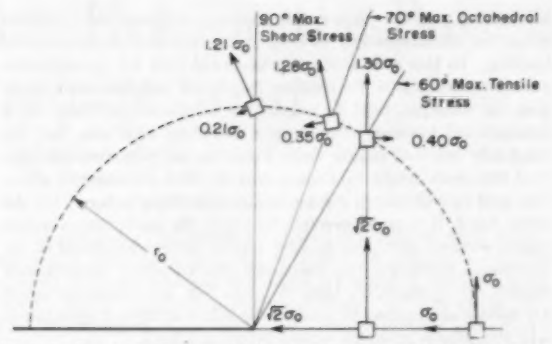

FIG. 6 CRITICAL PRINCIPAL STRESSES FOR THE LOWEST EVEN EIGENFUNCTION $\sigma_3 = -a_1 r_0^{-1/2}$

Again in this case the singular stress system varies as $r^{-1/2}$; the distortion-strain-energy-density variation is shown in Fig. 4. It is interesting to observe that in this case the energy drops on either side from a relative maximum in the direction of the crack to a minimum of 40 per cent of its $\psi = 0$ value at $\psi^\circ = \cos^{-1}(1/9)$.

It would be interesting to experiment photoelastically with the antisymmetric-loading condition, which is not too simple a matter, in an analysis similar to that of Post for the symmetrical case.

CONCLUSION

While it is not the intent to extend the range of validity of the elastic analysis by delving into the complicated phenomenon of failure or fracture mechanics, it does seem pertinent to remark upon some possible implications of the results obtained from elasticity theory.

First of all it seems that even in the presence of a partial (two-dimensional) hydrostatic-stress field there would be a reduced tendency for yielding at the base of the crack. Then, as the magnitude of the individual stresses increases as the inverse half power of the radius, the stress should become quite high with a tendency toward a cleavage failure. At the same time the elastic analysis indicates there should be a large amount of distortion off to the sides of the crack and presumably some yielding should take place in these areas which would tend toward a ductile failure. The character of failure actually occurring in a given specimen would depend upon the material. In this connection it is pertinent to mention some recent experimental evidence of Forsyth and Stubbington (8) called to the author's attention by S. R. Valluri, which tends to substantiate the remarks concerning an area of yielding off the crack direction, presumably ±70 deg for an exactly symmetrical loading.

In addition, because the stress becomes nonhydrostatic as the distance from the point of the crack increases, by Equation [35], there may be reason therefore to suspect a yielded region ahead of the crack also, although not as severe.

As a second remark, concerning the direction of cracking or forking, it is recognized that slow-moving cracks generally propagate more or less straight.[4] Because some cracks do fork,

[4] In an interesting piece of work Yoffe (9) has discussed the change of direction of a running crack due to its velocity and has found that if the material is such that a crack propagates in a direction normal to the maximum tensile stress (which, incidentally, is not σ_ψ as she apparently has assumed; indeed aside from the principal stresses, $\sigma_r \geq \sigma_\psi$), there is a critical velocity of about 0.6 times the velocity of shear waves in the material above which the crack tends to become curved. It may be of value to supplement her work by testing her hypothesis with respect to the maximum principal tensile stress; it is suspected, however, that the results will be qualitatively the same because, as she has remarked and as is shown in Fig. 6, the stress field is relatively uniform over a wide area in front of the crack.

however, it may be worth noting that any arbitrary crack will be subjected simultaneously to both symmetric and antisymmetric loading. In this connection it is observed that for the antisymmetric contributions the relative maximum and minimum energies, for example, tend to negate the effects which occur for a symmetrical loading. One might therefore conclude that for randomly oriented cracks there would be no preferred direction that the crack might take upon moving, with macroscopic structure and rate-of-energy release being controlling factors. On the other hand, it may be possible to relate the maximum principal tensile stresses occurring at ± 60 deg, in the neighborhood of the maximum distortion, to the angle crack-forking phenomenon shown, for example, by Post (6) or in Fig. 1(*b*), although again for metals as opposed to plastics the effect of crystal orientation and slip planes probably would be quite strong.

BIBLIOGRAPHY

1 "Stresses in a Plate Due to the Presence of Cracks and Sharp Corners," by C. E. Inglis, Transactions of the Institution of Naval Architects, London, England, vol. 60, 1913, p. 219.

2 "The Phenomena of Rupture and Flow in Solids," by A. A. Griffith, Philosophical Transactions of the Royal Society of London, England, vol. 221, 1921, pp. 163–198.

3 "Stresses at a Crack, Size of the Crack and the Bending of Reinforced Concrete," by H. M. Westergaard, Proceedings of the American Concrete Institute, vol. 30, 1934, pp. 93–102.

4 "Bearing Pressures and Cracks," by H. M. Westergaard, JOURNAL OF APPLIED MECHANICS, Trans. ASME, vol. 61, 1939, pp. A-49-53.

5 "Experimental Study of Stresses at a Crack in a Compression Member," by S. C. Hollister, Proceedings of the American Concrete Institute, vol. 30, 1934, pp. 361–365.

6 "Photoelastic Stress Analysis for an Edge Crack in a Tensile Field," by D. Post, Proceedings of the Society for Experimental Stress Analysis, vol. 12, no. 1, 1954, p. 99.

7 "Stress Singularities Resulting From Various Boundary Conditions in Angular Corners of Plates in Extension," by M. L. Williams, JOURNAL OF APPLIED MECHANICS, Trans. ASME, vol. 74, 1952, p. 526.

8 "The Slip Band Extrusion Effect Observed in Some Aluminum Alloys Subjected to Cyclic Stresses," by P. J. E. Forsyth and C. A. Stubbington, Royal Aircraft Establishment, MET Report 78, January, 1954.

9 "The Moving Griffith Crack," by E. H. Yoffe, *Philosophical Magazine*, vol. 42, part 2, 1951, pp. 739–750.

The Effect of a Circular Hole on the Pure Twist of an Infinite Strip

By OSAMU TAMATE,[1] SENDAI, JAPAN

In a previous paper by the author (1),[2] a theoretical solution for an infinite strip with a circular hole under plain bending is given by the method of successive approximation. This method demands laborious calculations. However, it seems that the labor can be diminished by employing the method of perturbation. In this paper, the effect of a circular hole in an infinite strip under the state of pure twist is investigated with the help of the perturbation method. The maximum deflections on the rim of the hole and the maximum stress couples in the strip are calculated and plotted versus hole-diameter strip-width ratio and Poisson's ratio of the plate material. Here the strip is considered subjected to the limitation of the Poisson-Kirchhoff theory of bending of thin plates.

Nomenclature

The following nomenclature is used in the paper:

x, y = rectangular co-ordinates
r, θ = polar co-ordinates
$x + iy = re^{i\theta}$ = middle plane of strip
E = Young's modulus
ν = Poisson's ratio
$D = Eh^3/12(1 - \nu^2)$ = flexural rigidity of strip
h = thickness of strip
$2b$ = width of strip
$2a$ = diameter of circular hole
w = deflection of strip
p = load intensity
$\xi = x/b$, $\eta = y/b$ = dimensionless rectangular co-ordinates
$\rho = r/b$ = dimensionless radial co-ordinate
$\lambda = a/b$ = hole-diameter strip-width ratio
$\epsilon = (1 - \nu)/(3 + \nu)$
M_x, M_y, M_{xy} / $M_r, M_\theta, M_{r\theta}$ = bending and twisting moments per unit length with reference to (x, y), (r, θ)-directions, respectively
Q_x, Q_y / Q_r, Q_θ = shearing force per unit length with reference to (x, y), (r, θ)-directions, respectively
V_x, V_y / V_r, V_θ = equivalent shearing force per unit length with reference to the (x, y), (r, θ)-directions, respectively
$\bar{\ }$ = overbar, indicating dimensionless quantities

Introduction

The problem of the stress distributions that arise when a perforated or notched isotropic plate is bent by transverse couples already has received some theoretical attention in certain special cases. Using the Poisson-Kirchhoff theory of thin plates (2), Goodier (3) has investigated the influence of circular and elliptic holes on the bending of thin plates. Lee (4) has given the theoretical solution of the problem in two fundamental cases when the plate is cut out by two symmetrically disposed hyperbolic notches. Neuber (5) also has discussed similar problems. Goland (6) has considered the effect of circular and elliptic inclusions on the bending of plates. Holgate (7) with the help of complex variables has solved the problem of a plate under transverse flexure with a cutout in the form of a square with rounded corners or a triangle with rounded corners.

Recently, Reissner (8, 9, 10) has extended and improved the classical (Poisson-Kirchhoff) theory. Reissner's theory takes into account the effect of shear deformation and transverse-normal stress, and contains the classical theory as the limiting case of vanishing plate thickness. This theory subsequently has been rederived from the general equations of elasticity by Green (11) who also has indicated a series method for the three-dimensional solution of flexure of plates (12). Using this theory, Reissner (9) has investigated the effect of a circular hole in an infinite plate under the state of both plain bending and pure twist. Stress-concentration factors are calculated and plotted versus ratio of hole diameter to plate thickness. The corresponding solution for the case of a rigid circular inclusion in an infinite plate subjected to plain bending has been given by Hirsch (13). Naghdi (14) has also applied Reissner's theory to the problems of the effects of an elliptic hole on both plain bending and pure twist of an elastic plate. In all of these investigations the plate is regarded as infinitely extended in two dimensions.

In a previous paper by the author (1), by use of the Poisson-Kirchhoff theory, a theoretical solution for an infinite strip with a circular hole under plain bending has been given. In the solution, the method of successive approximation is used which is analogous to that used by Howland (15, 16) for the two-dimensional elastic problems of such a strip. This method demands considerable labor in the numerical calculations. It seems, however, that the labor can be diminished by employing the method of perturbation.

In this paper the effect of a circular hole in an infinite strip under the state of pure twist is investigated with the help of the perturbation method. The solution of this problem seems also to be new.

Preliminary Results

We consider an infinitely long thin strip of isotropic, elastic material and take its middle plane, before twist occurs, as the x, y-plane. Let the strip be bounded in the plane by the lines $x = \pm b$. The hole will be supposed to have its center at the origin and to be of radius a. Polar co-ordinates (r, θ) also will be used which are defined by $re^{i\theta} = x + iy$ (Fig. 1).

We also will write

$$\xi = x/b, \eta = y/b, \rho = r/b, \lambda = a/b \quad [1]$$

---

[1] Assistant Professor of Mechanical Engineering, Tohoku University.

[2] Numbers in parentheses refer to the Bibliography at the end of the paper.

Contributed by the Applied Mechanics Division and presented at the Annual Meeting, New York, N. Y., November 25–30, 1956, of The American Society of Mechanical Engineers.

Discussion of this paper should be addressed to the Secretary, ASME, 29 West 39th Street, New York, N. Y., and will be accepted until April 10, 1957, for publication at a later date. Discussion received after the closing date will be returned.

Note: Statements and opinions advanced in papers are to be understood as individual expressions of their authors and not those of the Society. Manuscript received by ASME Applied Mechanics Division, May 31, 1956. Paper No. 56—A-17.

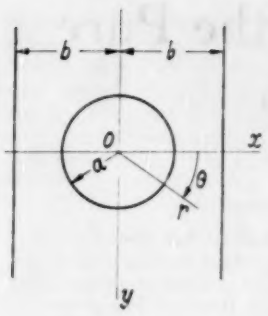

FIG. 1

so that ξ, η, ρ are co-ordinates measured in a unit equal to half the width of the strip and λ is the radius of the hole measured in the same unit. The strip will be considered subject to the limitations of the Poisson-Kirchhoff theory of thin plates. Accordingly, it is assumed that all lateral dimensions are large and all deflections small compared with the thickness of the strip. The differential equation for the transverse deflection w is then given by the theory as

$$D\nabla^4 w = p \quad \ldots\ldots [2]$$

where p is the pressure applied to the surface of the strip, and D is the flexural rigidity of the strip. The stresses are represented by their force and couple resultants. In Cartesian co-ordinates, they become

$$\left.\begin{aligned} M_x &= -D\left(\frac{\partial^2 w}{\partial x^2} + \nu\frac{\partial^2 w}{\partial y^2}\right), \qquad M_y = -D\left(\frac{\partial^2 w}{\partial y^2} + \nu\frac{\partial^2 w}{\partial x^2}\right) \\ M_{xy} &= -M_{yx} = D(1-\nu)\frac{\partial^2 w}{\partial x \partial y}, \quad Q_x = -D\frac{\partial}{\partial x}\nabla^2 w, \qquad Q_y = -D\frac{\partial}{\partial y}\nabla^2 w \end{aligned}\right\} \ldots [3]$$

where M_x and M_y are bending couples, M_{xy} and M_{yx} are torsional couples, and Q_x and Q_y are transverse shearing forces. Each is expressed per unit of arc length, and the x and y subscripts refer to action on the sections x = const and y = const, respectively; ν is Poisson's ratio of the plate material.

In the polar co-ordinates defined previously, Equations [3] are transformed into the following, for actions over the sections r = const

$$\left.\begin{aligned} M_r &= -D\left[\frac{\partial^2 w}{\partial r^2} + \nu\left(\frac{\partial w}{r\partial r} + \frac{\partial^2 w}{r^2\partial\theta^2}\right)\right] \\ M_{r\theta} &= D(1-\nu)\frac{\partial}{\partial r}\left(\frac{\partial w}{r\partial\theta}\right) \\ Q_r &= -D\frac{\partial}{\partial r}\nabla^2 w \end{aligned}\right\} \quad \ldots\ldots [4]$$

and for actions over the sections θ = const

$$\left.\begin{aligned} M_\theta &= -D\left[\frac{\partial w}{r\partial r} + \frac{\partial^2 w}{r^2\partial\theta^2} + \nu\frac{\partial^2 w}{\partial r^2}\right] \\ M_{\theta r} &= -M_{r\theta} \\ Q_\theta &= -D\frac{\partial}{r\partial\theta}\nabla^2 w \end{aligned}\right\} \quad \ldots\ldots [5]$$

With these notations, we shall seek the solution for the case where the strip is twisted, with Oy as the axis of twist, by torsional couples of a total amount $4H_y b$ at infinity. In this instance, since the middle plane of the strip is free from lateral loads, p is equal to zero; w is then a plane, single-valued, biharmonic function. Provided that the straight edges of the strip and the rim of the hole may both be stress-free, the boundary conditions of the present problem are expressed as follows

(a) $\eta \to \pm\infty$

$$\frac{\partial^2 \bar{w}}{\partial\xi\partial\eta} = 1, \quad \frac{\partial^2 \bar{w}}{\partial\xi^2} + \nu\frac{\partial^2 \bar{w}}{\partial\eta^2} = \frac{\partial^2 \bar{w}}{\partial\eta^2} + \nu\frac{\partial^2 \bar{w}}{\partial\xi^2} = 0$$

(b) $\xi = \pm 1$

$$\bar{M}_x = \frac{\partial^2 \bar{w}}{\partial\xi^2} + \nu\frac{\partial^2 \bar{w}}{\partial\eta^2} = 0, \quad \bar{V}_x = \frac{\partial^2 \bar{w}}{\partial\xi^2} + (2-\nu)\frac{\partial^2 \bar{w}}{\partial\xi\partial\eta^2} = 0$$

(c) $\rho = \lambda$

$$\bar{M}_r = \frac{\partial^2 \bar{w}}{\partial\rho^2} + \nu\left(\frac{\partial \bar{w}}{\rho\partial\rho} + \frac{\partial^2 \bar{w}}{\rho^2\partial\theta^2}\right) = 0$$

$$\bar{V}_r = \frac{\partial}{\rho\partial\rho}\left(\rho\frac{\partial^2 \bar{w}}{\partial\rho^2}\right) - \frac{\partial \bar{w}}{\rho^2\partial\rho} - \frac{\partial^2 \bar{w}}{\rho^2\partial\theta^2} + (2-\nu)\frac{\partial^2}{\rho\partial\rho\partial\theta}\left(\frac{\partial \bar{w}}{\rho\partial\theta}\right) = 0$$

where $\bar{w}$ is a dimensionless quantity related to the deflection w by the equation

$$\bar{w} = D(1-\nu)w/H_y b^2 \quad \ldots\ldots [6]$$

and in this instance, $\bar{w}$ must be a biharmonic function of ξ and η.

Deflection Function

Now the problem is reduced to the construction of a biharmonic function which satisfies all the boundary conditions (a), (b), and (c). As a first step in the solution, we shall introduce a fundamental biharmonic function $\bar{w}_0$ satisfying only the conditions (a) and (b). The term $\bar{w}_0$ corresponds to the deflection of an unperforated strip under the state of pure twist and can be written as

$$\bar{w}_0 = \xi\eta = \rho^2 \sin 2\theta/2 \quad \ldots\ldots [7]$$

To satisfy the condition (c) at the rim of the hole, we shall construct series of biharmonic functions, odd in both x and y, as required by symmetry, which do not disturb the boundary conditions on the straight edges nor at infinity. These functions are added to $\bar{w}_0$ and the boundary conditions at the rim of the hole are then satisfied by adjusting the parametric coefficients attached to the functions. The series of functions is derived by differentiation from the following two fundamental solutions for an unperforated strip having singularities at the center of the hole

$$\bar{w}_c = \frac{\cos\theta}{\rho} + \epsilon\int_0^\infty \frac{\cos u\eta}{\Delta'}\{(1 + 2u - \epsilon^{-1}e^{-2u})S - 2u\xi C\}\,du \quad \ldots [8]$$

$$\bar{w}_d = 2\rho\log\rho\cos\theta + \epsilon\int_0^\infty \left[\frac{\cos u\eta}{u^2\Delta'}\{(1 - \epsilon^{-2} - 4u^2)S - 2(1 - 2u + \epsilon^{-1}e^{-2u})u\xi C\} + \frac{\xi}{2\epsilon^2}\frac{e^{-u}}{n_z}\{(1+\epsilon) + (1-3\epsilon)u\}\right]du \quad \ldots [9]$$

where

$$S = \sinh u\xi, \quad C = \cosh u\xi, \quad \Delta' = \sinh 2u + 2\epsilon u, \quad \epsilon = (1-\nu)/(3+\nu)$$

The first terms in these expressions have singularities at the center of the hole, while the second terms are regular. The second terms are constructed so that they produce, on the straight edges of the strip, stress resultants canceling the values of $\bar{M}_x$ and $\bar{V}_x$ due to the first terms. It is also to be observed that differentiation with respect to η gives functions with the desired properties on the straight edges and at infinity, but even derivatives must be excluded since they are even in η and cannot enter into the antisymmetrical solution required. Since the use of any constant multiplier does not affect the desired properties, we may write the two sets of functions as follows: $n \geqslant 1$

$$\left.\begin{aligned} \bar{w}_{2n} &= (-1)^n \frac{1}{(2n-1)!} \frac{\partial^{2n-1}\bar{w}_c}{\partial \eta^{2n-1}} \\ \bar{w}_{2n+2}' &= (-1)^n \frac{1}{(2n)!}\left[\frac{\partial^{2n+1}\bar{w}_d}{\partial \eta^{2n+1}} - 2n\frac{\partial^{2n-1}\bar{w}_c}{\partial \eta^{2n-1}}\right] \end{aligned}\right\} \quad \ldots [10]$$

while

$$\bar{w}_2' = \frac{\partial \bar{w}_d}{\partial \eta}$$

To express the functions in terms of polar co-ordinates, the following formulas will be used

$$S \sin u\eta = \sum_{s=1}^{\infty} \frac{(u\rho)^{2s}}{(2s)!} \sin 2s\theta,$$

$$C \sin u\eta = \sum_{s=0}^{\infty} \frac{(u\rho)^{2s+1}}{(2s+1)!} \sin (2s+1)\theta \quad \ldots [11]$$

Hence we obtain

$$\left.\begin{aligned} \bar{w}_{2n} &= \rho^{-2n} \sin 2n\theta + \sum_{s=1}^{\infty} ({}^{2s}\kappa_{2n} + {}^{2s}\mu_{2n}\rho^2)\,\rho^{2s} \sin 2s\theta \\ \bar{w}_{2n}' &= \rho^{-(2n-2)} \sin 2n\theta + \sum_{s=1}^{\infty} ({}^{2s}\nu_{2n} + {}^{2s}\omega_{2n}\rho^2) \\ &\qquad \rho^{2s} \sin 2s\theta \end{aligned}\right\} \quad \ldots [12]$$

where

$$\left.\begin{aligned} {}^{s}\kappa_n &= -[(s-1)\epsilon I_{n+s-1}' - 2\epsilon I_{n+s}' \\ &\qquad + J_{n+s-1}']/(n-1)!\,s! \\ {}^{s}\mu_n &= -\epsilon I_{n+s+1}'/(n-1)!\,(s+1)! \\ {}^{s}\nu_n &= [\{(n-1)(s-1) + \epsilon^{-2}\}\,\epsilon I_{n+s-2}' - 2(n+s \\ &\qquad - 2)\,\epsilon I_{n+s-2}' + 4\epsilon I_{n+s-1}' + (n+s-2) \\ &\qquad J_{n+s-2}']/(n-2)!\,s! \\ {}^{s}\omega_n &= [(n-1)\epsilon I_{n+s-1}' - 2\epsilon I_{n+s}' + J_{n+s-1}']/ \\ &\qquad (n-2)!\,(s+1)! \end{aligned}\right\} \quad \ldots [13]$$

I_m' and J_m' being given by

$$I_m' = \int_0^{\infty} (u^m/\Delta')du, \quad J'_m = \int_0^{\infty} (u^m e^{-2u}/\Delta')du \quad \ldots [14]$$

Now, the required deflection function may be constructed in the form

$$\bar{w} = \bar{w}_0 + \sum_{n=1}^{\infty} (f_{2n}\bar{w}_{2n} + g_{2n}\bar{w}_{2n}') \quad \ldots [15]$$

where f_{2n} and g_{2n} are parametric coefficients to be determined from the boundary conditions at the rim of the hole. It is readily seen that the deflection function thus constructed gives a uniform twisting moment H_0 at infinity and zero values of $\bar{M}_x$ and $\bar{V}_x$ on the straight edges. Substituting Equations [12] into [15] and rearranging the terms, we have

$$\bar{w} = \sum_{n=1}^{\infty} [f_{2n}\rho^{-2n} + g_{2n}\rho^{-(2n-2)} + \{(\delta_{1,n}/2) + p_{2n}\}\,\rho^{2n} + q_{2n}\rho^{2n+2}] \sin 2n\theta \quad \ldots [16]$$

where

$$\left.\begin{aligned} p_{2n} &= \sum_{s=1}^{\infty} ({}^{2s}\kappa_{2n} f_{2s} + {}^{2s}\nu_{2n} g_{2s}) \\ q_{2n} &= \sum_{s=1}^{\infty} ({}^{2s}\mu_2 f_{2s} + {}^{2s}\omega_2 g_{2s}) \end{aligned}\right\} \quad \ldots [17]$$

$\delta_{1,n}$ being the Kronecker delta. The corresponding stress resultants $\bar{M}_r$ and $\bar{V}_r$ are

$$\begin{aligned} \bar{M}_r = \sum_{n=1}^{\infty} &[(1-\nu)2n(2n+1)f_{2n}\rho^{-(2n+2)} + (2n-1) \\ &\{(1-\nu)2n - 2(1+\nu)\}\,g_{2n}\rho^{-2n} + (1-\nu)2n(2n-1) \\ &\{(\delta_{1,n}/2) + p_{2n}\}\,\rho^{2n-2} + (2n+1)\{(1-\nu)2n \\ &+ 2(1+\nu)\}\,q_{2n}\rho^{2n}] \sin 2n\theta \end{aligned}$$

$$\begin{aligned} \bar{V}_r = \sum_{n=1}^{\infty} &2n[(1-\nu)2n(2n+1)f_{2n}\rho^{-(2n+1)} + (2n-1) \\ &\{(1-\nu)2n + 4\}\,g_{2n}\rho^{-(2n+1)} - (1-\nu)2n(2n-1) \\ &\{(\delta_{1,n}/2) + p_{2n}\}\,\rho^{2n-2} - (2n+1)\{(1-\nu)2n \\ &- 4\}\,q_{2n}\rho^{2n-1}] \sin 2n\theta \end{aligned}$$

The boundary conditions at the rim of the hole are thus satisfied if the coefficient of each term in the foregoing expressions vanishes identically when $\rho = \lambda$; that is

$$\left.\begin{aligned} &(1-\nu)2n(2n+1)f_{2n} + (2n-1)\{(1-\nu)2n \\ &\quad - 2(1+\nu)\}\lambda^2 g_{2n} + (1-\nu)2n(2n-1)\{(\delta_{1,n}/2) \\ &\quad + p_{2n}\}\lambda^{4n} + (2n+1)\{(1-\nu)2n + 2(1+\nu)\} \\ &\qquad q_{2n}\lambda^{4n+2} = 0 \\ &(1-\nu)2n(2n+1)f_{2n} + (2n-1)\{(1-\nu)2n + 4\} \\ &\quad \lambda^2 g_{2n} - (1-\nu)2n(2n-1)\{(\delta_{1,n}/2) + p_{2n}\}\lambda^{4n} \\ &\quad - (2n+1)\{(1-\nu)2n - 4\}q_{2n}\lambda^{4n+2} = 0 \end{aligned}\right\} (n \geqslant 1)$$

which may now be solved for f_{2n} and g_{2n} in the form

$$\left.\begin{aligned} f_{2n} &= -(2n-1)\epsilon\lambda^{4n}\{(\delta_{1,n}/2) + p_{2n}\} - [\{2n \\ &\qquad - (2n)^{-1}\}\epsilon + (2n\epsilon)^{-1}]\lambda^{4n+2}q_{2n} \\ g_{2n} &= 2n\epsilon\lambda^{4n-2}\{(\delta_{1,n}/2) + p_{2n}\} + (2n+1)\epsilon\lambda^{4n}q_{2n} \end{aligned}\right\} (n \geqslant 1)$$

$$\ldots [18]$$

The set of Equations [17] and [18] solves completely the problem of determining the parametric coefficients included in the deflection function $\bar{w}$.

Determination of Coefficients f_{2n} and g_{2n}

To solve the infinite set of Equations [17] and [18], the method of perturbation will now be used in which λ and ϵ are the perturbation parameters. As a first step in the solution, the integrals I_m' and J_m' are to be expanded into power series in ϵ. Since $\Delta' = \sinh 2u + 2\epsilon u$ and $\epsilon < 1$ for $0 \leqslant \nu \leqslant 0.5$

$$I_m' = \int_0^\infty \frac{u^m}{\Delta'}\,du = \int_0^\infty \frac{u^m}{\sinh 2u}\left(1+\epsilon\frac{2u}{\sinh 2u}\right)^{-1}du$$

$$= \frac{1}{2^{m+1}}\sum_{s=0}^{\infty}(-1)^s\epsilon^s\int_0^\infty \frac{x^{m+s}}{(\sinh x)^{s+1}}\,dx$$

Therefore we obtain $$I_m' = \sum_{s=0}^{\infty}(-1)^s i_{m,s}\epsilon^s \quad \ldots\ldots [19]$$

where

$$i_{m,s} = \int_0^\infty x^{m+s}(\sinh x)^{-(s+1)}dx/2^{m+1}$$

For $s = 0$ and $s = 1$, we have

$$i_{m,0} = \frac{m!}{2^m}\left(1-\frac{1}{2^{m+1}}\right)S_{m+1}, \quad i_{m,1} = \frac{(m+1)!}{2^{2m+1}}S_{m+1} \quad [20]$$

where

$$S_m = \sum_{n=1}^{\infty} n^{-m}$$

For $s \geqslant 2$, the following recurrence formula is obtained

$$i_{m,s} = \frac{(m+s)(m+s-1)}{s(s-1)}\,i_{m,s-2} - \frac{4(s-1)}{s}\,i_{m+2,s-2} \quad [21]$$

In a similar way, it can be proved that

$$J_m' = \sum_{s=0}^{\infty}(-1)^s j_{m,s}\epsilon^s \quad \ldots\ldots [22]$$

where

$$\left.\begin{aligned} j_{m,0} &= \frac{m!}{2^{2m+1}}S_{m+1},\\ j_{m,1} &= \frac{(m+1)!}{2^m}\left[S_{m+1} - S_{m+2} - \frac{1}{2^{m+1}}\left(S_{m+1} - \frac{1}{2}S_{m+2}\right)\right],\\ j_{m,s} &= \frac{(m+s)(m+s-1)}{s(s-1)}\,j_{m,s-2} - \frac{4(m+s)}{s(s-1)}\,j_{m+1,s-2} - \frac{4(s-2)}{s-1}\,j_{m+2,s-2} \end{aligned}\right\} \quad [23]$$

the last equation applying only for $s \geqslant 2$.

Substitution into Equations [13] now gives

$$\left.\begin{aligned} {}^{2s}K_{2n} &= \sum_{p=0}^{\infty}{}^{2s}K_{2n}^{(p)}\epsilon^p, \quad {}^{2s}\mu_{2n} = \sum_{p=1}^{\infty}{}^{2s}\mu_{2n}^{(p)}\epsilon^p\\ {}^{2s}\nu_{2n} &= \sum_{p=-1}^{\infty}{}^{2s}\nu_{2n}^{(p)}\epsilon^p, \quad {}^{2s}\omega_{2n} = \sum_{p=0}^{\infty}{}^{2s}\omega_{2n}^{(p)}\epsilon^p \end{aligned}\right\} \quad [24]$$

where

$$\left.\begin{aligned} {}^{s}K_n^{(p)} &= (-1)^p[(s-1)i_{n+s-1,p-1} - 2i_{n+s,p-1} - j_{n+s-1,p}]/(n-1)!\,s!\\ {}^{s}\mu_n^{(p)} &= (-1)^p i_{n+s+1,p-1}/(n-1)!\,(s+1)!\\ {}^{s}\nu_n^{(p)} &= (-1)^{p-1}[(n-1)(s-1)i_{n+s-2,p-1} + i_{n+s-3,p+1} - 2(n+s-2)i_{n+s-2,p-1} + 4i_{n+s-1,p-1} - (n+s-2)j_{n+s-3,p}]/(n-2)!\,s!\\ {}^{s}\omega_n^{(p)} &= (-1)^{p-1}[(n-1)i_{n+s-1,p-1} - 2i_{n+s,p-1} - j_{n+s-1,p}]/(n-2)!\,(s+1)! \end{aligned}\right\} \quad [25]$$

except for $p = 0$ and $p = -1$, when

$$\left.\begin{aligned} {}^{s}K_n^{(0)} &= -j_{n+s-1,0}/(n-1)!\,s!, \quad {}^{s}\nu_n^{(-1)} = i_{n+s-2,0}/(n-2)!\,s!\\ {}^{s}\nu_n^{(0)} &= 0, \quad {}^{s}\omega_n^{(0)} = j_{n+s-1,0}/(n-2)!\,(s+1)! \end{aligned}\right\} \quad [26]$$

We then seek a solution to Equations [17] and [18] in the form

$$\left.\begin{aligned} f_{2n} &= \sum_{r=0}^{\infty}\sum_{p=0}^{\infty}{}^{(p)}f_{2n}^{(r)}\lambda^{4n+2r}\epsilon^p, \quad p_{2n} = \sum_{r=1}^{\infty}\sum_{p=0}^{\infty}{}^{(p)}p_{2n}^{(r)}\lambda^{2r}\epsilon^p\\ g_{2n} &= \sum_{r=0}^{\infty}\sum_{p=1}^{\infty}{}^{(p)}g_{2n}^{(r)}\lambda^{4n+2r-2}\epsilon^p, \quad q_{2n} = \sum_{r=1}^{\infty}\sum_{p=1}^{\infty}{}^{(p)}q_{2n}^{(r)}\lambda^{2r}\epsilon^p \end{aligned}\right\} \quad [27]$$

where

$${}^{(p)}f_{2n}^{(r)},\ {}^{(p)}g_{2n}^{(r)},\ {}^{(p)}p_{2n}^{(r)},\ {}^{(p)}q_{2n}^{(r)}$$

are independent of λ and ϵ, and in particular

$$\left.\begin{aligned} {}^{(1)}f_2^{(0)} &= -1/2, \quad {}^{(1)}g_2^{(0)} = 1, \quad {}^{(p)}f_{2n}^{(0)} = {}^{(p)}g_{2n}^{(0)} = 0 \quad (n \geqslant 2)\\ {}^{(0)}f_2^{(0)} &= {}^{(p)}f_2^{(0)} = {}^{(p)}g_2^{(0)} = 0 \quad (p \geqslant 2) \end{aligned}\right\} \quad [28]$$

We now substitute Equations [24], [27], [28] into Equations [17] and [18], and then equate the coefficients of the same powers of λ and ϵ on both sides which result. This leads to the equations

$${}^{(p)}p_{2n}^{(1)} = {}^{2n}\nu_2^{(p-1)}, \quad {}^{(p)}q_{2n}^{(1)} = {}^{2n}\omega_2^{(p-1)} \quad \ldots\ldots [29]$$

$${}^{(p)}f_{2n}^{(1)} = -(2n-1)^{(p-1)}p_{2n}^{(1)}, \quad {}^{(p)}g_{2n}^{(1)} = 2n^{(p-1)}p_{2n}^{(1)} \quad \ldots\ldots [30]$$

$$\left.\begin{aligned} {}^{(p)}p_{2n}^{(r)} &= \sum_{u=0}^{p}\sum_{s=1}^{t}\left({}^{2n}K_{2s}^{(u)(p-u)}f_{2s}^{(r-2s)} + {}^{2n}\nu_{2s}^{(u-1)(p-u+1)}g_{2s}^{(r-2s+1)}\right)\\ {}^{(p)}q_{2n}^{(r)} &= \sum_{u=1}^{p}\sum_{s=1}^{t}\left({}^{2n}\mu_{2s}^{(u)(p-u)}f_{2s}^{(r-2s)} + {}^{2n}\omega_{2s}^{(u-1)(p-u+1)}g_{2s}^{(r-s2+1)}\right) \end{aligned}\right\} \quad (r \geqslant 2) \quad [31]$$

$$\left.\begin{aligned} {}^{(p)}f_{2n}^{(r)} &= -(2n-1)^{(p-1)}p_{2n}^{(r)} - \{2n - (2n)^{-1}\}^{(p-1)}q_{2n}^{(r-1)} - (2n)^{-1(p+1)}q_{2n}^{(r-1)}\\ {}^{(p)}g_{2n}^{(r)} &= 2n^{(p-1)}p_{2n}^{(r)} + (2n+1)^{(p-1)}q_{2n}^{(r-1)} \end{aligned}\right\} \quad (r \geqslant 2) \quad [32]$$

where the upper limit t of the summation in Equations [31] takes the value $(r-1)/2$ when r is an odd integer and $r/2$ when r is an even integer.

The procedure for the determination of the coefficients f_{2n}, g_{2n}, p_{2n}, and q_{2n} is then the following: We first determine ${}^{(p)}p_{2n}^{(1)}$ and ${}^{(p)}q_{2n}^{(1)}$ from Equations [29]. By using these values, ${}^{(p)}f_{2n}^{(1)}$ and ${}^{(p)}g_{2n}^{(1)}$ are computed from Equations [30]. Similar operations are carried out successively by the repeated applications of Equations [31] and Equations [32] for $r = 2, 3, \ldots\ldots$ It may be noted that the foregoing solution is valid in so far as the Series [27] is convergent. The proof of convergence seems rather difficult to achieve, although it seems unlikely from the physical considerations that there will be divergence when $\lambda < 1$ and $0 \leqslant \nu \leqslant 1/2$.

Numerical Examples

The foregoing solution will be worked out in some detail. In the calculation of $i_{m,s}$ and $j_{m,s}$, the values of S_m found by Stieltjes (17) are used. The calculation of ${}^{(p)}f_{2n}{}^{(r)}$, ${}^{(p)}g_{2n}{}^{(r)}$, ... is carried out until $p = 6$ and $r = 7$, but their values are not shown here for brevity.

It is now rather straightforward to compute the deflection and stress resultants at any point in the strip. It can be shown readily that the distribution of the deflection along the rim of the hole is given by

$$[w]_\lambda = \frac{6H_0a^2}{Eh^2}\left[2(1-\epsilon)\sin 2\theta + \sum_{n=1}^{\infty}\sum_{r=1}^{\infty}\sum_{p=0}^{\infty}\overline{W}_{n,r,p}\lambda^{2n+2r-2}\epsilon^p \sin 2n\theta\right] \quad [33]$$

where

$$\overline{W}_{n,r,p} = \sum_{s=0}^{p}(-1)^{p-s}(8-4\delta_{p,s}){}^{(s)}f_{2n}{}^{(r)} + {}^{(s)}g_{2n}{}^{(r)} + {}^{(s)}p_{2n}{}^{(r)} + {}^{(s)}q_{2n}{}^{(r-1)} \quad [34]$$

a and h being the radius of the hole and the thickness of the strip, respectively. From this, $[w]_\lambda$ in the case of infinite plate ($\lambda \to 0$) is easily found to be

$$[w]_{\lambda\to 0} = (12H_0a^2/Eh^3)(1-\epsilon)\sin 2\theta \quad [35]$$

which is the same as that obtained by Goodier (3). The maximum deflection on the rim of the hole occurs at the point $\theta = 45$ deg in the case of an infinite plate, while in the strip it occurs at θ less than 45 deg. But the amount of this shift is rather small. For instance, when $\nu = 0.3$ and $\lambda = 0.5$, the peak deflection on the hole rim occurs at $\theta = 44.8$ deg, the difference being only 0.2 deg. Thus the maximum deflection on the rim of the hole occurs practically at $\theta = 45$ deg, unless the diameter of the hole is considerable. From Equation [33], the deflection at the point ($\rho = \lambda$, $\theta = 45$ deg) is to be expressed as follows

$$[w]_{\lambda,45^\circ} = (6H_0a^2/Eh^3)\left[2(1-\epsilon) + \sum_{r=1}^{\infty}\sum_{p=0}^{\infty}\overline{W}_{r,p}\lambda^{2r}\epsilon^p\right] \quad [36]$$

where

$$\overline{W}_{r,p} = \sum_{s=0}^{t}(-1)^s\overline{W}_{2s+1,\,r-2s,\,p} \quad [37]$$

The upper limit t of the summation now takes the value $(r-1)/2$ when r is an odd integer and $(r-2)/2$ when r is an even integer. Fig. 2 shows the results graphically, from which it is readily seen that the effect of the Poisson's ratio on the values of $[w]_{\lambda,45^\circ}$ in the case of strip is almost the same as in the case of an infinite plate.

Next, we investigate the distributions of stress resultants in the strip. The most important is the bending couple along the rim of the hole; i.e., $[M_\theta]_\lambda$. Since $M_r = 0$ on the same rim, $[M_\theta]_\lambda$ is given by

$$[M_\theta]_\lambda = [M_\theta + M_r]_{r=a} = -D(1+\nu)[\nabla^2 w]_{r=a}$$
$$= 2H_0(\epsilon^{-1}-1)\sum_{n=1}^{\infty}[(2n-1)g_{2n}\lambda^{-2n} - (2n+1)q_{2n}\lambda^{2n}]\sin 2n\theta \quad [38]$$

Substituting for g_{2n}, q_{2n} the expressions given in Equations [27], we have

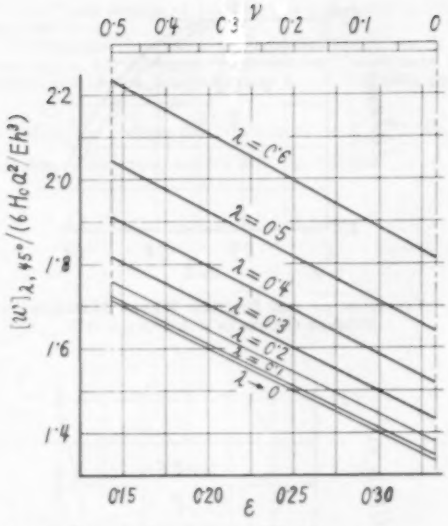

Fig. 2 Deflection at $r = a$, $\theta = 45$ Deg, Versus ϵ

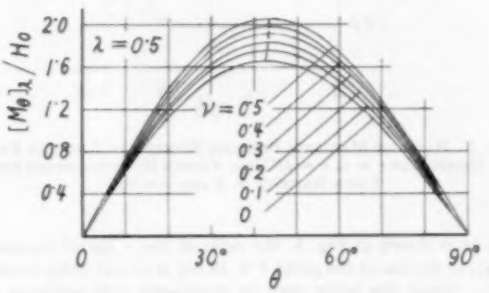

Fig. 3 Distribution of Angular Bending Moment Around the Hole ($a/b = 0.5$)

$$[M_\theta]_\lambda = H_0\left[2(1-\epsilon)\sin 2\theta + \sum_{n=1}^{\infty}\sum_{r=1}^{\infty}\sum_{p=0}^{\infty}M_{n,r,p}\lambda^{2n+2r-2}\epsilon^p \sin 2n\theta\right] \quad [39]$$

where

$$M_{n,r,p} = 2(2n-1)[{}^{(p+1)}g_{2n}{}^{(r)} - {}^{(p)}g_{2n}{}^{(r)}] - 2(2n+1)[{}^{(p+1)}q_{2n}{}^{(r-1)} - {}^{(p)}q_{2n}{}^{(r-1)}] \quad [40]$$

In the limiting case of $\lambda \to 0$, we obtain

$$[M_\theta]_{\lambda\to 0} = 2H_0(1-\epsilon)\sin 2\theta \quad [41]$$

which coincides with the value obtained by Goodier (3) and has the maximum value at the point $\theta = 45$ deg. The distribution of $[M_\theta]_\lambda$ is calculated for the case $\lambda = 0.5$ and shown in Fig. 3. In this case the maximum values of $[M_\theta]_\lambda$ occur at θ less than 45 deg. This shift becomes greater when ν becomes smaller. The variation of the position where the maximum $[M_\theta]_\lambda$ occurs is also plotted versus λ for the two limiting cases of $\nu = 0$ and $\nu = 0.5$ (Fig. 4). It can be seen that the change of the position under discussion becomes greater when λ becomes greater and ν smaller.

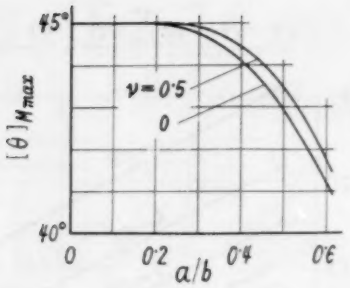

FIG. 4 VARIATION OF THE POSITION WHERE MAXIMUM BENDING MOMENT OCCURS ($\rho = 0$ AND $\nu = 0.5$)

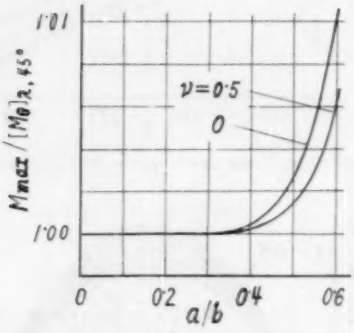

FIG. 5 RATIO OF MAXIMUM BENDING MOMENT TO ANGULAR BENDING MOMENT AT $r = a$, $\theta = 45$ DEG, VERSUS HOLE-DIAMETER STRIP-WIDTH RATIO ($\rho = 0$ AND $\nu = 0.5$)

But as is shown in Fig. 5, the ratio of the value of maximum $[M_\theta]_\lambda$ to the one at the point $\theta = 45$ deg is almost unity in every case. Hence the latter may be considered with sufficient approximation as the maximum. The value of M_θ at the point ($\rho = \lambda$, $\theta = 45$ deg) can be written from Equation [39] as follows

$$[M_\theta]_{\lambda,45°} = H_0 \left[2(1-\epsilon) + \sum_{r=1}^{\infty} \sum_{p=0}^{\infty} M_{r,p} \lambda^{2r} \epsilon^{2p} \right] \ldots [42]$$

where

$$M_{r,p} = \sum_{s=0}^{t} (-1)^s M_{2r+1,r-2s,p},$$

$$t = \begin{cases} (r-1)/2, \text{ if } r \text{ is an odd integer} \\ (r-2)/2, \text{ if } r \text{ is an even integer} \end{cases} \ldots\ldots [43]$$

Fig. 6 shows the results graphically. The maximum value of M_θ increases rapidly when λ increases, and for the same value of λ it becomes greater when ν becomes greater.

As the convergence of the Series [42] cannot be proved, we shall check the validity of [42] by comparing it with the results obtained by the successive-approximation method. The latter results are considered as correct to four decimal places, while they are obtained only for $\nu = 0.3$. The comparison is made in Table 1. It is clear that, within the limitation of four-figure

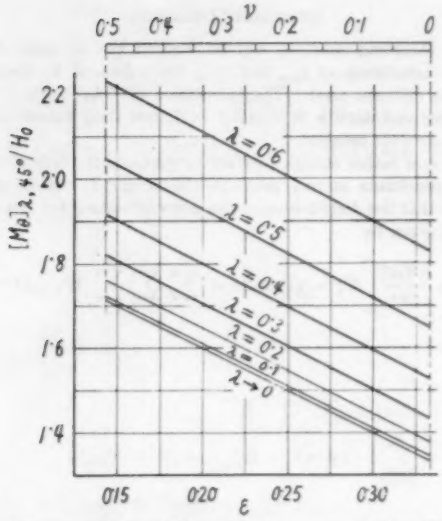

FIG. 6 ANGULAR BENDING MOMENT AT $r = a$, $\theta = 45$ DEG, VERSUS ϵ

tabulation, both results just coincide. But the result may be less reliable for $\nu \sim 0$, since then the terms of higher powers of ϵ are to be taken into account.

ACKNOWLEDGMENT

The author wishes to express his hearty thanks to Seiichi Higuchi, professor emeritus of Tohoku University, for his encouragement throughout the progress of the present investigation.

BIBLIOGRAPHY

1 "The Influence of a Circular Hole on the Transverse Flexure of Infinite Strip," by O. Tamate, Transactions of the Japan Society of Mechanical Engineers, vol. 20, 1954, pp. 687–692 (in Japanese with English summary).

2 "Theory of Plates and Shells," by S. Timoshenko, McGraw-Hill Book Company, Inc., New York, N. Y., 1940, Chapter 4.

3 "The Influence of Circular and Elliptical Holes on the Transverse Flexure of Elastic Plates," by J. N. Goodier, *Philosophical Magazine*, series 7, vol. 22, 1936, pp. 68–80.

4 "The Influence of Hyperbolic Notches on the Transverse Flexure of Elastic Plates," by G. H. Lee, JOURNAL OF APPLIED MECHANICS, Trans. ASME, vol. 62, 1940. p. A-53.

5 "Über das Kerbproblem in der Plattentheorie," by H. Neuber, *Zeitschrift für angewandte Mathematik und Mechanik*, vol. 20, 1940, pp. 199–209.

6 "The Influence of Shape and Rigidity of an Elastic Inclusion on the Transverse Flexure of Thin Plates," by M. Goland, JOURNAL OF APPLIED MECHANICS, Trans. ASME, vol. 65, 1943, p. A-69.

7 "The Transverse Flexure of Perforated Isotropic Plates," by S. Holgate, Proceedings of the Royal Society of London, England, series A, vol. 185, 1946, pp. 35–49.

8 "On the Theory of Bending of Elastic Plates," by E. Reissner, *Journal of Mathematics and Physics*, vol. 23, 1944, pp. 184–191.

9 "The Effect of Transverse Shear Deformation on the Bending of Elastic Plates," by E. Reissner, JOURNAL OF APPLIED MECHANICS, Trans. ASME, vol. 67, 1945, p. A-69.

10 "On the Bending of Elastic Plates," by E. Reissner, *Quarterly of Applied Mathematics*, vol. 5, 1947, pp. 55–68.

11 "On Reissner's Theory of Bending of Elastic Plates," by A. E. Green, *Quarterly of Applied Mathematics*, vol. 7, 1949, pp. 223–228.

12 "The Elastic Equilibrium of Isotropic Plates and Cylinders," by A. E. Green, Proceedings of the Royal Society of London, England, series A, vol. 195, 1949, pp. 533–552.

TABLE 1 $[M_\theta]_{\lambda,45°}$: $\nu = 0.3$

λ	0.1	0.2	0.3	0.4	0.5	0.6
By successive approx.	1.5866	1.6203	1.6800	1.7715	1.9027	2.0857
By Equation [42]	1.5866	1.6203	1.6801	1.7715	1.9028	2.0857

13 "The Effect of a Rigid Circular Inclusion on the Bending of a Thick Elastic Plate," by R. A. Hirsch, JOURNAL OF APPLIED MECHANICS, Trans. ASME, vol. 74, 1952, pp. 28–32.

14 "The Effect of Elliptic Holes on the Bending of Thick Plates," by P. M. Naghdi, JOURNAL OF APPLIED MECHANICS, Trans. ASME, vol. 77, 1955, pp. 89–94.

15 "On the Stresses in the Neighbourhood of a Circular Hole in a Strip Under Tension," by R. C. J. Howland, Philosophical Transactions of the Royal Society of London, England, series A, vol. 229, 1930, pp. 49–86.

16 "Bi-Harmonic Analysis in a Perforated Strip," by R. C. J. Howland and A. C. Stevenson, Philosophical Transactions of the Royal Society of London, England, series A, vol. 232, 1933, pp. 155–222.

17 "Tables des Valeurs des Sommes $S_k = \sum_{1}^{\infty} n^{-k}$," by T. J. Stieltjes, *Acta Mathematica*, vol. 10, 1887, pp. 299–302.

A Mixed Boundary-Value Problem of Elasticity With Parabolic Boundary

By GUNADHAR PARIA,[1] KHARAGPUR, INDIA

The problem of finding the stress distribution in a two-dimensional elastic body with parabolic boundary, subject to mixed boundary conditions, has been reduced to the solution of the nonhomogeneous Hilbert problem following the method of complex variable. The result has been compared with that for a straight boundary.

1 Introduction

THE plain strain distribution in an elastic body having the parabolic boundary has been found by the methods of complex variable and Fourier transforms when either the stresses or the displacements are prescribed on the boundary.[2-6] In the present paper the method of complex variable has been adopted to determine the stresses and displacements due to pressure of a rigid stamp, it being assumed that the friction at the common surface is sufficient to prevent any sliding. By conformal representation, the parabolic boundary is transformed to the straight boundary extending to infinity in both directions. The procedure leads to the solution of the nonhomogeneous Hilbert problem for holomorphic functions.

2 Formulation of Problem

Let L denote the parabolic boundary and s the region lying outside the parabola (i.e., not on the side of the focus). The elastic body occupies the region s. In the transformation

$$z = w(\zeta) = i(\zeta - ia)^2, \quad (a > 0)$$

$$z = x + iy, \quad \zeta = \xi + i\eta \qquad [1]$$

the real axis $\eta = 0$ in the ζ-plane corresponds in the z-plane to the parabola L given by

$$x^2 = 4a^2(y + a^2)$$

The curve corresponding to $\xi = \text{const} = l$ is a confocal parabola oriented in the opposite direction. Thus the region s is transformed into the lower half plane $\eta < 0$, which will be denoted by s^-, the upper half plane $\eta > 0$ being denoted by s^+. The superscripts + and — with the functions will indicate that they are defined in the regions s^+ and s^-, respectively. The part L' of the boundary L cut off by the confocal parabola $\xi = l$ will have the prescribed displacements

$$v_\xi = 0, \quad v_\eta = \text{const} = k \qquad [2]$$

where (v_ξ, v_η) are the displacements in the (ξ, η) co-ordinates. The remaining part of L is assumed to be stress free. Thus L' is placed symmetrically with respect to the vertex of L. (The method employed will however be independent of the position of L' on L.)

By using Equation [1], the stress components σ_ξ, $\tau_{\xi\eta}$, σ_η in (ξ, η) co-ordinates can be expressed as[2]

$$\left.\begin{aligned} \sigma_\xi + \sigma_\eta &= 2[\Phi(\zeta) + \overline{\Phi(\zeta)}] \\ \sigma_\eta - \sigma_\xi + 2i\tau_{\xi\eta} &= (\bar{\zeta} + ia)^{-1}\{(\bar{\zeta} + ia)^2 \Phi'(\zeta) \\ &\qquad - 2(\zeta - ia)\Psi(\zeta)\} \end{aligned}\right\} \qquad [3]$$

from which

$$(\zeta - ia)(\sigma_\eta - i\tau_{\xi\eta}) = (\zeta - ia)\{\Phi(\zeta) + \overline{\Phi(\zeta)}\} + \frac{1}{2}(\zeta - ia)^2 \overline{\Phi'(\zeta)} - (\bar{\zeta} + ia)\overline{\Psi(\zeta)} \qquad [4]$$

The displacement components (u, v) in Cartesian co-ordinates can be expressed as

$$2\mu(u' + iv') = 2i\nu(\zeta - ia)\Phi(\zeta) - i(\zeta - ia)\{2\overline{\Phi(\zeta)} + (\zeta - ia)\overline{\Phi'(\zeta)}\} + 2i(\bar{\zeta} + ia)\overline{\Psi(\zeta)} \qquad [5]$$

where

$$u' = \frac{\partial u}{\partial \xi} \quad v' = \frac{\partial v}{\partial \xi} \qquad [6]$$

(μ, ν) being constants characterizing the elastic property of the material.

Let

$$\Omega(\zeta) = -(\zeta + ia)\Phi(\zeta) - \frac{1}{2}(\zeta + ia)^2 \Phi'(\zeta) + (\bar{\zeta} - ia)\Psi(\zeta) \text{ for } \zeta \text{ in } s^- \qquad [7]$$

The function $(\zeta - ia)\Omega_*(\zeta)$ for ζ in s^+ is defined in such a way that

$$(\zeta - ia)\Omega_*(\zeta) = \overline{\Omega(\bar{\zeta})} = -(\zeta - ia)\overline{\Phi(\bar{\zeta})} - \frac{1}{2}(\zeta - ia)^2 \overline{\Phi'(\bar{\zeta})} + (\bar{\zeta} + ia)\overline{\Psi(\bar{\zeta})} \text{ for } \zeta \text{ in } s^+ \qquad [8]$$

Thus, from Equations [4] and [8] it is seen that $\overline{\Omega(\bar{\zeta})}$ is the analytic continuation of $\Omega(\zeta)$ through the unloaded part of the

---

[1] Indian Institute of Technology.

[2] "Some Basic Problems of the Mathematical Theory of Elasticity," by N. I. Muskhelishvili, P. Noordhoff Ltd., Groningen, Holland, 1953, §§ 95, 92, 114, 110.

[3] By R. Tiffen, *Quarterly Journal of Mechanics and Applied Mathematics*, vol. 5, 1952, p. 3.

[4] By K. L. Conrad, *Iowa State College Journal of Science*, vol. 23, no. 4, 1949, pp. 397–404.

[5] By G. Paria, (*a*) Bulletin Calcutta Mathematical Society, vol. 44, 1952, p. 4; (*b*) ibid., under publication.

Contributed by the Applied Mechanics Division and presented at the Annual Meeting, New York, N. Y., November 25–30, 1956, of The American Society of Mechanical Engineers.

Discussion of this paper should be addressed to the Secretary, ASME, 29 West 39th Street, New York, N. Y., and will be accepted until April 10, 1957, for publication at a later date. Discussion received after the closing date will be returned.

Note: Statements and opinions advanced in papers are to be understood as individual expressions of their authors and not those of the Society. Manuscript received by ASME Applied Mechanics Division, June 12, 1956. Paper No. 56—A-24.

boundary. A new function $\chi(\zeta)$ will now be defined for the whole plane as

$$\left.\begin{aligned}\chi(\zeta) &= (\zeta - ia)\,\Phi(\zeta) \quad \text{for} \quad \zeta \text{ in } s^-\\ &= (\zeta - ia)\,\Omega_*(\zeta) \quad \text{for} \quad \zeta \text{ in } s^+\end{aligned}\right\} \ldots\ldots [9]$$

The Relations [4] and [5] can be expressed in terms of the function $\chi(\zeta)$ with the help of Relations [7], [8], and [9]

$$\begin{aligned}(\zeta - ia)\,(\sigma_\eta - i\tau_{\xi\eta}) &= \chi(\zeta) - \{(\bar\zeta + ia)/(\zeta + ia)\}\,\chi(\bar\zeta)\\ &+ \frac{1}{2}\,\overline{\chi(\zeta)}\,\{2(\zeta - ia)/(\bar\zeta + ia) - (\zeta - ia)^2/(\bar\zeta + ia)^2\\ &-2(\bar\zeta - ia)/(\zeta + ia) + (\bar\zeta - ia)^2/(\bar\zeta + ia)\,(\zeta + ia)\}\\ &+ \frac{1}{2}\,\overline{\chi'(\zeta)}\,\{(\zeta - ia)^2/(\bar\zeta + ia) - (\bar\zeta - ia)^2/(\zeta + ia)\} \ldots [10]\end{aligned}$$

$$\begin{aligned}\mu(u' + iv') &= i\nu\chi(\zeta) + i\{(\bar\zeta + ia)/(\zeta + ia)\}\,\chi(\bar\zeta)\\ &- \frac{1}{2}\,i\,\overline{\chi(\zeta)}\,\{2(\zeta - ia)/(\bar\zeta + ia) - (\zeta - ia)^2/(\bar\zeta + ia)^2\\ &- 2(\bar\zeta - ia)/(\zeta + ia) + (\bar\zeta - ia)^2/(\bar\zeta + ia)\,(\zeta + ia)\}\\ &- \frac{1}{2}\,i\,\overline{\chi'(\zeta)}\,\{(\zeta - ia)^2/(\bar\zeta + ia) - (\bar\zeta - ia)^2/(\zeta + ia)\} \ldots [11]\end{aligned}$$

If t is a point on L, the boundary conditions can be written from Equations [10] and [11] as

$$\left.\begin{aligned}&\chi^+(t) - \chi^-(t) = 0 \quad \text{for} \quad t \text{ outside } L'\\ &\chi^+(t) + \nu\chi^-(t) = 2\mu\, g'(t) \quad \text{for} \quad t \text{ within } L'\end{aligned}\right\} \ldots [12]$$

where

$$2ig'(t) = u'^-(t) + iv'^-(t) \ldots\ldots [13]$$

Assuming that

$$u'^-(t) = \{u^-(t)\}', \quad v'^-(t) = \{v^-(t)\}'$$

i.e., the boundary values of the partial derivatives (u', v') are equal to the derivatives of the boundary values of (u, v), one finds from Equation [2], using the relation

$$|\omega'(\zeta)|\,(v_\xi + iv_\eta) = \overline{\omega'(\zeta)}\,(u + iv) \ldots\ldots [14]$$

that

$$2g'(t) = ik\left\{(t^2 + a^2)^{-\frac{1}{2}} - t(t - ia)\,(t^2 + a^2)^{-\frac{3}{2}}\right\}. [15]$$

The first of Relations [12] shows that $\chi(\zeta)$, defined in s^+ and s^-, is continuous across L, except in the part L' where the discontinuity is expressed by the second relation. Thus one arrives at the nonhomogeneous Hilbert problem of determining a holomorphic function $\chi(\zeta)$ with the line of discontinuity L'.

3 Solution of the Problem

The fundamental solution $\chi_0(\zeta)$ corresponding to the second of Boundary Condition [12] is given by[3]

$$\chi_0(\zeta) = (\zeta + l)^{-\frac{1}{2} + i\beta}\,(\zeta - l)^{-\frac{1}{2} - i\beta} \ldots\ldots [16]$$

where

$$2\pi\beta = \log_e \nu \ldots\ldots [17]$$

and the branch of $\chi_0(\zeta)$ has been chosen properly and

$$\chi_0^+(t) = (t + l)^{-\frac{1}{2} + i\beta}\,(t - l)^{-\frac{1}{2} - i\beta} \ldots\ldots [18]$$

$$\chi_0^-(t) = -\frac{1}{\nu}\,\chi_0^+(t) \ldots\ldots [19]$$

The complete solution $\chi(\zeta)$ is given by

$$\chi(\zeta) = C_0\chi_0(\zeta) + \frac{\mu\chi_0(\zeta)}{\pi i}\int_{L'}\frac{g'(t)\,dt}{\chi_0^+(t)\,(t - \zeta)} \ldots\ldots [20]$$

where C_0 is, in general, a complex constant to be determined later. After evaluation of the integral in Equation [20] by a special method given elsewhere,[3] one obtains

$$\chi(\zeta) = \frac{2\mu}{1 + \nu}\,g'(\zeta) + C_0\,\chi_0(\zeta) \ldots\ldots [21]$$

Thus $\chi(\zeta)$ being known, the stresses and displacements can be found from Equations [10] and [11]. On the boundary L' the stress components are given by

$$\begin{aligned}(t - ia)\,\{\sigma_\eta^-(t) - i\,\tau_{\xi\eta}^-(t)\} &= \chi^-(t) - \chi^+(t)\\ &= -\left(1 + \frac{1}{\nu}\right)C_0\,\chi_0^+(t) \ldots\ldots [22]\end{aligned}$$

If P_0 be the total pressure on L'

$$\begin{aligned}-P_0 &= \int_{L'}\{\sigma_\eta^-(t) - i\tau_{\xi\eta}^-(t)\}\,dt\\ &= -\left(1 + \frac{1}{\nu}\right)C_0\int_{L'}\frac{\chi_0^+(t)\,dt}{t - ia} \ldots\ldots [23]\end{aligned}$$

the total shearing force being zero.

Evaluating the integral in Equation [23] by the method already referred to, one obtains

$$C_0 = \frac{P_0}{2\pi}\,\{(l^2 + a^2)/\nu\}^{\frac{1}{2}}\,e^{2\beta\tan^{-1}\frac{a}{l}} \ldots\ldots [24]$$

Elimination of C_0 between Equations [22] and [24] gives

$$\left.\begin{aligned}P(t) &= \left(1 + \frac{1}{\nu}\right)\frac{P_0}{2\pi}\,e^{2\beta \text{ arc tan } (a/l)}\\ &\{(a^2 + l^2)/(a^2 + t^2)\,(l^2 - t^2)\}^{\frac{1}{2}}\\ &\cos\,[\beta \log_e \{(l + t)/(l - t)\} - \text{arc tan } (t/a)]\\ T(t) &= \left(1 + \frac{1}{\nu}\right)\frac{P_0}{2\pi}\,\exp\,\{2\beta \text{ arc tan } (a/l)\}\\ &\{(a^2 + l^2)/(a^2 + t^2)\,(l^2 - t^2)\}^{\frac{1}{2}}\\ &\sin\,[\beta \log_e \{(l + t)/(l - t)\} - \text{arc tan } (t/a)]\end{aligned}\right\} \ldots [25]$$

where

$$\sigma_\eta^-(t) = -P(t), \quad \tau_{\xi\eta}^-(t) = T(t) \ldots\ldots [26]$$

If $a \to \infty$ the parabolic boundary approaches the straight boundary and the problem reduces to that for a half plane. If P_s and P_s denote the values of $P(t)$ at $t = 0$ for the curved (parabolic) and straight boundaries, respectively

$$\begin{aligned}P_c = \{P(t)\}_{t=0} &= \left\{\left(1 + \frac{1}{\nu}\right)P_0(a^2 + l^2)^{\frac{1}{2}}\Big/(2\pi al)\right\}\\ &\exp\,\{2\beta \text{ arc tan } (a/l)\} \ldots\ldots [27]\end{aligned}$$

$$P_s = \lim_{a\to\infty} P_c = P_0(1 + \nu)\Big/\left(2\pi l\nu^{\frac{1}{2}}\right) \ldots\ldots [28]$$

TABLE 1 VALUES OF $\text{LOG}_{10}(P_c/P_s)$

a_1	0.1	0.2	0.3	0.4	0.5	0.6
$\text{Log}_{10}(P_c/P_s)$	0.7786	0.5754	0.3473	0.2493	0.1813	0.1321
					0.8	1.0
					0.0682	0.0312

Substituting $(a/l) = a_1$ and taking $\nu = 3$ one obtains

$$\log_{10}(P_c/P_s) = 0.1519 \text{ arc tan } a_1 + \frac{1}{2}\log_{10}(1 + a_1^2) - \log_{10}a_1 - 0.2386 \quad [29]$$

From Table 1, which gives the values of $\log_{10}(P_c/P_s)$ for different values of a_1, it is obvious that P_c is always greater than P_s and it increases as a_1 decreases; i.e., as the curvature increases.

Buckling of Initially Imperfect Cylindrical Shells Subject to Torsion[1]

By W. A. NASH,[2] GAINESVILLE, FLA.

An analytical solution based upon large-deflection shell theory is presented for the problem of the elastic instability of a thin cylindrical shell subject to torsion. The fundamental equations used are those presented by Donnell in 1934, and these equations together with the condition of stationary potential energy are employed to determine all arbitrary deflection parameters. Boundary conditions corresponding to clamped-end shells and also to shells having simply supported ends are considered. Load-deformation relations for various magnitudes of initial imperfection of the shell are determined for both boundary conditions. Lastly, values are presented for an imperfection factor based upon existing experimental evidence for clamped-end shells. The investigation described here is a continuation of work done earlier by Loo.

Introduction

In 1924 Schwerin (1)[3] presented the first analysis of the torsional buckling of thin elastic cylindrical shells. His study utilized classical, linear, small-deflection shell theory, but unfortunately actual calculations based upon his analysis would become extremely unwieldy. In 1933 Donnell (2) re-examined this problem and proposed a new simplified method of attack, still based upon small-deflection theory. His approach yielded simple relations between the critical buckling stress and the geometric parameters of the shell for several end conditions. However, analogous to the cases of axial compression and also hydrostatic pressure acting on thin cylindrical shells, these small-deflection analyses predict higher buckling loads than those actually found during test. For the case of torsional buckling the mean experimental value is about 75 per cent of the classical theoretical result, with a minimum of 60 per cent. These values are based upon tests conducted by Donnell (2) and Lundquist (3).

In an effort to explain the discrepancies between small-deflection theory and test for various loadings on cylindrical shells, Donnell (4) in 1934 introduced the concept of nonlinear terms due to finite deformations together with a consideration of the initial imperfections of the shell. In 1941 von Karman and Tsien (5) employed these nonlinear large-deflection equations to investigate the postbuckling behavior of axially compressed cylindrical shells. Their results reveal the existence of equilibrium positions with a buckled shape involving a lower load than given by classical theory. However, the maximum resistance of the cylinder was still found to be that indicated by classical theory. Their work did not specifically account for the initial imperfections present in the specimen but instead was based upon the hypothesis that the shell would "jump" into a configuration involving a lower level of potential energy. The work of von Karman and Tsien has been extended by Leggett and Jones (6), Michielsen (7), and Kempner (8).

In 1950 Donnell and Wan (9) considered the problem of axial compression of an initially imperfect cylinder and, by utilizing the finite-deflection equations developed by Donnell in 1934, obtained results that are in reasonable agreement with experimental evidence. In 1954 Loo (10) extended this analysis to include the case of torsional buckling of thin cylindrical shells. Finite-deflection theory together with a consideration of the initial imperfections of the shell formed the basis of this work.

In reference (10) the second approximation compatibility equation together with the principle of stationary potential energy was employed. However, the energy was actually made stationary with respect to only two of the four arbitrary deflection parameters and the other two parameters were assumed to have the values given by small-deflection shell theory. The effect of this simplifying assumption is not immediately obvious. The present investigation is an extension of Loo's work (10). The distinguishing features are:

(*a*) The potential energy is minimized with respect to all arbitrary deflection parameters with no results being drawn from small-deflection theory.

(*b*) The influence of the assumed buckling configuration on the load-deformation relations is studied by considering both clamped-end and also simply supported cylinders. This phase of the investigation is important because it is known that shell-buckling loads predicted by small-deflection theory depend critically upon the boundary conditions. It is logical to expect that the same situation exists when large-deflection theory is employed. Since reference (10) considered only one of many possible boundary conditions, this matter warrants additional analytical treatment.

(*c*) The condition of periodicity of circumferential displacement is enforced, whereas in reference (10) this question was only indirectly treated by assuming the number of waves present during buckling to be the same as indicated by small-deflection theory. Should the assumed buckling configuration be the exact one it would be satisfactory to consider the number of waves equal to that indicated by small-deflection theory. However, since this is unlikely, the simplification introduces an error of unknown magnitude.

(*d*) A parameter corresponding to a uniform radial displacement of the shell is introduced.

Analysis

Fundamental Equations. Let us consider a cylinder of mean radius R, length L, and thickness t. Let x, s, and z denote orthogonal co-ordinates in the axial, tangential, and radial directions, respectively. Further, let u, v, and w (positive inward) be the components of displacement (in the x, s, and z-directions, respectively) of any point in the middle surface of the shell. In the

[1] The results in this paper were obtained in the course of research conducted under Contract DA-01-009-ORD-404 between the Office of Ordnance Research, U. S. Army, and the University of Florida.

[2] Professor, Department of Engineering Mechanics, University of Florida. Mem. ASME.

[3] Numbers in parentheses refer to the Bibliography at the end of the paper.

Contributed by the Applied Mechanics Division and presented at the Annual Meeting, New York, N. Y., November 25–30, 1956, of The American Society of Mechanical Engineers.

Discussion of this paper should be addressed to the Secretary, ASME, 29 West 39th Street, New York, N. Y., and will be accepted until April 10, 1957, for publication at a later date. Discussion received after the closing date will be returned.

Note: Statements and opinions advanced in papers are to be understood as individual expressions of their authors and not those of the Society. Manuscript received by ASME Applied Mechanics Division, March 7, 1956. Paper No. 56—A-36.

thin cylinder the stress field may be considered to be composed of membrane and bending action and each system will be treated independently. The strain-displacement relations correct through all second-order terms are well known and involve derivatives of u, v, and w. However, the higher-order terms in u and v may reasonably be neglected in computing the membrane stresses and strains in a thin cylinder, since these displacements are small compared to w, and the membrane strain-displacement relations are taken in the form (4)

$$\left.\begin{aligned}\epsilon_x &= \frac{\partial u}{\partial x} + \frac{K}{2}\left(\frac{\partial w}{\partial x}\right)^2 \\ \epsilon_s &= \frac{\partial v}{\partial s} + \frac{K}{2}\left(\frac{\partial w}{\partial s}\right)^2 - \frac{w}{R} \\ \epsilon_{xs} &= \left(\frac{\partial u}{\partial s} + \frac{\partial v}{\partial x}\right) + K\,\frac{\partial w}{\partial x}\,\frac{\partial w}{\partial s}\end{aligned}\right\} \quad \ldots\ldots [1]$$

where $K = 1 + (2w_0/w) = 1 + (2a_0/a) = 1 + (V/a) = \text{const}$, where $V = 2a_0$, w_0 representing the initial radial deviation from perfect shape, $a_0 t$ the amplitude of w_0, and at the amplitude of w. The fact that K is taken to be constant implies that only the component of the initial deviation which is of the same shape as the displacements can be taken into account. This component of the initial deviation is by far the most important one. By assuming that the equations of equilibrium for an element in the plane of the cylinder wall are approximately the same as those in flat-plate theory and by introducing the Airy stress function, Donnell (4) obtained the following compatibility relation between the stress function F of the membrane stresses and the radial displacement w

$$\left(\frac{\partial^2}{\partial x^2} + \frac{\partial^2}{\partial s^2}\right)^2 F = EK\left[\left(\frac{\partial^2 w}{\partial x \partial s}\right)^2 - \left(\frac{\partial^2 w}{\partial x^2}\right)\left(\frac{\partial^2 w}{\partial s^2}\right)\right] - \frac{E}{R}\,\frac{\partial^2 w}{\partial x^2} \quad \ldots\ldots [2]$$

where E is the modulus of elasticity. The second-order terms on the right side of Equation [2] correspond to membrane stresses due to finite displacements, while the last term corresponds to membrane stresses due to the curvature. For an assumed w, F may be readily found from Equation [2]. The Airy function F will be the sum of a particular solution of this equation and the general solution of the corresponding homogeneous equation. For the case of pure torsion the latter solution is merely

$$F = -\tau_{xs} xs \quad \ldots\ldots [3]$$

where τ_{xs} denotes the mean shearing stress. Knowing F, the membrane energy of the cylinder may be expressed in terms of the stress function as follows (4)

$$E_m = \frac{t}{2E}\int_0^L \int_0^{2\pi R} \left\{\left(\frac{\partial^2 F}{\partial x^2} + \frac{\partial^2 F}{\partial s^2}\right)^2 + 2(1+\nu)\left[\left(\frac{\partial^2 F}{\partial x \partial s}\right)^2 - \frac{\partial^2 F}{\partial x^2}\,\frac{\partial^2 F}{\partial s^2}\right]\right\} dx\,ds \quad \ldots\ldots [4]$$

where ν denotes Poisson's ratio. The strain energy of bending is given by (4)

$$E_b = \frac{Et^3}{12(1-\nu^2)}\int_0^L \int_0^{2\pi R} \left\{\left(\frac{\partial^2 w}{\partial x^2} + \frac{\partial^2 w}{\partial s^2}\right)^2 + 2(1+\nu)\left[\left(\frac{\partial^2 w}{\partial x \partial s}\right)^2 - \frac{\partial^2 w}{\partial x^2}\,\frac{\partial^2 w}{\partial s^2}\right]\right\} dx\,ds \quad \ldots\ldots [5]$$

For rigid-testing machine loading, the variation of the potential energy of the external loads vanishes since no torsional displacements are permitted. Hence for this type of loading the total potential energy U_t may be taken to be the sum of E_m and E_b.

Displacement Pattern. Let us consider two buckling-displacement configurations, one corresponding to clamped ends of the cylindrical shell, the other implying simply supported ends. For the first case a suitable deflection function is

$$w = at\left[\sin\frac{n(s+\gamma x)}{R}\left(1 - \cos\frac{2\pi x}{L}\right) + d\left(\cos\frac{2\pi x}{L} - 1\right) + e\right] \quad \ldots\ldots [6]$$

where a, n, γ, d, and e are arbitrary parameters. This satisfies the important condition of vanishing slope at the ends. It does not necessarily satisfy the conditions $u = v = 0$ at the ends—but these last conditions are not important. The displacement parameter e is admitted in an effort to obtain the smallest possible buckling load, even though physically such a displacement at the ends of the shell would seldom be permitted in applications. Actually, it was found that the addition of this parameter e had only a very slight effect upon the final results.

For the second case we shall choose

$$w = a't\left[\sin\frac{n'(s+\gamma' x)}{R}\sin\frac{\pi x}{L} + d'\sin\frac{\pi x}{L} + e'\right] \quad \ldots [7]$$

Again, a', n', γ', d', and e' are arbitrary parameters. This pattern does not satisfy the condition of zero edge moment at the ends, as discussed in reference (2). However, the second term in Equation [7] does satisfy this condition and later in the paper it will be shown that it is precisely this term that becomes extremely important in the case of large displacements. Thus, even though the pattern indicated by Equation [7] does not correspond to simply supported ends for small deflections, it very closely represents this boundary condition for large displacements. For brevity this condition will be described as simple support even though it does not satisfy all of the requirements. Again, e' is introduced in an effort to obtain the minimum theoretical buckling load, but again it has only a negligible effect upon the final results.

In each of these analyses the origin of the x-co-ordinates is taken at one end of the shell. The second term in each of these expressions represents an axially symmetric deformation of the shell and becomes important in the case of large displacements where it reduces the circumferential stresses by balancing large deflection strains against strains due to change of radius.

For the displacement pattern corresponding to clamped ends the Airy function of the membrane stresses is found from Equation [2] to be

$$\begin{aligned}F = {} & c_1\cos\frac{2\pi x}{L} + c_2\cos\frac{4\pi x}{L} + c_3\cos\frac{2n(s+\gamma x)}{R} \\ & + c_4\,\frac{\cos 2n(s+\alpha_2 x)}{R} + c_5\cos\frac{2n(s+\beta_2 x)}{R} \\ & + c_6\sin\frac{n(s+\gamma x)}{R} + c_7\sin\frac{n(s+\alpha_1 x)}{R} \\ & + c_8\sin\frac{n(s+\beta_1 x)}{R} + c_9\sin\frac{n(s+\alpha_2 x)}{R} \\ & + c_{10}\sin\frac{n(s+\beta_2 x)}{R} - \tau_{xs} xs \quad \ldots\ldots [8]\end{aligned}$$

where

$$\alpha_1 = \gamma - m; \qquad \beta_1 = \gamma + m$$

$$\alpha_2 = \gamma - \frac{m}{2}; \qquad \beta_2 = \gamma + \frac{m}{2}$$

$$\alpha_3 = \gamma - 2m; \qquad \beta_2 = \gamma + 2m$$

$$m = \frac{2\pi R}{nL}$$

Here n denotes the number of circumferential waves. The constants in Equation [8] are given by

$$\left.\begin{aligned}
c_1 &= \frac{K_1 L^4}{32\pi^4} + \frac{K_2 m^2 d L^4}{16\pi^4} \\
c_2 &= -\frac{K_1 L^4}{512\pi^4}; \quad c_3 = \frac{K_1 R^4}{32n^4(\gamma^2+1)^2} \\
c_4 &= -\frac{K_1 R^4}{64n^4(\alpha_2^2+1)^2}; \quad c_5 = \frac{-K_1 R^4}{64n^4(\beta_2^2+1)^2} \\
c_6 &= \frac{K_1 d R^4}{2n^4(\gamma^2+1)^2} + \frac{K_2 \gamma^2 R^4}{n^4(\gamma^2+1)^2} \\
c_7 &= -\frac{K_1 d R^4}{2n^4(\alpha_1^2+1)^2} - \frac{K_2 \alpha_1^2 R^4}{2n^4(\alpha_1^2+1)^2} \\
c_8 &= -\frac{K_1 d R^4}{2n^4(\beta_1^2+1)^2} - \frac{K_2 \beta_1^2 R^4}{2n^4(\beta_1^2+1)^2} \\
c_9 &= \frac{K_1 d R^4}{4n^4(\alpha_2^2+1)^2}; \quad c_{10} = \frac{K_1 d R^4}{4n^4(\beta_2^2+1)^2}
\end{aligned}\right\} \quad \ldots [9]$$

where

$$K_1 = EKa^2t^2\frac{n^4}{R^4}m^2$$

$$K_2 = \frac{Eat}{R}\frac{n^2}{R^2}$$

Similarly, for the case of simply supported ends the Airy function is found from Equation [2] to be

$$\begin{aligned}
F' = {} & c_1' \cos\frac{2n'(s+\gamma' x)}{R} + c_2' \cos\frac{n'(s+\alpha_1' x)}{R} \\
& + c_3' \cos\frac{n'(s+\beta_1' x)}{R} + c_4' \sin\frac{n'(s+\gamma' x)}{R} \\
& + c_5' \sin\frac{n'(s+\alpha_2' x)}{R} + c_6' \sin\frac{n'(s+\beta_2' x)}{R} \\
& + c_7' \sin\frac{\pi x}{L} + c_8' \cos\frac{2\pi x}{L} - \tau_{xx} rs \quad \ldots [10]
\end{aligned}$$

where

$$\alpha_1' = \gamma' - m'; \quad \beta_1' = \gamma' + m'$$

$$\alpha_2' = \gamma' - 2m'; \quad \beta_2' = \gamma' + 2m'$$

$$m' = \frac{\pi R}{n'L}$$

The constants in Equation [10] are given by

$$\left.\begin{aligned}
c_1' &= \frac{K_1' R^4}{32(n')^4(1+\gamma'^2)^2}; \quad c_3' = \frac{K_1' d' R^4}{4(n')^4(\alpha_2'^2+1)^2} \\
c_2' &= \frac{K_2'(\alpha_1')^2 R^4}{2(n')^4(\alpha_1'^2+1)^2}; \quad c_4' = \frac{K_1' d' R^4}{4(n')^4(\beta_2'^2+1)^2} \\
c_5' &= -\frac{K_2'(\beta_1')^2 R^4}{2(n')^4(\beta_1'^2+1)^2}; \quad c_7' = \frac{K_2' d'(m')^2 L^4}{\pi^4} \\
c_6' &= -\frac{K_1' d' R^4}{2(n')^4(\gamma'^2+1)^2}; \quad c_8' = \frac{K_1' L^4}{32\pi^4}
\end{aligned}\right\} \quad \ldots [11]$$

where

$$K_1' = EK(a')^2t^2\frac{(n')^4}{R^4}(m')^2$$

$$K_2' = \frac{Ea't}{R}\frac{(n')^2}{R^2}$$

Knowing w and F, the total potential U_t is readily calculated for each of these cases by use of Equations [4] and [5].

Periodicity of Circumferential Displacement. From the strain-displacement relations, Equation [1], the stress-displacement relations may be formulated readily by use of the ordinary expressions for stress-strain relations in a biaxial field. From these relations the expression

$$\frac{\partial v}{\partial s} = \frac{1}{E}\left[\frac{\partial^2 F}{\partial x^2} - \nu\frac{\partial^2 F}{\partial s^2}\right] - \frac{K}{2}\left(\frac{\partial w}{\partial s}\right)^2 + \frac{w}{R} \quad \ldots [12]$$

is readily obtained. Since s is measured along the circumference of the shell, v must be a periodic function of s. Consequently, the constant term in Equation [12] must vanish. This leads to the determination of e and e' in each of the assumed displacement patterns. For the clamped-end shell, substitution in Equation [12] leads to

$$e = d + \frac{3K}{2}at\frac{\pi^2 R}{m^2 L^2} \quad \ldots [13]$$

and for the simply supported shell we obtain

$$e' = \frac{K}{8}a't\frac{\pi^2 R}{(m')^2 L^2} \quad \ldots [14]$$

Thus the coefficient corresponding to a uniform inward displacement is not an independent parameter.

Load-Deformation Relation. Let us consider the third Equation [1]. Let γ_{xs} denote the nonperiodic terms in

$$\left(\frac{\partial u}{\partial s} + \frac{\partial v}{\partial x}\right)$$

or physically, (R/L) multiplied by the mean angle of twist. Then by integration over the middle surface of the cylinder we readily obtain the relations

$$\frac{\tau_{xs}}{G} = \gamma_{xs} + 3K(a)^2t^2\frac{\pi^2\gamma}{m^2L^2} \quad \ldots [15]$$

for the clamped-end shell and

$$\frac{\tau_{xs}'}{G} = \gamma_{xs}' + \frac{K'}{4}(a)^2t^2\frac{\pi^2\gamma'}{(m')^2L^2} \quad \ldots [16]$$

for the shell with simply supported ends.

Minimization of Potential. From Equations [4], [5], and [15] the total potential energy for the clamped-end shell is found to be

$$\frac{(1+\nu)L^2}{8E\pi^4Rt^5}\,U_i = \frac{a^2}{12(1-\nu^2)}\,\frac{1}{m^4}\left\{\frac{1}{4}(1+\alpha_i^2)^2 + \frac{1}{4}(1+\beta_i^2)^2 + (1+\gamma^2)^2 + m^4d^2\right\} + (1+\nu)(a^4 + 2Va^3 + V^2a^2)$$
$$\left[\frac{17}{64m^4} + \frac{1}{64(1+\gamma^2)^2} + \frac{1}{256(1+\alpha_i^2)^2} + \frac{1}{256(1+\beta_i^2)^2} + \frac{d^2}{4(1+\alpha_i^2)^2} + \frac{d^2}{4(1+\beta_i^2)^2} + \frac{d^2}{16(1+\alpha_i^2)^2} + \frac{d^2}{16(1+\beta_i^2)^2}\right]$$
$$+ \frac{(1+\nu)}{4\pi^2}\left(\frac{L^2}{Rt}\right)(a^3 + Va^2)\left[\frac{d}{m^2} + \frac{d\gamma^2}{(1+\gamma^2)^2} + \frac{d\alpha_i^2}{2(1+\alpha_i^2)^2} + \frac{d\beta_i^2}{2(1+\beta_i^2)^2}\right] + \frac{(1+\nu)}{16\pi^4}\left(\frac{L^2}{Rt}\right)^2 a^2\left[d^2 + \frac{\gamma^4}{(1+\gamma^2)^2} + \frac{\alpha_i^4}{4(1+\alpha_i^2)^2} + \frac{\beta_i^4}{4(1+\beta_i^2)^2}\right] + \frac{1}{16\pi^4}\left[\frac{L^4}{t^4}(\gamma_{xx})^2 + 6(a^2 + Va)\frac{\pi^2\gamma}{m^2}\left(\frac{L^2}{t^2}\gamma_{xx}\right) + 9(a^4 + 2Va^3 + V^2a^2)\frac{\pi^4\gamma^2}{m^4}\right] \quad \ldots\ldots [17]$$

For the shell with simply supported ends it is

$$\frac{(1+\nu)L^2}{8E\pi^4Rt^5}\,U_i' = \frac{a'^2}{192(1-\nu^2)}\,\frac{1}{m'^4}\left\{\frac{1}{4}(1+\alpha_i'^2)^2 + \frac{1}{4}(1+\beta_i'^2)^2 + d'^2m'^4\right\} + \frac{(1+\nu)}{16}(a'^4 + 2Va'^3 + V'^2a'^2)\left[\frac{1}{64(1+\gamma'^2)^2} + \frac{d'^2}{4(1+\gamma'^2)^2} + \frac{d'^2}{16(1+\alpha_i'^2)^2} + \frac{1}{256m'^4} + \frac{(1+\nu)}{16\pi^4}\left(\frac{L^2}{Rt}\right)^2 a'^2\left[\frac{\alpha_i'^4}{4(1+\alpha_i'^2)^2} + \frac{\beta_i'^4}{4(1+\beta_i'^2)^2} + d'^2\right] + \frac{1}{16\pi^4}\left[\frac{L^4}{t^4}\gamma_{xx}'^2 + \left(\frac{L}{t}\right)^2\gamma_{xx}'\frac{(a'^2 + Va')\pi^2\gamma'}{4m'^2} + (a'^4 + 2Va'^3 + V^2a'^2)\frac{\pi^4\gamma'^2}{16m'^4}\right] \quad \ldots\ldots [18]$$

The deflection parameters a, n, γ, and d for the clamped-end shell, or a', n', γ', and d' for the simply supported case are determined from the condition that at equilibrium their values are such that the total potential energy of the system has a stationary value for any small variation of the parameters. In most large-deflection analyses involving the principle of stationary potential energy (5 through 10) the partial derivatives of the total potential energy, with respect to each of the parameters involved, are formed, equated to zero, and the resulting nonlinear equations solved simultaneously. In reference (10) only two of four possible such equations were considered directly. In the present investigation, the partial derivatives were not formed but instead each U_i and U_i' from Equations [17] and [18], respectively, was programmed on an IBM 602-A calculator. For the clamped-end shell, for example, for a given value of the parameter (L^2/Rt) the most expedient procedure was to assign values to V and $(L/t)^2\gamma_{xx}$ and then systematically adjust the values of a, m, γ, and d until a stationary value of the total potential energy was established. An analogous procedure was followed for the simply supported shell. Equations [15] or [16] were then used to determine $(L/t)^2\tau_{xx}/G$. In this manner one point on a load-deformation curve was established. Other values of $(L/t)^2\gamma_{xx}$ and V were then investigated until the families of curves appearing in Figs. 1 through 6 could be plotted. Shells having these values of $L^2/(Rt)$ are known from experimental evidence (2, 3) to be well within the elastic buckling range.

Certain results obtained from enforcing the condition that the total potential energy have a stationary value are plotted in Fig. 7 for the values $L^2/(Rt) = 2000$, $V = 0$ for the case of clamped-end shells. The curves shown there represent the variations of m, γ, and d with the amplitude a. Analogous curves could be plotted for other values of V and $L^2/(Rt)$ corresponding to the various plots shown in Figs. 1 through 6. Of particular interest are the variations of the parameters m and γ in contrast to the constant values assumed in reference (10). The values of m and γ used in reference (10) for $L^2/(Rt) = 2000$ are indicated by the dashed lines in Fig. 7 so that they may be compared to the values obtained in the present paper. These latter values are indicated by solid lines. Fig. 7 illustrates the increase in the value of m (i.e., the decrease in the number of circumferential waves) as the amplitude of the waves increases. This is in agreement with theoretical and experimental evidence regarding buckling of thin cylinders subject to axial compression. Thus the present treatment, in contrast to that of reference (10) does not assume that the number of circumferential waves is constant and equal to that indicated by small-deformation theory.

It is of interest to note that the load-deformation relations represented in Figs. 1 through 6 indicated a somewhat greater drop of resistance during the postbuckling stage than was found in reference (10). For example, the decrease in strength for a perfect specimen having $L^2/(Rt) = 2000$ was found in reference (10) to be 12 per cent, whereas, according to the present theory it is 26 per cent. The smaller decrease indicated by reference (10) is evidently one consequence of drawing two parameters from small-deflection theory.

From a study of the curves shown in Figs. 1 through 6, it was found that the ratio of the peak value of buckling stress for any given V to that for the corresponding perfect case ($V = 0$), denoted as $(\tau_{xx}/\tau_{xx_0})_{peak}$ is related to $L^2/(Rt)$ and V by the approximate relation

$$1 - \left(\frac{\tau_{xx}}{\tau_{xx_0}}\right)_{peak} = 4.25\left[\frac{V}{(L^2/Rt)^{0.2}}\right]^{0.6} \quad \ldots\ldots [19]$$

for clamped-end shells, and

$$1 - \left(\frac{\tau_{xx}}{\tau_{xx_0}}\right)_{peak} = 3.10\left[\frac{V}{(L^2/Rt)^{0.2}}\right]^{0.6} \quad \ldots\ldots [20]$$

for simply supported cylinders. It only remains to express the imperfection factor V as a function of the physical characteristics of the initially imperfect shell.

It is well known that the foregoing techniques yield true values of critical loads only if the assumed buckling configuration is exact. Perhaps a buckling configuration in which displacements are expressed as infinite series would be more general, but the solution of any such problem is now considered intractable. For any assumed buckling pattern other than the exact one, the foregoing analysis always indicates an excessive value of the buckling load. The magnitude of the discrepancy between the indicated value and that given by the exact buckling configuration is of course unknown. Consequently it is true that the reduction in the peak value of buckling stress is overestimated. However, the load-deformation relations indicated in Figs. 1 through 6 for perfect shells ($V = 0$) merely serve as reference lines from which the other curves are obtained. Since all shells contain some imperfections, only the curves $V \neq 0$ are actually used. The overestimates in reduction from the perfect cases are approximately ac-

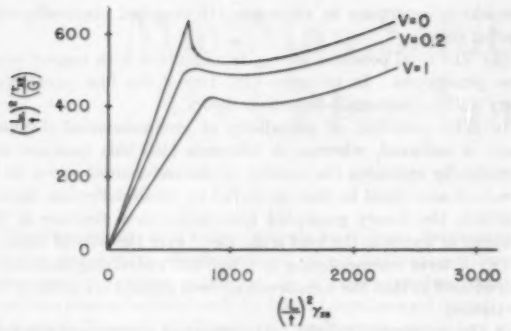

FIG. 1 RELATIONSHIP BETWEEN AVERAGE SHEARING STRESS AND AVERAGE ANGLE OF TWIST, FOR CLAMPED-END SHELLS WITH $L^2/(Rt) = 2000$

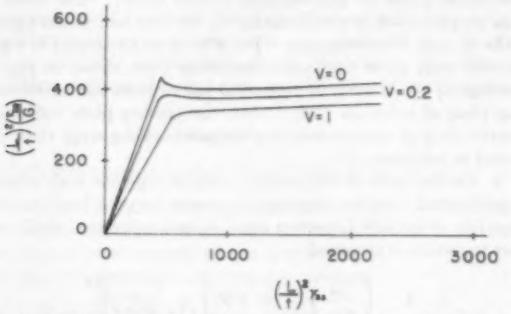

FIG. 2 RELATIONSHIP BETWEEN AVERAGE SHEARING STRESS AND AVERAGE ANGLE OF TWIST, FOR SIMPLY SUPPORTED SHELLS WITH $L^2/(Rt) = 2000$

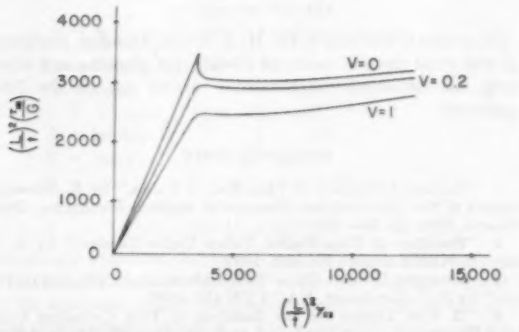

FIG. 3 RELATIONSHIP BETWEEN AVERAGE SHEARING STRESS AND AVERAGE ANGLE OF TWIST, FOR CLAMPED-END SHELLS WITH $L^2/(Rt) = 20{,}000$

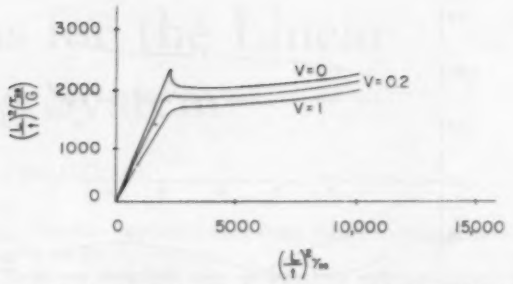

FIG. 4 RELATIONSHIP BETWEEN AVERAGE SHEARING STRESS AND AVERAGE ANGLE OF TWIST FOR SIMPLY SUPPORTED SHELLS WITH $L^2/(Rt) = 20{,}000$

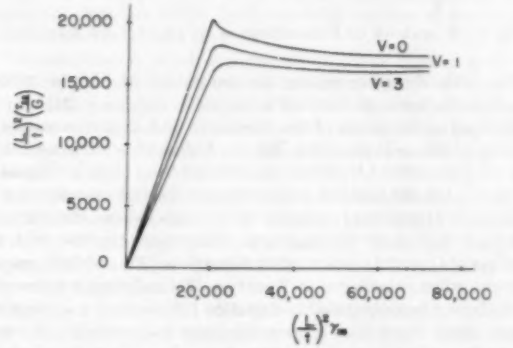

FIG. 5 RELATIONSHIP BETWEEN AVERAGE SHEARING STRESS AND AVERAGE ANGLE OF TWIST, FOR CLAMPED-END SHELLS WITH $L^2/(Rt) = 200{,}000$

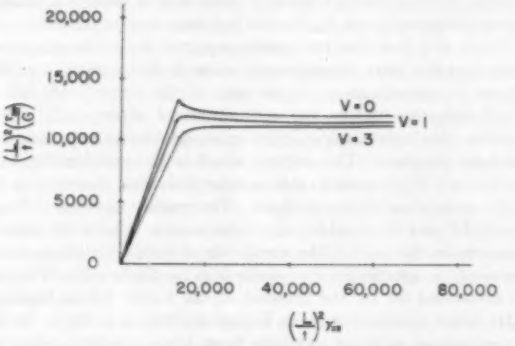

FIG. 6 RELATIONSHIP BETWEEN AVERAGE SHEARING STRESS AND AVERAGE ANGLE OF TWIST, FOR SIMPLY SUPPORTED SHELLS WITH $L^2/(Rt) = 200{,}000$

counted for by assigning appropriate values to V, the imperfection factor, when expressing V in terms of the parameters of the initially imperfect shell. In the absence of any treatment involving an exact buckling configuration this feature must be introduced into the analysis. Experimental studies currently being carried out are expected to indicate more nearly the exact nature of the true buckling configuration.

Donnell and Wan (9) and later Loo (10) employed the concept of an "unevenness" factor U_0 which for a thin cylinder is assumed to be related to $a_0 l$ (the amplitude of w_0) in the following manner

$$a_0 = U_0 \left[\left(\frac{L_x L_s}{L_x + L_s} \right) \frac{1}{t} \right]^\delta = V/2 \quad \ldots\ldots [21]$$

where L_x and L_s are the half wave lengths in the axial and circumferential directions, respectively. The factor U_0 is assumed to depend only on the method of fabricating the specimen. Let us adopt the value of $\delta = 2.0$, which is consistent with recommendations for strengths of columns (9). For a clamped-end cylindrical shell subject to torsion we have the relation

$$m = \frac{L_s}{L_x} = \text{wave-length ratio}$$

thus we have approximately

$$L_x = L/2 \quad \ldots\ldots [22]$$

and

$$L_s = \frac{m}{2} L \quad \ldots\ldots [23]$$

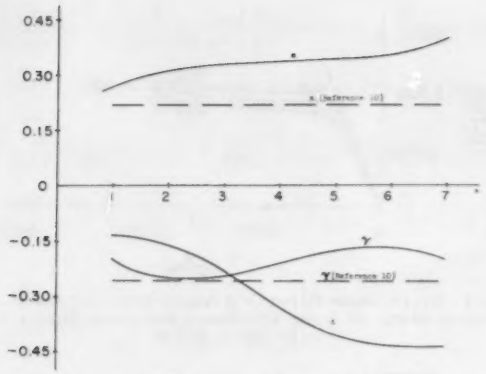

FIG. 7 VARIATION OF PARAMETERS m, γ, AND d WITH AMPLITUDE a

For shells characterized by the parameter $L^2/(Rt) = 2000$ a sufficiently accurate value of m for use in Equation [21] may be obtained as the mean of the maximum and minimum values of this variable as indicated in Fig. 7. Values of m for other values of the parameter $L^2/(Rt)$ are established from plots analogous to Fig. 7. On the basis of available experimental evidence due to Donnell (2) and also Lundquist (3) for clamped-end shells a value of $U_0 = 0.17 \times 10^{-6}$ is suggested. This value, together with the values of L_s and L_c indicated by Equations [22] and [23], respectively, when substituted in Equation [21] indicates a value of V which may be substituted in Equation [19] to yield a value of the peak shear stress that a given specimen may sustain. No data regarding the torsional buckling of simply supported cylindrical shells appear in the literature and consequently no value of U_0 is suggested for this boundary condition. An extensive experimental investigation is currently under way to provide a value of the unevenness factor U_0 for this last boundary condition.

While it is true that test results reported in the literature indicate that the mean experimental value of the torsional buckling stress is approximately 75 per cent of the value predicted by small-deflection theory, the wide scatter of experimental values renders this approximate figure unacceptable for any design or analysis purposes. This scatter, which is illustrated in Fig. 11 of reference (10), is considerably greater than that observed in stability tests of axially loaded bars. The results embodied in Equations [19] and [21] tend to reduce this scatter. One of the primary reasons for this is that the amplitude of initial deviations would certainly be greater for thin shells than for thick ones. This fact is accounted for by the presence of the factor L/t in Equation [21] (after substitution from Equations [22] and [23]). In fact experimental evidence available from tests currently being carried out by the author indicates that there exists a definite relationship between the ratio e/t, where e denotes the maximum deviation from true circularity as measured on the shell, and the ratio L/t. It is of course the ultimate aim to present relations predicting the strength of thin cylinders in terms of the measured initial imperfections and the geometric parameters of the shell. However, many additional test results are necessary for a complete solution.

CONCLUSIONS

1 The only existing treatment of the torsional buckling of thin cylindrical shells utilizing large-deflection theory together with a consideration of the initial imperfections of the shell has been extended in the following manner:

(a) Boundary conditions corresponding to clamped ends and also simply supported ends are specifically treated, whereas the boundary conditions in reference (10) implied elastically supported ends.

(b) The total potential energy is minimized with respect to all free parameters. In reference (10) two of the four parameters were drawn from small-deflection theory.

(c) The condition of periodicity of circumferential displacement is enforced, whereas in reference (10) this question was avoided by assuming the number of circumferential waves to be constant and equal to that predicted by small-deflection theory. Further, the theory presented here indicates a decrease in the number of waves as the load is increased over the critical value.

(d) A term corresponding to a uniform radial displacement is introduced so that the membrane stresses present are entirely due to torsion.

2 In reference (10) the total potential energy was rendered stationary with respect to only two of the four arbitrary deflection parameters and the other two parameters were assumed to have the values given by small-deflection shell theory. The effect of this simplification is not immediately obvious and would appear to be in need of investigation. The effects are illustrated in Fig. 7 as well as in all of the load-deformation plots shown in Figs. 1 through 6, which differ in numerical values from the corresponding plots of reference (10). Also, the present plots indicate a greater drop of resistance during the postbuckling stage than was found in reference (10).

3 On the basis of the present analysis together with existing experimental data the following expression for peak load-carrying capacity of initially imperfect clamped-end cylindrical shells subject to torsion is proposed

$$1 - \left(\frac{\tau_{xs}}{\tau_{xs_0}}\right)_{\text{peak}} = 4.25\left[\frac{V}{(L^2/Rt)^{0.3}}\right]^{0.6}$$

where V is obtained from Equation [21].

ACKNOWLEDGMENT

The author is indebted to Dr. H. A. Meyer, Director, Statistical Laboratory of the University of Florida, for planning and supervising the numerical computations carried out on the IBM equipment.

BIBLIOGRAPHY

1 "Torsional Stability of Thin-Walled Tubes," by E. Schwerin, Reports of the International Congress of Applied Mechanics, Delft, Holland, 1924, pp. 255–265.

2 "Stability of Thin-Walled Tubes Under Torsion," by L. H. Donnell, NACA Report No. 479, 1933.

3 "Strength Tests on Thin-Walled Duralumin Cylinders in Torsion," by E. E. Lundquist, NACA TN 472, 1932.

4 "A New Theory for the Buckling of Thin Cylinders Under Axial Compression and Bending," by L. H. Donnell, Trans. ASME, vol. 56, 1934, pp. 795–806.

5 "The Buckling of Thin Cylindrical Shells Under Axial Compression," by Th. von Karman and H. S. Tsien, *Journal of the Aeronautical Sciences*, vol. 8, June, 1941, pp. 303–312.

6 "The Behavior of a Cylindrical Shell Under Axial Compression When the Buckling Load Has Been Exceeded," by D. M. A. Leggett and R. P. N. Jones, ARC, R & M No. 2190, August, 1942.

7 "The Behavior of Thin Cylindrical Shells After Buckling Under Axial Compression," by H. F. Michielsen, *Journal of the Aeronautical Sciences*, vol. 15, December, 1948, pp. 738–744.

8 "Analysis of the Post-Buckling Behavior of an Axially Compressed Cylindrical Shell," by J. Kempner, Polytechnic Institute of Brooklyn, Brooklyn, N. Y., Report No. 212, 1953.

9 "Effect of Imperfections on Buckling of Thin Cylinders and Columns Under Axial Compression," by L. H. Donnell and C. C. Wan, JOURNAL OF APPLIED MECHANICS, Trans. ASME, vol. 72, 1950, pp. 73–83.

10 "Effects of Large Deflections and Imperfections on the Elastic Buckling of Cylinders Under Torsion and Axial Compression," by T. T. Loo, Proceedings of the Second U. S. National Congress of Applied Mechanics, 1954, pp. 345–357.

Min-Max Solutions for the Linear Mass-Spring System

By EUGENE SEVIN,[1] CHICAGO, ILL.

Absolute upper and lower bounds have been determined for the maximum displacement of an undamped linear mass-spring system acted on by a non-negative forcing function characterized only by total impulse and duration. The upper bound is shown to result from applying the total impulse to the mass as an initial blow. The lower bound is shown to depend upon the ratio of load duration to natural period of the system, and this response results from a forcing function consisting of an initial and final impulse and an intermediate constant force. In the latter case, for sufficiently short durations, the forcing function reduces simply to equal initial and final impulses.

Nomenclature

The following nomenclature is used in the paper:

x = co-ordinate of displacement
x_{max} = maximum displacement
$\max x_{max}$ = maximum-maximum displacement
$\min x_{max}$ = minimum-maximum displacement
$R = \dfrac{\min x_{max}}{\max x_{max}}$
m = mass
k = spring constant
$\omega = \sqrt{\dfrac{k}{m}}$ = circular frequency of system
$f(t)$ = forcing function
t = time
t_1 = duration of forcing function
I = impulse
E = energy
$\alpha = \omega t$

Introduction

There are numerous problems concerning the response of physical systems to dynamic forces in which the primary interest is not the time variation of the displacement,[2] but rather the maximum displacement attained. The maximum displacement is determined in most instances by computing the displacement-time relationship resulting from a solution of a differential equation, and then finding the maximum value of this function. This procedure requires, among other things, a complete knowledge of the forcing function.

There are occasions when it would be sufficient simply to obtain bounds on the maximum displacement on the basis of possibly incomplete but readily obtainable information regarding the forcing function. This information might include, for example, the duration of the force, the total impulse of the force, or the maximum value of the force.

Two situations in which such bounds would be of value are:

1 Only one differential equation is being studied, but solutions corresponding to many choices of the forcing function have to be considered in order to determine the particular forcing function for which the maximum displacement, say, exceeds a specified value.

2 It is required to find the maximum displacement corresponding to a given differential equation and forcing function. However, the forcing function is not too accurately known. For example, the time details of the forcing function may be known only approximately.

This paper is concerned with the following problem: If, for a given physical system (i.e., differential equation), the forcing functions are restricted to a certain class, what are the possible bounds for the maximum displacement? The solution of this problem requires the determination of the minimum-maximum displacement (minimax solution) and the maximum-maximum displacement (maximax solution) with respect to the class of forcing functions under consideration.

No general method of solving this type of problem seems to be available. To gain insight into the nature of such problems, with a view toward developing general methods of approach, a simple mechanical system was studied. Specifically, the problem considered was that of undamped forced motion of a mass on a linear spring. The forcing function was assumed to be non-negative and to be characterized only by total impulse and duration. The linear mass-spring system was chosen not only for its simplicity but also for its importance in many physical problems. The class of forcing functions considered is also of practical importance.

This paper is concerned primarily with the solution to the minimax problem, as the maximax solution is easily obtained. The former proceeds from a representation of the solution to the differential equation in a complex plane analogous to the familiar phase plane. The trajectory in this plane has the properties that (a) arc length is proportional to the impulse of the forcing function, (b) the radius vector is proportional to the square root of the energy of the system, and (c) the angle of turn of the tangent is proportional to the time. Moreover, this representation leads to an equivalent geometric problem of finding a curve which lies within or on the unit circle and joins the origin to a point on the circle such that the total angle of turn of the tangent is equal to a given value and the total length is a maximum.

Differential Equation

The differential equation governing the undamped motion of a mass on a linear spring is

$$m\ddot{x} + kx = f(t) \quad \ldots\ldots\ldots\ldots\ldots\ldots [1]$$

---

[1] Research Engineer, Department of Propulsion and Structural Research, Armour Research Foundation of Illinois Institute of Technology.

[2] "Displacement" and "force" are assumed here to include such analogous concepts as, for example, temperature and heat flux.

Contributed by the Applied Mechanics Division and presented at the Annual Meeting, New York, N. Y., November 25–30, 1956, of The American Society of Mechanical Engineers.

Discussion of this paper should be addressed to the Secretary, ASME, 29 West 39th Street, New York, N. Y., and will be accepted until April 10, 1957, for publication at a later date. Discussion received after the closing date will be returned.

Note: Statements and opinions advanced in papers are to be understood as individual expressions of their authors and not those of the Society. Manuscript received by ASME Applied Mechanics Division, June 11, 1956. Paper No. 56—A-26.

The initial conditions when the mass starts from rest are at

$$t = 0, \quad x = 0; \quad \dot{x} = 0 \qquad [2]$$

Let the forcing function $f(t)$, be restricted as follows

$$\left.\begin{aligned} &f(t) \geq 0 \quad \text{for} \quad 0 \leq t \leq t_1 \\ &f(t) = 0 \quad \text{for} \quad t \geq t_1 \\ &\int_0^{t_1} f(\tau)d\tau = I \end{aligned}\right\} \qquad [3]$$

Define the impulse function $F(t)$ as

$$F(t) = \int_0^t f(\tau)d\tau \qquad [4]$$

Then

$$\left.\begin{aligned} &F(0) = 0 \\ &F(t) \text{ monotonically nondecreasing} \\ &F(t) = I \text{ for } t \geq t_1 \end{aligned}\right\} \qquad [5]$$

The solution to Equation [1], subject to Condition [2], is[3]

$$\left.\begin{aligned} x(t) &= \frac{1}{m\omega}\int_0^t \sin\,\omega\,(t-\tau)dF(\tau) \\ \dot{x}(t) &= \frac{1}{m}\int_0^t \cos\,\omega\,(t-\tau)dF(\tau) \end{aligned}\right\} \qquad [6]$$

The expressions for displacement and velocity are in the form of Stieltjes integrals which permits consideration of impulse-type functions where the differential $dF(t)$ does not exist.

Let the maximum value of $x(t)$ from Equation [6] be denoted by x_{max}. The problem to be considered may now be stated in the following form: In the class of functions $F(t)$ satisfying Condition [5], find functions $F(t)$, or $f(t)$, for which

(*a*) x_{max} is a maximum

and for which

(*b*) x_{max} is a minimum

and, find x_{max} in (*a*) and (*b*).

Problems (*a*) and (*b*) will be referred to as the maximax and minimax problems, respectively.

Phase-Plane Representation

Define the complex variable $z(t)$ as

$$z(t) = m\dot{x}(t) + im\omega x(t) \qquad [7]$$

By Equation [6], this becomes

$$x(t) = \int_0^t [\cos\,\omega(t-\tau) + i\,\sin\,\omega(t-\tau)]\,dF(\tau)$$

$$= e^{i\omega t}\int_0^t e^{-i\omega\tau}dF(\tau) \qquad [8]$$

It will be noted that

$$|z(t)| = \sqrt{m^2\dot{x}^2(t) + m^2\omega^2x^2(t)} = \sqrt{2mE(t)} \qquad [9]$$

where

$$E(t) = \frac{1}{2}\,m\dot{x}^2(t) + \frac{1}{2}\,kx^2(t)$$

is the energy of the system. The complex plane $(m\dot{x}, m\omega x)$ is commonly referred to as the phase plane, and Equation [7] is a geometric representation of the system trajectory in the phase plane. Some familiar properties of the phase-plane representation of Equation [8] are summarized as follows:[4]

1 For an arbitrary continuous force, the phase-plane trajectory can be approximated by a series of circular arcs whose centers are always on the $m\omega x$-axis.

2 For a constant force, the phase-plane trajectory is exactly a circular arc. For zero force, the center of the circular arc is at the origin.

3 Positive time is proportional to the counterclockwise variation in the normal to the phase-plane trajectory. For a circular arc this corresponds to the angle swept out by the radius vector.

4 The length of the radius vector is proportional to the square root of the energy of the system.

5 An impulse-type forcing function is represented by a line segment parallel to the $m\dot{x}$-axis whose length is numerically equal to the impulse.

As an illustration, the phase-plane trajectory for the case in which $f(t)$ is a constant force f over the interval $0 \leq t < t_1 = \pi/2\omega$, plus an impulse I_1 at $t = t_1$, is shown in Fig. 1. Also shown

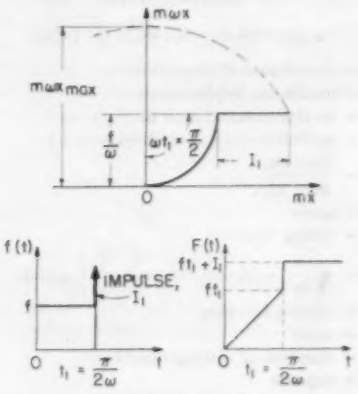

Fig. 1 Typical Phase-Plane Trajectory for Linear Mass-Spring System

in Fig. 1 is the impulse function $F(t)$ for this case. The maximum displacement is found directly from the geometry of the phase-plane trajectory to be

$$x_{max} = \frac{1}{m\omega}\sqrt{\left[\frac{f}{\omega}\right]^2 + \left[\frac{f}{\omega} + I_1\right]^2}$$

Maximax Solution

The maximax solution can be obtained in a simple fashion and it is convenient to do this before proceeding to the more interesting minimax problem. Using Equations [8] and [9], the following inequalities hold

$$\sqrt{2mE(t)} = |z(t)| \leq |e^{i\omega t}|\int_0^t |e^{-i\omega\tau}|\,dF(\tau) \leq \int_0^t dF(\tau). \qquad [10]$$

or, by Condition [3]

$$\sqrt{2mE(t)} \leq I$$

[3] "Vibration Problems in Engineering," by S. Timoshenko, D. Van Nostrand Company, Inc., New York, N. Y., 1951.

[4] "On a General Method of Solving Second-Order Ordinary Differential Equations by Phase-Plane Displacement," by L. S. Jacobsen, Journal of Applied Mechanics, Trans. ASME, vol. 74, 1952, pp. 543–553.

Hence, for all $t \geq 0$

$$E(t) \leq \frac{I^2}{2m} \quad \text{or} \quad E_{max} \leq \frac{I^2}{2m} \ldots\ldots\ldots\ldots [11]$$

Now if the mass is struck by a blow of impulse I at $t = 0$, then for all $t > 0$

$$E = \frac{I^2}{2m}$$

Thus Equation [10] yields as the solution to the maximax problem

$$\max E_{max} = \frac{I^2}{2m} \quad \text{and} \quad \max x_{max} = \frac{I}{m\omega} \ldots\ldots [12]$$

The associated forcing function is an initial impulsive load I.

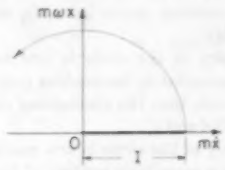

FIG. 2 PHASE-PLANE TRAJECTORY FOR MAXIMAX SOLUTION

The representation of this solution in the phase plane is simply a line segment of length I along the positive mx-axis, and the subsequent trajectory is a circle of radius I about the origin. This is shown in Fig. 2.

MINIMAX SOLUTION

A useful property of the minimax solution can be demonstrated easily by reference to the phase plane; namely

For the minimax solution the energy of the system must take on its maximum value at the duration of the loading, t_1 . . . . . [13]

The proof of this is as follows: Assume that Condition [13] does not hold, and let the phase-plane trajectory of the minimax solution be indicated as in Fig. 3. Let the impulse and duration

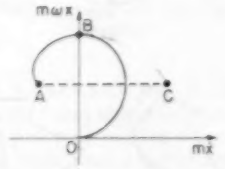

FIG. 3 PHASE-PLANE TRAJECTORY FOR ASSUMED MINIMAX SOLUTION WHICH VIOLATES CONDITION [13]

of the associated forcing function be denoted by I and t_1, respectively. Point A on the trajectory corresponds to the time t_1; for later times the trajectory is given by a circle with center at the origin and radius OA. For the particular case shown the maximum displacement is proportional to the length OB, and $OA < OB$.

It will now be shown that another forcing function, satisfying Condition [5] and having impulse I and duration t_1, can be found which will yield a lesser maximum displacement than that associated with OA. With reference to Fig. 3, the maximum displacement is not increased, owing to an impulsive load of magnitude AC applied at $t = t_1$, where $OC = OB$. Thus, the forcing function leading to the trajectory $OBAC$ will have a duration t_1 and lead to the same maximum displacement as the original forcing function, but will possess an impulse which exceeds I by the amount AC. Since this forcing function differs from the original only by the positive impulse AC, it too meets Condition [5].

Now it is clear from Equation [6] that the maximum displacement resulting from a particular forcing function is proportional to the scale of the forcing function; i.e., if x_{max} results from $f(t)$, cx_{max} results from $cf(t)$, where c is a constant. Therefore, if the forcing function leading to the trajectory $OBAC$ in Fig. 3 is scaled down so that its total impulse is equal to I, the maximum displacement attained must be less than that given by OB, contradicting the minimum property of the assumed minimax solution. The foregoing argument has been carried out for the particular case of Fig. 3 but is quite general. In fact, it further follows that the end point of the minimax trajectory (corresponding to the time $t = t_1$) must always lie in either the first or fourth quadrant of the phase plane.

It follows from Condition [9] that the maximum displacement is proportional to the square root of the maximum energy. Hence, the minimax (and maximax) solution for displacement is equivalent to the minimax (and maximax) solution for the total energy. This would not be true if the forcing function were allowed to be negative.

Geometric Equivalent of the Minimax Problem. Equation [8] leads to a geometric representation of the system trajectory in a complex plane closely related to the phase plane. Moreover, the nature of the trajectory in this plane yields a simple geometric equivalent, or analog, to the minimax problem. By Equations [8] and [9] one can write

$$\sqrt{2mE(t)} = \left| \int_0^t e^{-i\omega\tau}\, dF(\tau) \right| \leq I \ldots\ldots [14]$$

Define the quantity R by

$$R = \frac{x_{max}}{\max x_{max}} \quad (0 < R \leq 1)$$

Then

$$R = \frac{m\omega x_{max}}{I} = \frac{\sqrt{2mE_{max}}}{I} \ldots\ldots [15]$$

The solution to the minimax problem is thus obtained by finding a function $F(t)$, subject to Conditions [5], and satisfying the conditions

$$\left.\begin{aligned} \left| \int_0^t e^{-i\omega\tau}\, dF(\tau) \right| &\leq RI \\ \left| \int_0^{t_1} e^{-i\omega\tau}\, dF(\tau) \right| &= RI \end{aligned}\right\} \ldots\ldots [16]$$

such that the quantity R is a minimum. Then

$$\min x_{max} = \min R(\max x_{max}) = \frac{I}{m\omega} (\min R) \ldots [17]$$

In view of Condition [13], it will be noted that there is no loss in generality in the second of Conditions [16] which requires the energy to assume its maximum value at $t = t_1$.

Introduce the following change of variable

$$\alpha = \omega t; \quad \alpha_1 = \omega t_1; \quad F(t) = RIG(\alpha) \ldots\ldots [18]$$

Then Equation [16] becomes

$$\left.\begin{aligned} \left| \int_0^{\alpha} e^{-i\beta}\, dG(\beta) \right| &\leq 1 \\ \left| \int_0^{\alpha_1} e^{-i\beta}\, dG(\beta) \right| &= 1 \end{aligned}\right\} \ldots\ldots [19]$$

where $G(0) = 0$, $G(\alpha)$ monotonically nondecreasing; $G(\alpha_1) = 1/R$.

Let

$$w(\alpha) = \int_0^{\alpha} e^{-i\beta}\, dG(\beta) \quad \text{for} \quad 0 \leq \alpha \leq \alpha_1 \ldots\ldots [20]$$

Then $w(\alpha)$ represents a plane curve having the following properties, which can be verified easily from Equations [18–20]:

1 It starts at the origin; i.e., $w(0) = 0$.
2 It is within or on boundary of a unit circle; i.e., $|w(\alpha)| \leq 1$.
3 It ends on the periphery of the unit circle; i.e., $|w(\alpha_1)| = 1$.
4 The length of arc measured from the origin is $G(\alpha)$ which is proportional to the impulse function[5] $F(t)$.
5 It has total arc length

$$L_1 = \frac{1}{R} \ldots\ldots [21]$$

6 The parameter α is proportional to time and is the angle of turn of the tangent to the curve. A plot of $w(\alpha)$ is shown schematically in Fig. 4.

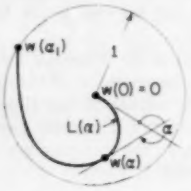

FIG. 4 GRAPHICAL REPRESENTATION OF EQUATION [20]

Equation [20] does not rule out curves containing straight-line segments and corners, and these have a simple physical interpretation. Over a straight-line segment there is a finite increase in length but no change in the angle of turn of the tangent. This corresponds to an increase in impulse in zero time, or a positive impulse load. At a corner there is no change in length of the curve but a finite rotation of the tangent. This corresponds to zero change in impulse over a finite time interval, or a period of time over which zero force acts.

A circular segment of arc also has a simple interpretation. Here there is both a change in length and angle of the tangent, but where the change in length is proportional to the angle change. This corresponds to a linear variation of impulse with time. Thus, a circular arc represents the application of a constant force.

The minimax problem can now be restated in terms of the following geometric problem:

Find a curve $w(\alpha)$ (the curve may have corners and contain straight-line segments) which joins the center of the unit circle to a point on the periphery and always remains within or on the circle, such that the total angle of turn of the tangent to the curve corresponds to a prescribed value α_1, and the total length of arc L_1 is a maximum. Also find the maximum arc length L_1.

That this is an equivalent statement of the minimax problem is clear since the prescribed angle of turn α_1 corresponds to the given duration of the load t_1 and, by Equations [21] and [17], a maximum total arc length L_1 corresponds to a minimum R and, in turn, a minimum-maximum displacement for a given total impulse I.

Properties of Minimax Solution to the Geometric Analog. A number of properties of the curve which is a solution to the above geometric problem will now be described. That these properties hold is based on the following condition:

[5] This is most easily seen by interpreting Equation [20] as the superposition of vectors of magnitude $dG(\beta)$.

If the curve $w(\alpha)$ is a minimax solution, it is impossible to modify $w(\alpha)$ to a curve $w^*(\alpha)$ having a greater length but the same total angle of turn of the tangent..... [22]

Proceeding from Condition [22], one determines that a minimizing curve has the properties indicated in the following: (The violation of the property stated is assumed and illustrated in the referenced figure by means of a solid line. The dotted line in this figure shows how the negation of the property to be proved implies a contradiction; i.e., Condition [22] is violated.)

1 In the interior of the unit circle no part of a minimizing curve is a convex arc, Fig. 5(*a*). Thus, in the interior of the circle the minimizing curve is a polygonal path.

2 The periphery of the circle is first reached by not more than two line segments, Fig. 5(*b*).

3 If the periphery of the circle is first reached by two line segments, the minimizing curve consists solely of these two line segments, Fig. 5(*c*).

4 If the periphery of the circle is first reached by one line segment and the immediately succeeding part of the minimizing curve is a line segment, then the minimizing curve consists of two line segments Figs. 5(*d* and *e*).

5 If the periphery of the circle is first reached by one line segment, then either the remaining portion of the minimizing curve lies entirely on the periphery of the circle, Fig. 5(*f*), or the remaining portion consists of two parts, one lying on the periphery of the circle and the other a line segment, Figs. 5(*g* and *h*).

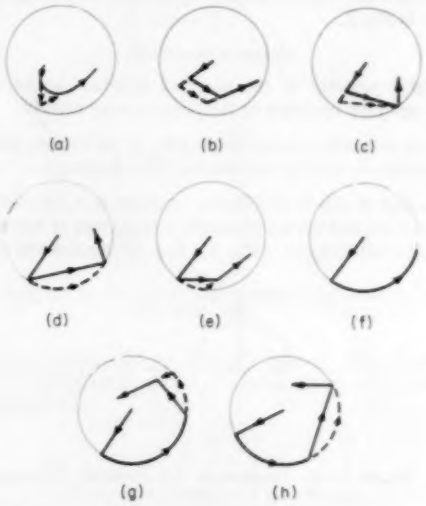

FIG. 5 PROPERTIES OF THE GEOMETRIC MINIMAX SOLUTION

Solution of the Minimax Problem. In view of the foregoing properties it is seen that a minimizing curve is always of the form shown in Fig. 6(*a*), or of the form shown in Fig. 6(*b*). Fig. 6(*b*) also includes the limiting cases in which the arc a or chord c reduces to a point. Thus, for $L_1 > 2$, a minimizing curve is of the general form shown in Fig. 6(*b*).

On the basis of Figs. 6(*a* and *b*) the minimax problem has been reduced to that of finding the appropriate combination of line segments and arcs which yields a maximum total length L_1 for a given total angle of turn α_1. This is a straightforward problem in which L_1 is a function only of α_1 and the ordinary methods of calculus can be applied.

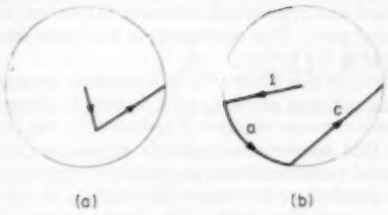

FIG. 6 POSSIBLE SOLUTIONS TO THE GEOMETRIC MINIMAX PROBLEM

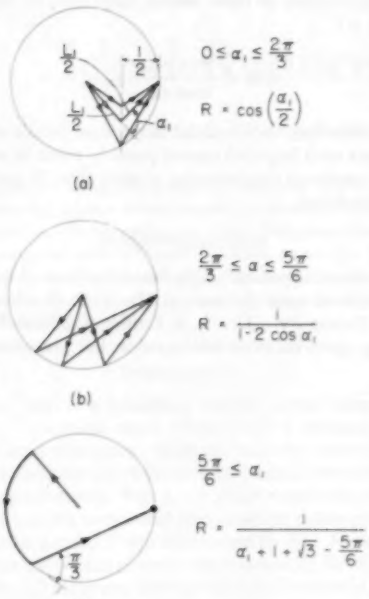

FIG. 7 SUMMARY OF SOLUTION TO THE GEOMETRIC MINIMAX PROBLEM

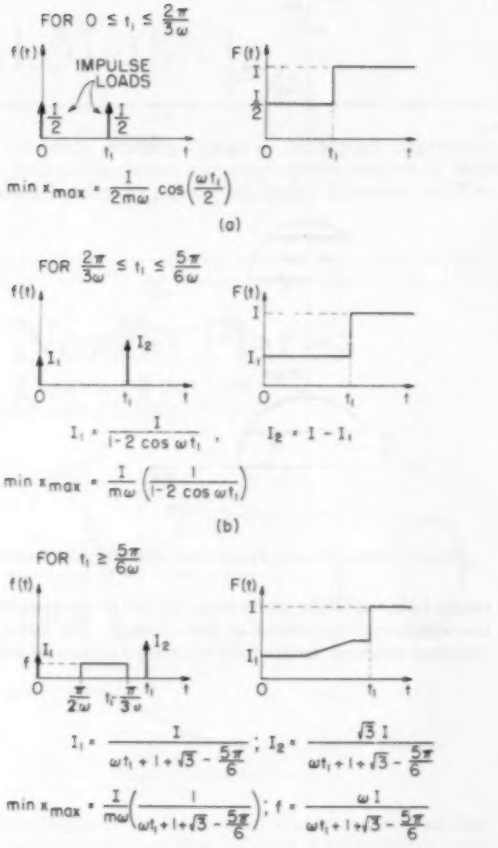
FOR $0 \le t_1 \le \frac{2\pi}{3\omega}$
f(t)
IMPULSE LOADS
$\frac{I}{2}$
$\frac{I}{2}$
F(t)
I
$\frac{I}{2}$
$\min x_{max} = \frac{I}{2m\omega}\cos\left(\frac{\omega t_1}{2}\right)$
(a)
FOR $\frac{2\pi}{3\omega} \le t_1 \le \frac{5\pi}{6\omega}$
I_1
I_2
$I_1 = \frac{I}{1-2\cos\omega t_1}$, $I_2 = I - I_1$
$\min x_{max} = \frac{I}{m\omega}\left(\frac{1}{1-2\cos\omega t_1}\right)$
(b)
FOR $t_1 \ge \frac{5\pi}{6\omega}$
$\frac{\pi}{2\omega}$
$\frac{\pi}{3\omega}$
$I_1 = \frac{I}{\omega t_1 + 1 + \sqrt{3} - \frac{5\pi}{6}}$; $I_2 = \frac{\sqrt{3}\,I}{\omega t_1 + 1 + \sqrt{3} - \frac{5\pi}{6}}$
$\min x_{max} = \frac{I}{m\omega}\left(\frac{1}{\omega t_1 + 1 + \sqrt{3} - \frac{5\pi}{6}}\right)$; $f = \frac{\omega I}{\omega t_1 + 1 + \sqrt{3} - \frac{5\pi}{6}}$
(c)

FIG. 8 SUMMARY OF SOLUTION TO THE PHYSICAL MINIMAX PROBLEM

The solution for the complete range of α_1 is summarized in Fig. 7, the details of the computations being omitted. The physical meaning of the geometric solution is summarized in Fig. 8. The response of the linear mass spring to several simple forcing functions is compared with the maximax and minimax displacements in Fig. 9.

In order to gain a better insight into the nature of the minimax solution obtained it may be helpful to consider the phase-plane representation shown in Fig. 10. The minimax solution is seen to result from a judicious choice of impulses and constant force that minimizes the total energy of the system. For durations $t_1 > 5\pi/6\omega$ (Fig. 10c) the mass is first displaced by an initial impulse and later held by a constant force at its position of maximum displacement. It is released at a time $t = \pi/3\omega$ prior to the duration t_1, and then the impulse remaining is applied as a blow at $t = t_1$. This causes the mass to oscillate within the maximum displacement first reached. The result of this loading is to keep the energy of the system constant throughout the motion and equal to the energy gained from the initial impulse. For shorter durations it is not possible to hold the mass at rest, and the forcing function reduces to an initial and final impulse. For $t_1 < 2\pi/3\omega$ these two impulses are numerically equal.

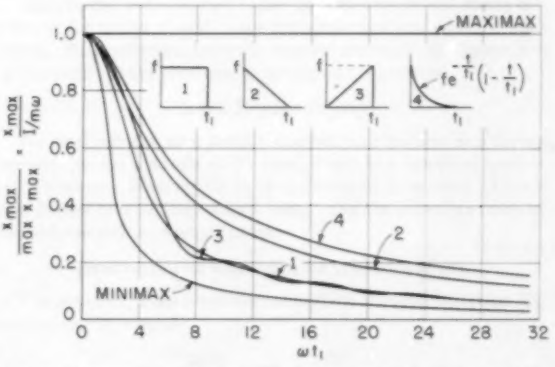

FIG. 9 COMPARISON OF MIN-MAX RESPONSE WITH THAT OF SEVERAL OTHER FORCING FUNCTIONS

SUMMARY

Absolute upper and lower bounds have been determined for the maximum displacement of an undamped linear mass-spring system acted on by a non-negative forcing function of specified duration and total impulse. The upper bound (maximax solution)

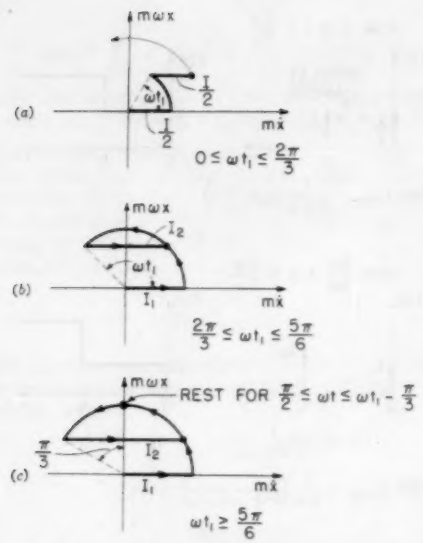

FIG. 10 PHASE-PLANE TRAJECTORY FOR MINIMAX SOLUTION

results from the total impulse being applied to the mass initially; the maximum displacement is then $I/(m\omega)$. The lower bound (minimax solution) results from a forcing function consisting of an initial and final impulse and intermediate constant force, in the most general case. The corresponding maximum displacement is shown in Fig. 9.

The intent of this study was to investigate general methods of handling min-max problems such as arise in connection with the dynamic response of physical systems. It was immediately apparent that conventional methods of analysis, such as the techniques of variational calculus, would be inadequate. It was therefore decided to investigate the nature of the min-max problem in particular cases. The linear mass-spring system discussed in this paper was chosen as a first example. The solution to this case was effected by means of a geometric analogy.

As one application of these results, inspection of Fig. 9 shows that for $\omega t_1 < 1$

$$0.88 < \frac{\min x_{max}}{\max x_{max}} \leq 1$$

That is, in this case, uncertainties in the time details of the loading (for fixed total impulse) cannot possibly result in error in the computed maximum displacement of more than 12 per cent, and probably much less.

ACKNOWLEDGMENTS

The geometric approach which forms the basis of the minimax solution is based upon the work of Mr. N. R. Goodman, now at Princeton University. Dr. R. A. Struble of Illinois Institute of Technology gave valuable assistance in the preparation of this paper.

Design Data and Methods

It is important that the data contained in technical papers be made readily available to design engineers. In order to satisfy these needs of industry, this section of the Journal includes a concise presentation of data and information drawn chiefly from papers previously published by the Applied Mechanics Division of The American Society of Mechanical Engineers.

Ideal Reducers and Nozzle Flares

By R. A. STRUBLE[1] and BERTHOLD SCHWEIZER,[2] CHICAGO, ILL.

The equation of a thin-walled reducer with constant circumferential plane stress under uniform internal pressure is derived. Such reducers were first conceived by Dr. H. C. Boardman[3] who referred to them as ideal. These reducers may be used either to connect two coaxial cylinders of different diameters or as nozzle flares for spherical heads and cone frustums.

Introduction

A REDUCER is a transition section joined tangentially to two cylindrical shells which have a common axis but different diameters. Such sections are characteristically surfaces of revolution about the common axis of the cylinders and are of double curvature, Fig. 1. A plane containing the axis of revolution is called a meridional plane and the radius of curvature in this plane at a point P will be denoted by R_2. A plane that is normal to the meridional plane in the direction of R_2 will be called a circumferential plane and the corresponding radius of curvature denoted by R_1. The principal tangential membrane stresses at P are given by the formulas[4]

$$\sigma_1 = \frac{pR_1}{h}\left(1 + \frac{R_1}{2R_2}\right) \quad \text{[1]}$$

$$\sigma_2 = \frac{pR_1}{2h} \quad \text{[2]}$$

where p and h are, respectively, the internal pressure and the thickness and where R_1 and R_2 are positive as shown in Fig. 1.

Ideal Reducers

An ideal reducer is defined as a thin-walled reducer of constant thickness having a shape such that, with uniform internal pressure, the circumferential plane stress σ_1 is constant throughout the reducer length. It will be shown that at any point of an ideal reducer the constant circumferential plane stress is always larger than the meridional plane stress σ_2, both being tensile, and that the shape and length of the ideal reducer are uniquely determined by the ratio of the radii of the cylinders to which it is joined.

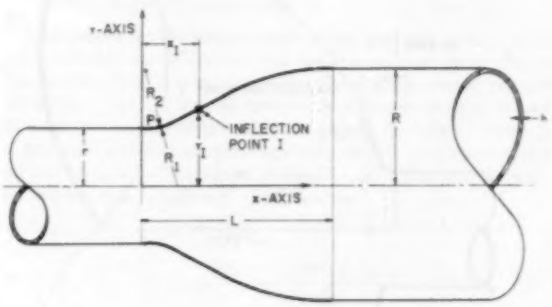

Fig. 1 Ideal Reducer

In a related work, F. von Tölke[5] has determined the shape of a reducer for which σ_1 and σ_2 are both constant and equal to each other. Such reducers, however, require artificial axial forces, not attributable to the pressure, to satisfy end conditions.

Ideal Nozzle Flares

An ideal reducer, or a portion thereof, may be used as a flaring section, joining a nozzle at the smaller end to a spherical head or cone frustum. Such nozzle flares are referred to as ideal. Figs. 2 and 3 show typical ideal nozzle flares using the inflection point of the reducer as the juncture point.

Derivation of Equation of Ideal Reducer

The equation of the ideal reducer is given through Equation [1], which may be written

$$\frac{2\sigma_1 h}{p} = 2R_1 + \frac{R_1^2}{R_2} \quad \text{[3]}$$

where $2\sigma_1 h/p$ is constant throughout the length of the reducer. In terms of the rectangular co-ordinates of Fig. 1, Equation [3] may be written

---

[1] Associate Professor of Mathematics, Illinois Institute of Technology.

[2] Instructor, Illinois Institute of Technology.

[3] Director of Research, Chicago Bridge and Iron Company.

[4] "Advanced Strength of Materials," by J. P. den Hartog, McGraw-Hill Book Company, Inc., New York, N. Y., 1952.

Discussion of this paper should be addressed to the Secretary, ASME, 29 West 39th Street, New York, N. Y., and will be accepted until April 10, 1957, for publication at a later date. Discussion received after the closing date will be returned.

Note: Statements and opinions advanced in papers are to be understood as individual expressions of their authors and not those of the Society. Manuscript received by ASME Applied Mechanics Division, June 12, 1956.

[5] "Über Rotationsschalen gleicher Festigkeit für konstanten Innen-order Aussendruck," by F. von Tölke, *Zeitschrift für angewandte Mathematik und Mechanik*, vol. 19, 1939, pp. 338–343.

$$\frac{2\sigma_1 h}{p} = 2y\sqrt{1+\left(\frac{dy}{dx}\right)^2} + \frac{y^2\dfrac{d^2y}{dx^2}}{\sqrt{1+\left(\frac{dy}{dx}\right)^2}} \quad [4]$$

The right-hand member of Equation [4] may be recognized as the y-derivative of the quantity

$$y^2\sqrt{1+\left(\frac{dy}{dx}\right)^2}$$

and hence, upon integrating from $y = r$ where $dy/dx = 0$, there results

$$kry = y^2\sqrt{1+\left(\frac{dy}{dx}\right)^2} + r^2(k-1) \quad [5]$$

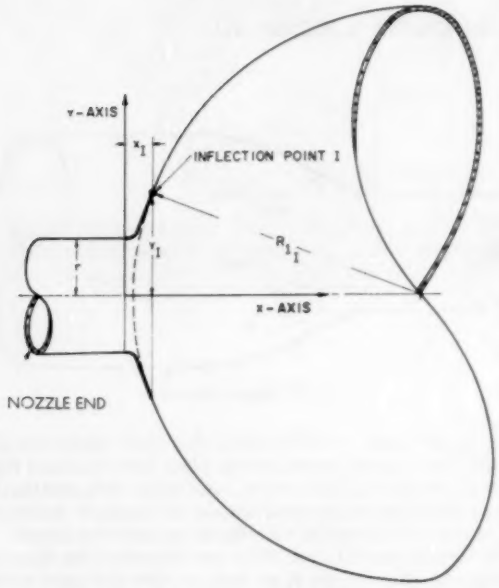

FIG. 2 IDEAL NOZZLE FLARE FOR SPHERICAL HEAD

where k is a dimensionless constant which determines the shape of the reducer

$$k = \frac{2\sigma_1 h}{rp} \quad [6]$$

It is useful to observe that Equation [5] may also be written in the form

$$R_1 = kr - \frac{r^2(k-1)}{y} \quad [7]$$

The variables in Equation [5] may be separated to yield

$$x = \int_r^y \frac{y^2 dy}{\sqrt{[rky - r^2(k-1)]^3 - y^4}} \quad [8]$$

The integral on the right-hand side of Equation [8] is elliptic. Its reduction to standard form is straightforward[6]; we give only the result

[6] "Handbook of Elliptic Integrals for Engineers and Physicists," by P. F. Byrd and M. D. Friedman, Springer-Verlag, Berlin, 1954.

$$x = \frac{-\sqrt{[rky - r^2(k-1)]^3 - y^4}}{y} + \frac{2r(k-1)}{z}\int_1^{\alpha(y)} \frac{dt}{\sqrt{(1-t^2)(1-mt^2)}} - \frac{rz}{2}\int_1^{\alpha(y)} \sqrt{\frac{1-mt^2}{1-t^2}}\,dt \quad [9]$$

where

$$m = \frac{(k-2)^2}{z^2}, \quad \alpha(y) = \frac{k}{k-2}\left[\frac{2r(k-1)}{ky} - 1\right]$$

and

$$z = \sqrt{k^2+4k-4}$$

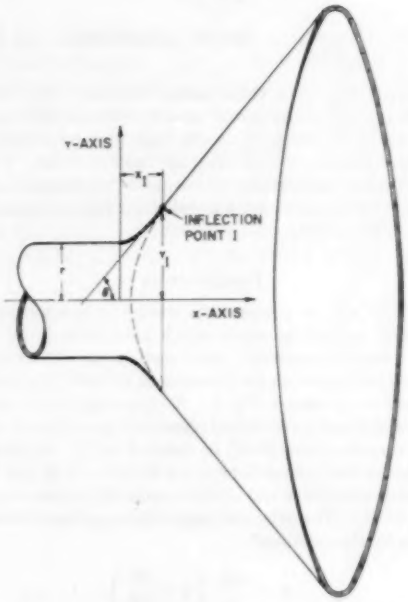

FIG. 3 IDEAL NOZZLE FLARE FOR CONE FRUSTUM

Equation [9] gives the equation of the ideal reducer in terms of tabulated elliptic integrals[6] of the first and second kind.

GEOMETRY OF THE IDEAL REDUCER

The radius R of the larger end of the reducer is given by the first root of the equation

$$\frac{dy}{dx} = \frac{\sqrt{[rky - r^2(k-1)]^3 - y^4}}{y^2} = 0$$

greater than r. We find

$$R = r(k-1) \quad [10]$$

Writing Equation [10] in the form

$$k = 1 + \frac{R}{r} \quad [11]$$

it follows that the shape of the ideal reducer is thus determined by the ratio R/r. The reducer shown in Fig. 1 is for a value of $k = 3$.

At the inflection point I of the reducer, $R_2 = \infty$, and from

Equations [3], [6], and [7] it follows that the y-co-ordinate (radius) of the reducer at this point is given by

$$y_I = \frac{2r(k-1)}{k} \quad [12]$$

The slope of the reducer and the length of the normal at the inflection point are of interest in the application to nozzle flares and are given through Equations [5] and [7], for $y = y_I$. Referring to Figs. 2 and 3 we have

$$\tan\theta = \frac{z(k-2)}{4(k-1)} \quad [13]$$

$$R_{1I} = \frac{kr}{2} \quad [14]$$

The flares shown in Figs. 2 and 3 are for values of $k = 10$ and $k = 5$, respectively.

The meridional stress along the reducer is given by Equations [2] and [7] and may be written

$$\frac{\sigma_2}{\sigma_1} = \frac{1 + \frac{R}{r} - \frac{R}{y}}{1 + \frac{R}{r}}$$

This ratio is less than unity for $r \leq y \leq R$ with a maximum of

$$\frac{R/r}{1 + R/r}$$

at the larger end of the reducer and with a minimum of

$$\frac{1}{1 + R/r}$$

at the smaller end.

Equation of the Ideal Reducer

The considerations of the preceding sections lead finally to the following expressions for the x-co-ordinate along the ideal reducer. For x between the left-hand end point (smaller end) and the inflection point: $(0 \leq \alpha \leq 1)$

$$x = \frac{rz}{2}[E(m) - E(m,\alpha)] - \frac{2(k-1)r}{z}[K(m) - F(m,\alpha)] - \frac{\sqrt{[rky - r^2(k-1)]^2 - y^4}}{y}$$

For x between the inflection point and the right-hand end point (larger end): $(-1 \leq \alpha \leq 0)$

$$x = \frac{rz}{2}[E(m) + E(m,-\alpha)] - \frac{2(k-1)r}{z}[K(m) + F(m,-\alpha)] - \frac{\sqrt{[rky - r^2(k-1)]^2 - y^4}}{y}$$

where $F(m, \pm\alpha)$ and $E(m, \pm\alpha)$ are incomplete elliptic integrals[6] of the first and second kind, respectively, with modulus m and argument $\pm\alpha$

$$m = \frac{(k-2)^2}{z^2}, \quad \alpha = \frac{k}{k-2}\left[\frac{2r(k-1)}{ky} - 1\right],$$

$$z = \sqrt{k^2 + 4k - 4}$$

and $K(m)$ and $E(m)$ are the corresponding complete elliptic integrals of modulus m.

In particular, the length L of the reducer (x-co-ordinate of the right-hand end point) is given by

$$L = rz\,E(m) - \frac{4(k-1)r}{z}K(m) \quad [15]$$

and the x-co-ordinate of the inflection point by

$$x_I = \frac{L}{2} - \frac{(k-2)r}{2k}z \quad [16]$$

For design purposes it is sufficient to lay out an ideal reducer by a well-known[6,7] semigraphical procedure which utilizes a geometric interpretation of Equation [3]. The simple expressions in Equations [12–16] then afford convenient checks on the accuracy of the layout, particularly near the inflection point where the graphical procedure degenerates. Complete details of such a layout appear in the reference.[7]

Volume and Surface Area of the Ideal Reducer

Expressions for the volume and surface area of a portion of an ideal reducer can be derived. In the general case, they involve incomplete elliptic integrals of the third kind, which are not tabulated. For the special case of the complete reducer or half reducer (to one side of the inflection point), the elliptic integrals of the third kind are complete and may be reduced to incomplete elliptic integrals of the first and second kind. The results, without derivations, are given in the following:

Volume of Complete Reducer

$$V_1 = 2\pi r^3\left\{\frac{k^3z}{3}E(m) - \frac{2(k-1)[2k^2 + 5(k-1)]}{3z}K(m) - \frac{\pi}{2}k(k-1)(1-\Lambda_0)\right\} \quad [17]$$

Volume of Reducer From Smaller End to Inflection Point

$$V_2 = \frac{V_1}{2} + \pi r^3\left\{\frac{k(k-1)}{2}\text{ arc cos}\frac{4(k-1)}{k^2} - (k-2)\frac{z[k^4 + 2(k-1)^2]}{3k^2}\right\} \quad [18]$$

Surface Area of Complete Reducer

$$S_1 = 2\pi r^2\left\{kE(m)z - \frac{4(k-1)[k^2 + 2(k-1)]}{kz}K(m) - \pi(k-1)(1-\Lambda_0)\right\} \quad [19]$$

Surface Area of Reducer From Smaller End to Inflection Point

$$S_2 = \frac{S_1}{2} + \pi r^2\left\{(k-1)\text{ arc cos}\frac{4(k-1)}{k^2} - (k-2)z\right\} \quad [20]$$

where $\Lambda_0 = \Lambda_0(m,\beta) = \frac{2}{\pi}\{K(m)E(1-m,\beta) - [K(m) - E(m)]F(1-m,\beta)\}$

is Heuman's lambda function[6,8] and

$$\beta = \frac{z}{\sqrt{2}\,k}$$

[7] "Ideal Reducers," by H. C. Boardman, *The Water Tower*, vol. 16, no. 3, January, 1955, pp. 8–9.

[8] "Tables of Complete Elliptic Integrals," by C. Heuman, *Journal of Mathematics and Physics*, vol. 20, 1941, pp. 127–206.

TABLE 1 DESIGN TABLE

k	L/r	x_1/r	Log* $\frac{V_1}{2\pi r^3}$	$\frac{V_2}{\pi r^3}$	Log* $\frac{S_1}{2\pi r^2}$	$\frac{S_2}{\pi r^2}$
2	2.221	1.111	0.04571	1.11	0.34655	2.22
3	3.286	0.956	0.63568	1.22	0.73878	2.30
4	4.306	0.830	1.07737	1.19	1.03342	2.38
5	5.309	0.734	1.41531	1.13	1.25864	2.43
6	6.305	0.658	1.68574	1.05	1.43949	2.48
7	7.298	0.598	1.91062	0.98	1.58984	2.52
8	8.290	0.548	2.10278	0.92	1.71842	2.56
9	9.282	0.507	2.27068	0.87	1.83052	2.59
10	10.27	0.472	2.41946	0.82	1.92988	2.62
11	11.27	0.442	2.55303	0.78	2.01912	2.64
12	12.26	0.415	2.67431	0.74	2.10003	2.66
13	13.25	0.392	2.78533	0.69	2.17406	2.68
14	14.24	0.372	2.88734	0.65	2.24229	2.70
20	20.21	0.285	3.37438	0.43	2.56738	2.76
40	40.14	0.165	4.30341	0.19	3.18696	2.86
100	100.08	0.077	5.51255	..	3.99317	2.94

* Logarithms are to the base 10.

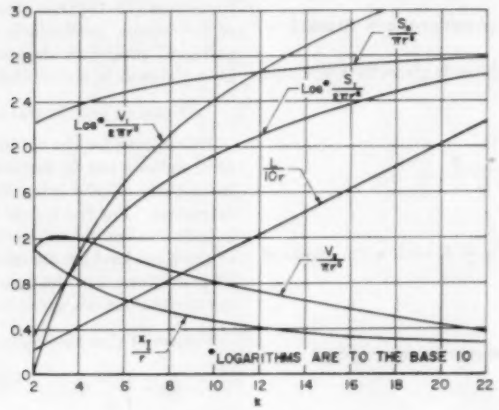

FIG. 4 DESIGN GRAPH

DESIGN TABLE

The formulas, Equations [15–20], developed in the preceding sections describe the ideal reducer in terms of tabulated functions. However, many of the expressions for the quantities involved are too complicated for design purposes. The design table (Table 1) and Fig. 4 give these quantities directly for a limited range of values of k.

Axisymmetrical Bending of Circular Plates Under Simultaneous Action of Lateral Load, Force in the Middle Plane, and Elastic Foundation

By YI-YUAN YU,[1] SYRACUSE, N. Y.

In this note the problem indicated in the title is solved in closed form on the basis of the classical small-deflection theory. As the problem is directly related to the stress analysis of tube sheets in heat exchangers, the present investigation also constitutes the preliminary step of a more exact analysis of the latter problem. Results of numerical examples are presented showing the influence of a tensile force in the middle plane and the rotation-resisting capability of the foundation on the deflection and bending moment of a uniformly loaded circular plate, either simply supported or clamped.

Introduction

PREVIOUS work on the bending of circular plates in the small-deflection theory, as may be found in Timoshenko's book (1),[2] deals with the simultaneous action of lateral load and force in the middle plane, or the simultaneous action of lateral load and an elastic foundation. Such problems were also discussed by Jen (2). Only in the corresponding beam problems has the simultaneous action of lateral load, axial force, and an elastic foundation been considered (3). The elastic foundation has been invariably taken to be one which can resist only the deflection of the beam or plate.

In the present note the axisymmetrical bending of circular plates under the simultaneous action of lateral load, force in the middle plane, and an elastic foundation will be discussed. The elastic foundation will be assumed to be capable of resisting not only the deflection but also the rotation of the plate; i.e., it will exert on the plate a reactive moment proportional to the maximum slope of the plate at any point in addition to the usual reactive force proportional to the deflection of the plate. In the axisymmetrical case the reactive moment is always proportional to the slope in the radial direction and acts in the same direction. The reactive moment of the foundation may also be shown to have the same effect as a tensile force in the middle plane of the plate; mathematically the two effects may therefore be treated together.

The problem to be solved is directly related to the stress analysis of tube sheets in heat exchangers. The latest development in this field has been given recently in another paper (4). Briefly, in a heat exchanger, the connecting flange and cylindrical shells exert, besides bending moments, also tensile forces on the tube sheet in the middle plane of the sheet; the tube bundle acts as an elastic foundation for the tube sheet and can resist rotation as well as deflection of the tube sheet. In the analysis given in (4) the bending moments exerted by the flange and shells and the deflection-resisting capability of the tube bundle have been taken into consideration. The additional effects due to the tensile force in the middle plane of the tube sheet and the rotation-resisting capability of the tube bundle on the stresses in the tube sheet remain to be determined. Thus the work presented here constitutes also another step further toward a more exact analysis of the tube-sheet problem.

Differential Equation of Problem and Its Solutions

Except the part concerning the rotation-resisting capability of the elastic foundation, the derivation of the governing equation of the problem is well known. For the sake of completeness, a simple derivation follows and the notations used are thereby introduced at the same time.

An element of the plate is shown in Fig. 1, in which q and m are, respectively, the resisting force and moment exerted by the foundation and are given by

$$q = kw, \qquad m = k_1(dw/dr)$$

k and k_1 being, respectively, the always positive deflection and rotation moduli of the foundation. By writing the equilibrium equations for the moments and forces acting on the element and by making use of the well-known formulas

$$M_r = -D[(d^2w/dr^2) + (\nu/r)(dw/dr)], \quad M_\varphi = -D[(1/r)(dw/dr) + \nu d^2w/dr^2] \ldots\ldots [1$$

the shearing force is obtained to be

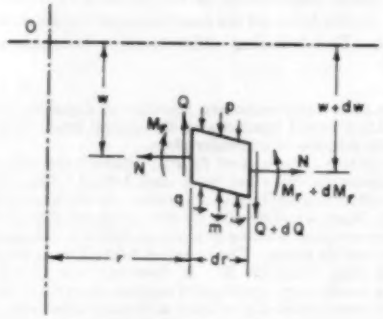

Fig. 1 Element of Plate

[1] Associate Professor of Mechanical Engineering, L. C. Smith College of Engineering, Syracuse University. Assoc. Mem. ASME.

[2] Numbers in parentheses refer to the Bibliography at the end of the paper.

Discussion of this paper should be addressed to the Secretary, ASME, 29 West 39th Street, New York, N. Y., and will be accepted until April 10, 1957, for publication at a later date. Discussion received after the closing date will be returned.

Note: Statements and opinions advanced in papers are to be understood as individual expressions of their authors and not those of the Society. Manuscript received by ASME Applied Mechanics Division, July 23, 1956.

$$Q = -Dd(\nabla^2 w)/dr + K(dw/dr) \quad [2]$$

and the lateral load intensity is given by

$$D\nabla^4 w - K\nabla^2 w + kw = p \quad [3]$$

which is also the governing equation of the problem. In Equations [2] and [3] we have used the notations

$$\nabla^2 = (d^2/dr^2) + r^{-1}(d/dr)$$

$$K = N + k_1$$

The effects due to N and k_1 are seen to be equivalent to each other.

Equation [3] is analogous to that for the corresponding beam problem; and, as in the beam problem, three cases will have to be considered according to whether $K^2 - 4kD$ is positive, zero, or negative. In the following, only the case of a tensile force N will be discussed, and K is therefore always positive.

When $K^2 - 4kD$ is positive, the complementary function of Equation [3] for the problem of a circular plate may be easily shown to have the form[3]

$$w = C_1 I_0(\alpha r) + C_2 I_0(\beta r) \quad [4]$$

in which C_1 and C_2 are arbitrary constants, I_0 are modified Bessel functions of the zero order and of the first kind, and

$$\alpha = \left[\frac{K + (K^2 - 4kD)^{1/2}}{2D}\right]^{1/2}, \quad \beta = \left[\frac{K - (K^2 - 4kD)^{1/2}}{2D}\right]^{1/2} \quad [5]$$

are real positive constants. When $K^2 - 4kD$ is zero, Equation [4] becomes of the form

$$w = C_1 I_0(\alpha r) + C_2 r I_1(\alpha r)$$

in which we now have

$$\alpha = [K/2D]^{1/2}$$

When $K^2 - 4kD$ is negative, Equation [4] still gives the solution. However, Equation [5] may now be written as

$$\alpha = \left[\frac{K + i(4kD - K^2)^{1/2}}{2D}\right]^{1/2}, \quad \beta = \left[\frac{K - i(4kD - K^2)^{1/2}}{2D}\right]^{1/2}$$

α and β are thus complex conjugates to each other, and so are $I_0(\alpha r)$ and $I_0(\beta r)$, which now have complex arguments. Equation [4] may therefore be written in the following more convenient form

$$w = C_1 I_0(\alpha r)_r + C_2 I_0(\alpha r)_i$$

where the subscripts r and i indicate the pure real and pure imaginary parts, respectively, of the function to which they are attached. In this form, all the functions and the constants C_1 and C_2 are real. The following differentiation formulas are easily obtainable[4]

$$\frac{d}{dr} I_0(\alpha r)_r = aI_1(\alpha r)_r - bI_1(\alpha r)_i$$

$$\frac{d}{dr} I_0(\alpha r)_i = aI_1(\alpha r)_i + bI_1(\alpha r)_r$$

$$\frac{d}{dr} I_1(\alpha r)_r = aI_0(\alpha r)_r - bI_0(\alpha r)_i - \frac{I_1(\alpha r)_r}{r}$$

$$\frac{d}{dr} I_1(\alpha r)_i = aI_0(\alpha r)_i + bI_0(\alpha r)_r - \frac{I_1(\alpha r)_i}{r}$$

in which the constants a, b, a_1, and b_1 are defined by

$$a + ib = \alpha, \qquad a_1 + ib_1 = \alpha^2$$

These formulas are useful in deriving expressions for the slope, moments, and shearing force.

The complete solution of Equation [3] is, needless to say, the sum of the complementary function and a particular integral. In the case of a uniform lateral pressure p on the plate, the particular integral is simply p/k.

Illustrative Examples

When the solution of the deflection w is known, the slope, moments, and shearing force may be obtained by straightforward differentiation, the last two according to Equations [1] and [2]. The problem of a circular plate on elastic foundation subjected to a uniform lateral pressure and a tensile force in the middle plane may then be solved in the usual manner, for both simply supported and clamped edges, and for all three cases of $K^2 - 4kD$ greater than, equal to, and smaller than zero. Based upon the solutions thus obtained, several numerical examples are calculated, the results of which give an indication of the influence of the tensile force in the middle plane and the rotation-resisting capability of the foundation. The data common to all these examples are

radius of plate = 10 in.
uniform pressure = 1000 psi
flexural rigidity of plate = $D = 10^6$ in. lb
deflection modulus of foundation = $k = 2 \times 10^4$ lb/in.^{3}

The values of $K = N + k_1$ are taken to be, respectively

$K = 3 \times 10^6$ lb/in. $(K^2 - 4kD > 0)$
$K = 2\sqrt{2} \times 10^5$ lb/in. $(K^2 - 4kD = 0)$
$K = 3 \times 10^4$ lb/in. $(K^2 - 4kD < 0)$

where no distinction between N and k_1 is made. In addition to these cases, the case in which $K = 0$ is also calculated according to the well-known solution of the problem of a uniformly loaded circular plate on an ordinary elastic foundation, without the action of any force in the middle plane. The result of this last case is used as a basis for comparison.

The numerical results for the deflection and radial bending moment are plotted in Figs. 2 and 3, respectively. Both the maximum deflection and the maximum moment for the case $K = 3 \times 10^4$ are about 10 per cent smaller than those for the case $K = 0$. The same quantities for the other two cases $K = 2\sqrt{2} \times 10^5$ and $K = 3 \times 10^6$ are further considerably smaller. As may be expected, the larger the value of K, the higher the reduction in the deflection and moment, and the bending stress becomes also correspondingly lower. However, a direct stress is at the same time induced due to any presence of the force N. Therefore, although the maximum final stress in the plate is always decreased through the additional consideration of k_1, this is not necessarily so when N is also taken into account.

[3] The complete complementary function of Equation [3] also includes modified Bessel functions of the second kind, which are not needed in the solution of a circular plate.

[4] The functions $I_0(\alpha r)_r$ and $I_0(\alpha r)_i$, which have rather general complex arguments, have not been used before. The notations as well as the differentiation formulas are new. On the basis of Reissner's plate theory, Naghdi and Rowley (5) derived an equation for the problem of axisymmetrical bending of plate on elastic foundation, without force in the middle plane. The equation takes a form similar to but less general than Equation [3]; it, however, was solved by these authors in a much more complicated manner in terms of the ber, bei, ker, and kei functions each combined with some other series function. See also reference (6) in connection with the functions used in this note and other similar functions.

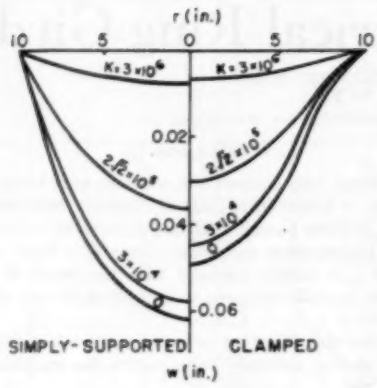

FIG. 2 DEFLECTIONS

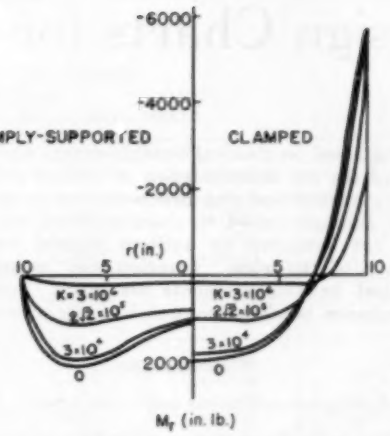

FIG. 3 RADIAL BENDING MOMENTS

As was shown in reference (4), the tube sheet in a heat exchanger is neither simply supported nor clamped. The value of the maximum radial bending moment in an actual tube sheet lies somewhere between those for the simply supported and clamped cases. According to the above results obtained for these latter cases, the maximum bending moment and the maximum stress in a tube sheet may also be expected to be lower than those calculated by the method described in reference (4); on the other hand, because of the presence of N, the maximum resultant stress is not necessarily lower. Incorporation of the effects of N and k_1 into the stress analysis of the tube sheet on the basis of the present result will be made in a future study.

BIBLIOGRAPHY

1 "Theory of Plates and Shells," by S. Timoshenko, McGraw-Hill Book Company, Inc., New York, N. Y., 1940.

2 "Bending of Circular Plates," by Shih-Min Jen, dissertation, University of Michigan, 1949.

3 "Beams on Elastic Foundation," by M. Hetényi, The University of Michigan Press, Ann Arbor, Mich., 1946, chapters VI and VII.

4 "Rational Analysis of Heat-Exchanger Tube-Sheet Stresses," by Yi-Yuan Yu, JOURNAL OF APPLIED MECHANICS, Trans. ASME, vol. 78, 1956, pp. 468–473.

5 "On the Bending of Axially Symmetric Plates on Elastic Foundations," by P. M. Naghdi and J. C. Rowley, Proceedings of the First Midwestern Conference on Solid Mechanics, Urbana, Ill., 1953, pp. 119–123.

6 "On the Generalized Ber, Bei, Ker, and Kei Functions with Application to Plate Problems," by Yi-Yuan Yu, *Quarterly Journal of Mechanics and Applied Mathematics*, forthcoming.

Design Charts for Symmetrical Ring Girders

By G. P. FISHER,[1] ITHACA, N. Y.

Charts, based on classical bending-energy analysis, are presented for the determination of critical design moments in symmetrical ring girders varying in shape from circular through round to sharp-cornered rings. The girders are subjected to uniform normal loading in the plane of the ring. Location and magnitude of all critical bending moments are given, from which the maximum bending moment is easily selected.

Nomenclature

The following nomenclature is used in the paper:

V = shear on transverse section; subscript locates section
T = axial force on section; subscript locates section
M = bending moment at section; subscript locates section
p = uniformly distributed normal internal load applied in plane of ring, per unit length of ring
a, b = ring dimensions, measured to centroidal axes
r = radius of curved segment of ring, measured to centroidal axis
θ = angular location in curved segment
γ = angle in curved segment
δ_x = displacement in x-direction at section 1
δ_y = displacement in y-direction at section 1
δ_r = rotational displacement at section 1
δ_{rx} = δ_r due to unit force in x-direction
δ_{ry} = δ_r due to unit force in y-direction
δ_{rr} = δ_r due to unit couple
δ_{rp} = δ_r due to applied load, p
R = moment coefficient = M/pb^2; subscript locates section
EI = flexural rigidity

Introduction

Ring girders commonly occur as elements of many types of structures; for example, as stiffening rings on pressurized ducts. The critical bending moments, shears, and axial forces required for ring design may be found in many handbook sources or simply computed for both circular rings and sharp-cornered rectangular rings, but are not generally available for round-cornered rectangular rings. Such rings occur in transition sections of pressurized ducts, notably those forming portions of wind tunnels. To satisfy this need, charts of critical bending-moment coefficients are presented (Fig. 4) for round-cornered rings and also for the limiting cases of circular and sharp-cornered rings, all of constant cross section and subjected to uniformly distributed normal load applied in the plane of the ring. Shears and axial forces are so simply computed by consideration of symmetry and static equilibrium that charts for these have been omitted. The coefficients used for construction of the charts are tabulated in Table 1 so that the reader may redraw the charts, if necessary, to suit his own purposes in calculation.

Analysis

The following brief analysis is a solution, considering bending energy only, of symmetrical rings of constant cross section subjected to a uniform normal internal load applied in the plane of the ring. Direct-stress and shear energy thus have been neglected, and it is tacitly assumed that the depth of the ring cross section is small compared to the radius of bend of the corners.

Imagine the ring, Fig. 1(*a*), to be cut at the origin. The forces on the cut section necessary to reproduce the conditions of the uncut ring are

$$V_1 = 0, \quad T_1 = -pb/2, \quad M_1 = \text{unknown}$$

positive in the sense of Fig. 1(*b*) and having such values as meet the three general conditions of continuity at the cut section

$$\delta_x = 0, \quad \delta_y = 0, \quad \delta_r = 0$$

That is, the three relative displacements between the cut ends must be zero to reproduce the uncut condition.

However, with V_1 and T_1 known in value, any single condition is sufficient for solution, say the rotational displacement

$$\delta_r = 0 = T_1\delta_{rx} + V_1\delta_{ry} + M_1\delta_{rr} + \delta_{rp} \quad \ldots\ldots [1]$$

where

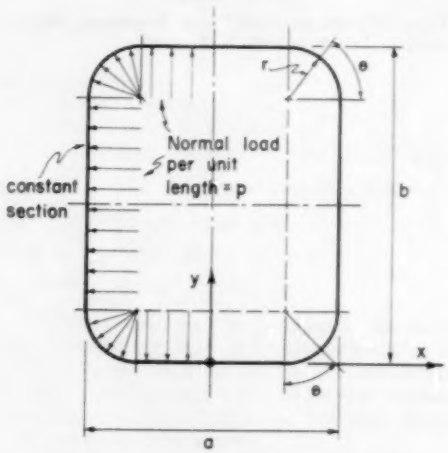

Fig. 1(*a*) Ring Dimensions and Loading

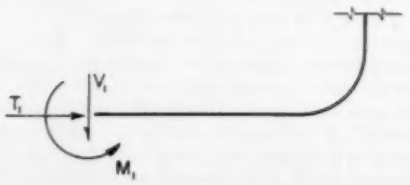

Fig. 1(*b*) Positive Sense of Redundants at Origin

[1] Associate Professor of Civil Engineering, Cornell University.

Discussion of this paper should be addressed to the Secretary, ASME, 29 West 39th Street, New York, N. Y., and will be accepted until April 10, 1957, for publication at a later date. Discussion received after the closing date will be returned.

Note: Statements and opinions advanced in papers are to be understood as individual expressions of their authors and not those of the Society. Manuscript received by ASME Applied Mechanics Division, May 15, 1956.

TABLE I

MOMENT COEFFICIENTS FOR SYMMETRICAL RING GIRDERS*

subjected to internal uniform normal load, p, per unit length

r/b	a/b	R_1	R_2	R_3	R_4	$R_{\theta\ max.}$	Θ for $R_{\theta\ max}$
0	0	+.0833	+.0833	+.0833	-.0417	+.0833	0°
	.2	+.0650	+.0700	+.0700	-.0550	+.0700	11°- 20'
	.4	+.0433	+.0633	+.0633	-.0617	+.0633	21°- 50'
	.6	+.0183	+.0633	+.0633	-.0617	+.0633	31°- 0'
	.8	-.0100	+.0700	+.0700	-.0550	+.0700	38°- 40'
	1.0	-.0417	+.0833	+.0833	-.0417	+.0833	45°
.1	.2	+.0711	+.0711	+.0311	-.0489	+.0711	0°
	.4	+.0482	+.0532	+.0232	-.0568	+.0544	14°- 0'
	.6	+.0227	+.0427	+.0227	-.0573	+.0474	26°- 35'
	.8	-.0057	+.0393	+.0293	-.0507	+.0493	36°- 50'
	1.0	-.0372	+.0428	+.0428	-.0372	+.0594	45°
.2	.4	+.0551	+.0551	-.0049	-.0499	+.0551	0°
	.6	+.0289	+.0339	-.0061	-.0511	+.0371	18°- 25'
	.8	+.0003	+.0203	+.0003	-.0447	+.0323	33°- 40'
	1.0	-.0309	+.0141	+.0141	-.0310	+.0389	45°
.3	.6	+.0371	+.0371	-.0229	-.0429	+.0371	0°
	.8	+.0083	+.0133	-.0167	-.0367	+.0203	26°- 35'
	1.0	-.0228	-.0028	-.0028	-.0228	+.0220	45°
.4	.8	+.0185	+.0185	-.0215	-.0265	+.0185	0°
	1.0	-.0125	-.0075	-.0076	-.0125	+.0091	45°
.5	1.0	0	0	0	0	0	-

* $R = M/pb^2$, positive for tension inside ring.

$$\frac{1}{2}EI\delta_{rr} = \int_0^{\pi/2} r^2(1-\cos\theta)d\theta + \int_r^{b-r} y\,dy + \int_0^{\pi/2}(b-r+r\sin\theta)r\,d\theta + \int_0^{a/2-r} b\,dx$$

$$= \frac{b^2}{2}\left[(\pi-4)\left(\frac{r}{b}\right) + \frac{a}{b} + 1\right]$$

and

$$\frac{1}{2}EI\delta_{rr} = 2\left[\int_0^{a/2-r} dx + \int_0^{\pi/2} r\,d\theta + \int_r^{b/2} dy\right]$$

$$= b\left[(\pi-4)\left(\frac{r}{b}\right) + \frac{a}{b} + 1\right]$$

Since V_1 is zero and the term of Equation [1] containing it vanishes, it is unnecessary to compute δ_{rp}.

It will be helpful in writing the term δ_{rp}, the rotational displacement at the cut section due to the applied load p, to find first the cantilever moment at any point of the curved segment of the ring (see Fig. 2)

$$dM_\theta = pr^2 d\gamma \sin\gamma(\cos\gamma - \cos\theta) + pr^2 d\gamma\cos\gamma(\sin\theta - \sin\gamma)$$

$$= pr^2(\sin\theta\cos\gamma - \cos\theta\sin\gamma)d\gamma$$

and

$$M_\theta = \int_0^\theta dM_\theta = pr^2[1-\cos\theta]$$

This is the cantilever moment due to the load p and will be recognized as the sum of the moments of the load acting on the vertical and horizontal projections. For example, at $\theta = \pi/2$

$$M_{\pi/2} = pr^2/2 + pr^2/2 = pr^2$$

Now

$$\frac{1}{2}EI\delta_{rp} = \int_0^{a/2-r}\left(\frac{px^2}{2}\right)dx + \int_0^{\pi/2}\left[\frac{p}{2}\left(\frac{a}{2}-r\right)^2 + p\left(\frac{a}{2}-r\right)r\sin\theta + pr^2(1-\cos\theta)\right]rd\theta$$

$$+ \int_r^{b-r}\left[\frac{pa^2}{8} + \frac{py^2}{2}\right]dy + \int_0^{\pi/2}\left[\frac{pa^2}{8} + \frac{p}{2}(b-r)^2 + p(b-r)r\sin\theta - \frac{pa}{2}r(1-\cos\theta) + pr^2(1-\cos\theta)\right]r\,d\theta$$

$$+ \int_0^{a/2-r}\left[\frac{p}{2}\left(\frac{a}{2}-r-x\right)^2 + \frac{p}{2}b^2\right]dx$$

$$= \frac{pb^3}{2}\left\{\left(\frac{r}{b}\right)^3\left(3\pi - \frac{28}{3}\right) + \left(\frac{r}{b}\right)^2\left(\frac{a}{b}-1\right)(3-\pi) + \left(\frac{r}{b}\right)\left(\frac{\pi}{4}-1\right)\left[\left(\frac{a}{b}\right)^2 + 2\right]\right.$$

$$\left. + \frac{1}{12}\left[\left(\frac{a}{b}\right)^3 + 3\left(\frac{a}{b}\right)^2 + 6\left(\frac{a}{b}\right) + 4\right]\right\}$$

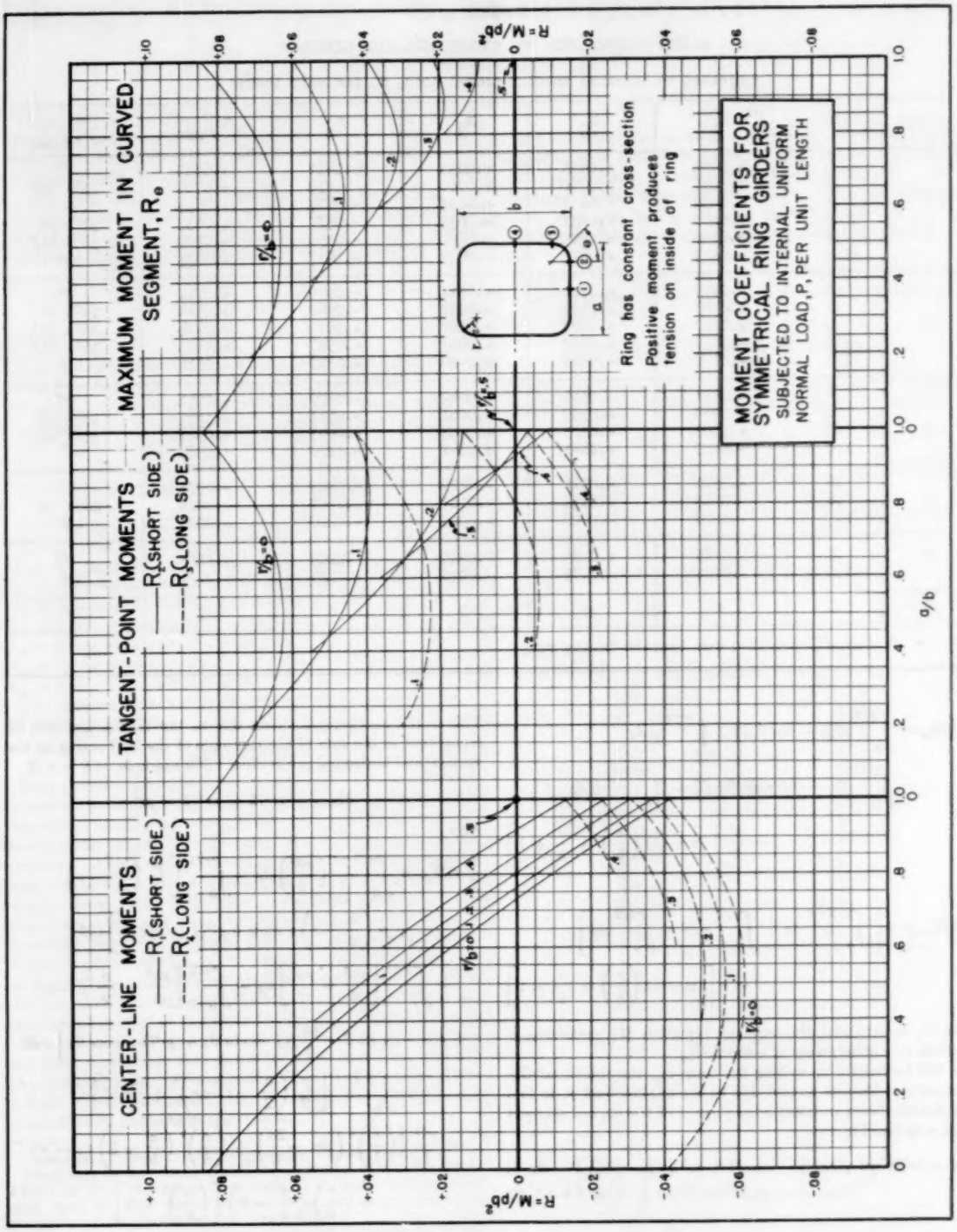
MOMENT COEFFICIENTS FOR SYMMETRICAL RING GIRDERS
SUBJECTED TO INTERNAL UNIFORM NORMAL LOAD, P, PER UNIT LENGTH
Ring has constant cross-section
Positive moment produces tension on inside of ring
MAXIMUM MOMENT IN CURVED SEGMENT, R_o
TANGENT-POINT MOMENTS
R_1 (SHORT SIDE)
R_2 (LONG SIDE)
CENTER-LINE MOMENTS
R_1 (SHORT SIDE)
R_2 (LONG SIDE)
$R = M/pb^2$
θ/b

FIG. 4

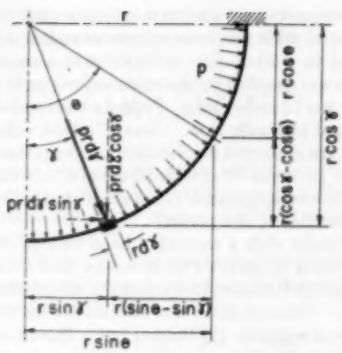

FIG. 2 CURVED CORNER ISOLATED AS CANTILEVER BAR

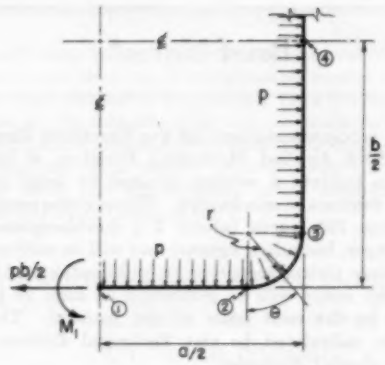

FIG. 3 QUARTER-RING SHOWING SECTIONS OF CRITICAL BENDING MOMENT

Substituting in Equation [1] for δ_{rx}, V_1, δ_{rr}, δ_{rp}

$$M_1 = \frac{-\frac{pb^2}{2}\left\{\left(\frac{r}{b}\right)^3\left(3\pi-\frac{28}{3}\right)+\left(\frac{r}{b}\right)^2\left(\frac{a}{b}-1\right)(3-\pi)+\left(\frac{r}{b}\right)\left(\frac{\pi}{4}-1\right)\left(\frac{a}{b}\right)^2+\frac{1}{12}\left[\left(\frac{a}{b}\right)^3+3\left(\frac{a}{b}\right)^2-2\right]\right\}}{(\pi-4)\frac{r}{b}+\frac{a}{b}+1}$$

$$= R_1 pb^2 \quad \text{or} \quad R_1 = \frac{M_1}{pb^2}$$

(where positive moment produces tension inside of ring).

Note from dimensional requirements (Fig. 1*a*) that if

$$a \le b, \text{ and } \frac{r}{a} \le \frac{1}{2} \ge \frac{r}{b}, \text{ then } \left(\frac{a}{b}\right)_{max} \ge 2\left(\frac{r}{b}\right)$$

Checking some known cases:

1 Circular ring (hoop stress only)

$$r/b = 0.5, \quad a/b = 1, \quad R_1 = 0 \quad \text{checks}$$

2 Square frame with sharp corners

$$r/b = 0, \quad a/b = 1, \quad R_1 = -\frac{1}{24} \quad \text{checks}$$

3 Fixed-ended beam

$$r/b = 0, \quad a/b = 0, \quad R_1 = +\frac{1}{12} \quad \text{checks}$$

With the redundant forces at the origin known, moments at the other critical points 2, 3, 4, and the curved corner may be computed statically as follows with reference to Fig. 3

$$M_2 = M_1 + \frac{p}{2}\left(\frac{a}{2}-r\right)^2$$

$$\therefore R_2 = \frac{M_2}{pb^2} = R_1 + \frac{1}{2}\left[\frac{1}{2}\left(\frac{a}{b}\right)-\frac{r}{b}\right]^2$$

$$M_3 = M_1 + \frac{pa^2}{8} + \frac{pr^2}{2} - \frac{pb}{2}r$$

$$\therefore R_3 = \frac{M_3}{pb^2} = R_1 + \frac{1}{2}\left[\frac{1}{4}\left(\frac{a}{b}\right)^2 + \left(\frac{r}{b}\right)^2 - \frac{r}{b}\right]$$

$$M_4 = M_1 + \frac{pa^2}{8} + \frac{pb^2}{8} - \frac{pb^2}{4}$$

$$\therefore R_4 = \frac{M_4}{pb^2} = R_1 + \frac{1}{8}\left[\left(\frac{a}{b}\right)^2 - 1\right]$$

$$M_\theta = M_1 + \frac{p}{2}\left(\frac{a}{2}-r\right)^2 + p\left(\frac{a}{2}-r\right)r\sin\theta - \frac{pb}{2}r(1-\cos\theta) + pr^2(1-\cos\theta)$$

$$\therefore R_\theta = \frac{M_\theta}{pb^2} = R_1 + \frac{1}{2}\left[\frac{(a/b)}{2}-r/b\right]^2 + \left[\frac{a/b}{2}-r/b\right](r\sin\theta)/b + \left[(r/b)^2-\frac{r/b}{2}\right](1-\cos\theta)$$

To find the angle θ at which maximum M_θ occurs, let

$$\frac{dM_\theta}{d\theta} = 0 = p\left(\frac{a}{2}-r\right)r\cos\theta - \frac{pb}{2}r\sin\theta + pr^2\sin\theta$$

whence

$$\theta = \tan^{-1}\left(\frac{a/b-2r/b}{1-2r/b}\right)$$

Brief Notes*

On the recommendations of the Executive Committee of the ASME Applied Mechanics Division, it has been decided to initiate a section devoted to brief notes on technical matters in mechanics. These notes must not be longer than 750 words (about 2½ double-spaced typewritten pages, including figures) and will be subject to the usual review procedure prior to publication. After approval such notes will be published as soon as possible, normally in the next issue of the Journal. The notes should be submitted to the Technical Editors of the *Journal of Applied Mechanics*.

Compressibility of a Sphere Pack—Comparison of Theory and Experiment

By I. FATT,[1] LA HABRA, CALIF.

BRANDT[2] has used Herta's theory[3] of the deformation of isotropic spheres in contact to derive a relation between the pressure applied to a sphere pack and the change in bulk and void volume. As part of a study of the compressibility of sedimentary rock, Brandt's equations have been tested experimentally.

Brandt's equations for the bulk volume and void volume of a sphere pack as a function of applied pressure are

$$V_{\text{bulk}} = \frac{4\pi NR^3}{3(1-\alpha)} - \frac{4\pi NR^3}{1-\alpha}\left(\frac{1.75(1-\delta^2)}{EC_\psi}\right)^{2/3} P^{2/3} \quad [1]$$

$$V_{\text{void}} = \frac{4\pi\alpha NR^3}{3(1-\alpha)} - \frac{4\pi NR^3}{1-\alpha}\left(\frac{1.75(1-\delta^2)}{EC_\psi}\right)^{2/3} P^{2/3} \quad [2]$$

where

- C_ψ = porosity factor = unity for pack of uniform size spheres
- E = modulus of elasticity of spheres
- N = number of spheres
- P = pressure on outside of enclosed sphere pack
- R = radius of spheres
- α = porosity = void volume per unit volume of sphere pack
- δ = Poisson's ratio of spheres

Three sphere packs were used to test these equations. The first was composed of 4000 neoprene spheres of radius 0.309 in. randomly packed in a 10-in-diam cylinder with a movable piston. The neoprene was specified by the manufacturer as 40 to 50 Shore. The cylinder was 10 inches long. Pressure was applied to the piston by means of hydraulic ram. Change in bulk volume was calculated from the measured displacement of the piston. The void volume of the pack was filled with kerosene which was displaced, when the pack was compressed, into a graduated cylinder through a tubing connection in the piston.

A rigid cylinder with a movable piston instead of a chamber with flexible walls (Brandt's Fig. 3) can be used if the stress applied by the piston is transmitted equally in all directions throughout the pack. This condition was fulfilled for the rubber sphere pack for several reasons: (1) Rubber has a Poisson ratio of 0.49. (2) There was no shear stress on the walls because (*a*) the spheres made only point contact on the walls, (*b*) the walls were of highly polished plastic, (*c*) the pack was filled with kerosene which acted as a lubricant, and (*d*) the cylinder length and diameter were equal. Visual observation showed that the spheres were distorted by the same amount at top and bottom of the pack during compression.

This sphere pack was used to test Brandt's equations and also his assumption that compression of the pack caused no change in volume of the spheres. The change in bulk volume should then be equal to the change in void volume. Void volume of the compressed pack was measured as a function of bulk volume from zero compression to a bulk volume 87.5 per cent of the original bulk volume. In this range the change in void volume was equal to the change in bulk volume.

The linear relation between bulk volume and $P^{2/3}$ shown in Fig. 1 is in agreement with Brandt's equation. The equation of the data of Fig. 1 is

$$V_{\text{bulk}} = 1.35 \times 10^4 - 230P^{2/3} \quad [3]$$

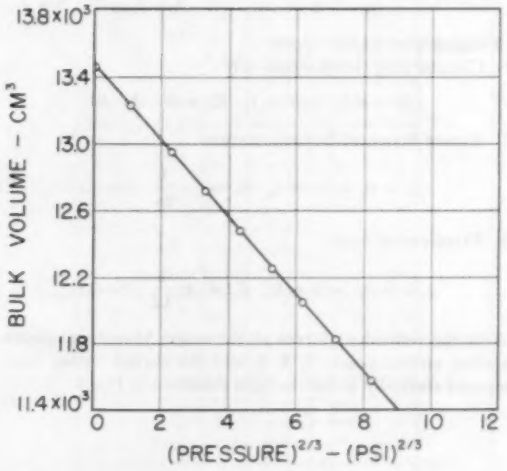

FIG. 1 BULK VOLUME OF SPHERE PACK AS A FUNCTION OF PRESSURE

Void volume as a function of pressure was similarly found to be

$$V_{\text{void}} = 5.015 \times 10^3 - 230P^{2/3} \quad [4]$$

The experimental data can be compared to theory if the modulus of elasticity and Poisson's ratio for the neoprene are known. Timoshenko and Goodier[3] show that the term $(1-\delta^2)/E$ can be

[1] Senior Research Chemist, California Research Corporation, a subsidiary of Standard Oil Company of California.

[2] "A Study of the Speed of Sound in Porous Granular Media," by H. Brandt, JOURNAL OF APPLIED MECHANICS, Trans. ASME, vol. 77, 1955, pp. 479–486.

[3] "Theory of Elasticity," by S. Timoshenko and J. H. Goodier, McGraw-Hill Book Company, Inc., New York, N. Y., 1951, pp. 372–377.

Presented at the West Coast Conference of the Applied Mechanics Division, Pasadena, Calif., June 11–16, 1956, of THE AMERICAN SOCIETY OF MECHANICAL ENGINEERS.

* Discussion of papers in Brief Notes should be addressed to the Secretary, ASME, 29 West 39th Street, New York, N. Y., and will be accepted until April 10, 1957, for publication at a later date. Discussion received after the closing date will be returned.

NOTE: Statements and opinions advanced in papers are to be understood as individual expressions of their authors and not those of the Society. Manuscript received by Applied Mechanics Division, December 13, 1955.

obtained directly from the deformation of a sphere between two blocks under a compressive force. For a neoprene sphere between steel blocks the relation is

$$\frac{1 - \delta^2}{E} = \frac{4}{3}\frac{R^{1/2}D^{3/2}}{F} \quad [5]$$

where D is the displacement under compressive force F and the other terms are as in Equations [1] and [2]. For the neoprene spheres used in the sphere pack, $(1 - \delta^2)/E$ was experimentally found to be 1.86×10^{-4} psi^{-1}.

Equations [1] and [2] can now be used to predict the relation between volume and pressure according to Brandt's theory. The predicted relations are

$$V_{\text{bulk}} = 1.28 \times 10^4 - 182P^{3/2} \quad [6]$$

$$V_{\text{void}} = 4.76 \times 10^3 - 182P^{3/2} \quad [7]$$

A comparison of Equations [6] and [7] with Equations [3] and [4] shows that Brandt's theory predicts the bulk and void volume within 5 per cent and the slope of the void volume versus $P^{3/2}$ line within 20 per cent.

The second sphere pack was composed of 1234 of the same neoprene spheres randomly packed into a thin-walled (about $^1/_{16}$ in. thick) polyethylene bottle 5.75 in. in diam and 10 in. long. The walls of the bottle were formed around the pack by immersing the evacuated bottle in boiling water for 10 minutes. The evacuated bottle was then chilled in ice water. The bottle was then placed into an oil tank in which the oil pressure could be raised as desired. The liquid produced from the compressed sphere pack was brought out of the bottle through a tubing fitting in the cap. This tubing led out of the oil-pressure tank so that the liquid produced from the compressed pack could be collected in a graduated cylinder. The change in bulk volume could not be measured.

The predicted relation of void volume to pressure for this pack of neoprene spheres is

$$V_{\text{void}} = 1425 - 55.8P^{3/2} \quad [8]$$

The observed relation in the range 0 to 50 psig was

$$V_{\text{void}} = 1560 - 60.5P^{3/2} \quad [9]$$

The third sphere pack was composed of 1500 high carbon chrome-steel spheres randomly packed into a thin-walled ($^1/_{16}$ in.) copper cylinder six in. in diam and eight in. long. The lid was silver-soldered onto the cylinder after the spheres were packed into it. A length of $^1/_4$-in-diam copper tubing was soldered into the lid.

The steel spheres were 0.297 in. in radius. The Poisson ratio and the modulus of elasticity were taken[4] as 0.275 and 30×10^6 psi, respectively.

The pack of steel spheres in the copper cylinder was compressed in the same way as just described for the rubber spheres in the polyethylene bottle. In the case of the copper cylinder an initial compression to 3000 psi was required to form the copper around the pack. After the initial forming the sphere pack produced and imbibed water completely reversibly when pressure was increased and then decreased.

The predicted relation of void volume to pressure for the steel sphere pack is

$$V_{\text{void}} = 1350 - 0.174P^{3/2} \quad [10]$$

The observed relation in the range 0 to 3000 psig was

$$V_{\text{void}} = 1420 - 0.242P^{3/2} \quad [11]$$

The difference between predicted and observed bulk and void volume at zero compression is attributable to edge effects. In a cylinder with diameter and length only 10 to 16 times the sphere diameter, the discontinuity at the wall can introduce the observed 5 per cent error. The error in the slope of the volume versus $P^{3/2}$ line is more difficult to explain. Part of the error is attributable to edge effects and part probably to the assumptions in the derivation of Brandt's equations.

[4] "Handbook of Physical Constants," Geological Society of America, Special Paper No. 36, 1942, p. 71.

Nonuniform Rim-Stress Conditions for a Rotating Solid of Uniform Stress

By L. V. KLINE,[1] HUNTSVILLE, ALA.

WHEN considering the rotating uniform-stress disk-and-rim combination as an energy-storage device, it may not be satisfactory to assume that a condition of uniform stress exists over the cross section of the rim. The following analysis permits the rim stresses to be nonuniformly distributed. It is shown that for any disk design it is possible to select a rim which will satisfy the conditions of uniform disk stress for all angular velocities. An explicit solution for the rim-radius ratio is given as a function of disk dimensions. Curves are presented showing the error which results from using the uniform rim-stress assumption.

By definition of a uniform-stress disk[2]

$$S_r = S_t = \frac{\rho\omega^2 r_1^2}{2 \ln \frac{x_1}{x_2}} \quad [1]$$

where

S_r = radial disk stress
S_t = tangential disk stress
ρ = density of the material
ω = angular velocity
r_1 = maximum disk radius (minimum rim radius)
x_1 = maximum axial disk width
x_2 = minimum axial disk width

A boundary condition which must be satisfied for the disk is that the radial stress at $r = r_1$ be given by Equation [1]. This condition can be satisfied by attaching a rim to the uniform-stress disk. The necessary dimensions of the rim are found by the following analysis:

Treating the problem as one of plane stress, the displacement of the outside radius of the disk is found from Hooke's law to be

$$\delta_d = \frac{r_1 S_r(1 - \mu)}{E} \quad [2]$$

where μ and E are the elastic constants of the material.

The displacement of the inside radius of the rim δ_r can be considered as the resultant of the displacement δ_m due to the centrifugal effect, and the displacement δ_{rp} due to the pull of the disk on the rim. If it is assumed that the displacement δ_{rp} is the same as

[1] Research Engineer, Research Laboratories, Research and Development Division, Ordnance Missile Laboratories, Redstone Arsenal. At present, Assistant Professor of Engineering Sciences, Purdue University, Lafayette, Ind.

[2] "Fundamentals of Machine Design," by C. A. Norman, E. S. Ault, and I. F. Zarobsky, The Macmillan Company, New York, N. Y., 1938, p. 287.

Manuscript received by ASME Applied Mechanics Division, July 12, 1956.

would be produced by an equivalent stress S_d/C, then this displacement[3] is given by

$$\delta_{rp} = -\frac{S_r r_1}{CE}\left[\frac{r_3^2 + r_2^2}{r_3^2 - r_1^2} + \mu\right] \quad [3]$$

where r_3 is the outside-rim radius. The parameter C must be an appropriate function of the axial rim width b and the disk width x_2. For this analysis it is assumed that $C = b/x_2$.

The displacement of the inside radius of the rim due to centrifugal force is given[4] by

$$\delta_{rs} = \frac{\rho\omega^2(1-\mu^2)}{8E}\left\{\frac{(3+\mu)(r_3^3 + r_1 r_2^2)}{(1+\mu)} - r_1^3 + \frac{(3+\mu)r_1 r_2^2}{(1-\mu)}\right\} \quad [4]$$

Eliminating ω from Equation [4] by using Equation [1], and using Equations [2], [3], and [4] to write the continuity relation

$$\delta_d = \delta_r = \delta_{rs} + \delta_{rp} \quad [5]$$

gives a relationship between rim dimensions and disk dimensions which can be solved easily for

$$\ln x_1/x_2 = f(r_1, r_2, C, \mu)$$

The explicit solution for a rim dimension function requires algebraic manipulation. This can best be done by letting

$$\gamma = r_2/r_1 \quad [6]$$

It can then be shown that

$$\gamma^4 - \varphi\gamma^2 + \theta = 0 \quad [7]$$

where

$$\varphi = \frac{2}{3+\mu}\left[1 + \mu + \frac{\mu+1}{C\ln\dfrac{x_1}{x_2}} + \frac{1-\mu}{\ln\dfrac{x_1}{x_2}}\right] \quad [8]$$

and

$$\theta = \frac{\mu-1}{3+\mu}\left[\frac{2\left(\dfrac{1}{C}-1\right)}{\ln\dfrac{x_1}{x_2}} + 1\right] \quad [9]$$

Solving Equation [7] for γ and eliminating those signs which have no physical significance give

$$\gamma = \left\{\frac{\varphi}{2} + \left[\left(\frac{\varphi}{2}\right)^2 - \theta\right]^{1/2}\right\}^{1/2} \quad [10]$$

Equation [10] is an expression for rim dimensions which is independent of angular velocity. For any combination of x_1/x_2 and r_1 (any given disk design), a combination of C and r_2 (rim design) can be selected which will satisfy Equation [10]. It follows that this rim design will insure that conditions of uniform stress will exist in the disk for all operating angular velocities.

The assumption of uniform stress over the rim cross section leads to

$$\ln\frac{x_1}{x_2} = \frac{3}{2(\gamma^3 - 1)}\left[\frac{1}{C} + \gamma - 1\right] \quad [11]$$

as the expression for γ which must be satisfied to insure uniform stress in the disk.

[3] "Strength of Materials," by S. Timoshenko, D. Van Nostrand Company, Inc., New York, N. Y., vol. 2, 1941, p. 241.

[4] Ibid., pp. 245–246.

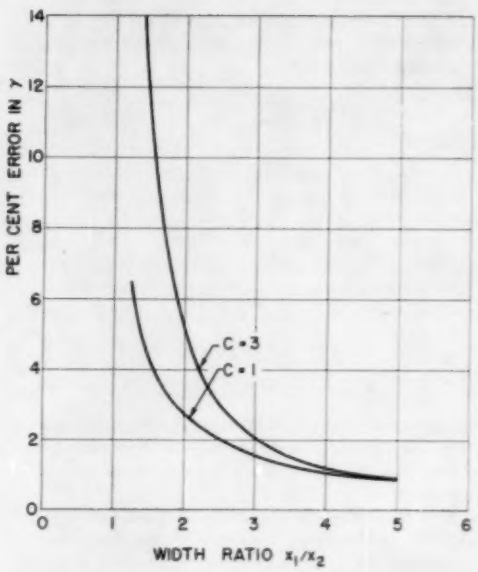

FIG. 1 ERROR IN γ FOR GIVEN x_1/x_2

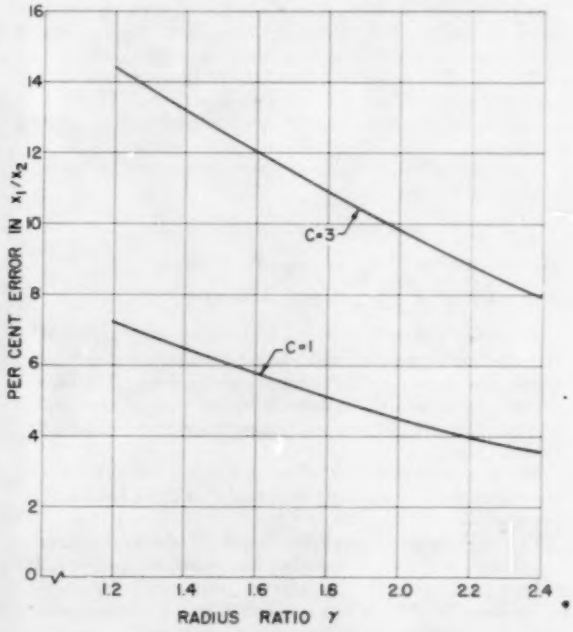

FIG. 2 ERROR IN x_1/x_2 FOR GIVEN γ

Fig. 1 shows the percentage error which results from using the approximation to select a rim when the disk-width ratio is given. Fig. 2 shows the percentage error which results in disk-width ratio when the rim-thickness ratio is given. The curves reveal that the error resulting from the approximation is less than 10 per cent for most of the design region. The permissible design error and the particular values of the design parameters will control whether or not the approximation can be used.

Note on Way's Large-Deflection Solution for the Uniformly Loaded and Clamped Circular Plate

By H. D. CONWAY,[1] ITHACA, N. Y.

EXACT solutions to the so-called "large-deflection" equations of plate theory are rare, one of the few being that of Way[2] for a uniformly loaded and clamped circular plate. As a result of bending, the radius of the edge tends to decrease and, as radial movement is prevented, the plate is subjected to radial tension. The question then arises as to whether the divergence of Way's results from the small-deflection solution is due mainly to induced radial tension or to using a large-deflection theory. It was the object of the present investigation to settle this point.

The linear theory of axially symmetrical plate bending gives

$$r^2\phi'' + r\phi' - \phi = -Qr^2/D \quad \ldots\ldots [1]$$

where ϕ is the slope at radius r. The shearing force Q is related to the radial tension N per unit circumferential length and uniformly distributed load q by

$$Q = qr/2 - N\phi$$

whence, after writing $N/D = \alpha^2$, the differential equation becomes

$$r^2\phi'' + r\phi' - (1 + \alpha^2r^2)\phi = -qr^3/2D \quad \ldots\ldots [2]$$

If N is assumed constant at all radii, α^2 is a constant and the general solution is

$$\phi = AI_1(\alpha r) + BK_1(\alpha r) + qr/2D\alpha^2 \quad \ldots\ldots [3]$$

where I_1 and K_1 are modified Bessel functions of the first order. For a solid plate K_1 becomes infinitely large at the center and hence B must be zero. The condition of zero slope at $r = a$ gives A and hence

$$\phi = dw/dr = \frac{-qa}{2D\alpha^2}\left[\frac{I_1(\alpha r)}{I_1(\alpha a)} - \frac{r}{a}\right] \quad \ldots\ldots [4]$$

Integrating this gives

$$\frac{w_{max}}{w_0} = \frac{32}{\alpha^2a^2}\left[\frac{1 - I_0(\alpha a)}{I_1(\alpha a)} + \frac{\alpha a}{2}\right] \quad \ldots\ldots [5]$$

where $w_0 = qa^4/64D$ is the maximum deflection for zero N. The maximum bending stress σ_e at the edge is

$$\frac{\sigma_e}{\sigma_e'} = \frac{4}{\alpha a}\frac{I_2(\alpha a)}{I_1(\alpha a)} \quad \ldots\ldots [6]$$

where $\sigma_e' = 3qa^2/4h^2$ is the bending stress at the edge for zero N. The radial bending stress σ_c at the center is given by

$$\frac{\sigma_c}{\sigma_c'} = \frac{8}{\alpha^2a^2}\left[1 - \frac{\alpha a}{2I_1(\alpha a)}\right] \quad \ldots\ldots [7]$$

where

$$\sigma_c' = \frac{3qa^2}{8}(1 + \nu)$$

is the bending stress at the center for zero N. Since the radius of the plate is invariant

$$\frac{1}{2}\int_0^a \phi^2 dr = \frac{Na}{Eh}(1 - \nu) \quad \ldots\ldots [8]$$

Hence from Equation [4] and after some simplification

$$\int_0^{\alpha a}\left[\alpha^2a^2\frac{I_1^2(\alpha r)}{I_1^2(\alpha a)} - 2\alpha^2 ar\frac{I_1(\alpha r)}{I_1(\alpha a)} + \alpha^2r^2\right]d(\alpha r) = \frac{\alpha^5a^9}{216(1 - \nu^2)^2(1 + \nu)}\left(\frac{Eh^4}{qa^4}\right)^2 \quad \ldots [9]$$

Integrating by parts, we may write

$$\int_0^{\alpha a}\alpha r I_1(\alpha r)d(\alpha r) = \alpha a I_0(\alpha a) - \int_0^{\alpha a} I_0(\alpha r)d(\alpha r)$$

The second integral, on the right-hand side of this equation, has been tabulated by Müller[3] and by Rothman.[4] The integral

$$\int_0^{\alpha a} I_1^2(\alpha r)d(\alpha r)$$

has not been tabulated but it is quite easy to show that it may be written in the series form

$$\sum_{z=0}^{z=\infty}\frac{(2 + 2z)!\left(\frac{1}{2}\right)^{2+2z}(\alpha a)^{3+2z}}{(3 + 2z)z!(2 + z)!(1 + z)!(1 + z)!}$$

which is sufficiently rapidly convergent for the values of αa necessary to compare with Way's calculations; that is, up to $\alpha a = 4$. The convergence of the series becomes increasingly slower with increase of αa, thus making calculations increasingly more laborious. It is probable that Way's method of solution will also present computational difficulties of this kind beyond this range.

Values of $\alpha a = 2$, 3, and 4 were selected and, assuming that $\nu = 0.3$, qa^4/Eh^4 was calculated from Equation [9] and the corresponding maximum deflection and stresses calculated from

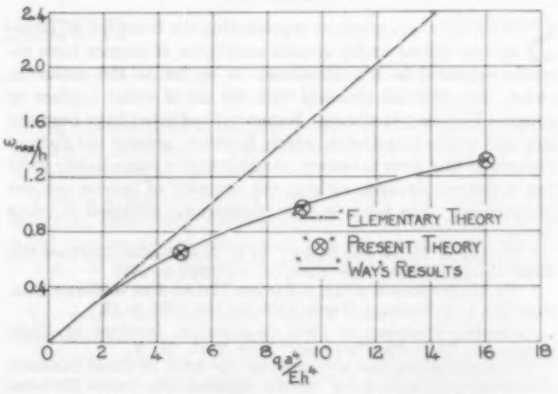

FIG. 1 DEFLECTION-LOAD CURVES FOR CIRCULAR PLATE

[1] Professor of Mechanics, Cornell University.

[2] "Bending of Circular Plates with Large Deflection," by S. Way, Trans. ASME, vol. 56, 1934, p. 627.

Manuscript received by ASME Applied Mechanics Division, July 25, 1956.

[3] "Über die zahlenmässige Beherrschung und Anwendung einiger den Besselschen verwandten Funktionen nebst Bemerkungen zum Gebiet des Bessel-funktionen," by R. Müller, *Zeitschrift für angewandte Mathematik und Mechanik*, vol. 19, 1939, p. 36.

[4] "Table of $\int_0^x I_0(x)dx$ for 0(0.1)20(1)25," by M. Rothman, *Quarterly Journal of Mechanics and Applied Mathematics*, vol. 2, 1949, p. 212.

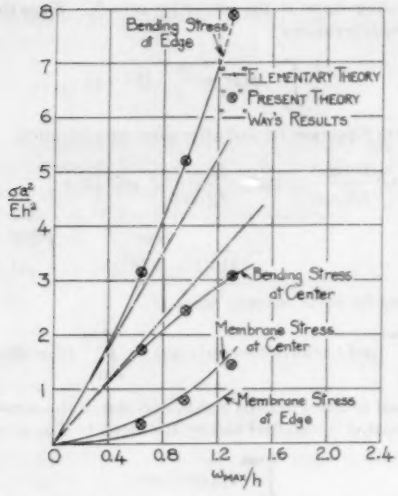

FIG. 2 STRESS-DEFLECTION CURVES FOR CIRCULAR PLATE

Equations [5], [6], and [7]. Figs. 1 and 2 show that the results are almost identical with Way's over the range of w_{max}/h considered and hence that the large-deflection terms have little effect in this range. It is likely that the same is true for the clamped square plate, which also has been discussed by Way.[5] However, a solution similar to the foregoing would be difficult to obtain in this case.

After completing the foregoing calculations, the author discovered that an investigation along similar lines was published in 1902 by I. G. Boobnov.[6] Unfortunately, Boobnov's paper contains errors which invalidate his results. Because of an incorrect definition of the equivalent of αa, the series used to evaluate the Bessel function integrals have insufficient terms and, additionally, $(1 - \nu)$ in the right-hand side of Equation [8] is omitted.

On the Use of Sine Transforms in Timoshenko-Beam Impact Problems

BY BRUNO A. BOLEY,[1] NEW YORK, N. Y.

INTRODUCTION

SEVERAL exact solutions representing the behavior of Timoshenko beams under various conditions of impact have recently appeared in the literature; in so far as the author is aware, they were all obtained with the aid of either Laplace or complex Fourier transforms. Somewhat neglected have been the sine and cosine transforms, which, however, present the distinct advantage that their inversion integrals can be immediately written in the real domain, without the necessity of tedious contour integrations. The result is then immediately obtained in terms of definite integrals which are usually evaluated numerically. This evaluation is often very difficult because of the unavoidable oscillations of the integrands; it is the purpose of this note to show that this disadvantage of the sine transform is not serious in this problem. To this end a known exact solution for a Timoshenko-beam impact problem is compared with one obtained with the aid of sine and cosine transforms; the exact solution chosen is that for a semi-infinite beam, whose end $x = 0$ is subjected to a step moment M_0, and is not allowed to displace.[8] It will be seen that no serious numerical difficulties arise and that, in fact, the integrals encountered here are no more difficult than those arising in a Laplace transform solution. The sine transform approach, when applicable, seems therefore definitely more advantageous.

SOLUTION

The Timoshenko beam equations for the deflection y and the rotation ψ due to bending may be written as

$$\left.\begin{aligned} \psi'' + (1/\gamma)(y_1' - \psi) - \ddot{\psi} = 0 \\ (1/\gamma)(y_1'' - \psi') - \ddot{y}_1 = 0 \end{aligned}\right\} \quad \ldots\ldots [1]$$

with the following nondimensional notation

$$y_1 = (y/r);\ \gamma = E/(k'G) \quad \ldots\ldots [1a]$$

and where primes and dots indicate differentiation with respect to the nondimensional variables

$$x_1 = x/r;\ t_1 = tc_1/r \quad \ldots\ldots [1b]$$

respectively. Here r is the radius of gyration of the beam cross section, k' the shear correction coefficient, c_1 the velocity of propagation of longitudinal waves, E and G the Young and shear moduli, respectively.

Let now

$$\left.\begin{aligned} Y(p, t_1) &= \left[\frac{2}{\pi}\right]^{1/2} \int_0^\infty y_1(x_1, t_1) \sin px_1 dx_1 \\ \Psi(p, t_1) &= \left[\frac{2}{\pi}\right]^{1/2} \int_0^\infty \psi(x_1, t_1) \cos px_1 dx_1 \end{aligned}\right\} \quad \ldots [2]$$

Multiplication of the first of Equations [1] by $\cos px_1$, of the second by $\sin px_1$, subsequent integration with respect to x_1 from 0 to ∞, and use of integration by parts gives the following result

$$\left.\begin{aligned} \Psi'' + \left(p^2 + \frac{1}{\gamma}\right)\Psi - \frac{p}{\gamma} Y &= \\ &- \left[\frac{2}{\pi}\right]^{1/2} \frac{M_0 r}{EI} = m_0 \\ Y'' + \frac{p^2}{\gamma} Y - \frac{p}{\gamma}\Psi &= 0 \end{aligned}\right\} \quad \ldots [3]$$

where the end conditions

$$y_1(0, t_1) = 0;\ \ \Psi'(0, t_1) = \frac{M_0 r}{EI} \quad \ldots\ldots [3a]$$

have been used. The solution of Equations [3], satisfying the initial conditions that

---

[4] "Theory of Plates and Shells," by S. Timoshenko, McGraw-Hill Book Company, Inc., New York, N. Y., 1940, p. 347.

[5] "On the Stresses in a Ship's Bottom Plating Due to Water Pressure," by I. G. Boobnov, Trans. INA, vol. 44, 1902, p. 15.

[1] Associate Professor of Civil Engineering, Institute of Flight Structures, Columbia University, New York, N. Y.

This investigation was supported by the Office of Naval Research.
Manuscript received by ASME Applied Mechanics Division, July 11, 1956

[8] This is Problem II of "Some Solutions of the Timoshenko-Beam Equations" by Bruno A. Boley and Chi-Chang Chao, JOURNAL OF APPLIED MECHANICS, Trans. ASME, vol. 77, Dec., 1955, pp. 579–586. It was solved there by means of Laplace transforms with respect to the time variable.

$$Y(p, 0) = \Psi(p, 0) = \dot{Y}(p, 0) = \dot{\Psi}(p, 0) = 0 \ldots [3b]$$

is easily found to be

$$\left.\begin{aligned} Y(p, t_1) &= \frac{m_0}{p^3}\left[1 + \frac{\lambda_2^2 \cos \lambda_1 t_1 - \lambda_1^2 \cos \lambda_2 t_1}{\lambda_1^2 - \lambda_2^2}\right] \\ \Psi(p, t_1) &= \frac{m_0}{p^3}\left[p + \right. \\ &\left. \frac{\lambda_2^2(p^2 - \lambda_1^2\gamma) \cos \lambda_1 t_1 - \lambda_1^2(p^2 - \lambda_2^2\gamma) \cos \lambda_2 t_1}{p(\lambda_1^2 - \lambda_2^2)}\right] \\ &= \frac{m_0}{p}\left[\frac{1}{p} + F(p, t_1)\right] \end{aligned}\right\} \ldots [4]$$

where

$$2\gamma\lambda_{1,2}^2 = p^2(1 + \gamma) + 1 \mp \{[p^2(\gamma - 1) + 1]^2 + 4p^2\}^{1/2} \ldots [4a]$$

The sine transform of the bending moment parameter (Mr/EI) is equal to $(-p\Psi)$; therefore the bending moment is given by

$$(Mr/EI) = \left[\frac{2}{\pi}\right]^{1/2} \int_0^\infty (-p\Psi) \sin px_1 dp \ldots\ldots [5]$$

Numerical Evaluation of the Bending Moment

With the aid of the second Equations [4], the moment of Equation [5] may be written in the convenient form

$$\frac{M(x_1, t_1)}{M_0} = \frac{2}{\pi}\int_0^\infty \frac{1 - \cos pt_1}{p} \sin px_1 dp - \frac{2}{\pi}\int_0^\infty \left[F(p, t_1) - \frac{\cos pt_1}{p}\right] \sin px_1 dp \ldots\ldots [5a]$$

The first term of the right-hand side of Equation [5a] is

$$\frac{2}{\pi}\int_0^\infty \frac{1 - \cos pt_1}{p} \sin px_1\, dp = \left\{\begin{array}{lll} 1 & \text{for} & t_1 > x_1 \\ 1/2 & \text{for} & t_1 = x_1 \\ 0 & \text{for} & t_1 < x_1 \end{array}\right\} \ldots [6]$$

and therefore represents the bending-moment propagation with a velocity c_1. The second term must be evaluated numerically; this was done in the following way. The function $F(p, t_1)$ may be expanded in powers of $(1/p)$ as follows

$$F(p, t_1) = \frac{\cos pt_1}{p} - \frac{t_1 \sin pt_1}{2p^2(\gamma - 1)} + \frac{1}{p^3(\gamma - 1)^2}\left[\gamma \cos \frac{pt_1}{\sqrt{\gamma}} - \left(\gamma + \frac{t_1^2}{8}\right)\cos pt_1\right] + \ldots\ldots [7]$$

For a value of p (say, p_0) sufficiently large, the relation

$$\int_0^\infty \left[F(p, t_1) - \frac{\cos pt_1}{p}\right] \sin px_1 dp = \int_0^{p_0} \left[F(p, t_1) - \frac{\cos pt_1}{p}\right] \sin px_1 dp - \frac{t_1}{2(\gamma - 1)}\int_{p_0}^\infty \frac{\sin pt_1 \sin px_1 dp}{p^2} \ldots\ldots [7a]$$

holds therefore in good approximation. The second integral on the right-hand side may be expressed in terms of the tabulated sine integral

$$Si(x) = \int_0^x (1/x) \sin x dx \ldots\ldots [7b]$$

as follows

$$\int_{p_0}^\infty \frac{\sin pt_1 \sin px_1}{p^2} dp = \frac{\cos p_0(t_1 + x_1) - \cos p_0(t_1 - x_1)}{2p_0} + \left(\frac{t_1 + x_1}{2}\right)\left[\frac{\pi}{2} - Si[p_0(t_1 + x_1)]\right] \mp \left(\frac{t_1 - x_1}{2}\right)\left[\frac{\pi}{2} - Si[p_0|t_1 - x_1|]\right] \ldots\ldots [7c]$$

The minus sign is to be used if $t_1 > x_1$, and the plus sign if $t_1 < x_1$.

The numerical evaluation of the first integral on the right-hand side of Equation [7a] was performed with the aid of Simpson's rule, with $p_0 = 5$ and the relatively coarse interval $\Delta p = 1/4$. The results obtained in this manner for the case of $t_1 = 5$ agreed with the previous ones within 1.5 per cent of the latter for all values of x_1. A check on the accuracy of the calculations may also be obtained by evaluating the bending moment for a value of $x_1 > t_1$ and comparing the result with the known value (i.e., zero). In this case, for $x_1 = 6$, the value $(M/M_0) = -0.002$ was obtained.

Discussion

Stiffness of Curved Circular Tubes With Internal Pressure[1]

E. C. Rodabaugh[2] and H. H. George.[3] The authors' valuable theoretical development and experimental confirmation of the effect of internal pressure on the flexibility and stresses in curved pipe subjected to in-plane bending moments are significant not only in aeronautical applications but also in many thin-wall industrial-piping applications.

Tests of a pipeline welding elbow of 30-in OD, 0.500-in. wall thickness, 45-in. bend radius conducted by the writers give additional confirmation to this theory, as is shown by the test results in Fig. 1 of this discussion. A significant reduction in flexibility and stress-intensification factors occurs in this elbow.

The writers have developed a similar theory which covers both in-plane and out-of-plane bending. By neglecting some of the less significant factors included in the paper, much simpler equations can be obtained which can be carried to higher-order approximations with relative ease; however, we would confirm the state-

[1] By P. G. Kafka and M. B. Dunn, published in the June, 1956, issue of the Journal of Applied Mechanics, Trans. ASME, vol. 78, pp. 247–254.

[2] Senior Research Engineer, Tube Turns, A Division of National Cylinder Gas, Louisville, Ky.

[3] Manager of Research Section, Tube Turns, A Division of National Cylinder Gas, Louisville, Ky.

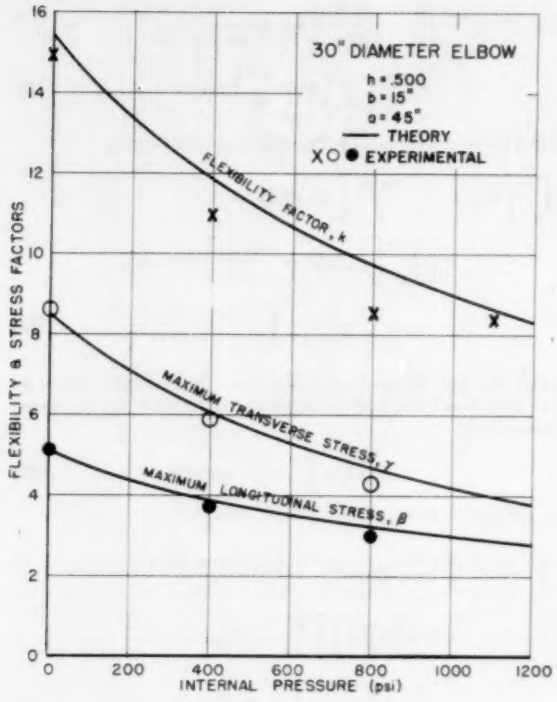

FIG. 1

ment that little gain in accuracy is achieved by using a higher-order approximation for the flexibility or longitudinal stress factor. The writers have applied their theory using a fourth-order approximation and obtained about the same results as those given in the paper. The series equations for the circumferential stress factor, on the other hand, converges less rapidly, and a fourth-order approximation gives markedly different results than a second-order approximation, as applied to the curved pipe tested by the authors.

It should be pointed out that where the stress-intensification factors are higher than about 2, the transverse stress factor is greater than the longitudinal stress factor; for small values of the parameter ha/b^2 at zero pressure the transverse-stress factor is double the longitudinal-stress factor. That the transverse stress is usually dominant is shown by the in-plane bending-fatigue tests reported by Markl.[4] Failure in fatigue consisted of longitudinal cracks along each side of the curved pipe ($\phi = 0$ or $\phi = 180$ deg). Fig. 2, herewith, shows the data from Fig. 5 of the paper along with the calculated transverse-stress factors using a fourth approximation. The zero pressure point on this curve is, of course, the same as that obtainable by a number of calculation methods such as those given by Gross (4), Beskin (7), or Clark and Reissner (9).[5] It would be of interest to know if the experimental transverse stresses measured by the authors would fall along this line.

AUTHORS' CLOSURE

The theoretical and experimental results submitted by Messrs. Rodabaugh and George appear to confirm the trend shown in the paper, namely, that the theory somewhat overestimates the flexibility factor, and that the error decreases with increasing pressure. That the transverse stress factor γ should require a higher-order approximation is not surprising because it is expressed in

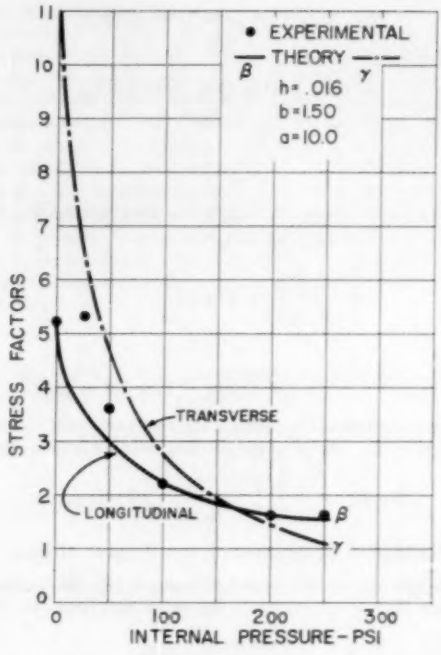

FIG. 2

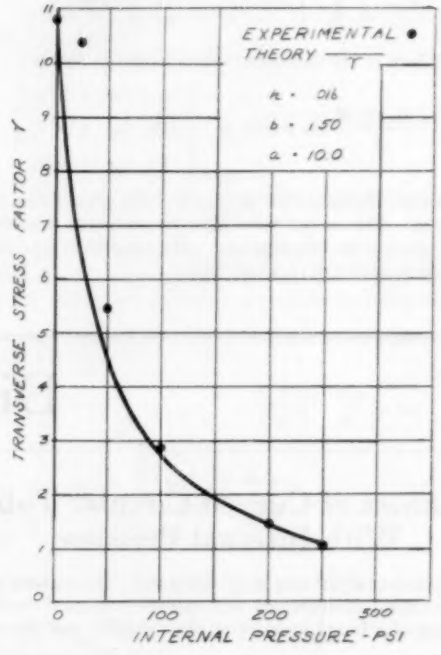

FIG. 3

[4] "Fatigue Tests on Piping Components," by A. R. C. Markl, Trans. ASME, vol. 74, 1952, pp. 287–303.

[5] Reference numbers in parentheses refer to the authors' Bibliography published with their paper.

terms of $(d^2v)/(d\varphi^2)$, whereas β, having neglected the quantity $(6M_\theta)/h^2$, is expressed in terms of $(dv)/d\varphi$. It is well known that if $\bar{v}$ is an approximate representation of a given function v, the discrepancy between the nth derivatives $\bar{v}^{(n)}$ and $v^{(n)}$ in general becomes larger with increasing n.

The graph (Fig. 3 herewith) shows how the authors' experimental values for γ match the Rodabaugh-George theoretical curve. The distribution and direction of the errors are very similar to those obtained for β, for the same tube.

The authors wish to thank Messrs. Rodabaugh and George for their valuable discussion.

Analysis of Creep in Rotating Disks Based on the Tresca Criterion and Associated Flow Rule[1]

P. G. Hodge, Jr.[2] The author has presented a most interesting comparison of three different theoretical solutions to the same problem, together with experimental results. Each of the theoretical solutions is based upon an extension of a corresponding theory of plasticity. In particular, the author's Method 3 represents the first time that the theory of plasticity based upon Tresca's yield condition and the associated flow rule has been extended to a creep problem. The author's Method 1 (Mises yield condition and associated flow rule) and Method 2 (Tresca yield condition and Mises flow rule) are taken from an earlier paper (author's reference 1).

All three methods yield predictions which are in qualitative agreement with the test results. However, it is evident from the author's curves that Method 1 gives the poorest agreement and Method 2 the best. The predictions of Method 3 are inferior to Method 2, but lie within the test scatter band in most cases.[3]

All of this is well presented by the author. In his concluding section, he cautions against drawing general conclusions until further test data are available, but tentatively concludes that (*a*) Method 2 is the most accurate method, but (*b*) the simplicity of Method 3 recommends it in cases where more tolerance is permitted.

To one who has followed the arguments of Hill[3] and Drucker,[4, 5] the seeming accuracy of Method 2 is quite disconcerting. In view of their strong theoretical arguments against the use of a flow rule other than the one properly associated with the yield condition, the writer is inclined to regard the excellent agreement as fortuitous and to seek for an alternative explanation.

Such an explanation is suggested by the work of Stockton and Drucker[6] who found that the actual yield condition of a real material was exceedingly complex but was reasonably well approximated by either the Mises or Tresca conditions. Thus it would appear that if better predictions than those given by Method 3 are desired, it is necessary to use a more accurate (and in general more complex) yield condition, rather than arbitrarily to combine a simple yield condition with an unjustified flow rule.

In view of the scatter generally associated with creep-test data, it is doubtful if this would be justified. Therefore, in the writer's opinion, the author's Method 3 is the only reasonable method for predicting creep in rotating disks. Thus the results of the author's paper are perhaps more valuable than he has indicated.

Author's Closure

The author would like to thank Professor Hodge for his very interesting and pertinent remarks which bring out several points not covered in the paper.

It should be mentioned that the author's primary purpose was to compare Methods 1, 2, and 3 on the basis of their utility and accuracy for design use in calculating creep deformations in rotating disks, without attempting to justify any particular method from a theoretical standpoint. The author agrees that the use of Method 2 is open to certain theoretical objections and that the excellent agreement with test data obtained by this method may be fortuitous, particularly in view of the scatter inherent in creep-test results. Also as indicated in the conclusions to the paper, further test data are needed before general conclusions may be drawn regarding the relative accuracy of the various methods used. The author has tended to favor the use of Method 3 over Method 2 primarily because of its simplicity and greater ease of application in design problems, and it is interesting to note that the former method is also preferable on theoretical grounds.

Theory of Yield Point and Transition Temperature of Mild Steel[1]

E. W. Hart.[2] The author proposes a conceptual framework in which to understand yield, and fracture of mild steel and a class of similar substances. This framework is set forth in something of the guise of a microscopic model since the central concept and working variable is the number of "relaxation centers" per unit volume. The writer feels there are numerous points on which such a model and the author's treatment of it must be criticized.

The author purports to derive $\partial n/\partial\sigma$ in the first part of the Appendix. The result as obtained in Equation [32] is due to a mathematical error. The second term in the parentheses of Equation [32] is really identical with the first term, but it has been replaced by an approximation, and so that equation should be identically zero. It is clear that no deduction of the derivative could have been made anyway, since nothing is known of the form of n, and no assumption is made about it.

Further, some constants in Equation [35] are made equal to each other by requiring that dn be a perfect differential. This requirement is certainly not physical and leads to unreal possibilities. By requiring integrability independent of the $\sigma - t$ path, the same concentration of relaxation centers at some σ and t may be achieved whether all the time t is spent at the stress σ or at a stress infinitesimally above σ_0.

Furthermore, there is some uncertainty about the effect of neglecting $e^{-\alpha(\sigma-\sigma_0)}$ since many problems of interest are concerned with small stress behavior. Also, if it is the author's intention that $\sigma = \sigma_0$ when $t = t_0$ (possibly with the restriction that σ thereafter never fall below σ_0), it is not so simple a matter to blankly assume n equal to zero at $t = t_0$, since most materials of concern to the author have quite complex histories. In connec-

---

[1] By A. M. Wahl, published in the June, 1956, issue of the Journal of Applied Mechanics, Trans. ASME, vol. 78, pp. 231–238.

[2] Professor of Applied Mechanics, Polytechnic Institute of Brooklyn, Brooklyn, N. Y. Mem. ASME.

[3] "Plastic Distortion of Non-Uniform Sheets," by R. Hill, *Philosophical Magazine*, vol. 40, 1949, pp. 971–983.

[4] "Some Implications of Work Hardening and Ideal Plasticity," by D. C. Drucker, *Quarterly of Applied Mathematics*, vol. 7, 1950, pp. 411–418.

[5] "A More Fundamental Approach to Plastic Stress-Strain Relations," by D. C. Drucker, Proceedings of the First National Congress of Applied Mechanics, Chicago, 1951, J. W. Edwards, Ann Arbor, Mich., 1952, pp. 487–491.

[6] "On Fitting Mathematical Theories of Plasticity to Experimental Results," by F. D. Stockton and D. C. Drucker, GDAM Report No. A11-44, Brown University, Providence, R. I., 1949.

[1] By F. Forscher, published in the June, 1956, issue of the Journal of Applied Mechanics, Trans. ASME, vol. 78, pp. 219–224.

[2] General Electric Research Laboratory, Schenectady, N. Y.

tion with this, it should be noted further that the "const" in Equation [36] which is equated to zero by the foregoing assumption is not a constant but is a function of σ.

The complaints of the immediately preceding paragraph are in effect protests against the indefinite nature of the model. As employed in the paper, it is little more than a way of talking about the empirical results. The fictitious relaxation centers are introduced as very vaguely defined entities, and the attempt to identify them with Frank-Read sources is only verbal. No restrictive defining properties are enunciated for these entities which might guide one in determining their role in various processes. And so, the specific application of the model to various phenomena is so discretionary and arbitrary that the writer feels the model satisfies none of the logical requirements on the structure of a theory.

Author's Closure

Dr. Hart's criticism concerns itself with the appendix and is due mainly to a difference of opinion as to the proper choice of the mathematical model.

It would be of little practical value to set down Equation [27] without being able to integrate it. By requiring dn to be a perfect differential the solution n becomes, of course, independent of the path, which is criticized as "unphysical." The author recognized this (in the paragraph following Equation [36]) but felt that the agreement of prediction with experiments was the criterion by which to judge the validity of the theory. The good agreement is probably due to the fact that n is only slightly dependent on the path in tension tests or yield delay experiments and thus can be represented by a point function. On the other hand, the phenomenon of the endurance limit of mild steel could not be represented by the point function model. The latter case is an example where, besides the path requirements, neither the term $\exp[-a(\sigma - \sigma_0)]$ nor the aging effect could be neglected.

There is no mathematical error in Equation [32]. The two terms in the bracket cannot be identical since the local stress σ_L (first term) must be larger than the shear stress σ_{ij} (second term) in the presence of any relaxation centers (see Equation [28]).

The constant in Equation [36] represents the effects of the past history (i.e., the time before $t = t_0$ and $\sigma = \sigma_0$) on the experiment under consideration and does not depend on stress. For if the stress σ would be high enough to generate relaxation centers it would have to be above σ_0 and thus past $t = t_0$. There exists, however, the possibility that σ_0 also depends on the history—a consideration which requires much further experimental work.

In summary, the author feels that this semiempirical theory, like many other theories, has necessarily some shortcomings due to the idealization of the process. However, it has proved its usefulness by the simple expressions from which the many aspects of the yield phenomenon can be derived, consistent with experimental results. It also represents an example of a type of model which seems promising for applications in mechanics though it may not appear attractive to the solid-state physicist.

A Suction Device Using Air Under Pressure[1]

M. Zaid.[2] The author has investigated an interesting physical problem, and since there is good agreement between theory and experiment, it appears that he has included the essential elements in his analytical approach. However, the following corrections should be noted.

Equation [7] neglects both the ambient and tube pressures. In the spirit of technical fluid mechanics, on which the author's paper is based, this is changed as follows:

With reference to Fig. 1 of this discussion, considering equilibrium on the disk for the region $0 \leq r \leq r_1$ we have

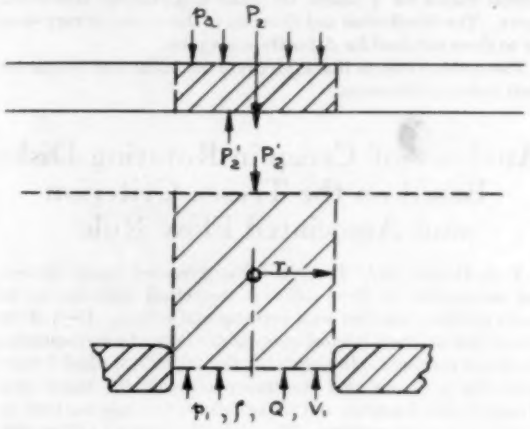

Fig. 1

$$P_2 = p_a \pi r_1^2 - P_2' \quad [1]$$

From momentum considerations

$$P_2' = p_1 \pi r_1^2 + \rho Q V_1 \quad [2]$$

However, using the general energy equation (since $V_0 = 0$)

$$p_0 = p_1 + \frac{\rho}{2} V_1^2 \left(1 + \frac{fl}{2r_1}\right) \quad [3]$$

Using Equations [3] and [2] in [1] results in

$$P_2 = -\frac{1}{2} \frac{\rho Q^2}{\pi r_1^2} \left(1 - \frac{fl}{2r_1}\right) + (p_a - p_0)\pi r_1^2 \quad [4]$$

This should replace the author's Equation [7]

The total force on the disk is the sum of the author's P_1 (Equation [6] of his paper) and P_2, Equation [4], herewith.

In the author's ψ and χ notation this becomes

$$\psi_{\text{corrected}} = \psi_{\text{author's}} + \frac{\chi^2}{2\gamma^2} \left(1 + \frac{f}{2} \frac{\lambda}{\gamma}\right) - \gamma^2 \quad [5]$$

Fig. 2 of this discussion is a graph of ψ versus χ showing experimental data, the author's ψ, and the corrected ψ for various friction factors.

It will be seen for the case under examination that $\psi_{\text{correction}}$ and ψ_{author} do not differ greatly.

It is interesting to examine two limit cases.

Case I

$$r_1 \to r_2 \quad (\gamma \to 1) \quad \text{(Fig. 3)}$$

In this case

$$\psi_{\text{author}} = -\chi^2$$

$$\psi_{\text{correction}} = -\frac{\chi^2}{2} \left(1 - \frac{f}{2}\lambda\right) - 1$$

[1] By L. F. Welanetz, published in the June, 1956, issue of the Journal of Applied Mechanics, Trans. ASME, vol. 78, pp. 269–272.

[2] Technical Consultant, Ford Instrument Corp., Division of Sperry Rand Corp., Missile Division, N. Y. Assoc. Mem. ASME.

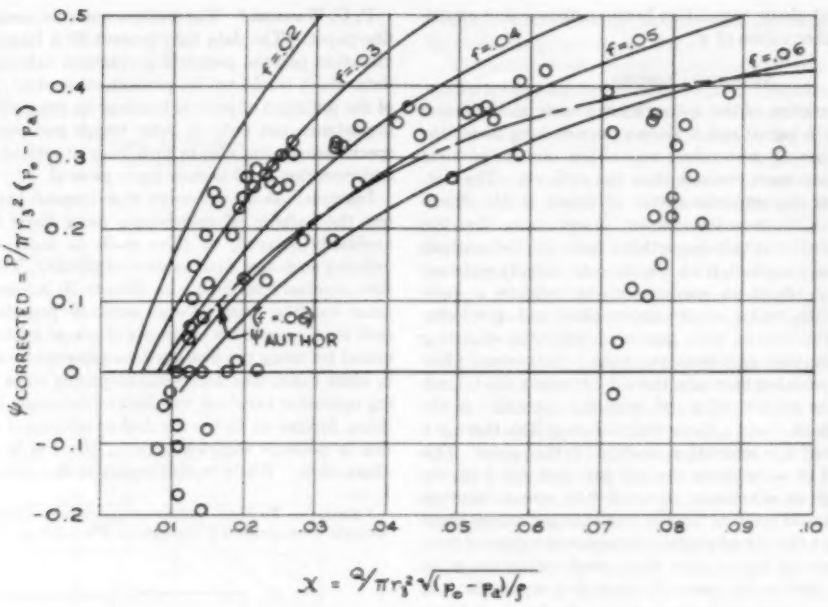

FIG. 2

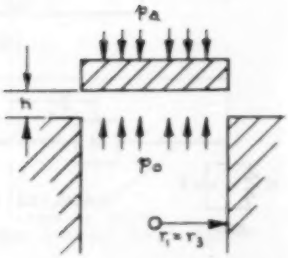

FIG. 3

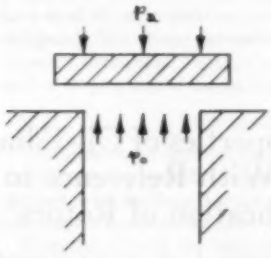

FIG. 4

Now let the upper disk and plate opening be closed so that $\eta \to 0$ then

$$\chi \to 0$$

and

$$\psi_{\text{author}} \to 0$$

$$\psi_{\text{correction}} \to -1$$

Thus both results would predict that

$$Q \to 0$$

but the author's would predict

$$P \to 0$$

While the correction shows

$$P \to \pi r_3^2(p_a - p_0)$$

which one expects if $h \to 0$ in Fig. 3.

Case II

$$(\eta \to 0) \quad \text{(Fig. 4)}$$

In this case $\chi \to 0$

and

$$\psi_{\text{author}} \to -\gamma(1 - \gamma)$$

$$\psi_{\text{correction}} \to -\gamma$$

thus

$$P_{\text{author}} \to -(p_0 - p_a)\pi r_1(r_3 - r_1)$$

$$P_{\text{correction}} \to -(p_0 - p_a)\pi r_1 r_3$$

Now since $Q \to 0$ and $p_0 > p_a$, we expect that the pressure will grade from p_0 to p_a for $r_1 \leq r \leq r_3$.
Thus

$$|P| > (p_0 - p_a)\pi r_1^2$$

However, for the case of $(r_3 - r_1) < r_1$

$$|P_{\text{author}}| < (p_0 - p_a)\pi r_1^2$$

whereas, since $r_3 > r_1$, in all cases

$$|P_{\text{correction}}| > (p_0 - p_a)\pi r_1^2$$

as expected.

In the theory of the paper both compressibility and the effect of variation of f with Q, V, Δp, h, and so on were neglected. Can the author comment on whether the inclusion of these factors

would bring about closer correlation between theory and experiment for the smaller values of η?

AUTHOR'S CLOSURE

Mr. Zaid's correction of the author's force term on the center area of the plate is logical and it gives values of force under the limiting conditions of zero plate separation and large tube diameter which are more realistic than the author's. The fact, that the resulting characteristic curves as shown in Mr. Zaid's Fig. 2 depart from the experimental results even more than the original curve, is believed to indicate that a more detailed analysis of the flow in the transition from the tube to radially outward flow is necessary. Such an analysis would indicate a stagnation point at the center of the upper plate and a velocity gradient across the stream, with maximum velocities occurring along the bell-mouthed exit from the tube. With small plate separation, even with low flow rate, the velocity along this boundary may reach the velocity of sound, with the possibility of the formation of a shock wave. Even with subsonic flow there is a strong possibility of flow separation, as stated in the paper. This may be expected to occur along the bell-mouthed exit from the tube, resulting in an effectively narrower flow stream between the plates. It would account for the fact that for intermediate values of flow rate the experimentally determined values of force on the upper plate are higher than those predicted by the equations. At high flow rates, probably both flow separation and shock waves occur, resulting in the fact that the flow-rate factor fails to continue to increase with plate separation. It is believed that shock waves and flow separation are major factors as compared with variation in the pipe friction factor in causing the difference between the experimental results and the simple theory.

Some Dynamic Properties of Oil-Film Journal Bearings With Reference to the Unbalance Vibration of Rotors[1]

P. R. TRUMPLER.[2] The limitations of ordinary critical-speed calculations, which ignore bearing-support complexities and other significant factors, are becoming rather evident to many turbomachinery designers. The authors have presented important new information on the manner in which bearings may influence rotor motion. The writer agrees with the authors in their feeling that the proportioning of bearings for low vibration levels is an important new design concept.

The linearization of the bearing problem is a good first step. With the use of modern computers the removal of this limitation should not be too difficult. Linearization of the dynamic bearing equations leads to some important questions which cannot be answered until better solutions are available. The oil-whip phenomenon, for instance, is quite important and cannot be explained by equations of the form of the authors' Equation [1].

Stodola felt that fluid friction at the disk surfaces provided the damping which limited rotor motion at critical speeds; the authors say that damping in bearings does the job. It would be interesting to consider the applications in which each form is predominant. Also, the effect of seals and internal (hysteresis) damping may not be negligible.

P. C. WARNER.[3] The authors are to be congratulated on their fine paper. The data they present fill a large gap in the rotor-vibration picture, permitting practical calculations of vibration data which would not be possible otherwise. An understanding of the influence of journal bearings on rotor vibration is of prime importance not only in rotor design and rotor-stator-clearance specifications, but also in such later situations as field balancing, and vibration trouble-shooting in general.

Inasmuch as an extensive experimental program designed to test the validity of calculations using these data has been unavoidably delayed, we have made as many checks as possible utilizing such test data as were available. The range of bearing sizes checked runs from 3 in. diam to 20 in. diam, with a range of rotor weights from several hundred pounds to 90 tons. In each case, reasonable estimates of actual critical speeds were obtained by using the bearing data reported by the authors. This, in some cases, was somewhat surprising since the range of bearing operation involved was below the range tested by the authors, forcing us to use the dashed sections of the curves. While this is perhaps somewhat risky, there is in fact currently no alternative. While we still expect to do rather extensive testing,

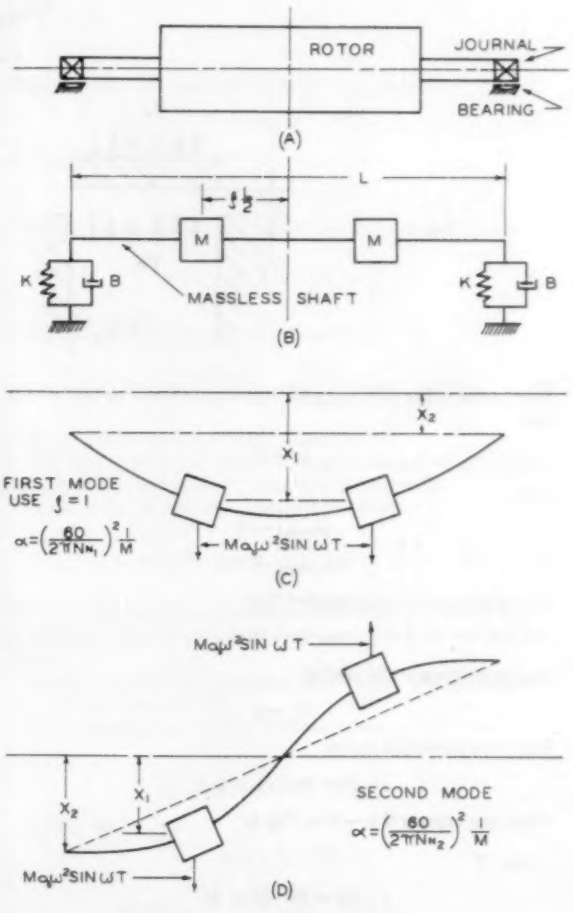

FIG. 1

[1] By A. C. Hagg and G. O. Sankey, published in the June, 1956, issue of the JOURNAL OF APPLIED MECHANICS, Trans. ASME, vol. 78, pp. 302–306.

[2] Professor of Mechanical Engineering, Illinois Institute of Technology Chicago, Ill. Mem. ASME.

[3] Medium Turbine Engineering, Steam Division, Westinghouse Electric Corporation, Philadelphia, Pa. Assoc. Mem. ASME.

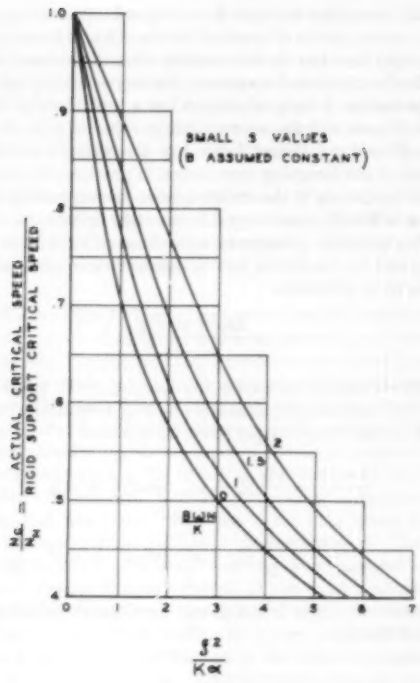

FIG. 2(a)

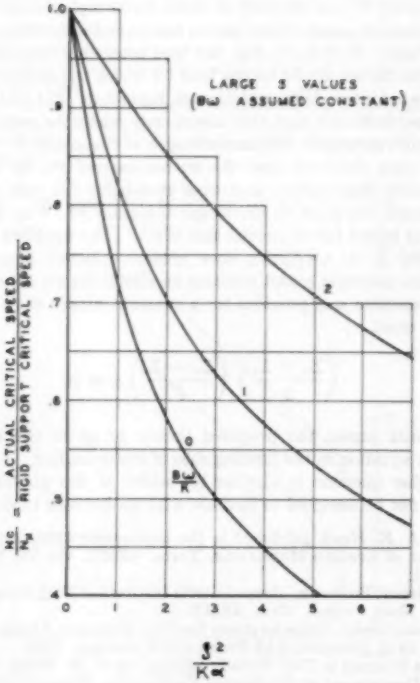

FIG. 2(b)

we feel at this time that realistic rotor-vibration calculations may be made using the authors' data.

The writer would like to take issue with the statement by the authors, that the inclusion of bearing conditions in critical-speed calculations was probably not practical until the advent of modern high-speed computers. It is strongly felt that simplified calculations of certain one and two-degree-of-freedom systems are not only sufficiently accurate when representing many actual rotors, but also afford a valuable insight into the rotor-vibration picture. This greatly increases the value of the bearing data since many people who are engaged in rotor design do not have a computer readily available. In the only cases available to the writer at this time, single-degree-of-freedom calculations of critical speeds deviated from high speed-digital computer calculations by 1.7 and 2.9 per cent.

The writer has considered the vibration of a rotor system similar to that considered by the senior author in reference (5), extending the calculations to include the second mode of vibration. Fig. 1 (*a* through *d*), herewith, indicates the system considered, and Figs. 2 (*a*) and (*b*) indicate some results. Two curves are required because of the essential difference in bearing action at high and low values of the Sommerfeld variable, as evidenced in the authors' Figs. 3 and 4.

The writer has found the charts of Fig. 2 of this discussion to be quite useful, particularly when a quick, reasonable estimate is needed. It is agreed however, that in those cases where a multirotor unit with many bearings is to be considered, a high-speed computer is a necessity. Even in such cases, if each rotor is supported in its own bearings, surprisingly good estimates may be made from Fig. 2.

Again, the authors are to be congratulated for presenting a paper of immediate practical importance which is of interest to such a large group of mechanical engineers.

AUTHORS' CLOSURE

The authors are grateful for the comments and suggestions of Prof. Trumpler and Mr. Warner, both of whom have made important contributions toward a better understanding of the vibration of rotating machines.

Equation [1] and the tests were designed to provide "equivalent" linear properties of oil films for the specific case of unbalance vibration. Stability considerations were deliberately avoided, and in the application of these dynamic properties to vibration calculations it is assumed that we have a stable system. This approach may have its defects, as Prof. Trumpler suggests; however, it seems that more general procedures await the time when operation of real bearings are more accurately specified.

Professor Trumpler also points out that sources of rotor damping other than the bearing oil films may be important. Friction of the surrounding medium can certainly be significant, as Stodola suggests, when the geometry of the rotor is favorable and when the density of the surrounding medium is high. A centrifugal water pump is an example in this category. On the other hand, the vibration magnification of a machine operating in air, hydrogen, or steam is usually far lower than would be expected on the basis of damping other than that provided by bearing oil films. Modern machines have quite rigid bearing supports, and hysteresis damping in nonrotating parts is believed to be very small. Rotor hysteresis is, of course, inoperative for unbalance vibration and has no effect on vibration magnification.

The experience reported by Mr. Warner is encouraging and lines up with our own experience in East Pittsburgh. Mr. Warner suggests that high-speed computers are not always essential, and he includes interesting and valuable charts based on simplified rotor systems. This should prove to be of especial interest to engineers concerned with critical speed calculations.

An Improved Nomogram for the Ratios of the Octahedral to the Maximum Shearing Stresses[1]

G. A. Zizicas.[2] The author should be commended for the nomographic version of the writer's original analysis.[3] When the value of the ratio $\rho = \tau_{oct}/\tau_{max}$ of the octahedral to the maximum shear for given values of parameters α and β is sought, his nomogram is simpler and in general easier to use. That of the earlier paper[3] still may be more advantageous, however, when the most appropriate value of ratio ρ is desired for a specific problem. Then, the value of ρ appearing in such a problem can be placed in the writer's nomogram and found to be contained within a closed-plane area. The centroid of that area, the center of the smallest circle containing it, or some other appropriate mean point, is easily chosen as the representative value of ρ for the problem under consideration. If all the points fall along a straight line, as in the author's nomogram, the choice of an effective value of ρ may not be made as conveniently. Moreover, for values of both α and β close to unity, the author's nomogram requires two lines at a very small angle. Their point of intersection may not be evaluated as accurately as by the writer's version. It should be noted also that the writer's version gives the values of the parameter μ, for which the author's approach requires an additional nomogram.

The relation of the author's nomogram to the writer's analysis, referred to in the author's paper, can be made clearer, by considering Equations [10] or [11] of his development,[3] either one of which can be written

$$2\alpha - 1 - \beta = \pm(1-\beta)\sqrt{\left[\frac{3}{2}(3\rho^2 - 2)\right]} \quad \ldots\ldots [1]$$

or

$$2(\alpha - 1) + (1 - \beta) = \pm(1-\beta)\sqrt{\left[\frac{3}{2}(3\rho^2 - 2)\right]} \quad [2]$$

The latter equation gives for the ratio of $1-\alpha$ to $1-\beta$

$$\frac{1-\alpha}{1-\beta} = \frac{1}{2}\left\{1 + \sqrt{\left[\frac{3}{2}(3\rho^2 - 2)\right]}\right\} \quad \text{for} \quad \alpha > \beta \quad [3]$$

$$\frac{1-\alpha}{1-\beta} = \frac{1}{2}\left\{1 - \sqrt{\left[\frac{3}{2}(3\rho^2 - 2)\right]}\right\} \quad \text{for} \quad \alpha < \beta \quad [4]$$

Now the values $1-\alpha$ and $1-\beta$ represent the vertical side of the triangles formed in the author's nomogram by joining by a straight line a value of α to a value of β and adding the inclined scale joining the points (+1.00) of his two vertical scales. Hence the common vertex of these triangles can be located on the inclined scale by the values of the right-hand side of foregoing Equation [3] or [4]. Such values are readily calculated from Table 1 of writer's paper.[3] For an appropriately chosen length of the inclined scale of the author's nomogram (chosen as, say, 5 in. or 10 cm to simplify calculations), these values locate points on the inclined scale corresponding to various values of ρ. To such points the associated value of ρ is assigned. Alternately, or as a check, various points of specified values of α and β can be joined by a straight line and its intersection with the inclined scale of the author's nomogram be assigned the corresponding value of ρ; such a procedure is most effective when a typical value of β and ρ is first chosen and the corresponding value of α is computed by, say, Equation [11] and Table 1 of the writer's paper.[3] By either one of the foregoing approaches, in practice one only needs to locate the points of the inclined scale corresponding to $\rho = 0.8165$, $\rho = 0.9428$, and integral hundredths in between.

Finally, a similar nomogram with three straight lines, as the one proposed by the author, can be constructed to give the values of the index of deviation

$$\mu = \frac{2s_2 - s_1 - s_3}{s_1 - s_3}$$

It is only necessary to adjust the inclined scale by observing that, as the foregoing Equations [3] and [4] combined with Equation [18] of the writer's paper show, for instance

$$\frac{1-\alpha}{1-\beta} = \frac{1}{2}(1+\mu) \quad \text{when} \quad \alpha > \beta \quad \ldots\ldots [5]$$

$$\frac{1-\alpha}{1-\beta} = \frac{1}{2}(1-\mu) \quad \text{when} \quad \alpha < \beta \quad \ldots\ldots [6]$$

The actual nomogram is not shown here but it could be drawn without difficulty.

[1] O. P. Kharbanda, published in the June, 1956, issue of the Journal of Applied Mechanics, Trans. ASME, vol. 78, p. 312.

[2] Assistant Professor of Engineering, University of California, Los Angeles, Calif.

[3] "A Simple Nomogram for the Ratios of Octahedral to Maximum Shearing Stresses and Its Physical Interpretation," by G. A. Zizicas, Journal of Applied Mechanics, Trans. ASME, vol. 76, 1954, pp. 291–293.

The Propagation of Fatigue Cracks[1]

F. A. McClintock.[2] Since the author's model is based on elements behaving in a macroscopically plastic manner, valid results should still be obtained at stress levels high enough so that the crack propagates all the way to failure under the first application of load. In other words, the load producing fracture under static conditions should be the load for which the rate of growth becomes infinite. Differentiation of Equations [27] and [28] of the paper indicates that this occurs only when the nominal applied load reaches the ultimate strength of the material. Experimental data obtained since the author carried out his analysis have shown that fracture may occur even below the yield stress in some cases, the more so the longer the crack.[3,4] Why does the proposed model fail to predict this effect? The modified Griffith equation, $\Sigma = \sqrt{(Ep/b)}$, does predict a length dependence. Since the proposed model contains an elastic matrix fitted to the elastic solution and provides for a constant plastic work per unit area of crack

$$\left(\frac{\Sigma_1 + \Sigma_0}{2}\right)\left(\frac{\Sigma_1 - \Sigma_0}{F}\right)a = p$$

one would expect the proposed theory to go to the modified Griffith equation in the limiting case of static loading.

Another question is whether the width of the plastic zone a should not be assumed to increase with an increase in the length

[1] By A. K. Head, published in the September, 1956, issue of the Journal of Applied Mechanics, Trans. ASME, vol. 78, 1956, pp. 407–410.

[2] Assistant Professor, Massachusetts Institute of Technology, Cambridge, Mass. Assoc. Mem. ASME.

[3] "Some Design Considerations for Tear Resistant Airplane Structures," by A. Sorenson, IAS Preprint 618, January, 1956.

[4] "On Fracture in Thin Metallic Sheets," by F. M. White, Master's thesis, Department of Mechanical Engineering, Massachusetts Institute of Technology, Cambridge, Mass. May, 1956.

of the zone, as can be observed experimentally and has been shown theoretically for shear.[5]

Finally, the writer now realizes that it should have been pointed out, in the reference given by footnote 2 of the paper, that the length of the cracks was not entirely negligible compared to the size of the specimens, so that the close agreement obtained between those experiments and the older theory may have been rather coincidental.

Pending exact solutions from the theory of plasticity, it is only by inventing, analyzing, and, where necessary, modifying models such as the author's, that an understanding of the mechanics of crack growth can be obtained.

N. J. Wadsworth.[6] The writer has made a few observations on the rate of growth of fatigue cracks in annealed copper which may be of interest. Cylindrical polycrystalline specimens (grain size about 0.1 mm) were tested under reversed axial tensile-compressive stress. The peak force applied to the specimens was held constant during the test. The fatigue stress used was 8.4×10^8 dynes cm^{-2}, the ultimate tensile strength of the specimens calculated on the original area was 2.1×10^9 dynes cm^{-2}, and the original yield stress was less than 3×10^8 dynes cm^{-2}. Fatigue cracks were detected when they were one grain long about halfway through the test. (Other changes were seen earlier.[7]) The length of the crack on the surface of the specimen was measured at intervals and the results of measurements on two specimens are shown in Fig. 1 of this discussion. (Length of crack)$^{-1/2}$ decreases approximately linearly with increasing cycles until the length of the crack is an appreciable fraction of the specimen diameter (4 mm) when the rate increases. All four cracks observed on specimen 58 grew at the same rate, and the proposed growth law fits the observations well. Even when the cracks were 0.5 mm long the rate of growth of each end was still less than 1 atom per cycle.

No measurements were made on the variation of rate of propagation with stress, but it seems that the rate must be more stress-dependent than is given by Equation [28] of the paper. At 8.4×10^8 dynes cm^{-2} the spreading of a crack already one grain long took about 2 million of the total 3.6 million cycles. Using this, Equation [28] would predict that the same growth would take one million cycles at a stress of 10.5×10^8 dynes cm^{-2}, if the observed U.T.S. is used for Σ_1, and longer if a higher value is used. A slight extrapolation of the *S-N* curve for these specimens[8] indicates that the total life would in fact be less than this. It would be of interest to have the author's views on this and also on the cracks studied by Frost[9] which stop growing when they are a few tenths of a millimeter long.

The measurements described were made when the writer was at the Physics Department of the University of Bristol.

[5] "Elastic-Plastic Stress and Strain Distribution Around Sharp Notches Under Repeated Shear," by J. A. H. Hult and F. A. McClintock, Ninth International Congress of Applied Mechanics, Brussels, Belgium, 1956.

[6] Royal Aircraft Establishment, Farnborough, Hants, England.

[7] "The Origin of Fatigue Fracture in Copper," by N. Thompson, N. Wadsworth, and N. Louat, *Philosophical Magazine*, 8th series, vol. 1, 1956, p. 113.

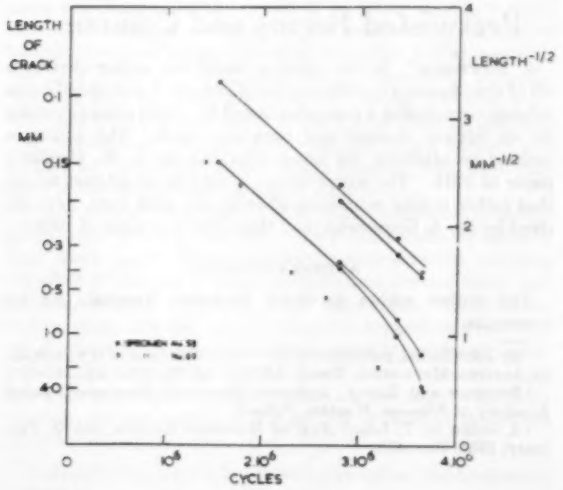

Fig. 1

Author's Closure

I would like to thank Professor McClintock and Dr. Wadsworth for their interest in this paper. Professor McClintock has raised an apparent discrepancy in the behavior of the model crack under tensile loading. The reason for this is as follows. In analyzing the behavior of the model crack under fatigue a number of approximations were necessary. Although these approximations were reasonable for fatigue, they are not all reasonable for fracture in a single loading; e.g., the first approximation made (leading to Equation [PM5]) was that the plastic deformation per half cycle was small. To analyze the tensile fracture of this model crack it is therefore necessary to start at the fundamental Equations [PM1–4]. I have now done just this and find that the Griffith-Orowan equation given by Professor McClintock follows directly, without any approximations being used. Although straightforward, the derivation is rather too lengthy to give here.

Professor McClintock's second question is one which has been the cause of much argument. For the model crack, the elastic stress concentration, the opening of the crack under load, and the static fracture strength all depend on the length of the crack through the factor $[b/a]^{1/2}$. There appear to be two reasonable choices, either that a is proportional to b, or that a is constant. In the first case it would mean that a crack remains geometrically similar as it grows and that a large crack has the same stress concentration as a small crack. As would be expected, the growth of a fatigue crack in this case follows an exponential law. The original reason for keeping a constant was the feeling that as a fatigue crack grows it does not remain geometrically similar but that the tip of the crack has a constant configuration, probably determined at an atomic level, which is independent of the length of the crack. It seemed reasonable then to keep a constant, especially as this implied that the stress concentration then increased as the square root of the crack length. For the original purpose of this model, to describe a fatigue crack, I think the choice of a constant is appropriate even if this means abandoning the literal interpretation of a as the width of the plastic zone.

It appears very difficult to make allowance for the finite size of the specimen, so I have no comment on Professor McClintock's final point.

I would like to thank Dr. Wadsworth for his data, as published measurements on the growth of fatigue cracks are very few. His observation on the stress dependence of the crack growth rate appears to be correct, although in view of the scatter of fatigue data it is a borderline case. However, this aspect appears to require further investigation. His final point is one for which I can offer no explanation.

[8] Footnote 7, Fig. 2, line C.

[9] "Crack Formation and Stress Concentration Effects in Direct Stress Fatigue," by N. E. Frost, *The Engineer*, vol. 200, 1955, pp. 464 and 501.

Vibrations of Cylindrical Shells With Rotatory Inertia and Shear[1]

E. H. KENNARD.[2] The principal interest of this paper lies in those vibrations, not usually considered, in which the motion varies predominantly in the radial direction within the thickness of the shell. Perhaps a misgiving may be expressed, however, concerning an inconsistency in the approximate equations that are used. "Radial lines remain straight," yet in Equation [8] of the paper, shear is introduced, as a consequence of which radial lines must distort. In the Timoshenko beam theory a similar obscurity affects only the significance and value of K, but the consequences might be more serious when local motions play a predominant role.

In the case of ordinary long-range vibrations, where the motion can be described adequately in terms of the displacements of the median surface, it would seem that a better estimate of the effects of rotatory inertia and transverse shear could be obtained with use of more complete equations such as those of Epstein [in reference (3) of authors' Bibliography].

AUTHORS' CLOSURE

In the authors' opinion, one need have no misgiving concerning the inconsistency mentioned by Dr. Kennard, since the principal aim of the paper is not to study the vibrations in which variations across the wall thickness play a predominant role, but, rather, to obtain a first approximation of the influence of shear and rotatory inertia on the first two modes of vibration. In this approximation, the assumption that "radial lines remain straight" is valid. The use of Epstein's equations to study these modes would lead to greater mathematical and computational complexity, which, the authors believe, is probably not warranted.

An Elastoplastic Thermal-Stress Analysis of a Free-Plate[1]

PAUL SEIDE.[2] To some extent the author restricted himself unnecessarily in this recent paper since for this problem a solution could have been obtained, in principle at least, for a strain-hardening material with temperature-dependent properties. Because of the assumptions inherent in the formulation of the problem—that we are considering the interior of a free plate subjected to a uniform heat input and are sufficiently removed from the edges—considerations of symmetry and equilibrium indicate that the stresses are given by (using the author's notation)

$$\sigma_{yy} = \sigma_{zz} = \bar{\tau}(\bar{x})$$

$$\sigma_{xx} = \sigma_{xy} = \sigma_{xz} = \sigma_{yz} = 0 \quad \ldots\ldots\ldots\ldots [1]$$

But this would indicate that the stresses are in constant ratio and hence that the strains are in constant ratio, so that deformation theory can be used. Since we have only one unknown, $\bar{\tau}(\bar{x})$, the plate problem is somewhat analogous to the problem of a long, thin rectangular beam subjected to a temperature distribution which is uniform along the length of the beam but varies throughout its depth. For this problem there need be no restriction on material properties or, indeed, on the form of the temperature variation throughout the depth. It can be shown from the stress-strain and strain-displacement relations that the displacements u and v must be linear functions of the co-ordinate $\bar{x}$ and that the stress distribution for monotonically increasing stresses is given by

$$\bar{\tau}(\bar{x}) = -\frac{\alpha T(\bar{x})}{\dfrac{Y_2 - \nu}{E} + \dfrac{Y_2}{E_s}} + A + B\bar{x} \quad \ldots\ldots\ldots [2]$$

where E is Young's modulus as a function of temperature, E_s is the secant modulus for the uniaxial stress-strain curve as a function of $\bar{\tau}(\bar{x})$ and temperature, and A and B are constants determined by the condition that the stress distribution $\bar{\tau}(\bar{x})$ yields zero resultant force and zero resultant moment over the thickness. It can be seen that in general the determination of A and B is quite difficult and that trial-and-error methods are necessary. When unloading of any portion of the thickness occurs the solution must, of course, be modified to take into account the change in stress-strain relations in that region.

These remarks should not detract from the paper which contains an interesting approximation for the temperature distribution through the plate and a quite complete discussion of the stresses for both the loading and unloading conditions in a plate of a perfectly plastic material. The main purpose of these comments is to indicate that the author's solution could have been obtained in a more straightforward manner and could have been generalized, in principle, beyond the assumption of perfect plasticity.

AUTHOR'S CLOSURE

The author agrees with Dr. Seide that, for this particular problem, the deformation and flow theories would yield identical results. However, he wished to formulate this problem in a manner which would allow a completely analytical treatment and which would permit extension to other thermal and residual stress problems for which the deformation theory would be inadmissible. Such extensions have been made and will be reported on shortly.

Pretwisted Beams and Columns[1]

J. NOWINSKI.[2] In his valuable paper the author derives a set of simultaneous equilibrium equations for a pretwisted beam column, constituting a generalization of the well-known equations for an initially straight and untwisted beam. The author is inclined to attribute the latter equations to J. N. Goodier's paper of 1941. The writer thinks it may be of interest to say that rather similar equations, although for solid bars, were derived by Dr. A. Grzedzielski and the writer in a paper of 1938.[3]

AUTHOR'S CLOSURE

The author wishes to thank Professor Nowinski for his comments.

---

[1] By T. C. Lin and G. W. Morgan, published in the June, 1956, issue of the JOURNAL OF APPLIED MECHANICS, Trans. ASME, vol. 78, pp. 255–261.

[2] David Taylor Model Basin, Washington, D. C.

[1] By Jerome Weiner, published in the September, 1956, issue of the JOURNAL OF APPLIED MECHANICS, Trans. ASME, vol. 78, 1956, pp. 395–402.

[2] Member of Technical Staff, The Ramo-Wooldridge Corporation, Los Angeles, Calif. Assoc. Mem. ASME.

[1] By John Zickel, published in the June, 1956, issue of the JOURNAL OF APPLIED MECHANICS, Trans. ASME, vol. 78, 1956, pp. 165–175.

[2] Professor and Editor, *Archiwum Mechaniki Stosowanej*, Polish Academy of Sciences, Warsaw, Poland.

[3] A review by T. Leser, *Applied Mechanics Reviews*, vol. 9, February, 1956, Rev. 436.

Book Reviews

Fifty Years' Boundary-Layer Research

50 Jahr Grenzschichtforschung. Edited by H. Görtler and W. Tollmien. Friedr. Vieweg & Sohn, Braunschweig. (Sole distributors in U.S.A., United Kingdom, and Indonesia, I. R. Maxwell & Co., Ltd., 4 & 5 Fitzroy Square, London W.1, England; 122 East 55th Street, New York 22, N. Y.) Cloth, 6½ × 9½ in., viii and 499 pp., 236 figs., D.M. 66.

Reviewed by William R. Hawthorne[1]

THIS memorial volume marks the fiftieth anniversary of Prandtl's epoch-making paper which, in 1904, introduced the concept of the boundary layer. It is nearly 500 pages long and contains 44 papers by 56 authors nearly all of them describing original work. This collection of papers is intended to illustrate the features of boundary-layer research which are attracting attention today and thereby show how much progress has been made in the first 50 years. It is indeed a mixed bag which lacks any arrangement except that of printing the papers in the order in which the manuscripts were received. The editors present a disarming excuse for this apparent untidiness. It is the untidiness of the subject which in spite of 50 years of useful work still evades either full mathematical description or control of its phenomena in practice. The reader, after an attempt to marshal the papers in some consistent pattern for himself, will agree that their variety is remarkable. Sixteen of the papers are in German and one is in French; the remainder are in English. Translations of the abstracts would have been helpful.

The first paper in the volume is an able and concise review of the 50 years of research, by W. Tollmien. There are about five theoretical papers on the laminar, incompressible, and two-dimensional boundary layer which deal with the conditions at its outer edge (A. Betz has a new computational method), the calculation of separation, the effect of equation of state for liquids, and the treatment of boundary layers in electron stream. Porous walls are treated mathematically in two papers. Unsteady laminar boundary layers are analyzed by two authors, and one paper gives some measurements of the growth of boundary layer in a shock tube. There is great interest in three-dimensional, incompressible laminar boundary layers. The effect of sudden lateral perturbation of a boundary layer, rotationally symmetrical boundary layers on rotating bodies and in conical nozzles, flow over ellipsoids, and the question of flow direction at separation are analyzed.

H. Görtler and G. Hammerlein discuss Görtler vortexes and present an interesting theory which suggests that they may occur in the neighborhood of a stagnation point.

There are about eight papers on laminar compressible boundary layers, some with heat transfer. One of them treats the effect of weak shock interaction; three offer theoretical results including the effect of Prandtl Number, viscosity-temperature index, and frictional heating on velocity and temperature distributions; another deals with the boundary layer in hypersonic flow. The use of a Stanton tube as a skin-friction meter in compressible flow is the subject of another paper. Experiments on the boundary layers of supersonic jets are described. The heating of a flat plate suddenly set into motion is the subject of another theoretical analysis.

Transition is discussed in seven papers of which two are primarily analytic and the remainder contain some description and analysis of experiments. In particular, A. Fage summarizes results obtained in the past 25 years with the fluid-motion microscope. F. X. Wortman describes the visualization and measurement of stream-line position with tellurium, noting the existence of three as well as two-dimensional oscillations near transition. Eckert and his co-workers report experimental results on transition on a vertical heated plate.

Papers by D. Coles, E. R. van Driest, and C. Ferrari on the turbulent boundary offer methods of estimating skin friction and heat transfer based on certain empirical assumptions. This is naturally an area of great interest.

It is evident from the above summary that theorists still have much to discuss on even the simplest type of boundary layer and that considerable effort is being devoted to transition, compressibility, and three-dimensional effects.

Eight other papers not easily categorized in the above list include the analysis of radial jets, the boundary-layer growth at entry to a pipe, the measurement of turbulence in a diffusing channel, the analysis of flow under gravity in a duct with heating from below, the use of sailplanes for boundary-layer research, the flow of lubricant in journal bearings, and A. D. Young and S. Kirby's calculations of the drag of biconvex wing sections at supersonic speeds.

On the whole the volume achieves its object, although for the lay reader less exhausting and more instructive ways of obtaining a summary of the present state of boundary-layer research probably could be devised. It has the quality of a still taken from a motion-picture film. It will disappoint some; others may find it a stimulus for further exploration. However difficult it may be for the general reader, there is no doubt that the volume presents an appropriate tribute to Prandtl's genius which is dignified by the authors' efforts to contribute their original work. The research worker will inevitably find this an interesting volume for both reference and study.

[1] University Engineering Laboratory, Cambridge, Cambridgeshire, England.

Engineering Mechanics

Engineering Mechanics. By S. Timoshenko and D. H. Young. McGraw-Hill Book Company, Inc., New York, N. Y., Fourth Edition, 1956. Cloth, 9 × 6 in., x and 478 pp., plus appendixes, illus., $7.50.

Reviewed by N. O. Myklestad[2]

THE body of this book is divided into two equal parts: part one, statics; and part two, dynamics. Almost all the headings of this new edition are identical with the ones of the third edition; however, the material arrangement and the presentation of the subject matter have been thoroughly revised. In doing this the authors have had these objectives: (1) simplification of the text proper, (2) improved arrangement of subject matter, and (3) de-emphasis of the algebraic treatment of problems. The problem sets have been completely revised, and they contain a high percentage of new problems. The reviewer is sorry to see the algebraic treatment of problems de-emphasized; but the book as a whole is outstanding and makes a well-balanced textbook of mechanics.

[2] 5346 Calle Del Norte, Phoenix, Ariz. Mem. ASME.

Suspension Bridges

STATISCHE UND DYNAMISCHE BERECHNUNG ERDVERANKERTER HÄNGEBRÜCKEN MIT HILFE VON GREENSCHEN FUNKTIONEN UND INTEGRALGLEICHUNGEN. By Hugo Moppert. Veröffentlichungen des Deutschen Stahlbau-Verbandes. Heft 9. Stahlbau-Verlags GMBH, Köln, Germany, 1955. Paper, 6½ × 9½ in., 114 pp., Dm 18.

REVIEWED BY ALI KYRALA[3]

THIS dissertation systematically treats the static and dynamic problems of suspension-bridge design from a mathematical viewpoint. The first section of 47 pages is devoted to formulating the static problems in terms of Green's functions and to determining the influence functions for the bending and torsion of solid web girders. There is a very brief final article on the extension to framed girders.

In the second section the integral equations for bending and torsional vibrations are set up and the Rayleigh principle applied to the determination of characteristic frequencies for a variety of special cases. The last section is a numerical application of the methods expounded in the preceding sections to the Cologne-Mülheim bridge. Antisymmetric characteristic frequencies for bending are determined by replacing the integral equation concerned with a set of linear equations and also by the Rayleigh method. The two methods agreed to within 1.1 per cent. Further computations of the characteristic frequencies for symmetrical bending and symmetrical and antisymmetrical torsional vibrations are carried out by the Rayleigh method.

Although the equations read smoothly, the text is not distinguished by any striking expository style. The printing is excellent. The publication can be recommended as a class reference for courses in suspension-bridge design and also as a professional reference for practicing engineers in this field.

High-Speed Aeronautics

PROCEEDINGS OF THE CONFERENCE ON HIGH-SPEED AERONAUTICS, Polytechnic Institute of Brooklyn, Jan. 20–22, 1955. Edited by Antonio Ferri, N. J. Hoff, and P. A. Libby. Polytechnic Institute of Brooklyn, Brooklyn, N. Y., 1955. Cloth, 8½ × 6 in., vi and 392 pp., illus., $5.25.

REVIEWED BY W. R. HAWTHORNE[4]

THIS volume contains the papers presented at a conference on high-speed aeronautics which was part of the centennial celebration of the Brooklyn Polytechnic Institute. The volume consists of the 16 papers given during the three-day session, an account of the conference by N. J. Hoff, and a list of the participants.

Libby and Bloom describe the facilities for experimental research available at the Institute's Laboratory in Freeport, N. Y. Air-storage capacity up to 2800 psi is used to supply both supersonic and hypersonic tunnels. Some theoretical work at the Institute described by Antonio Ferri has concerned itself with analytical solutions of the high-speed flow around bodies of aeronautical interest without the normal linearization of the equations of motion. Examples are given of solutions in which linearized disturbances are superposed on a basic nonlinearized flow approximating to the actual flow field. The paper includes descriptions of methods of dealing with transonic regions and with interferences.

N. J. Hoff analyzes a redundant framework, a rigid frame, and a thick-walled tube in the presence of steady creep in a paper which presents the beginning of a method of creep stress analysis to the engineer.

The first guest paper is that of Dr. von Karman who surveys the solutions in sub and supersonic wing theory. His brilliant summary of the state of understanding of compressible flow, including transonic and hypersonic flow and shock-boundary layer interaction as well as other pertinent topics, is likely to be of great value to the student. Another valuable summary is given in H. L. Dryden's paper on transition at sub and supersonic speeds. This promises a rapid development of our knowledge of the origin of turbulence. L. Crocco presents an original contribution to the theory of shock-boundary-layer interaction with complementary experimental results. Oswatitsch and Keune present a new method of computing the flow around bodies of revolution at Mach number unity. Experimental results show that the theory is satisfactory in practice. In a short paper Busemann discusses the noise from supersonic aircraft and suggests some simple methods of analyzing it. R. T. Jones discusses the factors affecting the design of supersonic jet transports.

Michel and Sirieix present experimental results on the effect of incidence on the characteristics of an airfoil at transonic speeds. H. Schlichting gives an interesting summary of analyses of the two-dimensional performance of turbine and compressor cascades.

In three papers L. Broglio, J. Duberg, and W. H. Horton present some aspects of the problems set by the thermal effects on aircraft structures in high-speed flight. Broglio's thermal balance method is of interest. Duberg's review of NACA work includes a discussion of the effects of creep and of transient temperature distributions in typical structures. Horton described similar effects but also summarizes work on heat transfer in various constructional features.

In the hypersonic field Smelt discusses the problem of designing wind tunnels for very high Mach numbers, and Kantrowitz surveys the properties of air in shock waves of very high temperature.

The papers in this volume are on the whole of a high standard and can be recommended both to the student for reference and to the lay reader as a summary of the state of the art in a rapidly moving field.

---

[3] Mathematician-Physicist, Lessells and Associates, Inc., Boston, Mass.

[4] Professor, University Engineering Laboratory, Cambridge University, Cambridge, England.

Information for Authors

• Manuscripts should be submitted in final form to the Technical Editors. Each manuscript must be accompanied by a statement that it has not been published elsewhere nor has it been submitted for publication elsewhere. A paper which would occupy more than five pages of the Journal may be returned to the author for abridgment.

• The author should state his business connection, the title of his position, and his mailing address. A short abstract (50 to 100 words) should be included on the first page immediately preceding the introductory paragraph of the paper.

• Three copies of the manuscript are required. One of these must be a carefully prepared printer's copy, typed in double spacing, on one side of the page only, with wide margins, on 8½ by 11-in. opaque white paper. Mimeographed manuscripts, if prepared with exceptional care, can be accepted provided they are completely edited.

• All mathematical expressions should be written by hand in ink or set out by typewriter in a way which would define each symbol unambiguously. Care should be taken to distinguish between capital and lower-case letters, between (0) and the letter (*O*), between the numeral (1) and the letter (*l*), etc. A list of symbols carefully marked, if it has not been included in the body of the paper, should accompany the manuscript on a separate page.

• Before preparing a manuscript the author should study printed articles in the Journal, with special attention to the form and style of mathematical expressions, tables, footnotes, references, and abstract. Care should be taken to arrange all tables and mathematical expressions in such a way that they will fit into a single column when set in type. Equations that might extend beyond the width of one column (fractions that should not be broken or long expressions enclosed in parentheses) should be rephrased to go on two or more lines within column width. Fractional powers are preferred to root signs and should always be used in more elaborate formulas.

• A normal paper should not exceed five pages in the Journal. It is about 6000 words or twenty to twenty-five double-spaced typewritten pages inclusive of drawings. A Brief Note should not exceed 750 words or about one column in the Journal inclusive of drawings.

• Originals and two copies of figures must accompany the manuscript. Line drawings should not be larger than 8½ × 11 inches, and should be planned for reduction to column width. Lettering should be large enough to be clearly legible when the illustration is reduced. The originals of line drawings must be in India ink on white or pale blue tracing paper or tracing cloth. Photographs of equipment or test specimens must be glossy prints and should be used sparingly. Captions for figures should be typed double-spaced and included as the last page of the manuscript. The figure number and author's name should be written in the margin or on the back of each illustration.

• Titles of papers should be brief. If an adequate description of the subject requires a title which, along with the authors' names, would occupy more than one line on the cover of the Journal, a separate shorter title should be submitted.

• Authors can obtain copies of the ASME Manual MS-4, "An ASME Paper," from the Technical Editors and are urged to do so before drafting their papers in final form.

• Papers published in the Journal of Applied Mechanics must first be presented at a Meeting, either in person or by title. Scheduling of papers is in the hands of the Secretary of the Applied Mechanics Division. Authors should indicate their preference in this respect to the Technical Editors when submitting a paper.

• An author is entitled to 25 preprints free of charge (in the case of two authors, 15 each; three or more authors, 10 each). Larger quantities of preprints or reprints can be ordered from Editorial Department, The American Society of Mechanical Engineers, 29 West 39th Street, New York 18, N. Y. Quotations will be sent on request.

D. C. Drucker and J. Kestin, *Technical Editors*

Please address all communications to: Technical Editors
Journal of Applied Mechanics, ASME
Division of Engineering
Brown University
Providence 12, R. I.

To Be Published [illegible]

CUMULATIVE INDEX TO ASME TECHNICAL PAPERS

Price [illegible]

This Index to ASME [illegible] formerly published in the Transactions, the Journal of Applied Mechanics, and Mechanical Engineering will consist of two sections: The first will cover approximately 2200 papers published in these magazines from 1940 to 1956. This subject index will list the titles of the papers alphabetically under as many headings as are necessary and include extensive cross-references for quick orientation to related material. Its chronologically arranged authors' index will give the headings and the page under which each paper is listed in the subject index. The second section will be a reprint of the Sixty-Year (1880–1939) Index originally published in 1940 and now out of print. The size of the volume will be 9" x 12" and the binding, dark blue fabrikoid with title stamped in gold on the spine.

To Be Published [illegible]

GLOSSARY OF TERMS IN NUCLEAR SCIENCE AND TECHNOLOGY

Price, $5.00*

This book consolidates in a single alphabetical listing some 1500 terms and definitions originally published in nine separate sections entitled: Atomic Reactor Theory, Nuclear Engineering, Chemistry, Chemical Engineering, Biophysics, Radiobiology, Instrumentation, Isotope Separation, and Metallurgy. These are special terms peculiar to the fields of nuclear energy and the respective fields in a different sense or with different emphasis from what is commonly understood in other connections, and also definitions in the same way, but so frequently or so to be unfamiliar.

While this 1957 Edition includes no new terms, it has been greatly improved by the removal of ambiguities in the former definitions, simplification and modification of over [illegible] definitions, and the correction of typographical errors.

Published [illegible]

CREATIVE ENGINEERING

Price $1.00*

Originality, intuition, and creative ability in the engineering profession and how these qualities may be encouraged and developed are the subjects here discussed.

[illegible]

*20% discount [illegible]

AMERICAN SOCIETY OF MECHANICAL ENGINEERS

[illegible] New York 36, N. Y.